Determining Upper Limb Kinematics and Dynamics During Everyday Tasks

Ingram A. Murray, B.Sc. (Hons.), M.Sc.

This thesis is submitted in fulfilment of the requirements for the Degree of

Doctor of Philosophy

Centre for Rehabilitation and Engineering Studies

Department of Mechanical, Materials and Manufacturing Engineering

University of Newcastle upon Tyne

November 1999

Declaration

This Thesis describes work carried out by the author in the Department of Mechanical, Materials and Manufacturing Engineering of the University of Newcastle upon Tyne, United Kingdom, during the period December 1996 to November 1999, under the supervision of Professor G. R. Johnson.

This Thesis describes original work which has not been submitted for a higher degree at any other University and is the work solely of the undersigned author, except where acknowledged in the text.

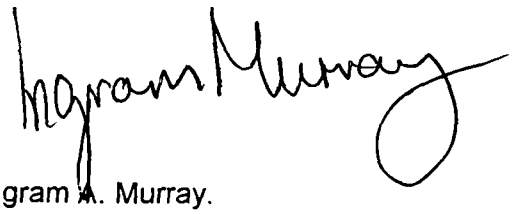

Ingram A. Murray.

ABSTRACT

In planning orthopaedic procedures or designing joint replacements for the upper limb, detailed knowledge on the kinematic and dynamic behaviour of the shoulder, elbow and wrist joints during the performance of everyday tasks is essential.

Previous studies have included kinematic analyses of everyday activities involved in feeding and personal hygiene though none have included both the kinematic and dynamic analyses of these tasks. This study has involved the development, validation and application of experimental methods and analysis techniques, enabling the measurement and modelling of upper limb kinematics and dynamics.

A four camera video-based motion analysis system was used to track reflective spheres attached at specific locations on the upper limb and trunk. Novel methods for the definition of the embedded trunk frame and glenohumeral rotation centre were incorporated. Joint attitudes, cadences, angular velocities and angular accelerations were calculated prior to the determination of external forces and moments through the dynamic modelling of the upper limb.

The procedures developed have been validated against known measurements and the results of previous studies. These have been applied to obtain kinematic and dynamic data from unimpaired subjects and subjects with shoulder impairment during performance of ten everyday tasks involved in feeding, personal hygiene and the use of everyday objects.

Elbow and shoulder flexion were found to be the primary components for the successful completion of the selected tasks.

Reaching to the opposite side of the neck was identified as being the most complex of the activities tested in terms of rotation at the shoulder and elbow.

Characteristic patterns of motion at the joints of the upper limb were identified during anterior targeted lifting.

Differences in performance between the unimpaired and impaired subjects were identified, particularly in the results for cadence and the individual joint velocities and accelerations.

ACKNOWLEDGEMENTS

The following people deserve my gratitude for their involvement in my work in Newcastle over the past three years.

Firstly I would like to thank the Engineering and Physical Sciences Research Council and DePuy International, for providing the funding that enabled me to carry out this work.

I would equally like to thank Professor Garth Johnson for the initial opportunity to come to Newcastle, for supervising this work and for his advice and encouragement throughout its completion.

Thanks to John Williams, Senior Lecturer in the Department of Trauma & Orthopaedic Surgery in the University of Newcastle Medical School and shoulder surgeon in the Freeman Hospital, who provided access to impaired subjects and whose previous research experience was extremely useful.

Thanks also to Mary Stewart, Senior Bioengineer with DePuy International in Leeds, for her time spent discussing this work both in Leeds and Newcastle and her suggestions.

Grateful thanks to those brave subjects who 'volunteered' for my study.

Thanks to Germano Gomes, who occupied the other half of my office and aided on many occasions when confusion reigned and to all of my other fellow CREST members who provided technical and moral support throughout the period of my work, from the early days of Nick, Mike, Paul and Jeanne to the current crowd David, Iain, Fred, Patric, Jose and Eve.

Last but not least, thanks to the family Murray for their support, Mum, Dad and Calum too and most of all, thanks and apologies to Rachel, who put up with my lab induced absence on so many occasions.

TABLE OF CONTENTS

CHAPTER 1 : INTRODUCTION

1.1 Foreword

The measurement of human motion involves obtaining and comparing the position and orientation of the involved limb segments during movement. The relative motion between these segments may be described in terms of the kinematic descriptors; joint angles and linear and angular velocities and accelerations.

External forces and moments at or around the joints may be calculated by combining information on the mass of the limb segments and any additional load with the kinematic results. These forces and moments are the dynamic or kinetic descriptors of human motion, relating segment motion to its causes.

Knowing the external kinematics and dynamics, properties such as the moments and contact forces at each of the joints may be obtained through calculation of the associated muscle forces. The measurement and modelling of such parameters for the lower limb have been performed extensively to determine the loading cycle and kinematics of the hip and knee during gait.

Less frequently studied, probably due to its complexity, have been the same properties of upper limb motion. Upper limb joints and particularly the shoulder, are subjected to larger ranges of motion than the lower limb and involve highly complex three-dimensional task specific motions. In comparison, lower limb motion is primarily two-dimensional during gait, having more of a cyclic nature with relatively simple and consistent patterns of motion largely associated with a single activity.

A major procedural difference between upper and lower limb studies is that the latter usually involves the measurement of ground reaction forces which are not relevant in upper limb studies.

As highlighted in the President's Lecture at the International Society of Biomechanics, XVIIth Congress (Rau (1999)), there is a lack of a standardised marker attachment pattern for upper limb studies and of detailed biomechanical models of the upper limb. The scarcity of databases of information from upper limb studies on unimpaired subjects was also highlighted.

Such databases of information are essential in the investigation of shoulder impairment and injury as well as in the development of design specifications for artificial joint implants. Joint implants for the upper limb can in general be considered to be at an earlier stage of development than those for the lower limb and studies of the kinematics and dynamics of upper limb motion can play a key role in rectifying this.

The majority of previous upper limb studies have been related to the performance of standard tests such as abduction rather than genuine every day tasks, making the results of limited practical use in, for instance, the development of implants. Before significant changes can take place there is a requirement for data on the kinematics and dynamics of the upper limb, associated with its every day use.

1.2 Objectives

The objective of this study was to address the measurement and modelling of the kinematics and dynamics of the segments and joints of the upper limb associated with normal every day tasks. This would lead to data truly representative of that experienced during normal daily life.

Kinematic and dynamic data from unimpaired subjects would be obtained, serving as a basis for development of implant designs or for comparison with data from subjects with pathological or traumatic impairment. Results from such impaired subjects would be obtained in order to allow a comparison. In order to achieve these aims, certain objectives were required to be met :

- The development of a suitable laboratory arrangement for human upper limb testing.
- The development of a suitable testing method in terms of marker attachment pattern, selection of suitable tests and their protocol.
- The development of suitable analysis methods in terms of the definition of embedded frames and subsequent calculation of angles, forces and moments through modelling of the upper limb segments.

- The performing of a thorough validation of the test methods and analysis techniques developed.
- The investigation of the normal daily patterns and ranges of upper limb joint angles and the associated external forces and moments for unimpaired subjects.
- The investigation of the same properties during impaired upper limb motion.

This study may be seen as the first step towards a more complete view of the upper extremity and addresses most of the issues raised by Rau (1999). Further advancement might be achieved through the subsequent performance of musculoskeletal modelling of the internal structures of the upper limb joints.

1.3 Thesis layout

Throughout the early chapters of this thesis, several topics and their relevance to the process of analysing upper limb motion will be introduced. These include information on the anatomical structures and necessary background theory. The following chapters then discuss the methods employed and the results obtained using these methods.

Chapter 2 introduces the underlying anatomical structures of the upper limb and their articulations. Chapter 3 also relates to these structures, discussing the anthropometry of the upper limb segments.

Chapter 4 'sets the scene' for the study by reviewing the literature concerning previous studies of upper limb motion in general and in particular those involving studies of everyday tasks.

Chapter 5 introduces background theory, necessary for an understanding of the discussion in Chapter 6 of the materials and methods used during the study.

Chapter 7 presents the results of preliminary testing carried out in order to assess the analysis system and to validate the methods developed. Chapter 8 presents the results obtained through testing of upper limb motion during the performance of a set of activities selected for their relevance to everyday tasks.

A discussion of these results is also given in Chapter 8. Chapter 9 describes a further experimental study and a discussion of the results obtained.

Conclusions drawn from this entire body of work and recommendations for further work are given in Chapter 10.

CHAPTER 2 : THE PECTORAL GIRDLE AND UPPER LIMB ANATOMY

2.0 Introduction

The purpose of this chapter is to describe each of the bony elements involved in the shoulder complex and upper limb as shown in Fig.2.1. and the interaction of these components at the articulations between them.

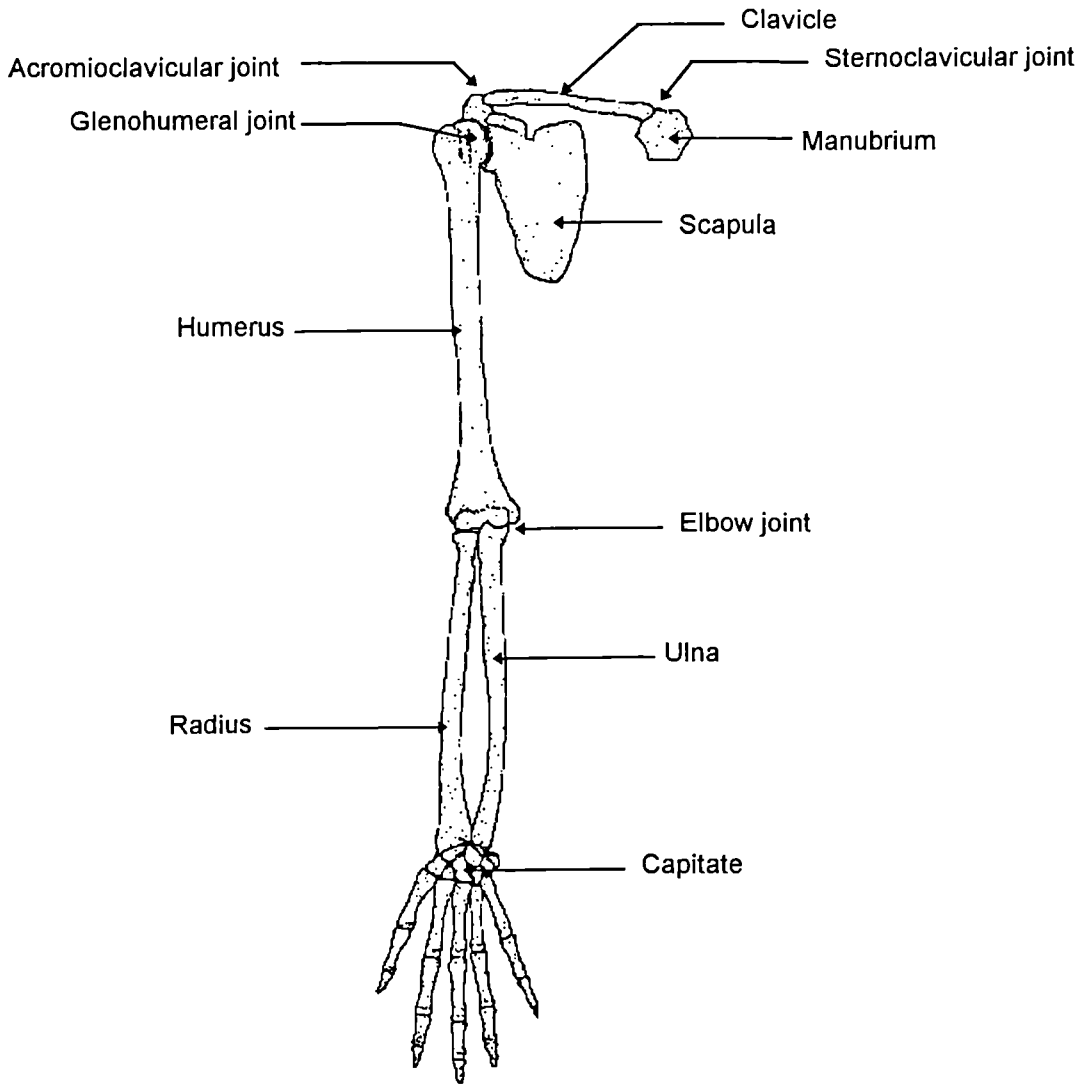

Fig. 2.1 The pectoral girdle and upper limb (adapted from Palastanga et al (1994))

The human shoulder complex involves a series of joints with a mobility greater than any other joint in the human body. Four skeletal segments are involved, these being the humerus, sternum, scapula and clavicle, the latter two combining to make up the shoulder girdle. All but the sternum move

simultaneously and in combination to permit the large range of motion between trunk and humerus.

As well as permitting the greatest range of motion, the shoulder joint is also the most frequently dislocated joint in the human body (Martini (1995)), and thus it can be said that to a certain extent the stability of the joint has been sacrificed in order to achieve the high degree of joint mobility.

It is of little relevance to this work to enter into the time-consuming process of a detailed description of the soft tissues of the upper limb, the main focus of interest being the kinematics of the hard tissues. Some indication of the complexity of the musculature of the shoulder and upper limb can be taken from Karlsson & Peterson (1992) however. This paper described the modelling of thirty muscular components thought to contribute to the carrying of an internal load, as shown in Fig. 2.2. As shown in this figure, the description of the muscular involvement at the shoulder joint is a complicated one, details of which can be found in many published anatomical works.

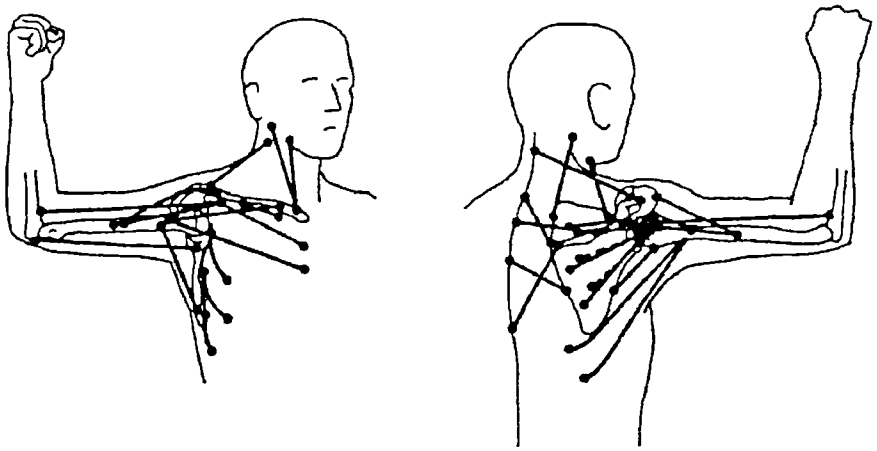

Fig. 2.2 The muscles of the shoulder complex shown as stretched strings along the shortest path between their attachment points. (Karlsson & Peterson (1992))

To meet the demands imposed in allowing the large range of movement at the shoulder, the surrounding skeletal muscles and the rotator cuff musculature within the joint must interact with bone, ligament and tendon in order to provide dynamic stability. In combination with the mobility of the elbow

joint, this allows the placing of the hand in an almost universal range of positions within its workspace.

2.1 Commonly used anatomical terminology

Any discussion of anatomical structure requires the use of certain standard descriptive terminology. Before proceeding, it is necessary to introduce some of this terminology as shown in Fig. 2.3. Slight variations in terminology exist between published descriptions, but the following definitions will be used throughout this work.

The definitions of various directions and planes are given in Table 2.1 and illustrated in Fig. 2.3.

Anterior (Ventral)	The front
Posterior (Dorsal)	The back
Superior (Cephalic/ Cranial)	Above (Towards the head)
Inferior (Caudal)	Below or away from the head (Towards the coccyx)
Medial	Toward the body's longitudinal axis or medial plane
Lateral	Away from the body's longitudinal axis or medial plane
Proximal	Toward an attached base
Distal	Away from an attached base
Sagittal plane	Any vertical plane passing through the body in an anterior-posterior direction and thus separating right and left portions of the body
Coronal plane	Any vertical plane passing through the body in a superior-inferior direction and thus separating anterior and posterior portions of the body
Transverse plane	Any horizontal plane passing through the body at right angles to the previous two and thus separating superior and inferior portions of the body

Table 2.1 Definitions of planes and directions used in anatomical descriptions.

Along with the anatomical planes, three anatomical axes are also defined. These are named the superior-inferior axis, anterior-posterior axis and medial-lateral axis, and their directions can be ascertained from Fig. 2.3 and Table 2.1.

It is also necessary to clarify the terminology used when describing human movement at this stage. Complex geometric rotations like those which occur at the joints of the human body are not additive but are sequence dependent and this can result in highly complicated methods for the description of the motion. Traditionally however, the standard approach is to describe any motion as a projection in one of the anatomical planes previously discussed.

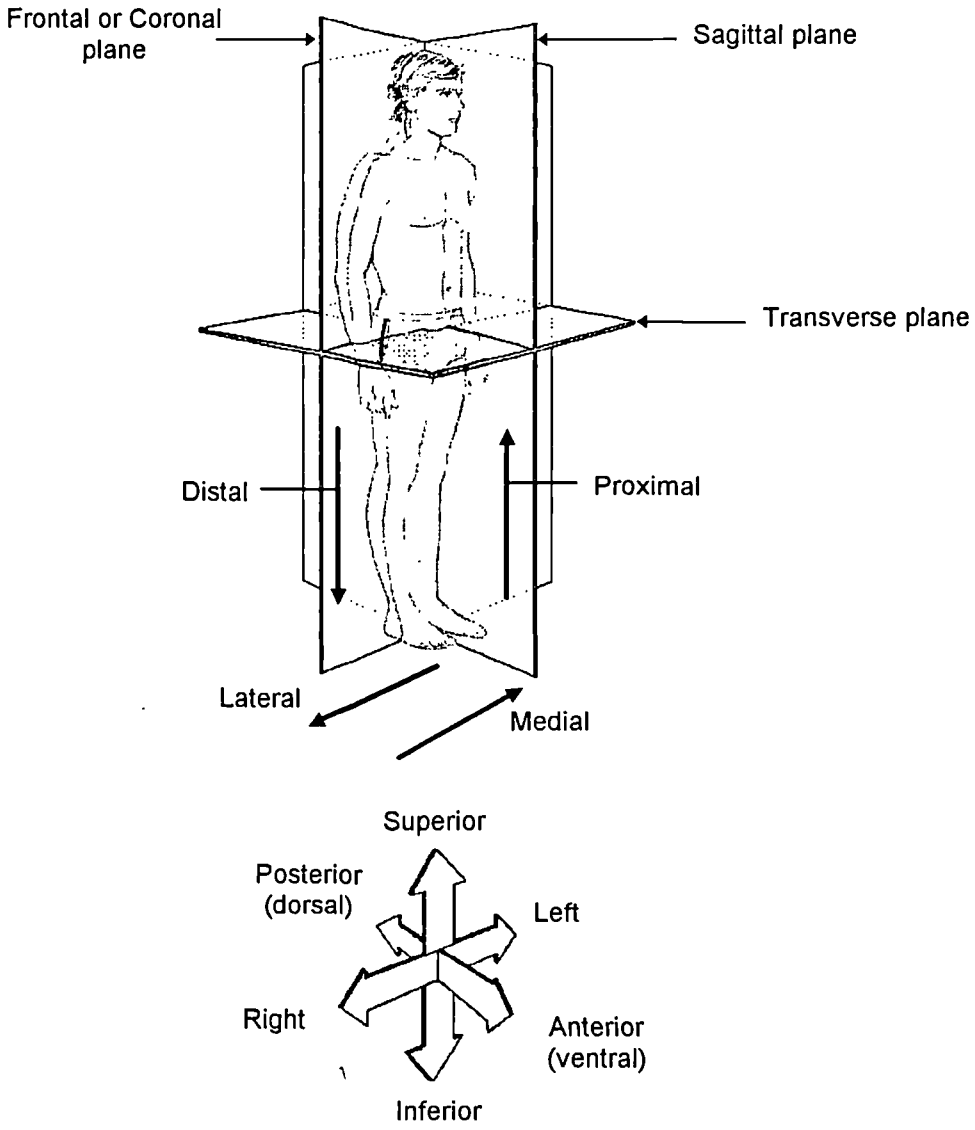

Fig. 2.3 Planes of section and terms used in anatomical descriptions (adapted from Martini et al (1995))

To aid in this description it is necessary to define the 'anatomical position'. In this position the body is viewed from the anterior surface with the hands at the sides, palms facing forward. This is often used as a reference

position when studying or describing motion of the upper limb. Fig. 2.4 aids in the understanding of the following descriptions of upper limb motion, showing rotations in relation to the anatomical position.

Flexion\ Extension: These describe the motion of the upper limb forwards (flexion) or backwards (extension) in the sagittal plane and also the bending or straightening of the elbow respectively, as shown in the anterior view in Fig. 2.4 where the right elbow is flexed to 90°, while the left elbow is extended. Similarly, a rotation of the hand about the wrist in the direction in which the palm faces is termed wrist flexion, the opposite being wrist extension. These movements can occur in the transverse as well as the sagittal plane, being termed 'horizontal' flexion and extension.

Abduction\ Adduction: These describe the motion of the upper limb medially (adduction) or laterally (abduction) in the coronal plane. Most studies assume no abduction or adduction at the elbow, though as discussed in Section 2.5.2 there is an apparent abduction when the elbow is fully extended, known as the carrying angle. At the wrist, a rotation of the hand in the direction of the thumb side is termed radial deviation, the opposite being ulnar deviation.

The term 'elevation' may also be used to describe raising of the arm in any plane, up to or beyond 90°, therefore flexion and abduction may be termed elevation in the sagittal and coronal planes respectively.

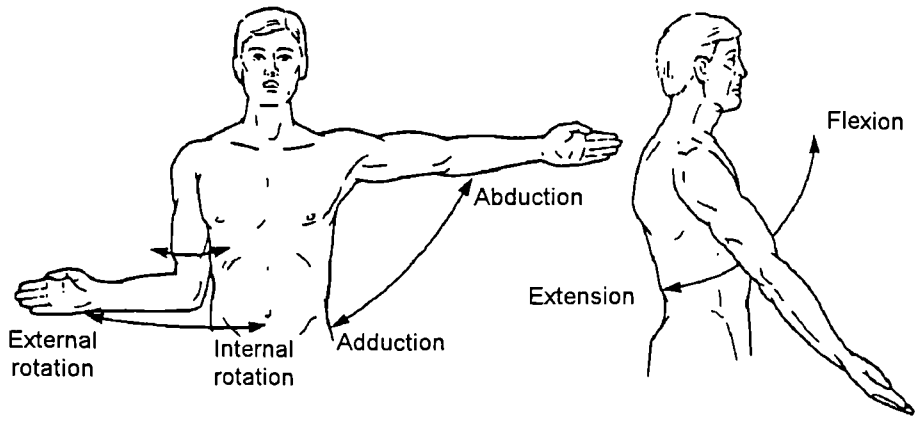

Fig. 2.4 The movements of the shoulder (adapted from Hollinshead (1991))

Internal\ External Rotation: This is the motion that turns the upper limb about its own longitudinal axis. In the anatomical position viewed from above,

internal rotation of the humerus moves the hand medially, while external rotation moves the hand laterally. At the elbow, the internal rotation causing medial motion of the hand is termed pronation. The reverse movement, which returns the hand to the anatomical position is called supination.

2.2 The bones of the shoulder girdle

2.2.1 The scapula

The scapula is a broad, flat bone the body of which has a triangular shape to its anterior aspect and is positioned posterior to the shoulder over ribs two to seven as can be seen in Fig. 2.5.

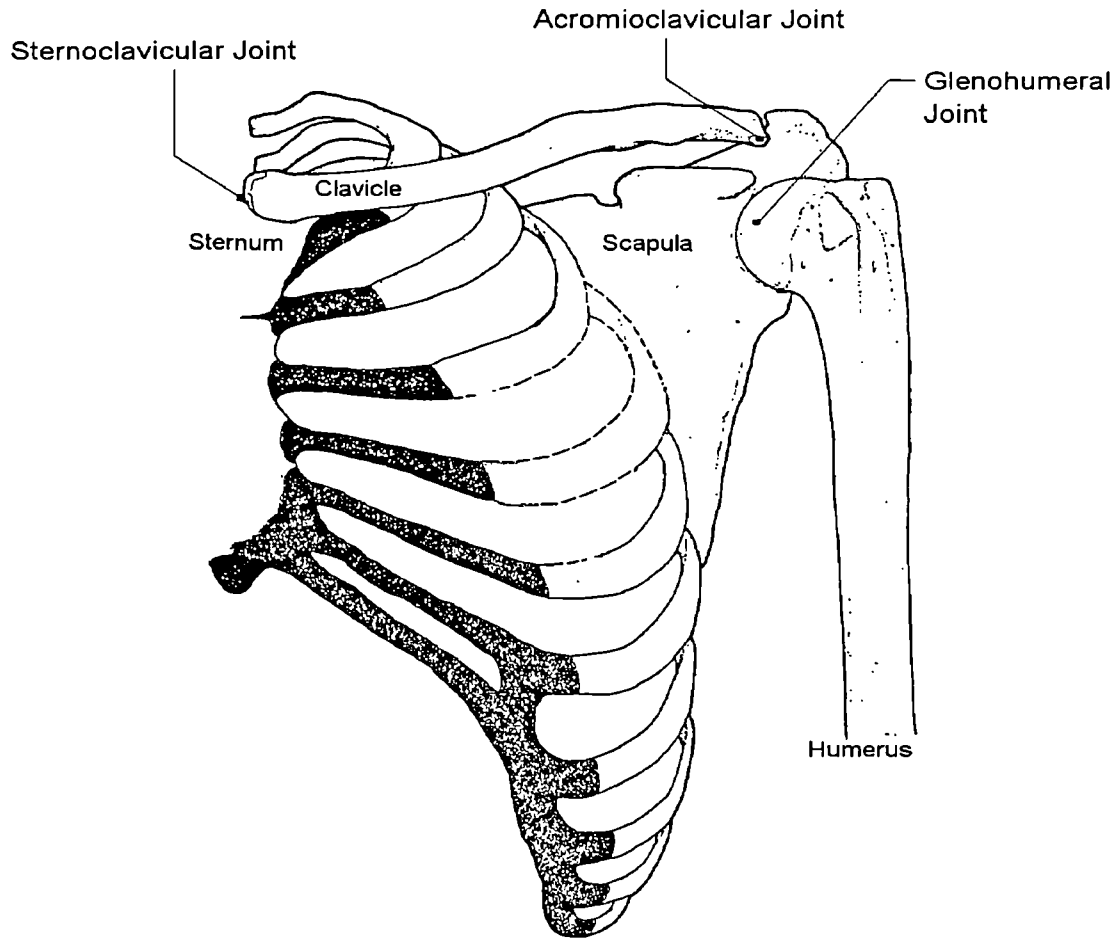

Fig.2.5 Skeletal system of the shoulder (Adapted from Palastanga et al. (1994))

The scapula is dynamically moored to the axial skeleton by muscles, there being no direct bony or ligamentous connection linking it to the thoracic cage. It is allowed to glide over the fascia-covered thorax during upper limb movement, giving rise to the "scapulothoracic articulation" described later and provides the humerus with a stable yet mobile base.

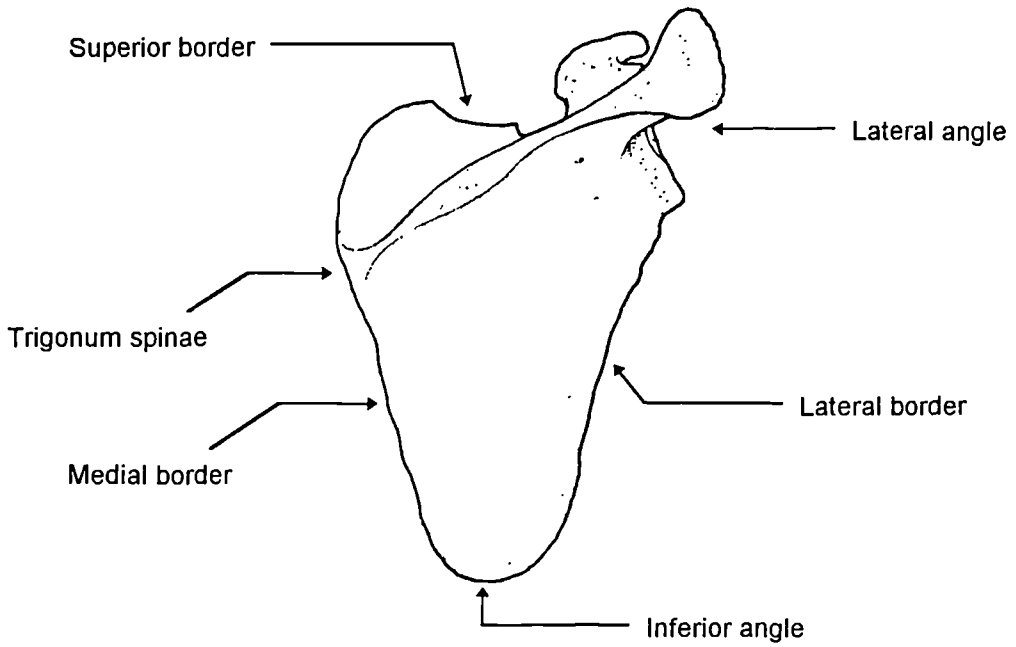

Fig. 2.6 Posterior surface of the scapula (adapted from Palastanga et al (1994))

The three sides of the triangular shaped scapula are named the superior, medial and lateral borders with the corners being termed the medial, inferior and lateral angles, as shown in Fig. 2.6 and Fig. 2.7.

Adjacent to the lateral angle the scapula thickens and becomes rounded to form a neck which supports the shallow pear-shaped glenoid fossa, as shown in Fig.2.8. The glenoid fossa is tilted slightly upwards at an angle of approximately 15° to the vertical, providing some support to the humeral head.

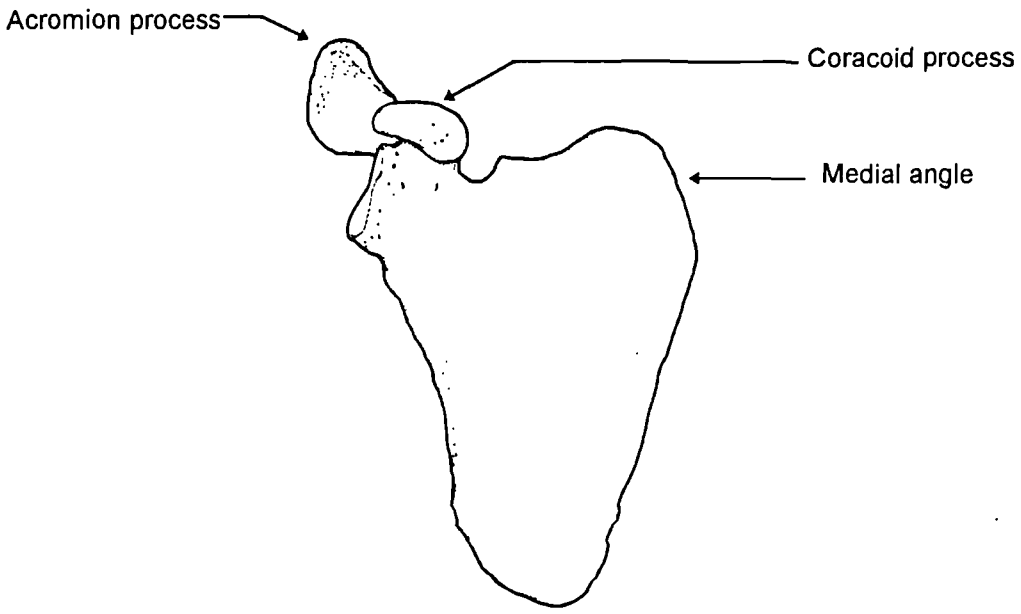

Fig. 2.7 Anterior surface of the scapula (adapted from Palastanga et al (1994))

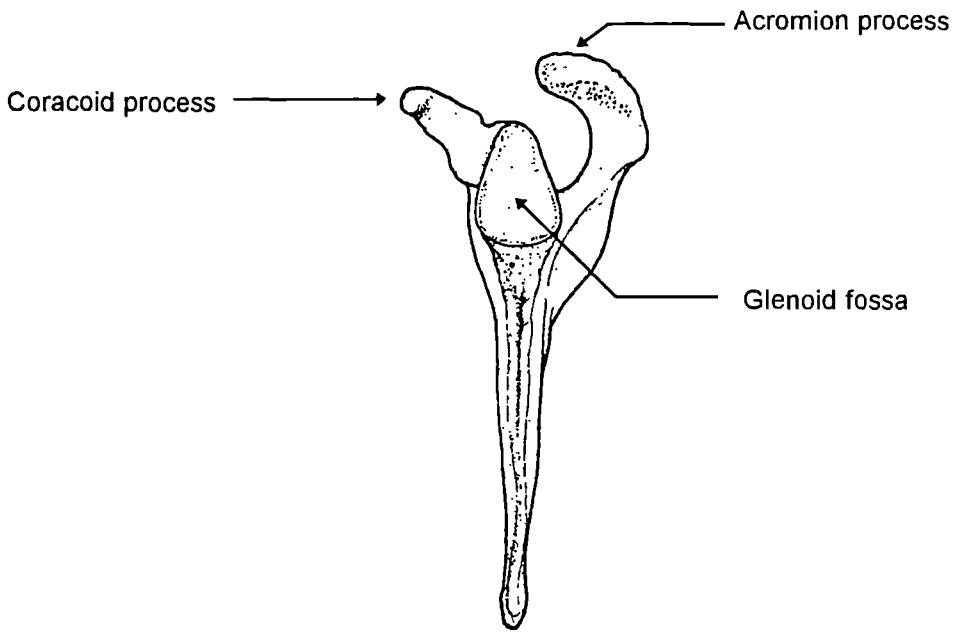

Fig. 2.8 Lateral view of the scapula (adapted from Palastanga et al (1994))

2.2.2 The clavicle

The clavicle lies almost horizontally in the upper thorax and is the only direct connection between the axial skeleton and upper limb. It is an s-shaped

bone as shown in Fig.2.9, curving laterally and dorsally from its roughly triangular sternal (medial) end to the larger, broad, flat acromial (lateral) end.

The lateral end of the clavicle is constrained to move about the surface of a sphere defined by its length and thus holds the scapula laterally and enables the arm to be clear of the trunk.

The clavicle articulates at the sternoclavicular joint with the superior and lateral border of the manubrium of the sternum (shown in Fig.2.10) lateral to the jugular notch, and at the acromioclavicular joint with the acromion of the scapula (see Fig.2.7 and Fig.2.8). Together with the scapula the clavicle forms the *'shoulder' or 'pectoral' girdle*.

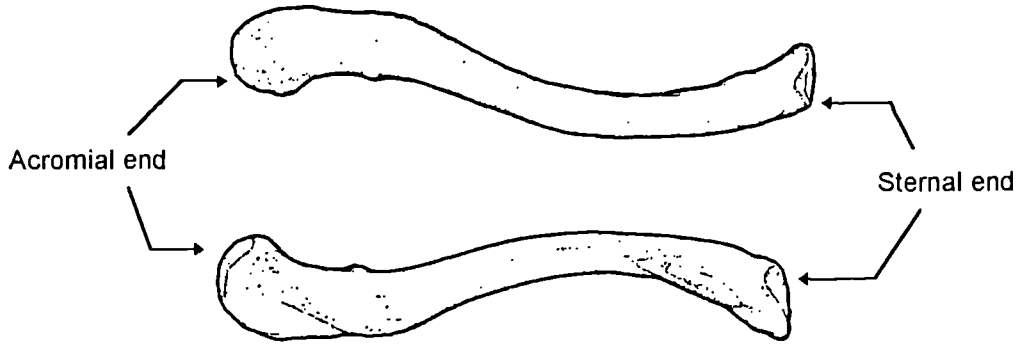

Fig.2.9 The clavicle (adapted from Palastanga et al (1994))

2.2.3 The sternum

The adult sternum or "breastbone" is a flat bone that forms the anterior midline of the thoracic wall. It acts as the base on the trunk for the hard tissues of the upper extremity and has three components, as shown in Fig.2.10.

The broad, triangular manubrium, the widest and most superior portion of the sternum, articulates with the clavicle at the sternoclavicular joint and also with the first pair of ribs. The jugular notch (level with the lower border of the body of the second thoracic vertebra) is the shallow indentation between the clavicular articulations and on either side of this are the smaller, oval, clavicular notches for articulation with the sternal ends of the clavicles.

The tongue shaped gladiolus (body) attaches to the inferior surface of the manubrium at the sternal angle (level with the lower border of the body of the fourth thoracic vertebra).

The smallest of the three components, the xiphoid, attaches at the inferior surface of the gladiolus, level with the ninth thoracic vertebra.

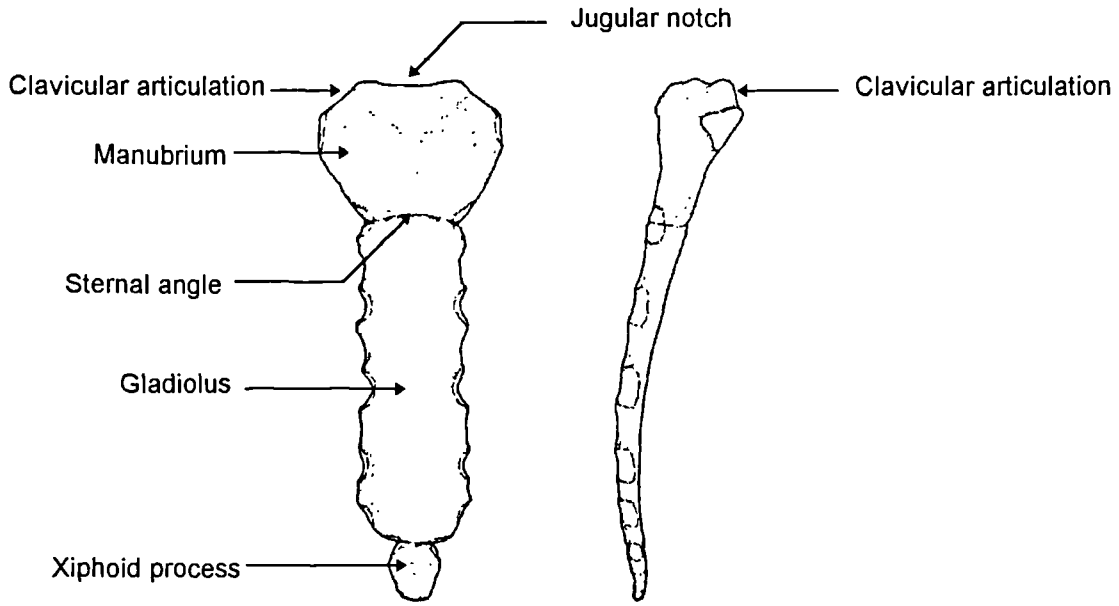

Fig.2.10 Sternum anterior and lateral views (adapted from Palastanga et al (1994))

2.3 The articulations of the pectoral girdle

The following sections seek to discuss in more detail some of the joints and articulations touched on briefly in the preceding sections.

2.3.1 The acromioclavicular joint

The acromioclavicular joint is a synovial joint linking the clavicle and scapula. All movement at this joint is passive, there being no muscle present which might enable an active relative movement between the bones.

The shape of lateral end of the clavicle is that of an oval flat or slightly convex facet and this articulates with a flat or slightly concave facet of a similar shape on the anterior and medial border of the acromion process. A wedge-

shaped fibrocartilaginous articular disc is present, compensating for the small degree of incongruity between the articular surfaces.

Attached at the articular margins of this joint is a relatively loose fibrous capsule. This capsule is strongest at the top where it is thickened and reinforced by the muscular fibres of the trapezius. Additional strength is supplied by thickenings of the capsule known as the superior and inferior acromioclavicular ligaments, upon which the stability of the joint depends.

Further strength is supplied by the coracoclavicular ligament, anchoring the lateral end of the clavicle to the coracoid process of the scapula. The function of this extremely strong ligament is to stabilise the clavicle with respect to the acromion. It is made up of two parts, the anterolateral trapezoid and the posteromedial conoid ligaments, restraining movements of the scapula with respect to the clavicle in the backwards and forwards directions respectively.

The most important function of the acromioclavicular joint is to provide an additional range of movement for the pectoral girdle after the limits of the range of motion of the sternoclavicular joint have been reached. Movement with three degrees of freedom is allowed about the superior, anterior and lateral axes.

2.3.2 The sternoclavicular joint

The sternoclavicular joint links the medial end of the clavicle with the manubrium of the sternum. The clavicle is allowed three degrees of freedom of motion by this joint, elevation and depression, protraction and retraction, and axial rotation. Functionally the sternoclavicular joint behaves as a ball and socket joint though its form is not that of such a joint.

As mentioned in Section 2.2.2, the lateral end of the clavicle may describe an area represented by the surface of a sphere with radius equal to the length of the clavicle. The centre of rotation for the movements other than axial rotation is not at the sternoclavicular joint centre, but through the costoclavicular ligament. This is a short, dense ligament attached between the medial end of the clavicle and the first rib, and limits the elevation of the clavicle as well as preventing any excessive movement in the anterior/ posterior direction of its medial end.

The articulating surfaces of the clavicle and sternum do not have similar radii of curvature and therefore do not form a particularly congruous joint. Some degree of congruence is provided by an intra-articular fibrocartilaginous disc which also provides cushioning as well as contributing to the stability of the joint.

A fibrous joint capsule surrounds the entire joint attaching to the articular margins of the sternum and clavicle. This capsule is relatively strong gaining reinforcement anteriorly, posteriorly and medially by thickenings of the capsule, the anterior and posterior sternoclavicular ligaments and the interclavicular ligament respectively.

2.3.3 The scapulothoracic articulation

In addition to the two true synovial joints already described, a third articulation contributes to the kinematics of the pectoral girdle. This is the "translational joint" between the scapula and thorax.

The mobility afforded to the scapula through its association with the clavicle would initially appear to allow it six degrees of freedom, three rotational from the acromioclavicular joint and three translational from the translations of the lateral end of the clavicle. The previously mentioned constraint of the lateral end of the clavicle to move about the surface of a sphere defined by its length however, imposes a similar constraint on the acromioclavicular joint, reducing the available degrees of freedom to five.

In order to allow this freedom of movement it is necessary for the scapula to be free to move on the posterior wall of the thorax. It is this movement that leads to the description of a translational scapulothoracic articulation, though the conditions of a true joint are not met.

Normally, the scapula moves across the surface of the thorax, gliding on an interface between the ribs and their covering musculature and the covering musculature of the scapula. Both the anterior and posterior articular surfaces of the scapula are lined with a soft fibrous fascia which allows the gliding motion to occur. The contact between the scapula and thorax places further limitation on the range of scapular motion.

A further physiological though not a true anatomical joint is also defined in some anatomical descriptions of the shoulder (McCullagh (1995), Culham & Peat (1993)) named the sub-deltoid, or subacromial joint.

2.4 The bones of the upper limb

The skeletal structure of the upper limb includes the bones of the upper arm, forearm, wrist and hand. The motion at the wrist between the forearm and hand was not considered and so the upper limb is described from its connection to the pectoral girdle at the humeral head, to its connection with the hand at the wrist.

The upper arm contains a single bone, the humerus extending distally from the glenohumeral joint to the elbow joint. The forearm contains two bones, the ulna and the radius extending distally from the elbow joint to the wrist joint.

2.4.1 The humerus

The humerus (Fig. 2.11) extends from the scapula proximally, where its smooth approximately hemispherical head articulates with the glenoid fossa. At its distal end is the elbow, where the humerus articulates with the two bones of the forearm, the radius and ulna.

In the resting position the head of the humerus faces upwards, inwards towards the medial line of the body and in a posterior direction, with a retroversion on its shaft of approximately 30°. This retroversion allows the humerus to move in the plane of the scapula which lies approximately 30° anterior to the coronal plane of the body.

The greater tubercle of the humerus is located near the head and can be used to locate the lateral contour of the shoulder, being located a few centimetres anterior and inferior to the tip of the acromion.

The lower end of the humerus is expanded laterally, flattened anteroposteriorly and bent slightly forwards. It presents two articular surfaces, the capitulum being the lateral of these, providing a rounded, convex surface for articulation with the proximal end of the radius.

Medial to the capitulum is the trochlea which articulates with the proximal end of the ulna. This presents a grooved surface with an anterolateral projection on its medial edge, which causes a lateral deviation between the long axis of the ulna in relation to that of the humerus, the previously mentioned carrying angle.

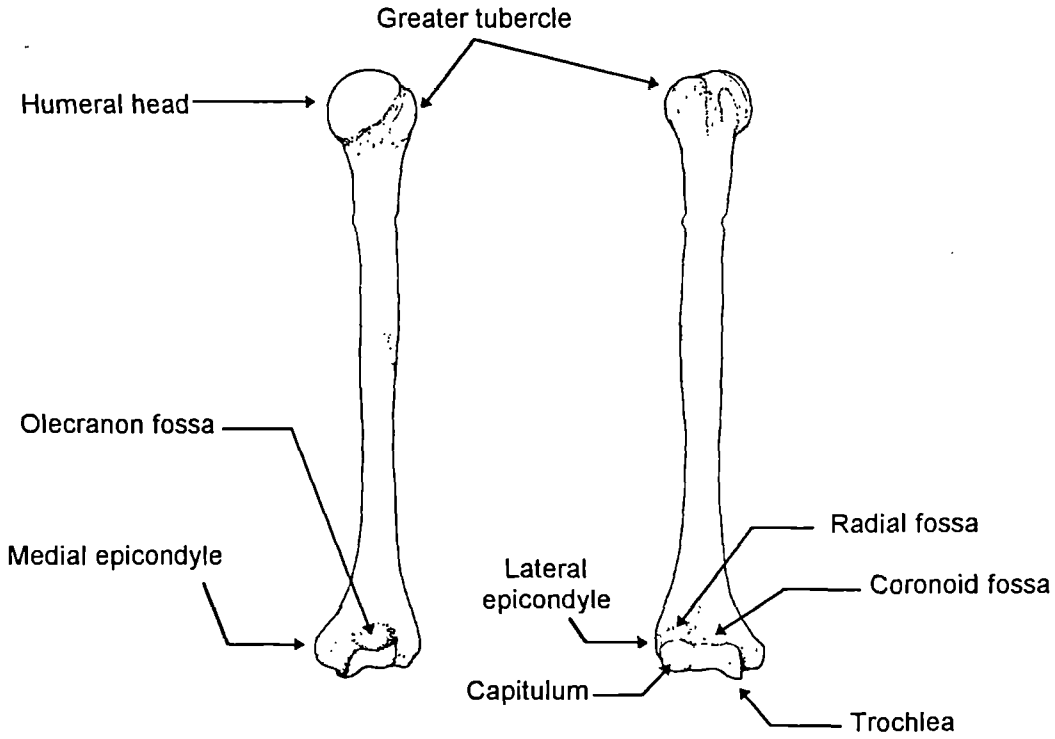

Fig.2.11 Humerus posterior and anterior views (adapted from Palastanga et al (1994))

The lateral and medial epicondyles of the humerus lie lateral to the capitulum and medial to the trochlea respectively. The distal end of the humerus also presents three fossae, one for the olecranon on the posterior of the bone and two on the anterior of the bone on the medial and lateral sides for the coronoid process and radius respectively.

2.4.2 The ulna

The ulna is the longer of the two bones of the lower arm, lying medial to the radius in the anatomical position and articulating laterally with it at each end. The proximal end of the bone is larger than the distal end and has two projecting processes enclosing a cavity.

The larger of these two processes is the olecranon process (the tip of the elbow) which points forward with the elbow in full extension and which forms the proximal part of the bone. Anteriorly it is concave forming the upper part of the articular surface of the trochlear notch. This notch is completed by the coronoid process on the front of the ulnar shaft and articulates with the trochlea of the humerus at the elbow joint, known as the olecranal or humeroulnar joint. On the lateral side of this process is the concave radial notch which accepts the head of the radius.

The distal end of the ulna has a narrow neck expanding into a small rounded head which has a smooth articular surface for the radius on its anterior and lateral aspects. The styloid process projects downwards from the posterior part of the ulnar head.

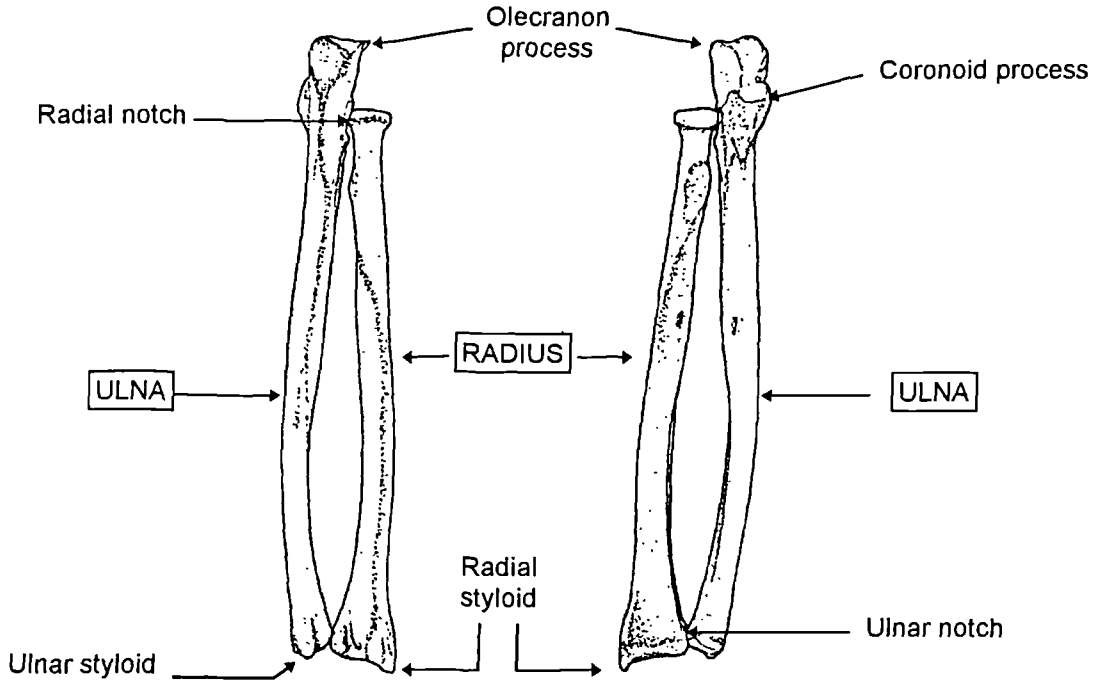

Fig.2.12 Right radius and ulna - posterior and anterior views (adapted from Palastanga et al (1994))

2.4.3 The radius

The radius is shorter than the ulna and lies laterally to it in the anatomical position as shown in Fig. 2.12. The proximal end is the smaller of the two and presents a thick concave disc for articulation with the capitulum of

the humerus. The lateral side of the proximal head is flattened and articulates with the radial notch of the ulna.

The distal end of the radius is expanded having five distinct surfaces, the lateral surface extending distally to the radial styloid. This assists in the stability of the wrist joint, while the medial surface forms the concave ulnar notch for articulation with the distal head of the ulna.

The radial shaft is convex laterally allowing it to move around the ulna during forearm pronation.

2.5 The articulations of the upper limb

2.5.1 The glenohumeral joint

The glenohumeral joint is the articulation between the rounded head of the humerus and the shallow glenoid fossa of the scapula and is an extremely mobile synovial ball and socket joint.

The articular surface of the humeral head is smooth, round and several times the diameter of the glenoid fossa. The disproportionate size and lack of congruency of the articular surfaces make the joint inherently unstable, necessitating additional support. This is provided through a deepening of the fossa effected by the glenoid labrum, fibrocartilaginous tissue attached around the circumference of the fossa.

As the glenoid offers little in the way of a kinematic constraint for the head of the humerus and as ligaments would severely limit joint movement, muscle tension is employed to supply kinematic control of the joint and allow its great range of motion. Active muscular support is provided by all of the muscles between the pectoral girdle and the humerus but in particular, the stability of the joint depends on the muscles of the rotator cuff, consisting of four muscles which act as extensible ligaments.

The joint is surrounded by a loose cylindrical fibrous capsule, which in contrast to those at other joints discussed, offers no improvement to the stability of the joint. It is strong in places however, strengthened by the thickened sections of the capsule anteriorly, the superior, middle and inferior glenohumeral ligaments and also posteriorly by the coracohumeral ligament.

Combined with the freedom of the scapula associated with the sternoclavicular and acromioclavicular joints, the glenohumeral joint contributes greatly to the complexity of the shoulder mechanism and its large range of movement.

The glenohumeral joint has a greater range of movement than any other joint in the human body (Martini (1995)) with five degrees of freedom, these being rotation in three planes as well as sliding of the humeral head over the glenoid in both vertical and horizontal directions.

2.5.2 The Elbow Joint

As discussed in Palastanga et al (1994), the elbow joint is the synovial joint between the arm and forearm and for practical purposes can be regarded as a pure hinge joint. A fibrous capsule completely encloses the elbow joint, this capsule being shared with the superior radioulnar joint (see Section 2.5.3).

The capsule is strengthened by the collateral ligaments, strong triangular bands which blend in with the sides of the joint capsule. They are relatively tense in all positions of flexion and provide strong support for the elbow in all directions of movement.

On the anterior of the capsule there is a thickening referred to as the capsular ligament, posteriorly however, the capsule is weak and membranous.

The shape of the articular surfaces combining at the elbow joint provides it some stability but the joint is greatly reinforced by the collateral ligaments and the surrounding cuff of skeletal muscles including the triceps and biceps muscles.

The articular surfaces come into closest contact when the forearm is flexed to 90° and in a position of mid pronation-supination. This position lends itself to allowing the elbow joint maximum stability and is the position naturally assumed when fine manipulation of the fingers and hand is required.

The possible movements at the elbow joint are those of flexion and extension which occur about an axis through the humeral epicondyles. This axis is not at right angles to either of the humeral or forearm long axes. As mentioned previously there is a carrying angle between the arm and forearm due to the geometry of the articular surfaces, the medial end of the

flexion/extension axis being slightly lower than the lateral. The deviation of this axis leads the hand to move medially during flexion, ultimately lying over the shoulder.

Several studies have investigated the carrying angle. Beals (1976) carried out a radiographic study of fifty six male and fifty female adults. The mean carrying angle at full elbow extension for this group was found to be 17.8°, with no significant difference between males and females. Morrey et al (1976) used similar techniques and implanted wires on two upper limbs from unembalmed cadavers. They found a linear change in the carrying angle from 10° in full extension to between 6° and 10° in full flexion. Deland et al (1987) studied five cadaver specimens and found the carrying angle in full extension to vary between 13° and 22°, with an average of 15.4°. The angle was found to be close to zero in full flexion.

A small amount of abduction and adduction and lateral and medial rotation may occur at the elbow, though these will be extremely small.

2.5.3 The radioulnar Joints

As well as articulating with the humerus at the elbow, the radius and ulna also articulate with each other. This occurs via synovial pivot joints at their proximal and distal ends and by an interosseous membrane along their length which contributes to the stability of the radius and ulna during rotation.

The superior radioulnar joint is the articulation between the head of the radius and the radial notch of the ulna, and as previously mentioned shares a joint capsule with the elbow joint. The main movement is the rotation of the radial head within the radial notch of the ulna though some movement occurs between the radial head and humerus.

The inferior radioulnar joint is the articulation between the head of the ulna and the ulnar notch on the lower end of the radius, principally united by a triangular fibrocartilaginous disc between the lateral side of the root of the ulnar styloid process and the ulnar notch.

The loose fibrous joint capsule of the inferior radioulnar joint is relatively weak, allowing movement between the radius and ulna. The joint is afforded a high degree of stability however, primarily by the presence of the articular disc.

The major movement that the distal radioulnar articulation permits is the rolling of the ulnar notch of the radius across the rounded surface of the ulnar head. This occurs in pronation where the radius and ulna cross, the radius lying anterior to the ulna.

During pronation there is also an extension and lateral displacement of the ulna caused by a magnification through the length of the bone of the very slight extension and medial displacement of the ulna at the elbow.

The interosseus membrane is a strong, fibrous sheet which joins the lateral margin of the ulna to the radius. It contributes to the stability of the inferior radioulnar joint and provides a firm connection between the radius and ulna. The interosseus membrane also allows the transmission of forces from the hand through the radius to the ulna, and thereafter up through the humerus.

CHAPTER 3 : TECHNIQUES FOR THE PREDICTION OF BODY SEGMENT PARAMETERS: A REVIEW OF THE LITERATURE

3.0 Introduction

In carrying out a quantitative biomechanical analysis of human upper limb motion it is necessary to estimate certain characteristics of the body segments under analysis. These characteristics include segment lengths, masses, centre of mass (CM) locations and mass moments of inertia and are known as the body segment parameters (BSPs).

The objective in analysing upper limb motion, is to combine these segment parameters with segmental kinematic data obtained from a video motion analysis system, in order to allow the computation of kinetic quantities such as the forces and moments at the joints of the upper limb.

Hinrichs (1985) stated that;

"use of indirect estimates of body segment masses, centres of mass, and moments of inertia is arguably one of the biggest sources of error in biomechanics research."

It is clear then that the selection of an appropriate and accurate method for estimation of the various BSPs is an essential part of any motion analysis method that seeks to minimise errors.

The forces and moments that cause movements in the upper limb fall into one of two categories. Internal forces and moments are those transmitted by body tissues as muscular or joint contact forces and tensions in the ligaments. External forces and moments are all the physical interactions between the upper limb and its environment including gravitational and loading contributions.

Gravitational contributions to the external forces and moments can be determined knowing the mass and the location of the centre of mass of each of the segments of the upper limb. Such quantities can be calculated, together with the required segmental mass moments of inertia about the principal axes, by means of prediction techniques. These are based on measured

anthropometric dimensions and take the form of ratios or regression equations obtained through statistical analysis of data.

The following chapter contains an introduction to the process of predicting the BSPs, including a review of literature related to the development of predictive ratios and regression equations. The topic will be discussed in two broad categories, the estimation of the mass and centre of mass of the segment being the first, the calculation of the moments of inertia being the second. Within these categories the literature is discussed in a largely chronological order.

3.1 Some initial definitions

Before entering into a discussion of the various techniques it is first necessary to introduce some definitions for the parameters that will be discussed.

3.1.1 The Centres of Gravity and Mass

The centre of gravity (CoG) is the location of the centroid of all gravitational forces of the mass elements of an object, the point through which the weight of the object acts. The centre of mass (CM) is the location of the centroid of all mass elements of an object, weighted by their individual mass. These are not identical properties, particularly for very large objects where gravitational forces may vary, but for the purposes of biomechanical analysis can be regarded as the same point.

3.1.2 The Segment Moments of Inertia

The moment of inertia of a body segment is a measure of its opposition to change in angular motion associated with rotational motion and is the rotational analogue to mass. The entire inertial system of a rigid body can be described by specifying six parameters in relation to a reference co-ordinate frame embedded in the segment. These parameters are the three mass moments of inertia I_{xx}, I_{yy} and I_{zz} about the X,Y and Z axes and the three products of inertia I_{xy}, I_{xz} and I_{yz} with respect to the XZ & YZ, XY & YZ and XY & XZ planes respectively.

If the embedded anatomical axis systems selected for rotation are chosen to be coincident with the principal axes (longitudinal, anteroposterior, mediolateral) then the product terms are no longer a factor, only being necessary where the principal axes are rotated relative to the embedded co-ordinate axes.

3.2 The prediction of body segment mass and centre of mass location

Many measurement techniques have been used in obtaining body segment parameter data. Drillis et al (1964) produced a detailed review of these techniques, as well as some of the data obtained using these methods. The following discussion concentrates mainly on the results obtained rather than the techniques used in individual studies.

Harless (1860) segmented the cadavers of two executed criminals (average age 29years, average height 170.2cm, average weight 55.5kg) into arm, forearm, hand, thigh, shank and foot segments. The head, neck and trunk were considered as three segments of which the uppermost segment (the head and neck) was treated in essentially the same manner as the limb segments.

The separation of adjoining segments was made tangent to their planes of articulation and the soft tissues at the end of each segment were sutured over the bone. Each limb segment was then weighed on a precision balance, and its centre of gravity determined.

In their pioneering work, Braune & Fischer (1889) dissected the frozen cadavers of three males (average: age 47.5years, height 168.3cm, weight 64kg) into 14 segments, separated through the appropriate joint centres.

Each of the individual segments was weighed before thin metal rods were driven into them perpendicular to the three principal planes. The location of the centre of gravity of each segment was determined by suspending them from these rods. The planes of intersection of the rods with the segment were marked and the centre of gravity of the segment located where these three planes intersected.

Using the same methods as those reported by Braune & Fischer (1889), Fischer (1906) dissected a small cadaver (height 150cm weight 44.057kg) and determined the weight and CM location of 14 body segments.

Dempster (1955) dissected the frozen cadavers of eight males (average: age 68.5years, height 166.9cm, weight 59.6kg). The cadavers were separated through the joint centres and each segment weighed. The longitudinal CM location was determined using a balance plate which could pivot around one of its diagonals.

The predictive ratios for the masses and centres of gravity (mass) for upper limb segments from the papers discussed till now can be seen in Table 3.1 along with those from the study of Clauser et al (1969), discussed later.

	Relative Mass (m_i/m) Relative Distance (L_i/L)									
Segment	Harless (1860)		Braune & Fischer (1889)		Fischer (1906)		Dempster (1955)		Clauser (1969)	
	m_i/m %	L_i/L %	m_i/m %	L_i/L %	m_i/m %	L_i/L %	m_i/m %	L_i/L %	m_i/m %	L_i/L %
Arm	5.7	-	6.2	52.6	5.4	44.6	4.9	51.2	4.9	41.3
Upper arm	3.2	-	3.3	47.0	2.8	45.0	2.7	43.6	2.63	51.3
Forearm & hand	2.6	-	3.0	47.2	2.6	46.2	2.2	67.7	2.27	62.6
Forearm	1.7	42.0	2.1	42.1	-	-	1.6	43.0	1.61	39.0
Hand	0.9	39.7	0.8	-	-	-	0.6	50.6	0.65	18.0

Table 3.1 Relative segment mass (given as a percentage of total body mass) and centre of gravity location (given as a percentage of the distance along the longitudinal axis from the proximal joint) from selected cadaver studies. (Adapted from Nigg & Herzog (1995))

Contini (1972) derived data with reference to surface landmark measurements on living subjects using some of the methods discussed in Drillis et al (1964). This is in contrast to many of the studies discussed in this chapter which use cadaver dissection and measurement for data. Harless (1860), Braune & Fischer(1889), Fischer (1906), Dempster(1955), Clauser et al (1969) and Chandler et al (1975) discussed later, all used cadaver studies to determine mass, volume, density and centre of mass of the total human body and of selected segments.

The data in Contini (1972) were drawn from two studies, those of Drillis & Contini (1966) & Contini (1970). In the former paper, data were obtained from twelve males in the age range 20-40 years, while in the latter nine males

(20-30 years), five females (17-20 years), three females (40-50 years) and nineteen subjects with hemiplegia or amputation were measured.

The work of Contini (1972) provides data on the location of the centres of mass of the upper limb, assumed to be coincident with the centres of volume. The author opined that data obtained from cadaver studies probably represented true mass centres, while data obtained from live subjects probably represented volume centres. The data provided gives the average location of each of the segment centres of mass as a percentage of the overall segment length from the proximal joint as shown in Table 3.2.

Similar data were given by Pheasant (1986), shown in Table 3.3.

Segment	%	Segment Definition
Entire arm	43.1	Glenohumeral joint/ Ulnar styloid
Upper arm	44.9	Glenohumeral axis/ Elbow axis
Forearm and hand	38.2	Elbow axis/ Ulnar styloid
Forearm	42.3	Elbow axis/ Ulnar styloid
Hand	39.2	Wrist axis/ Knuckle II middle finger

Table 3.2 Average location of segment centre of mass, as a percentage of segment length from the proximal joint. (Contini (1970))

Segment	Location of centre of gravity
Upper arm	48% of distance from shoulder to elbow joint
Forearm	41% of distance from elbow to wrist joint
Hand	40% of the hand length from the wrist joint (at the centre of an object gripped)

Table 3.3 Location of the centres of gravity of the segments of the upper limb. Quoted from Reynolds (1978) or calculated using the data of Dempster (1955), together with anthropometric estimates for British adults aged 19-65 years. (Pheasant (1986))

The work of Drillis & Contini (1966) also includes data on the average mass of each of the upper limb segments as a percentage of the total body mass, as given in Table 3.4.

Segment	%age
Upper extremities	5.97
Upper arms	3.57
Forearm & hand	2.40
Forearms	1.80
Hands	0.60

Table 3.4 Average mass of the segments of the upper limb as a percentage of the total body mass. (Drillis & Contini (1966))

Again similar data can be found in Pheasant (1986) and is shown in Table 3.5.

Segment	%age of Total Body Weight
Total arm	5.0
Upper arm	2.8
Forearm and Hand	2.2
Forearm	1.7/1.6
Hand	0.6

Table 3.5 Average weight of the segments of the upper limb as a percentage of the total body mass. Quoted from Reynolds (1978) or based on calculations using the data of Dempster (1955), together with anthropometric etimates for British adults aged 19-65 years. (Pheasant (1986), Winter (1990))

Clauser et al (1969) sought to discover whether anthropometric dimensions could be used to predict body segment parameters.

Thirteen male cadavers of average weight 66.52kg, average height 172.2cm and average age 49.31 years, were dissected into fourteen segments. Preserved cadavers were used in order to allow the selection of a representative range of the population. The dissection cuts were sealed with aerosol plastic spray to reduce seepage and *evaporation.*

The weight, volume and centre of mass of each of the segments was determined and extensive anthropometric measurements taken to describe their length, breadth and circumference, left and right side data being averaged.

The foremost assumption made in using these measurements for the estimation of segment parameters on living subjects, is that relationships found

for cadavers are equally valid for the living. Changes in the tissues and body fluids after death will almost certainly affect the validity of this assumption.

The mean values of segment masses and CM location were determined and a set of regression equations were derived for the prediction of segment weight, volume and CM location from more than 30 anthropometric measurements. The equations were produced by selecting the variables that had most power to predict a specific segment variable. Body mass was found to be the most common predictor, with circumferences good for weight estimation and lengths good for centre of mass prediction. The regression equations were found to be much more effective than the ratios, the three-step regression having half the error or less than the ratio method.

Clauser et al (1969) compared their data with the estimation of the centre of mass at the centre of volume point from Drillis & Contini (1966). It was found that the volume and mass centres were not coincident and that if the centre of volume were used it would predict the centre of mass proximal to its true location, imparting an error of constant direction of around 2-3cm.

Hinrichs (1990) made adjustments to the ratio data of Clauser et al (1969). The mean segment centre of mass ratios for each of the segments were adjusted in an attempt to allow their application to segments with estimated joint centres rather than bony landmarks as endpoints.

The elbow joint centre of rotation was taken to lie midway between the medial and lateral epicondyles of the humerus, the shoulder joint centre of rotation at the humeral head centroid and the wrist centre of rotation at a point mid way between the distal portions of the radial and ulnar styloids. These are similar locations to those chosen by many upper limb motion studies.

The adjusted ratios for the centres of mass in relation to the corrected proximal endpoints at the joint centres are given in Table 3.6.

Segment	Endpoints	%age
Upper arm	Shoulder joint centre-Elbow joint centre	0.4910
Forearm	Elbow joint centre-Wrist joint centre	0.4176

Table 3.6 Average location of segment centre of mass, as a percentage of segment length from the proximal joint centre. (Hinrichs (1990))

Clarys & Marfell-Jones (1986a) used experimental anthropometric data from the embalmed cadavers of three females and three males (ages 79, 79, 81, 69, 78, 15 respectively) in their study of the component tissues of the limb segments. 182 anthropometric measurements were made bilaterally and the cadavers severed into 14 segments. The segmentation and dissection procedures used are outlined in Clarys & Marfell-Jones (1986b).

The upper limb was divided into arm, forearm and hand segments and each of these further fractionated into four components by removing the skin, adipose tissue, muscle and bone.

The limb segments and dissected tissues were weighed both in air and under water, these weights being corrected for fluid loss and various anthropometric measurements were taken during the process of dissection.

The recorded data were then used to develop regression models for the prediction of segmental component tissue masses from anthropometric measurements on the limb segments.

The data given in Clarys & Marfell-Jones (1986b) are for the gross weights of each of the segments and were used to develop regression equations for predicting the segment masses. It is possible however to calculate percentage values for each of the segments in relation to the total body mass from the data given. This produces the results given in Table 3.7, which are comparable to those from other studies discussed.

Segment	%age of Total Body Mass
Upper Arm	2.70
Forearm	1.33
Hand	0.62

Table 3.7 Average mass of the segments of the upper limb as a percentage of the total body mass. (Clarys & Marfell-Jones (1986b))

Clarys & Marfell-Jones (1986b) found their regression model to be as good as that of Clauser et al (1969) and significantly better than the ratio method of Barter (1957). They expressed reservations on its use however, as it was

unable to predict the masses of all subject segments to within 5% of their measured mass.

3.3 The prediction of body segment moments of inertia

If a segment is suspended from a fixed point, for instance a bar through its proximal joint centre and then set in motion, the period of its oscillation can be measured. The moment of inertia about an axis through the point of suspension can then be found and from this the moment of inertia about an axis through the centre of mass.

Such a technique has been adopted in several studies. The relevant moment data obtained in this way by Dempster (1955) is shown in Table 3.8.

Hatze (1980) developed a 17 segment model whereby the human body was represented and inertial properties determined mathematically. 262 anthropometric measurements were made on each subject in order that the rigidly modelled segments could be fitted. Data from one of the four subjects used to test the model can be seen in Table 3.8, along with data for a cadaver of similar structure from Dempster (1955).

Other methods include the 'quick release method' (Fenn (1938), Bouisett & Pertuzon (1967)) whereby the moment of inertia of the forearm on a living subject can be determined. The subject's limb is required to exert a constant force against a device which is then released. The angular acceleration of the forearm after release can be measured and the moment of inertia determined from this.

	Dempster (1955)	Hatze (1980)
Segment	Transverse Moment of Inertia [kgm^2]	Transverse Moment of Inertia [kgm^2]
Left arm	0.0222	0.0203
Right arm	0.0220	0.0229
Left Forearm	0.0055	0.0086
Right Forearm	0.0072	0.0093
Left Hand	0.0009	0.0010
Right Hand	0.0011	0.0010

Table 3.8 Transverse moments of inertia for the upper limb segments based on data from Dempster (1955) and Hatze (1980). (From Nigg & Herzog (1995)).

The 'relaxed oscillation' method employed by Peyton (1986) and Allum & Young (1976) also allowed determination of the moment of inertia of the forearm of a living subject. A single impulse or oscillating force was applied to a resting limb and its response allowed calculation of the moment of inertia.

A summary of data on the moment of inertia of the forearm including that obtained with the previous methods are given in Table 3.9.

Study		Moment of Inertia of the Forearm [kgm^2]	
	Number of Subjects	Mean	Range
Braune & Fischer (1889)	2	0.0505	-
Fenn (1938)	1	0.0590	-
Hill (1940)	1	0.0277	-
Wilke (1950)	1	0.0530	-
Dempster (1955)	8	0.0577	0.0397 - 0.0852
Bouisset & Pertuzon (1968)	11	0.0599	0.0430 - 0.080
Kwee (1971)	4	-	0.03 - 0.051
*Allum & Young (1976)	4	0.0740	0.0690 - 0.0820
Peyton (1986)	8	0.0646	0.0476 - 0.0862

Table 3.9 Moments of inertia of the forearm and hand segment about the humeral axis from the experimental investigations of several authors. (N.B. * - moment of inertia of the entire limb about the humeral axis). (Taken from Nigg & Herzog (1995)).

Chandler et al (1975) used similar procedures to those of Clauser et al (1969). Data regarding mass distribution characteristics of the human body as described by the principal moments of inertia and their orientation to body and segment anthropometry were produced.

The weight, centre of mass location and principal moments of inertia were determined for six adult male cadavers, selected and paired for similarity of body configuration (mass: 50.6 - 89.2 kg, height: 1.64 - 1.82m).

All specimens were shaved and 116 anthropometric and landmark measurements were taken on each cadaver in the supine position using x-rays and flouroscopy, a type of radiography in which x-rays emerging from a patient impinge directly on a fluorescent screen.

Each cadaver was strapped onto a positioning board and frozen prior to being cut into 14 segments in the planes shown in Fig 3.1, similar to those of Clauser et al (1969). One of each pair of matched cadavers was treated in a standing (anatomical) position, the other in a sitting position. Each of the cadaver segments then had their mass, centre of mass location, moments of inertia and volume measured.

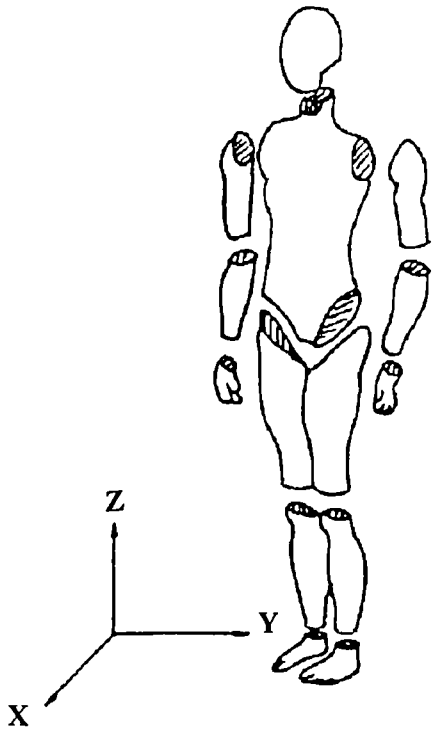

Fig 3.1 14 primary body segments with their appropriate cut plane locations (Reynolds et al (1975))

The human body is not composed of rigid segments, but of tissues which distort as muscles contract and the body changes position or is subject to varying acceleration. This makes measurement of body segment moments of inertia difficult and led Chandler et al (1975) to make the assumption that the segments were rigid, an assumption necessary for the purposes of most biomechanical studies. In order to make this assumption more reasonable Chandler et al (1975) determined the segment parameters of frozen cadaver segments strapped to holders in insulating styrofoam specimen boxes.

Axis systems were defined in relation to the specimen boxes. For the upper arm the Z-axis was defined as passing through the centre of the humeral

head and the mid-point of the epicondyles. The X axis was perpendicular and anteriorly directed with the Y axis normal to these.

For the forearm the Z-axis passed through a proximal point similar to the mid-point of the epicondyles and the centre of the cut surface of the capitate, the largest bone of the wrist. The X axis was perpendicular and laterally directed with the Y axis normal to these. A composite pendulum technique was used, the pendulum comprising the segment and holder. The holder was suspended from a rigid stand and the box swung round X,Y and Z axes and axes in each of the XY, XZ and YZ planes.

The mass, effective length and period of oscillation of the specimen and holder were all measured over fifty cycles, allowing calculation of the three principal moments of inertia about axes through the centre of mass. The volume of each segment was also measured by measuring their weight while immersed in alcohol.

Chandler et al (1975) specifically stated that their study design did not attempt to provide a statistically valid sample for establishing population estimates for the body segment parameters. It was suggested however that the differences between the principal moments of inertia of their specimens and those of living male subjects of similar physical characteristics would be small.

The segment volume was found in general to be the best predictor of the moments of inertia. The I_{xx} and I_{yy} values were found to be of approximately the same magnitude for the major limb segments, with I_{zz} around 20% of I_{xx} values. Differences in the principal moments of inertia between seated and standing positions were found to be small. It was concluded that estimates of the segment moments of inertia in one orientation could be used in any other segment orientation for the purposes of modelling.

The work of Chandler et al (1975) is also documented in a second paper, that of Reynolds et al (1975). The upper limb segment moments of inertia about the centre of mass from the latter paper are shown compared to those of Dempster (1955) in Table 3.10.

	Study	Reynolds et al (1975)			Dempster (1955)
Segment		I_{xx} ($\times 10^{-3}$ kgm^2)	I_{yy} ($\times 10^{-3}$ kgm^2)	I_{zz} ($\times 10^{-3}$ kgm^2)	I_{x-y} ($\times 10^{-3}$ kgm^2)
Upper arm	Right	13.5	13.27	2.01	14.20
	Left	15.21	13.77	2.28	13.90
Forearm	Right	6.69	6.45	0.88	5.60
	Left	6.47	6.30	0.86	5.50
Hand	Right	0.754	0.615	0.215	0.50
	Left	0.684	0.557	0.179	0.45

Table 3.10 Transverse moments of inertia for the upper limb segments compared with data from Dempster (1955). NB: I_{x-y} for Dempster data is an axis perpendicular to the longitudinal axis, passing through the centre of mass. (Reynolds (1975)).

McConville et al (1980) aimed to demonstrate that mass distribution properties of the human body and its segments could be predicted from anthropometric dimensions taken from living subjects as opposed to cadavers.

Data on 31 male subjects were obtained using three-dimensional photography from cameras placed at strategic locations to photographically segment their bodies into 24 parts.

The co-ordinates of selected anatomical landmarks allowed the computer reconstruction of the segments. The volume, centre of volume and principal moments of inertia were determined stereophotometrically. Seventy five body dimensions were anthropometrically measured and multiple regression equations developed for each of the body segments.

Anatomical co-ordinate axes were defined in each of the segments based on anatomical landmarks, with Z being directed proximally, X anteriorly and Y towards the left of the body, as in Fig 3.1. The centres of volume and mass were assumed coincident and regression equations were developed in a similar way to those in the earlier paper of Clauser et al (1969).

Hinrichs (1985) set out to develop a set of regression equations for the estimation of segmental moments of inertia about both the transverse and longitudinal axes of living subjects. The basis for this was the study of Chandler et al (1975) with anthropometric measurements used as predictors.

Symmetry about the segment longitudinal axes was assumed, the justification being the similar moments of inertia about the axes perpendicular to the long axis found by Chandler et al (1975).

Hinrichs (1985) averaged the two transverse moments of inertia for each segment, as well as the anthropometric and moment of inertia data from left and right extremities. The original data for each segment was thus reduced to the segment moments of inertia about its longitudinal axis and a transverse axis through its centre of mass, as well as several anthropometric dimensions specific to the segment.

Linear regression equations for the estimation of the moment of inertia from the anthropometric dimensions were then computed. It was suggested that these equations might not be suitable for use on subjects with anthropometric dimensions outside the ranges of those on which the original data was obtained by Chandler et al (1975).

Hinrichs (1985) expressed some concern about the very small sample size on which his equations were based and Nigg (1995) expressed the view that these equations should be used with caution for this reason.

Forwood et al (1985) also used the data of Chandler et al (1975) in their effort to validate methods of scaling data for the segment moment of inertia about the transverse principal axis through the centre of gravity.

The mean moments of inertia for each segment were scaled using subject body mass and segment length and also using subject body mass and standing height. The latter method was found to give the best results and this should hold for the frontal as well as the transverse axis.

Doubt was cast on the validity of using such scaling techniques for the longitudinal axis, due to the questionable correlation between standing height and segment diameters. This would suggest that the use of a technique which includes segment circumference measurements might be most useful.

Such a technique was developed by Yeadon & Morlock (1989) in their comparison of linear and non-linear methods of estimating the segmental moments of inertia from anthropometric measurements.

Segmental moments of inertia about anatomical axes were again derived from the data of Chandler et al (1975). Linear and non-linear regression

equations for the moments of inertia of the body segments about the anterior-posterior, medial-lateral and longitudinal axes were determined. Right limb data were used to develop the regression equations and left limb data used to validate them.

Equal transverse moments of inertia for each segment (I_x=I_y) were assumed as Chandler et al (1975) gave no segment depth or width dimensions. These transverse moments of inertia were averaged to give the mean transverse moment of inertia I_t.

Linear equations for the upper limb were based on the length and given circumference values for each segment (2 for the hand, 3 for all other segments). Non-linear equations were based on the length and a mean perimeter value, the latter calculated giving double weighting to the mid-point perimeter over the end-point perimeters where three were given. Neither set of equations involved a mass predictor.

The linear and non-linear methods were compared, the linear equations being found to determine the inertia values for the limb on which the equations were based more accurately than the non-linear equations. When comparing the equations on the left arm as an independent sample, the non-linear equations were more accurate by some margin. The linear equations appeared to be accurate for the sample on which they are based, but less so on another sample. The equations were then compared outside the anthropometric range of the original sample of Chandler et al (1975), on a 10 year old boy. The non-linear equations were found to perform to a much greater degree of accuracy than the linear equations.

The non-linear equations were considered superior to the linear ones, giving reasonable segmental moment of inertia estimates even when the anthropometric measurements lay outwith the original sample range upon which they were based. The final non-linear regression equations (equations 3.1 and 3.2) of Yeadon & Morlock (1989) for the non-torso segments are based on both left and right limb data from Chandler (1975).

$$I_z = k_1 p^4 h \qquad (3.1)$$

$$I_t = \tfrac{1}{2} I_z + k_2 p^2 h^3 \qquad (3.2)$$

Where I_z and I_t are the moments of inertia about the longitudinal axis and transverse axes respectively in kgm^2. Table 3.11 gives other necessary values.

The regression techniques of both Yeadon & Morlock (1989) and Clauser et al (1969) were used in the paper of Veeger et al (1997) to estimate segment moments of inertia, mass and centre of mass location. This paper is discussed in Chapter 7 in relation to location of the glenohumeral joint centre.

Segment	Variable	Definition / Value	p
Upper arm	h	Length : shoulder centre to elbow centre	
	p_1	Perimeter : below axilla	
	p_2	Perimeter : maximum	$p=(p_1+2p_2+p_3)/4$
	p_3	Perimeter : elbow	
	k_1	0.979	
	k_2	6.11	
Forearm	h	Length : elbow centre to wrist centre	
	p_1	Perimeter : elbow	
	p_2	Perimeter : maximum	$p=(p_1+2p_2+p_3)/4$
	p_3	Perimeter : wrist	
	k_1	0.810	
	k_2	4.98	
Hand	h	Length : wrist centre to tip of finger III	
	p_1	Perimeter : wrist	
	p_2	Perimeter : metacarpal-phalangeal joints	$p=(p_1+p_2)/2$
	k_1	1.309	
	k_2	7.68	

Table 3.11 Definitions and values of the variables required in the non-linear approach of Yeadon & Morlock (1989). (N.B. Linear measurements are in metres and the hand is in a flexed/ relaxed orientation)

The preferred solution for the estimation of segment parameters would be to base these on cross sectional segment data from different body types and for both men and women, none of the papers discussed till now providing a completely satisfactory solution. In future, Computerised Tomography (CT), or more so Magnetic Resonance Imaging (MRI) technology may become more widely used in such studies, allowing the different densities of bone, muscle and fat to be taken into account. These however are more expensive and invasive than the more traditional methods and would involve greater ethical consideration. More recent studies have attempted to use such technologies to measure body segment parameters however.

Zatsiorsky & Seluyanov (1983) obtained data from one hundred male subjects (age23.8±6.2 years, height 174.1±6.2cm, mass 73.0±9.1kg), fifty six of whom were physical education students, twenty six students and eighteen researchers. A radioactive isotope gamma ray scanning technique was used to determine mass and inertial characteristics of their segments.

The intensity of a gamma ray beam decreases as it passes through a substance and the density of that substance can be determined by the level of attenuation. It is therefore possible to measure the intensity on either side of substance (in this case a human subject) and from this calculate its density.

Subjects were placed in a supine position on a couch. A gamma ray emitter passed over and scanned the entire body. A collimated detector passing underneath the subject detected the attenuated radiation. A surface density profile was produced for the entire body, the locations of each of the measured intensities being recorded in relation to previously defined anatomical reference points.

The regression equation (3.3) was developed:

$$y = B_0 + B_1X_1 + B_2X_2 \qquad (3.3)$$

Where X_1 is the body mass in Kg, X_2 is the body height in centimetres and y is the predicted value of the variable.

Segment	Mass (kg)	CoG (%)	M (%)	K_1 (%)	K_2 (%)	K_3 (%)
Hand	0.447	63.09	0.614	28.50	23.3	18.2
	(0.072)	(4.85)	(0.083)	(2.16)	(1.71)	(2.30)
Forearm	1.177	57.26	1.625	29.50	28.4	13
	(0.161)	(3.26)	(0.140)	(0.86)	(0.65)	(1.51)
Upper arm	1.980	55.02	2.707	32.80	31	18.20
	(0.319)	(4.19)	(0.243)	(1.61)	(1.245)	(3.27)

Table 3.12 Mean values of Mass and Inertial characteristics of the upper limb, with SD in brackets. M(kg)=mass of segment, CoG (%)=centre of gravity along longitudinal axis, M(%)=mass of segment as a percentage of body mass, K_1, K_2, K_3 are the ratios of the radius of gyration about the anteroposterior axis, transverse axis and longitudinal axis of the segment respectively, to the length of the segment (Zatsiorsky & Seluyanov (1983))

This equation was applied to allow prediction of the relative masses and centre of gravity locations of the body segments along with their radii of gyration. The three principal moments of inertia about the anteroposterior, transverse and longitudinal axes with respect to the segment CoG of living subjects were then calculated. The regression equation coefficients for these values are given in the original paper, the results are shown in Table 3.12.

In their later paper, Zatsiorsky & Seluyanov (1985) produced regression equation (3.4) for mass, centre of gravity and principal moments of inertia based on the results of their previous tests. Again the regression coefficients for these values can be found in the original paper.

$$y = B_0 + B_1X_1 + B_2X_2 + B_3X_3 + B_4X_4 \qquad (3.4)$$

This equation was developed with the "most predictable" anthropometric features as the predictors as opposed to the weight and height which are not necessarily the best predictors for the individual body segments. A total of 67 anthropometric measurements were taken, the best predictors for each of the segments of the upper limb being:

Hand X_1 = length of straight hand (cm)
X_2 = width of the hand (cm)
X_3 = mean circumference of the hand (cm) ($=D_1+D_2 / 2$)
where D_1 = circumference of the hand (cm)
D_2 = the smallest circumference of the distal forearm (cm)

Forearm X_1 = length of forearm (cm)
X_2 = width of the hand (cm)
X_3 = mean circumference of the forearm (cm) ($=D_1+D_2+D_3 / 3$)
where D_1 = the smallest circumference of the distal forearm(cm)
D_2 = middle circumference of the forearm (cm)
D_3 = the maximum circumference of the proximal forearm (cm)

Upper arm X_1 = biomechanical length of the upper arm (cm)

X_2 = circumference of the relaxed upper arm (cm)

$X_3 = D_1+D_2 / 2$

where D_1 = lower diameter of the upper arm (cm)

D_2 = lower diameter of the forearm (cm)

Pearsall & Reid (1994) carried out a comprehensive review of body segment parameter studies, the works of Dempster (1955), Clauser et al (1969) and Chandler et al (1975) being found to be the most commonly cited.

The studies of Zatsiorsky & Seluyanov (1983), (1985) along with the supplementary data for female subjects (age 20-27 years, nine swimmers, six fencers) in Zatsiorsky et al (1990) were considered among the best sources of data, since they had a substantially large number of subjects and measured in vivo.

De Leva (1993) also advocated the use of the data of Zatsiorsky & Seluyanov (1983) and Zatsiorsky et al (1990) above cadaver based data for the same reasons. Considered a further advantage of these studies were the younger average age of the subjects (23.8 years for males, 19 years for females) and therefore a greater relevance to a young, living population, most subjects being physical education undergraduates.

In his later paper, de Leva (1996a) carried out a correction process on the data of Zatsiorsky & Seluyanov (1983) similar to that carried out by Hinrichs (1990) on the data of Clauser et al (1969). The motivation for this was the fact that the original data were not referenced in terms of joint centres but by bony landmarks and for this reason were rarely utilised.

The mean relative centre of mass positions were adjusted to relate to joint centres, using the data of Chandler et al (1975) in the case of the upper arm. The resulting values for the relevant dimensions are given in Table 3.13.

		Mass %		Centre of Mass %	
Segment	End points	Females	Males	Females	Males
Upper arm	Shoulder JC-Elbow JC	2.55	2.71	57.54	57.72
Forearm	Elbow JC-Wrist JC	1.38	1.62	45.59	45.74
Hand	Wrist JC-Met III	0.56	0.61	74.74	79.00

Table 3.13 Relative segment mass (given as a percentage of total body mass) and centre of gravity location (given as a percentage of the distance along the longitudinal axis from the proximal joint centre). (de Leva (1996a)

3.4 The location of joint centres

The joint centres for the work of de Leva (1996a), are defined using the methods described in de Leva (1996b). This technique for estimating the joint centre locations was developed using a selection of the data of Chandler et al (1975). Percentage longitudinal distances of the joint centres from neighbouring bony landmarks were calculated, relative to the lengths of the proximal and/ or distal segments. The basis for this were the assumptions that the human joints are perfect hinge or ball-and-socket joints and that the joint centres lie on the respective segment longitudinal axes. The resulting locations of the joint centres are shown in Fig 3.2 where:

Shoulder Joint Centre (SJC) = The centre of the humeral head.

Elbow joint Centre (EJC) = The centre of the transverse section of the humerus, at the level of the greatest projection of the medial humeral epicondyle (near the level of the skin crease at the anterior surface of the elbow).

Wrist Joint Centre (WJC) = The centre of a transverse section of the capitate bone, at the level of the palpable groove between the lunate and capitate bone

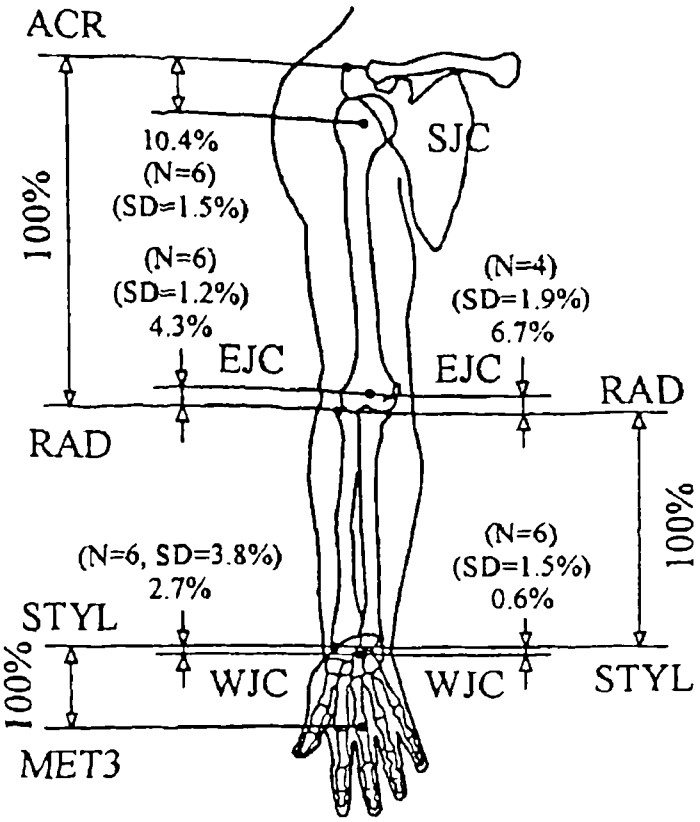

Fig 3.2 Percentage longitudinal distances of joint centres from neighbouring bony landmarks. Each percentage is relative to the closest 100% distance (N=number of subjects; SD= standard deviation). (de Leva (1996b))

As can be seen in Fig 3.2, these percentages are based on either four or six subjects, small samples when trying to develop data representative of the wider population.

3.5 The prediction of body segment lengths

One of the most common of the anthropometric measurements studied are the lengths of each of the segments of the body between the joints at either end. The previously discussed work of Contini (1972) produced data for the average lengths of the various segments of the body, expressed as a percentage of the height of the subjects, given for male subjects in Fig.3.3.

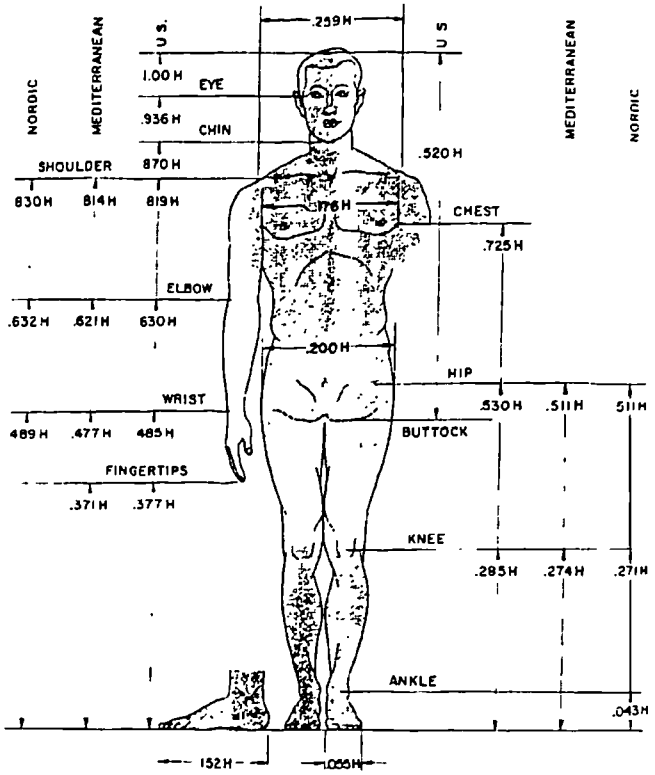

Fig.3.3 Body segment lengths (Contini (1972))

Pheasant (1986) also provides some data for anthropometric segment length measurements taken from the re-analysis of Dempster (1955) by Reynolds (1978), the data for the upper limb are shown in Table 3.14.

Segment	Males	Females
Upper arm	17.4 %	17.2 %
Forearm	15.6 %	14.9 %
Hand	10.9 %	10.8 %

Table 3.14 Average length of the links of the upper limb as a percentage of the total height (Pheasant (1986)).

3.6 Summary and Conclusions

In considering all of the work discussed over the preceding pages, there seems good reason to be sceptical of BSP data from cadaver studies, where sample sizes are generally small, average ages high and tissues not necessarily in a condition similar to that during life. In this respect the more recent of the cadaver papers discussed may offer little that is superior to the earlier data provided in the late 19th century.

The advocation of the use of the data of Zatsiorsky & Seluyanov (1983) by de Leva (1993) and Pearsall & Reid (1994) would seem reasonable. The sample size on which these data were based was larger than other studies and thus would lead to more generally relevant average data. The study was carried out on living and therefore intact subjects and thus the data were not subject to changes or loss of tissues and fluids after death or in the process of dissection as occurs during cadaver studies. The younger average age of the sample also supports their use for similar reasons, the data being more relevant than cadaver studies for a living population. The modifications by de Leva (1996a) to the work of Zatsiorsky & Seluyanov (1983) relate the data to landmarks appropriate to a study of the upper limb. The only comparable work is that of Drillis & Contini (1966) and Contini (1972), which were carried out on a much smaller sample and with methods which appear less rigorous than those of Zatsiorsky & Seluyanov (1983).

For these reasons the data of Zatsiorsky & Seluyanov (1983), modified by de Leva (1996a), were selected for the calculation of upper limb segment parameters; segment mass, centre of mass location and mass moments of inertia. The data used are given in Table 3.15, the segment end points of the upper arm and forearm being the same as those in Table 3.13. For the hand the segment end points are the wrist joint centre proximally and the tip of the third digit distally. The lengths of the upper arm and forearm were obtained directly from the motion analysis co-ordinate data, the length of the hand being calculated as 10.79% of the subject height from de Leva (1996a).

Segment	End Points	Mass (%)	CM (%)	K1 (%)	K2 (%)	K3 (%)
Upper Arm	SJC-EJC	2.71	57.72	28.5	26.9	15.8
Forearm	EJC-WJC	1.62	45.74	27.6	26.5	12.1
Hand	WJC-DAC3	0.61	36.24	28.8	23.5	18.4

Table 3.15 Segment parameters of the upper limb, Mass(%)=Relative segment mass (as a percentage of total body mass), CM(%)=centre of mass location (as a percentage of the distance along the longitudinal axis from the proximal joint centre), K_1, K_2, K_3 are the radii of gyration. (de Leva (1996a)).

Equation (3.5) was then used to calculate the moment of inertia of each segment about given principal axes.

$$I = (M \times m) \times (L \times K)^2 \qquad (3.5)$$

Where M is the total body mass of the subject, m is the mean relative mass of the segment from Table 3.15, L is the segment length and K is the mean relative radius of gyration of the segment about the chosen axis.

CHAPTER 4 : UPPER LIMB MOTION STUDIES: A REVIEW OF THE LITERATURE

4.0 Introduction

Having discussed the anatomy and anthropometrics of the pectoral girdle and upper limb, the next stage was to investigate how the various components interrelate. This chapter contains a review of previous studies involving the measurement of human upper limb motion, providing a summary of relevant results from previous studies and of possible activities for analysis.

Of particular interest are those studies which have involved analyses of activities of daily living and those which provide data on the shoulder, the latter having traditionally been regarded as extremely difficult due to the complex nature of the shoulder joint.

Several analysis systems are available and have been used for the study of upper limb motion. The most commonly used of these are introduced through discussion of general upper limb studies, before focusing on those that have investigated activities of daily living or provide data of direct relevance to such studies. All the systems and analysis techniques discussed are based on the principle of tracking anatomical landmarks or surface markers affixed in relation to these landmarks. In most studies, landmark co-ordinates are found in relation to some laboratory fixed co-ordinate system and used to define local segment-embedded co-ordinate systems.

In such studies the limb segments are treated as rigid bodies in which the segment-embedded frames are assumed fixed. The position and orientation of the embedded frames can then be described with respect to the global co-ordinate system using a position vector and orientation matrix or a combination of these in a transformation matrix.

Angular changes through time at the joints of the upper limb may be investigated by comparing the relative movements of embedded co-ordinate systems in the proximal and distal segments. Angular velocities and accelerations at these joints can then be calculated to obtain dynamic information.

4.1 Motion analysis systems applied in upper limb studies

4.1.1 Electromagnetic systems

Several upper limb motion analyses have been carried out using electromagnetic devices. The principal on which these operate is the generation of three orthogonal low frequency electromagnetic fields from a transmitter and the detection of these fields through multiple smaller receivers.

Biryukova et al (1996) used a 'Polhemus FASTRAK' device in order to locate the centre of rotation at the shoulder and axes of rotations at the elbow and wrist. In their later work Biryukova et al (1998) measured the kinematics of reaching movements using the same methods.

Johnson et al (1993), Barnett (1996) and Barnett et al (1999) used 'Polhemus' systems for measurement of scapulohumeral motion. Similar work was carried out by Meskers et al (1998b) and Meskers et al (1999) using a 'Flock of Birds' system. Similarly to Biryukova et al (1996) and Biryukova et al (1998), Djupsjobacka et al (1999) used a Polhemus 'Fastrak' system for the measurement of upper limb kinematics.

Electromagnetic systems have the benefit of producing virtually real time data giving fast access to three-dimensional data. Disadvantages are a sensitivity to metal in the environment, a limited range of around three metres and the tethering of the subject to the central hardware unit through the receiver connections. The data output are also dependent on the positioning of a single sensor on each segment, ruling out the application of optimisation to overcome the problems of skin movement.

4.1.2 Video-based systems

The most commonly used systems in upper limb studies are those based on the filming and recording of the motion using video cameras.

The simplest application of this technique is to track anatomical landmarks with little or no additional external marker, using personal judgement to locate the defined points of interest on the recorded video images.

Elliot et al. (1985) used such a method for the analysis of baseball pitching technique, where test subjects had paint applied over anatomical landmarks and were then filmed during motion before digitising of the images.

Whiting et al (1988) studied the kinematics of the upper extremity during boxing. Points on the shoulder, elbow, wrist and glove were marked with tape to indicate the centres of the joints and these were filmed using phase-locked cameras. Phase-locking of the cameras ensured that the correct frames from each camera would coincide during the process of combining the camera views to obtain three-dimensional information.

Payton & Bartlett (1995) marked anatomical locations with black tape prior to capturing kinematic data during swimming, where externally fixed markers of any reasonable size would obviously be unsuitable. Light emitting diodes (LEDs) mounted on the camera lenses were used to synchronise the camera views.

Neither Elliot et al. (1985) nor Whiting et al (1988) defined segment embedded axes, in contrast to the majority of papers in this field. Two cameras were used in each of these studies as well as that of Payton & Bartlett (1995).

These studies rely on the tracking of two-dimensional markers in order to reconstruct three-dimensional trajectories. It is therefore possible that each camera observes a target of a different size, which could introduce errors in identification during manual or automatic digitising.

It would seem reasonable that when three-dimensional information is required, the markers identifying anatomical landmarks should be three-dimensional in order to present the same size and shape in each camera view.

As neither anatomical landmarks nor painted or taped markers exhibit this property, the only solution is to attach some form of external marker to the segment which can be related to the underlying anatomical landmarks.

One frequently used method of achieving this aim is the use of active LED markers attached to the limb segments of the subject. Mann & Antonsson (1983) used an infra-red LED-based 'Selspot I' system for measuring human motion. Samuelson et al. (1987) used an updated version ('Selspot II') of the same system, attaching forty-three infra-red LEDs at various locations on an

elastic polyester suit fitted to the contours of the subject's body. In a further study, Scholz (1989) used the WATSMART™ infra-red LED system.

One problem with such active systems is the necessity for only one infra-red emitting diode to be visible at each instant during sampling. A sequential firing of the LEDs at intervals of several microseconds is thus required. This can introduce difficulties in identifying the active diode and problems with reflections causing spurious data.

A further problem is the power supply to the LEDs which require the subject to move while tethered with cable connections from the LEDs and the analysis system. Some of the most up to date systems such as the infra-red LED based CODA system have managed to overcome this problem, removing the direct connections between LED and the analysis unit.

Passive three-dimensional external markers which reflect light, either from spotlights or camera mounted lights back towards the camera, as opposed to actively emitting light, may also be used. Such markers can be quick and easy to apply and interfere less with patient movement than the tethered markers of some active systems. Passive marker systems operate using either infra-red light or visible light and many studies have involved their use, some of which are discussed on the following pages.

Kadaba et al (1989) used a five camera 'Vicon' system incorporating passive infra-red reflecting markers. The repeatability of gait measurements from forty subjects was assessed. A similar system was used by Khoo et al (1995) in their assessment of loads on the lumbar spine during walking.

Peterson & Palmerud (1996) used passive infra-red reflecting markers and a 'MacReflex' system in order to investigate sources of error in the measurement of upper extremity orientation in relation to an initial reference pose. Testing was carried out on a calibration frame, a mechanical link model of the upper limb and a human volunteer fitted with a cuirass and cuffs around the distal humerus and forearm, to which were attached reflective spheres.

Scholz & Millford (1993) evaluated the accuracy of a two camera 'PEAK Performance Technologies' system, synchronising two cameras using LEDs mounted on the camera lens hood.

Langrana (1981) tested students carrying out a diagonal reach movement with and without an orthosis using a two camera system. Wooden marker triads were attached on the humerus and wrist and aligned with the underlying segment longitudinal axes.

Wang et al (1996) assessed the kinematics of the soft-tennis forehand drive using a six camera 'Motion Analysis Corp.' system. Thirteen reflective markers were placed on each subject as given in Chapter 6, Table 6.1.

Rao et al (1996) used a six camera 'Vicon' system to investigate the upper limb kinematics of sixteen paraplegics performing wheelchair propulsion. Accurately defined relationships between ten surface marker positions and the underlying joint centres were established as given in Chapter 6, Table 6.2.

In this study values of forearm carrying angle were included in contrast to most studies in which they are disregarded. A more rigorous method of locating the glenohumeral joint centre than in other studies was also employed.

Sprigings et al (1994) used three cameras in their analysis of the contributions of upper limb segment rotations to racket head speed in the tennis serve. Ten markers were attached on the shoulder, elbow, wrist, hand and racket, their locations again given in Chapter 6, Table 6.1.

Having introduced some of the available motion analysis systems and their use for studies of the upper limb, the review of previous studies will now focus on studies that have involved investigation of the upper limb during activities of daily living or are of direct relevance to such studies.

4.2 Kinematic studies of the upper limb

An early attempt was made to carry out a three-dimensional study of the kinematics of the upper limb during activities of daily living by Dol'nikov (1965). The upper limb was allocated seven degrees of freedom, these being abduction\ adduction, flexion\ extension, and internal\ external rotation at the shoulder, elbow flexion\ extension, forearm internal\ external rotation, ulnar\ radial deviation and wrist flexion\ extension.

An instrumented orthosis was constructed for the upper limb, secured on the subject by means of a shoulder harness or vest. This allowed the measurement of all seven above mentioned degrees of freedom by means of

potentiometers built into the joints of the orthosis. The joint angles were found and from these the velocities and accelerations were calculated.

Tests were carried out on thirty-four able-bodied subjects (thirty-one males, three females) with ages ranging from 17 to 63 years. The subjects were asked to carry out seven activities associated with everyday living. These included seated testing of; pouring from a bottle into a glass, drinking from a glass and eating with a spoon and standing tests of; combing hair and working with a screwdriver, a hammer and a file.

Kinematic parameters were determined and the means of each of these were found. The results provided were the mean values of the angular excursion (θ), maximum angular velocity (ω) and maximum angular acceleration (α), for each of the seven degrees of freedom previously described and are shown in Table 4.1.

Movement		Everyday Tasks				Working Tasks		
		Pouring from a bottle	Drinking from a glass	Eating with a spoon	Combing	Screw-driver	Hammer	File
Hand Flexion /	θ	3	3	4	10	7	10	3
Extension	ω	94	74	94	238	221	656	147
	α	1994	1885	1937	5598	5168	24557	4360
Hand Abduction /	θ	25	25	33	47	67	53	36
Adduction	ω	119	124	201	606	652	1350	366
	α	2647	2217	2722	4584	5512	20838	3724
Forearm Rotation	θ	74	21	34	52	119	22	11
	ω	660	363	440	660	1719	837	286
	α	13522	7678	8136	13923	31169	22460	8938
Elbow Flexion /	θ	22	71	37	97	9	54	34
Extension	ω	92	269	126	584	97	842	309
	α	1318	2292	1375	4183	1833	13063	3495
Shoulder Rotation	θ	0	22	25	50	46	37	30
	ω	0	321	418	980	768	1031	619
	α	0	4412	5443	18335	13178	23778	12032
Shoulder Flexion /	θ	0	10	10	41	6	19	17
Extension	ω	0	54	1226	195	80	269	155
	α	0	974	917	3610	1375	5500	3151
Shoulder Ab /	θ	5	3	5	11	9	10	9
Adduction	ω	40	50	56	172	92	241	138
	α	688	802	802	2120	1375	3724	3037

Table 4.1 Angular Excursion, Velocity and Acceleration for Seven Different Tasks, where θ = arc of movement (Degrees), ω = max. angular velocity (Degrees/s), α = max. angular acceleration (Degrees/s^2). Dol'nikov, (1965).

In the original paper the results were expressed in radians, radians/s and radians/s^2, but can be found expressed in units of degrees in Buckley et al (1996).

For the tasks chosen to represent necessary activities of daily living, elbow flexion and forearm rotation showed the greatest arc of movement, reaching maximum values of 97° and 74° respectively. Shoulder flexion and abduction can both be seen to have relatively low values throughout the everyday tasks, the maximum value reached being 41° of shoulder flexion during the combing test.

Safaee-Rad et al (1990b) used a biplanar video analysis technique described in Safaee-Rad et al (1990a). Studies of the function of the whole upper limb during the activities of eating with spoon, eating with a fork and drinking from a cup were carried out. Ten healthy male subjects in the age range 20-29 years were assessed.

Seven markers were placed on the shoulder, elbow, wrist and hand and an initial position was defined. Deviation of the upper limb joints during testing was referenced to this position and expressed in terms of Euler angles.

Eight different rotations; shoulder flexion, shoulder abduction, shoulder rotation, elbow flexion, forearm rotation, wrist flexion, wrist deviation and wrist rotation were measured. The carrying angle at the elbow was considered insignificant. The mean and standard deviation of the maximum and minimum angles for each joint during each task were given and from these, the arc of motion required to carry out the task. These results can be seen in Table 4.2.

The values shown for elbow flexion can be seen to compare favourably with those of two studies discussed in Section 4.3. In particular the results for the drinking test and the fork test compare favourably with those of Morrey et al (1981) for similar tests, though the values for eating with a spoon do not compare quite as well with a similar test discussed by Packer et al (1990).

Cooper et al (1993) discussed a continuation of this work using identical experimental techniques. The same three feeding tasks were carried out by ten male and nine female subjects aged between 18 and 50 years, first with the normal freedom of movement and then with a splint fixing the elbow in 110° of flexion. The results are given in Table 4.3.

Movement		Task					
		Drinking from a cup		Eating with a fork		Eating with a spoon	
		Mean (°)	SD (°)	Mean (°)	SD (°)	Mean (°)	SD (°)
Wrist flexion\extension	Min.	-7.5	6.1	3.3	8.2	7.7	9.0
	Max.	5.9	8.0	17.7	7.2	20.4	8.7
	Arc	13.4	6.3	14.4	3.8	12.8	4.1
Wrist deviation	Min.	-16.1	7.2	-3.2	8.2	-4.2	6.2
	Max.	-8.3	6.4	4.9	6.7	4.4	5.9
	Arc	7.8	3.7	8.0	3.0	8.6	2.4
Wrist rotation	Min.	-0.5	0.8	-0.2	1.0	-0.3	1.0
	Max.	2.0	1.7	1.9	2.3	2.2	1.3
	Arc	2.4	1.6	2.1	1.6	2.5	0.8
Forearm rotation	Min.	-31.2	7.2	-58.8	7.9	-58.7	5.8
	Max.	-3.4	11.1	38.2	7.9	22.9	14.6
	Arc	27.8	8.9	97.0	8.8	81.6	17.5
Elbow flexion\extension	Min.	71.5	5.9	93.8	6.0	101.2	8.1
	Max.	129.2	2.5	122.3	3.6	123.2	5.0
	Arc	57.7	5.2	28.5	5.3	22.0	7.9
Shoulder rotation	Min.	5.2	8.0	5.1	9.8	4.8	12.0
	Max.	23.4	12.0	18.1	10.0	16.8	11.9
	Arc	18.2	8.0	13.0	2.2	12.0	5.1
Shoulder flexion\extension	Min.	15.8	4.4	10.7	5.2	7.8	7.7
	Max.	43.2	16.3	35.2	11.9	36.1	13.7
	Arc	27.4	13.9	24.4	9.1	28.3	10.0
Shoulder abduction\adduction	Min.	12.7	7.7	7.1	7.8	6.6	9.9
	Max.	31.2	9.2	18.6	6.0	21.8	7.1
	Arc	18.5	9.5	11.5	2.6	15.2	7.2

Table 4.2 Average Joint Rotations During Three Feeding Tasks. (N.B. shoulder internal rotation - positive, pronation - positive, wrist extension -positive, radial deviation - positive, wrist external rotation - positive). Safaee-Rad et al (1990b)

	Males						Females					
Movement	Unrestricted			Restricted			Unrestricted			Restricted		
	Min (°)	Max (°)	Arc (°)	Min (°)	Max (°)	Arc (°)	Min (°)	Max (°)	Arc (°)	Min (°)	Max (°)	Arc (°)
Shoulder												
Flexion	9.0	36.1	27.1	12.4	69.3	56.9	3.9	31.1	27.2	-3.2	57.5	60.7
Abduction	5.9	22.7	16.8	2.5	28.7	26.2	12.7	27.6	14.9	13.1	35.8	22.7
Internal rotation	-1.3	22.1	23.4	2.2	49.1	46.2	1.9	27.9	29.8	-4.8	39.6	44.4
Elbow Flexion	77.3	125.6	48.3	105.7	120.4	14.7	85.7	135.7	50.0	104.8	122.4	17.6
Forearm Rotation	-52.8	47.1	99.9	-48.4	34.9	83.3	-51.2	37.5	88.7	-34.1	17.8	51.9
Wrist												
Flex /extension	-6.8	20.9	27.7	-9.1	22.0	31.1	-7.7	22.3	30.0	-10.1	24.6	34.7
Deviation	-18.7	2.4	21.1	-22.9	4.8	27.7	-3.0	18.4	21.4	-12.2	12.2	24.4
Rotation	-1.8	1.1	2.9	-4.0	1.6	5.6	-2.4	1.1	3.5	-3.6	1.8	5.4

Table 4.3 Average Joint Rotations Required During Three Feeding Tasks with Restricted and Unrestricted Elbow Joint - Males and Females (19 subjects) (N.B. shoulder internal rotation - positive, pronation - positive, wrist extension -positive, radial deviation - positive, wrist external rotation - positive). Cooper et al (1993).

It can be seen from these results that a restriction of movement at the elbow joint resulted in an increase of movement at the other joints compensating for the restriction. This is indicated by an increase in male shoulder flexion and rotation and female shoulder flexion for all tasks. Male abduction increased only during use of the spoon, with female abduction and internal rotation increasing only during drinking. The results in Table 4.3 for the unrestricted set of tests compare well with those in Table 4.2 from the work of Safaee-Rad et al (1990b).

Buckley et al (1996) suggested that differences in the experimental protocol may be the cause of variations in results between different studies. Of particular importance are the initial positioning of objects involved in the study and the definition of a neutral limb position as a reference for the study.

Romilly et al (1994) also carried out a study using the work of Safaee-Rad et al (1990a) as the basis for their technique. The entire upper extremity was studied during daily activities of normal adult life as a preparatory step to developing a powered upper limb orthosis.

Six able-bodied subjects (three males) in the age range 22 to 44 years carried out 22 different tasks. Five markers were attached at the shoulder, elbow, wrist and hand. Anthropometric measurements were made on each of the subjects in order to translate between surface markers and joint centres. Movements were analysed by means of a video camera system incorporating two cameras at an angle of 50°.

The tasks included four activities involved in eating and drinking; with hands, a fork, a spoon, from a glass, six reaching activities, nine activities of daily living; pouring from a jug, lifting a telephone receiver, turning a doorknob, using a light switch and three activities of personal hygiene; combing the hair, brushing the teeth and washing the face.

The arm was modelled with seven active degrees of freedom using a global co-ordinate system similar to that of Pearl et al (1992) discussed later. This included measures of azimuth (rotation about a fixed vertical axis through the shoulder), elevation (rotation about any horizontal axis through the shoulder), roll (internal\ external rotation of the upper arm), elbow flexion,

forearm rotation, ulnar deviation and wrist flexion. The forearm carrying angle was modelled as a further passive degree of freedom.

The average values for each of the joint rotations during performance of the tasks is shown in Table 4.4. Values for the standard deviations of each of the values are included in the original paper.

	Joint													
	Shoulder						Elbow		Forearm		Wrist			
	Azimuth		Elevation		Roll		Flexion		Rotation		Flexion		Yaw	
Task	Min	Max	Min	Max	Min	Max	Min	Max	Min	Max	Min	Max	Min	Max
Hands	39	65	33	47	-49	0	67	134	-70	36	-18	12	-12	10
Fork	32	49	34	54	-40	1	73	129	-37	50	-6	35	-13	10
Spoon	34	54	32	76	-61	-4	75	123	-24	57	-7	53	-7	17
Cup	37	56	32	63	-62	-21	68	136	-14	37	-24	16	-11	8
Reach1	7	40	29	35	-38	-23	71	84	-24	-11	-30	-6	-7	9
Reach2	38	76	31	39	-32	-19	66	78	-26	-15	-32	-19	-2	4
Reach3	35	108	30	42	-33	-20	57	81	-29	-15	-33	-15	-2	5
Reach4	8	43	31	36	-28	-17	67	80	42	49	-17	-5	-1	7
Reach5	40	80	32	40	-27	-19	64	77	39	47	-13	-6	-2	4
Reach6	38	107	32	44	-28	-19	58	79	37	47	-14	-6	-2	5
Pour	36	66	32	85	-45	-16	65	86	-49	36	-32	-1	-12	4
Door	39	72	34	58	-50	-20	58	78	-2	47	-32	-11	-4	11
Knob	37	69	37	64	-45	-15	42	76	7	52	-38	-11	-10	9
Tap	33	65	34	64	-45	-17	57	77	19	48	-17	22	-39	9
Light	37	69	32	96	-56	-21	45	88	-47	41	-19	3	-23	1
Button	39	68	31	90	-57	-27	51	88	20	40	-19	2	-8	2
Page	7	73	30	45	-26	-4	86	98	42	61	-13	30	-23	14
Phone	36	71	35	53	-82	-26	74	151	-26	48	-32	9	-14	11
Lap	7	81	15	34	-31	20	49	84	31	45	-30	2	0	10
Wash	32	86	28	51	-75	-18	73	148	-86	50	-42	14	-19	15
Brush	35	68	34	69	-78	-22	72	146	-46	41	-32	39	-22	17
Comb	35	86	31	77	-85	-13	71	143	-52	47	-35	36	-18	24
Extremes	7	108	15	96	-85	20	42	151	-86	61	-42	53	-39	24
SD (%)	7.8	8.1	4.1	6.3	9.9	8.3	6.1	7.1	11.0	9.4	8.9	11.6	7.3	5.6

Table 4.4 Average Joint Rotations During 22 Different Tasks (N.B. pronation - positive, wrist flexion -positive, radial deviation (yaw) - positive) Romilly et al (1994)

Romilly et al (1994) obtained results of a similar magnitude to those of Safaee-Rad et al (1990b) for the feeding tasks. These papers employ different angular conventions however and thus the results cannot be directly compared. Both papers found greater values than those from the Russian survey of Dol'nikov (1965). Buckley et al (1996) concluded that Romilly et al (1994) recorded much greater shoulder rotations overall, due to the fact that they looked at reaching tasks as opposed to activities of personal hygiene or feeding. For the elbow joint, Romilly's results correspond fairly closely with

both Morrey et al (1981) and Packer et al (1990), particularly the latter when using a telephone, giving more elbow extension than Safaee-Rad et al (1990b).

Cheng (1996) described an investigation of the kinematic and kinetic characteristics of the upper limb during four activities. Seated tests included the lifting of 1kg and 2kg weights in the shape of a book to table height, shoulder height, head height and maximum height, along with the controlling of a steering wheel (right hand forces) and cutting with a knife. The opening and closing of a door was tested in a standing position.

	M_x		M_y		M_z		Total	Grav.	Inert.	Load
Activity	Max	Min	Max	Min	Max	Min	M_t	M_g	M_i	M_h
1kg Book										
Table Hgt	-1.87	-9.98	6.74	-5.69	13.17	-0.35	16.12	13.12	10.68	
SD	1.16	2.27	2.25	1.66	1.99	1.93	1.64	1.63	1.78	
Shoulder Hgt	-1.34	-11.54	5.83	-6.18	16.64	-0.33	19.73	14.51	12.37	
SD	1.53	3.83	3.37	2.46	3.51	2.25	3.17	1.43	3.32	
Head Hgt	-0.23	-12.53	5.28	-5.67	17.64	-0.85	21.14	14.01	13.97	
SD	2.52	3.07	2.97	1.84	3.39	2.95	3.22	1.37	3.31	
Maximum Hgt	0.85	-14.3	6.58	-6.45	18.08	-1.1	23.1	12.62	15.75	
SD	1.98	4.19	3.86	2.23	3.87	4.21	4.39	2.44	4.46	
2kg Book										
Table Hgt	-2.85	-12.88	6.24	-7.06	18.89	3.5	21.35	19	11.68	
SD	2.11	2.72	3.75	2.75	2.14	2.07	1.58	2.03	2.07	
Shoulder Hgt	-2.07	-13.4	4.8	-6.1	21.69	3.44	24.59	20.91	13.62	
SD	4.41	4.2	2.71	2.77	1.91	2.77	2.54	1.64	2.88	
Head Hgt	-1.22	-14.14	5.35	-6.38	22.52	3.07	25.87	20.07	14.91	
SD	3.35	4.7	3.98	2.28	3.71	3.22	4.95	2.15	3.98	
Maximum Hgt	0.07	-17.59	5.66	-6.84	21.31	1.7	26.69	18.61	15.24	
SD	2.74	3.95	2.18	1.92	3.85	3.03	5.29	3.35	4.22	
Door										
Open\Close	0.6	-5.61	3.04	-2.35	10.93	-0.9	11.61	8.27	3.79	5.94
SD	2.12	1.37	0.93	1.29	1.94	1.97	1.78	0.98	2.11	1.3
Driving										
Steering	10.04	-9.18	32.62	-3.21	18.4	-7.5	35.44	9.42	3.22	38.07
SD	7.78	4.13	6.41	2.64	3.65	7.03	5.51	1.3	0.86	8.53
Cutting										
Cutting	1.3	-5.22	2.8	-3.3	9.51	-2.99	10.7	5.7	6.35	6.87
SD	2.24	2.55	1.58	1.56	2.78	3.68	2.61	1.37	2.67	3.65

Table 4.5 Maximum moments and standard deviations at the shoulder for various activities. M_x, M_y, and M_z are the abduction\adduction, internal\external rotation and flexion\extension moments at the shoulder respectively. M_t is the maximum resultant shoulder moment, M_g is the gravitational shoulder moment, M_i is the inertial shoulder moment and M_h is the resultant moment from the hand load. Cheng (1996).

A strain-gauged transducer was used for the measurement of hand loads during control of a simulated steering wheel system, with an instrumented

door rig and cutting plate being used in the other tests. The three dimensional movements of the upper limb were measured with a six camera 'Vicon' system as used by Runciman (1993). The data obtained were combined with the force data to allow calculation of the moments at the shoulder and elbow joints. Six normal, right-handed subjects with ages ranging from 27 to 38 years were tested on their dominant side. The resulting shoulder and elbow moments can be seen in Table 4.5 and Table 4.6. The gravitational component given incorporates the mass of the book and the arm.

	M_x		M_y		M_z		Total	Grav.	Inert	Load
Activity	Max	Min	Max	Min	Max	Min	M_t	M_g	M_i	M_h
1kg Book										
Table Hgt	1.09	-3.36	-0.08	-4.42	8.72	0.66	10.05	6.48	5.23	
SD	1.1	1.6	0.53	0.93	1.36	0.96	1.14	0.6	0.87	
Shoulder Hgt	1.24	-3.93	0.32	-4.28	9.89	-0.38	11.1	6.6	5.71	
SD	0.74	1.09	0.64	1.18	1.914	1.26	1.69	0.55	1.3	
Head Hgt	1.1	-4.82	0.1	-4.63	10.17	-0.33	11.61	6.67	6.2	
SD	1.27	1.2	0.85	0.81	1.88	1.76	1.66	0.66	1.46	
Maximum Hgt	2.06	-5.32	1.01	-5.27	10.54	-0.68	12.11	6.72	6.73	
SD	2.63	0.87	1.7	1.16	1.93	1.31	1.93	0.62	1.61	
2kg Book										
Table Hgt	1.07	-5.21	-1.07	-6.08	12.97	2.85	14.53	10.99	6.19	
SD	1.41	1.69	0.86	0.97	1.87	1.77	1.52	0.8	0.94	
Shoulder Hgt	1.19	-5.38	-1.19	-6.86	15.04	1.87	16.66	11.15	7.29	
SD	1.67	1.67	1.1	1.53	1.47	2.88	1.19	0.91	1.05	
Head Hgt	1.19	-7.06	-0.96	-7.6	14.86	0.4	16.72	11.14	7.63	
SD	2.47	1.45	0.94	1.71	2.34	2.89	2.03	1	1.62	
Maximum Hgt	1.31	-7.56	-0.06	-7.75	14.68	0.03	17.16	11.26	7.95	
SD	2	0.91	0.78	1.11	3.25	1.81	2.74	1.15	1.54	
Door										
Open\Close	0.43	-2.91	1.37	-2.72	5.61	0.69	6.28	2.73	0.98	4
SD	0.99	-0.75	0.96	1.75	1.76	1.14	2.02	0.42	2.01	1.78
Driving										
Steering	13.53	-3.44	8.27	-2.05	14.04	-1.99	21.04	2.72	1.04	22.19
SD	7.48	1.38	2.44	1.16	3.38	3.03	4.83	0.43	0.24	5.43
Cutting										
Cutting	2.38	-0.86	1.94	-2.91	4.38	-1.73	6.35	2.32	2.58	5.02
SD	1.3	0.98	2.66	1.19	2.16	1.8	1.83	0.34	1.12	2.73

Table 4.6 Maximum moments and standard deviations at the elbow for various activities. M_x, M_y, and M_z are the abduction\adduction, internal\external rotation and flexion\ extension moments at the elbow respectively. M_t is the maximum resultant elbow moment, M_g is the gravitational shoulder moment, M_i is the inertial elbow moment and M_h is the resultant moment from the hand load. Cheng (1996).

High moments due to hand load in steering were obtained and elbow flexion and extension was the major component in the activities analysed.

The difficulty of the activities was graded by the magnitude of the resultant total shoulder moment. In ascending order these were cutting, door opening\ closing, lifting and driving. The difficulty of lifting increased with the increase in mass and height of lift. The major component of shoulder moment in all activities other than driving is seen to be the flexion\ extension moment. Cheng (1996) also gave the data for the 1kg book lift in Table 4.7.

Rotation Angle	Table Height		Shoulder Height		Head Height		Max. Height	
	Mean (°)	SD (°)	Mean (°)	SD (°)	Mean (°)	SD (°)	Mean (°)	SD (°)
Flexion	37.3	8.0	65.2	5.3	100.7	8.2	118.7	6.7
Abduction	25.6	10.3	44.2	11.6	113.1	6.6	137.0	7.2
Internal Rotation	64.6	14.9	66.6	8.5	63.6	8.3	63.3	4.1

Table 4.7 Mean and standard deviation of maximum rotation angles of upper arm for lifting a 1kg book to four heights. Cheng (1996).

4.3 Kinematic studies of the elbow

Several studies have been carried out with specific focus on the elbow joint. Morrey et al (1981) used an electrogoniometer to study the elbow motion of eighteen men and fifteen women carrying out fifteen activities of daily living. Subjects were asked to touch various points on their body that were thought to reflect possible positions of the hand during activities of dressing and personal hygiene, these were the top and rear of the head, the waist, chest and neck, the sacrum and the shoe. The results obtained are shown in Table 4.8.

Task	Elbow Flexion (degrees)	Forearm Supination (degrees)	Forearm Pronation (degrees)
Moving hand to :			
Head (vertex)	118.6 ± 6.1	46.6 ± 16.0	-
Head (occiput)	144.0 ± 7.0	2.0 ± 23	-
Shirt (waist)	100.4 ± 13.2	11.9 ± 23.8	-
Shirt (chest)	120.0 ± 8.2	29.4 ± 19.2	-
Shirt (neck)	134.7 ± 5.2	40.9 ± 16.3	-
Sacrum	69.7 ± 12.4	55.8 ± 20.1	-
Shoe	16.0 ± 6.3	-	19.0 ± 17.2

Table 4.8 Position of the elbow joint during routine activities of personal care and hygiene. Average values of mean and standard deviation for 33 subjects. (Morrey et al (1981)).

Eight activities of daily living were also analysed, these being; pouring from a jug, raising a glass to the mouth, cutting with a knife, putting a fork to the mouth, using a telephone, reading a newspaper, rising from a chair and opening a door. The results obtained are shown in Table 4.9.

Task	Mean Flexion (Degrees)			Mean Rotation (Degrees)		
	Min.	Max.	Arc.	Pronat.	Supinat.	Arc.
Pour from jug	35.6	58.3	22.7	42.9	21.9	64.8
Put glass to mouth	44.8	130.0	85.2	13.4	10.1	23.5
Cut with knife	89.2	106.7	17.5	41.9	-26.9	15.0
Put fork to mouth	85.1	128.3	43.2	10.4	51.8	62.2
Use the telephone	42.8	135.6	92.8	40.9	22.6	63.5
Read a newspaper	77.9	104.3	26.4	48.8	-7.3	41.5
Rise from a chair	20.3	94.5	74.2	33.8	-9.5	24.3
Open a door	24.0	57.4	33.4	35.4	24.3	58.8

Table 4.9 Amount of elbow motion required to carry out selected daily activities. Maximum, Minimum and Arc values for 33 subjects where negative supination represents pronation. (Morrey et al (1981)).

It was concluded that the functional arc of elbow flexion\extension was 100°, between limits of 30° and 130°, and the arc of forearm rotation was around 100° evenly distributed between pronation and supination.

Packer et al (1990) also carried out a study of elbow function using electrogoniometry. This study looked at elbow flexion in five rheumatoid arthritis subjects (three males, two females) awaiting elbow arthroplasty, and five control subjects (three males, two females), all in the age range 54 to 81 years. Three activities were carried out; standing and sitting using chair arms for support, eating with a spoon and lifting a telephone receiver to the ear, the latter two in a seated position. It is important to note that these tests were partly chosen for the lack of involvement of hand and shoulder function in their performance. The joint angles, arc and duration of each of the tests were recorded. The results obtained for the five control subjects with no known shoulder pathology are shown in Table 4.10.

The results obtained were similar to those of Morrey et al (1981), the largest discrepancy being in the telephone test, where Packer observed a much smaller range of movement (75°-140°) in comparison to that obtained by Morrey et al. (43°-137°). Any comparison made between such papers must

however be made while remembering that the experimental protocol might have varied in each case, with factors such as the height of the table having some effect.

Movement		Task					
		Sit-Stand-Sit		Use Telephone		Eat With Spoon	
		Median	Range	Median	Range	Median	Range
	Min. (°)	15	-10-25	75	45-85	70	35-100
Flexion	Max. (°)	110	85-120	140	130-160	115	90-140
	Arc (°)	95	70-110	65	55-115	45	15-70

Table 4.10 Required elbow flexion in degrees for three selected activities of daily living carried out by five control subjects, where extreme extension is denoted by the lowest angle. (Packer et al (1990))

The inter-subject variation can be seen to be quite large, most obviously in the case of the spoon test, showing that the target end position of a movement can be achieved with a variety of joint orientations.

Williams (1996) investigated upper limb motion with a particular focus on the elbow joint. Six activities were analysed using a six camera 'Vicon' system, these being reaches from table to mouth, to the vertex of the head, to the back of the neck, to the perineum, forward to a shelf and to maximum height. Graphical data from eleven unimpaired and eight impaired subjects were presented. These data, along with that from Cheng (1996), were used for the validation of the experimental methods and analysis techniques developed in the current study, as discussed in Section 7.8.

4.4 Musculoskeletal modelling studies

Several studies have obtained kinematic data during performance of upper limb tasks as the basis for the development of musculoskeletal models and the subsequent calculation of internal muscle and joint forces.

An early shoulder study was undertaken by Inman et al (1944), who investigated the relationships between the bony elements of the shoulder using roentgenography and the insertion of pins into the bones of living subjects. Forces were calculated at various stages during abduction in the coronal plane, over a range of elevations between 30° and 180°, though details of the steps involved between these limits are not given.

The maximum calculated compressive force on the glenoid was found to occur at 90° of elevation, reaching 10.2 times the weight of the extremity. Given that the authors estimated the extremity weight amputated at the glenohumeral joint as being 9% of the total weight of the body, this would correspond to a force of around 0.92 times body weight. No details are given of the mass of the subjects or the number involved in the study, but this force would be equivalent to approximately 676N for a subject of mass 75kg.

Poppen & Walker (1976) also carried out a roentgenographic study of the shoulder. Abduction of the arm in the plane of the scapula was studied in steps of 30°, from the relaxed arm position to an elevation of 150° and then maximum elevation. A total of 27 subjects comprising twelve normals (age range 22-63) and fifteen with shoulder problems (age range 17-72) were tested. The movement and rotation of the scapula, arm angle, glenohumeral angle, scapulothoracic angle and the movement of the humeral head on the face of the glenoid were all investigated.

The instantaneous centre of motion about which the humerus appeared to rotate was also identified. This is possible only if the motion is assumed to be two-dimensional, no such points existing in three-dimensional movement, where motion occurs about instantaneous axes of rotation.

Maximum Arm Angle (Degrees)	30° to Max. GH:ST Ratio	Instantaneous Centre (mm)	Excursion of Ball on Glenoid (mm)
150	1.25 ± 0.25	6.0 ± 1.85	1.09 ± 0.475

Table 4.11 Averages of the results for the normal volunteers in the work of Poppen & Walker (1976). The first column shows the angle between the longditudinal axis of the humerus and an axis parallel with the vertical axis of the body. The second column shows the ratio between the angle of deviation of the humeral longditudinal axis from the scapular vertical axis and the deviation of the scapular vertical axis from a line parallel to the vertical axis of the body. The third column shows the distance between the instantaneous rotation centre of the humeral head and its geometric centre. The final column shows the excursion of the humeral head on the glenoid in the superior/inferior plane between each 30° movement.

This study was limited to two-dimensions though the data in Table 4.11, the average data for the normal volunteers, is still of interest and of use for comparison with other results.

Poppen & Walker (1978), again carried out an investigation of 'isometric' abduction (or elevation) in the plane of the scapula. The term isometric means that each of the individual measurements was taken with the arm maintained in a constant position. The aim was to calculate the force vectors at the glenohumeral joint for the abduction movement, taking into account the muscles active at each phase of the motion.

The results from their previous paper, Poppen & Walker (1976) were combined with data concerning the lines of action of the muscles involved. This was obtained during a radiographic study of three male upper quarter cadaveric specimens. The lines of action of the muscles were displayed on the radiographs first by attaching elastic wires between their insertions and repeating the radiographs and later by implanting radiopaque elastic wires along the muscle centres prior to taking the radiographs.

A further group of data included were a set of electromyograph (EMG) results for the activity of the muscles involved at each angle studied. The method of calculating the muscle forces is not fully explained in the paper, but the assumption was made that "the relative force in a given muscle is proportional to its cross-sectional area times the integrated electromyographic signal". Information on the integrated EMG of the muscles is cited as coming from the work of Jones (1970), where 37 normal subjects were tested during isometric scapular plane abduction. The level of activity of each of the active muscles was indicated by a value on a scale from 0 to 4.

The results given from this work after combining and processing the data discussed above, are the averages over the three specimens of the compressive, shear and resultant forces at the glenohumeral joint for abduction in neutral rotation at six discrete positions ranging in 30° steps from 0° to 150°.

The maximum resultant force was found to rise to 0.89 times body weight at 90° of abduction, decreasing thereafter to 0.4 times body weight at 150° of elevation. For a subject of mass 75kg, these values would correspond to 655N and 294N respectively. The compressive force peaked at around 0.83 times body weight (610N) at 90°, the shearing force peaking at 0.42 times body

weight (309N) at 60°. The authors estimated a 60% increase in the force values if a hand load of 1kg was present.

On estimating the forces in rotation it was found that in external rotation they were around the same value as those obtained in neutral rotation. For abduction in internal rotation however, the forces were found to be higher, the resultant force at 90° being twice the value for external rotation. All force values are in the scapular plane, thus the quoted shearing force is in the superior/inferior direction.

Karlsson & Peterson (1992) again focused on elevation in the scapular plane in their discussion of a shoulder model which included all components attached to the humerus, nineteen muscular elements, one ligamentous element and the x, y and z components of the contact force between the scapula and humerus. The aim was to determine whether such a model could be used to predict all the internal musculoskeletal forces acting on the humerus under different conditions of loading.

An idealised mechanical model of the shoulder was used, where the bones of the shoulder were modelled as rigid bodies, the joints as ball joints and the muscles or muscle sections as stretched strings between attachment points. Normalised cross-sectional areas of the muscles were obtained by expressing the cross-sectional area of each muscle as a percentage of the total sum of the cross-sectional areas of the shoulder muscles.

Six force and moment equilibrium equations were formulated for the internal muscular and external gravitational forces, incorporating twenty-three unknown internal forces and therefore having no unique solution. This indeterminate problem was solved using an optimisation process for which the sum of the squared muscle stresses (internal muscle forces/ normalised muscle cross-sectional areas) was the objective function minimised. Having solved for the internal muscle forces it was possible to determine the joint contact forces.

In theory the above model could be used to assess the complete range of shoulder motion. In this paper however, only elevation in the scapular plane was modelled, between 0° and 120° in steps of 15° for a hand load set at 1kg. At each step a numerical solution was found for the force levels in each of the involved components. Anthropometric data for a young male of mass 75kg was

used as input to the model. The calculated contact force rose to a value of 650N (0.88 times body weight) at a level of 60° of abduction, before falling at higher elevations. A level of around 600N (0.82 times body weight) was found between 60° and 90° of elevation for the subject modelled.

Poppen and Walker (1978) estimated a 60% increase in their calculated force with a 1kg hand load. This would take their maximum resultant contact force to around 1.4 times body weight, some way above the value obtained by Karlsson & Peterson (1992). The latter paper is in closer agreement with the 0.92 times body weight of Inman et al (1944), though their investigation involved abduction in the coronal plane with no hand load. In comparison with these other papers the value of Karlsson & Peterson (1992) would appear relatively low.

The development of another three-dimensional shoulder model was described by van der Helm (1994). In this model each morphological structure was represented by an appropriate element, the mechanical behaviour of which was well defined. The clavicle and humerus for instance were modelled as rigid beam elements, the scapula by two tightly connected beam elements, with the joints modelled by three perpendicular hinge elements. Muscles were modelled by one to six active force-generating elements, representing muscle lines of action and connected between the muscle origin and insertion. Knowing the mechanical behaviour of these elements the behaviour of the whole system could be assessed by connecting them.

The model incorporated 16 muscles, three joints, three extracapsular ligaments and the kinematic constraint of the scapulothoracic gliding plane. The parameters for the model described the mass and rotational inertia of the upper limb, data on the physiological cross-section of the muscles and geometric parameters describing the positions of muscle and ligament attachment sites and bony landmarks, as well as joint rotation centres.

Cadaveric studies were used to find many of the geometric parameters required (details of these studies can be found in Van der Helm & Veenbaas (1991), Veeger et al (1991) and van der Helm et al (1992)). The position of the acromioclavicular joint and trigonum spinae (see Fig.2.1and Fig.2.5) at each of

the positions chosen were used as the input for the model, as were the mean humeral rotation angles.

Position and rotation information was obtained during a study described in van der Helm & Pronk (1995). This study involved the use of the "palpator" (as described in Pronk & van der Helm (1991)). This was a spatial digitiser made up of an open chain mechanism which consisted of four links and four hinge joints, with a rigidly fixed base. Rotations at the hinge joints were recorded using high precision potentiometers, the output of which could be used to determine the position of the end point of the final link. By touching the endpoint of the palpator to a palpated landmark and pressing a foot trigger, the three-dimensional co-ordinates of the landmark were calculated to an accuracy of 1.43mm standard deviation.

Humeral frontal plane abduction and sagittal plane flexion were measured, both unloaded and with a 0.75kg hand load, for 10 healthy male subjects. The mean age of these subjects was 23.1±1.9years, the mean height 181.7±3.7cm and the mean weight 71.3±3.9kg. The positions of eleven bony landmarks on the thorax (jugular notch, transition from gladiolus to xiphoid process, 7^{th} cervical vertebra, 8^{th} thoracic vertebra), clavicle (jugular notch, most dorsal point of the acromioclavicular joint), scapula (acromioclavicular joint, acromial angle, inferior angle, trigonum spinae) and humerus (lateral and medial epicondyle) were recorded at 30° intervals of elevation from 0° to 180°.

These experimental data were used by van der Helm (1994) in the modelling process. The model was used to produce information on the orientations of the clavicle and scapula and the muscle forces necessary to counterbalance the external load on the upper extremity. Resultant contact forces at the glenohumeral joint were calculated, outputs being expressed about the axes with their origin at the jugular notch (incisura jugularis), the X axis medial to lateral, Y axis inferior to superior and the Z axis ventral to dorsal. The highest values found were at 90° of elevation in all tests. The resulting glenohumeral contact forces at this elevation are shown in Table 4.12.

It can be seen that there is an increase of 56% in the resultant force between unloaded and loaded abduction, close to the increase predicted for a

slightly higher hand load by Poppen and Walker (1978). The force obtained for loaded abduction is close to that of Karlsson and Peterson (1992), though for a slightly different hand load.

	X component	Y component	Z component	Resultant
Unloaded abduction	344N	83N	-156N	387N
Loaded abduction	533N	144N	-239N	602N
Unloaded anteflexion	111N	33N	-328N	348N
Loaded anteflexion	118N	56N	-478N	496N

Table 4.12 Resultant glenohumeral contact forces at 90°. (N.B. Values are taken from graphical information and thus approximate). (van der Helm (1994)).

If the mean body weight of the subjects tested is taken, the resultant force values in Table 4.12 are equivalent to 0.55 times body weight and 0.86 times body weight for the unloaded and loaded abduction tests respectively. The latter value can be seen to agree with those previously documented.

The papers discussed to this point all suffer from the same limitation, being restricted to analysis of two dimensional motion and the associated kinematics. This simplifies the analysis of a three-dimensional situation. In order to obtain truly relevant data a study should be made in three dimensions.

Anglin et al (1996) carried out a study into three-dimensional movements, involving the assessment of five activities in order to gain a measure of the contact forces on the glenohumeral joint. The activities assessed were :

1. standing up from a chair using the arms
2. sitting down into a chair using the arms
3. walking with a cane
4. lifting a 5kg box from floor to shoulder height using both hands
5. lifting and carrying a 10kg suitcase

These activities were chosen as they were regarded to be similar to common daily activities which would lead to a high force at the shoulder joint. An infrared 'Optotrak' system was used in order to determine arm and trunk angles, markers being attached as previously described by Romilly et al

(1994). Forces were measured by means of a transducer on the chair arm during standing and sitting and a force platform during the walking test. The box lifting test included a force component due to gravity, the suitcase lift included a dynamic force component based on the accelerations of the hand.

The average age, body weight and height of the six subjects were 55years (51-64years), 73kg (52-89kg) and 168cm (152-187cm) respectively, evenly divided between males and females and none had a history of shoulder problems. The subjects were asked to repeat the tests five times and the contact forces obtained are shown, normalised to body weight, in Table 4.13. Included are the overall average force values, the overall range of all of the trials for each task and the average of the maximum values across each run of five trials for each of the tasks, as well as the maximum five-trial average force for each task from all the subjects.

	Standing	Sitting	Cane	Box	Suitcase
Average (all trials & subjects)	1.8	2.0	1.7	1.8	2.4
Range (all trials & subjects)	0.5 - 4.3	0.3 - 6.9	0.4 - 3.2	1.5- 2.3	1.3 - 4.3
Avg.Max. (across trials)	2.7	2.9	2.0	1.9	2.7
Max. Avg. (across subjects)	3.1	5.1	2.8	2.2	3.5

Table 4.13 Glenohumeral contact forces as a multiple of body weight (Anglin (1996)).

Another study of real-life activities is that of Runciman & Nicol (1994), who outlined the development of a biomechanical model of the glenohumeral joint. This model was developed in an attempt to investigate muscle and joint loading during three dimensional activities. The authors used muscle origin and insertion data from the work of Johnson (1990).

This information was combined with a dry bone study, as well as anthropometric and real time kinematic data for the trunk, clavicle scapula and forearm in the modelling process. The kinematic information was obtained using a six camera 50Hz Vicon system to trace markers of known placements on the body. A force platform and strain gauged transducer were also used to measure hand loading.

Several real life activities involving dynamic, three-dimensional movement were investigated. Results were quoted for a preliminary test of frontal plane abduction, carried out on a single male subject of age 25 years,

weight 65kg and height 1.75m. The net overall effect of the external forces and moments on the glenohumeral joint were calculated, this including the gravitational contribution knowing the relative size and positioning of the segments with respect to the glenohumeral joint centre. The contribution of any hand load could be similarly calculated. The maximum compressive force from the humeral head on the glenoid was predicted by the model to be approximately 1.2 times body weight at a frontal plane abduction of 80°. This is higher than results previously quoted, for instance Poppen & Walker (1978) who predicted the value to be 0.83 times body weight.

More detailed information on the tests carried out and the results obtained can be found in Runciman (1993). This thesis details the work on which the previous paper was based and gives the full description of the testing process. Five male subjects were tested carrying out a variety of activities, firstly abduction and flexion with a 2kg hand load to allow comparison with previous two-dimensional modelling and then some three dimensional exercises, push-ups, press-ups and chin-ups. The subjects were each required to carry out two sets of two repetitions of each exercise and from the information obtained using the Vicon system, the model was used to predict the joint forces. A summary of the relevant results is shown in Table 4.14.

Test	Range of compressive GH contact forces (× body weight)	Maximum compressive GH contact force (× body weight)	Maximum Anterior/Posterior shearing force (× body weight)	Maximum Superior shearing force (× body weight)
Abduction	0.9 - 1.8	> 1.2	0.5	0.3
Flexion	1.4 - 2.0	> 1.4	0.1	0.2
Push-up	3.0 - 7.5	> 5.0	1.0	1.0
Press-up	2.3 - 5.4	> 3.0	2.0	1.0
Chin-up	3.1 - 4.9	> 4.0	< 1.0	< 1.0

Table 4.14 Glenohumeral contact forces as a multiple of body weight. Results taken from Runciman (1993). In the above table both abduction and flexion tests were carried out with a hand load of 2kg. For the data in the third column the shearing force is always anterior except in the case of the chin-up test where it is posterior.

Runciman (1993) also used the data for the abduction tests to make an approximation for unloaded abduction in order to allow comparison with the earlier work of Poppen & Walker (1978). Based on the results, a maximum compressive joint force of approximately 0.7 - 0.8 times body weight was

calculated. This corresponds well with the two-dimensional model of Poppen and Walker (1978) and the three-dimensional models of Karlsson & Peterson (1992) and van der Helm (1994).

4.5 Summary of results

Tables 4.15 to 4.17 summarise comparable results from the studies discussed.

	Author	Dol'nikov	Safaee-rad	Romilly
Activity		degrees	degrees	degrees
Pouring	rotation arc	0	-	-45→ -16 (roll)
	flex/ext arc	0	-	32→85 (elev)
	abd/add arc	0	-	36→66 (az)
drinking	rotation arc	22	5.2→23.4	-62→ -21 (roll)
	flex/ext arc	10	15.8→43.2	32→63 (elev)
	abd/add arc	3	12.7→31.2	37→56 (az)
fork	rotation arc	-	5.1→18.1	-40→1 (roll)
	flex/ext arc	-	10.7→35.2	34→54 (elev)
	abd/add arc	-	7.1→18.6	32→49 (az)
spoon	rotation arc	25	4.8→16.8	-61→ -4 (roll)
	flex/ext arc	10	7.8→36.1	32→76 (elev)
	abd/add arc	5	6.6→21.8	34→54 (az)
telephone	rotation arc	-	-	-82→ -26 (roll)
	flex/ext arc	-	-	35-53 (elev)
	abd/add arc	-	-	36→71 (az)
combing	rotation arc	50	-	-85→ -13 (roll)
	flex/ext arc	41	-	31→77 (elev)
	abd/add arc	11	-	35→86 (az)
sit-stand	rotation arc	-	-	-
	flex/ext arc	-	-	-
	abd/add arc	-	-	-
door	rotation arc	-	-	-50→ -20 (roll)
	flex/ext arc	-	-	34→58 (elev)
	abd/add arc	-	-	39→72 (az)

Table 4.15 Comparison of shoulder motion for selected activities, in degrees. (N.B. Internal rotn. +ve, values from Romilly are in terms of azimuth, elevation and roll)

	Author	D'olnikov	Morrey	Packer	Romilly	Safaee-rad
Activity		degrees	degrees	degrees	degrees	degrees
Pouring	flexion arc	22	35.6→58.3	-	65→86	-
	forearm rotn	74	42.9→ -21.9	-	-49→36	-
drinking	flexion	71	44.8→130	-	68→136	71.5→129.2
	forearm rotn	21	13.4 → -10.1	-	-14→37	-31.2→ -3.4
fork	flexion	-	85.1→128.3	-	73→129	93.8→122.3
	forearm rotn	-	10.4 → -51.8	-	-37→50	-58.8→38.2
spoon	flexion	37	-	70→115	75→123	101.2→123.2
	forearm rotn	34	-	-	-24→57	-58.7→22.9
telephone	flexion	-	42.8→135.6	75→140	74→151	-
	forearm rotn	-	40.9→ -22.6	-	-26→48	-
combing	flexion	97	-	-	71→143	-
	forearm rotn	52	-	-	-52→47	-
sit-stand	flexion	-	20.3→94.5	15→110	-	-
	forearm rotn	-	33.8→9.5	-	-	-
door	flexion	-	24→57.4	-	58→78	-
	forearm rotn	-	35.4 → -23.4	-	-2→47	-

Table 4.16 Comparison of elbow motion for selected activities, in degrees. (N.B. Pronation +ve)

Author (year)	Plane	Force (×B.W.)	Angle	Hand Load
Inman (1944)	Frontal	0.92	90°	0
Poppen (1978)	Scapular	0.89	90°	0
		1.4 (†)	90°	1kg
Karlsson (1992)	Scapular	0.88	60°	1kg
Runciman (1993)	Frontal	>1.2	-	2kg
		0.7-0.8 (†)	-	0
van der Helm (1994)	Frontal	0.55	90°	0
		0.86	90°	0.75kg

Table 4.17 Maximum resultant glenohumeral joint contact forces as a multiple of body weight for abduction of the arm. († = estimated from previous result)

Pheasant (1986) also gave relevant data on the maximum ranges of joint movement as given in Table 4.18.

Wang et al (1998) found the range of a particular joint motion to be strongly dependent on the position of the limb. The range of humeral axial

rotation for seven male subjects aged between 23 and 34 years was studied. The average range was found to vary from 94° to 157° dependent on humeral position, the maximum occurring when the upper arm was in its natural vertically downward position, the minimum when it was near vertically upwards.

Movement	5^{th} %ile (degrees)	50^{th} %ile (degrees)	95^{th} %ile (degrees)	SD (degrees)
Shoulder flexion	168	188	208	12
Shoulder extension	38	61	84	14
Shoulder abduction *	106	134	162	17
Shoulder adduction	33	48	63	9
Shoulder Int.rotn.	61	97	133	22
Shoulder Ext.rotn.	13	34	55	13
Elbow flexion	126	142	159	10
Forearm pronation	37	77	117	24
Forearm supination	77	113	149	22
Wrist flexion	70	90	110	12
Wrist extension	78	99	120	13
Radial deviation	12	27	42	9
Ulnar deviation	35	47	59	7

Table 4.18 Ranges of upper limb joint motion. From the survey of Dempster (1955) re-analysed by Barter et al (1957). (Pheasant (1986)). N.B. * - increased to 180° through accessory movements of the scapula.

4.6 Possible activities for analysis

A variety of tasks have been assessed in previous upper limb studies and have been discussed in the preceding pages.

McWilliam (1970) carried out a study in which seventeen able-bodied males and females were requested to complete a questionnaire in which they indicated the activities they regarded as important in daily living. Many of the high scoring activities have been analysed in the studies discussed. These include eating, personal hygiene and the use of door handles and telephones.

Table 4.19 contains a summary of activities previously analysed, others deemed important during the study of McWilliam (1970) and some anatomical

locations in which the limb can be placed. This represents a pool of activities from which a selection might be made for analysis. To the right of some activities are a grading of their importance carried out by a member of staff at DePuy International, the sponsors of this work.

Activities previously studied		**Tasks from McWilliam (1970)**	
		getting in/ out of bed *	5
Feeding		dressing†	2
eating with hands		tucking/ adjusting clothes †	
eating with fork	4	using lavatory *	1
eating with spoon	2	walking with hand rail *	
cutting with knife *	3	spreading with knife *	
drinking from a glass/ mug	1	lifting pots/ pans	6
pouring from a jug/ kettle	5	shaving †	7
		towelling dry †	4
Personal Hygiene		using hairdryer	
brushing teeth †	4	writing *	3
brushing/ combing hair †	3	removing objects from pocket †	
washing face †	2	vacuuming *	
turning tap *	1	ironing *	
		using drawers / hangers *	
General		using a brush / mop *	
using a screwdriver/ hammer/ file*			
standing/ sitting from/ into chair *	1	**Relevant anatomical locations**	
opening/ closing door *	4	abduction	
lifting a box		flexion	
lifting a suitcase		hand behind back	
using a telephone	3	hand in opposite axilla	
reading a newspaper †	8	reach to shoe	
using walking stick *	6	reach to opposite hip	
driving *	7	reach to chest	
turning doorknob/ lever *	4	reach to neck	
pressing switch/ button *	2	hand behind head, elbow forward	
push-up *		hand behind head, elbow back	
press-up *		hand on top of head, elbow forward	
chin-up *		hand on top of head, elbow back	

Table 4.19 A summary of activities, * = activities requiring extra instrumented apparatus, † = activities requiring force application other than lifting. Grading: 1 = most important. (N.B. Of the reaching activities, abduction, flexion and reaching to shoe, waist, chest neck, top of head and behind head have been analysed previously)

CHAPTER 5 : THEORETICAL ASPECTS OF MOTION ANALYSIS

5.0 Introduction

In order to analyse the motion of the upper limb by modelling its segments as rigid bodies and affixing markers at relevant landmark points, it was necessary to apply numerous theoretical elements between the stages of filming tests and obtaining joint angle, force and moment data.

The following pages provide an introduction to the relevant theory and available alternatives involved in the analysis process. This serves as background for the complete discussion of methodology in Chapter 6.

The various topics are introduced in the chronological order in which they feature during the analysis process.

5.1 Camera calibration

In order that information on the three-dimensional position of markers can be obtained, it is necessary to employ an algorithm to transform the digitised two-dimensional video image data. The Direct Linear Transformation (DLT) introduced by Abdel-Aziz & Karara (1971) is the algorithm favoured in the Ariel Performance Analysis System (APAS) and used in the current study.

Prior to the introduction of the DLT, the analysis of photogrammetric data was carried out on "comparators", through projection of the image onto a grid of known dimensions for instance. Two steps were required to transform firstly from projected co-ordinates to image data and then to object space co-ordinates. This involved filming of known fixed landmarks throughout testing and initial approximations of internal camera parameters and their locations.

The DLT improved the efficiency of the process, transforming between projected and object space in one step by determining the relative location of the camera film plane and the orientation of the camera. This information is combined with two-dimensional co-ordinate data from each camera image to derive the three-dimensional co-ordinates of the target markers.

An initial requirement of the DLT is the filming by a minimum of two cameras of non coplanar control points with known 3D co-ordinates in the

measurement space. Such control points are usually attached to some sort of rigid calibration frame. The control points are removed prior to filming the motion analysis study in the same test space. It is critical that camera positioning and lens settings are unchanged after calibration.

The two-dimensional images of the calibration frame and subject are then digitised prior to calculating the three-dimensional co-ordinates of the target markers. It is assumed for the DLT that the co-ordinates of a marker image in any two-dimensional camera image plane are a linear function of the co-ordinates of the marker in the three-dimensional object space. These co-ordinates are found by solving Equations 5.1 and 5.2 which contain a total of eleven unknown coefficients, a_{kj}, which for each camera *j* are proportional to an amplification factor of the camera and define the linear transformation between object space and image planes.

For *m* markers the method provides a relationship between the two-dimensional co-ordinates of a marker *i* (*i=1,...,m*) on the film and its three-dimensional location in space. For *n* cameras the relationship between the co-ordinates of the markers on the film of the camera *j* (*j=1,...,n*) and the spatial three-dimensional co-ordinates of this marker are determined by :

$$x_{ij} = \frac{a_{1j}x_i + a_{2j}y_i + a_{3j}z_i + a_{4j}}{a_{9j}x_i + a_{10j}y_i + a_{11j}z_i + 1} \qquad (5.1)$$

$$y_{ij} = \frac{a_{5j}x_i + a_{6j}y_i + a_{7j}z_i + a_{8j}}{a_{9j}x_i + a_{10j}y_i + a_{11j}z_i + 1} \qquad (5.2)$$

Where for marker *i* :

x_{ij} = x co-ordinate of marker *i* on the film measured with camera *j*

y_{ij} = y co-ordinate of marker *i* on the film measured with camera *j*

x_i = x co-ordinate of marker *i* in the three-dimensional space

y_i = y co-ordinate of marker *i* in the three-dimensional space

z_i = z co-ordinate of marker *i* in the three-dimensional space

a_{kj} = coefficient k in the transformation formulas for marker *i*

The calibration process establishes the unknown coefficients a_{kj}, provided the calibration frame includes a minimum of six well distributed and defined reference points. Each calibration marker yields two equations, six markers thus provide an overdetermination of the unknowns for each camera, allowing a least-squares solution to be found. A summary of the DLT method of Abdel-Aziz & Karara (1971) can be found in Nigg & Herzog (1995).

Several studies have investigated the accuracy when using the DLT including those of Wood & Marshall (1986), Challis & Kerwin (1992), Chen et al (1994) and Hinrichs & McLean (1995). In order to achieve the best results it was found that calibration points should be distributed throughout the test volume. Accuracy was greatest when the activity under analysis was performed within the calibrated volume, but decreased as points further outside the calibrated volume were analysed.

The advantages of the DLT are its relative simplicity and the flexibility it allows in camera arrangement. It does not require initial knowledge of the location or orientation of the cameras, the distance between cameras and subject, or any information about the camera or projection lenses such as focal length and magnification. By directly determining the relationship between the image space and each of the digitised views, all the intervening image changes are eliminated and need not be considered.

The DLT is the most commonly used algorithm in motion analysis systems based on the reconstruction of three-dimensional co-ordinates from two-dimensional images. Modified versions have been proposed by several authors including Gazzani (1992), (1993), Hatze (1988) and Yu et al (1993).

Hinrichs & McLean (1995) discuss an alternative to the DLT, the Non-linear Transformation (NLT) proposed by Dapena et al (1982) with a later correction by Dapena (1985). Multiple frames of data were collected while two markers attached to a bar were moved around the test space. Static points were used to define the location and orientation of the co-ordinate system allowing the 'building' of any size control object desired. The NLT has advantages of flexibility of calibration volume and portability of necessary apparatus, though determination of camera internal parameters by a separate

procedure is required. Some systems, such as the most recent 'Vicon 512' system have adopted derivations of the NLT as their default calibration method.

Tsai (1986) also developed a two step calibration method, claimed to deal with lens distortion more efficiently than the DLT and to be more accurate outwith the calibration volume, a method recently adapted by Schmid (1998). *Cerveri et al (1998) outlined a further adaptation, a one step process whereby* all internal and external camera parameters were determined by surveying a moving calibration object similar to that used for the NLT.

5.2 Position and orientation descriptors

Having obtained the three-dimensional marker co-ordinates, the next stage was to use these co-ordinates to determine the position in space and orientation of the segments to which they were attached. In order to achieve this it was necessary to define the orthogonal segment embedded and global co-odinate frames previously mentioned. By determining the relationships between these frames, the segment positions and orientations could be found.

The 3D kinematic relationship between frames is completely described by a position vector and a rotation or direction cosines matrix relating the two frames. These will be discussed in the following pages using the notation of Craig (1989) as follows :

- variables written in uppercase represent vectors or matrices
- variables written in lowercase represent scalars
- Leading subscripts and superscripts identify which co-ordinate system a quantity is written in. For example, ${}^{A}P$ represents a position vector written in co-ordinate system *{A}*, and ${}^{A}_{B}R$ is a rotation matrix that specifies the relationship between co-ordinate systems *{A}* and *{B}*
- Trailing superscripts indicate the inverse or transpose of a matrix. For example, R^{-1}, R^{T}

5.2.1 The Position Vector for describing displacements

Having defined co-ordinate frames, the position of the origin of one frame may be specified in relation to another by means of a position vector as shown in Fig. 5.1. Following the prescribed convention the three component column vector shown is identified as ${}^{A}P$.

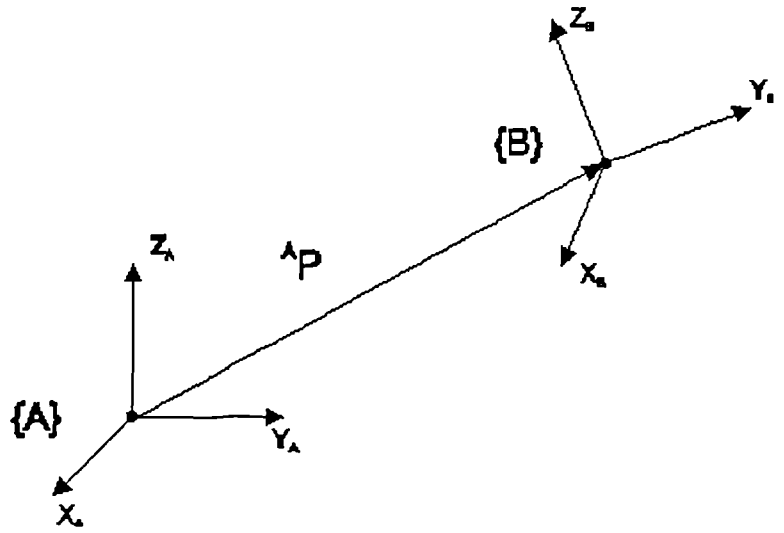

Fig 5.1 Position vector ${}^{A}P$, the origin of {B} in relation to co-ordinate system {A}

The components of the 3×1 column vector define the co-ordinates of the origin of *{B}* in the frame of *{A}* and can be denoted:

$$ {}^{A}P = \begin{bmatrix} p_x \\ p_y \\ p_z \end{bmatrix} \qquad (5.3) $$

5.2.2 The Rotation Matrix for describing orientations

The position vector locates a single point in frame {B}, though this frame could be in an infinite number of orientations. In order to describe all six degrees of freedom of the frame, the position vector must be used in tandem with a rotation matrix which describes the orientation of one frame with respect to the other.

The scalar product of two unit vectors yields the cosine of the angle between them. The rotation matrix consists of these direction cosines between

each of the axes of frame {B} and the axes of frame {A}. The nine direction cosines are combined in a 3x3 rotation matrix.

In order to determine the direction cosines a unit vector in the direction of any of the axes can be considered, unit vector $\hat{X}_B$ along the *X* axis of co-ordinate frame *{B}* in Fig 5.2 for instance.

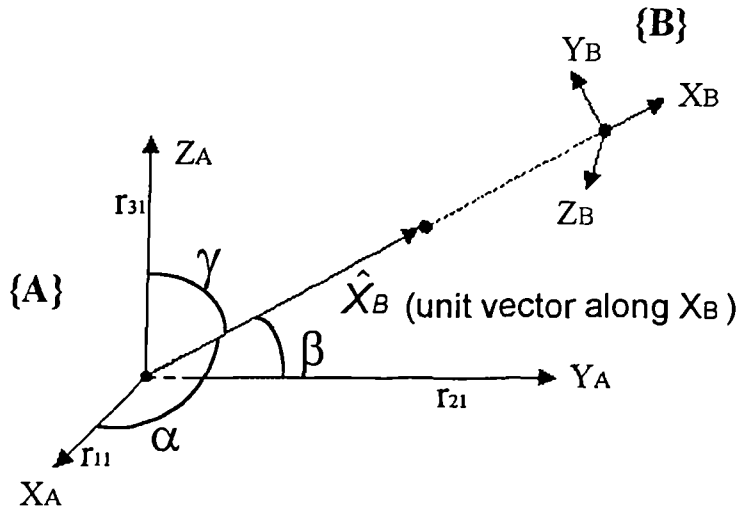

Fig 5.2 Direction cosines of a unit vector

The cosines of the angles α, β and γ are the direction cosines of vector $\hat{X}_B$, relative to the co-ordinate system *{A}*. An alternative representation uses the scalar displacements where $cos(\alpha)=r_{11}$, $cos(\beta)=r_{21}$ and $cos(\gamma)=r_{31}$. Hence the *X* axis of *{B}* relative to the co-ordinate system of *{A}* is described by equation 5.4.

$$ {}^{A}\hat{X}_B = \begin{bmatrix} \cos(\alpha) \\ \cos(\beta) \\ \cos(\gamma) \end{bmatrix} = \begin{bmatrix} r_{11} \\ r_{21} \\ r_{31} \end{bmatrix} \qquad (5.4) $$

The same process can be carried out for the *Y* and *Z* axes of *{B}*. Combining all three yields Equation 5.5, the rotation matrix describing the orientation of *{B}* relative to *{A}*, ${}^{A}_{B}R$.

$$ {}^{A}_{B}R = \begin{bmatrix} {}^{A}\hat{X}_B & {}^{A}\hat{Y}_B & {}^{A}\hat{Z}_B \end{bmatrix} = \begin{bmatrix} r_{11} & r_{12} & r_{13} \\ r_{21} & r_{22} & r_{23} \\ r_{31} & r_{32} & r_{33} \end{bmatrix} \qquad (5.5) $$

The position and orientation of *{A}* or *{B}* may be described relative to any known co-ordinate system. The rotation matrix which describes the orientation of *{A}* relative to *{B}*, ${}^{B}_{A}R$ is the transpose of ${}^{A}_{B}R$ as given in Equation 5.6.

$$ {}^{B}_{A}R = {}^{A}_{B}R^{T} \qquad (5.6) $$

Similarly, the position of the origin of *{A}* in the frame of *{B}*, the vector ${}^{B}P$, may be defined as in Equation 5.7.

$$ {}^{B}P = -{}^{A}_{B}R^{T} \cdot {}^{A}P \qquad (5.7) $$

5.2.3 The homogeneous transform combining position and orientation

The position vector and orientation matrix descriptions of one frame in relation to another can be combined in one 4×4 matrix known as a homogeneous transform. The first 3x3 elements of this matrix are the rotation matrix, followed by the 3x1 position vector as given in equation 5.8.

$$ {}^{A}_{B}T = \left[\begin{array}{ccc:c} & {}^{A}_{B}R & & {}^{A}P \\ \hdashline 0 & 0 & 0 & 1 \end{array}\right] = \begin{bmatrix} r_{11} & r_{12} & r_{13} & p_x \\ r_{21} & r_{22} & r_{23} & p_y \\ r_{31} & r_{32} & r_{33} & p_z \\ 0 & 0 & 0 & 1 \end{bmatrix} \qquad (5.8) $$

This matrix can be used to describe a general transformation mapping of a vector or point from its description in one frame to a description in another frame. It can also be utilised, as in the current study, to describe one frame in relation to another and was used extensively in the MATLAB analysis routines described in Chapter 6.

5.2.4 The orientation vector

The columns of a 3×3 rotation matrix are mutually orthogonal and have unit magnitude and the determinant of such matrices is always +1. These facts

allow the application of Cayley's formula (Equation 5.9), which gives that for any such matrix *R*, there exists a skew symmetric-matrix *S*, such that

$$R = (I_3 - S)^{-1} (I_3 + S) \qquad (5.9)$$

Where I_3 is the 3×3 unit matrix.

A skew-symmetric matrix of dimension three such as *S* is specified by just three independent parameters, with the result that it is possible to specify any 3×3 rotation matrix with three parameters.

It is advantageous to reduce the orientation matrix into some more compact form described in terms of just three elements. Various parametrisations exist that enable this, one of the most commonly used being the Euler angles described later in Section 5.4.1. Such a description of an orientation, defined using three elements as opposed to the nine of the original orientation matrix is known as an orientation vector.

5.3 Calculation of transformations

The co-ordinates for a set of points associated with each segment were measured at some initial time and at some later time after motion had occurred. The segments were regarded as rigid bodies and therefore the final positions were related to the initial positions by some rotation and translation.

The aim of the motion analysis was to establish the rotation and translation from marker co-ordinate data, allowing the segment motion to be found. Various options were available to find the transformation matrices that describe the relationships between the segments in each sampled instant.

The assumption could have been made that the experimental co-ordinate data for each segment's three surface skin-fixed markers was noise-free. The technical axes would then be defined directly from this data. There will always be some relative motion between the markers however, the measured marker trajectories being perturbed in comparison to the displacement of the underlying bony landmarks and causing the rigid body assumption to be inaccurate. Cappozzo et al (1993) found markers over bony

landmarks to move by as much as two centimetres in relation to the underlying bone in their lower limb videofluoroscopic study.

An alternative is to employ some optimisation process in order to correct for the noise introduced by inter-marker movement and make the positional data from individual markers conform to the rigid body assumption. Such optimisations generally involve the estimation of the transformation matrix which optimally maps the configuration of a cluster of an arbitrary number of markers (equal to or greater than three) in an initial static calibration data set, to the analogous noisy configuration of the cluster in the laboratory frame at each sampled instant during motion. This can be achieved by finding the values of R (a 3×3 orthogonal rotation matrix) and P (a 3×1 3D translation vector) which minimise the discrepancy between the true final landmark location and the transforms of the initial locations in a least squares sense, as shown in Equation 5.10. The notation '||' indicates the *frobenius norm* of the resultant matrix, which involves the sum being computed over all the elements of the matrix.

$$\Sigma^2 = \Sigma||\text{final positions} - (R\times(\text{initial positions}) + P)||^2 \qquad (5.10)$$

Knowing the rotation matrix and translation vector allows the construction of a transformation matrix. After finding the best estimate of the transformation that maps the locations of the landmarks from their initial to their final position, the technical frames would then be defined from the optimised marker cluster co-ordinates.

Spoor & Veldpaus (1980) introduced a least-squares algorithm for obtaining translation and rotation matrices from the spatial co-ordinates of markers. The use of the helical axis method for the characterisation of body movements, discussed later, was also described. Veldpaus, Woltring & Dortmans (1988) refined the algorithm of Spoor & Veldpaus (1980), their unweighted least squares method avoiding some of the disadvantages of the original algorithm.

Söderkvist and Wedin (1993) also describe a least-squares method for determining the motion of a rigid body from landmark positions based on that of

Spoor & Veldpaus (1980). It was concluded to be superior to the earlier method as it was more stable and hence superior for ill-conditioned problems.

Their method involved computing the solution to the minimisation process using quantities that derive from the singular value decomposition (SVD) of a matrix related to the rotation matrix. The SVD is a technique for the orthogonal decomposition of a single matrix into three, and is discussed in numerous textbooks, including those of Lawson & Hanson (1974) and Golub & Van Loan (1991), the theorem for this process being :

> If A is a real $m \times n$ matrix, then there exists an $m \times m$ orthogonal (unitary) matrix $U=[u_1, \ldots, u_m] \in R^{m \times m}$ and an $n \times n$ orthogonal (unitary) matrix $V=[v_1, \ldots, v_n] \in R^{n \cdot n}$, such that $A= USV^T$. Where S is an m by n orthogonal matrix ($diag(\sigma_1, \ldots, \sigma_{min(m,n)}) \in R^{m \times n}$) with real diagonal elements, σ_i, such that $\sigma_1 \geq \sigma_2 \geq \ldots \sigma_{min(m,n)} \geq 0$ (i.e. decreasing non-negative diagonal elements). The σ_i are the *singular values* of A and the first (m,n) columns of U and V are the left and right singular vectors of A.

The relationship can be written as $A= USV^T$ or alternatively $U^TAV=S$.

Derivations for this method have been described in Hanson & Norris (1981), Arun et al (1987) and also in the more recent work of Challis (1995). Söderkvist & Wedin (1993) discuss this method and give a step by step algorithm for carrying it out, an algorithm similarly described by Challis (1995).

Chèze et al (1995) also described a procedure to numerically solidify an attached marker configuration. The three markers on each segment were selected which came closest to representing the corners of a rigid triangle over the range of movement. A best-fit solid triangular shape was defined from these markers over the range of images, after removing those in which the shape was most deformed. The least squares minimisation of Söderkvist & Wedin (1993) was then used to fit the best-fit solid triangle to the measured markers at each point in the motion.

5.4 Angular parametrisations

Having calculated the rotation matrices the next stage in the analysis process was to obtain some visualisation of their meaning, for instance as a sequence of three rotations about defined axes as discussed in Section 5.2.4.

5.4.1 Euler angles

Probably the most commonly utilised method for describing biomechanical orientations are the Euler angles, which may be defined relative to any axis sequence as long as at least two axes are used. For the purposes of introducing the relevant theory a three axis *Z, Y', X"* sequence will be discussed, as given in Fig. 5.3.

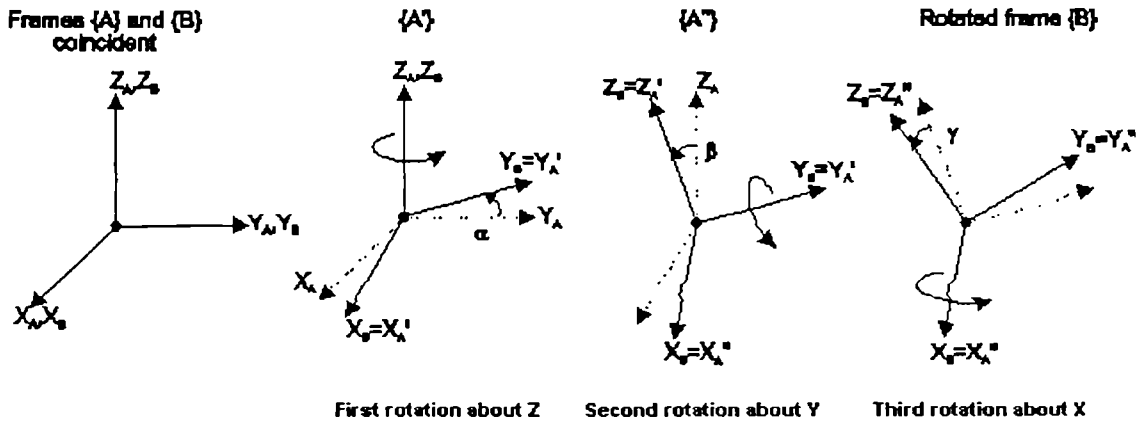

Fig 5.3 Definition of the *Z, Y', X"* Euler sequence.

The Euler angle rotations between frames *{A}* and *{B}*, initially coincident, are firstly a rotation of {B} about the Z_B axis by an angle α, followed by a rotation about the displaced Y_B axis by an angle β and finally about the twice displaced X_B axis by an angle γ. The orientation of the fixed axis system being rotated is altered each time a rotation is carried out, the frame lying in two intermediate positions before reaching its final orientation.

Each rotation occurs not about the axes of the fixed frame *{A}*, but about those of the moving frame *{B}*. Each of the intermediate frames *{A'}* and *{A"}* are therefore dependent on the preceding rotations. The second rotation β occurs about the axis Y_B, the position of which depends upon the first rotation

α. Similarly, the position of the final axis of rotation X_B is dependent on both of the previous rotations α and β.

Such three dimensional rotations are sequence dependent. The given sequence of rotations about the *Z*, *Y*, and *X* axes does not result in the same final position of frame *{B}* as would the same rotations about the sequence *X*, *Y*, *Z*. The non-commutative nature of rotations is unsurprising given their derivation from rotation matrices, the multiplication of which are non-commutative.

In order to apply the Euler angle notation, it is necessary to decompose the calculated rotation matrices in terms of a selected Euler angle sequence, achieved in the following manner.

Again referring to Fig. 5.3, a rotation matrix ${}^A_BR$ can be constructed relating frames *{A} and {B}*. This matrix can be broken down as a multiplication of three component matrices representing each of the individual rotations, ${}^A_BR={}^A_BR_{Z,Y',X''}(\alpha,\beta,\gamma)$. Expanding to provide a rotation matrix comprised of the three constituent rotations, α *about the Z axis,* β *about the Y' axis and* γ *about* the *X''* axis gives Equation 5.11.

$$ {}^A_BR_{Z,Y',X''}(\alpha,\beta,\gamma) = R_Z(\alpha)\cdot R_{Y'}(\beta)\cdot R_{X''}(\gamma) \qquad (5.11) $$

Multiplying the matrices gives Equation 5.12.

$$ \begin{aligned} {}^A_BR_{Z,Y',X''}(\alpha,\beta,\gamma) &= \begin{bmatrix} \cos\alpha & -\sin\alpha & 0 \\ \sin\alpha & \cos\alpha & 0 \\ 0 & 0 & 1 \end{bmatrix} \cdot \begin{bmatrix} \cos\beta & 0 & \sin\beta \\ 0 & 1 & 0 \\ -\sin\beta & 0 & \cos\beta \end{bmatrix} \cdot \begin{bmatrix} 1 & 0 & 0 \\ 0 & \cos\gamma & -\sin\gamma \\ 0 & \sin\gamma & \cos\gamma \end{bmatrix} \\ &= \begin{bmatrix} \cos\alpha\cdot\cos\beta & \cos\alpha\cdot\sin\beta\cdot\sin\gamma-\sin\alpha\cdot\cos\gamma & \cos\alpha\cdot\sin\beta\cdot\cos\gamma-\sin\alpha\cdot\sin\gamma \\ \sin\alpha\cdot\cos\beta & \sin\alpha\cdot\sin\beta\cdot\sin\gamma+\cos\alpha\cdot\cos\gamma & \sin\alpha\cdot\sin\beta\cdot\cos\gamma-\cos\alpha\cdot\sin\gamma \\ -\sin\beta & \cos\beta\cdot\sin\gamma & \cos\beta\cdot\cos\gamma \end{bmatrix} \end{aligned} \qquad (5.12) $$

The matrix given in Equation 5.12 may be equated with the general form of the rotation matrix as given in Equation 5.5. This allows the *Z*, *Y'* and *X''* axis rotations to be obtained by solving Equation 5.12 for α, β, and γ giving;

$$\beta = A\tan 2\left(-r_{31}, \sqrt{r_{11}^2 + r_{21}^2}\right) \qquad (5.13)$$

$$\alpha = A\tan 2\left(\frac{r_{21}}{\cos\beta}, \frac{r_{11}}{\cos\beta}\right) \qquad (5.14)$$

$$\gamma = A\tan 2\left(\frac{r_{32}}{\cos\beta}, \frac{r_{33}}{\cos\beta}\right) \qquad (5.15)$$

Twelve possible Euler angle sequences for rotations around the co-ordinate axes are available. The six classic Euler two axis systems describe sequences in which the first rotation occurs about an initial axis, the second about a displaced intermediate axis and the third about the twice displaced first axis, i.e. Z, Y', Z''. The second subset of the Euler angles are the six three axis systems in which the rotations occur about all three axes i.e. Z, Y', X''. These have been termed the Cardan or Bryant angles (Woltring (1991)).

For the purpose of motion analysis, the aim would be to calculate the Euler angles between two adjacent segments. A 'zero' position would be defined in which the embedded co-ordinate frames were parallel. The Euler angles representing rotations at the joint about perpendicular axes would then be calculated in relation to this zero position.

When using such systems the occurrence of 'gimbal lock' is a problem, where a rotation of 90° about the second axis in either direction causes singularity to occur, two axes becoming parallel and the matrix solutions becoming unobtainable.

Also in each non-singular case there are two possible angular solutions, giving rise to the phenomenon of "Codman's Paradox" in anatomy (Codman (1934)), where different combinations of numerical values of the three angles produce similar physical orientations of the segment. This is not actually a paradox, but a consequence of the non-commutative nature of three-dimensional rotations and can be mathematically explained through the properties of rotation matrices (Politti et al (1998)).

5.4.2 Joint Co-ordinate System (JCS)

One perceived limitation of the Euler or Cardan rotations is that they occur about axes fixed in each segment. Such systems are not regarded as clinically representative, as flexion is thought to occur about an axis in the proximal segment and rotation about an axis in the distal segment.

Suntay et al (1978) and Grood & Suntay (1983) presented an alternative representation, a derivation of a three axis Euler system, the Joint Co-ordinate System (JCS). Their method involved the definition of bone embedded co-ordinate frames in the proximal and distal segments at the knee.

One body fixed axis from each of the three available in the proximal and distal segment systems and a third 'floating' axis, the common perpendicular to the first two, were used to construct a third co-ordinate system describing the joint orientation. The floating axis was fixed in neither body segment and moved in relation to both. A representation of this system is shown in Fig. 5.4.

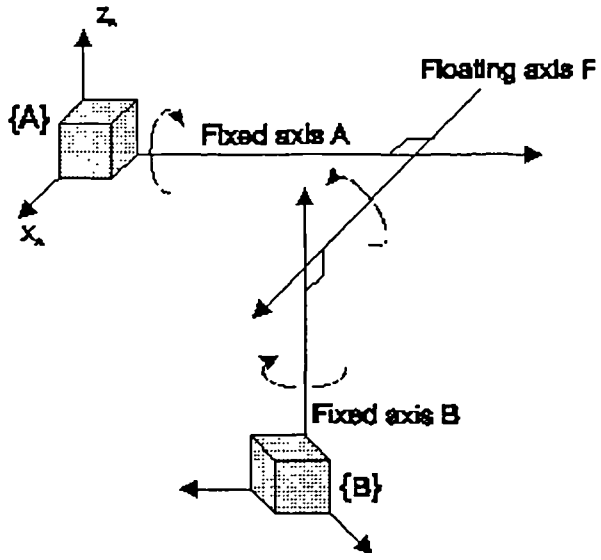

Fig 5.4 The Joint Co-ordinate System of Grood & Suntay (1983).

Using such a method overcomes the problem of temporal sequence dependence inherent in the standard Euler angle definitions, as the three axes about which rotations occur are independent. A sequence effect is imposed however, though this sequence is established prior to analysis on selection of axes or the choice of axis geometry. The axes can be selected so the angles correspond to clinical descriptions of joint motion.

Again, gimbal lock can be a problem when the second rotation reaches ±90°, though this can be made to occur about an axis where little rotation occurs.

5.4.3 The "global" angles - azimuth, elevation and roll

An et al (1991) discussed an alternative description of motion in which the glenohumeral centre was viewed as the centre of an imaginary sphere described by the distal end of the humerus and with a radius equal to its length.

The position of the elbow may be described on this sphere in terms of an angle of azimuth about a vertical axis which defines the plane of elevation, an elevation about an axis perpendicular to the first and finally an axial rotation or roll of the humerus about its longitudinal axis.

This description, incorporating the angles of azimuth and elevation are often termed the 'global' angles, due to their similarity to the terms of longitude and latitude used to describe position on a globe.

Angles of azimuth specify circumferential lines of longitude, while angles of elevation specify circumferential lines of latitude, the centres of which all lie on the polar axis of the globe, as shown in Fig 5.5.

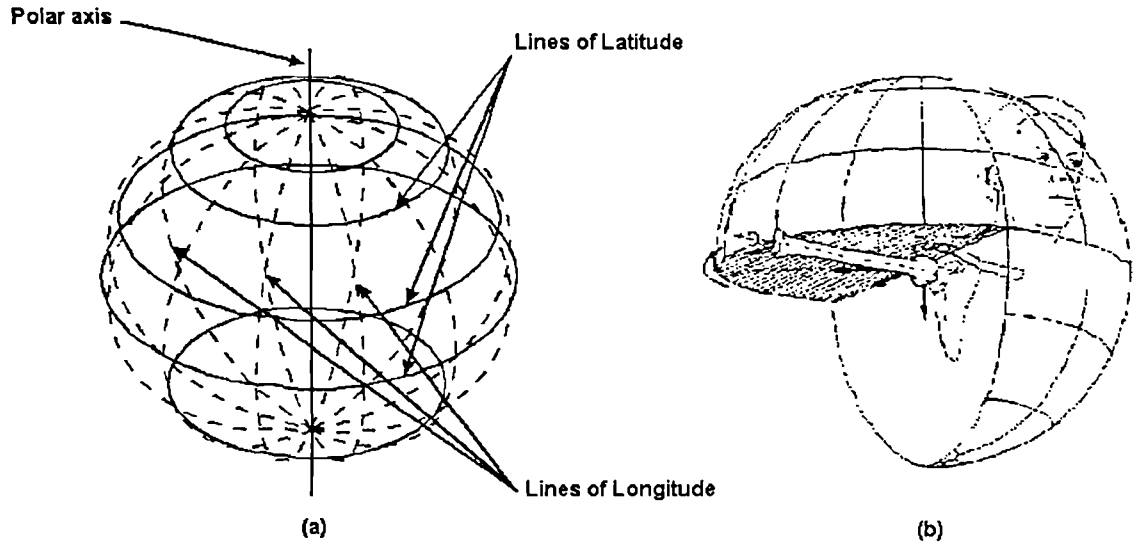

Fig 5.5 (a) Lines of longitude and latitude and (b) their similarity to the spherical representation of shoulder rotations from An et al. (1991)

Selecting appropriate axes makes the computation of the global angles identical to the *Z*, *Y'*, *X''* Euler system discussed in Section 5.4.1. This is

achieved by selecting the *Z* axis as the vertical polar or azimuthal axis, the Y' axis as the horizontal elevation axis and the X'' axis as the humeral rotation or roll axis.

Various papers on upper limb task analysis have used variations of this system (Buckley, 1996) including those of Kapandji (1982) (first published in 1970), Benati (1980) and Engin & Chen (1986), Davis (1998) and Barnett (1999). Pearl et al (1992) discussed a similar method and found that most activities of daily living occurred in an anterior plane of elevation as opposed to the sagittal and coronal planes. Crawford et al (1999) also used a similar description for spinal motion.

Global angles allow a more visual representation and comprehension of humeral motion than the Euler angles and allow an unambiguous description of elevation in any plane. Problems of gimbal lock exist for this method however, due to a singularity at the poles where the axes of azimuth and roll are coincident. In this position any amount of azimuth may be measured, but compensated for by the roll component, making it impossible to accurately determine these angles.

5.4.4 Projected angles

A further alternative for description of orientation is the projection of the axes of the local embedded frames onto the planes of a reference co-ordinate system. The differences in the projections of the axes can be interpreted as the joint angle between proximal and distal segments.

Using this system, pure flexion of the humerus would be measured as the projection of the humeral longitudinal axis on the sagittal plane. Abduction would be the projection of this axis on the frontal plane. The relevant angle would then be calculated from the components of the vector in the plane representing the longitudinal axis.

Braune & Fischer (1889) represented the upper arm orientation by the projection of line connecting the elbow and shoulder centres onto specified planes. More recently a similar technique was used by Cheng (1996).

Cheng & Pearcy (1999) found this method to cause overestimation and misinterpretation of 3D joint flexion and adduction rotations, due to the

influence of longitudinal axis motion out of the planes of projection and the interdependence of these angles. An alternative method was suggested whereby flexion/ extension was represented as an angle between the longitudinal axis of a segment and its projection on the frontal plane. Abduction/ adduction was then represented as an angle between the longitudinal segment axis and its projection on the sagittal plane. These definitions allowed the independent description of flexion at any abduction and vice versa. Using such a method, rotation about the longitudinal axis would be calculated by a separate process.

5.4.5 Helical axis motion descriptors

The descriptors of orientation discussed so far require additional information on the translational components of motion involved in order to provide a complete description of the position of an embedded frame in three dimensional space. There are however some methods that allow a complete kinematic description.

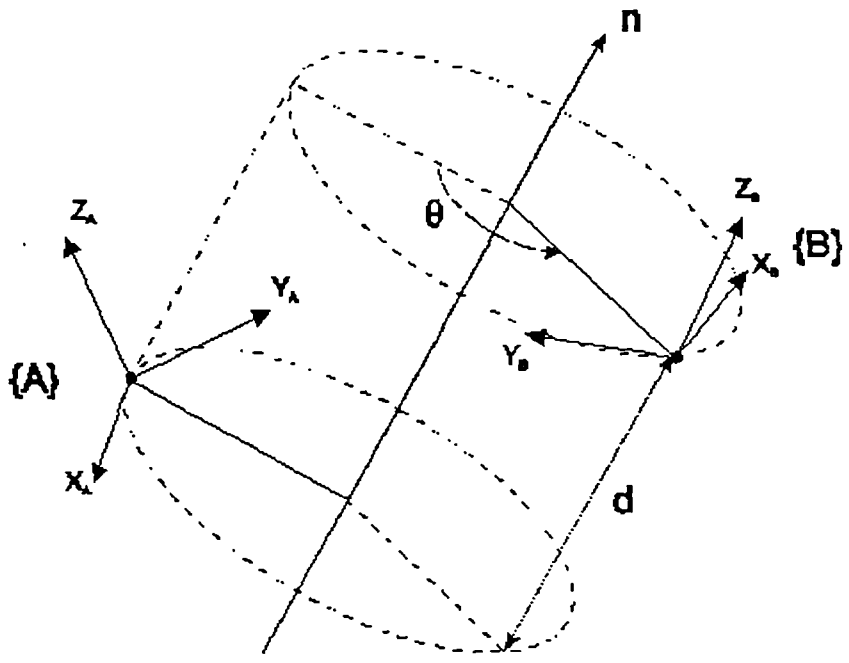

Fig 5.6 Illustration of the finite helical axis.

One such option is the 'equivalent screw displacement axis' (ESDA) or 'finite helical axis' (FHA). Chasles' Theorem as given in Woltring et al (1994), states that the current position and attitude of a rigid body can be described as

if attained from the reference pose by a single displacement about and along a directed line in space. A mathematical interpretation of this, using vector algebra, was presented by Bisshopp (1969). Fig. 5.6 illustrates this theorem.

Knowing the start and end points it is possible to completely describe all six degrees of freedom of the motion of the body between *{A}* and *{B}*. This is achieved by determining the position and direction of the axis with unit direction vector n, together with the displacement d along it and the rotation θ about it.

Woltring et al (1985) found that the determination of the position and the direction of the axis was very sensitive to errors in landmark measurement. Stochastic errors frequently occurred, having magnitude inversely proportional to the finite rotation magnitude between the two frames. Veldpaus et al (1988) made similar conclusions.

Chèze et al (1998) also found that the errors involved were inversely proportional to the rotation magnitude and hence unsuited to calculation over successive samples. They advised modelling joint kinematics using successive rotations about a three axis system, such as the JCS of Grood & Suntay (1983).

Woltring et al (1994) introduced the use of the "Instantaneous Helical Axis" (IHA), the mean axis of rotation about and along which a segment can be considered to be instantaneously moving with respect to another segment. The advantage of the use of the IHA as opposed to the FHA is that the latter fails to convey any detail of the movement during its occurrence, merely relating the initial and final positions. The FHA is calculated between successive positions of two adjacent body segments without regard to route or trajectory between these points. A series of IHAs can be calculated and displayed for continuous motion. A further development discussed by Woltring (1991) and Woltring et al (1994) allows the output of 'helical angles' where the helical axis vector n is decomposed along the axes of a global or segment embedded cartesian system.

This technique can be applied to give a functional representation of the relative motion between two segments and is considered by some to be more mathematically rigorous than the Euler-based techniques, though is highly sensitive to measurement error and magnitude of rotation. A disadvantage of

the helical axis descriptions is that they are not necessarily related to the mechanical structure of the joint itself. Their general lack of a physical interpretation calls into question their use in the clinical environment, Euler angles being more intuitive.

The papers of Ramakrishnan & Kadaba (1991) and Woltring (1991) provide sources of information on the Euler and helical motion models, the latter discussing several descriptors of segment position and orientation.

5.5 Velocity and acceleration calculations

In order to determine the dynamics of the upper limb segment motion it was necessary to calculate linear and angular velocities and accelerations from the joint angle data.

Numerical differentiation methods can be employed to determine approximate values of linear velocity and acceleration from displacement data and are frequently used in motion analysis studies. Several formulas for performing numerical differentiation exist and the topic is discussed in various texts, including those of Lanczos (1967), Hildebrand (1974), Kreysig (1983), Yakowitz (1989), Gerald & Wheatley (1989) and Winter (1990).

Numerical differentiation is an unstable process, approximate values of derivatives will be less accurate than the data from which they are derived. Small errors made during the process cause greatly magnified errors in the final result, any noise in the original data is raised by a power of two on each differentiation. Truncation errors also affect the accuracy of the technique. These are due to the reduction of a calculation that might require an infinitely long series, to a series of limited length. Rounding errors are also a problem, due to imprecision in representing numbers in a computer where the final digit after the decimal point is either rounded off or removed.

The most accurate numerical approximations are obtained by differentiating suitable Lagrange interpolation formulas. Of these the least susceptible to errors are the central difference equations, involving a calculation of the derivative at the central point in the relationship.

Derivatives taken over a span of five data points are among the most appropriate for motion analysis purposes. Relationships exist using fewer than five points but these are less reliable.

Equation 5.16 gives a numerical approximation for the first derivative used by Khoo et al (1995) and Cheng (1996). Equation 5.17 gives a numerical approximation for the second derivative used by Gagnon & Gagnon (1992) and Cheng (1996). Each of these approximations are derived from five point lagrangian polynomials.

$$f'(xi) = \frac{x_{i-2} - 8x_{i-1} + 8x_{i+1} - x_{i+2}}{12h} \qquad (5.16)$$

$$f''(xi) = \frac{-x_{i-2} + 16x_{i-1} - 30x_i + 16x_{i+1} - x_{i+2}}{12h^2} \qquad (5.17)$$

In Equations 5.16 and 5.17, x_i is the data point at which the numerical differentiation is calculated, where the suffixes denote equal time intervals. The unit time interval between adjacent data points is denoted *h* and depends on the sampling frequency of the motion analysis system.

Worden (1990) carried out an investigation into the merits of various numerical methods for integration and differentiation. Differentiating displacement data twice using the five point centred difference formula was found to give a good estimate of velocity though the acceleration data were less satisfactory.

It was suggested that the measurement of accelerations followed by numerical integration rather than numerical differentiation of displacement data might be more appropriate.

The angular velocities and accelerations of the segments are required for the calculation of the moments of inertia of the segment and as input for the calculation of rigid body joint dynamics as discussed in Section 5.7.

Having established the rotation matrix of a moving segment, its absolute angular velocity can be established using Equation 5.18, the 'Poisson Equation' discussed in Roberson & Schwertassek (1988).

$$\frac{d({}^{A}_{B}R)}{dt} = {}^{A}_{B}\dot{R} = -{}^{A}_{B}\tilde{\omega}_{B}\,{}^{A}_{B}R \qquad (5.18)$$

The Poisson equation relates the time derivative of the rotation matrix and the angular velocity of the segment, where ${}^{A}_{B}R$ is the rotation matrix describing the rotation of a segment embedded frame *{B}* with respect to the reference frame *{A}*.

${}^{A}_{B}\dot{R}$ is the time derivative of this matrix, a matrix of the time derivatives of the individual elements of the rotation matrix ${}^{A}_{B}R$ at time *t*, which can be calculated using numerical differentiation.

${}^{A}_{B}\tilde{\omega}_{B}$ is thus the angular velocity of frame *{B}* with respect frame *{A}*, the right subscript here indicating that the angular velocity is written in frame *{B}*.

The explicit expression of the above equation can be developed as discussed in Likins (1973):

$$({}^{A}_{B}\dot{R})({}^{A}_{B}R)^{-1} = -\begin{bmatrix} 0 & -\omega_z & \omega_y \\ \omega_z & 0 & -\omega_x \\ -\omega_y & \omega_x & 0 \end{bmatrix} \qquad (5.19)$$

The matrix on the right of Equation 5.19 is the angular velocity matrix where ω_i (i=x, y, z) are the angular velocities of the segment with respect to the reference frame *{A}* as expressed in the segment frame *{B}*, i.e. x, y and z are the axes of the segment co-ordinate frame.

Because $({}^{A}_{B}R)^{-1}=({}^{A}_{B}R)^{T}$, then Equation 5.19 can be written as:

$$\begin{bmatrix} \dot{r}_{11} & \dot{r}_{12} & \dot{r}_{13} \\ \dot{r}_{21} & \dot{r}_{22} & \dot{r}_{23} \\ \dot{r}_{31} & \dot{r}_{32} & \dot{r}_{33} \end{bmatrix} \begin{bmatrix} r_{11} & r_{21} & r_{31} \\ r_{12} & r_{22} & r_{32} \\ r_{13} & r_{23} & r_{33} \end{bmatrix} = -\begin{bmatrix} 0 & -\omega_z & \omega_y \\ \omega_z & 0 & -\omega_x \\ -\omega_y & \omega_x & 0 \end{bmatrix} \qquad (5.20)$$

The matrix on the right of Equation 5.20 has the properties of skew-symmetry, all elements on the main diagonal are zero and off-diagonal elements exist in pairs with opposite signs. The transpose of such a matrix is its negative, i.e. $({}^{A}_{B}\dot{R})({}^{A}_{B}R)^{T} = -({}^{A}_{B}R)({}^{A}_{B}\dot{R})^{T} = -(({}^{A}_{B}\dot{R})({}^{A}_{B}R)^{T})^{T}$.

From Equation 5.20 the components of angular velocity of frame *{B}*, with respect to frame *{A}*, written in frame *{B}* can be obtained as:

$$\begin{aligned}\omega_x &= -\left(r_{21}\dot{r}_{31} + r_{22}\dot{r}_{32} + r_{23}\dot{r}_{33}\right)\\ \omega_y &= -\left(r_{31}\dot{r}_{11} + r_{32}\dot{r}_{12} + r_{33}\dot{r}_{13}\right)\\ \omega_z &= -\left(r_{11}\dot{r}_{21} + r_{12}\dot{r}_{22} + r_{13}\dot{r}_{23}\right)\end{aligned} \qquad (5.21)$$

The numerical differentiation techniques previously described can then be used to obtain the angular acceleration of the segment with respect to the laboratory frame expressed in the segment co-ordinate system *{B}*:

$$\begin{aligned}\varepsilon_x &= \frac{d\omega_x}{dt}\\ \varepsilon_y &= \frac{d\omega_y}{dt}\\ \varepsilon_z &= \frac{d\omega_z}{dt}\end{aligned} \qquad (5.22)$$

The matrix of components of the angular velocity matrix may be obtained for any parametrisation of the rotation matrix. The same process might be carried using a rotation matrix parametrised by the Euler angles for instance.

This method has been used previously by Ramey & Yang (1981), Kromodihardjo & Mital (1987), Gagnon & Gagnon (1992) and Cheng (1996).

This method involves simple calculations and is independent of rotational sequence. Knowing the rotation matrix the angular velocity of a moving segment can be calculated, followed by its angular acceleration by numerical differentiation of the angular velocity.

An alternative when differentiating linear or angular displacement data is to utilise a smoothing and differentiating filter. An example of this is discussed

in Dohrmann et al (1988) who used a dynamic programming spline method for smoothing and differentiating data.

An estimate of the optimal smoothing parameter, a trade-off between the closeness of the fit and smoothness of the line, was required for this method. Dohrmann et al (1988) used the method of Generalised Cross Validation (GCV) to automatically estimate this parameter.

Craven & Wahba (1979) found that an estimate of the optimal smoothing parameter could be obtained from the data itself by minimising an approximate error function (the GCV function) and thus the mean-squared error between the data points and an underlying estimated smooth curve. The GCV function can be written as:

$$GCV(B) = \frac{\frac{1}{N}\sum_{k=1}^{N}\left(x_k - d_k\right)^2}{\frac{1}{N^2}trace\left(\mathrm{I} - A(B)\right)^2} \qquad (5.23)$$

Where N is the number of data points, x_k are the estimated positions, d_k the measured positions, B the smoothing parameter and A the influence matrix which depends on B and relates the estimates to the measured data by x=Ad. The trace of a matrix is the sum of the elements on the main diagonal of that matrix.

The matrix A in the GCV function was calculated by Dohrmann et al (1988) through a dynamic programming solution of another minimisation process for each value of B, described by Busby & Trujillo (1985). The value of B at which the minimum of the GCV function occurs is then selected as the optimum estimate of the smoothing parameter for the cubic spline smoothing process.

Woltring (1986) described a technique similar to that of Dohrmann et al (1988), involving the GCV. Corradini et al (1993) tested several filtering techniques, including that of Woltring (1986) which they found to be the most flexible and accurate technique.

Giakas & Baltzopolous (1997) compared and evaluated six of the most commonly used automatic filtering techniques in biomechanics. Their assessment was based on simulated gait analysis kinematic data for eight

surface fixed markers, sampled at 50Hz using a video based system. One of the selected algorithms was that of Dohrmann et al (1988), chosen as it does not require zero accelerations at the end points and was considered computationally faster than the algorithm of Woltring (1986). It was concluded that no one filtering method was optimal for the filtering of biomechanical data or for all derivative domains, though the GCV method was considered one of the most appropriate for filtering of kinematic data.

Barth et al (1998) compared the performance of the GCV of Woltring (1986) with that of a second order Butterworth filter, along with three methods of calculating the angular velocity of a rigid body. Data for comparison were obtained from five shank markers during a gait analysis trial using the least squares technique of Challis (1995). Orientations were parametrised using Cardan angles and the corresponding velocities and accelerations calculated using the method of Kane (1983) which involves parametrisation of the orientation matrix using Cardan angles and operating on their time derivatives followed by 7-point numerical differentiation.

During testing the angular velocity calculations were made firstly using Poisson's equation. The second method used was that of Kane (1983). The final technique was that described by Angeles (1996), using the relationship between two body points and the angular velocity of that body and the positions and velocities of all markers in a least squares sense. The method of Kane (1983) was found to be superior to the use of Poisson's equation. The method of Angeles (1996) only compared with that of Kane (1983) when endpoint errors were removed.

The GCV was found to be superior to the Butterworth filter when smoothing orientation angles on considering the whole data set, though this was reversed when several endpoints were removed from the data. A similar pattern was found for the values of angular acceleration when using these filters. Both methods provided improved acceleration values on filtering both marker and angular velocity data after correcting for endpoint errors. In general the GCV was found to perform much better at the endpoints, though the Butterworth filter produced smoother results, particularly for the angular velocity and acceleration.

Hodgson (1994) developed and suggested improvements to the GCV method of Dohrmann et al (1988) and developed a MATLAB version of the generalised cross validation based cubic spline.

5.6 Denavit-Hartenberg (D-H) parameters

In order to calculate the upper limb segment dynamics it was necessary to model the upper limb as an open kinematic chain. Such modelling of the human body as a series of interconnected rigid links is a standard biomechanical approach (Cappozzo (1984)).

Denavit & Hartenberg (1955) developed a notation to describe the relationship between successive links in any kinematic chain in terms of four parameters. These uniquely determine the positions of the joint axes of two adjacent single degree of freedom joints. This notation has been applied to create a model of the upper limb by both Chèze et al (1996) and Barker et al (1997). The D-H parameters are:

θ_i - the joint rotation (rotation of one link w.r.t. the next about the joint axis)

d_i - the link offset (distance from one link to the next along the axis of the joint)

a_i - the link length

α_i - the link twist

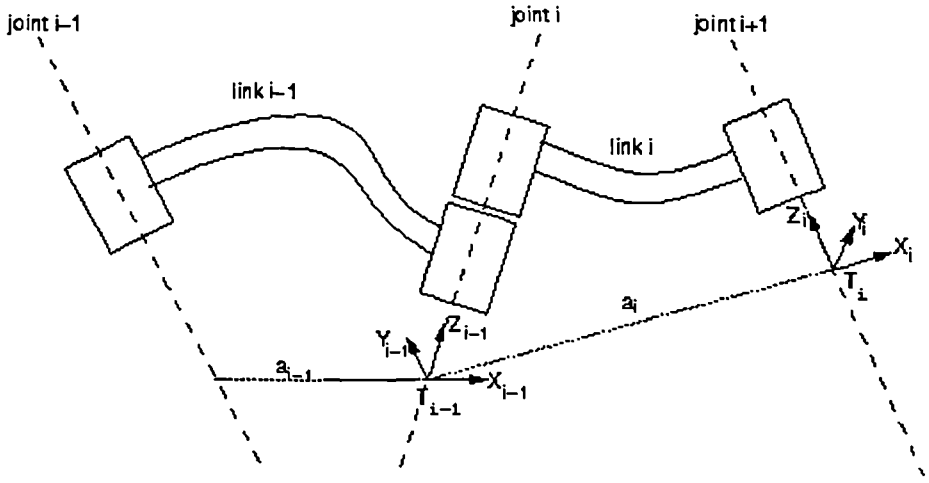

Fig 5.7 The standard Denavit-Hartenberg notation. (adapted from Corke (1996))

It is important when using the D-H parameters that a consistent method of frame (and hence parameter) assignment is followed. From the links shown in Fig. 5.7, we may define the frames in the following way:

Fix an origin (frame 0) with its z axis along the axis of motion of the first joint.
$\mathbf{Z}_{i-1}$ (or Z_0) is assigned along the axis of the i^{th} joint.
$\mathbf{X}_i$ is assigned along the common perpendicular between the $\mathbf{z}_{i-1}$ and the $\mathbf{z}_i$ axes. If two joint axes are arranged so that their joint axes intersect, there can be no common normal connecting them, thus a_i is zero. In this case the $\mathbf{x}_i$ axis may be defined along either of the two directions normal to both $\mathbf{z}_{i-1}$ and $\mathbf{z}_i$ axes. $\mathbf{Y}_{i-1}$ is chosen to complete a right handed set.

The link parameters are then assigned thus:
θ_i - the angle between the $\mathbf{x}_{i-1}$ and $\mathbf{x}_i$ axes, measured about $\mathbf{z}_{i-1}$.
$\boldsymbol{d}_i$ - the distance from the $\mathbf{x}_{i-1}$ to the $\mathbf{x}_i$ axis measured along $\mathbf{z}_{i-1}$.
$\boldsymbol{a}_i$ - the distance from $\mathbf{z}_{i-1}$ to $\mathbf{z}_i$ measured along the $\mathbf{x}_i$ axis.
α_i - the angle between $\mathbf{z}_{i-1}$ and $\mathbf{z}_i$ measured about the axis $\mathbf{x}_i$.

The forward solution when calculating the position and orientation of the hand relative to the base frame given a set of joint angles may be stated as:

$$^{i}P = {}^{i}_{i+1}T \cdot {}^{i+1}P \qquad (5.24)$$

i.e. points expressed in terms of reference frame i = transformation $\times$ points expressed in terms of reference frame $i+1$.
Where ${}^{i}_{i+1}T$ is formed from a rotation θ_i about the z_{i-1} axis, a translation d_i along the z_{i-1} axis, a translation a_i along the x_i axis and a rotation α_i about the x_i axis. The transformation matrix ${}^{i}_{i+1}T$ may then be calculated as :

$$^{i}_{i+1}T = Rot(z_{i-1},\theta_i)\,Trans(0,0,d_i)\,Trans(a_i,0,0)\,Rot(x_i,\alpha_i) \qquad (5.25)$$

$$ {}^{i}_{i+1}T = \begin{bmatrix} \cos\theta_i & -\sin\theta_i & 0 & 0 \\ \sin\theta_i & \cos\theta_i & 0 & 0 \\ 0 & 0 & 1 & 0 \\ 0 & 0 & 0 & 1 \end{bmatrix} \begin{bmatrix} 1 & 0 & 0 & 0 \\ 0 & 1 & 0 & 0 \\ 0 & 0 & 1 & d_i \\ 0 & 0 & 0 & 1 \end{bmatrix} \begin{bmatrix} 1 & 0 & 0 & a_i \\ 0 & 1 & 0 & 0 \\ 0 & 0 & 1 & 0 \\ 0 & 0 & 0 & 1 \end{bmatrix} \begin{bmatrix} 1 & 0 & 0 & 0 \\ 0 & \cos\alpha_i & -\sin\alpha_i & 0 \\ 0 & \sin\alpha_i & \cos\alpha_i & 0 \\ 0 & 0 & 0 & 1 \end{bmatrix} \qquad (5.26) $$

$$ {}^{i}_{i+1}T = \begin{bmatrix} \cos\theta_i & -\cos\alpha_i \sin\theta_i & \sin\alpha_i \sin\theta_i & \cos\theta_i \cdot a_i \\ \sin\theta_i & \cos\alpha_i \cos\theta_i & -\sin\alpha_i \cos\theta_i & \sin\theta_i \cdot a_i \\ 0 & \sin\alpha_i & \cos\alpha_i & d_i \\ 0 & 0 & 0 & 1 \end{bmatrix} \qquad (5.27) $$

Equation 5.27 gives the general form of the transformation matrix ${}^{A}_{B}T$, which relates frame *{B}* relative to frame *{A}* using the D-H parameters.

Once all the D-H parameters have been found, the individual transformation matrices can be worked out for each link. These matrices can then be multiplied together to find the single transformation that relates the final frame *N* to the base frame *0*.

$$ {}^{0}_{N}T = {}^{0}_{1}T\,{}^{1}_{2}T\,{}^{2}_{3}T \ldots\ldots {}^{N-1}_{N}T \qquad (5.28) $$

5.7 Dynamic calculations

There are several techniques originally developed in the field of robotics and manipulator dynamics, which may be used for derivation of the equations of motion of the upper limb, modelled as an open loop kinematic chain.

Luh et al (1980) discussed some options for the formulation of the equations of motion of manipulators, assigning their co-ordinate systems according to the D-H convention. They described a Recursive Newton-Euler (RNE) formulation based on consideration of the forces involved.

The RNE involves the successive transformations of velocities and accelerations from the base of a link model out to the end, link by link using the relationships of moving co-ordinate systems. Knowing this kinematic information and incorporating mass distribution information, forces are then

transformed back from the end to the base to obtain the joint moments required to cause the motion.

These calculations are more efficient than traditional methods as they reference the i^{th} link velocities, accelerations, forces and moments to the i^{th} link co-ordinate system as opposed to the base co-ordinate system.

The options of using a free-body method was considered too laborious, as was the use of a Lagrangian formulation, based on energy considerations in which the explicit inclusion of forces is avoided. The method of virtual work (Williams & Seireg (1979)) was also dismissed for similar reasons, there being no computational difference between it and the Lagrangian formulation, only a different sequence of steps.

Walker & Orin (1982) also describe the RNE method in their investigation of techniques for forward dynamics solutions, again using the D-H convention to assign link co-ordinate systems. Hollerbach (1980) discussed the RNE formulation and outlined a similar method for a computationally efficient recursive Lagrangian formulation. It was concluded that recursive formulations based on either Lagrangian or Newton-Euler dynamics offered the best method of dynamics calculation. The RNE formulation was found to reduce the number of necessary additions and multiplications and therefore to be the more efficient.

The procedure employed for the RNE formulation of the dynamic equations of motion is to first write the equations which define the outward recursion. These iteratively calculate the angular and linear velocities and accelerations of each defined link from proximal to distal end of the model. The equations which define the inward recursion are then written. These allow calculation of the forces and moments exerted on successive links under the prescribed motion for each link from the distal to the proximal end of the model. Fig 5.8 Shows the notation used for the RNE applied to a D-H parameter link model.

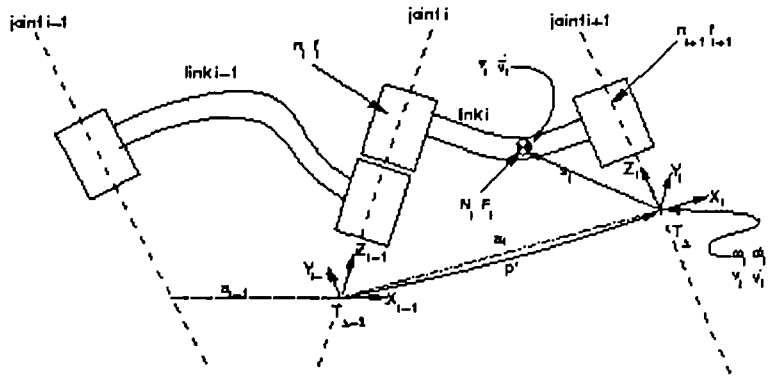

Fig 5.8 Notation for RNE formulation inverse dynamics. (adapted from Corke (1996))

The following equations define the outward RNE recursion, $1 \leq i \leq n$, where n is the number of defined joints and axis i+1 is rotational. The notation used is that employed by Corke (1996) combining those of Hollerbach (1980) and Walker & Orin (1982), modified to include the rotation matrix definition of Craig (1989).

$$ {}^{i+1}\underline{\omega}_{i+1} = {}^{i+1}_{i}R({}^{i}\underline{\omega}_{i} + \underline{z}_o\dot{\underline{q}}_{i+1}) \tag{5.29} $$

$$ {}^{i+1}\dot{\underline{\omega}}_{i+1} = {}^{i+1}_{i}R\left\{{}^{i}\dot{\underline{\omega}}_{i} + \underline{z}_o\ddot{\underline{q}}_{i+1} + {}^{i}\underline{\omega}_{i} \times (\underline{z}_o\dot{\underline{q}}_{i+1})\right\} \tag{5.30} $$

$$ {}^{i+1}\underline{v}_{i+1} = {}^{i+1}\underline{\omega}_{i+1} \times {}^{i+1}\underline{p}_{i+1}{}^{*} + {}^{i+1}_{i}R\,{}^{i}\underline{v}_{i} \tag{5.31} $$

$$ {}^{i+1}\dot{\underline{v}}_{i+1} = {}^{i+1}\dot{\underline{\omega}}_{i+1} \times {}^{i+1}\underline{p}_{i+1}{}^{*} + {}^{i+1}\underline{\omega}_{i+1} \times \left\{{}^{i+1}\underline{\omega}_{i+1} \times {}^{i+1}\underline{p}_{i+1}{}^{*}\right\} + {}^{i+1}_{i}R\,{}^{i}\dot{\underline{v}}_{i} \tag{5.32} $$

$$ {}^{i}\bar{\dot{\underline{v}}}_{i} = {}^{i}\dot{\underline{\omega}}_{i} \times \underline{s}_i + {}^{i}\underline{\omega}_{i} \times \left\{{}^{i}\underline{\omega}_{i} \times \underline{s}_i\right\} + {}^{i}\dot{\underline{v}}_{i} \tag{5.33} $$

$$ {}^{i}\underline{F}_{i} = m_i\,{}^{i}\bar{\dot{\underline{v}}}_{i} \tag{5.34} $$

$$ {}^{i}\underline{N}_{i} = J_i\,{}^{i}\dot{\underline{\omega}}_{i} + {}^{i}\underline{\omega}_{i} \times (J_i\,{}^{i}\underline{\omega}_{i}) \tag{5.35} $$

Note that the COM linear velocity given by Equation 5.31 does not need to be computed as no other expression depends upon it.

The following equations define the inward recursion, $n \geq i \geq 1$.

$$ {}^{i}\underline{f}_i = {}_{i+1}^{i}R\,\underline{\quad}^{i+1}\underline{f}_{i+1} + {}^{i}\underline{F}_i \tag{5.36} $$

$$ {}^{i}\underline{n}_i = {}_{i+1}^{i}R\left\{{}^{i+1}\underline{n}_{i+1} + ({}_{i}^{i+1}R\,{}^{i}\underline{p}_i^{*}) \times {}^{i+1}\underline{f}_{i+1}\right\} + ({}^{i}\underline{p}_i^{*} + \underline{s}_i) \times {}^{i}\underline{F}_i + {}^{i}\underline{N}_i \tag{5.37} $$

$$ \underline{Q}_i = ({}^{i}\underline{n}_i)^T ({}_{i+1}^{i}RZ_o) \tag{5.38} $$

where, referring to Fig. 5.8 :

- i is the link index, in the range 1 to n
- $\underline{J}_i$ is the moment of inertia of link i about its COM
- $\underline{s}_i$ is the position vector of the COM of link i with respect to frame i
- m_i is the mass of link i
- $\underline{\dot{q}}_i$ is the angular velocity at joint I (about axis Z_{i-1})
- $\underline{\ddot{q}}_i$ is the angular acceleration at joint I (about axis Z_{i-1})
- $\underline{\omega}_i$ is the angular velocity of link i
- $\underline{\dot{\omega}}_i$ is the angular acceleration of link i
- $\underline{v}_i$ is the linear velocity of frame i
- $\underline{\dot{v}}_i$ is the linear acceleration of frame i
- $\underline{\bar{v}}_i$ is the linear velocity of the COM of link I
- $\underline{\dot{\bar{v}}}_i$ is the linear acceleration of the COM of link i
- Z_o Z_o is a unit vector in the Z direction, Z_o =[0 0 1]
- $\underline{n}_i$ is the moment exerted on link i by link i-1
- $\underline{f}_i$ is the force exerted on link i by link i-1
- $\underline{N}_i$ is the total moment at the COM of link i
- $\underline{F}_i$ is the total force at the COM of link i
- $\underline{Q}_i$ is the moment required to be exerted at joint i

${}^{i-1}_{i}R$ is the rotation matrix defining the orientation of frame i with respect to frame i-1 and can be seen in Equation 5.39 to be the same as the rotation matrix part of the generalised transformation matrix in Equation 5.27 .

$$ {}^{i-1}_{i}R = \begin{bmatrix} \cos\theta_i & -\cos\alpha_i \sin\theta_i & \sin\alpha_i \sin\theta_i \\ \sin\theta_i & \cos\alpha_i \cos\theta_i & -\sin\alpha_i \cos\theta_i \\ 0 & \sin\alpha_i & \cos\alpha_i \end{bmatrix} \qquad (5.39) $$

With ${}^{i}\underline{p}_{i}^{*}$ being the displacement from the origin of frame i-1 to frame i with respect to frame i.

$$ {}^{i}\underline{p}_{i}^{*} = \begin{bmatrix} a_i \\ d_i \sin\alpha_i \\ d_i \cos\alpha_i \end{bmatrix} \qquad (5.40) $$

Boundary conditions can be used to introduce the effect of gravity loading on the links by setting the linear acceleration of the base link, $\dot{v}_o = -\underline{g}$, where $\underline{g}$ is the gravity vector in the reference co-ordinate frame. This is equivalent to saying that the base of the linkage is accelerating upwards with an acceleration equal to gravity, causing the same effect on the links as gravity would. The base velocity is set as zero, $v_o = 0$, $\omega_o = 0$ and $\dot{\omega}_o = 0$.

A further alternative for the derivation of the equations of motion of the upper limb are Kane's dynamical equations, described by Kane et al (1983) and Kane & Levinson (1983). Kane's equations are a vector based method, generating a minimal set of equations of motion through the use of generalised speeds, partial linear and angular velocities of the system and generalised inertia and active forces. This method has been found to be highly efficient and has been used to form the basis of the dynamic analysis software Pro/MECHANICA.

5.8 Spline smoothing

When fitting a curve to data it is possible to employ a single equation that provides a reasonable approximation to the entire data set. Fitting a single

equation may be difficult however if the data set is long or complex.

The use of 'splines' offers an alternative to the fitting of a single equation, using a series of equations to fit the complete data set, with each equation fitting only a portion of the data. When these equations are connected together they provide a mathematical approximation to the entire data set. It is important for each section of the fitted curve to be free of discontinuities, its slope and curvature blending smoothly at each boundary. Third order or cubic equations are the lowest order equations which allow this and along with quintic (fifth order) splines are frequently used in biomechanical studies. Splines are mathematicallly equivalent to digital filters with a cubic spline being roughly equivalent to a 2nd order Butterworth filter applied twice. A quintic spline would be equivalent to a 3rd order Butterworth filter applied twice.

Chapter 6 : MATERIALS AND METHODS

6.0 Introduction

The aim of this study was to use video cameras to track the positions and orientations through time of bone-embedded co-ordinate frames, rigidly associated with and directly related to the underlying bones of the upper limb and to describe this motion in terms of a global laboratory co-ordinate frame.

Having made the assumption that the limb segments could be treated as rigid bodies for the purposes of kinematic analysis, such tracking would then allow the movement of the bones in relation to some reference position and the relative motion between bones to be assessed.

In order to use such techniques in a laboratory setting, several issues had to be addressed. These included the identification of landmarks on the body segments under analysis and the size and positioning of external markers. It was also necessary to establish the marker attachment pattern and thereafter the definitions of the segment embedded frames.

A further issue was the method by which the marker co-ordinates obtained from the motion analysis system should be manipulated in order to reconstruct the body fixed axes and best describe the relative motion of the body segments.

The following sections discuss the equipment, software, experimental methods and subsequent analysis procedures utilised to achieve these aims. As far as possible these will be introduced in the order in which each element of the experimental method was carried out, beginning with the Ariel Performance Analysis System (APAS) and its software.

6.1 The Ariel Performance Analysis System (APAS) - Hardware

6.1.1 Introduction

The APAS is a three-dimensional video motion analysis system supporting the use of multiple video cameras and automatic or manual marker digitising. The image sequences obtained from video were stored in picture form on a computer for subsequent processing.

Richards (1998) found the APAS system to be superior to several similar systems available in analysing valid and reliable data for human movement.

6.1.2 The computer

The AST® Bravo® LC P75 computer was the primary hardware component of the system used and included an 'Intel Smart Video Recorder Pro Board', a 'Matrox Millenium II Graphics Card' and a '3COM 3C900-COMBO PCI Ethernet Network Interface Card' and a board for the connection of a monochrome monitor.

6.1.3 Monitors

Two monitors were connected to the APAS system, a Panasonic PanaSync/Pro™ 7G TX-D2162 21" color display monitor, used to display the video images for capture and digitising and an ARCUS™ CH-3423W 13" monochrome monitor used for displaying option menus in the Transform, Smoothing and Print modules discussed later.

6.1.4 Video playback unit (VCR)

A Panasonic Hi-Fi Professional Video, model AG-7350 was used for playback of videotape recordings of the upper limb activities in order to allow high precision freeze-frame video imaging.

6.1.5 Video cameras

Standard compact VHS camcorders were used to record motion sequences for subsequent analysis. Four were selected from a group of three JVC GR-AX400 and three JVC GR-AX460 video cameras.

6.2 The APAS - Software

A typical movement analysis using the APAS consists of several distinct operations; Data Collection (Filming and Capturing), Digitising, Transforming, Smoothing and the Presentation of Results. After filming and recording a test

on video tape, a series of software modules were used to carry out the above operations and these will now be discussed in order of their use.

6.2.1 The Capture Module

Initially, each recorded video image was displayed on the monitor and stored on the computer hard disk in digital form using the Capture Module. The stored image sequences could then be retrieved and displayed one frame at a time for the purposes of digitising, eliminating the need for video apparatus during this process.

The maximum sampling frequency was 50Hz as the system allowed the analysis of fields rather than entire frames. The capturing of image sequences from video tape at varying sample intervals was enabled however, through the selection of 'skip' values. For activities performed at slower speeds, the definition of skip value of one allowed every second image to be captured from tape, thus doubling the sampling interval. It was also necessary to specify a 'step delay', the time delay between successive commands to step the VCR when skipping of images had been specified. The step delay had no effect when every image was being captured.

6.2.2 The Digitising Module

To produce computer image sequences from the stored video images it was necessary to convert the recorded patterns to numbers or digits, hence the term digitising.

Each marker appeared as a two dimensional circle in each camera view. Using a video cursor controlled via the mouse, the location of each of the attached markers were identified and digitised, a red cross indicating when a marker had been digitised successfully.

Both manual and automatic digitising modes were supported, the latter requiring high contrast between the markers and background. Four views were opened and digitised simultaneously with manual control of the digitising process providing an opportunity for error checking and visual feedback.

The automatic digitising software used contrast, brightness and kinematic parameters, such as velocity and acceleration, to locate specific

markers. The centre of each marker image was located through identification of the centroid of pixels whose threshold exceeded a user-defined level. After manually digitising several fields, the algorithm would "learn" the characteristics of each point and operate under the automatic mode.

It was possible to label markers as 'missing' in a particular camera view if they became obscured. Such markers would then be ignored in the digitising process for that particular camera and image. If obscured for several images, markers were labelled 'invisible' as an alternative to using the 'missing' option in every image. The software then skipped the marker and proceeded to the next sequential marker for digitising. Digitising with the marker included was resumed when it became visible again.

With every frame digitised, it was necessary to digitise a fixed marker, which provided a reference against which all other markers were measured and compensated for small variations in the horizontal and vertical positions of the captured images. This marker had to remain stationary and be clearly visible in every frame including those for the system and anatomical calibrations discussed later.

6.2.3 The Transformation Module

After digitising all camera views, it was necessary to compute the true three-dimensional co-ordinates of the attached markers from the two-dimensional digitised image co-ordinates. This computation was performed in the APAS using the Direct Linear Transformation (DLT) introduced by Abdel-Aziz & Karara (1971) and discussed in Section 5.1. Time synchronisation of all camera views was followed by computation of the 3D image co-ordinates of the markers.

6.2.4 The Smoothing Module

Smoothing of the image co-ordinates was necessary to remove small random digitising errors or noise from the transformed image sequence. A choice from five different types of smoothing functions were available, these being cubic spline, digital filter, polynomial, quintic spline and Fourier smoothing. Displacement curves for each marker were displayed along with

their velocity and acceleration curves. As previously mentioned, taking successive derivatives has the effect of emphasising or highlighting the variations or noise in the data. Included in the smoothing module was an option to use a linear interpolation algorithm between the endpoints of an interval. This was useful where a section of the data curve contained erroneous values through digitising errors or obscuring of markers.

6.2.5 Printing Module

Once the sequences had been digitised, transformed and smoothed, the printing module was used to produce output files. These contained the three-dimensional data for marker motion in the global Cartesian co-ordinate system.

These reports included marker displacement components along each global co-ordinate axis, along with velocity and acceleration information calculated using an in-built system algorithm very similar to the five-point numerical differentiation of Equations 5.16 and 5.17.

6.2.6 The APAS 'Anthro' Program

This module allowed the calculation of segment mass, location of CM and principal moments of inertia with respect to the CM, requiring user input of body mass and height or additional anthropometrical parameters. Algorithms based on the work of Harless (1860), Braune & Fischer (1889), Fischer (1906), Bernstein (1947), Dempster (1955), Clauser et al (1969), Marion (1979) and Zatsiorsky & Seluyanov (1983) were offered, a number of these studies being discussed in Chapter 3. The modifications to the data of Zatsiorsky & Seluyanov (1983), made by de Leva (1996a) were not offered and therefore the 'Anthro' module was not utilised for the upper limb study.

6.3 An overview of the motion analysis experimental procedures

6.3.1 Laboratory Preparation

The initial preparation of the testing environment is a crucial step in the motion analysis process, one of the most basic necessities being the provision

of multiple electrical outlets in order to power the cameras and computing equipment.

Suitable lighting conditions were essential as the APAS was dependent on marker contrast for its accuracy. Alaways et al. (1996) studied the effect on accuracy of variation in lighting conditions and concluded that line of sight lighting should be used to evenly illuminate the side of the marker facing each camera. For this reason built-in camera spotlights were used to illuminate the test space, some of which were filtered to reduce skin glare. A ceiling mount and three camera tripods were required to allow a suitable arrangement of the cameras around the test space.

In order to maximise the contrast between markers and their background, reflections in the room were minimised. The walls and fittings were painted with a matte black finish or draped with black cloth and the windows were covered to darken the room.

6.3.2 Camera Positioning

According to photogrammetrical theory (Ghosh (1979)), the optimal camera arrangement is one in which the object distances are small, corresponding to larger scale photographs and the viewing planes or optical axes of each of the cameras intersect at 90°.

Alaways et al. (1996) also recommended a 90° camera intersection angle. In practice however a ten or twenty degree variation from this is not critical, anything over 60° (less than 120°) being considered sufficient. For arrangements in which the viewing planes differ by less than 30 degrees, small errors in digitising can lead to large errors in the 3D co-ordinates.

Thornton et al (1998) carried out a systematic analysis of the effects of camera positioning on the error when using a 'Kinemetrix' system. It was found that in general the precision of the system increased with increasing angle between the cameras in the horizontal plane from 15° to 45° and in the vertical plane from 0° to 30°.

Due to the complex motion of the upper limb, attached segment markers can become obscured by other parts of the body and are thus not necessarily seen by the same cameras throughout the measured motion. A minimum

of two cameras must view each marker in each sampled instant or marker trajectory information can be lost.

In order to minimise the occurrence of occluded markers during critical phases of the activity the number of cameras was increased to four rather than the minimum two. In order to reach as near to the recommended 90° intersection angles the cameras were carefully positioned, three around the front and right side of the subjects with one mounted on the ceiling above.

The cameras were also mounted at differing heights in order to avoid their axes being coplanar, another situation which can lead to frequent marker occlusion. Object distances were kept as short as recommended by Ghosh (1979), as much of the field of view of each camera as possible being filled with subject activity to ensure maximum resolution when viewing and digitising.

6.3.3 Calibration of test volume

As previously mentioned, the DLT was used to provide a relationship between the two-dimensional co-ordinates of the markers on the captured video sequences and their three-dimensional locations in space. In order to use the DLT the first stage in the experimental process was the calibration of the test volume. A rigid two-level calibration frame of approximate base dimensions 0.97×0.96m, a height of 0.88m and upper level dimensions 0.98×0.72m was used. This frame was placed in the test volume on a raised platform 0.46m above floor level.

A total of ten calibration markers were attached, one at each corner of the upper and lower levels and one in the centre of each level, arranged so as to cover the experimental volume. Their co-ordinates were measured to an accuracy of 1mm using a 'Stäubli Unimation Puma 700' robot arm. Using more than the minimum of six non-coplanar control points, increased the accuracy of the DLT transformation, the redundancy making the system more robust.

This arrangement allowed the calibration of a volume large enough for upper limb studies and followed the recommendations of previous work discussed in Section 5.1, having the calibration points distributed about and within this volume. One corner of the frame was designated as the global

laboratory frame origin, the other points having known locations relative to this point.

After filming the calibration frame, the camera field of view, position and focal length were fixed for the duration of each motion sequence recorded for analysis. It was not necessary for the control points to be seen during the filming so the frame was removed prior to commencing the activity.

As mentioned in Section 6.2.2 it was necessary to include a fixed point in each of the camera views during filming of both the calibration frame and subject motion. This was achieved by attaching a 35mm diameter reflective spherical marker to the tip of a 1.2m long rod rigidly fixed in a vertical position.

After calibration, a set of reflective markers were attached to the limb segments of each of the subjects under analysis. The construction and positioning of these markers will be discussed in the following sections.

6.3.4 Marker construction - considerations

When considering the construction of markers for motion analysis two options are available, as discussed by Cappozzo et al (1995).

The first involves the construction of individual markers which are attached directly to the skin on, or related to, definable landmarks. These lead to the definition of flexible skin-fixed marker clusters known as deformable arrays. These arrays suffer from deformation due to variations in skin displacement, though such artefacts can be corrected using numerical techniques, discussed in Section 5.3.

Such least-squares and solidification techniques were discussed by Chèze et al (1998). They allow correction of the relative displacements between markers belonging to the same segment but not the global displacements of the set of external markers with respect to the underlying bone.

The alternative to the use of individual skin-fixed markers and numerical artefact correction is to use clusters of markers at skin level or raised from the skin, attached to common rigid or flexible plates which are fixed on the subject. The lack of variation in marker spacing during movement in these clusters leads to them being termed rigid arrays. Such arrays have previously been

used in studies of upper limb motion by Langrana (1981), Peterson & Palmerud (1996), Williams et al (1996) and Davis et al (1998). Schmidt et al (1999) adopted a similar method, mounting markers on foam rubber bandages.

One benefit of rigid arrays is the improved visibility of the markers on scaling them for differing arm size and they may also be more convenient and quicker to apply. The rigid relationship between markers also avoids the inter-marker movement and array deformation that can occur when using individual markers.

Rigid arrays are still susceptible to movement of the entire array with respect to the underlying bone however and thus do not necessarily overcome the effects of skin deformation, but may only hide these effects. The use of algorithms for the correction of skin movement artefacts is also made impossible by the use of rigid arrays.

Other disadvantages of rigid arrays are a potential loss of longitudinal rotation information if arrays are placed near the proximal segment end and possible greater hindrance to the subject than individual markers, due to the size and mass of the array.

It was decided for this study to use the option of skin-fixed deformable arrays obtained by the attachment of individual markers on the skin. Marker locations were selected for visibility, ease of tracking and minimal relative motion between skin surface and the underlying bone.

As discussed later in section 6.5.5, an option in the analysis software was included to allow the use of an algorithm for 'solidification' of skin movement.

6.3.5 Marker construction

In previous studies a range of marker diameters from 15-25mm had been used. It was decided that markers of diameter 25mm would be suitable for investigating the motion of the upper limb.

Twelve single markers were constructed from 25mm diameter wooden spheres, coated in strips of Scotchlite™ reflective tape. A 1mm thick pliable polythene disc of diameter 25mm was attached to the base of each sphere.

Three lightweight markers were made from 25mm compressed paper balls coated in reflective tape. These were mounted on extended wands of lengths 25mm, 35mm and 45mm, attached to 50mm×15mm polyethene bases.

The markers were fixed to each subject with double-sided non-allergenic 'wig' tape.

6.3.6 Methodologies from previous studies

Tables 6.1-6.3 outline the marker placement, joint centre location and bone embedded frame definition methodologies used in previous studies.

6.3.7 Marker placement - considerations

As previously discussed, at least three markers were required on each segment of the upper limb to fully describe its position and orientation in three dimensions.

Söderkvist and Wedin (1993) calculated a condition number, based on singular values, indicating the effect on computed rotation matrices of landmark measurement errors. The conclusion reached on calculating this condition number for several marker configurations, was that the markers should be as widely spaced as possible and non-collinear. Cappozzo (1991) and later Cappozzo et al (1997) also outlined several criteria for the selection of marker position based on their visibility, separation, offset, convenience and skin movement.

The selection of the marker locations on the segments of the upper limb and trunk was crucial to the success of the method, as even using four cameras some marker loss is inevitable.

In some studies such as that of Turner-Stokes & Reid (1999), individual markers are attached directly over the joint centres. This is insufficient however if the aim is to track frames embedded in each upper limb segment.

It was therefore necessary to consider how to define the embedded frames. The most apparent solution in terms of relating surface markers to the underlying bone and defining and tracking embedded frames, would be to attach individual markers directly over palpated bony anatomical landmarks on each of the segments and define embedded frames from these landmarks.

Paper	Lower Arm	Upper Arm	Trunk
Runciman (1993)	Dorsal and ventral wrist.	Placed over deltoid insertion, double marker over back of the elbow	markers over manubriosternal joint, horiz opposite this, nominally at T4 spinous process, marker over xiphoid process Measured distance between marker centre and manubriosternal joint
Van der Helm and Pronk (1995)	none	Cuff round lateral and medial epicondyles.	Jugular notch, xiphisternal joint seventh cervical vertebra.
Sprigings et al (1994)	Medial and lateral epicondyles, radial and ulnar styloids.	Medial and lateral epicondyles, anterior and posterior deltoid muscle.	none
Williams (1996)	Placed over the bony subcutaneous border of the proximal ulna at a level 2 inches from the tip of the olecranon. Placed directly over the most distal part of the ulnar styloid. Placed directly over the most distal part of the radial styloid.	Placed over the most inferior insertion of the deltoid muscle fibres onto the bone of the humerus. Placed over the most proximal insertion of the brachioradialis muscle fibres onto the bone of the distal humerus. Placed directly over the bony prominence of the medial epicondyle.	Placed in the mid-line half way from the sterno-manubrial joint to the sternal tip. Placed on the mid-line over the maximum convexity of the thoracic kyphosis. Placed on the mid-line over the maximum concavity of the lumbar lordosis.
Cheng, Pei Lai (1996)	Double marker on ulnar styloid, single marker on radial styloid.	Double marker on acromial process, double marker fixed at rear of elbow joint.	double-marker wand over manubrium sterni, single marker over xiphoid.
Rao et al (1996)	Medial and lateral epicondyles, radial and ulnar styloids.	Greater tubercle, medial and lateral epicondyles.	Third thoracic spinous process, manubrium, xiphoid.
Wang,X.G. (1996)	Double marker on ulnar styloid	Single marker on acromio-clavicular joint and lateral epicondyle	Double markers on Jugular notch, seventh cervical vertebra.
Wang et al (1996)	Medial and lateral epicondyles, radial and ulnar styloids. Three on triangular plate	Acromion, lateral and medial epicondyles. Three markers on triangular plate	Xiphoid process, jugular notch, seventh cervical vertebra.
Wang et al (1998)	Medial and lateral epicondyles, radial and ulnar styloids.	Acromion, lateral and medial epicondyles.	Xiphoid process, jugular notch, seventh cervical vertebra.
ISB Stand'n Committee (1993)	none	Lateral and medial epicondyles, cuff over upper arm.	Jugular (suprasternal) notch, Xiphoid process, seventh cervical vertebra, eighth thoracic vertebra.

Table 6.1 Marker Placement Methodologies

Paper	Wrist Centre	Elbow Centre	GH Centre
Rao et al (1996)	Mid-point between Radial Styloid and Ulnar styloid markers	Mid-point between lateral and medial epicondyle markers	30° posterior rotation about a line joining markers over the greater tubercle and the lateral epicondyle
Wang et al (1996)	"	"	none
Sprigings et al (1994)	"	"	mid-point between markers on the anterior and posterior side of the deltoid
Runciman,R. J. (1993)	none	calculation from double-marker wand attached at rear of the elbow using epicondyles measure to give elbow centre. Arm in anatomical position	none
ISB Standard'n Committee (1994/98)	none	Mid-point between lateral and medial epicondyle markers	obtained using regression equations on scapular landmarks (Meskers et al (1997))
Cheng, P.L. (1996)	calculation from markers attached over radial and ulnar styloids	calculation from double-marker wand attached at rear of the elbow	calculation from double-marker wand attached at the acromial process
Wang,X.G. (1996)	Extrapolation of double marker attached to ulnar styloid.	Half width of elbow from lateral epicondyle to epitrochlea along cross-product of arm and forearm longitudinal axes	Minimisation of distance of arbitrary points from calculated helical axes during humeral circumduction movements
Wang et al (1998)	calculation from markers attached over radial and ulnar styloids	Mid-point between lateral and medial epicondyle markers	Average centre of rotation of the 'lumped' shoulder joint between thorax and humerus. From fitting of elbow positions to a sphere using acromion as first estimate.
Engin et al (1984)	locates position of the glenohumeral centre by assuming it lies a predetermined distance along a line between markers over the oleocranon and the acromion		

Table 6.2 Joint Centres Location Methodologies

Paper	Lower Arm	Upper Arm	Trunk
Runciman (1993)	line through elbow centre and the mid point of markers placed on the dorsal and ventral wrist. Parallel to line through markers on dorsal and ventral wrist. Third from these. (both of the upper and lower arm co-ordinate systems are defined from the same set of markers and then applying transformations)	Axis along line joining elbow centre and palpated point on humeral shaft centre line directly under deltoid insertion marker. Cross product of this line with line through elbow centre and the mid point of markers placed on the dorsal and ventral wrist. third from these.	Technical axis through markers over manubriosternal joint and T4. Perpendicular to plane containing above line and marker over xiphoid, third using these origin at manubriosternal joint. In neutral position assume anatomical frame parallel with laboratory frame and calculate orientation between marker and anatomical frame.
Van der Helm and Pronk (1995)	none	Axis defined from longitudinal axis of cuff attached at lateral and medial epicondyles. Axis defined as normal to plane including first axis and line between epicondyles, third using these Origin at glenohumeral centre	Axis defined along line from jugular notch to transition between body and xiphoid of scapula. Axis defined as perpendicular to plane including above line and the seventh cervical vertebra, third using these origin at jugular notch. Global frame defined at jugular notch with vertical axis.
Sprigings et al (1994)	All axes using lines joining joint centres and lines between external markers and cross products of these origin at humeral/ulnar joint	All axes using lines joining joint centres and lines between external markers and cross products of these origin at glenohumeral centre	none
Williams (1996)	Long axis from distal radio-ulnar joint (0.57 of vector from RS to US markers) to subcutaneous border of the ulna marker. Second from cross of first with RS-US vector. Third from these. Rotate frame forward about flexion axis by 15°	Long axis from mid-point of medial epicondyle to origin of brachioradialis vector to mid point of medial epicondyle to deltoid insertion vector. Axis from cross of first axis with ME-OBR vector. Third axis by cross product and then rotate frame backwards about flexion axis by 15°	Axis from lumbar to thoracic spine, axis along cross product of first axis and line between lumbar spine and sternum, third from these. Rotated forward about flexion axis by 20° to bring into line with global vertical.

Table 6.3(a) Bone-embedded Axes Methodologies

Cheng, Pei Lai (1996)	Axis defined along line joining elbow and wrist centres. Axis defined along cross-product of first line with line joining radial and ulnar styloid markers, third from these origin at wrist centre	Axis defined along line joining elbow and shoulder centres. Axis defined along cross-product of first line with line joining elbow wand double markers, third using these origin at elbow centre	Axis defined along line joining double jugular notch marker. Axis defined along cross-product of first line with line joining xiphoid and manubrium markers, third using these origin at manubrium sterni
Rao et al (1996)	Define plane between the radial and ulnar styloids and the elbow joint centre. One axis normal to this plane, one along line of elbow and wrist centres, third using these	Define plane using glenohumeral centre and lateral and medial epicondyles. One axis normal to this plane, one along line of glenohumeral and elbow centres, third using these	Define sagittal plane using three markers, assume coplanar. Project lateral epicondyle and greater tubercle line onto this plane in neutral posn (zero flexion wrt trunk), One axis normal to the plane, third using these
Wang et al (1996)	Axis defined along line joining lateral and medial epicondyles. Axis defined as cross-product of first line and line joining elbow centre and ulnar styloid marker, third using these, origin at midpoint of lateral and medial epicondyles	Axis defined along line joining elbow centre and acromial marker. Axis defined as cross-product of first line with line joining acromial and lateral epicondyle markers origin at acromion marker, third axis from these	Axis between xiphoid process and jugular notch defined. Axis defined by cross product of first line and line joining jugular notch and 7th cervical vertebra, third using these origin at jugular notch marker
Wang,X.G. (1996)	Longitudinal axis from wrist centre to elbow centre. Elbow flexion axis cross-product of upper arm and forearm longitudinal axes. Third from these.	Longitudinal axis from elbow centre to glenohumeral centre. Elbow flexion axis cross-product of upper arm and forearm longitudinal axes. Third from these.	Global vertical with subjects sitting erect in seat Axis defined by cross product of first axis and plane of jugular notch, xiphoid and 7th cervical vertebra, third using these origin at jugular notch
Wang et al (1998)	none	Axis defined along line joining elbow centre and shoulder centre. Axis defined as normal to plane formed by longitudinal axes of upper arm and forearm, third axis from these	Vertical axis same as global axis from calibration procedure. Axis defined by cross product of first axis and plane of jugular notch, xiphoid and 7th cervical vertebra, third using these origin at jugular notch marker
ISB Standard'n Committee (1993/97)	none	Long axis from mid-point of lateral and medial epicondyle markers to GH rotation centre. Second axis by cross product of first axis with EM-EL vector. Third from these.	Long axis from mid-point of xiphoid and T8 markers to mid-point of jugular notch and C7 markers. Perpendicular to plane defined by previous markers, third from these.

Table 6.3(b) Bone-embedded Axes Methodologies (continued)

These markers could be applied in such positions that they would allow the determination of the location of the joint centres to which they relate, for instance, so as their mid-point lies at the joint centre.

Knowing the co-ordinates of the joint centres and the markers with respect to the global laboratory frame, a set of orthogonal vectors can be defined and a bone embedded Cartesian frame constructed. Such an embedded frame is known as an anatomical frame. The instantaneous position and orientation of the segment in relation to the calibrated laboratory co-ordinate system would then be described through calculation of the transformation between the global and embedded frames.

Embedded frames created directly from experimental co-ordinate information on markers positioned over anatomical landmarks, do not provide the best characteristics for motion analysis purposes however. This is largely due to problems of poor marker visibility in many such positions. If the embedded axes were to be defined by placing markers on either side of the joint, as is common in many upper limb studies, problems would arise for instance at the elbow, where a marker on the medial epicondyle would often be obscured. A marker on this location might also interfere with the natural performance of the activity. The medial epicondyle is also susceptible to large movement between skin and underlying bone.

The definition of an intermediate co-ordinate system between the laboratory and anatomical frames as described by Cappozzo et al (1995), can help overcome some of these problems. A minimum of three non-collinear surface markers were still required per segment. In this instance however, it was not necessary to attach the markers at particular, identifiable bony landmarks and they could in fact be attached in arbitrary positions with no apparent geometric relationship to anatomical landmarks.

The main criteria here are that the markers, known as technical markers, be positioned and fixed in such a way as to minimise their motion with respect to the underlying bone and that the visibility of the attached markers to the cameras should be maximised. Data on the position of the technical markers in the calibrated laboratory reference frame at each sampled instant of time can

be obtained from the system. From these point co-ordinates in laboratory space a bone embedded frame is again defined, termed a technical frame.

As with the anatomical frame, the technical frame is described with respect to the laboratory co-ordinate system in each instant by a transformation matrix. This represents the displacements and rotations necessary to move the technical frame from a reference position coincident with the laboratory frame to its true position in space.

The location of bony anatomical landmarks can then be identified in relation to the technical frames using the technique of 'anatomical calibration', discussed in detail in section 6.3.11. Embedded anatomical frames can be constructed in relation to these landmarks in a similar manner to the anatomical frame previously discussed. The transformation matrix describing the anatomical frame in relation to the technical frame can then be found.

The extra step of defining a technical frame helps overcome the problems of the first option as it allows the fixation of markers at positions of minimum skin movement and maximum visibility and can aid in reducing the instances of occluded markers. The constraint of placing the markers over anatomical landmarks is not imposed, the most suitable marker positions being chosen.

This latter method was utilised for the analysis of the upper limb. The points identified by markers or through anatomical calibration during this process are discussed in the following sections.

6.3.8 Markers attached to the forearm

Three markers were attached on the forearm in order to define the embedded frames as shown in Fig. 6.1.

According to Keogh & Ebbs (1984), the ulnar styloid process may be identified by lying the hand flat on the table palm down in ulnar deviation to highlight the tendon of the extensor carpi ulnaris on the ulnar side of the head of the ulna. By radially deviating the hand it can be seen that the tendon runs in a groove between the head of the ulna and a smaller palpable bony prominence continuous with the subcutaneous border of the ulna, this is the styloid process. The ulnar styloid was the site for the first forearm marker.

The second forearm marker was placed on the most distal point of the radial styloid, the distal prolongation of the lateral surface of the radius (Keogh & Ebbs (1984)), which according to Moore & Agur (1996) can be palpated on the lateral side of the wrist about 1cm more distal than the ulnar styloid process, between the tendons of the wrist and also anteriorly. Knowing the locations of the styloid markers, the wrist centre was defined at their mid-point.

The third forearm marker was attached on the proximal ulna at a palpable point slightly distal to the tip of the olecranon. This was similar to the positioning used in the upper limb study of Williams (1996).

In addition to these, the lateral (LE) and medial (ME) epicondyles of the humerus were also located during anatomical calibration. The elbow joint centre was defined at their mid-point.

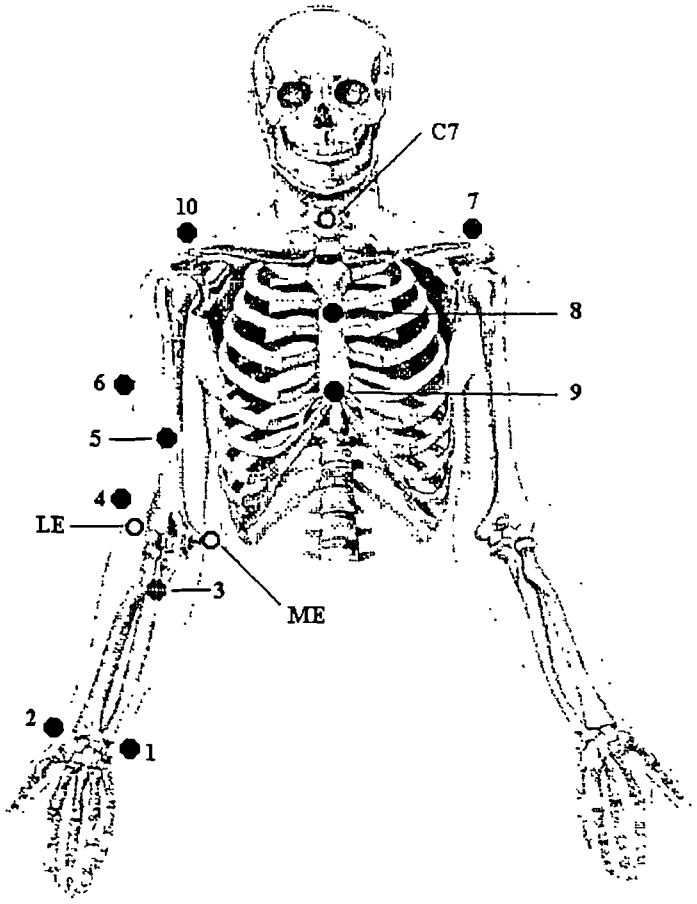

Fig 6.1 Surface fixed marker locations.

6.3.9 Markers attached to the upper arm

Three markers were attached on the upper arm as shown in Fig. 6.1. Again similarly to the work of Williams (1996), a marker was placed

approximately over the insertion of the deltoid muscle on the proximal humerus and another approximately over the insertion of the brachioradialis muscle on the distal humerus.

A third marker was attached on the lateral side of the biceps at a position approximately midway along a line connecting the other two markers on the upper arm and anterior to this line with the arm in the anatomical position.

In addition to these, the lateral and medial epicondyles, palpable at the distal end of the humerus, were located during anatomical calibration in order to allow location of the elbow centre at their mid-point and definition of the humeral longitudinal axis.

According to Keogh & Ebbs (1984), the medial epicondyle is the easily palpable distal extremity of the medial supracondylar ridge and is more easily palpated from the posterior aspect, being masked anteriorly by the common origin of the forearm flexor muscles. The lateral epicondyle is also more easily palpable from behind, being masked anteriorly by the common origin of the forearm extensor muscles.

6.3.10 Markers attached to the trunk

Four markers were placed on the trunk during testing as shown in Fig. 6.1, three of these being used for the definition of the trunk embedded frame. The first marker was placed over the left acromion (the curved continuation of the spine of the scapula) which, as described in Keogh & Ebbs (1984) is subcutaneous and is easily palpable in the summit of the shoulder. The tip of the acromion is the most anterior point and is readily palpated about one finger's breadth lateral to the lateral end of the clavicle.

The second marker was attached approximtely over the the xiphoid process, which according to Moore & Agur (1996) lies in a slight depression where the converging costal margins form the infrasternal angle (the angle between ribs and xiphoid).

According to Backhouse & Hutchings (1998), the manubrium slopes a little in comparison to the vertical sternum below, giving the join between them a slight palpable angulation, the sternal angle.

With the subject standing vertically with their back against the wall, a third marker was attached over the manubrium. The most suitable of the lightweight wand mounted markers was selected and its attachment position adjusted until it lay vertically above the xiphoid marker, measured using a spirit level. Establishing a vertical line between the xiphoid and manubrium markers allowed the definition of the trunk vertical axis between these.

Additional to these, the prominent vertebral spine of the seventh cervical vertebra (C7) was located during anatomical calibration. Moore & Agur (1996) state that the tips and spinous processes of some cervical and all thoracic vertebra are palpable when the vertebral column is flexed. Keogh & Ebbs (1984) describe the spine of C7 as the upper of the two prominences found in the root of the neck, the lower being the spine of T1. The spines can usually not be seen but can be felt. With the subject bent forwards the spines project more and can be identified.

A fourth trunk marker was attached over the right acromion. This marker was used to identify the location of the centre of rotation of the glenohumeral joint to allow the definition of the humeral longitudinal axis. The process of locating the glenohumeral rotation centre is discussed in detail in section 6.5.4.

6.3.11 Anatomical calibration

Section 6.3.7 describes the definition of 'technical' embedded co-ordinate frames assumed rigid with the underlying bone, from skin-fixed marker arrangements which may be arbitrary and non-repeatable in their relationship to the bone.

A requirement of this technique is that a preliminary "anatomical calibration" as described by Cappozzo et al (1995) be carried out. In this process the geometrical relationships between the surface fixed technical markers and selected bony anatomical landmarks are found. Knowing or assuming the relationship between these landmarks and the associated joint centres then allows the definition of the bone embedded 'anatomical' reference frames, constructed in relation to these centres.

The relationship between the defined technical frame and the chosen anatomical landmarks can be found under the most advantageous conditions,

not necessarily during limb movement, as the anatomical landmark co-ordinates should be constant with respect to the embedded technical frame. Points may thus be tracked which would normally be obscured from view or which might cause the motion to become unnatural if a marker was attached.

The anatomical calibration may be carried out by attaching temporary markers over the anatomical landmarks as well as the usual technical markers elsewhere, and recording a single frame. By calculating the three-dimensional co-ordinates of all the markers, the position of the bony landmarks with respect to surface technical markers could be determined.

Prior to continuing with the process of filming the motion the temporary anatomical landmark markers would be removed, their location in reference to the surface markers being saved on the single frame. Assuming that the skin-fixed marker array is rigid with the underlying bone, the location of the anatomical landmarks could thus be calculated at any time during movement. Such a method was used by Schmidt et al (1999a, 1999b).

As an alternative to attaching temporary extra markers to locate the positions of the anatomical landmarks in relation to the technical markers, a pointer can be used, to which are affixed two markers of known separation and distance from the pointer tip. The tip of the pointer would be placed on the anatomical landmark allowing both the pointer markers and the surface markers to be visible. Again a single frame would be recorded and the location of the anatomical landmarks calculated using the reconstructed image before proceeding with filming of motion.

The latter method was chosen for the purposes of the upper limb motion study, having the benefit of allowing calibration of markers in awkward positions which might be obscured from the view of the camera using the first method. Using a pointer also removes the need to incorporate a correction for the size of the marker when locating the anatomical landmark, as its tip rests directly upon it.

A pointer was constructed from a 79cm long, 6mm diameter steel rod painted black, to which were attached two 35mm reflective markers. The first marker was attached at a distance of 25cm from the pointer tip, the second a further 25cm along the length of the pointer.

During the anatomical calibration process, subjects were asked to flex their elbow to around 90° and place their forearm in the neutral forearm pronation position defined for the current study (90° pronated from the 'anatomical position' forearm position).

6.3.12 Filming the activities

Video recording took place using four cameras, initially for the purposes of anatomical landmark calibration and then during performance of the selected activities. A requirement that had to be met in order to combine simultaneous camera views using the APAS, was that all cameras must record a single distinct event called the synchronising event. This event had to be seen by all cameras simultaneously in order to time match the image sequences.

This was achieved using an LED system as shown in Fig 6.2, similar to those used by Scholz & Millford (1993) and Payton & Bartlett (1995). Four LEDs were connected to a purpose made timing device which allowed varying durations of LED firing, between 0.04s and 1s depending on the selected data sampling rate. The LEDs could be placed anywhere in the test volume to maximise their visibility to each camera and triggered simultaneously.

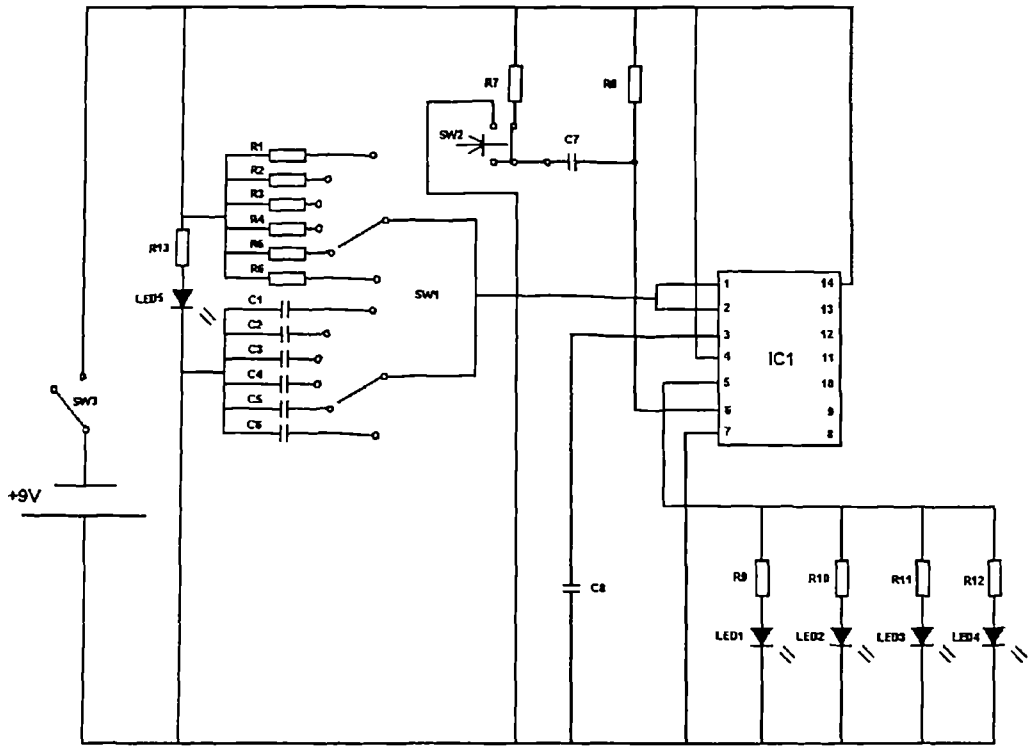

Fig. 6.2 Circuit diagram for LED synchronising device.

Where :

IC1 =	Timer - NE556N	R6 =	910K
SW1 =	2 pole 6 way (RS320-685)	R7, R8 =	10K
SW2 =	Microswitch (1NO,1NC)	R9 - R12 =	330K
SW3 =	1 pole rocker (320-017)	R13 =	470K
LED 1-5 =	Std 5mm red	C1, C3, C6 =	1000nF
R1 =	36K	C2 =	2200nF
R2 =	33K	C4 =	4700nF
R3 =	130K	C5 =	1500nF
R4 =	39K	C7 =	1nF
R5 =	300K	C8 =	10nF

As discussed in Section 6.3.3 a fixed point was also placed within the test volume. Details of the activities the subjects were asked to perform and the protocol for each of these are discussed in Section 8.1.

6.4 An overview of the APAS data processing procedures

6.4.1 APAS analysis - obtaining the marker co-ordinates

The APAS software modules described in Section 6.2 were used after filming of the activities in order to obtain the three-dimensional co-ordinates of the markers through time.

The 'Capture' module described in Section 6.2.2 was used to create an image file from the recorded activities from each camera, as well as capturing images for the calibration frame and anatomical calibration process.

When capturing the motion data the repetition for analysis was selected and some images from the previous and subsequent cycles captured in order to allow data leading in and out of the selected repetition.

For the purposes of the anatomical calibration process, four frames of data were captured for each of the three landmarks located.

The image sequences captured were digitised using the software described in section 6.2.2. Four views were shown on the monitor simultaneously for 3D digitising and a digitised sequence was created using a combination of the automatic and manual digitising features.

In addition to digitising the subject markers and fixed point, the control point locations used to calibrate the image space were also digitised for each camera view. The known Cartesian co-ordinate locations of each of the control points in relation to the selected calibration frame origin were also entered in the same order in which their images were digitised. During the digitising process, the frame in each view showing the LED synchronising device to be active was noted to allow synchronising of the data.

The transformation module described in section 6.2.3 was then used to carry out the DLT process on the digitised image sequences, using the actual measured locations as well as the digitised co-ordinates of the control points. This module utilised the defined synchronising event (LED flash) from each of the views as a basis for time matching the sequences. The time for each frame in each view was adjusted relative to the synchronising event so that in all four views the synchronising events occurred at the same absolute time.

The cubic spline algorithm from the Smoothing module described in section 6.2.4 was considered sufficient for positional data and applied on the transformed data. This algorithm is based on traditional spline function theory, but enhanced to allow approximate fitting rather than the traditional exact fitting to the data points. By viewing the marker acceleration curves, the extent of random error remaining in the data could be determined and smoothing values were adjusted to reduce this.

The printing module described in section 6.2.5 was then used to output the three-dimensional marker co-ordinates in the global laboratory frame through time, along with their velocities and accelerations. The output data were transferred into the "Excel" package where a macro was written to select the co-ordinate data for each marker, the velocity and acceleration data being disregarded. The macro arranged this data in a suitable format before saving it to a file for input into several MATLAB procedures for further analysis.

6.5 An overview of the MATLAB data processing procedures

After obtaining the marker co-ordinates through time the next stage in the process was to define the local segment embedded Cartesian frames and from these to calculate the inter-segment angles, forces and moments.

The necessary analyses were carried out using MATLAB™ routines which were a combination of newly written and public domain routines as well as some adapted from sources in literature. Routines that fall within the latter categories are credited to their original author where appropriate.

The "apas.m" file orchestrates the analysis process, reading in the files output by the Excel macro and running the analysis procedures.

6.5.1 Obtaining landmark locations from anatomical calibration

In order to obtain the three-dimensional co-ordinates of the lateral and medial epicondyles and the seventh cervical vertebra, information from the frames captured for each landmark were averaged. A vector was defined between the two pointer markers and this vector was then added to the pointer marker nearest its tip. Thus the pointer tip and therefore the bony landmark to which it was applied was located.

Each of the three landmarks was then related to an embedded technical frame, C7 to the trunk frame and the epicondyles to both the upper arm and forearm frames. The definitions of these embedded technical frames are given in the following section.

6.5.2 Defining the embedded Technical frames

Embedded technical frames were defined in relation to the surface fixed markers with one marker selected as the origin for the frame. For each segment two vectors were defined between one of the three attached markers and each of the other two by the subtraction of their position vectors in the laboratory frame.

The two unit vectors then defined a plane and their cross-product gave the normal to this plane. By taking the cross-product of this normal vector with one of the two original vectors it was possible to obtain three orthogonal unit vectors related to the underlying bone, as required.

For the trunk (Fig.6.3) the xiphoid (XI) marker was selected as the origin. A vector was defined from XI to the manubrium (MA) marker and this was taken as the trunk technical z-axis (Ttz). Another vector was defined from XI to the left acromial (LA) marker (Ttx'). By finding the cross product of Ttx' and Ttz it

was then possible to calculate the trunk technical y-axis (Tty). By finding the cross product of Tty and Ttz it was then possible to calculate the trunk technical x-axis (Ttx).

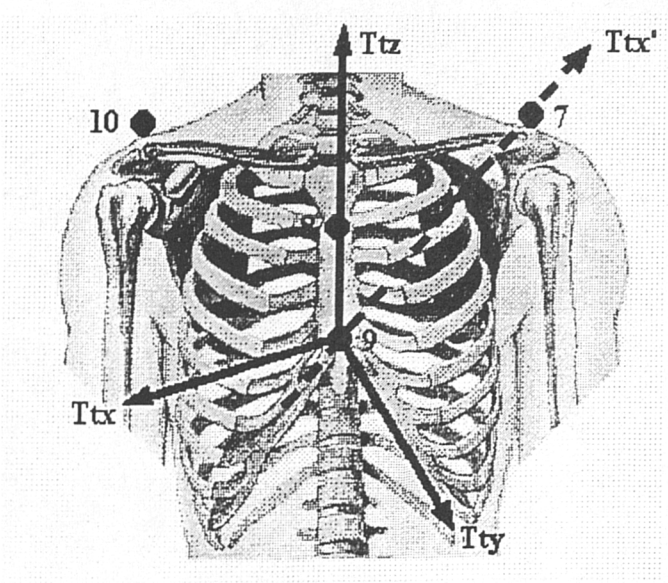

Fig. 6.3 Trunk embedded 'technical' axes.

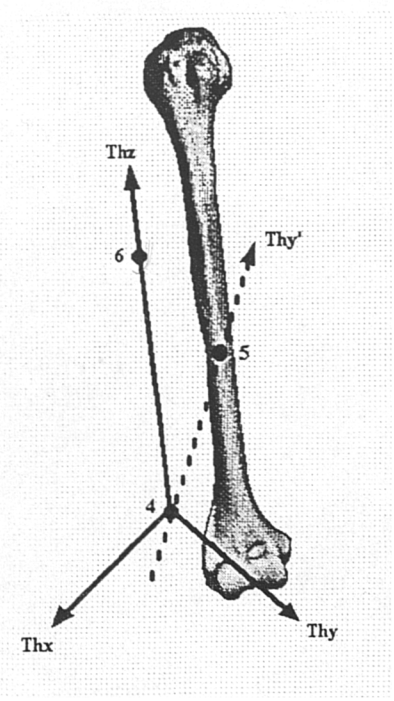

Fig. 6.4 Upper arm embedded 'technical' axes.

For the upper arm (Fig.6.4) the brachioradialis insertion (BI) marker was selected as the origin. A vector was defined from BI to the deltoid insertion (DI)

marker and this was taken as the humeral technical z-axis (Thz). Another vector was defined from BI to the biceps (BB) marker (Thy'). By finding the cross product of Thy' and Thz it was then possible to calculate the humeral technical x-axis (Thx). By finding the cross product of Thz and Thx it was then possible to calculate the humeral technical y-axis (Thy).

For the forearm (Fig.6.5) the ulnar styloid (US) marker was selected as the origin. A vector was defined from US to the radial styloid (RS) marker and this was taken as the forearm technical x-axis (Tfx).

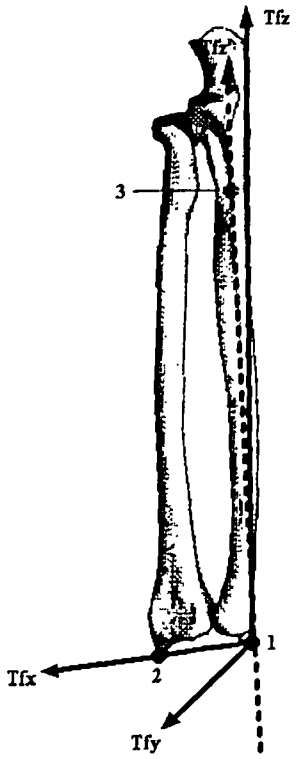

Fig. 6.5 Forearm embedded 'technical' axes.

Another vector was defined from RS to the proximal ulna (PU) marker (Tfz'). By finding the cross product of Tfz' and Tfx it was then possible to calculate the forearm technical y-axis (Tfy). By finding the cross product of Tfx and Tfy it was possible to calculate the forearm technical z-axis (Tfz).

Each of the trunk, humeral and forearm technical axes were then unitised, by dividing each of them by their magnitude. The orientation between the global and technical frames for any sampled instant could then be calculated.

The reconstruction of the motion of each bone in the global reference frame involved estimating, at each sampled instant throughout the motion, the position of each of the bony anatomical landmarks by using the measured co-ordinates of the markers which formed the technical cluster.

From anatomical calibration, the transformation matrix that linked the global and technical frames was known, as well as the locations of the epicondyle and C7 landmarks in the global frame. It was then possible to calculate the locations of these landmarks in relation to the technical frames by dividing their position vectors in the global frame by the calculated transformation matrix.

This then allowed the definition of the bone embedded anatomical frames as described in the following section.

6.5.3 Defining the embedded Anatomical frames

Knowing the co-ordinates of the epicondyle and C7 bony anatomical landmarks in relation to the technical frames from anatomical calibration, it was possible to define embedded anatomical frames in relation to the technical frame as opposed to the global laboratory frame.

For the trunk (Fig.6.6), the xiphoid (XI) marker was chosen as the origin of the embedded anatomical frame. The longitudinal anatomical axis (Atz) was defined first as lying along the line connecting the xiphoid and manubrial markers, the same as the trunk technical z-axis. Another vector was defined from the xiphoid marker to the C7 landmark identified during anatomical calibration in relation to the trunk technical frame (Aty'). By finding the cross product of Atz and Aty' it was then possible to calculate the trunk anatomical x-axis (Atx). By finding the cross product of Atz and Atx it was then possible to calculate the trunk anatomical y-axis (Aty). Each of the trunk anatomical axes were then unitised.

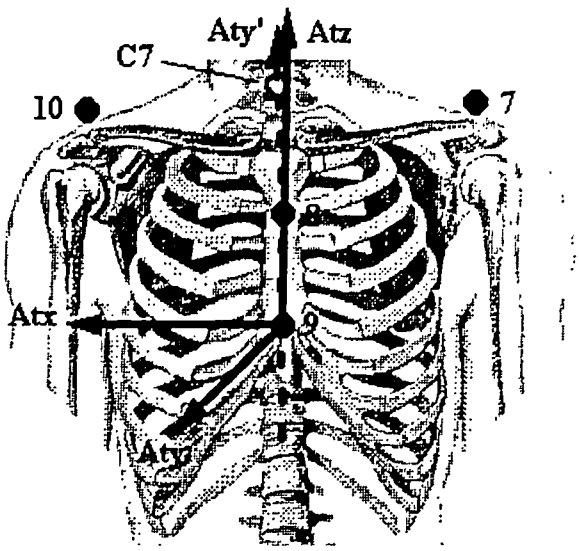

Fig. 6.6 Trunk embedded 'anatomical' axes.

The location of the right acromial (RA) marker was identified in relation to the trunk anatomical frame. From this location and using the method discussed in section 6.5.4, the glenohumeral centre was identified in relation to the trunk frame. It was then possible to find the relationship between trunk anatomical and humeral technical frames and thus define the glenohumeral centre in relation to the humeral technical frame.

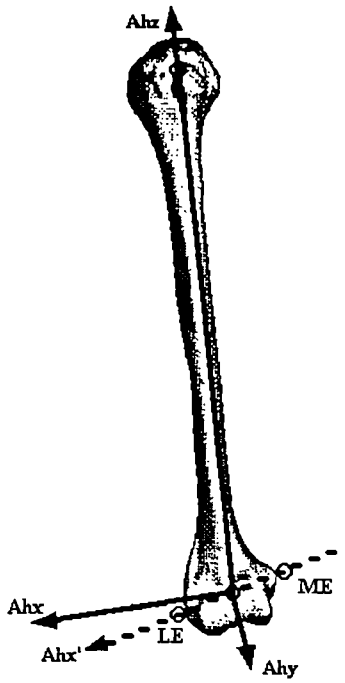

Fig. 6.7 Upper arm embedded 'anatomical' axes.

The embedded humeral anatomical frame (Fig.6.7) could then be defined, the elbow joint centre being chosen as its origin. The longitudinal anatomical axis (Ahz) was defined first as lying along the line connecting the elbow and glenohumeral centres, identified in relation to the humeral technical frame during anatomical calibration. Another vector was defined from the ME landmark to the LE landmark (Ahx'). By finding the cross product of Ahz and Ahx' it was then possible to calculate the humeral anatomical y-axis (Ahy). By finding the cross product of Ahy and Ahz it was then possible to calculate the humeral anatomical x-axis (Ahx). Each of the humeral anatomical axes were then unitised.

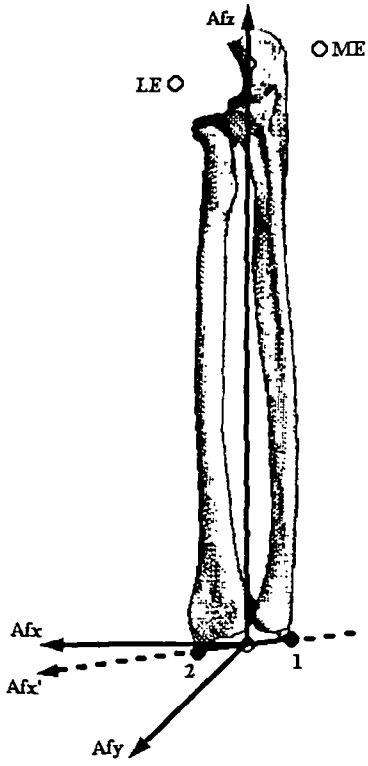

Fig. 6.8 Forearm embedded 'anatomical' axes.

For the forearm (Fig. 6.8) the wrist joint centre was chosen as the origin of the embedded anatomical frame. The longitudinal anatomical axis (Afz) was defined first as lying along the line connecting the wrist and elbow centres. The latter was defined as the mid-point of the medial epicondyle (ME) and lateral epicondyle (LE) landmarks in relation to the forearm technical frame, identified during anatomical calibration, the former as the mid-point of the RS

and US markers. Another vector was defined from the US marker to the RS marker (Afx'). By finding the cross product of Afz and Afx' it was then possible to calculate the forearm anatomical y-axis (Afy). By finding the cross product of Afy and Afz it was then possible to calculate the forearm anatomical x-axis (Afx). Each of the forearm anatomical axes were then unitised.

Having defined the anatomical axes, the transformation matrices relating the technical and anatomical embedded frames could be found, similarly to the transformation between global and technical frames.

The position of the anatomical landmarks was assumed to be invariant with respect to the technical frames. Thus at any sampled instant, the three-dimensional surface marker locations could be found. The embedded technical frames could be defined in relation to these and the embedded anatomical frames found knowing the transformation from technical to anatomical frames.

To this stage in the analysis process, all manipulations were carried out using the 'tech.m' MATLAB procedure, which takes as input the skin-fixed and pointer marker co-ordinate information and outputs the transformation matrices between technical and anatomical embedded frames. This includes a calculation of the glenohumeral joint centre as discussed in the following section.

6.5.4 Defining the centre of the glenohumeral joint

In order to define the humeral anatomical embedded frame it was necessary to locate a landmark representing the centre of rotation of the glenohumeral joint, in line with the recommendations of the International Society of Biomechanics (ISB) Standardisation Committee Recommendations (Van der Helm & Dapena (1993), Van der Helm (1997)).

Van Der Helm et al (1992) estimated the position of the rotation centre of the humerus with respect to the scapula by calculating the location of the centre of a sphere fitted to the glenoid, using the radius of a sphere fitted to the humeral head. This approach was first suggested in the earlier work of Van Der Helm et al (1989), who found that the articular surfaces of the glenohumeral joint could be assumed to be two concentric spheres.

Fourteen shoulders from seven cadaver specimens were studied and their estimated glenohumeral rotation centre was found to be laterally, inferiorly and anteriorly displaced from the most posterior palpable point on the acromioclavicular joint as given in Table 6.4. From the data given in the paper the average distance between acromion and elbow centre was 35.43cm, which corresponds well with the later data of Veeger et al (1997).

It has been suggested that an alternative to finding the joint centres through marker positioning, is to locate a functional joint centre by moving the limb in question and calculating the centre of rotation of this movement. Such a method had been proposed by Cappozzo (1984), (1991) for locating the "functional" joint centre of the hip.

Wang (1996) modelled the glenohumeral joint as a ball and socket joint and located its 'functional' centre with respect to surface landmarks. This was carried out by minimising the sum of the square distance from an arbitrary point in space to finite helical axes calculated from data obtained using a two camera, infra-red optoelectronic system.

Five healthy subjects aged between 17 and 47 were told to sit erect in a seat, their backs supported, torsos stationary. Upper arm circumduction movements were repeated three times, limited to a level of humeral elevation inferior to 90°. The calculated average centre of rotation in relation to the acromio-clavicular surface point is given in Table 6.4, relative to a set of axes that coincide with those in which the other results are quoted.

Veeger et al (1997) used a similar method, in their study of five upper extremity specimens from four fresh cadavers and carried out a similar procedure to that of Van Der Helm et al (1992) in calculating the centre of a sphere fitted to the glenoid.

Keeping the scapulohumeral region intact, the scapulae of the specimens were mounted on a measuring board and the relative movement between scapula and humerus analysed. This was carried out using an electromagnetic tracking system, the sensors of which were fixed on the shafts of the humerus, radius and ulna as well as on the spine of the scapula.

The rotation centre of the glenohumeral joint was determined during passive abduction/ adduction, flexion/ extension and internal/external rotation

of the humerus. Three trials for each motion were carried out, each trial involving two full cycles of the motion. Instantaneous helical axes (IHAs) were determined for the shoulder from the recorded data. From the calculated IHAs the optimal pivot point was found.

After studying the humeral motion, positional information for various bony structures was found by digitising their locations during dissection of the cadaver specimens. Joints were disarticulated and muscles removed while leaving the electromagnetic sensors untouched. The locations of the bony structures were expressed in the global reference frame of the electromagnetic tracking system, thus allowing direct comparison of their positions with those on adjacent body segments and the joint rotation centres.

Resulting locations for the glenohumeral centre in relation to the acromion from this process are given in Table 6.4, after manipulation of the data in order to relate them to standard anatomical axes. Veeger et al (1997) state that in fixing the scapulae to the experimental apparatus, they were rotated -45° around the Z axis and 20° around the X axis in comparison to the average resting position of the scapula, taken from the work of Pronk (1991) who measured the rest positions of the scapula and clavicle in eighteen subjects. A least-squares method was used to calculate a mean orientation matrix relating the mean scapular resting position to a global anatomical co-ordinate system centred at the jugular notch.

Initially in the process of manipulating the data of Veeger et al (1997) it was assumed that the rotations of the scapula from its resting position occurred in the order in which they are given in the original paper, first about the Z-axis and then about the X-axis. The order of rotations was checked by attaching a scapula to a jointed arm in a similar position to the test position of Veeger et al (1997) and carrying out the two possible sequences of the two rotations in order to return the scapula to its resting position. It was found that the given order (X then Z, as this is the reverse direction of the rotations quoted in the paper) oriented the scapula in a reasonable representation of its resting position.

The process was later modified to improve its accuracy using the data of Pronk (1991). The embedded frame of Pronk (1991) was defined in each of the

scapulae of the five cadavers studied by Veeger et al (1997). The differences between global frames were corrected and thus it was possible to rotate each of the scapular data sets of Veeger et al (1997) to lie in the resting position as defined by Pronk (1991). After carrying out this process it was found that the order of rotations was the same as that quoted by Veeger et al (1997), but that the magnitudes varied greatly form those quoted for all except one subject.

On investigating the data it was also found that the left arm data for the second specimen had not been corrected by Veeger et al (1997) for the reversal of the y-axis due to the attachment of the scapula facing in the opposite direction to the right arm specimens. The co-ordinates were adjusted to account for this and the resulting locations for the corrected glenohumeral centre locations in relation to the acromion from this improved process are again given in Table 6.4.

Meskers et al (1998a) outlined a method for the in vivo calculation of the rotation centre of the glenohumeral joint. Their technique uses linear regression equations based on bony landmarks and surface data points of the scapula and humerus, measured on thirty-six scapulae and humeri sets from nineteen cadaver specimens. This technique was specifically developed for those studies where palpation techniques are utilised for the location of scapular bony landmarks in three dimensions, for example in the work of Meskers et al (1998b). The position of the glenohumeral rotation centre shown in Table 6.4 was first estimated using the method of Van Der Helm et al (1992).

The co-ordinates given in Table 6.4 from the work of Meskers et al (1998a) are expressed in relation to a scapular co-ordinate system with its origin at the acromion, x-axis along the line from trigonum spinae (TS) to the most dorsal point of the acromioclavicular joint (AC), z-axis perpendicular to the plane through TS, AC and the most inferior point of the scapula, the inferior angle (AI) and the y-axis the cross-product of the x and z axes.

The authors constructed a regression model using linear least squares to describe the relationship between the rotation centre and palpable landmarks on the scapula in their local scapular co-ordinate system. They validated this model against a sample of the original cadaver data and concluded that an accurate in vivo prediction of the glenohumeral rotation

centre could be obtained from palpable bony landmarks when required for kinematic studies of the upper limb.

Paper	Acromion to :	X (cm)	Y (cm)	Z (cm)	Mag. (cm)
Van der Helm et al (1992)*	Humeral Head	1.79	3.39	-4.44	5.87
Wang, X.G. (1996)‡	Rotation centre	1.38	0.82	-3.66	3.9965
	range	-0.29-2.68	-0.02-1.38	0.63	1.08
Veeger et al (1997)**	Glenoid	0.97582	-0.66234	-3.86238	4.038428
	SDev	1.139193	1.158843	0.693073	1.766643
Veeger et al (1997)***	Humeral Head	0.74668	-0.34984	-4.4593	4.534895
	SDev	1.179747	0.610679	0.82123	0.629503
Veeger et al (1997) ****	Rot. Centre	0.68448	-0.82444	-3.7289	3.879808
	SDev	0.946897	0.809161	0.847892	1.506743
Veeger et al (1997)!(corr)	Rot. Centre	0.9045	-0.4333	-3.8745	4.0
	SDev	0.4631	0.3907	0.8349	1.03
Meskers et al (1998a)*****	Humeral Head	0.998†	1.90†	-4.58†	5.06
	±	0.416	0.756	0.48	0.99

Table 6.4 Relationships between : Most posterior palpable point on the acromioclavicular joint and centre of sphere fitted to glenoid with radius of sphere fitted to humeral head (*, *****). Surface point of acromioclavicular joint (‡). Most cranial point on the acromioclavicular joint and centre of sphere fitted to glenoid (**) and sphere fitted to humeral head (***). Most cranial point on the acromioclavicular joint and calculated rotation centre of glenohumeral joint (****,!). († - co-ordinates expressed in non-standard frame - see text)

Laursen et al (1998) defined the centre of the glenohumeral joint as being 2cm below the inferior edge of the acromion in their study of the calculation of shoulder muscle forces based on electromyographic studies. The source of this information is given as the paper by Iannotti et al (1992), though in this paper no direct measurement of this distance was made and it appears that Laursen et al (1998) may have used the dimensions given for the radius of the humeral head.

Wang et al (1998) used a sonic digitiser in their study of upper arm axial rotation. The average centre of rotation of the 'lumped' shoulder joint between the thorax and the humerus was defined as the proximal andmark for the definition of the humeral embedded axis. This point was found as the centre of

a sphere to which the measured elbow positions were fitted using an optimisation procedure, with the acromio-clavicular joint as an initial estimate.

An alternative method to those above would be the direct estimation of the glenohumeral joint in relation to a surface fixed marker or markers. This approach has been adopted by several authors (Sprigings et al (1994), Rao et al (1996), Cheng (1996)) as shown in Table 6.2. Other authors (Runciman (1993), Van der Helm & Pronk (1994), Williams (1996)) have avoided using the glenohumeral centre to define the longitudinal axis of the humerus, by locating this axis directly in relation to surface markers, as shown in Table 6.3.

Cheng (1996) used a method for determining the centre of the shoulder joint developed by Nicol (1977). A double marker was attached on the acromial process. By extrapolating the line joining the markers by the radius of the shoulder joint ball, the centre of the joint could be located.

The radius of curvature of the shoulder joint ball was defined as the distance from the acromial process to the estimated centre of the glenohumeral joint, using the semicircular form of the surface contour at the shoulder region. The centre of shoulder ball was palpated with the upper arm in different positions, and the radius of shoulder ball measured in each position manually using a ruler. The resulting measurements were then averaged to find the required radius.

The key elements in the successful use of such a method would seem to be that the double marker be as light and as securely attached as possible in order to minimise swinging of the marker and that it should be carefully positioned on the acromion to minimise error in the location of the glenohumeral centre.

Schmidt et al (1999a) defined the centre of the shoulder to be 7cm inferior to a marker attached on the acromion, this distance being the average of visually determined distances using a ruler. Schmidt et al (1999b) also used a method similar to that of Wang et al (1998), locating the functional centre of the glenohumeral joint during shoulder flexion and abduction.

The data in Table 6.4 allows an estimate of the distance between acromion and glenohumeral rotation centre to be made, and thus gives an idea of the expected value when measuring the radius of the shoulder joint ball.

From the given data, the distance between the acromion and the glenohumeral centre is between 3.87cm and 5.87cm with an average of around 4.5cm.

On considering the options available it was decided not to utilise the method of identifying the humeral longitudinal axis directly as carried out by Runciman (1993), Van der Helm & Pronk (1994), Williams (1996). This method might be prone to the errors in marker positioning, differing soft tissue bulk and does not include the location of the glenohumeral centre as suggested in the ISB recommendations (Van der Helm & Dapena (1993), Van der Helm (1997)).

The method of Sprigings et al (1994) was dismissed as its accuracy again appears to be dependent on marker placement and would be affected by muscular movement and differing tissue bulk. The method of Rao et al (1996) was dismissed as it involves the use of a standard angular correction which cannot be assumed correct for all subjects. The method of Cheng (1996) was dismissed as it seemed prone to errors in positioning and angle of attachment of the double marker and the measurement of the radius of the shoulder joint ball. The processes used by Wang (1996) and Veeger (1997), locating the rotation centre through the calculation of instantaneous or finite helical axes are promising, though would require the addition of an extra stage in the analysis process.

In order to limit the inconvenience to the subject in terms of time taken to film the tests and minimise the time taken to analyse the data, it was decided that the addition of such an extra phase during testing should be avoided.

The similar method of Wang et al (1998), locating the centre of rotation of the 'shoulder' is not as suitable however as the calculated centre over extensive upper limb movements would include a large component due to scapular movement. Again the location of the 'shoulder' as opposed to GH centre is a deviation from the ISB recommendations (Van der Helm & Dapena (1993), Van der Helm (1997)).

The method may be adapted to locate the centre of the glenohumeral joint by the exclusion of certain movements as in the earlier work of Wang (1996), though again an extra stage in the analysis process would be required.

The regression equations of Meskers et al (1998a) were considered unsuitable as they are based on a process of estimation from scapular

landmarks, which are not easily identified with surface fixed markers. This process would also require positioning of cameras both anteriorly and posteriorly to the subject which was not convenient in the laboratory arrangement.

It was finally decided that the most suitable method of locating the glenohumeral centre, taking into account the limiting factors of laboratory equipment and test duration would be to use existing data from previous studies. A standard practice for the calculation of segment masses, centres of mass and inertias in biomechanical studies as discussed in Chapter 3, has been the use of generalised values obtained during anatomical studies and it was decided to apply a similar method in the location of the glenohumeral centre.

On selecting the previous work as a basis for this process the data of Meskers et al (1998a) is unsuitable as it is given in reference co-ordinate frame which is not in line with a standard global frame. After applying the equations of Meskers et al (1998a) to the cadaver data of Veeger et al (1997) it was also found that the calculated results varied from those measured.

It was decided to use those data on a calculated rotation centre (Wang (1996), Veeger et al (1997)) as opposed to fitting of spheres to the articulating surfaces (Van der Helm (1992)). The data of Wang (1996) and Veeger et al (1997) correspond very well for the Z (vertical) co-ordinate and reasonably well for the X (medial-lateral) co-ordinate. The correspondence is not so close for the Y (anterior-posterior) co-ordinate, though they are within the error limits of each other. This difference may be due to any variation in the definition of the acromial point, though there is a variability within the five individual data sets for both papers. The data of Veeger et al (1997) was finally chosen for several reasons.

Wang (1996) collected his data using only two cameras which as previously discussed is not the optimum arrangement. The resulting data, being based on marker locations through time, would be prone to the combined errors of marker movement and digitising errors.

The data of Veeger et al (1997), being based on a study involving the attachment of sensors directly to the bony elements of the upper limb and

scapula, would not be susceptible errors due to relative motion between skin and underlying bone. The scapula also remained fixed in this study and so no contribution could be made to the resulting data by scapular movement, not necessarily the case with the data of Wang (1996).

When adopting a generalised approach it is necessary to scale the data against known anthropometric dimensions, a process made possible by the extensive anthropometric information supplied by Veeger et al (1997) but not by the information given in Wang (1996).

The method for utilising the data of Veeger et al (1997) for the location of the glenohumeral rotation centre involved finding the vectors directly linking the most cranial point on the acromioclavicular joint with the rotation centre for each of the five sets of shoulder data, after re-locating the co-ordinate data in the scapular resting position of Pronk (1991).

These vectors were normalised in each case, by dividing them by an appropriate scaling dimension, the corresponding distance between the mid-point of the epicondyles (MP) and the acromion (AC) calculated from the cadaver data. This dimension was chosen after plotting the vector magnitudes against the MP-AC distance and finding a trend for the vector sizes to increase with increasing MP-AC distance. The resulting vectors were then averaged to give a normalised average position vector for the glenohumeral rotation centre with respect to the acromion.

Thereafter, the normalised vector can be multiplied by the measured distance between the mid-point of the epicondyles and the most cranial point on the acromioclavicular joint from any subject. This will yield the vector between the most cranial point on the acromioclavicular joint and glenohumeral rotation centre in relation to the trunk embedded frame. The average normalised position vector for the glenohumeral rotation centre in relation to the most cranial point on the acromion was found to be :

	[0.0261	-0.0126	-0.1115]
SDs	[0.0130	0.0111	0.0233]

The exact location of the joint centre of rotation will move with activity due to variation in the joint structures and articular surfaces which are not perfect curved surfaces. The location of a constant centre of rotation is therefore not truly representative of the joint behaviour. Because of this, the method presented is not ideal, but is considered reasonable and is similar to standard methods for the estimation of anatomical and anthropometric parameters in biomechanical studies.

The method is based on the definition of embedded scapular frames from accurate landmark locations from the cadaver study of Veeger et al (1997) and the definition of the scapular resting position from Pronk (1991) and is thus considered to represent a more rigorous location of the glenohumeral centre than alternative methods.

6.5.5 Calculation of transformation matrices

In order to calculate optimised transformation matrices between marker locations, the SVD based algorithm given in Söderkvist & Wedin (1993) and discussed in Section 5.3 was used as the basis of a MATLAB procedure, 'soder.m', included in the 'KineMat' toolbox of Reinschmidt & van den Bogert (1997). This toolbox is available for download on the International Society of Biomechanics (ISB) Internet site.

This procedure requires as input, the co-ordinates through time of three or more non-collinear marker points, expressed as the rows of a matrix. The singular value decomposition of a 3×3 matrix derived from the positions of the markers is then calculated. Output are the optimised 4×4 transformation matrices describing the rigid body segments.

According to Söderkvist & Wedin (1993), the advantages of this SVD algorithm are that it does not require an initial estimate for the unknown transformation parameters and is thus computationally efficient. It is also more stable in the presence of noise than other methods.

The 'soder.m' procedure was incorporated in the upper limb analysis process in order to allow calculation of transformation matrices. It was considered an advantage to include the flexibility in the analysis process to

allow optimisation if required and the procedure was incorporated for use in two ways.

The first was to optimise the segment positions and orientations in relation to an initial reference position and orientation obtained during anatomical calibration of C7. The transformations between global and anatomical frames were found for this reference data.

Thereafter the transformations linking the marker clusters at each instant to their initial position could be found using the optimisation process. The latter transformations were then multiplied into the initial transformations between global and anatomical frames, resulting in a sequence of transformation matrices describing, at each sampled instant, the orientation and position of the embedded anatomical frames in relation to the global laboratory frame.

The second use of the SVD procedure was to calculate transformation matrices in a non-optimising fashion where the embedded technical frames were simply defined in relation to the marker co-ordinate data with no correction for relative marker movement.

By using the unit vectors representing each of the axes of the technical frames as input to the SVD procedure, it was possible to calculate the transformation between these frames. As the transformations in this case were calculated between predefined axes and not a cluster of markers, the algorithm had no optimisation effect on the data.

6.5.6 Kinematic Analysis

The next step in the process of analysing the data was to calculate the joint attitudes through time from the 3D positions and orientations of the defined embedded frames.

The MATLAB procedure "tech2.m" was written to calculate the positions and orientations of the embedded technical frames with respect to global laboratory frame at each sampled instant and express these in terms of transformation matrices. Knowing the relationship between embedded technical and anatomical frames from anatomical calibration and calculation in the "tech.m" procedure, it was then possible to calculate the transformation matrices relating global and anatomical frames at each instant.

These matrices were then decomposed using a chosen angular parametrisation, several options being available as discussed in Section 5.4. The chosen sequence was the flexion-adduction-internal rotation sequence of the JCS. This choice was based on the results of preliminary testing, discussed in Section 7.4. As stated by Woltring (1994), this JCS convention was recommended by the Committee on Standardisation of the International Society of Biomechanics.

The angles were calculated in two ways in order to provide a check on the calculations. The first was to determine them directly from the calculated matrices using the 'Rzyxsolv.m' function from the Kinemat toolbox. The second method for calculating the angles was to employ the general algorithm for the JCS described by Cole et al (1993). The "cole.m" MATLAB procedure was written in order to carry out the calculation of the joint angles from the orientations of the embedded frame axes in the global frame.

6.5.7 Calculation of velocities and accelerations

Having calculated the joint orientations through time and prior to calculating the dynamic parameters associated with the movement, it was then necessary to find further kinematic variables, the joint velocities and accelerations.

The generalised cross validation based cubic spline filter of Hodgson (1994) was obtained from the author as two MATLAB routines "dpf.m" and "dpfsweep.m". The filter was tested against 5-point numerical differentiation for upper limb data and found to be superior in that it did not force the endpoint data to zero.

These MATLAB procedures were incorporated in the analysis program "numdiff.m". They enabled the filtering and differentiation of the joint angle data in order to obtain the joint angular velocities and accelerations in a similar process to that which forms the basis of the technique of Kane (1983). These velocities and accelerations were output directly, while also being utilised for the calculation of the upper limb dynamics discussed in the following section.

6.5.8 Dynamic analysis

Having calculated the kinematics, the next step in the analysis process was to calculate the dynamics involved in the activity under analysis. The "numdiff.m" procedure was written to carry out this process, taking as input the joint angles through time. Included in this procedure were the calculations of the various body segment parameters.

Segment lengths were calculated as the distance between proximal and distal joint centres when defining the embedded frames, for example from glenohumeral centre to elbow centre for the humerus.

Segment masses and centre of mass (CM) locations were calculated from the measured subject weight using the data from de Leva (1996a) discussed in Chapter 3. Finally, segment moments of inertia were calculated, again using the data of de Leva (1996a).

The next stage was to combine the kinematic information obtained as discussed in Sections 6.5.6 and 6.5.7, with the segment length, mass, CM, inertia and loading information in order to allow calculation of the 3-D external joint forces and moments.

6.5.9 The dynamic upper limb model

In order to calculate the external forces, a generalised dynamic model of the upper limb as a mechanical linkage was developed. Similar models have been described by Chèze et al (1996) and Barker et al (1997) for the glenohumeral and elbow joints. More recently Bao & Willems (1999) extended these to include the sternoclavicular and acromioclavicular joints.

The segments of the limb were modelled as rigid bodies using the D-H notation to specify the location and orientation of the axes of rotation, represented by revolute joints. Coincident degrees of freedom as found in the shoulder were represented using links with 90° link twist but zero link length.

The model consisted of three segments, representing the upper arm, forearm and hand, as shown in Fig. 6.9. Seven degrees of freedom were included, three at the shoulder, two at the elbow and two at the wrist. Fig 6.10 indicates the rotations represented by the model. The lengths of the upper arm

and forearm were defined by specifying a link offset equivalent to the appropriate dimension, the length of the hand by a link length.

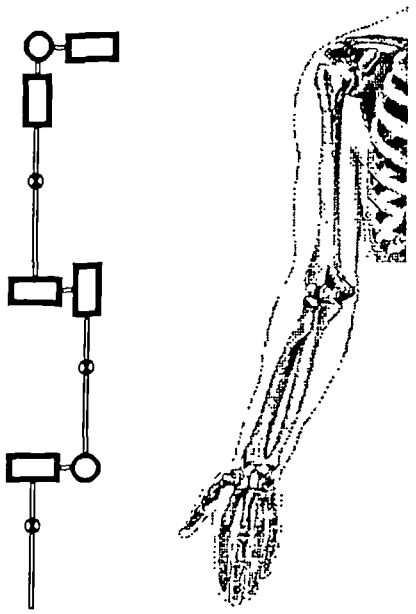

Fig 6.9 The modelled upper arm linkage and the anatomical structure. Rectangles and circles in bold represent rotations about axes parallel with and perpendicular to the page respectively.

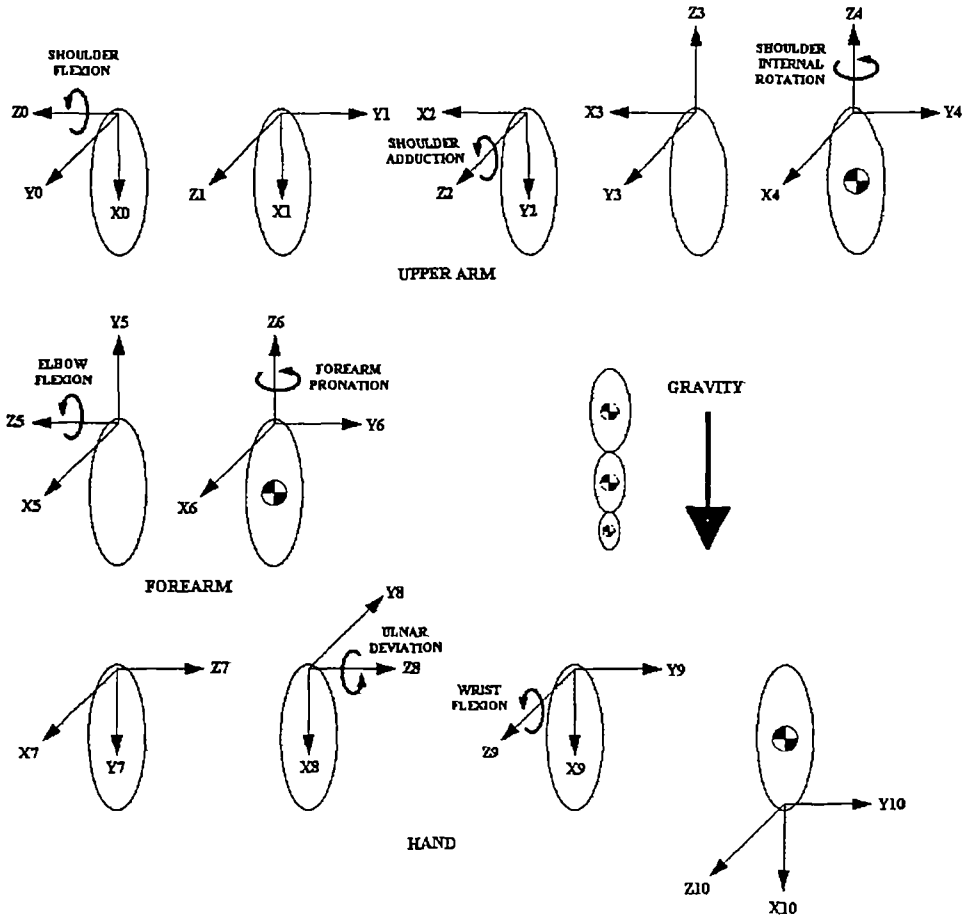

Fig 6.10 The motions represented by the upper arm linkage model

The first axis of rotation was defined as shoulder flexion as opposed to the shoulder adduction of Barker et al (1997). Thus the order of rotations of the model were made to correspond with the JCS sequence used to calculate the rotations at the shoulder.

A modification of the upper limb model was also developed to allow application of the JCS sequence at the wrist as shown in Fig 6.11. This modification was not adopted as no wrist angles were measured.

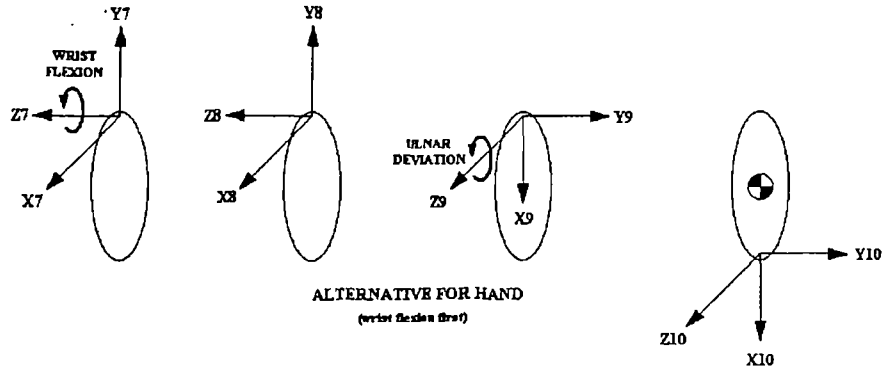

Fig.6.11 Modification to allow application of the chosen JCS sequence at the wrist

Having developed the link model of the upper limb, Barker et al (1997), used the Robotics Toolbox described by Corke (1995, 1996) in order to carry out inverse dynamics calculations. This toolbox comprises many functions required in robotics, the one used in this analysis being the "rne.m" routine which allowed computation of the inverse dynamics using the RNE formulation of the dynamic equations of motion described in section 5.7.

This procedure was modified to output calculated values of the forces at each of the upper limb joints relative to their local co-ordinate system. Also output were the joint moments required to achieve a given set of joint angles and linear and angular velocities and accelerations, at each point in the limb trajectory, as well as the forces and moments due to any additional hand load.

The inputs to the inverse dynamic process were vectors containing the previously calculated angular displacements, velocities and accelerations at each of the joints through time. A vector representing the standard acceleration due to gravity was also required, the value used being that

adopted in the International Service of Weights and Measures, 9.80665ms^{-2} (HMSO (1986)).

The other input was a 10×20 'dyn' matrix as shown in Fig 6.12, which completely described the kinematics and dynamics of the limb model using D-H parameters. Each row represents one link in the model, each column represents one of the necessary input parameters, though for the upper limb model only the first twelve columns are used, the final eight containing zeros.

The first four columns contain all the D-H parameter information for the construction of the linkage representing the upper limb, as discussed in Section 5.6. The fifth column (σ) defined the joints as revolute. Also shown are the motions represented by each defined link.

D-H Parameters						CM Locations			Inert.Mmts.			
α	a	θ	d	σ	mass	r_x	r_y	r_z	I_{xx}	I_{yy}	I_{zz}	Functional Motion
-pi/2	0	θ_1	0	0	0	0	0	0	0	0	0	Shoulder Flex/Ext
0	0	-pi/2	0	0	0	0	0	0	0	0	0	-
pi/2	0	θ_3	0	0	0	0	0	0	0	0	0	Shoulder Ab/Add
0	0	pi/2	0	0	uam	0	0	-uac	A	T	L	-
pi/2	0	θ_5	-ual	0	0	0	0	0	0	0	0	Shoulder Int/Ext Rotn
-pi/2	0	θ_6	0	0	fam	0	0	-fac	A	T	L	Elbow Flex/Ext
-pi/2	0	θ_7	-fal	0	0	0	0	0	0	0	0	Forearm Int/Ext Rotn
0	0	pi/2	0	0	0	0	0	0	0	0	0	-
pi/2	0	θ_9	0	0	0	0	0	0	0	0	0	Wrist Rad/Uln Dev.
0	hl	θ_{10}	0	0	hm	-hc	0	0	L	A	T	Wrist Flex/Ext

Fig 6.12 Matrix showing necessary content of 'dyn' matrix.

In the matrix given in Fig 6.12, ual, fal and hl are the upper arm, forearm and hand lengths respectively, uam, fam and hm their masses and uac, fac and hc the longitudinal locations of their centres of mass with respect to the co-ordinate frame. A, T and L are the mass moments of inertia about the Anteroposterior, Transverse and Longitudinal axes of each of the segments respectively. Any hand-held mass was added to that of the hand in the matrix.

The matrix differs from that of Barker et al (1997) due to the changes for the angular order at the shoulder. Other differences are the combining of the final two rows of the matrix as well as a reversal of the sign of the link twist of the eighth link.

The MATLAB routine 'numdiff.m' was written to calculate the various body segment parameters and then insert the values into a correctly formatted matrix before applying the RNE for the calculation of forces and moments.

Matrices of output data were then compiled for each test, containing all the angle, force and moment data. The 'plots.m' procedure was written to allow plotting of the trajectories of the wrist, elbow and shoulder centres, the angles, forces and moments through time at each of the joints and the resultant forces.

6.5.10 Normalisation of the data output

The 'data_sdd.m' MATLAB procedure was written to normalise angle, force and moment data to one hundred percentage points of a complete cycle.

Normalising time-series data is a convenient way of comparing time history curves and is a standard procedure in many biomechanical studies. Normalising is carried out in order to overcome offsets between structurally similar data curves due to differences in, for instance, the speed of performance of the movements between subjects. This normalisation then allows 'average' curves to be calculated without removing real properties of these curves.

The technique employed is a modification of that used by Williams (1996) who used the 'interpft' MATLAB command to normalise angle data. This function returns a vector of data of a specified length (100 samples for normalisation purposes), obtained by 1-D interpolation in the discrete Fourier Transform of the raw data vector, computed by another in-built MATLAB function.

The modifications made were to include normalisation of the force and moment data and to utilise an alternative MATLAB command, 'interp1'. This function was used to return a normalised vector, determined by cubic spline interpolation within the raw data vector to find the value of an underlying 1-D function. A comparison was made between the use of the two methods for interpolation of a sine function. The 'interp1' was found to be superior to the 'interpft' function in that the latter method introduced noisy 'end-effects' to the data whereas the former did not. Using the 'interp1' function it was possible to

re-sample the raw data to one hundred percentage steps between cycle start and end points selected on screen with a user controlled cursor.

Alternative, more complex normalisation methods are available, based on structural averaging (Wang & Gasser (1996), Sadeghi et al (1998)), dynamic time warping (Wang & Gasser (1997)) and also the 'local proportional scaling' technique of Kanatani-Fujimoto et al (1997).

For the purposes of the current study the performance of the cubic spline based technique in MATLAB was found to be sufficient after comparing the normalised angle, force and moment plots with those of the raw data. The normalised curves were found to accurately represent the curve patterns of the raw data.

6.6 Presentation of the data

For the purposes of plotting the normalised data, a Microsoft Excel macro was written which read in the normalised data matrices output from MATLAB and plotted graphs of the angles, forces and moments through time. A further macro was written which opened and read each of the normalised data sheets and plotted various graphs as given in Table 8.6, comparing data for each of the repetitions of a particular activity.

Where necessary the sample standard deviations (SD) were calculated. Based on a normal distribution a ±2SD boundary will contain approximately 95% of the observations at any point in the cycle, indicating how widely values are dispersed from the mean value and therefore the variability in that data. The SD was calculated using the "nonbiased" or "n-1" method in Equation 6.1.

$$SD = \sqrt{\frac{n\sum x^2 - (\sum x)^2}{n(n-1)}} \qquad (6.1)$$

The ±2SD boundaries were utilised as only fourteen sets of subject data were analysed. For larger data samples, more complex statistical analyses may be employed such as the 'Bootstrap' (Olshen et al (1989), Lenhoff et al (1999)) or 'Principal Components Analysis' (Jackson (1991), Deluzio et al

(1997)) methodologies. Each of these allows the calculation of confidence intervals based on the data curves in their entirety as opposed to breaking them into their individual data points as occurs when using the ±2SD boundaries.

6.7 Summary of methods

A four camera video-based motion analysis system was used to track 25mm diameter, reflective spheres attached at specific locations, three on each of the forearm and upper arm and four on the trunk. Selected anatomical landmarks were located in relation to these markers through anatomical calibration (Cappozzo et al (1995)). Activities were filmed, image sequences digitised and three-dimensional marker co-ordinates obtained.

Purpose-written MATLAB™ procedures incorporating some public domain routines (KINEMAT, Robotics Toolbox) were used to process and analyse the co-ordinate data. Transformation matrices were calculated using the optimisation process of Söderkvist & Wedin (1993).

Wrist and elbow centres were estimated as the mid-points of surface fixed markers and anatomical landmarks respectively and the shoulder centre using data adapted from the cadaver study of Veeger et al (1997). From the surface fixed markers and the anatomical landmarks it was then possible to define technical and anatomical embedded frames.

The Joint Co-ordinate System (JCS) of Cole et al (1993) was used to calculate joint orientations and the smoothing and differentiation filter of Hodgson (1994) employed in order to obtain the joint kinematics.

A model of the upper limb was constructed using the notation of Denavit & Hartenberg (1955), using similar robotics-based techniques to those of Chèze et al (1996) and Barker et al (1997).

This model combined joint kinematic data with segment inertia, mass and loading information to give the upper limb rigid body dynamics through the recursive Newton-Euler formulation of Luh et al (1980) incorporated in the Robotics Toolbox of Corke (1995, 1996).

Data were standardised to one hundred percentage points of a cycle using a cubic spline method in MATLAB and presented using Excel macros.

CHAPTER 7 : PRELIMINARY TESTING

7.0 Introduction

In order that the methods described in the preceding chapters might be used with confidence it was necessary to assess their accuracy and repeatability. As discussed in the following pages, this was carried out initially for some of the most basic APAS functions and then for the methodological and analytical techniques.

7.1 Testing of APAS 'skip' function

As discussed in section 6.2.1, the APAS Capture module for capturing image sequences from video tape allows varying sampling intervals through the selection of 'skip' values and the definition of a 'step delay'.

It was necessary to establish what ranges of step delay were necessary in order to make the skip values consistent with those specified. Any deviation from the specified values would lead to varying time steps between sampled data, introducing errors in data time histories and the process of calculating velocities and accelerations.

It was decided to compare sampled image sequences against known time steps. A video tape was obtained on which time codes had been read and recorded, allowing individual fields to be specifically identified. This then allowed the capturing of fields from the tape while providing visual evidence of the interval between each sample.

When capturing image sequences the first image was captured at 'zero time' as opposed to one specified skip from zero. Therefore there was an expected shortfall of the captured sequence in comparison with the theoretical time, equivalent to the number of images being skipped.

The results obtained are shown in Table 7.1 for the capturing of three hundred fields with a skip value of four (every fifth field captured). The expected timecode reading was thus thirty seconds minus four skipped fields, bearing in mind that fifty fields represent one second.

SKIP NO.	FRAMES	STEP DELAY	THEORY (secs)	TIMECODE (secs..fields)
4	300	150ms	30	29..46
4	300	125ms	30	29..46
4	300	115ms	30	29..46
4	300	112ms	30	29..46
4	300	111ms	30	29..46
4	300	110ms	30	17..26
4	300	109ms	30	16..06
4	300	100ms	30	15..25

Table 7.1 Results obtained from testing of skip value and step delay.

As can be seen, when the step delay was set equal to or below 110ms the skip function became unreliable. At the lower delay values there was insufficient time for the video capture mechanism to successfully skip the specified number of fields. This testing showed that skip values and therefore timing information were consistent with those specified at step delays of 111ms and above. For all further testing the step delay was set to a minimum of 200ms.

7.2 Robot arm testing of velocity measurement

The computation of velocity and acceleration values was necessary for the implementation of the dynamic model discussed in Section 6.5.9.

In order to test the accuracy of the APAS system in establishing the velocity of a moving target marker during a well defined movement, a 38mm diameter spherical plastic marker coated in reflective tape was placed on a wand in the grip a 'Stäubli Unimation Puma 700' robot arm.

The precise velocity of the motion of the robot arm could not be specified, only percentages of a maximum value. The arm was programmed to describe a horizontal or vertical arc across a range of velocities as given in Table 7.2. Its motion was analysed using the APAS, two cameras being used due to limitations of space around the robot arm. These were arranged at an intersection angle of approximately 90°.

Test No.	Plane of Arc	%ages of Maximum Velocity Tested	Angular Range	Approximate Radius of Curvature
1	Horizontal	20, 40, 60, 80 %	20°	1.00 m
2	Vertical	20, 40, 60, 80 %	30°	1.09 m
3	Vertical	20, 40, 60, 80 %	45°	0.95 m

Table 7.2 Details of the robot arm test repetitions analysed.

A comparison with the experimental data obtained from the APAS could then be made. Between the tests at 40% and 80% of maximum robot arm velocity for instance, a doubling of the experimentally obtained velocity would be expected.

The average peak velocities were calculated from the APAS data for each test. It was then possible to calculate and compare the projected 100% velocities of the robot arm during each of the tests, as shown in Table 7.3.

	Test1	Test2	Test3
20% Max Velocity	153.25	133.26	118.12
40% Max Velocity	153.04	133.11	118.05
60% Max Velocity	153.40	132.95	117.91
80% Max Velocity	152.75	133.55	118.44
Mean	153.11	133.26	118.13
St.Dev.	0.3	0.28	0.22

Table 7.3 Projected 100% velocities calculated from experimental velocities.

The standard deviation of the projected 100% velocities calculated for each percentage setting can be seen to be very low for all three tests. These results show that changes in the velocity of a moving marker were accurately established using the APAS, the accuracy of such calculations being a key element in any marker based analysis of human motion.

7.3 Pendulum testing of acceleration measurement

In order to test the accuracy of the APAS system when establishing the acceleration of a moving target marker, it was initially attempted to analyse the

motion of a free-falling object. A plaster filled 38mm diameter spherical marker coated in reflective tape was dropped from rest at a height of around 2.5m. When analysing the captured video sequences of these tests however, it was found that the camera shutter speed was too low, causing the images of the falling marker to be elongated.

The difficulties in accurate digitising of the falling marker location from the elongated images led to the development of an alternative dynamic test. A simple pendulum was constructed by attaching a 38mm diameter plaster filled, spherical plastic marker, coated in reflective tape, to a cotton thread and connecting this to a rigid frame.

The mean stride frequency for male gait was calculated at 0.92Hz from the data of Inman et al (1981) and the corresponding frequency of arm oscillation assumed to be the same. It was considered that most upper limb daily activities would occur at a frequency lower than that of the free arm swing during gait, complex targeted daily activities requiring more precise control. A pendulum length (l) of approximately one metre and frequency 0.5Hz was therefore selected.

The pendulum was released from a consistent starting position, by the cutting of a loop of thread securing it to the rigid frame on one side. Its initial angular deflection from its vertical rest position (θ) was around 15°. The first ten seconds of each test were filmed, this being the period during which the amplitude was greatest. Capturing of images was initiated towards the end of the first swing to allow any perturbations due to the release of the pendulum to die down. The period of the pendulum (T) was obtained from the digitised data using the 'pends.m' routine, through calculation of the average time difference between maximum horizontal and vertical displacements in its cycle.

Taking the idealised model of the pendulum as a mass suspended by a weightless, unstretchable string in a uniform gravitational field and making the small amplitude assumption that the restoring force is proportional to θ as opposed to $\sin\theta$, equations 7.1 and 7.2 were then employed to calculate g, the acceleration due to gravity. For an idealised pendulum initially deflected by

θ=15°, the true period differs from that given by Equation 7.1 by less than 0.5% (Sears et al (1987)).

$$T = 2\pi\sqrt{\frac{l}{g}} \qquad (7.1)$$

$$g = 4l\left(\frac{\pi}{T}\right)^2 \qquad (7.2)$$

The results obtained for three repetitions of the pendulum trial, each involving five full oscillations of the pendulum, are given in Table 7.4 along with the average and standard deviation (SD) of these results. Also given are the theoretical period required to obtain the true value of g and that required to obtain the experimental average value.

Plane of Maxima	Trial 1	SD	Trial 2	SD	Trial 3	SD
Horizontal	9.6727 ms^{-2}	0.059	9.6432 ms^{-2}	0.068	9.6432 ms^{-2}	0.068
Vertical	9.6727 ms^{-2}	0.059	9.6732 ms^{-2}	0.114	9.6727 ms^{-2}	0.059
Average	**Standard Deviation**		**Theoretical Period**		**Experimental Period**	
9.6630 ms^{-2}	0.0668 ms^{-2}		2.0368s		2.0519s	

Table 7.4 Acceleration values obtained during pendulum testing.

The average value of 9.663 ms^{-2} for g, is less than 1.5% from the true value of 9.8062 ms^{-2}. As can be seen, the period obtained through experimentation differs from that necessary to obtain the exact value of g by around 0.015s. This is a small margin considering that the minimum APAS sampling interval is 0.02s.

The results showing the period of the pendulum as less than the theoretical value might have been expected, as the force due to air drag, resisting the motion of the pendulum bob and thus lengthening its period, was not incorporated in the calculations.

The results of the analysis of pendulum motion again show the accuracy with which displacement data obtained using the APAS can be used to calculate parameters derived from these displacements.

7.4 Jointed arm testing of angle measurement

During the analysis process described in Chapter 6, relative angles between body segments were to be calculated from embedded frames defined in relation to patterns of surface attached markers. Having established that the APAS could be reliably employed for the tracking of marker motion, the next step was to assess the degree of accuracy with which the APAS and the MATLAB routines allowed angles to be calculated. In order to carry this out, a full-size model of the upper limb was constructed from 20mm diameter plastic tubing and mounted on a wooden frame, as shown in Fig 7.1.

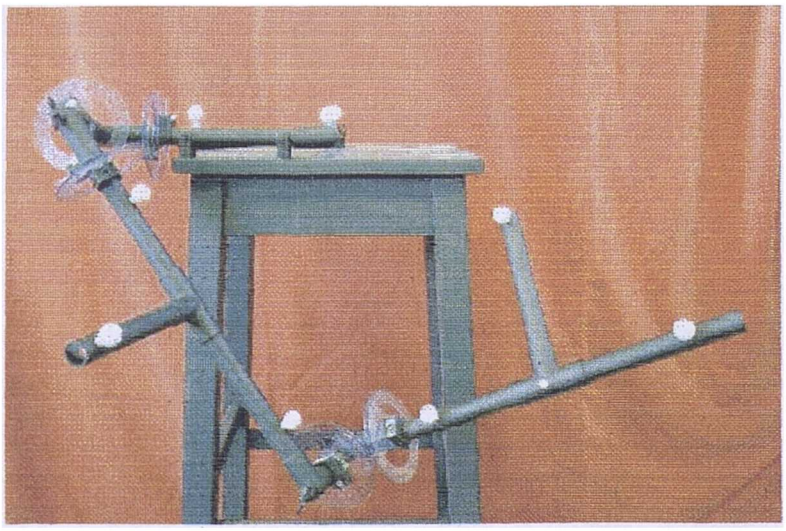

Fig.7.1 Five degree of freedom model of the human upper limb with markers attached.

Five joints incorporating 360° protractors were included in the model to represent three degrees of freedom at the shoulder and two at the elbow. These then allowed the direct measurement of the joint rotations for comparison with those obtained using the APAS.

Reflective markers were positioned on the model in a similar arrangement to that described in Chapter 6 for the upper limb motion analysis.

The arm model and the wooden frame on which it was mounted were painted black so as to maximise the contrast between the markers and background.

After the initial orientations were established using a spirit level, twelve stationary orientations of the model joints were then selected as shown in Table 7.5. Two images were captured by three cameras in each position and some positions were repeated. This allowed the assessment of the reliability and repeatability of the data.

The magnitude of each of the angles was measured directly using the attached protractors and experimentally using the APAS. Elbow abduction was assumed to be zero as no allowance was made in the arm model for such a movement.

	ELBOW			SHOULDER		
Position	Adduction	Flexion	Int. Rot.	Adduction	Flexion	Int. Rot.
1	0	90	0	0	0	0
2	0	0	0	0	45	0
3	0	0	45	0	45	0
4	0	0	-45	0	45	0
5	0	45	0	0	45	0
6	0	45	0	0	45	45
7	0	45	0	45	45	45
8	0	90	0	0	0	0
9	0	135	0	0	0	0
10	0	90	0	0	0	0
11	0	90	45	0	0	0
12	0	90	- 45	0	0	0

Table 7.5 Orientations of the mechanical arm model joints at each sampled position.

In order to establish the joint orientations from the marker co-ordinate data, the JCS (Grood & Suntay (1983), Cole et al (1993)) as discussed in Section 5.4.2 was used. This technique was developed in order to overcome the sequence dependence of the joint rotations when using traditional Euler angle methods and to allow description of joint movement in terms of clinically defined motions.

Using the JCS leads to results that are independent of the rotation sequence, but are subject to a sequence effect imposed by the initial selection of the axes about which these rotations occur. Different axis sequence

selections will result in different numerical results for the same joint attitude in the same way that selecting different Euler sequences leads to differing results.

Cole et al (1993) found the magnitude of the differences in the joint attitude representations between selected axis sequences to be dependent on the range of motion during the movement, differences being more pronounced at joints with large ranges of motion. It was thus necessary to establish the most suitable of the six available sequences for obtaining a measure of the joint orientations at the shoulder and elbow.

For each of the twelve stationary positions of the model arm, the components of joint attitude were calculated from the APAS data for each of the six defined angular sequences and compared with the protractor measurements. Table 7.6 gives the RMS difference between the two for each rotation sequence, where 'RFA' represents the sequence; internal rotation - flexion - adduction, the other sequences being similarly labelled.

	ELBOW RMS DIFFERENCE (°)				SHOULDER RMS DIFFERENCE (°)			
SEQ.	Adduc.	Flex.	Int.Rot.	Total	Adduc.	Flex.	Int.Rot.	Total
RFA	48.88	18.80	35.32	103.00	2.83	1.24	2.02	6.09
ARF	18.81	1.16	17.85	37.82	2.82	1.95	1.24	6.01
RAF	18.77	2.15	17.41	38.33	2.95	1.05	1.09	5.09
AFR	57.97	2.19	42.89	103.05	0.46	0.90	2.26	3.62
FRA	1.72	1.40	1.90	5.02	0.52	2.23	0.81	3.56
FAR	1.46	1.75	1.89	5.1	0.26	0.18	0.26	0.7

Table 7.6 RMS differences between experimental and protractor measured results.

Large differences can be seen in the accuracy of the results obtained when different angle sequences are chosen. The results clearly indicate that flexion - adduction - rotation (FAR) is the most suitable JCS sequence for the determination of the angles at the shoulder. This represents the selection of the flexion/extension axis of the proximal segment for the first rotation, the abduction/adduction axis as the floating axis for the second rotation, with the distal segment long axis for the third rotation.

For the elbow, the flexion - rotation - adduction (FRA) sequence appears to be marginally the most suitable sequence though there is little appreciable

difference between this and the FAR sequence. This is due to the fact that the abduction/ adduction angle was defined as zero for the model.

In their discussion of the use of Cardan angles, Tupling & Pierrynowski (1987) suggested that when selecting a sequence, the first rotation should be the largest, the second rotation should be the smallest and the third rotation is the remaining one. This proposal is supported by the jointed arm results where the two most suitable sequences for both shoulder and elbow have joint flexion as the first rotation.

Grood & Suntay (1983) defined the FAR axis sequence with specific reference to the knee joint. Similar sequences were also used by Ramakrishnan & Kadaba (1991) and Capozzo (1984). The same sequence was again selected by Cole et al (1993) in their standardisation proposal for the JCS, along with the suggestion that these axis selections would give attitude components consistent with the anatomical definitions of joint movement.

The RMS values for the FAR sequence given in Table 7.6, show that the angles obtained for elbow rotation provide the poorest match with those in Table 7.5. All the RMS values are within 2° for the elbow however and are within 0.5° for the shoulder. These results indicate the high accuracy and repeatability of the angular orientation results obtained using the APAS and MATLAB angle calculation routines, digitising errors, reading errors and sag in the jointed arm notwithstanding.

7.5 Comparison of moment calculation with a previous study

Having validated some basic properties of the analysis process involving the APAS and the MATLAB software for calculation of angles, it was attempted to validate the method for calculation of the various joint moments described in Section 6.5.9, through comparison with a previous study.

Runciman (1993) calculated external moments during a preliminary validation study of his method. Pure abduction in the frontal plane was analysed, performed as a series of four static positions by a male subject, aged 25, mass 65kg and height 1.75m. As no numerical data were supplied, the data values for comparison were obtained by measurement of the graphs given in Runciman (1993) with an accuracy of around ± 0.1Nm.

Starting with the angles measured from the graphs and using the body segment parameter data of Drillis & Contini (1966) as specified by Runciman (1993), it was possible to re-analyse the tests for the purposes of comparison by inputting the same initial data into the 'numdiff.m' MATLAB routine.

The motion was modelled as pure abduction in the frontal plane with no shoulder flexion, shoulder rotation or elbow flexion. The results obtained can be seen in Fig 7.2 along with those of Runciman (1993) whose axes of rotation having been modified to correspond with those defined for the shoulder in Section 6.5.3. The moments shown are the those required to be applied about *the joint to perform the action.*

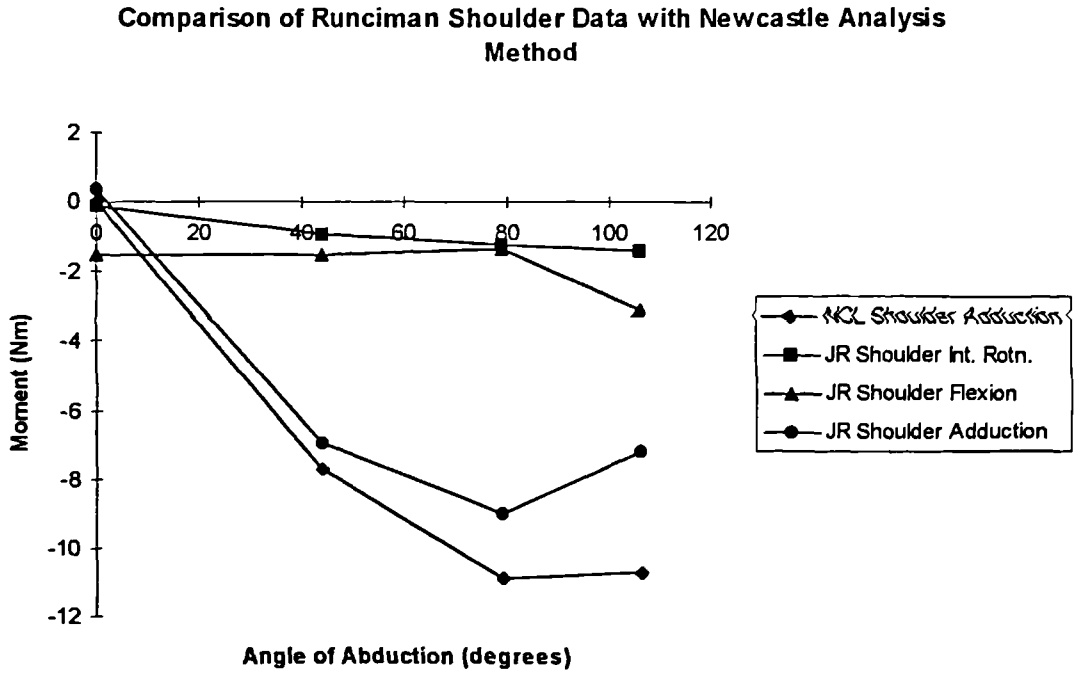

Fig 7.2 Comparison of Runciman (1993) and MATLAB data, showing moments at the glenohumeral joint due to external loading of the arm during frontal plane humeral abduction. (JR = Runciman (1993), NCL = Matlab method)

The abduction moment pattern obtained using the MATLAB method is similar in shape to that of Runciman (1993) though is of greater magnitude. This difference in magnitude is due to rotations about the shoulder flexion and rotation axes and the elbow flexion axis in the data of Runciman (1993), who stated that "External humeral rotation was kept to a minimum,..." and "The subject was seated with a slightly bent elbow posture throughout data collection".

The effect of the rotations at the shoulder is indicated by the moments about these axes in Fig 7.2. As previously stated however, the MATLAB model assumed ideal abduction with a fully extended elbow.

The greatest deviation between the results occurs at the final data point where the shoulder flexion and rotation moments of Runciman (1993) are at their greatest. In order to assess the extent of their effect, values of elbow flexion and shoulder flexion were input into the MATLAB model in order to find how big an angle would be required to bring these results into line with those of Runciman (1993). The results shown in Fig 7.3 were obtained.

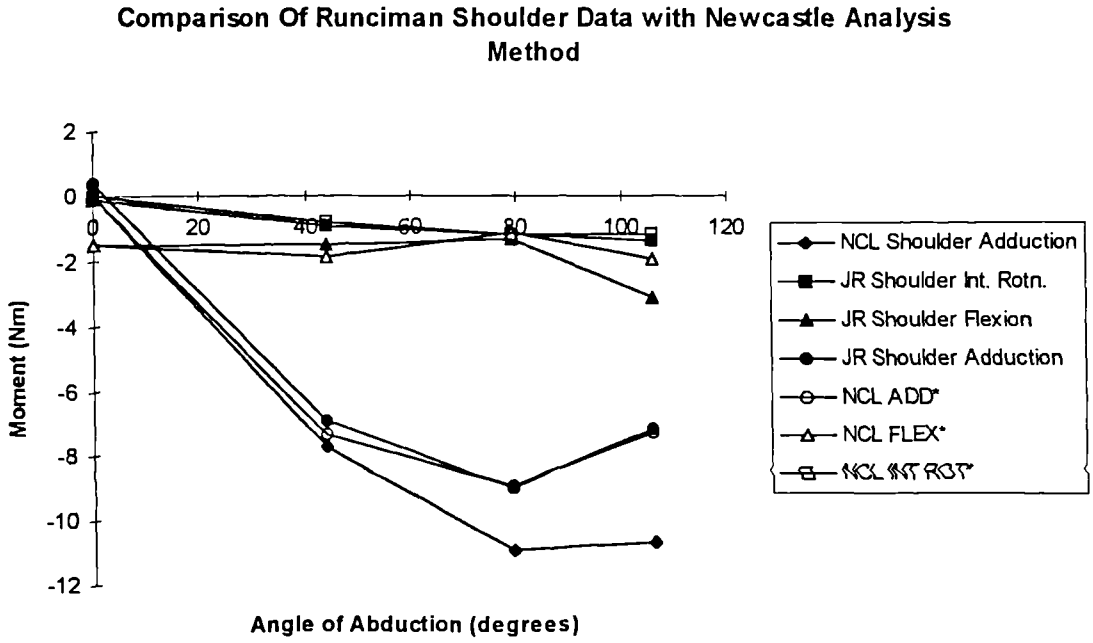

Fig 7.3 Comparison of Runciman (1993) glenohumeral joint moment data with that obtained using Matlab method, (JR = Runciman (1993), NCL = Matlab method, NCL...* = corrected for elbow and shoulder flexion)

The values of the angles of flexion at the shoulder and elbow, input in order to produce these results are given in Table 7.7.

Angle of Abduction	0°	44°	79°	106°
Shoulder Flexion	-14°	-20°	-40°	40°
Elbow Flexion	25°	25°	25°	25°

Table 7.7 Values of shoulder and elbow flexion input in Matlab model at each step of abduction in order to obtain results shown in Fig 7.3.

The change of sign for shoulder flexion at the highest angle of abduction in Table 7.7 is due to the abduction angle being greater than 90°, leading to an extension moment rather than a flexion moment being required about the shoulder to maintain the position. From Table 7.7 and Fig 7.3, it is clear that relatively small amounts of flexion at the shoulder and elbow were required in order to bring the results from the MATLAB procedure close to those of Runciman (1993). The contribution of the rotation at the shoulder indicated in Fig 7.3 would further influence these results.

It was concluded that the MATLAB routine was reliable and accurate for use in the calculation of joint moments, comparable results to the shoulder moments of Runciman (1993) being obtained for the same input data. In the absence of any standardised or definitive directly measured joint moment values, obtaining similar results to those of Runciman (1993) was as close as could be achieved to a validation of the MATLAB method.

7.6 Testing of measurement repeatability

In order to assess the repeatability of the motion analysis method it was decided to film and analyse repetitions of a test selected from those that would be carried out by all subjects. Any differences arising between the results from such repetition would be due to variations in marker positioning, anatomical calibration, test protocol and inconsistencies in the digitising process.

The activity chosen for the validation study was a right hand reach from a position in which the hand rested palm downwards on a table surface, to a position in which the hand cupped the left side of the neck. The table was set at seated elbow height and at a distance from the subject equal to the length of the forearm and hand with the fingers extended.

This activity was repeated by a single subject at the same time on three consecutive days, using the same technique on each occasion. The subject was a male, age 43, height 1.76m, weight 81.5kg. A sample of the data obtained can be seen in Fig 7.4, Fig 7.5 and Fig 7.6.

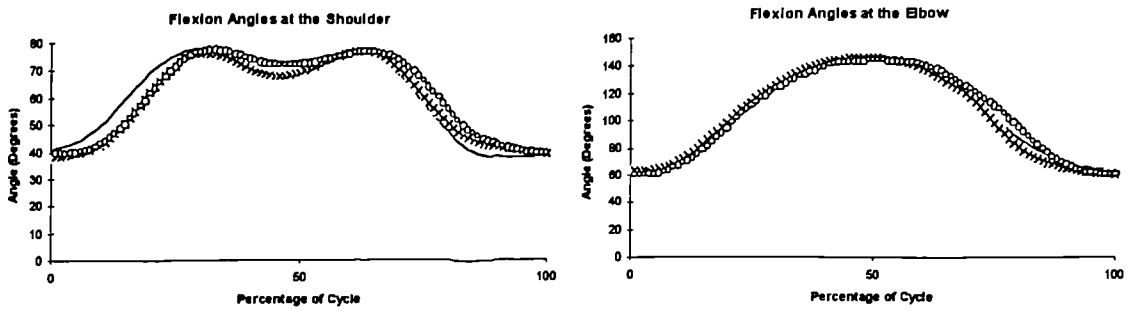

Fig 7.4 Flexion angles at the shoulder and elbow for validation tests.

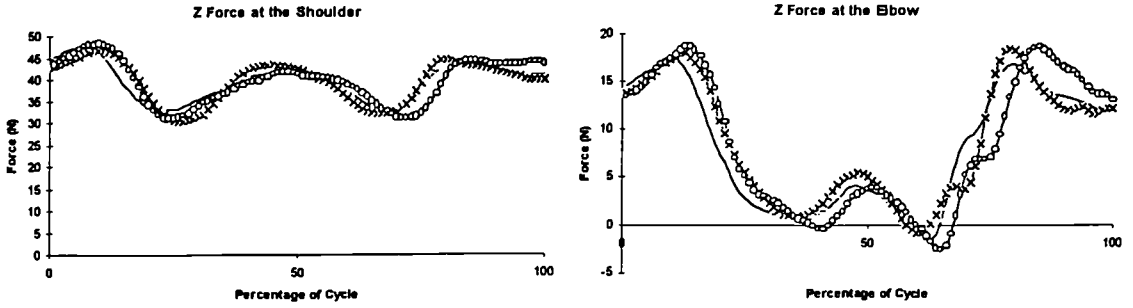

Fig 7.5 Longitudinal axes forces at the shoulder and elbow for validation tests.

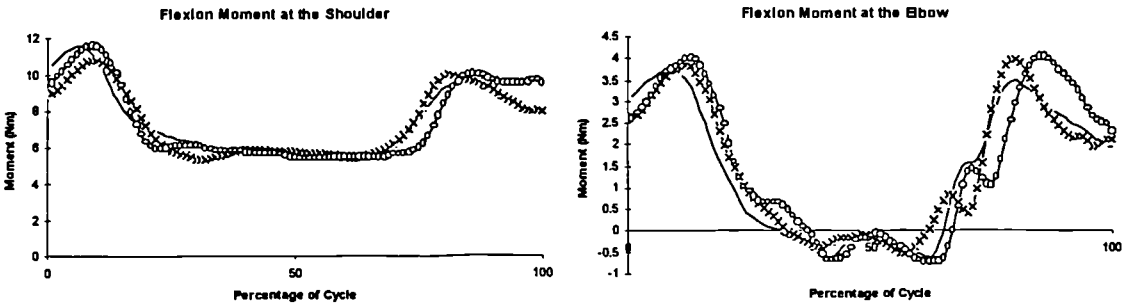

Fig 7.6 Flexion moments at the shoulder and elbow for validation tests.

As can be seen the trials were found to produce results that showed a relatively consistent pattern of angles, moments and forces, the ranges of the measured parameters from all three tests corresponding well.

The validation tests were normalised to one hundred percentage points of a cycle using the elbow angle data, which can be seen to be reasonably consistently aligned across all three tests. Slight misalignments are observable in the normalised shoulder angles however and these are due to the difficulty in normalising the measurements of the various parameters for each test.

For any subject there will be a natural variability between repetitions when performing complex upper limb activities, slight differences in the sequence and timing of the various movements involved which make normalisation of the data difficult. Such normalisation problems are inherent in any study that involves normalisation of multiple variables for comparative purposes while attempting to retain the natural structure of the data.

Cheng (1996) carried out a validation involving three repeated measurements of elbow flexion and forearm rotation on each of two subjects. As discussed in Section 7.5, Runciman (1993) tested one subject carrying out pure abduction in the frontal plane as a series of four static positions. Similarly Barnett (1996) took five stationary samples on each of five subjects during abduction of arm in the coronal plane at 10° increments from 0° to 90°.

The reach to the neck activity was highly complex in comparison with these, involving ranges of shoulder abduction (~60°), shoulder rotation (~30°), elbow pronation (~100°) and elbow adduction (~15°), in addition to those angles given in Figs 7.4-7.6.

The data obtained over three repetitions of this complex upper limb activity show the experimental methods and analytical techniques, discussed in Chapter 6, to allow high levels of repeatability between tests.

7.7 Comparison of angle measurement with flexible electrogoniometer

In a further validation study, the methods described in Chapter 6 were used to measure flexion angle at the elbow, the results being compared with simultaneous measurements of the same angle using two other devices.

The first of these was a measurement device incorporating a 360° potentiometer as shown in Fig. 7.7. An aluminium strip was attached on each side of the potentiometer. Cuffs were made to fit around the circumference of the upper arm and forearm and one of these was attached to each aluminium strip allowing the device to be secured to the arm. The attachment position of these cuffs could be altered for use of the device on a range of arm sizes.

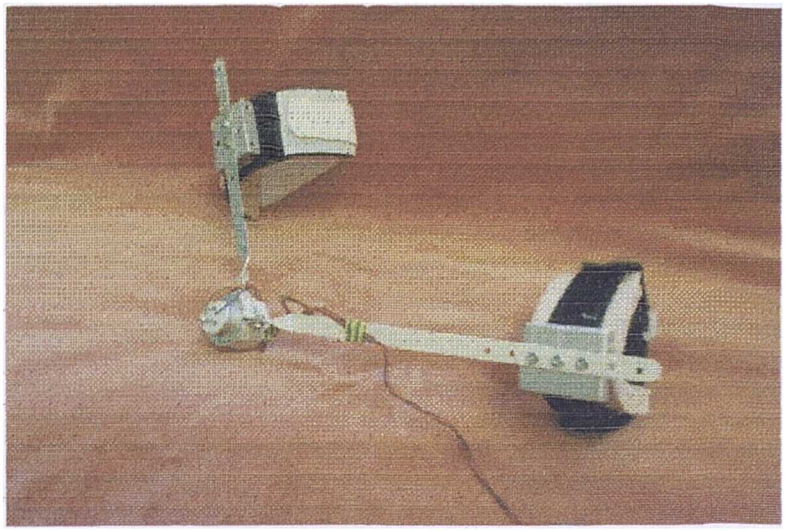

Fig 7.7 Potentiometer device for measurement of elbow flexion.

The device was calibrated against a protractor goniometer for twelve points at 30° intervals from 30° up to 180° and back down to 30°. The linearity of the device can be seen in the calibration graph shown in Fig. 7.8.

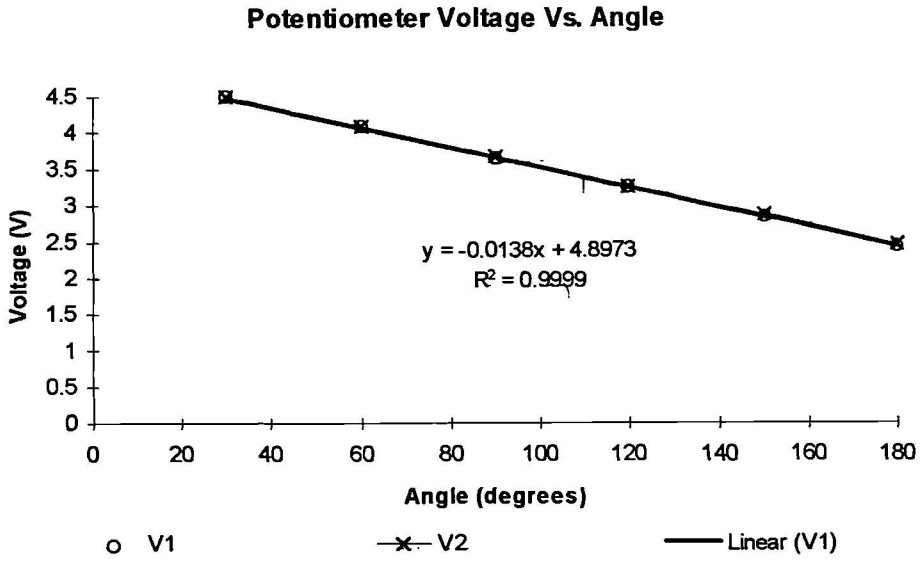

Fig 7.8 Calibration graph for the potentiometer device.

When mounted on the arm the potentiometer was held to the lateral side of the elbow. The positioning of the device was adjusted, a good alignment with the flexion axis of the elbow being judged to be where flexion of the joint caused minimal movement of the device other than rotation of the potentiometer. During elbow flexion the aluminium strips of the device flexed

slightly to accommodate the carrying angle, allowing deflection of the potentiometer to closely follow the rotation of the joint. During testing, the potentiometer device was regarded as the 'gold standard'. It was considered the most accurately aligned with the true elbow rotation axis and was minimally affected by skin movement.

The second device used for comparison was a Biometrics XM110 flexible electrogoniometer as used by Pandyan et al (1999), the signal from which was amplified using a custom built amplifier. One end was attached on the posterior of the upper arm, the other on the posterior of the forearm in the anatomical position.

The angular values from both the flexible electrogoniometer and potentiometer were collected via an Elan AD132 PCMCIA analogue to digital converter (ADC) using the Hewlett Packard 'HPVee' software package.

Reflective markers were attached as described in Chapter 6, allowing the simultaneous measurement of the elbow flexion by the potentiometer, flexible electrogomiometer and APAS.

In order to synchronise the data from all three measurement devices, a connection was made from the LED device described in Section 6.3.12 to the ADC. When triggered this activated LEDs in front of each APAS camera while simultaneously producing a spike in the data collected by the ADC. During analysis these spikes were matched with the corresponding LED flash in order to time match the data sets.

Elbow flexion was performed in two positions, the first at around 90° of humeral flexion, the second at around 135° of humeral flexion. The forearm was maintained in a supinated position. The elevation of the humerus was necessary in order to maximise the visibility of the attached reflective markers amidst the various cables and connections of the other two attached devices.

One subject performed pure flexion of their elbow as specified. Five repetitions in each position of humeral flexion were performed. From each set of five, the middle repetition was selected for analysis using the APAS. The results obtained are shown in Fig.7.9 and Fig.7.10.

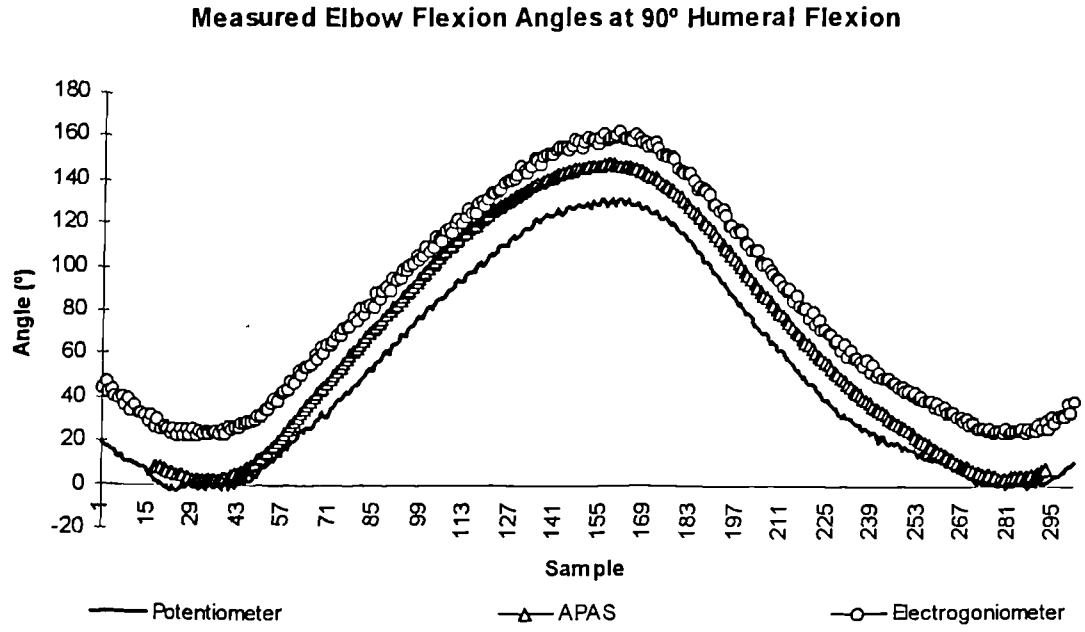

Fig 7.9 Measured elbow flexion angles at 90° humeral flexion.

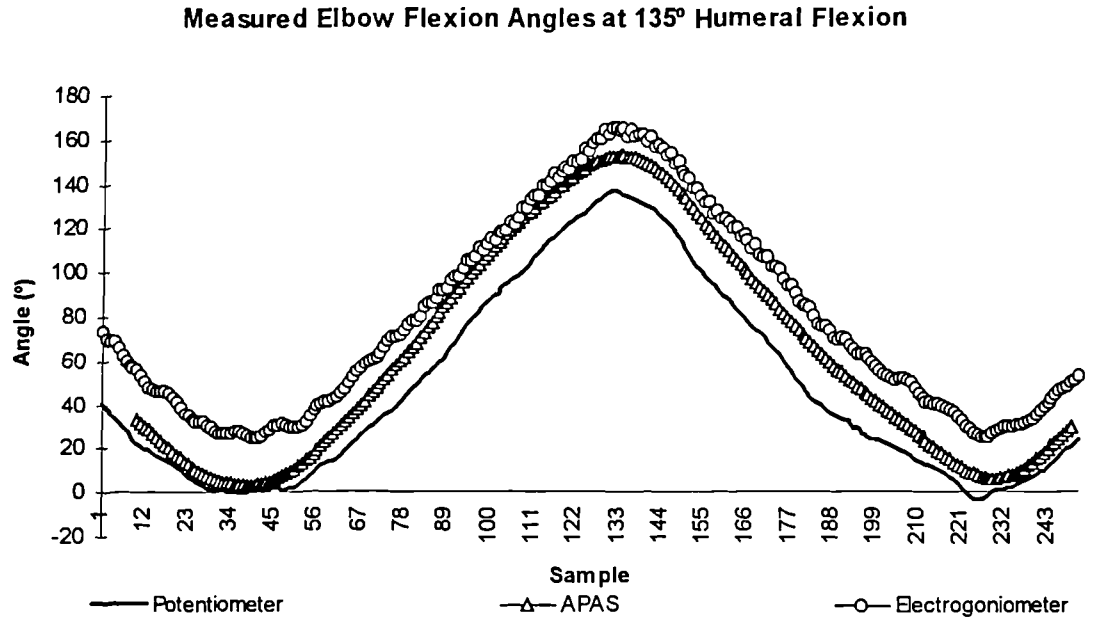

Fig 7.10 Measured elbow flexion angles at 135° humeral flexion.

It can be seen from these graphs that the patterns of elbow flexion are similar from all three measurement devices. The graphs indicate an offset of the APAS and flexible electrogoniometer data from the potentiometer data however. These offsets would be due to differing definitions of the zero flexion position between each of the methods used.

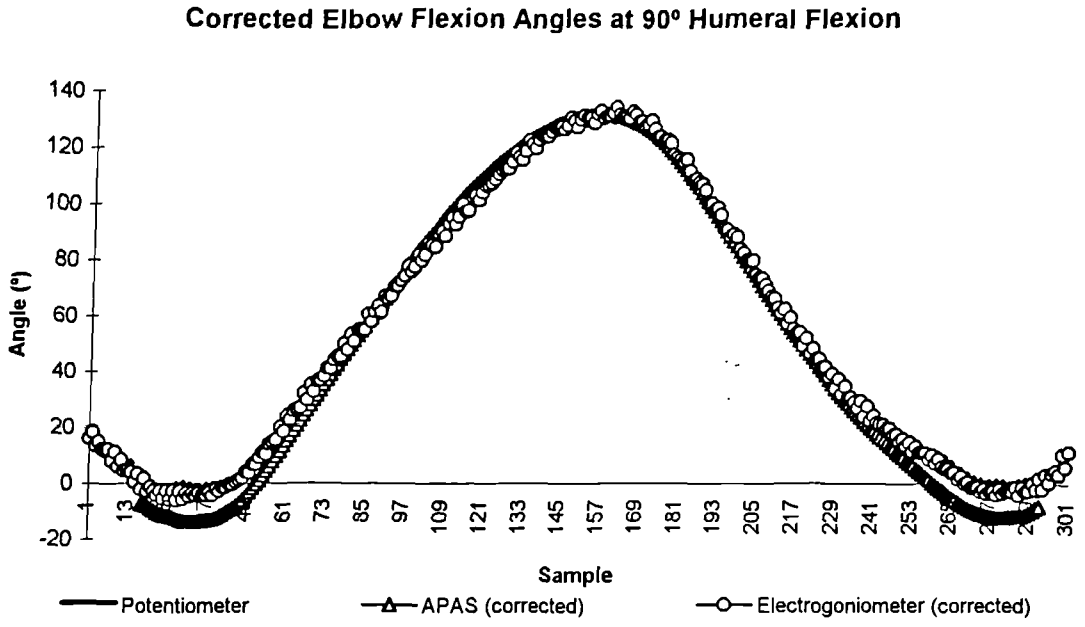

Fig 7.11 Elbow flexion angles at 90° humeral flexion corrected for zero offsets.

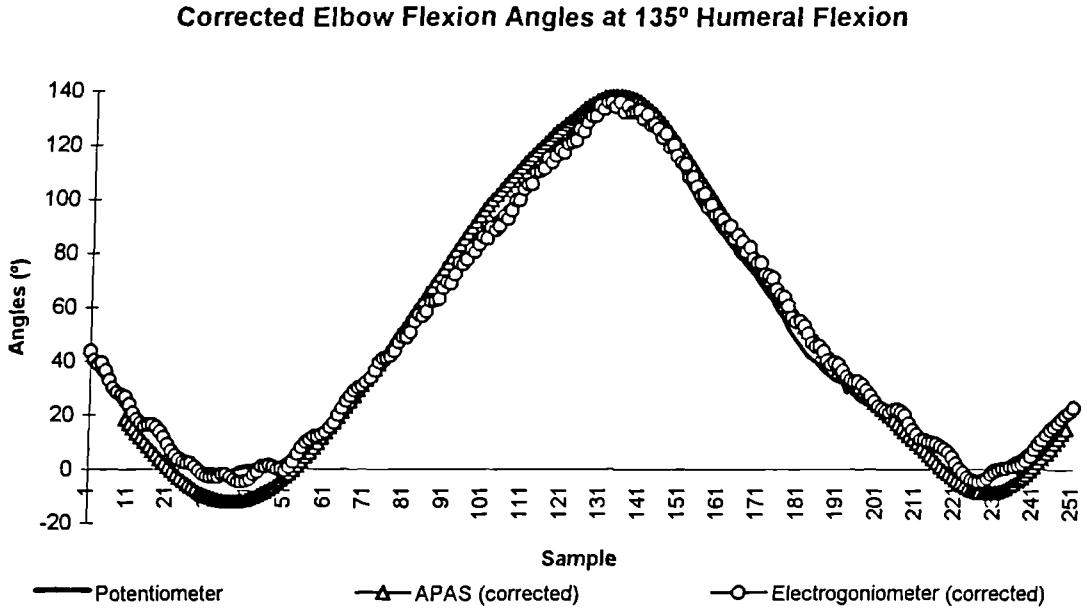

Fig 7.12 Elbow flexion angles at 135° humeral flexion corrected for zero offsets.

On correcting the APAS and flexible electrogoniometer data for these offsets by 16° and 28.6° respectively, the graphs shown in Fig. 7.11 and Fig. 7.12 were obtained. From these corrected graphs it can be seen that the data from the potentiometer and flexible electrogoniometer correspond very closely. The range of the APAS data is slightly greater than the others in both instances.

The source of this problem was thought to be the fact that the APAS analysis involved the measurement of flexion about an embedded axis orthogonal to the longitudinal axis of the humerus. In common with all similar studies involving embedded frame definition, this axis does not necessarily exactly replicate the true anatomical flexion axis.

The difference in measured angles was investigated further by trying to draw a measure of the rotation about the true elbow flexion axis from the APAS data, this being attempted in two ways. First the helical axis (HA) was calculated between the upper arm and forearm embedded frames for each sampled instant, as well as the relative rotation of the frames about this axis. In theory the HA should correspond with the true elbow flexion axis at each instant. It was found using the 'screw.m' MATLAB routine of Reinschmidt & van den Bogert (1997).

The second method used was that described by Charlton (1999), in which a total linear least squares problem as described in van der Helm et al (1992) was solved in order to identify a plane fitted through the sampled positions of the ulnar styloid throughout each test. The axis of elbow flexion was then defined as the normal to this plane (SPN). Having identified this axis, a time history of the flexion angles was calculated by rotating the position of the ulnar styloid at each sampled instant about the axis until it lay coplanar with the glenohumeral joint centre and epicondyles. It was assumed that this position represented zero elbow flexion.

The results from both these methods are shown for each test in Fig 7.13 and Fig. 7.14, again incorporating a compensation for the zero position offset, 18.25° in the case of the helical axis and 12° for the styloid plane normal.

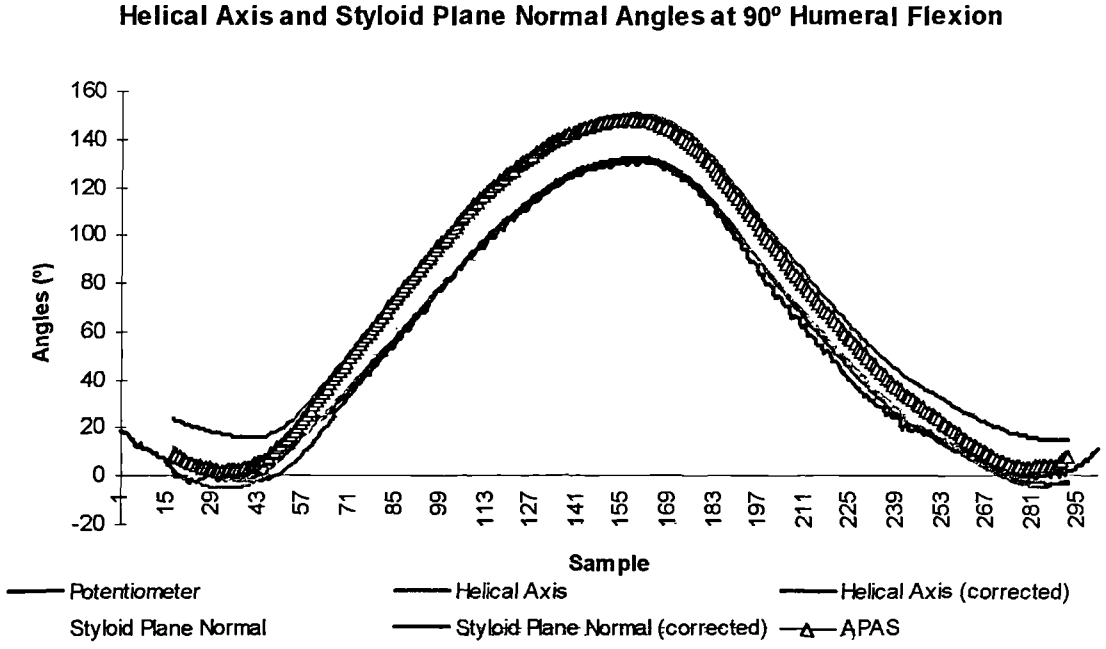

Fig 7.13 Rotation about helical axis & normal to styloid plane (90° humeral flexion).

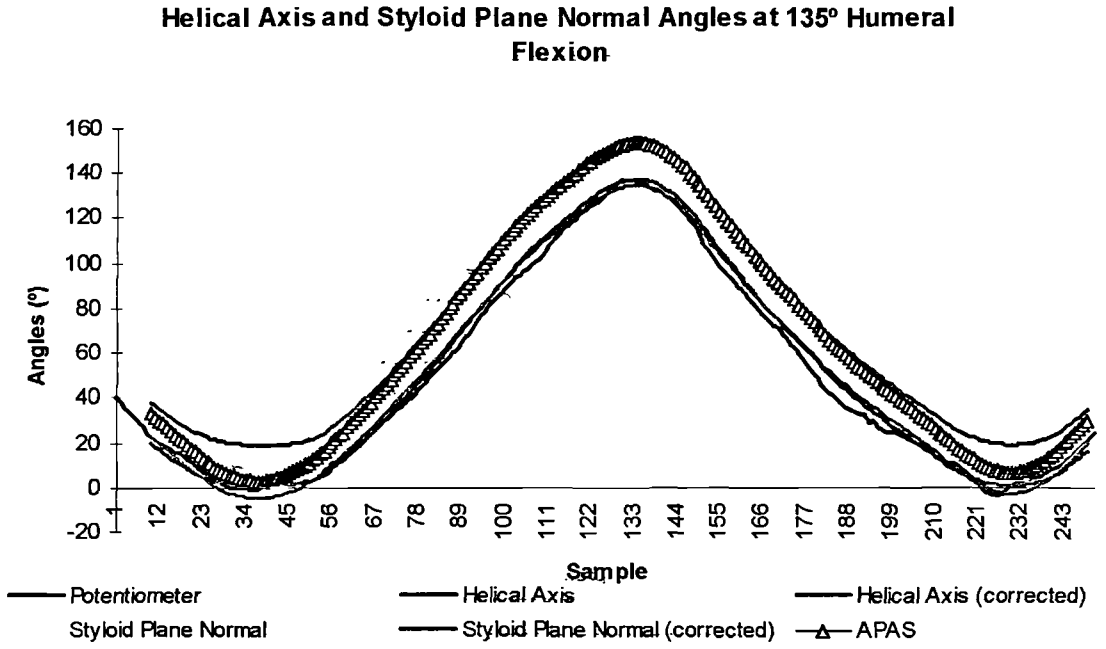

Fig 7.14 Rotation about helical axis & normal to styloid plane (135° humeral flexion).

These graphs show that both the methods employed to identify the rotation about the true elbow flexion axis produce results similar to each other and to the potentiometer measured angle. The HA appears to have greatest effect on the lower angles of flexion, raising these angles slightly. The SPN has a similar effect though also decreases the maximum flexion angles to a certain extent. Both methods decrease the overall range of angles, bringing it

into line with that measured by the potentiometer. It would thus appear that the original difference in the range of angles was indeed due to the forced measurement of the flexion angle about an axis that was displaced from the true axis of flexion.

The difference in orientation of the axes need only be small to cause this effect. The average calculated HAs and SPNs, defined in relation to the humeral embedded frame are given in Table 7.8. The approximate rotations of these axes in relation to the humeral embedded x-axis are also given.

	X	Y	Z	Anterior Rotn.	Superior Rotn.
HA - 90°	0.9665	-0.2523	0.0406	14.6°	2.3°
HA - 135°	0.9702	-0.2411	0.0037	14°	0.2°
SPN - 90°	0.9624	-0.2161	0.1646	12.7°	9.5°
SPN - 135°	0.9776	-0.1779	0.1123	10.3°	6.4°

Table 7.8 Unit vectors and rotations of the HA and SPN for elbow flexion at 90° and 135° humeral flexion in relation to humeral embedded frame.

The major component of the HA and SPN axes given in Table 7.8 can be seen to lie in the direction of the humeral embedded x-axis, about which the APAS elbow flexion was measured. The rotations relating the HA and SPN axes to the humeral embedded x-axis are seen to be reasonably small.

It can be said then, that the bone embedded forearm frame discussed in Section 6.5.3 includes a representation of the elbow flexion axis which, though not exactly coincident with the true anatomical rotation axis, provides a reasonable representation of it.

Ramakrishnan & Kadaba (1991) and Hollerbach & Hollister (1995) both found that significant errors could be introduced into kinematic analyses if the co-ordinate reference frame was not correctly aligned with the joint mechanism. When trying to define axes of rotation from surface markers however and when those axes of rotation vary with joint movement, it becomes extremely difficult to align the defined embedded frame axes with the true anatomical axes of rotation. Embedded frame definitions in all such studies can therefore only ever be an estimate of the underlying anatomical axes.

It has been shown that imposing the orientation of the axes about which rotations occur by the definition of orthogonal embedded frames introduces some inconsistency between measured angles and the true anatomical rotations. Such inconsistencies are inherent in any study that involves the definition of embedded orthogonal axes about which rotations are measured.

The results of the comparison with the potentiometer and electrogoniometer devices have shown however, that the methods developed allow a sufficiently accurate measure of angular rotation to be obtained.

7.8 Comparison with results from two previous studies

In order to test the validity of the overall method from marker attachment to the final output of angles, forces and moments, activities were included in the testing process which would allow comparison with results from two previous studies. These activities were performed by all subjects tested during data collection as discussed in Chapter 8.

The first of these activities was similar to the "hand to mouth" test of Williams (1996), for which only angular data were compared. The results from the repetition of this test are given with the other subject test data in the following chapter. *Fig 7.15 and Fig 7.16 show the data of Williams (1996) for* shoulder and elbow flexion angle respectively, used for the comparison process.

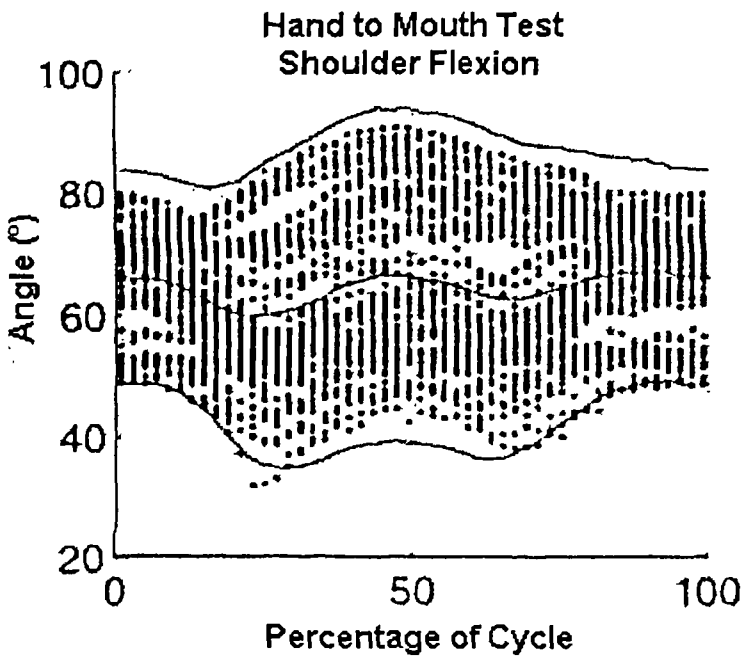

Fig 7.15 Shoulder flexion for 'hand to mouth' test from Williams (1996).

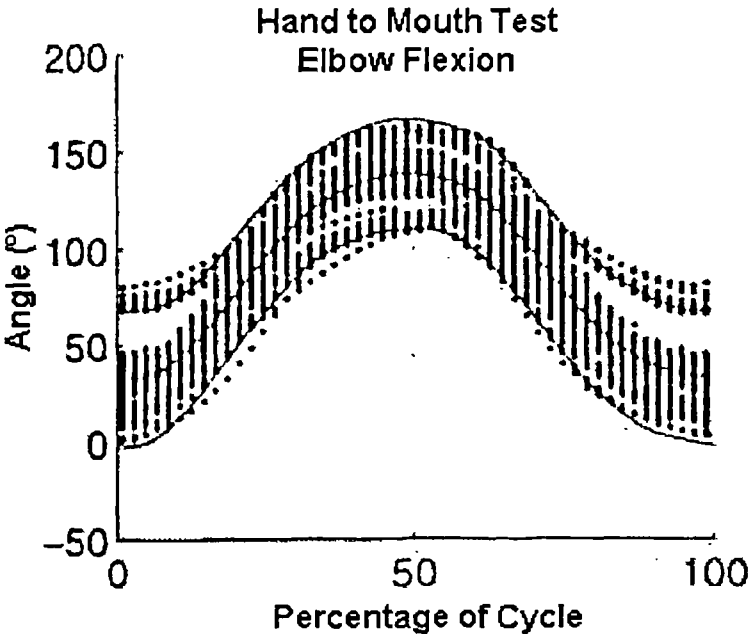

Fig 7.16 Elbow flexion for 'hand to mouth' test from Williams (1996).

The other activities were similar to the "book lift" tests of Cheng (1996), for which both angular and moment data were compared. Again the results from the repetition of this test are given with the other subject test data in the following chapter.

Fig 7.17 and Fig 7.18 show the data of Cheng (1996) for shoulder and elbow flexion angle respectively, used for the comparison process. The reference position of Cheng (1996) was with the elbow in a position of 180° elbow flexion in comparison with that from the current study. For this reason the data of Cheng (1996) in Fig 7.18 have been inverted to correct for this difference.

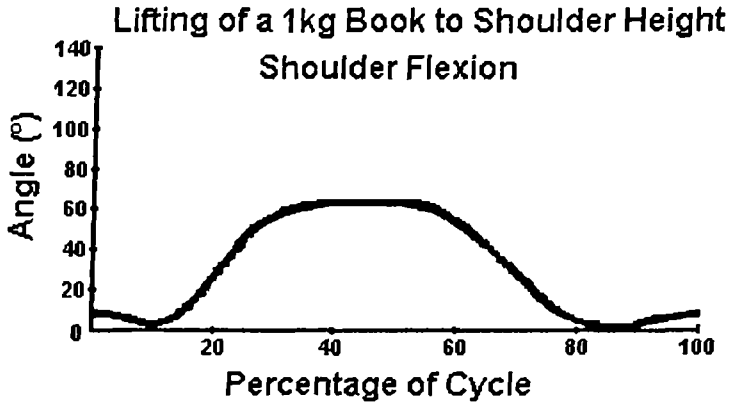

Fig 7.17 Shoulder flexion for 'book lift to shoulder height' from Cheng (1996).

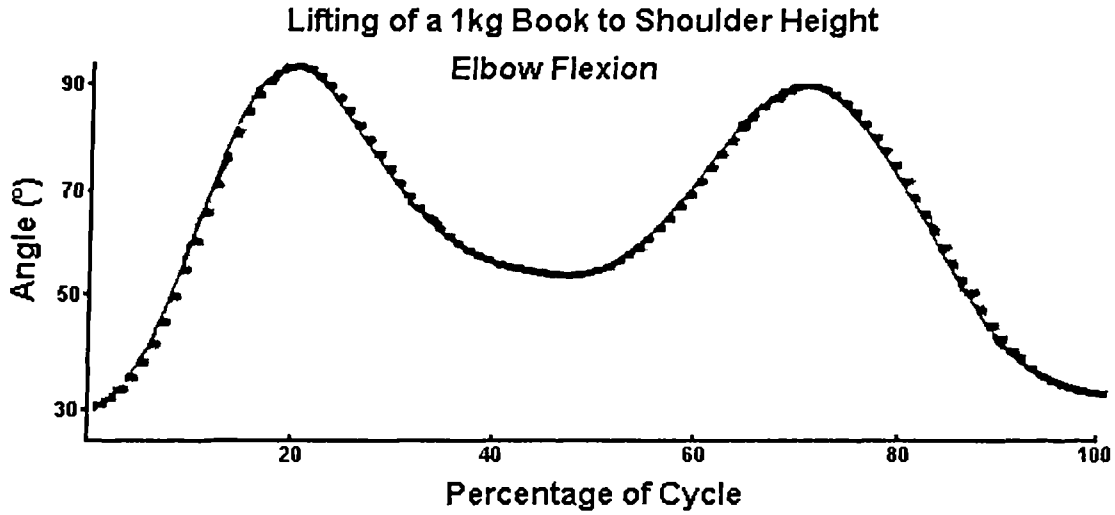

Fig 7.18 Elbow flexion for 'book lift to shoulder height' from Cheng (1996).

When comparing the data of Cheng (1996) with that in Chapter 8 from the current study, it must be noted that the starting position for the tests of Cheng (1996) was with elbow almost fully extended by the side.

Fig 7.19 and Fig 7.20 show the data of Cheng (1996) for shoulder and elbow flexion moment respectively, used for the comparison process.

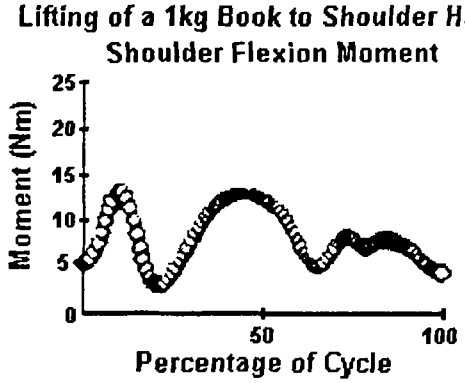

Fig 7.19 Shoulder flexion moment for 'book lift to shoulder height' from Cheng (1996).

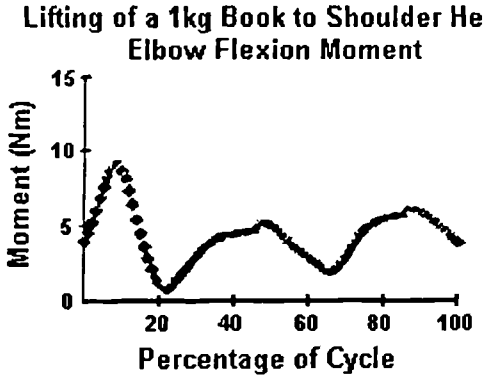

Fig 7.20 Elbow flexion moment for 'book lift to shoulder height' from Cheng (1996).

This validation involved a comparison with data obtained during subject testing and the results are included in the discussion of that testing in Chapter 8.

7.9 Summary of preliminary testing

In several previous studies, validation of analysis methods has taken the form of showing repeatability of results. The work discussed in this chapter comprises a more comprehensive and rigorous assessment of the validity of a set of motion measurement methods and analysis techniques, involving the comparison of measurements with known quantities.

It has been shown that reliable timing information can be obtained during the Capture process and that smoothing and differentiation of the

displacement data obtained allows the reliable calculation of the velocities and accelerations of moving markers.

Both the APAS and the MATLAB analysis routines have been shown to allow the accurate and reliable determination of angles from patterns of attached reflective markers.

On assessing all six available JCS sequences using an experimental arrangement specifically related to the upper limb, results in agreement with the standardisation proposal of Cole et al (1993) were obtained, indicating the selection of the Flexion-Adduction-Rotation JCS axis sequence for the description of shoulder and elbow motion.

The MATLAB analysis routines for the calculation of moments from angular displacements were shown to be accurate and a high level of repeatability between tests was achieved.

Through comparison with two other measurement devices, the methods for the measurement of joint angles were shown to be reliable within the limitations of the rotation axis positioning imposed by the definition of embedded frames.

Repetition of tests from previous studies allowed an assessment of the entire process from the camera positioning, attachment of markers and anatomical calibration through synchronising, capturing and digitising of the image sequences to the definition of embedded frames and calculation of angles, body segment parameters, forces and moments. The comparison of the data from these repeated tests is discussed in the following chapter.

CHAPTER 8 : SUBJECT TRIALS, RESULTS AND DISCUSSION

8.0 Introduction

The purpose of this chapter is to present and discuss the results obtained during the testing of ten unimpaired and two impaired subjects. A comparison with results from previous studies introduced in Section 7.8 is included.

8.1 Selection of activities for analysis

It was decided that a selection of activities from the list presented in Table 4.19 should be identified for the purposes of subject testing. In order to assess which of these might be suitable in terms of simplicity of filming, repeatability and range of motion, test recordings of twenty-three activities were made using three cameras. These were performed by a single subject on whom markers were placed as specified in Chapter 6. All the activities were performed in a seated position in order to minimise trunk movement and therefore isolate motion of the upper limb from that of the trunk, while also ensuring that the activities were performed within the calibrated test volume, the dimensions of which are given in Section 6.3.3.

Each activity was given a score from one to three, indicating increasing range of movement at the shoulder and elbow joints. The score for each activity was established by visual estimation of the ranges on viewing the recorded image sequences. The overall visibility of the attached markers for each test was also judged.

The resulting assessment of all twenty-three activities is given in Table 8.1. During the viewing of image sequences it was clear that the ranges of joint motion were highly dependent on the initial positioning of any object involved and the positioning of the hand and arm in relation to these objects, indicating that careful initial positioning of both the subject and any object used was essential in order to ensure test repeatability.

Activity	Shoulder R.O.M			Elbow R.O.M			Marker Visibility
	1	2	3	1	2	3	
Eating with hands		✓				✓	good
Eating with fork	✓					✓	reasonable
Eating with spoon		✓				✓	good
Drinking from cup		✓				✓	reasonable
Pouring from jug		✓			✓		good
Brushing teeth		✓				✓	good
Brushing hair			✓			✓	poor
Washing face		✓				✓	reasonable
Using Telephone		✓				✓	good
Block lift to varying heights			✓			✓	good
Lifting pots and pans			✓			✓	good
Shaving		✓				✓	reasonable
Using hairdryer			✓		✓		poor
Ab/ Adduction			✓	✓			good
Flex/ extension			✓	✓			good
Hand behind back		✓				✓	poor
Hand to opposite axilla			✓		✓		good
Hand to opposite shoulder			✓		✓		good
Hand to opposite hip		✓			✓		good
Hand to chest	✓					✓	good
Hand to neck	✓					✓	good
Hand to head (elbow forward)			✓			✓	poor
Hand to head (elbow back)			✓			✓	poor

Table 8.1 A selection of filmed tasks, the degree of rotation at shoulder and elbow graded on an ascending scale from 1 to 3, with marker visibility also judged.

The results displayed in Table 8.1 enabled a reduction in the number of activities selected for the purposes of subject testing, based on the ranges of joint motion involved, marker visibility and whether their analysis would require additional apparatus, for example instrumented transducers, which would have made the analysis process more complex.

Initially sixteen activities were selected for performance by the subjects during testing, as given in Table 8.2. Only subject No.1 performed all sixteen however, the number of activities being subsequently reduced to ten, the six

discarded activities being adjudged to involve movements similar to and already analysed during other tests given in Table 8.2. Activities involving positioning of the hand behind the back were not included due to the limitations in marker visibility when filming such activities with only four cameras.

Activity	Area of use	Activity	Area of use
1. Reach to opposite axilla	Hygiene	9. Lift block to shoulder height	Everyday object
2. Reach to opposite side of neck	Hygiene	10. Lift block to head height	Everyday object
3. Reach to side and back of head	Hygiene	11*.Brush hair right side of head	Hygiene
4. Eat with hand to mouth	Feeding	12*.Brush hair back of head	Hygiene
5. Eat with a spoon	Feeding	13*.Brush hair top of head	Hygiene
6. Drink from a mug	Feeding	14*.Reach to throat	Hygiene
7. Answer telephone	Everyday object	15*.Reach to top of head	Hygiene
8. Brush left side of head	Hygiene	16*.Place hand over mouth	Feeding

Table 8.2 List of activities performed by subjects. (* indicates activities performed by subject No.1 only)

An adjustable table was set at the seated elbow height of each subject and at a distance from them equal to the length of their forearm and hand with the fingers extended, a position similar to that described in Section 7.6 for the tests of repeatability. For the tests involving lifting to seated acromion and head heights, an adjustable projector stand acted as a shelf.

During testing, all subjects were instructed to perform tests at a speed and manner with which they felt comfortable. Only the initial position and the aim of each task were defined, in order to minimise any variation from the subjects' natural movement patterns. Similar testing procedures were adopted in the studies of Barker et al (1996), Cheng (1996) and Williams (1996).

Ten repetitions of each activity, divided as two sets of five, were performed by each subject while seated and as specified in Section 6.3.12 these were recorded using four video cameras. The middle repetition of the second set of five was selected for analysis. This ensured consistency in the analysis process and allowed the subjects to become familiar with each activity

and the laboratory environment, ensuring that their movements were as natural and representative of their normal everyday motion as possible.

8.2 Subject details

Subject No.1 performed all the activities given in Table 8.2, with a further nine unimpaired male subjects performing activities Nos.1-10. All subjects were right-handed and performed the activities with their right arm. Details for each subject are given in Table 8.3, including their upper arm and forearm lengths. These were the only BSPs not calculated using the data of De Leva (1996a), but were measured between the shoulder, elbow and wrist centres identified from marker data during the process of anatomical calibration.

Subject	Age (years)	Height (m)	Mass (kg)	U.Arm Lgth. (cm)	Forearm Lgth. (cm)
No.1	43	1.76	81.5	31.20	26.57
No.2	23	1.85	88.5	33.39	27.31
No.3	36	1.70	60.0	29.78	26.59
No.4	31	1.71	81.0	30.77	26.07
No.5	23	1.79	82.5	31.98	27.21
No.6	58	1.72	82.5	30.93	25.78
No.7	43	1.77	82.0	30.62	25.45
No.8	30	1.71	79.0	31.83	26.70
No.9	30	1.78	81.5	31.92	28.37
No.10	26	1.77	66.0	32.63	28.51
Mean	**34.30**	**1.76**	**78.45**	**31.50**	**26.85**
SD	**11.00**	**0.05**	**8.61**	**1.06**	**1.01**

Table 8.3 Subject details for unimpaired subjects.

In addition to the ten unimpaired subjects, two further right-handed male subjects were analysed, the relevant details for whom are given in Table 8.4. Both had subacromial impingement in their right shoulder with a "painful arc" that had been resistant to steroid injections and were due to have surgery. These impaired subjects performed the ten selected activities with their affected arm.

Subject	Age (years)	Height (m)	Mass (kg)	U.Arm Lgth. (cm)	Forearm Lgth. (cm)
No.11	45	1.79	82.0	35.82	28.00
No.12	39	1.69	66.0	30.83	25.97
Mean	**42.00**	**1.74**	**74.00**	**33.32**	**26.98**
SD	**4.24**	**0.07**	**11.31**	**3.53**	**1.43**

Table 8.4 Subject details for subacromial impingement subjects.

8.3 Experimental apparatus introducing additional hand loading

During performance of activities Nos.5 - 10 by all subjects and Nos.11 - 13 by subject No.1 only, additional loading on the upper extremity was introduced by objects held in the hand. The details of these objects and their masses measured using a precision calibrated electronic balance are given in Table 8.5.

Activity	Object	Mass (kg)
No. 5	Spoon	0.048
No. 6	Mug	0.275
No. 7	Telephone Receiver	0.215
Nos. 8, 11, 12, 13	Hairbrush	0.045
No. 9, 10	Wooden Block	0.452

Table 8.5 Masses of hand-held objects during testing.

In order to gauge its relevance during performance of activities Nos.9 and 10, the moments of inertia of the wooden block were calculated using Equation 8.1 for the moment of inertia (I) of a parallelepiped about an axis through its centre of mass, where m was the mass of the block, l was its length and b its breadth.

$$I = \frac{m\left(l^2 + b^2\right)}{12} \qquad (8.1)$$

The value for the largest moment of inertia was around 0.001kgm^2, insignificant for activities performed at the velocities and accelerations achieved during everyday tasks and some way below the moments of inertia of

the limb segments, discussed in Section 3.3 and which are generally neglected during such studies (Runciman (1993)). The inertial properties of the hand-held objects were therefore ignored for the purposes of the dynamic calculations of the activities involving their use, only their mass being considered to contribute. The contributions of the segment moments of inertia were incorporated in the overall force and moment values.

8.4 Protocol for the ten selected everyday activities

8.4.1 Reach to opposite axilla

The reach to the opposite axilla started from an initial position with the right hand palm downwards on the table surface, placed to the right of the trunk mid line, anterior to the right shoulder. One full repetition was considered to involve a reach to place the hand in the left axilla, followed by a return to the initial position.

8.4.2 Reach to opposite side of neck

The reach to the opposite side of the neck started from the same initial position as the reach to the opposite axilla. One full repetition was considered to involve a reach to enclose the left side of the neck with the right hand, followed by a return to the initial position.

8.4.3 Reach to side and back of head

The reach to head side and back started from the same initial position as the reach to opposite axilla. One full repetition was considered to involve a reach to and passing of the right hand around the right side and posterior of the head, followed by a return to the initial position.

8.4.4 Eat with hand to mouth

The eat with hand to mouth started from an initial position with the right hand anterior to and in line with, the mid line of the trunk. The hand was initially held at rest on the table surface, the fingers directed downwards in a grabbing position simulating the picking of food from a plate. One full repetition

was considered to involve the raising of the hand to the mouth, followed by a return to the initial position.

8.4.5 Eat with a spoon

The eat with a spoon started from an initial position with the right hand anterior to and in line with, the mid line of the trunk, the spoon gripped in the subjects' preferred manner. One full repetition was considered to involve the raising of the spoon to the mouth, followed by a return to the initial position.

8.4.6 Drink from a mug

The drink from a mug started from an initial position with the right hand anterior to and in line with, the mid line of the trunk, the mug gripped in the subjects' preferred manner. One full repetition was considered to involve the raising and tilting of the mug to the mouth, followed by a return to the initial position.

8.4.7 Answer telephone

The answer the telephone activity started from an initial position with the right hand resting palm downwards on the receiver of a telephone placed to the right of the trunk mid line, anterior to the right shoulder. One full repetition was considered to involve the raising of the telephone receiver to the right ear, followed by a return to the initial position.

8.4.8 Brush hair left side of head

The brush the left side of the head activity started from an initial position with the right hand lateral to the trunk mid line, anterior to the right shoulder, clasping a hair brush in the subjects' preferred manner. One full repetition was considered to involve the raising and one pass of the brush from anterior to posterior of the left side of the head, followed by a return to the initial position.

8.4.9 Lift to shoulder height

The raising of the block to shoulder height started from an initial position with the right hand placed lateral to the trunk mid line, anterior to the right shoulder, gripping a wooden block of dimensions 14cm×9cm×6cm between thumb and fingers as if holding a book upright. One full repetition was considered to involve the raising and placing of the block on a shelf set at shoulder height and at approximately arm's length anterior to the right shoulder of the subject while introducing no forward movement of the trunk, followed by a return to the initial position.

8.4.10 Lift to head height

The raising of the block to head height started from the same initial position as the raise to shoulder height. One full repetition was considered to be similar to the raise to shoulder height though with the shelf set at head height.

8.4.11 Activities performed by subject No.1 only

For the activities performed by the first subject only, the brushing of the right side, back and top of the head activities had the same initial position as for brushing of the left side of the head. One full repetition was considered to involve the raising of the brush and one pass of the brush from anterior to posterior of the right side of the head, from top to bottom of the posterior of the head, or from anterior to posterior of the top of the head respectively, followed by a return to the initial position. The reach to the throat, reach to the top of the head and the placing of the hand over the mouth had the same starting position as the reach to opposite axilla activity. One full repetition was considered to involve the raising of the right hand to the throat, to the top of the head or a reach to and placing of the hand over the mouth respectively, followed by a return to the initial position.

8.5 Results obtained for ten selected everyday activities

The following sections detail the results obtained during testing of all subjects while performing each of the activities given in Table 8.2. The first section presents the subject cadences from all ten activities. Each subsequent section includes a discussion of the other kinematic and dynamic data obtained for a particular activity. For the reach to opposite axilla activity discussed in Section 8.5.2, time histories of the angles, forces and moments are presented for both the unimpaired and impaired subjects, along with the average maxima and minima of these data and the global and the average maxima and minima of the joint angular velocities and accelerations. It was considered preferable to establish the ranges in this fashion than to take the maximum and minimum values from the mean data curve, these being affected by any offset in the time normalisation of the curves.

For subsequent activities these graphical results are included in Appendix II and are referred to in the body of the text by a figure number prefixed with the letter 'A'. Forces and moments at the wrist were calculated and appear in Appendix III though are not discussed in detail.

For those activities involving an additional hand load, the absolute and the average maxima and minima of the force and moment contribution of that hand load are also presented. In some sections where they were considered of value and clear patterns emerged, angle vs. angle, velocity vs. angle, acceleration vs. angle, moment vs. angle or velocity vs. velocity graphs are included. Table 8.6 summarises all the data output permutations for each test.

Cadences	Acceleration Vs. Acceleration Plots
Shoulder, Elbow & Wrist Trajectories	External Joint Forces
Joint Angles	External Joint Moments
Angle Vs. Angle Plots	Moment Vs. Angle Plots
Velocity Vs. Angle Plots	Moment Vs. Moment Plots
Acceleration Vs. Angle Plots	Forces & Moments Due To Hand Load
Velocity Vs. Velocity Plots	Impaired Vs. Unimpaired Comparisons

Table 8.6 All permutations of the data initially output from the analysis process.

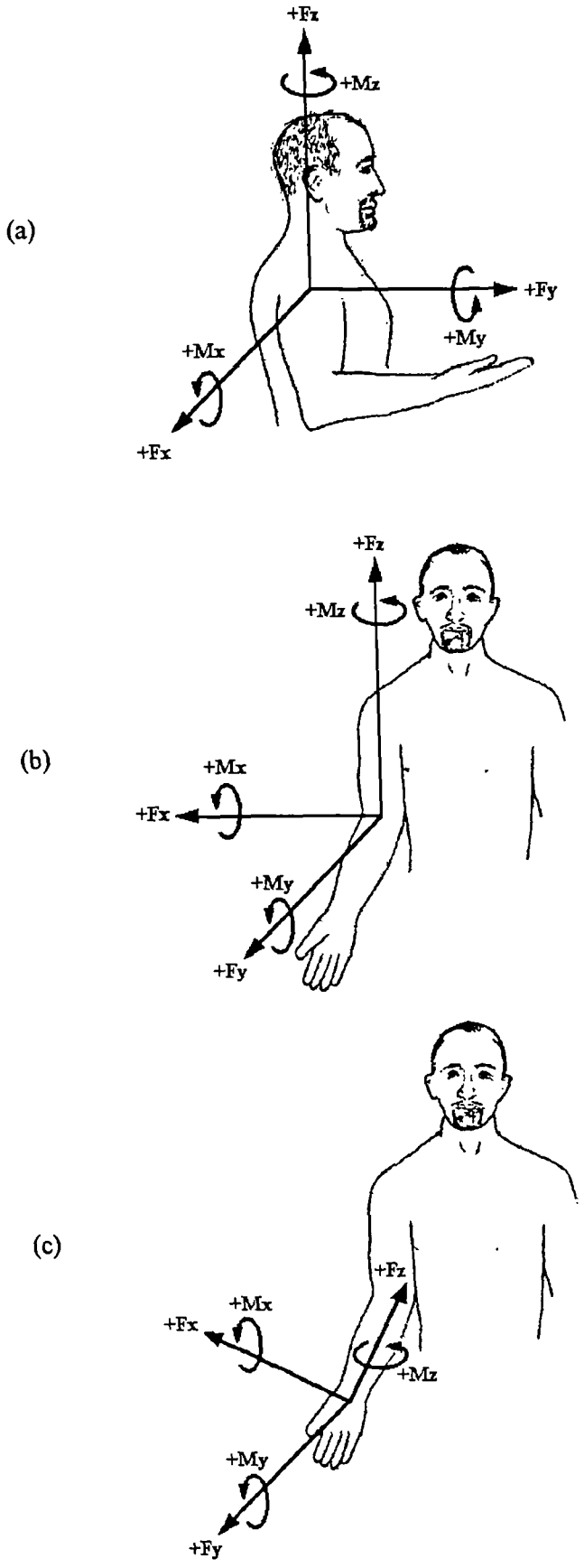

Fig.8.1 Sign conventions for the (a) shoulder, (b) elbow and (c) wrist.

The sign convention utilised during the discussion of all results in this chapter is given in Fig.8.1. Forces were taken to act positively along the positive direction of the embedded axes and represent those applied on the proximal end of the segment distal to the frame. Moments were taken to act positively about the axes following the convention of the right hand rule and represent those applied about the joint to perform the action. Positive angular rotations, velocities and accelerations act in the same direction as the positive moments about the axes.

When discussing the rotation about an axis, the axis is referred to in accordance with the positive rotation which occurred about it. Therefore when discussing forearm pronation or supination for instance, the rotations are described in terms of a positive and negative rotation respectively about the pronation axis.

8.5.1 Cadences

The cadence of each subject while performing the activities was calculated and these are summarised in Fig. 8.2. The maximum, mean and minimum values for the ten unimpaired subjects are presented along with the values for each of the two impaired subjects.

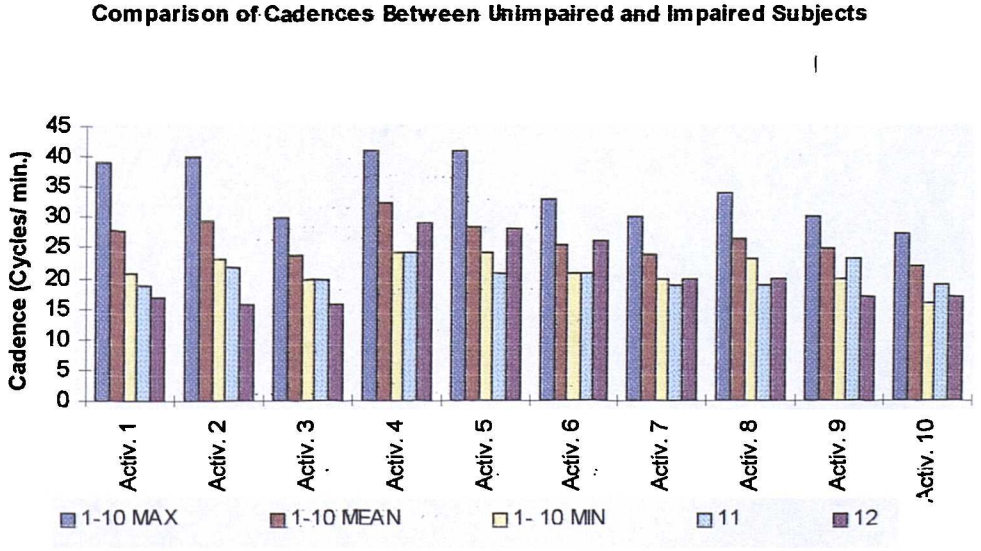

Fig 8.2 Maximum, Mean and Minimum cadences for unimpaired subjects (1-10) along with those for the impaired subjects (11, 12) during performance of all tested activities. Activity numbers are those given in Table 8.2.

The mean of all the unimpaired cadences was 0.44Hz, corresponding well with the value of 0.5Hz suggested during the discussion of the pendulum preliminary test in Section 7.3.

It can be seen that during five of the ten tested activities (1, 2 ,3, 7 & 8) the cadences of the impaired subjects were below the minimum measured cadence for the unimpaired subjects for the same activity. That this was the case for the first three activities might have been due to an early hesitation on the part of the impaired subjects through fear of causing themselves pain. The impaired subject cadences were below the mean cadence for the unimpaired subjects in all cases except that of subject No.12 for the drink from a mug activity (No.6) which was around 1% greater than the unimpaired mean.

Overall, a definite trend can be seen for the impaired subjects to have performed all of the activities at a lesser cadence than those without impairment. A reduced impaired subject cadence was expected, as these subjects would be likely to try and reduce or remove the possibility of experiencing pain.

8.5.2 Activity 1 - Reach to opposite axilla

The trajectories of the elbow and wrist joint centres are shown in Fig.8.3, the most notable feature being the similarity between the wrist trajectories from all subjects in comparison to the much less regular pattern of the elbow trajectories. Figs. 8.4, 8.5 show the angles, forces and moments at the shoulder and elbow, with the mean ±2SD boundaries in bold. These data are also summarised along with the joint angular velocities and accelerations in Tables 8.7 - 8.11.

At the shoulder, internal rotation was the major component of the motion, reaching the greatest maximum in mid-cycle from any of the ten activities. The greatest force at the shoulder was along the vertical Z axis force, with the forces applied along the X axis as the hand reached the axilla and moved away from it being among the highest values from any of the ten activities. Flexion was the greatest moment at the shoulder, though reached the lowest maximum from the unimpaired mean for any of the ten activities.

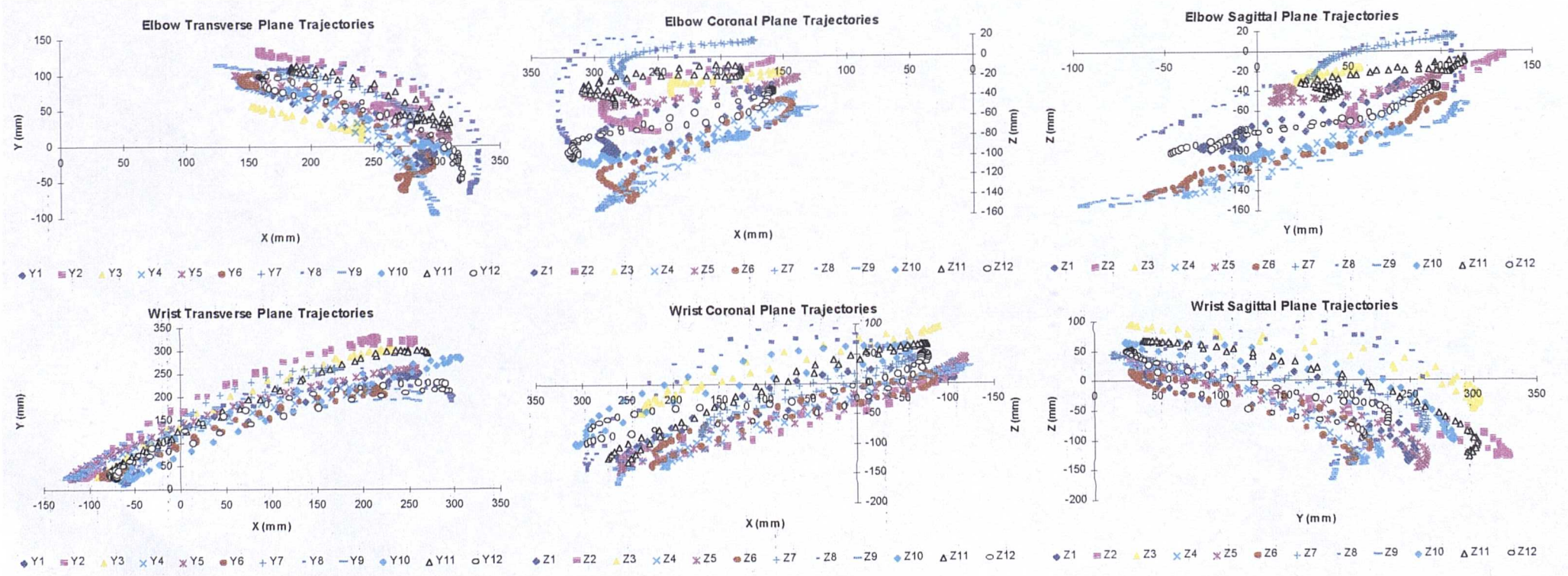

Fig.8.3 Trajectories of Elbow and Wrist in the Trunk Frame during performance of Activity 1.

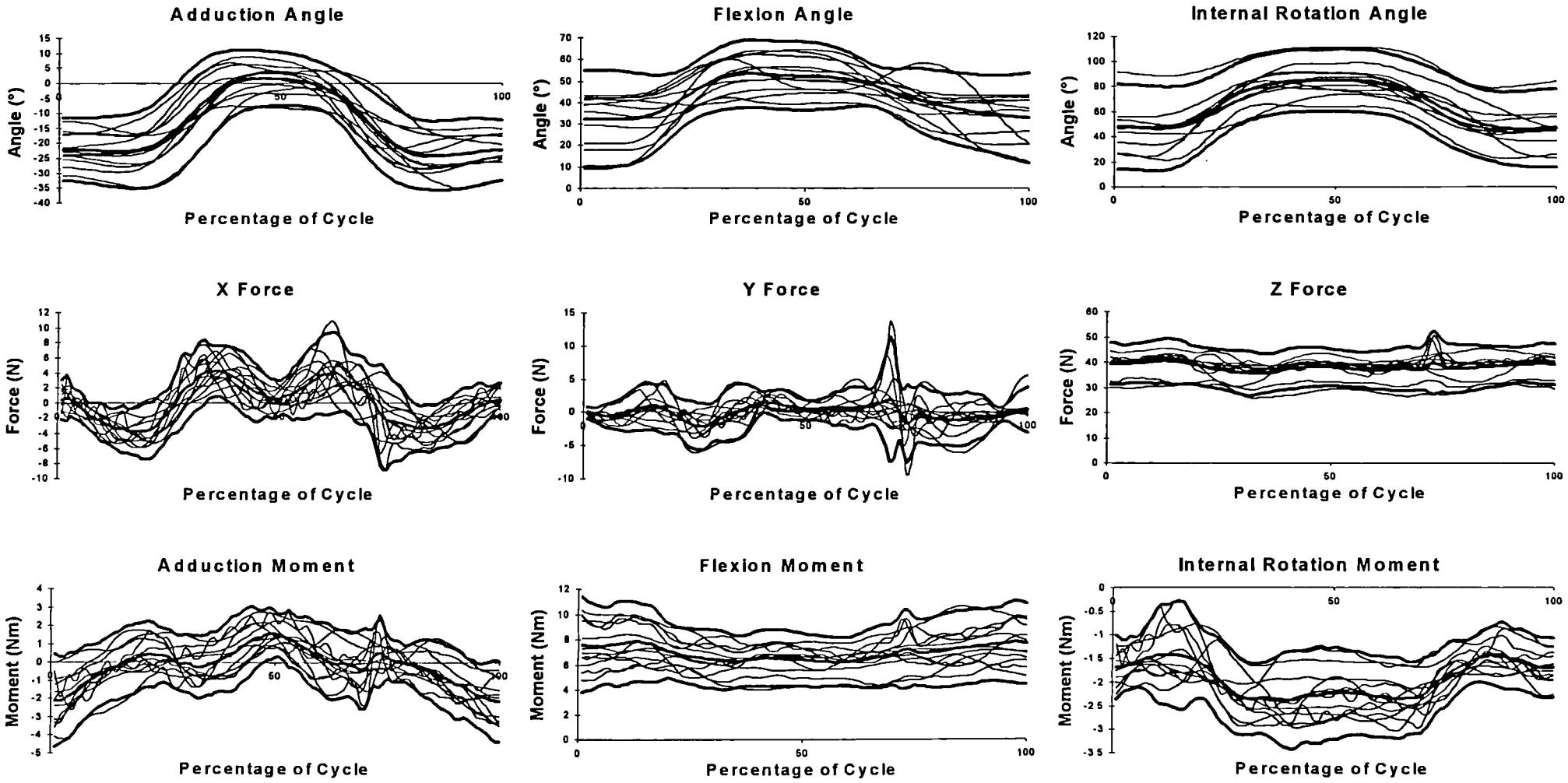

Fig 8.4 Angle, Force and Moment graphs for the Shoulder during performance of Activity 1, showing mean +/- 2SD in bold.

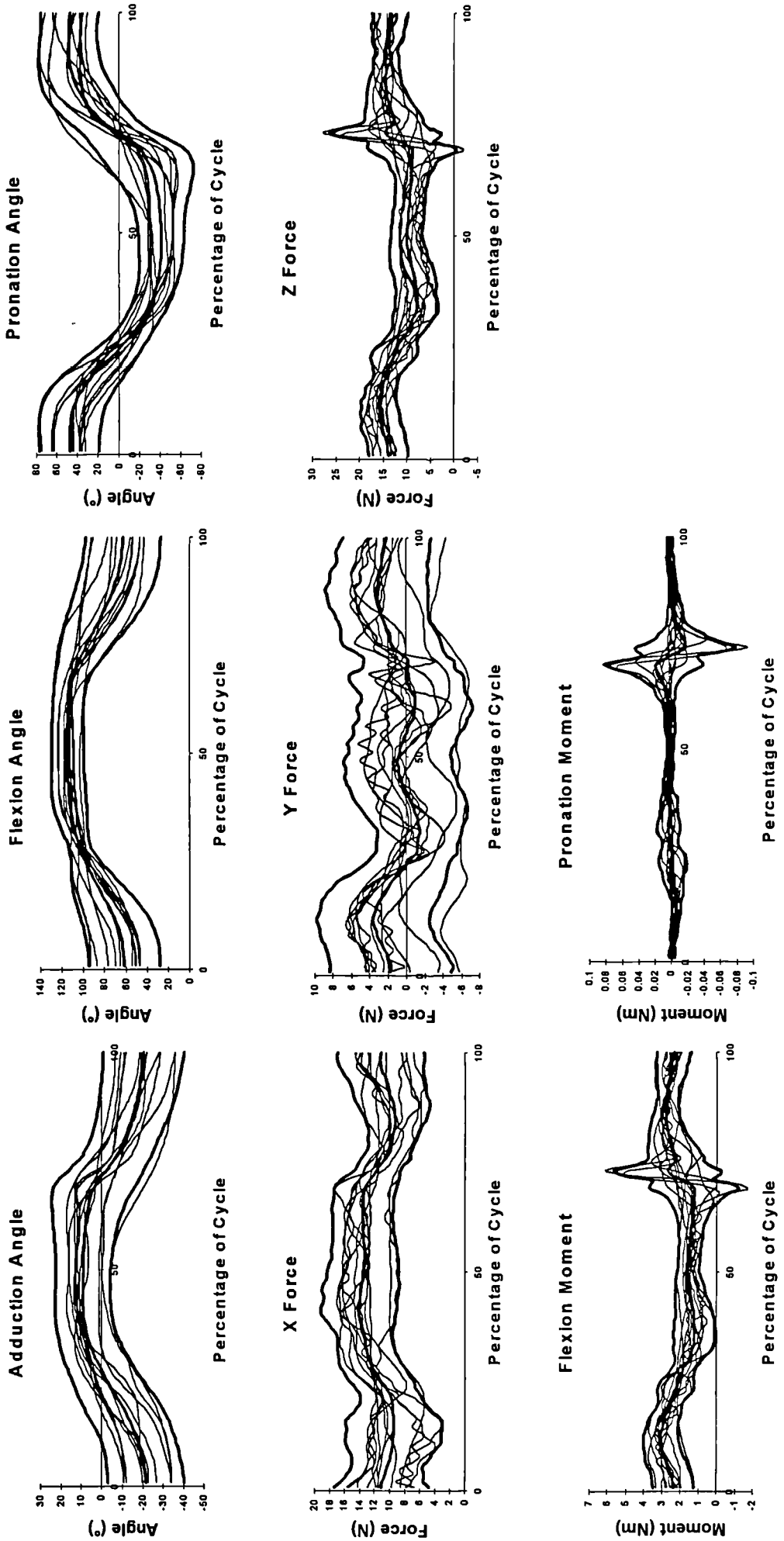

Fig 8.5 Angle, Force and Moment graphs for the Elbow during performance of Activity 1, showing mean +/- 2SD in bold.

		Sh.Add.	Sh.Flex.	Sh.Int.Rot	Elb. Add.	Elb.Flex.	Elb.Pron.
Activity 1	Max.	2.0	54.3	85.9	9.8	115.8	51.2
	SD	4.6	7.6	11.7	6.9	7.0	14.6
	Min.	-25.3	31.0	43.9	-22.2	60.5	-42.8
	SD	5.3	10.5	15.0	9.8	16.7	11.5

Table 8.7 Mean maximum and minimum joint rotations (°).

		Sh.X	Sh.Y	Sh.Z	Elb.X	Elb.Y	Elb.Z	Wr.X	Wr.Y	Wr.Z
Activity 1	Max.	6.0	4.8	42.3	14.5	4.3	18.2	5.6	-1.2	1.1
	SD	2.1	3.5	5.5	2.3	2.8	4.0	2.4	0.6	1.0
	Min.	-5.0	-3.9	34.6	7.8	-2.7	6.5	-0.2	-5.6	-1.1
	SD	1.7	2.3	4.0	2.6	2.2	3.6	0.6	0.5	0.9

Table 8.8 Mean maximum and minimum joint forces (N).

		Sh.Add.	Sh.Flex.	Sh.Int.Rot.	El.Flex.	Wr.U.Dev.	Wr.Flex.
Activity 1	Max.	1.9	8.2	-1.1	3.6	0.0	-0.1
	SD	0.6	1.5	0.5	1.0	0.0	0.0
	Min.	-2.4	5.6	-2.6	0.7	-0.4	-0.4
	SD	1.1	1.0	0.4	1.0	0.2	0.0

Table 8.9 Mean maximum and minimum joint moments (Nm).

		Sh.Flex.	Sh.Add.	Sh.Int.Rot.	Elb.Flex.	Elb.Pron.
Activity 1	Max.	1.1	1.2	1.9	2.0	4.8
	SD	0.6	0.3	0.7	0.9	2.5
	Min.	-1.0	-1.2	-1.6	-1.9	-4.0
	SD	0.5	0.2	0.4	0.9	1.5

Table 8.10 Mean maximum and minimum joint angular velocities ($rads^{-1}$).

		Sh.Flex.	Sh.Add.	Sh.Int.Rot.	Elb.Flex.	Elb.Pron.
Activity 1	Max.	5.8	5.9	9.8	9.7	30.9
	SD	2.7	1.8	4.2	7.0	29.5
	Min.	-5.4	-6.2	-8.3	-11.4	-29.5
	SD	3.1	1.3	3.5	9.8	28.4

Table 8.11 Mean maximum and minimum joint angular accelerations ($rads^{-2}$).

At the elbow the second largest range of pronation and the narrowest range of flexion from the unimpaired subjects for any of the ten activities were obtained. The major component of force was along the humeral longitudinal (Z) axis. A negative force along the Y axis occurred as the hand reached the axilla and moved away from it. Flexion was the greatest moment at the elbow.

Figs. 8.6 and 8.7 show the angles, forces and moments at the shoulder and elbow obtained from the impaired subjects, along with the unimpaired subject mean and ± 2SD boundaries. The unimpaired and impaired maxima and minima are given in Fig. 8.8 the key for which is given in Table 8.12 and is the same for all such plots presented for the ten activities.

No.	Angle Plots	No.	Force Plots	No.	Moment Plots
1	Shoulder Adduction	1	Shoulder X	1	Shoulder Adduction
2	Shoulder Flexion	2	Shoulder Y	2	Shoulder Flexion
3	Shoulder Int. Rotn.	3	Shoulder Z	3	Shoulder Int. Rotn.
4	Elbow Adduction	4	Elbow X	4	Elbow Flexion
5	Elbow Flexion	5	Elbow Y	5	Elbow Pronation
6	Elbow Pronation	6	Elbow Z	6	Wrist Ulnar Deviation
		7	Wrist X	7	Wrist Flexion
		8	Wrist Y		
		9	Wrist Z		

Table 8.12 Key for angle, force and moment maxima and minima plots.

At the shoulder subject No.11 failed to reach the adducted position of the unimpaired mean but reached a greater maximum of elbow flexion. Subject No.12 failed to reach a maximum shoulder flexion close to that of the unimpaired mean, though had a greater range of pronation at the elbow, reaching a greater maximum value than the unimpaired mean from any of the ten activities.

At the shoulder, as with the unimpaired subjects, the Z axis force was the greatest, with that of subject No.11 maintaining a constant level greater than subject No.12. At the elbow both impaired subjects exhibited negative Y axis forces similar to the unimpaired mean, the only negative Y axis forces from these subjects for any of the ten activities. The X axis became vertically

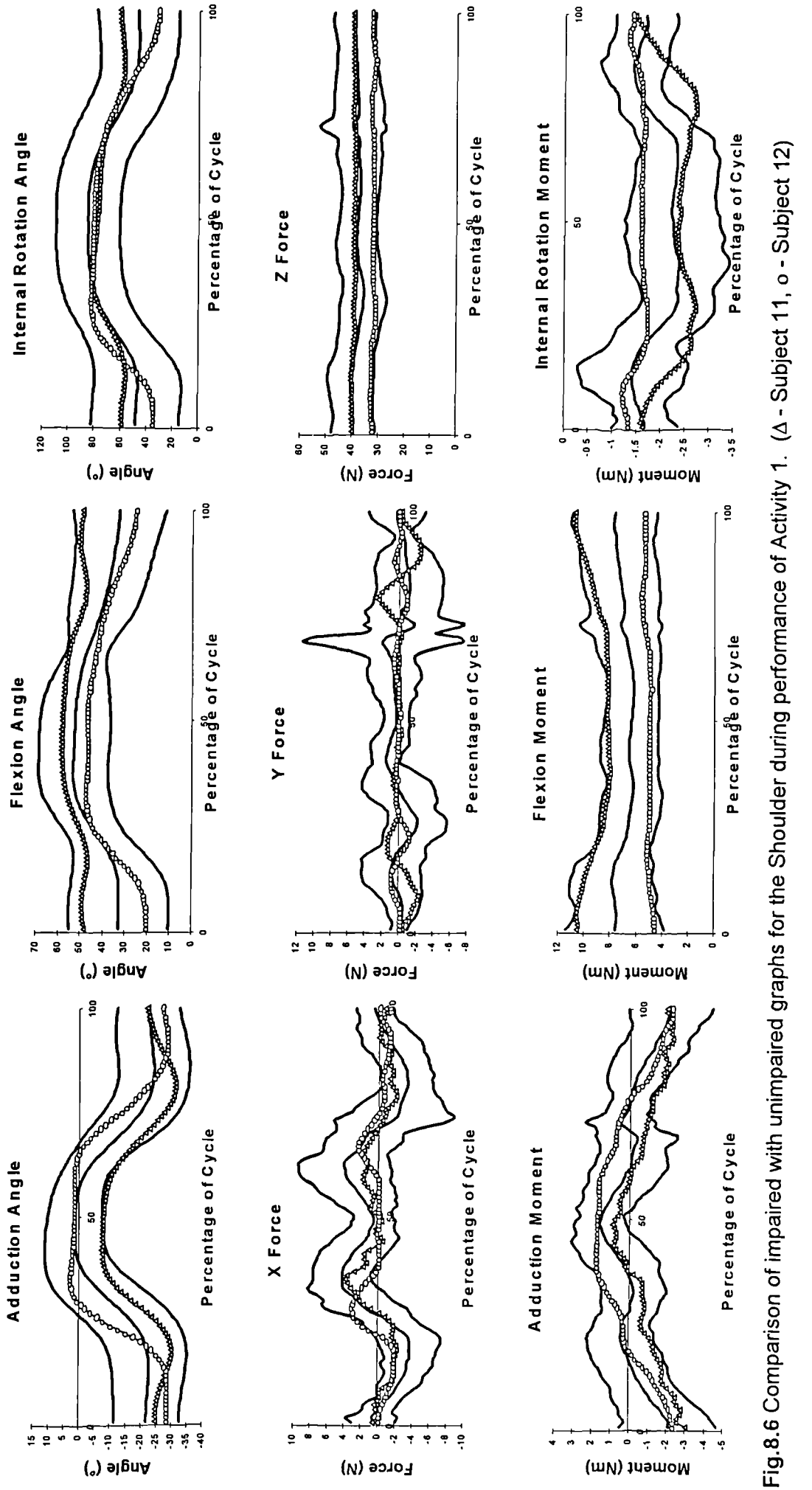

Fig.8.6 Comparison of impaired with unimpaired graphs for the Shoulder during performance of Activity 1. (Δ - Subject 11, o - Subject 12)

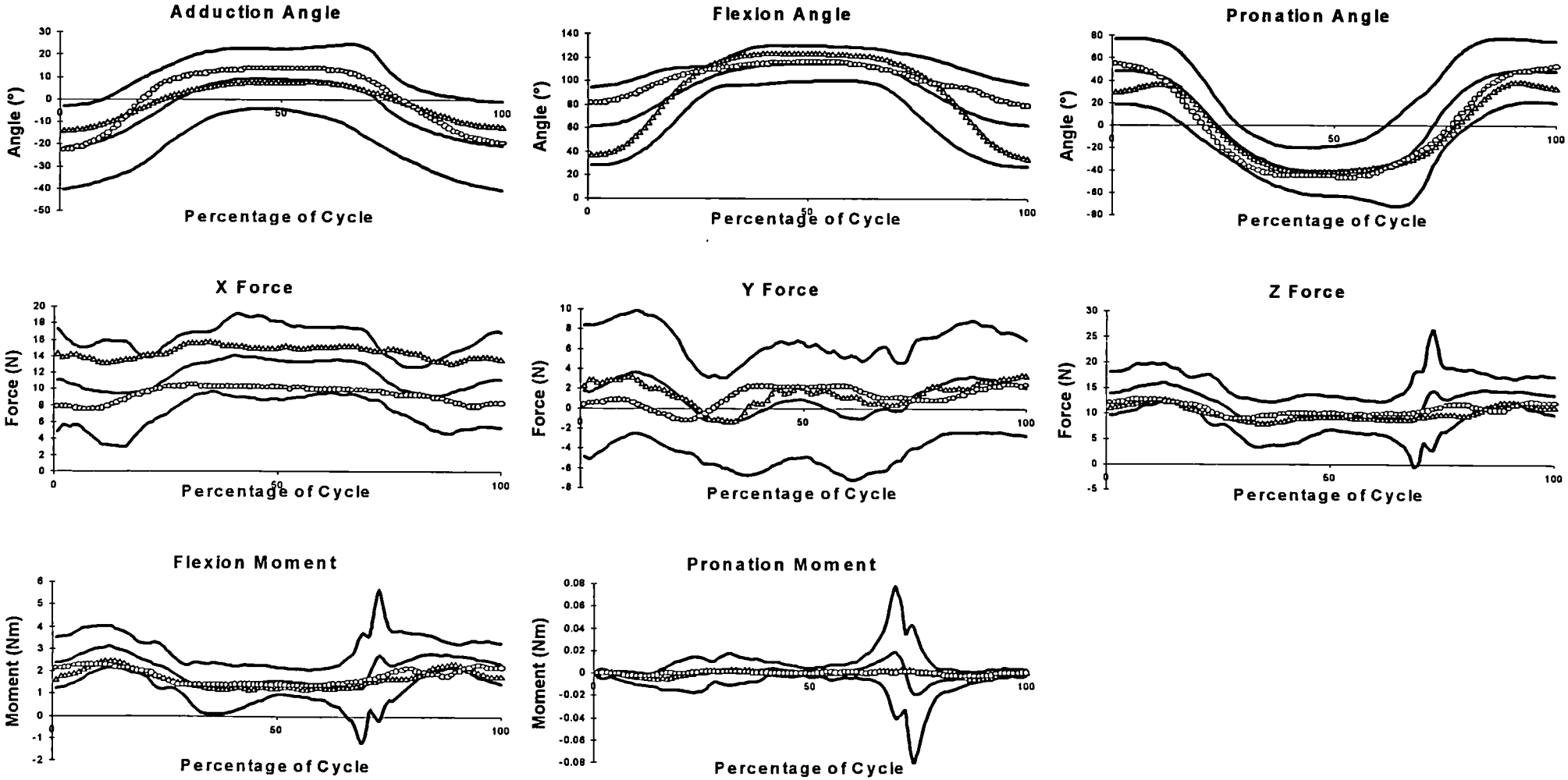

Fig.8.7 Comparison of impaired with unimpaired graphs for the Elbow during performance of Activity 1. (Δ - Subject 11, o - Subject 12)

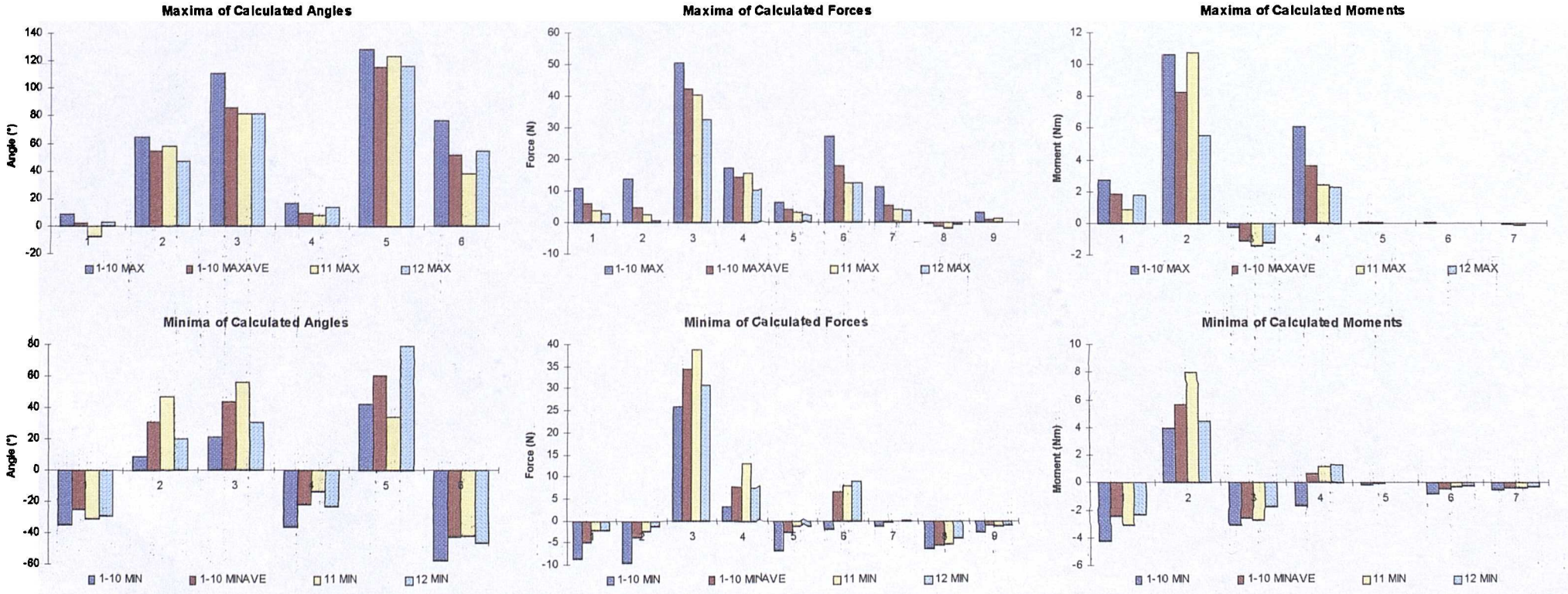

Fig.8.8 Unimpaired global maximum (1-10 Max), global minimum (1-10 Min), mean maximum (1-10 Maxave) and mean minimum (1-10 Minave) Angle, Force and Moment values, along with impaired maximum (11 Max, 12 Max) and minimum (11 Min, 12 Min) during performance of Activity 1. Key as in Table 8.12.

oriented in mid-cycle leading to a wider variation in the forces along this axis between subjects due to the difference in their masses. A similar effect can be seen in the shoulder flexion and internal rotation moment patterns in Figs. 8.6 and 8.8.

The global and mean maxima and minima of the velocities and accelerations for the unimpaired subjects at each of the modelled joints, along with the maxima and minima of the impaired subjects, are given in Fig.8.9, the key for which is given in Table 8.8 and is the same for all such plots discussed.

No.	Velocity Plots	No.	Acceleration Plots
1	Shoulder Flexion	1	Shoulder Flexion
2	Shoulder Adduction	2	Shoulder Adduction
3	Shoulder Int. Rotn.	3	Shoulder Int. Rotn.
4	Elbow Flexion	4	Elbow Flexion
5	Elbow Pronation	5	Elbow Pronation

Table 8.13 Key for angular velocity and acceleration maxima and minima plots.

The average maximum impaired velocity was between 40% and 45% lower than the mean of the unimpaired subjects. The maximum elbow flexion velocity of subject No.11 was greater than the unimpaired mean though the range of flexion for this subject was around 34° greater than for the unimpaired subjects. The average maximum impaired accelerations were between 50% and 55% lower than the mean of the unimpaired subjects.

8.5.3 Activity 2 - Reach to opposite side of neck

A similarity between the wrist and elbow trajectories from all subjects for this activity was apparent as shown in Fig.A.8.10 for this activity.

Fig.A.8.11 and A.8.12 show the angles, forces and moments at the shoulder and elbow, with these data also summarised along with the joint angular velocities and accelerations in Tables 8.14 - 8.18. At the shoulder, flexion and internal rotation contributed similarly with adduction having the greatest range and reaching the most adducted position from any of the ten activities performed. The forces along the X axis reached their maximum

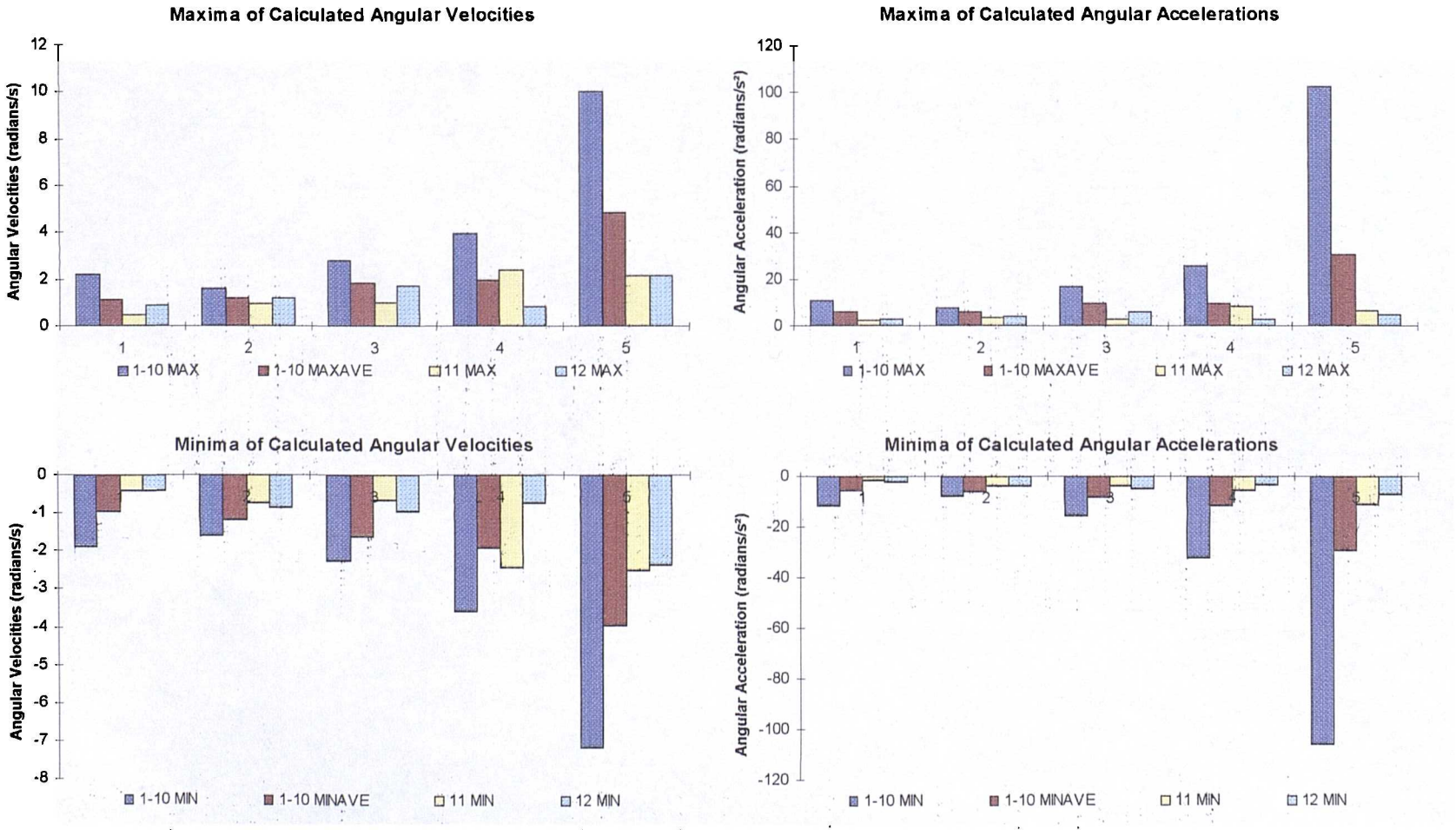

Fig.8.9 Unimpaired global maximum (1-10 Max), global minimum (1-10 Min), mean maximum (1-10 Maxave) and mean minimum (1-10 Minave) Angular Velocity and Acceleration, along with impaired maximum (11 Max, 12 Max) and minimum (11 Min, 12 Min) during performance of Activity 1. Key as in Table 8.13.

		Sh.Add.	Sh.Flex.	Sh.Int.Rot	Elb. Add.	Elb.Flex.	Elb.Pron.
Activity 2	Max.	20.1	76.8	85.2	3.1	138.9	52.0
	SD	9.2	11.9	8.2	5.7	5.2	13.0
	Min.	-23.4	28.4	42.1	-23.8	63.3	-53.7
	SD	10.2	11.1	12.4	12.3	16.3	12.6

Table 8.14 Mean maximum and minimum joint rotations (°).

		Sh.X	Sh.Y	Sh.Z	Elb.X	Elb.Y	Elb.Z	Wr.X	Wr.Y	Wr.Z
Activity 2	Max.	8.3	5.8	45.2	17.0	6.4	19.5	5.6	-0.8	1.8
	SD	3.3	2.5	4.6	2.5	1.8	2.5	1.1	1.1	1.0
	Min.	-7.4	-7.9	31.0	6.6	-3.3	-0.3	0.1	-6.3	-1.7
	SD	2.4	3.4	4.1	3.0	2.2	3.3	0.7	0.8	0.8

Table 8.15 Mean maximum and minimum joint forces (N).

		Sh.Add.	Sh.Flex.	Sh.Int.Rot.	El.Flex.	Wr.U.Dev.	Wr.Flex.
Activity 2	Max.	2.0	9.5	-0.9	4.0	0.0	0.0
	SD	0.9	1.3	0.6	0.5	0.1	0.1
	Min.	-2.5	4.9	-2.5	-0.5	-0.4	-0.4
	SD	1.0	0.7	0.3	0.5	0.1	0.1

Table 8.16 *Mean maximum and minimum joint moments (Nm).*

		Sh.Flex.	Sh.Add.	Sh.Int.Rot.	Elb.Flex.	Elb.Pron.
Activity 2	Max.	2.2	1.8	1.9	2.7	5.4
	SD	0.8	0.5	0.7	1.0	1.8
	Min.	-1.8	-1.7	-2.0	-2.8	-4.3
	SD	0.7	0.7	0.7	0.8	1.1

Table 8.17 Mean maximum and minimum joint angular velocities ($rads^{-1}$).

		Sh.Flex.	Sh.Add.	Sh.Int.Rot.	Elb.Flex.	Elb.Pron.
Activity 2	Max.	9.6	8.8	11.1	12.9	34.2
	SD	4.2	3.0	5.2	3.5	20.9
	Min.	-8.9	-8.9	-10.6	-13.6	-29.8
	SD	2.7	3.6	5.3	5.0	12.0

Table 8.18 Mean maximum and minimum joint angular accelerations ($rads^{-2}$).

positive and negative values from any of the ten activities with the Y axis force reaching the greatest negative value from any of these tests.

At the elbow flexion was a major component and pronation had the greatest range with the most supinated position from any of the ten activities being reached. The force in the direction of the X axis reached the third highest maximum and the force along the Y axis the greatest negative value for any of the ten activities performed due to the vertical orientation of these axes during the cycle. An extension moment was required at the elbow in mid-cycle.

Figs.A.8.13 and A.8.14 show the angles, forces and moments at the shoulder and elbow, obtained during performance of this activity by the impaired subjects with Fig.A.8.15 showing the unimpaired and impaired maxima and minima.

At the shoulder, subject No.11 had lower ranges of flexion and internal rotation than the unimpaired mean and failed to reach the adducted position of that mean. At the elbow, this subject reached a considerably greater maximum flexion than the unimpaired mean and a more supinated position than the maximum supination of the unimpaired mean from any of the ten activities.

Subject No.12 reached a lower maximum of internal rotation at the shoulder in mid-cycle than the unimpaired mean though reached a greater maximum of flexion. Similar elbow flexion and supination maxima to the unimpaired mean were reached but a lower maximum pronation.

The shoulder Z axis forces for subjects No.11 and No.12 varied in the upper and lower levels of the mean unimpaired force range respectively, with the magnitudes of the minimum for subject No.12 being lower for this activity than the unimpaired mean from any activity. The moments about each of the modelled degrees of freedom exhibited similar patterns. The shoulder internal rotation moment of subject No.11 varied considerably as shown in Fig.A.8.13, due to the large ranges of elbow flexion and pronation and had a greater negative magnitude than the unimpaired mean.

The absolute and mean unimpaired maxima and minima of the angular velocities and accelerations about each joint axis, along with the maxima and minima from the impaired subjects are given in Fig.A.8.16. The average maximum velocity for this activity was between 40% and 45% less than the

unimpaired mean for subjects No.11 and No.12, the elbow flexion velocity of subject No.11 being an exception. The average maximum acceleration at all modelled joints was between 50% and 60% lower for the impaired subjects than the unimpaired mean.

8.5.4 Activity 3 - Reach to side and back of head

Due to the high complexity of this activity subjects adopted varied strategies. This made finding a suitable camera arrangement difficult, resulting in marker visibility problems in mid-cycle for some subjects where both anterior and posterior views were required. It was necessary to interpolate between the trajectories of the markers prior to and following the frames in which they were obscured. For subjects No.3, No.4 and No.8 the data obtained in this way was found to be unsatisfactory, interpolation being necessary across several frames and resulting in a section of unreliable data. It was therefore decided that for this activity only, the data from these three subjects would not be included, the data presented in this section being that obtained from subjects Nos.1, 2, 5, 6, 7, 9, 10,11 and 12.

Fig.A.8.17 shows little repeated pattern in the elbow and wrist trajectories for this activity with the exception of the sagittal plane wrist trajectory. Figs.A.8.18 and A.8.19 show the angles, forces and moments at the shoulder and elbow with these data also summarised along with the joint angular velocities and accelerations in Tables 8.19 - 8.23. At the shoulder, flexion and abduction both reached their second highest maximum values from any of the ten activities, the shoulder maintaining an abducted position throughout. The minimum vertical Z axis force was the lowest from the unimpaired subjects for any of the ten activities as was the minimum of the shoulder flexion moment.

At the elbow, flexion and pronation both reached their greatest maxima from any of the ten activities. A negative force occurred along the Z axis in mid-cycle, the shoulder flexing past 90°, taking the humeral longitudinal axis past horizontal. The maximum force in the Y direction was the greatest from the unimpaired subjects for any of the ten activities performed. The greatest extension moment from the unimpaired subjects for any of the ten activities

		Sh.Add.	Sh.Flex.	Sh.Int.Rot	Elb. Add.	Elb.Flex.	Elb.Pron.
Activity 3	Max.	-16.9	107.9	63.2	-0.9	164.8	65.3
	SD	7.6	9.0	13.0	13.7	8.0	8.2
	Min.	-35.7	26.7	21.9	-25.7	61.4	7.3
	SD	11.0	9.3	11.4	7.4	14.8	19.9

Table 8.19 Mean maximum and minimum joint rotations (°).

		Sh.X	Sh.Y	Sh.Z	Elb.X	Elb.Y	Elb.Z	Wr.X	Wr.Y	Wr.Z
Activity 3	Max.	4.4	6.1	47.0	14.5	14.0	21.8	4.8	2.1	0.9
	SD	1.7	1.9	2.5	3.3	3.5	2.1	1.1	0.9	0.7
	Min.	-4.3	-5.4	30.1	6.0	0.2	-4.8	-5.8	-7.2	-3.2
	SD	1.3	1.7	3.9	2.9	1.5	2.1	0.9	0.7	0.5

Table 8.20 Mean maximum and minimum joint forces (N).

		Sh.Add.	Sh.Flex.	Sh.Int.Rot.	El.Flex.	Wr.U.Dev.	Wr.Flex.
Activity 3	Max.	1.2	9.5	-0.5	4.5	0.4	0.2
	SD	0.5	1.5	0.4	0.6	0.1	0.1
	Min.	-2.8	3.9	-2.0	-2.8	-0.4	-0.5
	SD	1.2	1.0	0.4	0.9	0.1	0.1

Table 8.21 Mean maximum and minimum joint moments (Nm).

		Sh.Flex.	Sh.Add.	Sh.Int.Rot.	Elb.Flex.	Elb.Pron.
Activity 3	Max.	1.7	0.7	1.1	3.6	2.3
	SD	0.6	0.5	0.4	0.9	0.8
	Min.	-2.8	-0.5	-1.9	-3.8	-2.4
	SD	1.1	0.2	1.3	0.9	1.1

Table 8.22 Mean maximum and minimum joint angular velocities ($rads^{-1}$).

		Sh.Flex.	Sh.Add.	Sh.Int.Rot.	Elb.Flex.	Elb.Pron.
Activity 3	Max.	10.9	4.9	11.0	17.1	19.1
	SD	5.5	2.7	7.1	6.4	9.6
	Min.	-11.7	-4.0	-10.2	-16.1	-20.9
	SD	6.1	3.0	10.1	6.0	11.6

Table 8.23 Mean maximum and minimum joint angular accelerations ($rads^{-2}$).

tested was required around mid-cycle as the humeral longitudinal axis passed horizontal with the elbow fully flexed.

Figs.A.8.20 and A.8.21 show the angles, forces and moments at the shoulder and elbow, obtained from the impaired subjects with the maxima and minima of these data given in Fig.A.8.22. At the shoulder subject No.11 reached a considerably lower maximum of internal rotation and a lower level of abduction than the unimpaired mean, though flexion reached a maximum in mid-cycle similar to the greatest value from the unimpaired mean for any of the ten activities. The elbow became supinated in mid-cycle unlike the unimpaired mean and reached a lower maximum pronation, though flexion reached a similar maximum to the unimpaired mean and the greatest value for this subject from any activity.

For subject No.12 the maximum shoulder flexion in mid-cycle was considerably less than the unimpaired mean as was the maximum level of abduction. Internal rotation was considerably less than the unimpaired mean initially and reached a lower minimum. At the elbow the maximum of pronation was around half that of the unimpaired mean and flexion reached a lower maximum.

The shoulder Z axis force for subject No.11 had greater maximum and minimum values than the unimpaired mean with a greater negative maximum for the X axis force. Those of subject No.12 were considerably lower than the unimpaired mean. At the elbow, subject No.11 had greater maximum Y axis force and a greater negative Z axis force than any values from the unimpaired mean for any activity. The elbow extension moment of subject No.11 in mid-cycle was greater than any from the unimpaired mean for any activity.

The absolute and mean unimpaired maxima and minima of the angular velocities and accelerations about each joint axis, along with the maxima and minima from the impaired subjects are given in Fig.A.8.23. The average maximum angular velocity at all modelled joints for subject No.12 was between 46% and 48% less than the unimpaired mean, with the average maximum acceleration between 60% and 70% less. For subject No.11 the average maximum upward (positive) velocity was 2% greater than the unimpaired mean, though the downward (negative) velocity was around 25% lower. The average

maximum upward acceleration was around 17% less than the unimpaired mean and the downward acceleration some 31% less.

8.5.5 Activity 4 - Eat with hand to mouth (repetition from Williams (1996))

The trajectories of the elbow and wrist joint centres for this activity are shown in Fig.A.8.24 to have had little repeated pattern other than that of the sagittal plane wrist trajectory. Figs.A.8.25 and A.8.26 show the angles, forces and moments at the shoulder and elbow with these data also summarised along with the joint angular velocities and accelerations in Tables 8.24 - 8.28. At the shoulder the smallest ranges for all three rotations from any of the ten activities were obtained and the adduction moments were among the lowest measured.

At the elbow, flexion was the primary rotation with the major component of force being along the Z axis. An extension moment at the elbow was required around mid-cycle as the forearm longitudinal axis passed vertical with the shoulder flexed. Fig.8.27 shows the relationship between elbow flexion moment and angle. As elbow flexion began from the initial position a large moment was necessary to counteract the action of gravity on the forearm mass centre, maximally horizontally displaced from the axis of rotation. As flexion increased, this horizontal displacement was reduced leading to a decrease in the moment required.

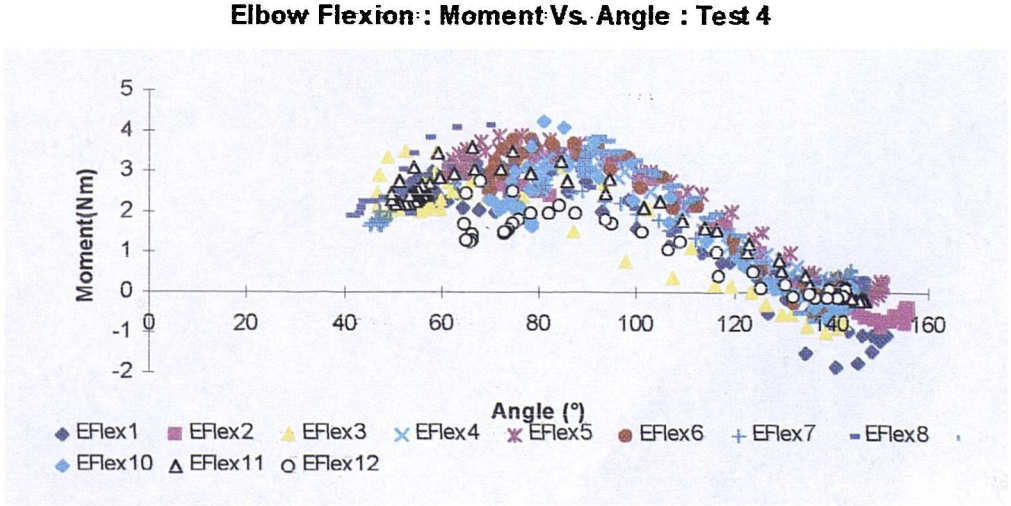

Fig 8.27 Elbow flexion Moment Vs. Angle during eat with hand to mouth.

		Sh.Add.	Sh.Flex.	Sh.Int.Rot	Elb. Add.	Elb.Flex.	Elb.Pron.
Activity 4	Max.	-9.2	51.0	54.7	-1.3	144.0	49.9
	SD	6.5	7.7	11.1	5.1	4.1	14.6
	Min.	-16.2	38.0	42.0	-18.3	60.4	-24.2
	SD	7.7	9.7	11.8	9.4	15.5	18.3

Table 8.24 Mean maximum and minimum joint rotations (°).

		Sh.X	Sh.Y	Sh.Z	Elb.X	Elb.Y	Elb.Z	Wr.X	Wr.Y	Wr.Z
Activity 4	Max.	2.1	4.8	42.3	12.3	9.0	16.8	4.5	-1.6	-0.4
	SD	0.8	2.3	3.2	2.8	2.5	2.2	0.8	0.9	0.8
	Min.	-1.8	-4.0	35.4	8.9	2.9	7.4	-0.8	-5.9	-3.5
	SD	0.9	1.7	4.2	2.7	1.9	2.7	0.6	0.5	0.6

Table 8.25 Mean maximum and minimum joint forces (N).

		Sh.Add.	Sh.Flex.	Sh.Int.Rot.	El.Flex.	Wr.U.Dev.	Wr.Flex.
Activity 4	Max.	0.9	9.5	-1.1	3.5	0.1	-0.1
	SD	1.0	1.4	0.3	0.4	0.1	0.1
	Min.	-0.7	5.4	-2.0	-0.6	-0.3	-0.4
	SD	0.8	0.9	0.5	0.6	0.1	0.0

Table 8.26 Mean maximum and minimum joint moments (Nm).

		Sh.Flex.	Sh.Add.	Sh.Int.Rot.	Elb.Flex.	Elb.Pron.
Activity 4	Max.	0.7	0.3	0.6	3.1	3.9
	SD	0.2	0.2	0.3	0.7	1.7
	Min.	-0.6	-0.4	-0.7	-3.3	-3.3
	SD	0.3	0.2	0.3	0.8	1.3

Table 8.27 Mean maximum and minimum joint angular velocities ($rads^{-1}$).

		Sh.Flex.	Sh.Add.	Sh.Int.Rot.	Elb.Flex.	Elb.Pron.
Activity 4	Max.	4.7	2.5	4.8	14.4	22.2
	SD	2.8	1.1	2.6	6.2	11.4
	Min.	-3.4	-2.1	-3.8	-13.3	-24.7
	SD	1.5	0.8	2.1	4.1	10.9

Table 8.28 Mean maximum and minimum joint angular accelerations ($rads^{-2}$).

The shoulder and elbow angular data were compared with graphs presented by Williams (1996), examples of which are given in Fig.7.15 and Fig.7.16. The values were corrected for differences in embedded axes definitions and initial limb orientations and are shown in Tables 8.29 and 8.30 in relation to the axes defined for the current study.

	Mean Range	**± 2SD boundaries**
Shoulder Flexion	60° → 67°	34° → 94°
Shoulder Adduction	5° → -11°	21° → -35°
Shoulder Internal Rotation	52° → 24°	88° → -11°.

Table 8.29 Approximate mean shoulder angles ranges from Williams (1996).

	Mean Range	**± 2SD boundaries**
Elbow Flexion (Max)	137°	109° → 166°
Elbow Flexion (Min)	*33°*	*-2° → 68°*
Elbow Adduction	-15° → -9°	-32° → 11°
Elbow Pronation	32° → -13°	71° → -81°

Table 8.30 Approximate mean elbow angle ranges from Williams (1996).

The mean ranges of shoulder flexion and adduction from the current study were slightly lower than those of Williams (1996), though the mean range of internal rotation from both studies corresponds closely. The initial minimum elbow flexion from Williams (1996) was lower as the table surface in that study was set at waist height, lower than the elbow height used for the current study. The elbow flexion maxima from both studies were similar, with the mean range of pronation at the elbow from the current study being slightly greater.

Figs.A.8.28 and A.8.29 show the angles, forces and moments at the shoulder and elbow obtained from the impaired subjects, with the unimpaired and impaired maxima and minima of these data given in Fig.A.8.30. Subject No.11 had a lesser amount of shoulder internal rotation than the unimpaired mean, particularly in mid-cycle where the hand reached the mouth, with a lower

flexion also being reached at this point. A steady level of abduction greater than the unimpaired mean was maintained. At the elbow the maximum supination as the hand reached the mouth was considerably greater than the unimpaired mean, with the maximum of flexion similar to the unimpaired mean.

Subject No.12 was more internally rotated and abducted at the shoulder than the mean of unimpaired subjects throughout the cycle and also reached a greater maximum flexion. At the elbow a greater supination than the unimpaired subject mean was reached in mid-cycle though the flexion maximum was similar.

The shoulder Z axis force and all moments for subject No.11 can be seen to have varied in the upper levels of the mean unimpaired range with those of subject No.12 considerably lower. The maximum forces and moments at shoulder and elbow from both subjects were comparable to the unimpaired mean however.

The absolute and mean unimpaired maxima and minima of the velocities and accelerations of rotation about each joint axis, along with the maxima and minima from the impaired subjects are given in Fig.A.8.31. The maximum angular velocities at the shoulder were generally lower than those resulting from the larger range of motion at the elbow. The average maximum upward velocity at the shoulder from subjects No.11 and No.12 was around 36-37% less than the unimpaired mean, with the downward velocity around 3-4% less. At the elbow the average maximum velocity was around 8-9% less than the unimpaired mean.

The relationship between the elbow flexion angular velocity and angle in the phase plane diagram in Fig.8.32, shows the large elbow flexion range and a similar pattern from all subjects, indicating the importance of the rotation to this activity. The area above the X axis represents increasing elbow flexion moving the hand towards the mouth, the area below represents elbow extension as the hand moves away, returning to its initial position. The maximum velocity clearly occurs around the mid-point in both phases of the motion and the X-axis symmetry for the unimpaired subjects indicates the general similarity in the flexion and extension velocities. A decrease in the extension phase velocities for the impaired subjects is also apparent.

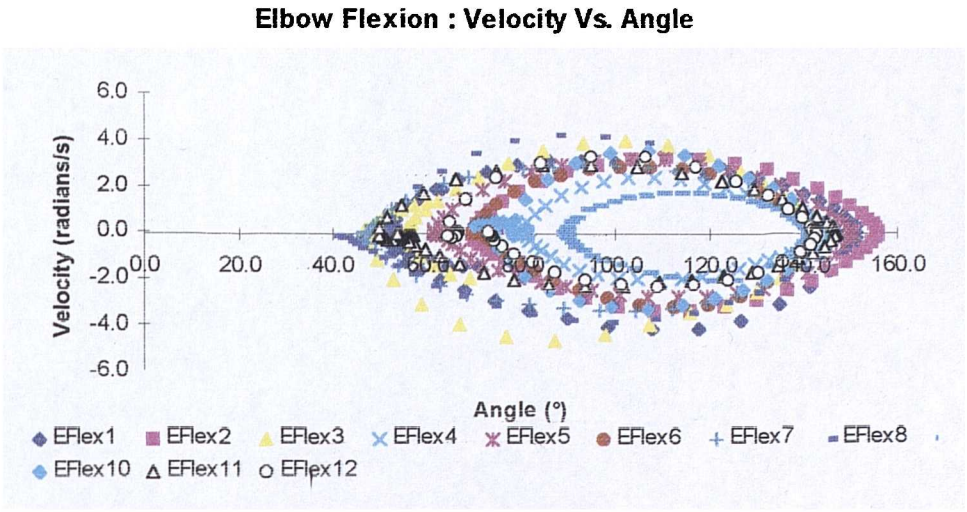

Fig.8.32 Elbow flexion Velocity Vs. Angle during eat with hand to mouth.

The acceleration plots in Fig.A.8.31 show the average maximum acceleration at all modelled joints for subject No.11 to be between 30% and 35% lower than the unimpaired mean. Subject No.12 showed average maximum shoulder accelerations between 70% and 75% lower than the unimpaired mean with those at the elbow between 15% and 20% greater.

8.5.6 Activity 5 - Eat with spoon

The trajectories of the elbow and wrist joint centres given in Fig.A.8.33 show little repeated pattern other than that of the sagittal plane wrist trajectory. Figs.A.8.34 and A.8.35 show the angles, forces and moments at the shoulder and elbow during this activity with these data also summarised along with the joint angular velocities and accelerations in Tables 8.31 - 8.35. At the shoulder, flexion and internal rotation had the lowest maximum values for any activity and the shoulder remained abducted throughout. All three rotations at the shoulder had similar ranges of around 16°, among the lowest from any activity. The shoulder Z axis force maintained a constant level while the force along the X axis had the lowest magnitudes in both positive and negative directions from any activity. Those along the Y axis were similarly low. The maximum and minimum flexion moments were the second lowest from all ten activities and this was one of only two activities for which an abduction moment was required throughout.

		Sh.Add.	Sh.Flex.	Sh.Int.Rot	Elb. Add.	Elb.Flex.	Elb.Pron.
Activity 5	Max.	-17.6	49.8	46.3	-0.7	147.6	7.3
	SD	9.8	10.7	8.2	5.9	1.8	29.9
	Min.	-34.3	33.6	30.1	-14.5	62.2	-26.8
	SD	12.5	12.5	8.1	13.1	12.2	15.5

Table 8.31 Mean maximum and minimum joint rotations (°).

		Sh.X	Sh.Y	Sh.Z	Elb.X	Elb.Y	Elb.Z	Wr.X	Wr.Y	Wr.Z
	SD	0.9	1.7	4.2	2.7	1.9	2.7	0.6	0.5	0.6
Activity 5	Max.	1.6	3.8	42.1	13.2	9.1	15.9	6.3	-1.0	0.1
	SD	0.6	1.7	3.7	3.4	2.2	3.1	0.8	0.7	0.8
	Min.	-1.7	-3.6	35.5	9.4	2.0	7.5	-0.6	-4.0	-3.7
	SD	0.7	1.8	4.4	3.0	1.5	3.0	1.2	0.9	0.7

Table 8.32 Mean maximum and minimum joint forces (N).

		Sh.Add.	Sh.Flex.	Sh.Int.Rot.	El.Flex.	Wr.U.Dev.	Wr.Flex.
Activity 5	Max.	-0.8	9.0	-1.1	3.2	0.1	-0.1
	SD	1.5	1.7	0.3	0.5	0.1	0.1
	Min.	-2.0	4.7	-2.2	-0.8	-0.4	-0.3
	SD	0.9	0.7	0.6	0.6	0.1	0.1

Table 8.33 Mean maximum and minimum joint moments (Nm).

		Sh.Flex.	Sh.Add.	Sh.Int.Rot.	Elb.Flex.	Elb.Pron.
Activity 5	Max.	0.7	0.6	0.5	2.6	1.6
	SD	0.4	0.3	0.2	0.6	1.2
	Min.	-0.7	-0.5	-0.4	-3.0	-1.6
	SD	0.4	0.3	0.2	0.8	1.3

Table 8.34 Mean maximum and minimum joint angular velocities ($rads^{-1}$).

		Sh.Flex.	Sh.Add.	Sh.Int.Rot.	Elb.Flex.	Elb.Pron.
Activity 5	Max.	4.5	2.8	2.9	10.3	9.6
	SD	2.9	1.4	2.0	5.5	5.6
	Min.	-4.0	-2.1	-2.4	-10.1	-11.9
	SD	3.0	1.0	1.5	4.2	9.6

Table 8.35 Mean maximum and minimum joint angular accelerations ($rads^{-2}$).

At the elbow, flexion was by far the greatest rotation, reaching the third highest maximum value from any activity. Pronation reached the lowest maximum value from any activity with the maximum of supination being among the greatest. The force at the elbow along the Z axis reached a lower maximum than for any other activity with that along the X axis having a greater minimum than for any other activity. The maximum flexion moment required was lower than for any other activity and an extension moment at the elbow was required around mid-cycle as the forearm longitudinal axis passed the vertical with the shoulder flexed. The relationship between elbow flexion angle and moment is given in Fig.8.36 and shows the decrease in the moment required as the elbow became more flexed.

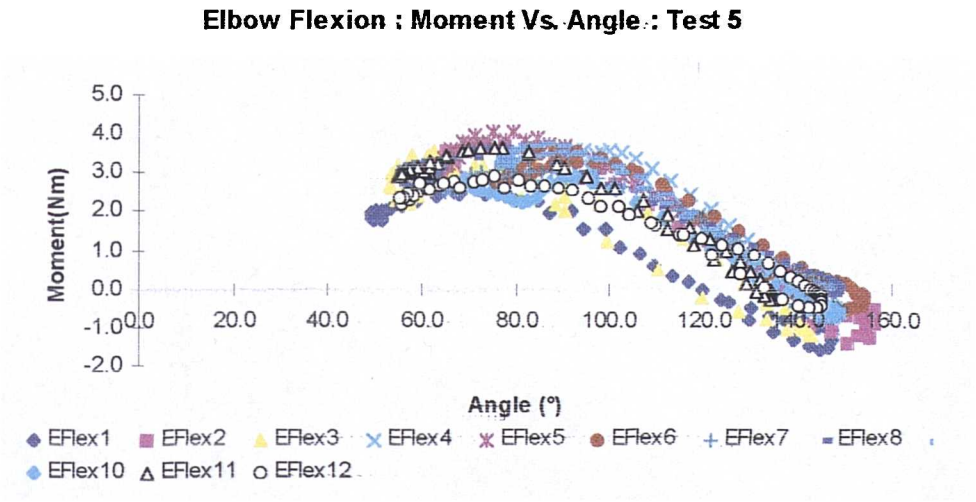

Fig.8.36 Elbow flexion moment Vs. Angle during eat with spoon.

This activity involved additional loading due the mass of the spoon and the maxima and minima of the contributions of this mass to the forces and moments at each of the modelled joints is shown in Fig.A.8.37. The contribution of the spoon mass was around 3% on average to the forces and moments at the shoulder and elbow and around 9% on average to the forces and moments at the wrist.

Figs.A.8.38 and A.8.39 show the angles, forces and moments at the shoulder and elbow obtained from the impaired subjects, with the maxima and minima of these data given in Fig.A.8.40. For subject No.11, shoulder internal

rotation was less than that of the unimpaired mean throughout the cycle and reached a considerably lower maximum, while flexion reached a similar maximum. The maximum abduction reached was slightly greater than the unimpaired mean. The elbow reached a greater maximum supination than the unimpaired mean and unlike the unimpaired mean was supinated throughout the cycle, with flexion reaching a lower maximum than the unimpaired mean.

For subject No.12, shoulder internal rotation and flexion reached slightly lower maxima than the unimpaired mean and the level of abduction was considerably lower throughout. At the elbow, as with subject No.11, a greater supination maximum than the unimpaired mean was reached and the forearm remained supinated throughout, while flexion was similar to the unimpaired mean.

The shoulder Z axis force and all moments for subject No.11 varied in the upper levels of the mean unimpaired range with those of subject No.12 considerably lower. The maximum Y axis force for subject No.11 was lower than the maximum unimpaired mean Y axis force from any of the ten activities.

The absolute and mean unimpaired maxima and minima of the angular velocities and accelerations about each joint axis, along with the maxima and minima from the impaired subjects are given in Fig.A.8.41.

The maximum angular velocities at the shoulder were considerably lower than those at the elbow due to the comparatively low range of motion at the shoulder. The average maximum velocities at the shoulder and elbow for subject No.11 were around 2% and 35%-45% lower than the unimpaired mean respectively, with those for subject No.12 around 8% and 18% lower than the unimpaired mean respectively. Fig.8.42 shows the phase plane relationship between the flexion angular velocity and angle at the elbow. The area above the X axis represents increasing elbow flexion as the spoon was raised to the mouth, the area below represents extension of the elbow, moving the spoon from the mouth and back to its initial position. The maximum velocity occurred around the mid-point of each phase, the similarity between velocities in each phase being shown in the X-axis symmetry.

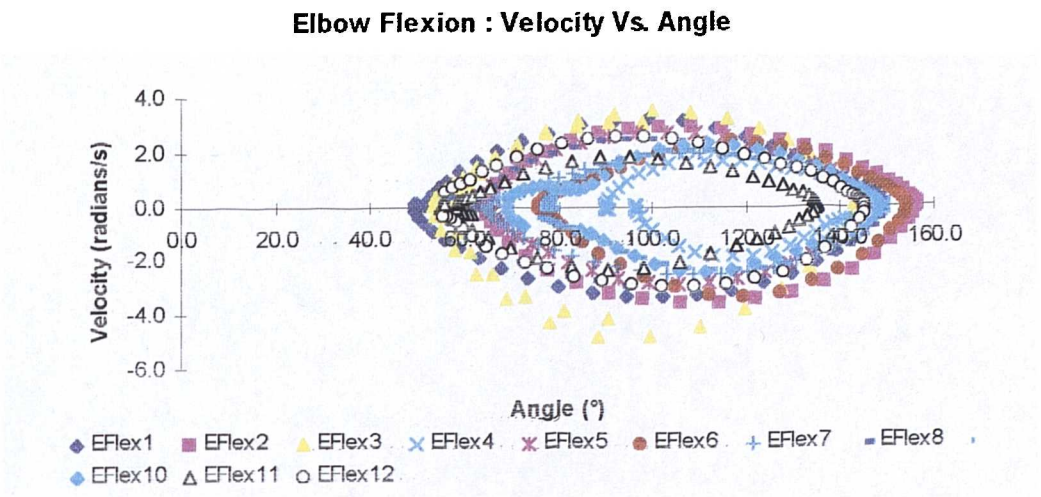

Fig.8.42 Elbow flexion Velocity Vs. Angle during eat with spoon.

The acceleration plots in Fig.A.8.41 show the average maximum accelerations at the shoulder and elbow for subject No.11 to be around 10% and 56% lower than the unimpaired mean respectively. For subject No.12 the average maximum upward and downward accelerations at the shoulder were around 16% less and 12% greater than the unimpaired mean respectively. At the elbow the average maximum upward and downward accelerations were around 40% and 3% less than the unimpaired mean respectively.

8.5.7 Activity 6 - Drink from mug

The trajectories of the elbow and wrist joint centres during this task are given in Fig.A.8.43 and show little repeated pattern other than that of the sagittal plane wrist trajectory.

Figs.A.8.44 and A.8.45 show the angles, forces and moments at the shoulder and elbow during this activity with these data also summarised along with the joint angular velocities and accelerations in Tables 8.36 - 8.40. At the shoulder no rotation was particularly great, flexion being the main component, with internal rotation having the second narrowest range from all activities and the second lowest maximum value. The forces along the X and Y axes were low with the Z axis force maintaining a relatively constant level. An abduction moment was required throughout the cycle, this being one of only two activities for which this was the case.

		Sh.Add.	Sh.Flex.	Sh.Int.Rot	Elb. Add.	Elb.Flex.	Elb.Pron.
Activity 6	Max.	-14.8	55.3	46.7	-4.1	144.3	22.6
	SD	7.3	9.2	7.3	6.8	6.0	24.6
	Min.	-33.5	36.0	33.7	-15.1	61.1	-9.0
	SD	12.2	7.9	8.5	11.0	10.9	15.3

Table 8.36 Mean maximum and minimum joint rotations (°).

		Sh.X	Sh.Y	Sh.Z	Elb.X	Elb.Y	Elb.Z	Wr.X	Wr.Y	Wr.Z
Activity 6	Max.	2.1	3.6	45.8	15.0	10.8	19.4	8.8	-1.8	0.2
	SD	0.8	1.8	4.2	3.3	1.8	2.1	1.5	1.4	1.2
	Min.	-1.4	-4.2	37.2	10.6	2.9	7.5	-2.9	-5.5	-5.5
	SD	0.5	2.3	4.1	2.7	1.6	3.1	1.8	1.4	0.8

Table 8.37 Mean maximum and minimum joint forces (N).

		Sh.Add.	Sh.Flex.	Sh.Int.Rot.	El.Flex.	Wr.U.Dev.	Wr.Flex.
Activity 6	Max.	-0.3	10.8	-1.5	4.4	0.2	-0.1
	SD	1.5	1.9	0.3	0.4	0.1	0.1
	Min.	-1.8	5.6	-2.8	-1.0	-0.6	-0.4
	SD	0.9	0.7	0.7	0.6	0.1	0.1

Table 8.38 Mean maximum and minimum joint moments (Nm).

		Sh.Flex.	Sh.Add.	Sh.Int.Rot.	Elb.Flex.	Elb.Pron.
Activity 6	Max.	0.7	0.5	0.4	2.7	1.1
	SD	0.2	0.3	0.2	0.5	0.5
	Min.	-0.8	-0.6	-0.4	-2.9	-1.4
	SD	0.3	0.3	0.1	0.8	0.8

Table 8.39 Mean maximum and minimum joint angular velocities ($rads^{-1}$).

		Sh.Flex.	Sh.Add.	Sh.Int.Rot.	Elb.Flex.	Elb.Pron.
Activity 6	Max.	3.9	2.2	2.5	11.5	8.2
	SD	2.0	1.1	1.3	4.0	3.8
	Min.	-3.3	-2.5	-1.9	-9.2	-7.8
	SD	1.5	1.6	1.0	3.8	2.9

Table 8.40 Mean maximum and minimum joint angular accelerations ($rads^{-2}$).

At the elbow, flexion made the greatest contribution with the range of pronation being the second lowest from any activity. The major force components occurred along the Z and X axes. An extension moment was required around mid-cycle as the forearm longitudinal axis passed the vertical with the shoulder flexed. Fig.8.46 shows the decrease in the elbow flexion moment as flexion increased for all subjects.

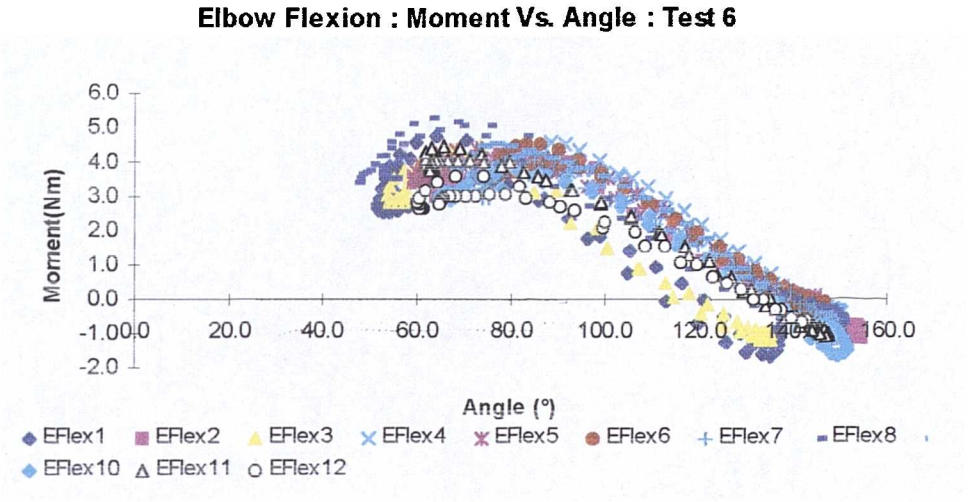

Fig.8.46 Elbow flexion Moment Vs. Angle during drink from mug.

This activity involved additional loading due the mass of the mug and the maxima and minima of the contributions of this mass to the forces and moments at each of the modelled joints is shown Fig.A.8.47. This mass contributed around 12%-14% on average to the forces and moments at the shoulder and elbow and around 30%-35% to the forces and moments at the wrists.

Figs.A.8.48 and A.8.49 show the angles, forces and moments at the shoulder and elbow, obtained during performance of this activity by the impaired subjects, with Fig.A.8.50 showing the maxima and minima of these data.

Subject No.11 reached a less internally rotated position in mid-cycle than the minimum from the unimpaired mean from any of the ten activities, with a maximum some 20° lower than that of the unimpaired mean for this activity. A lower flexion maximum was also reached in mid-cycle and the shoulder of subject No.11 was in greater abduction than the unimpaired mean throughout

the activity. At the elbow the pronation maximum was greater than the maximum from the unimpaired mean for any activity and unlike the unimpaired mean was pronated throughout the cycle. A slightly greater maximum of elbow flexion than the unimpaired mean was also achieved.

Subject No.12 reached a lower maximum of shoulder flexion and a considerably lower maximum abduction than the unimpaired mean in mid-cycle as the mug reached the mouth, though was less abducted throughout the cycle than the mean. At the elbow a greater pronation than the unimpaired mean was reached as the mug was tilted to the mouth with flexion being similar to that mean.

The shoulder Z axis force and all moments for subject No.11 can be seen to vary in the upper levels of the mean unimpaired range with those of subject No.12 considerably lower. Both impaired subjects had lower maxima along the shoulder X and Y axes and the elbow X and Z axes than the unimpaired mean.

The absolute and mean unimpaired maxima and minima of the angular velocities and accelerations about each joint axis, along with the maxima and minima from the impaired subjects are given in Fig.A.8.51.

The maximum angular velocities at the shoulder were considerably lower than those at the elbow. The average maximum shoulder and elbow velocities for subject No.11 were around 39% and 29% less than the unimpaired mean respectively, with those of subject No.12 being around 52% and 15% less than the unimpaired mean at the shoulder and elbow respectively.

Fig.8.52 shows the phase plane relationship between the elbow flexion velocity and angle, the area above the X axis representing increasing elbow flexion as the mug was raised to the mouth, the area below representing elbow extension as the mug was returned to its initial position. The impaired subjects can be seen to have reached lower magnitudes during the extension phase.

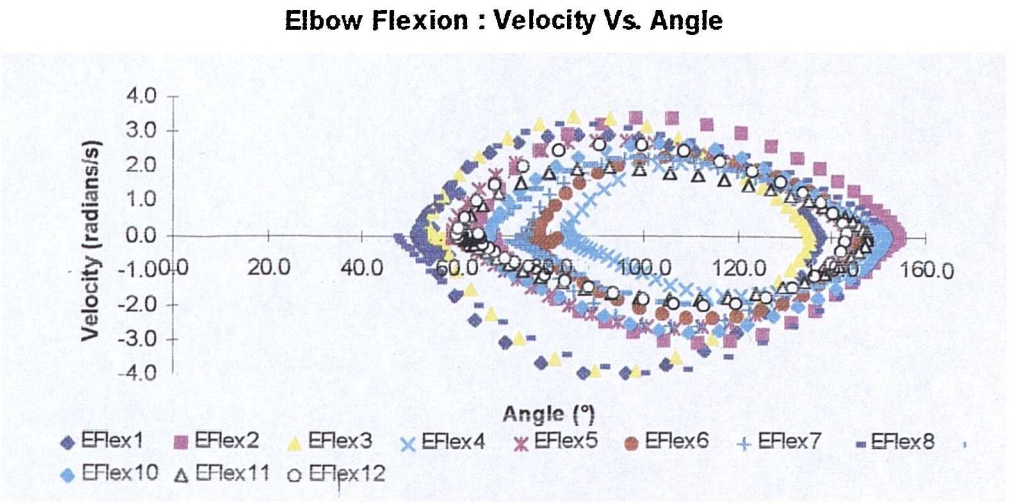

Fig.8.52 Elbow flexion Velocity Vs. Angle during drinking from mug.

As shown in Fig.A.8.51 the average maximum shoulder and elbow accelerations for subject No.11 were between 60% and 65% lower than the unimpaired mean. Subject No.12 showed average maximum shoulder accelerations differing by around the same amount as those for subject No.11, with those at the elbow being 36% lower than the unimpaired mean.

8.5.8 Activity 7 - Answer telephone

Fig.A.8.53 shows the trajectories of the wrist joint centres during this task to have been relatively consistent between subjects in each of the transverse, coronal and sagittal planes, whereas those for the elbow were inconsistent.

Figs.A.8.54 and A.8.55 show the angles, forces and moments at the shoulder and elbow during this activity with these data also summarised along with the joint angular velocities and accelerations in Tables 8.41 - 8.45. The shoulder stayed in a position of abduction throughout the cycle with the second narrowest mean range from any activity. The mean shoulder Z axis force maintained a relatively consistent level with the maximum along the Y axis being the largest from the unimpaired subjects for any of the ten activities tested at the point where the shoulder stopped extending and flexed slightly to bring the receiver to the ear. The flexion moment at the shoulder had a high maximum due to the extension of the elbow in the initial position

		Sh.Add.	Sh.Flex.	Sh.Int.Rot	Elb. Add.	Elb.Flex.	Elb.Pron.
Activity 7	Max.	-12.6	60.2	48.2	-5.8	152.3	53.1
	SD	4.2	9.9	10.2	5.0	7.9	17.1
	Min.	-23.0	39.7	27.7	-23.7	36.3	22.9
	SD	7.7	8.5	9.6	8.6	15.8	8.9

Table 8.41 Mean maximum and minimum joint rotations (°).

		Sh.X	Sh.Y	Sh.Z	Elb.X	Elb.Y	Elb.Z	Wr.X	Wr.Y	Wr.Z
Activity 7	Max.	2.9	7.2	44.3	14.7	12.6	17.5	4.9	0.3	-0.2
	SD	0.9	2.4	4.0	3.3	2.1	2.4	1.1	1.4	1.1
	Min.	-2.0	-6.0	37.1	8.8	5.0	8.0	-4.2	-8.3	-5.8
	SD	0.7	1.9	4.2	2.8	1.8	2.8	0.8	0.9	0.6

Table 8.42 Mean maximum and minimum joint forces (N).

		Sh.Add.	Sh.Flex.	Sh.Int.Rot.	El.Flex.	Wr.U.Dev.	Wr.Flex.
Activity 7	Max.	0.2	12.3	-0.9	4.1	0.3	0.0
	SD	0.8	1.6	0.2	0.4	0.1	0.1
	Min.	-1.6	5.1	-2.7	-1.3	-0.3	-0.6
	SD	0.8	0.9	0.7	0.6	0.1	0.1

Table 8.43 Mean maximum and minimum joint moments (Nm).

		Sh.Flex.	Sh.Add.	Sh.Int.Rot.	Elb.Flex.	Elb.Pron.
Activity 7	Max.	0.7	0.3	0.7	3.5	1.0
	SD	0.4	0.2	0.3	1.5	0.6
	Min.	-0.9	-0.4	-0.8	-3.3	-1.2
	SD	0.4	0.3	0.4	1.4	1.1

Table 8.44 Mean maximum and minimum joint angular velocities ($rads^{-1}$).

		Sh.Flex.	Sh.Add.	Sh.Int.Rot.	Elb.Flex.	Elb.Pron.
Activity 7	Max.	6.4	2.2	5.5	14.0	10.5
	SD	3.6	1.3	2.9	6.8	9.4
	Min.	-4.7	-2.2	-3.9	-11.9	-11.1
	SD	2.4	1.9	2.9	6.7	9.6

Table 8.45 Mean maximum and minimum joint angular accelerations ($rads^{-2}$).

At the elbow the major component of rotation was flexion with the greatest mean range from the unimpaired subjects for any of the ten activities tested and reaching the second greatest maximum from any activity. Pronation covered the narrowest mean range, though included the second greatest maximum from the unimpaired subjects for any of the ten activities tested, the forearm remaining pronated throughout. The major component of force at the elbow was along the Z axis, though considerable forces also occurred along both X and Y axes. An extension moment was required around mid-cycle as the forearm longitudinal axis passed the vertical with the shoulder flexed. The relationship between the elbow flexion moment and angle is given in Fig.8.56 and shows an initial rise as the elbow flexed, raising the forearm from a downward oriented position, to a maximum moment as the forearm was horizontal before falling as elbow flexion increased.

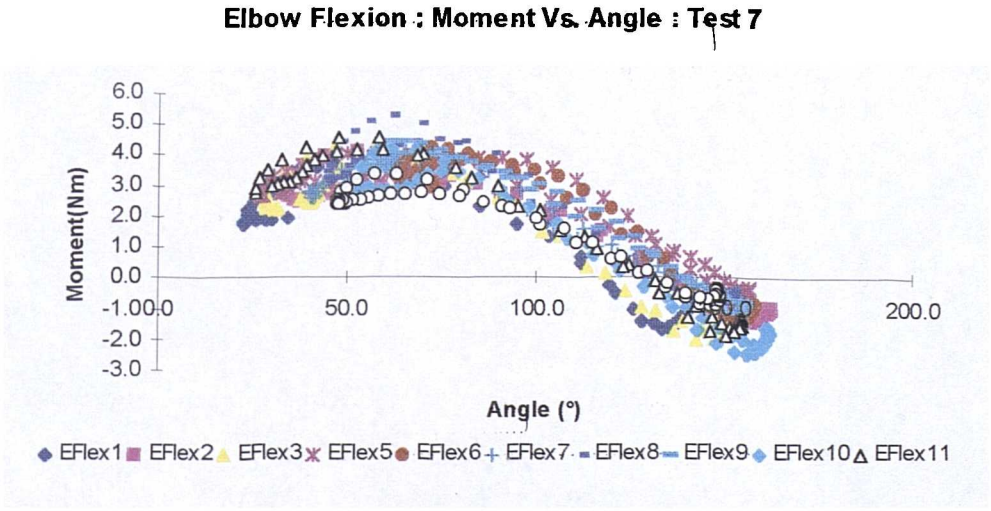

Fig.8.56 Elbow flexion Moment Vs. Angle during answering telephone.

This activity involved additional loading due to the mass of the receiver and Fig.A.8.57 shows the maxima and minima of the contributions of this hand held load to the forces and moments at each of the modelled joints. The contribution of this mass was around 10%-12% on average to the forces and moments at the shoulder and elbow and around 30%-35% to the forces and moments at the wrist.

Figs.A.8.58 and A.8.59 show the angles, forces and moments at the shoulder and elbow, obtained during performance of this activity by the impaired subjects, with the unimpaired and impaired maxima and minima of these data given in Fig.A.8.60.

For subject No.11 shoulder internal rotation was considerably lower than the unimpaired mean throughout, though particularly in mid-cycle, with flexion also slightly lower. Shoulder adduction exhibited a pattern different to that for the unimpaired mean, being abducted initially and becoming less so in mid-cycle. At the elbow, pronation was less than the unimpaired mean throughout with flexion reaching a slightly greater maximum than that mean.

Subject No.12 had a narrow range of shoulder internal rotation and reached a lesser maximum of flexion and a lesser abduction in mid-cycle as the receiver reached the ear than the unimpaired mean. At the elbow, the mean pronation range reached a maximum around half that of the unimpaired mean with flexion reaching a similar maximum to that mean.

The maximum forces at the shoulder and elbow from both impaired subjects was comparable to the unimpaired mean, with the shoulder forces for subjects No.11 and No.12 varying in the upper and lower levels respectively of the mean unimpaired force range. The moments about each of the modelled degrees of freedom for these subjects exhibited a similar pattern.

The absolute and mean unimpaired maxima and minima of the angular velocities and accelerations about each joint axis, along with the maxima and minima from the impaired subjects are given in Fig.A.8.61.

The maximum angular velocities at the shoulder were considerably lower than those at the elbow. The average maximum shoulder velocity for subject No.12 was between 45% and 50% less than the unimpaired mean, with that of subject No.11 around 18% less. At the elbow the average maximum pronation velocity from subject No.11 was around 14% less than the unimpaired mean, with that from subject No.12 around 39% less. At the elbow the average maximum flexion velocities from subjects No.11 and No.12 were around 5% greater and 24% less respectively than the unimpaired mean. Fig.8.62 shows the phase plane relationship between the elbow flexion velocity and angle.

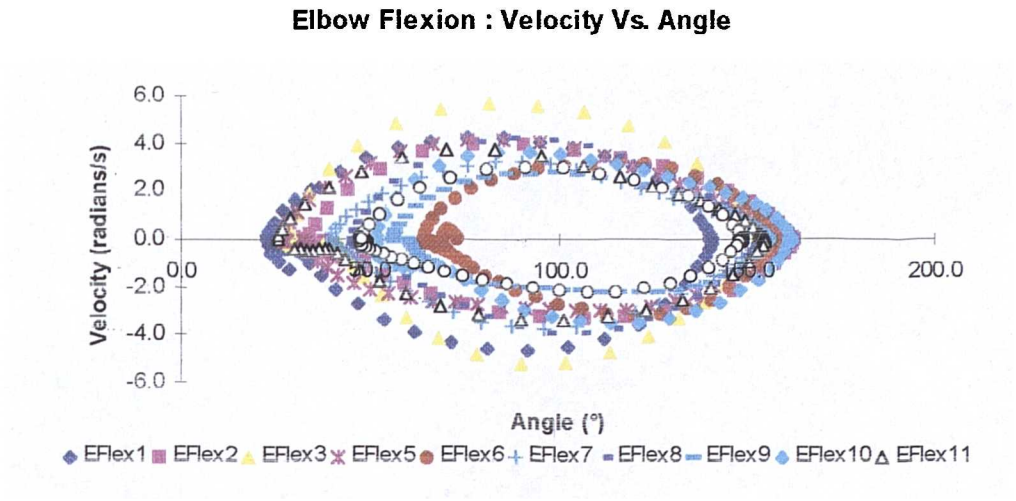

Fig.8.62 Elbow flexion Velocity Vs. Angle during answering telephone.

The area above the X axis in Fig.8.62 represents increasing elbow flexion as the telephone receiver was raised to the ear, the area below representing extension as the receiver was returned to the telephone cradle.

Fig.A.8.61 shows the maximum accelerations at all modelled joints for both impaired subjects to have been less than the unimpaired mean. For subject No.11 the average maximum shoulder and elbow accelerations were around 30% and 25% lower than the unimpaired mean respectively, with those of subject No.12 around 72% and 51% lower than the unimpaired mean respectively.

8.5.9 Activity 8 - Brush hair left side of head

The trajectories of the elbow and wrist joint centres during this task are given in Fig.A.8.63 and show relatively consistent patterns of wrist trajectory in each of the transverse, coronal and sagittal planes with less consistent elbow trajectories.

Figs.A.8.64 and A.8.65 show the angles, forces and moments at the shoulder and elbow with these data also summarised along with the joint angular velocities and accelerations in Tables 8.46 - 8.50. At the shoulder flexion and internal rotation were the primary rotations though an adduction was required in mid-cycle, one of only three activities for which this was the

		Sh.Add.	Sh.Flex.	Sh.Int.Rot	Elb. Add.	Elb.Flex.	Elb.Pron.
Activity 8	Max.	0.4	83.9	72.7	-2.4	126.3	19.3
	SD	16.9	18.9	10.7	8.1	8.1	31.9
	Min.	-18.7	32.7	37.2	-27.0	59.9	-25.8
	SD	13.1	13.6	13.6	14.9	12.3	20.6

Table 8.46 Mean maximum and minimum joint rotations (°).

		Sh.X	Sh.Y	Sh.Z	Elb.X	Elb.Y	Elb.Z	Wr.X	Wr.Y	Wr.Z
Activity 8	Max.	3.9	3.1	45.6	16.3	8.7	18.6	6.5	-0.6	-0.1
	SD	0.6	1.2	4.3	2.9	1.5	3.7	1.1	1.7	0.8
	Min.	-4.3	-3.1	32.7	6.9	2.9	0.2	-1.2	-5.7	-3.4
	SD	1.2	1.3	4.3	3.2	1.4	5.7	1.4	1.1	0.7

Table 8.47 Mean maximum and minimum joint forces (N).

		Sh.Add.	Sh.Flex.	Sh.Int.Rot.	El.Flex.	Wr.U.Dev.	Wr.Flex.
Activity 8	Max.	1.7	10.1	-1.1	4.0	0.1	-0.1
	SD	1.1	2.0	0.6	0.6	0.1	0.1
	Min.	-1.5	5.6	-2.6	-0.8	-0.5	-0.4
	SD	1.3	0.9	0.5	0.9	0.1	0.1

Table 8.48 Mean maximum and minimum joint moments (Nm).

		Sh.Flex.	Sh.Add.	Sh.Int.Rot.	Elb.Flex.	Elb.Pron.
Activity 8	Max.	1.8	0.7	1.1	2.8	1.9
	SD	0.5	0.2	0.3	0.9	1.7
	Min.	-2.0	-1.0	-1.7	-2.4	-2.0
	SD	0.6	0.3	0.4	0.6	1.3

Table 8.49 Mean maximum and minimum joint angular velocities ($rads^{-1}$).

		Sh.Flex.	Sh.Add.	Sh.Int.Rot.	Elb.Flex.	Elb.Pron.
Activity 8	Max.	9.1	5.7	8.3	13.5	14.6
	SD	2.5	2.0	2.6	5.7	13.6
	Min.	-7.6	-4.2	-8.7	-11.5	-14.7
	SD	2.6	1.3	3.0	5.3	9.6

Table 8.50 Mean maximum and minimum joint angular accelerations ($rads^{-2}$).

case. The mean shoulder Z axis force maintained a consistent level with the maxima along the Y axes in both positive and negative directions having the lowest magnitude from any of the ten activities. The adduction moment had quite large variations between subjects for the moments at the beginning and end of the cycle due to differing starting and finishing upper limb positioning.

At the elbow the major component of rotation was flexion which had the second narrowest mean range form any of the ten activities. The major force components were those along the Z and X axes. An extension moment at the elbow was required in mid-cycle as shown in the relationship between the elbow flexion moment and angle given in Fig.8.66. Some inconsistency between subjects is shown due to the complex nature of this activity involving more than simply flexion of the elbow.

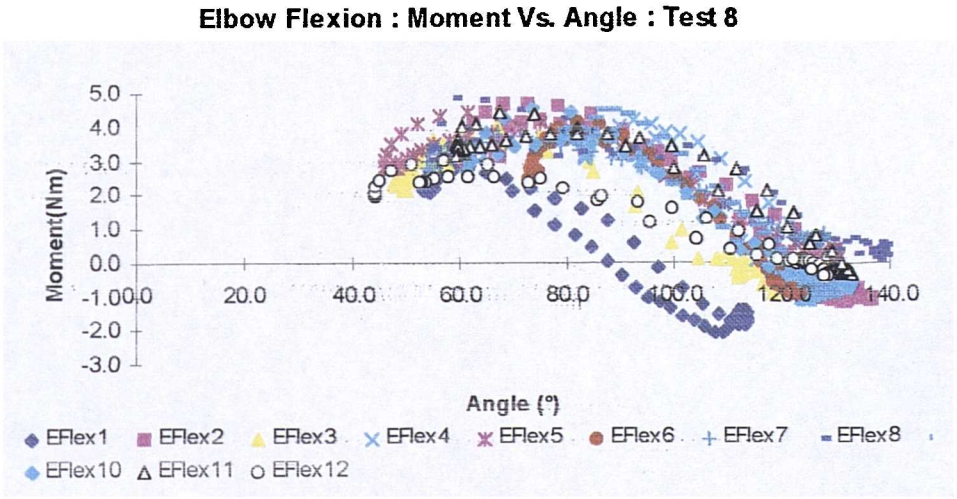

Fig.8.66 Elbow flexion Moment Vs. Angle during brushing left side of head.

This activity involved additional loading due to the mass of the brush and the maxima and minima of the contributions of this hand held load to the forces and moments at each of the modelled joints are given in Fig.A.8.67. This mass contributed around 3%-5% on average to the forces and moments at the shoulder and elbow and around 8%-9% to the forces and moments at the wrist.

Figs.A.8.68 and A.8.69 show the angles, forces and moments at the shoulder and elbow, obtained during performance of this activity by the

impaired subjects, with the unimpaired and impaired maxima and minima of these data given in Fig.A.8.70.

For subject No.11 shoulder internal rotation and flexion were both lower than the unimpaired mean by a considerable margin throughout the cycle. The maximum abduction was slightly lower than the unimpaired mean with the maximum adduction being slightly greater. At the elbow subject No.11 had greater initial supination than the unimpaired mean and became pronated in mid-cycle as the unimpaired mean became supinated. Subject No.11 also reached a greater maximum flexion around mid-cycle than the unimpaired mean.

For subject No.12, the shoulder was more internally rotated initially and less internally rotated in mid-cycle, than the unimpaired mean with a similar pattern for flexion. This subject reached a greater abduction in mid-cycle than the unimpaired mean as the brush reached the left side of the head, having been initially less abducted. At the elbow, in contrast to the unimpaired mean, the forearm remained pronated throughout and a slightly greater maximum of flexion was reached.

The maximum forces at shoulder and elbow from subjects No.11 and No.12 were found to vary in the upper and lower levels of the mean unimpaired force range respectively. At the elbow the minimum X axis force for subject No.11 was lower than the minimum from the unimpaired mean for any activity. The moments were greater for subject No.11 than those for subject No.12.

The absolute and mean unimpaired maxima and minima of the angular velocities and accelerations about each joint axis, along with the maxima and minima from the impaired subjects are given in Fig.A.8.71.

The maximum angular velocity for each of the modelled rotations from the impaired subjects were generally lower than those from the unimpaired subjects. The average maximum shoulder angular velocity for subject No.11 was around 26% less than the unimpaired mean, with that of subject No.12 around 50% less. At the elbow the average maximum flexion and pronation velocities from subject No.11 were around 15% and 41% less than the unimpaired mean respectively, with those from subject No.12 around 4% and 64% less respectively.

Fig.A.8.71 shows the average maximum accelerations at all modelled joints for both subjects to be less than the unimpaired mean. Those of subject No.11 were around 37% and 47% lower than the unimpaired mean at the elbow and shoulder respectively, with those of subject No.12 around 62% and 49% lower respectively.

8.5.10 Activity 9 - Lifting to shoulder height (repetition from Cheng (1996))

Fig.A.8.72 shows the trajectories of the elbow and wrist joint centres during this task, reasonable consistency between subjects for both being apparent. Of particular note are the laterally curved elbow coronal plane trajectories due to abduction of the shoulder during lifting.

Figs.A.8.73 and A.8.74 show the angles, forces and moments at the shoulder and elbow during this activity with these data also summarised along with the joint angular velocities and accelerations in Tables 8.51 - 8.55. The maximum of shoulder flexion was the third highest from the unimpaired subjects for all activities with the minimum being the second lowest, as was the minimum of internal rotation. The mean shoulder Z axis and Y axis forces reached their second greatest maxima from any of the ten activities. Fig.8.75 gives the relationship between the shoulder flexion moment and angle. The initial moment appears to be low but is actually the greatest minimum from any activity. As the shoulder extended and the elbow flexed the moment reached its greatest maximum values from all ten activities. The second greatest abduction and internal rotation moments were also achieved.

At the elbow the major component of rotation was flexion and this was one of only two activities involving an extension of the elbow from its initial position, the second most extended position for any of the ten activities being reached. The maximum forces along the X, Y and Z axes all reached their second highest values from all ten activities, as did the elbow flexion moment and this was one of only three activities that required no elbow extension moment.

		Sh.Add.	Sh.Flex.	Sh.Int.Rot	Elb. Add.	Elb.Flex.	Elb.Pron.
Activity 9	Max.	-10.6	88.2	57.9	-16.9	99.7	38.0
	SD	8.2	9.5	11.8	9.5	7.6	15.9
	Min.	-32.7	14.9	19.2	-32.2	22.0	-10.6
	SD	11.9	6.1	8.1	9.1	7.7	13.4

Table 8.51 Mean maximum and minimum joint rotations (°).

		Sh.X	Sh.Y	Sh.Z	Elb.X	Elb.Y	Elb.Z	Wr.X	Wr.Y	Wr.Z
Activity 9	Max.	3.8	6.6	50.2	18.8	13.7	24.2	8.6	-2.5	-1.5
	SD	1.2	1.9	4.0	2.3	2.1	1.9	1.5	1.8	0.9
	Min.	-4.4	-6.9	34.5	7.0	3.1	1.2	1.2	-8.7	-7.0
	SD	1.7	2.6	5.8	3.5	1.6	3.3	2.2	1.5	1.1

Table 8.52 Mean maximum and minimum joint forces (N).

		Sh.Add.	Sh.Flex.	Sh.Int.Rot.	El.Flex.	Wr.U.Dev.	Wr.Flex.
Activity 9	Max.	1.5	14.3	-1.1	5.4	0.0	-0.3
	SD	1.1	1.4	0.3	0.5	0.2	0.1
	Min.	-3.3	7.1	-3.3	1.5	-0.6	-0.7
	SD	1.4	1.2	0.9	0.9	0.1	0.1

Table 8.53 Mean maximum and minimum joint moments (Nm).

		Sh.Flex.	Sh.Add.	Sh.Int.Rot.	Elb.Flex.	Elb.Pron.
Activity 9	Max.	2.6	0.9	1.3	3.6	2.0
	SD	0.7	0.3	0.6	0.9	0.9
	Min.	-2.6	-1.0	-1.5	-2.8	-1.8
	SD	0.5	0.4	0.4	0.6	0.8

Table 8.54 Mean maximum and minimum joint angular velocities ($rads^{-1}$).

		Sh.Flex.	Sh.Add.	Sh.Int.Rot.	Elb.Flex.	Elb.Pron.
Activity 9	Max.	9.7	5.9	7.6	14.8	10.8
	SD	2.7	2.3	2.4	5.0	4.8
	Min.	-9.6	-4.3	-6.0	-17.7	-11.6
	SD	3.2	1.9	2.4	5.5	6.7

Table 8.55 Mean maximum and minimum joint angular accelerations ($rads^{-2}$).

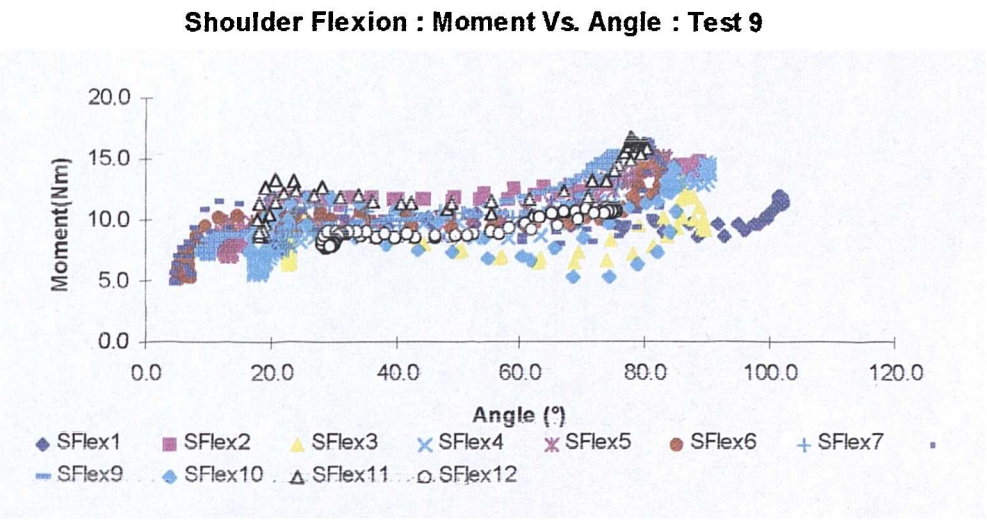

Fig.8.75 Shoulder flexion Moment Vs. Angle during raise of block to shoulder height.

All possible combinations of angle against angle for both unimpaired and impaired subjects were plotted for each activity and were of interest for this activity as shown in Fig.8.76. In particular repeated relationships are visible for the elbow flexion angles, the shoulder internal rotation angles and the elbow pronation angles, all in relation to shoulder flexion. Of particular note is the increase in shoulder internal rotation and decrease in the elbow pronation as the shoulder was flexed.

This activity involved additional loading due to the mass of the wooden block and the maxima and minima of the contributions of this mass to the forces and moments at each of the modelled joints is given in Fig.A.8.77. This mass contributed around 20%-25% on average to the forces and moments at the shoulder, around 15%-20% on average to the forces and moments at the elbow and around 50% to the forces and moments at the wrists.

The shoulder and elbow angle and moment data were compared with graphs presented by Cheng (1996), examples of which are given in Figs.7.17-7.20. The values were corrected for differences in embedded axes definitions and initial limb orientations, the subjects of Cheng (1996) having raised a 1kg block from a surface around 20cm above floor level, considerably lower than the elbow height initial position used for the current study and requiring a lower initial elbow flexion of around 30°. Data from the relevant portions of the cycle

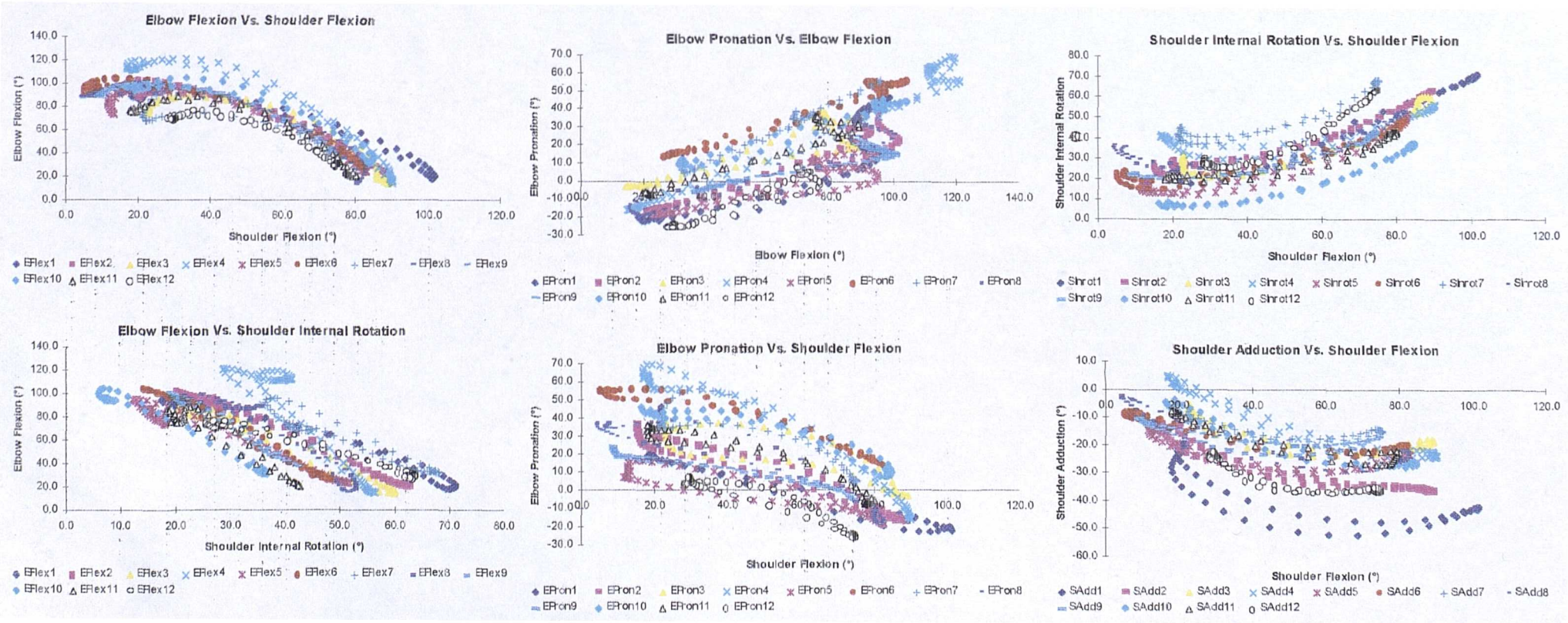

Fig.8.76 Angle Vs. Angle relationships during performance of Test 9. (Δ - Subject 11, o - Subject 12)

are shown in Tables 8.56 and 8.57 in relation to the axes defined for the current study. No standard deviation or uncertainty boundaries were given.

	Mean Range
Shoulder Flexion	3° → 67°
Shoulder Adduction	-16° → -44°
Shoulder Internal Rotation	2° → 64°

Table 8.56 Approximate mean shoulder angles ranges from Cheng (1996).

	Mean Range
Shoulder Flexion	3Nm → 13Nm
Shoulder Adduction	-3Nm → -5Nm
Shoulder Internal Rotation	-3Nm → 1Nm

Table 8.57 Approximate mean shoulder moment ranges from Cheng (1996).

All of the ranges of Cheng (1996) at the shoulder are seen to lie comfortably within the ±2SD boundaries from the current study, shown in Fig.A.8.73. The mean ranges of shoulder flexion and adduction from Cheng (1996) show slightly greater abduction and slightly lower flexion than the unimpaired mean from the current study, with internal rotation showing a greater range, being less internally rotated initially. The mean range of the shoulder flexion moment from Cheng (1996) is similar to that from the current study, though has a lower minimum value due to the greater extension of the elbow in the initial position. The shoulder internal rotation and adduction moments from Cheng (1996) compare less well, with values outside the ±2SD boundaries from the current study, shown in Fig.A.8.73. This variation could be explained by differences in the initial positions of the subjects and in the arrangement of the shelf to which they reached.

At the elbow, Cheng (1996) obtained an approximate mean range of flexion between 93° and 54° the maximum of which corresponds well with that obtained in the current study though the minimum, obtained in mid-cycle as the block was placed on the shelf, does not compare as well. This difference is

almost certainly due to a difference in the horizontal distance between subjects and shelf in the two studies. Cheng (1996) established this as the subjects' preferred distance after practising the movement, whereas it was defined for the current study as approximately equal to arm's length. The closer the shelf was to the subject the less extension of the elbow would be required. Cheng (1996) did not present elbow adduction angles and forearm pronation was presented in terms of a rotation from an initial position and thus could not be compared.

For the elbow flexion moment, Cheng (1996) obtained an approximate mean range for the relevant section of the cycle starting at around 5Nm, dropping to around 1Nm before rising to around 5Nm in mid-cycle. No standard deviation or uncertainty boundaries were given. These values again correspond well with the unimpaired mean from the current study though have a greater value around the mid-point of the cycle, probably due to the mass of the hand held block in the work of Cheng (1996) being more than twice that of the block used in the current study.

Figs.A.8.78 and A.8.79 show the angles, forces and moments at the shoulder and elbow, obtained during performance of this activity by the impaired subjects, with Fig.A.8.80 showing the maxima and minima of these data.

For subject No.11 shoulder internal rotation reached a considerably lower maximum value than the unimpaired mean as did flexion and both had narrower ranges. Subject No.11 showed lower abduction angles than the unimpaired mean throughout the cycle. At the elbow this subject achieved lesser magnitudes of pronation and supination and a considerably lower flexion maximum.

For subject No.12, the shoulder was more internally rotated and abducted than the unimpaired mean throughout the cycle and was more flexed initially though reached a lesser maximum. At the elbow, this subject was considerably more supinated than the unimpaired throughout the cycle and had a lower initial flexion though reached a similar minimum to the unimpaired mean in mid-cycle.

The shoulder Z axis forces for subjects No.11 and No.12 varied in the upper and lower levels of the mean unimpaired force range respectively. Forces in each of the X and Y axes directions for subject No.11 were comparable to the unimpaired mean with those for subject No.12 being lower, with the magnitude of the negative Y axis force being smaller than the minimum from the unimpaired mean for any activity. The moments exhibited a similar pattern with the shoulder flexion moment for subject No.11 being the greatest maximum value from any subject for any activity. The adduction moment of subject No.12 stayed negative throughout the cycle where a slight adduction moment was apparent in mid-cycle for all other subjects.

The absolute and mean unimpaired maxima and minima of the angular velocities and accelerations about each joint axis, along with the maxima and minima from the impaired subjects are given in Fig.A.8.81. The average maximum angular velocities for all modelled rotations from the impaired subjects were lower than those from the unimpaired subjects. Subject No.11 achieved average maximum velocities around 33% and 23% lower than the unimpaired mean at the shoulder and elbow respectively, with those for subject No.12 around 38% and 51% lower respectively.

Fig.8.82 shows the phase plane relationship between the shoulder flexion velocity and angle for all subjects. The area above the X axis represents increasing shoulder flexion as the wooden block was raised to the shelf, with the area below representing shoulder extension as the block was returned to its initial position on the table. Of note is the distinctly different pattern of shoulder flexion from subject No.12, showing a marked reduction in both the range of flexion angles and the magnitudes of the velocities.

Similarly interesting was the plot of elbow flexion velocity against shoulder flexion velocity shown in Fig.8.83 in which the right hand loop represents the raising of the block to the shelf, the left hand loop represents the lowering of the block to its initial position. The upper portion of each loop represents the acceleration phase in that direction, with the lower portion representing deceleration to rest.

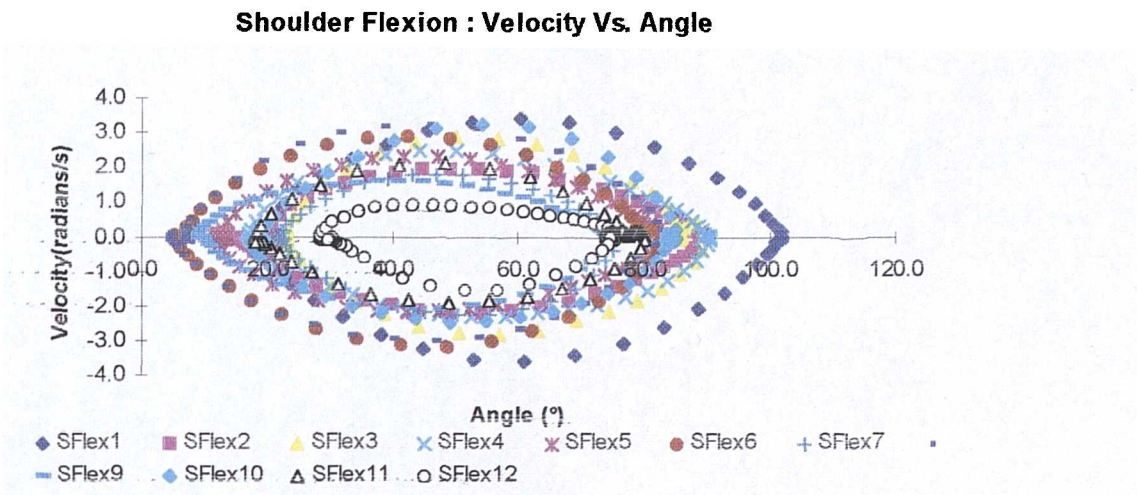

Fig.8.82 Shoulder flexion Velocity Vs. Angle during raise of block to shoulder height.

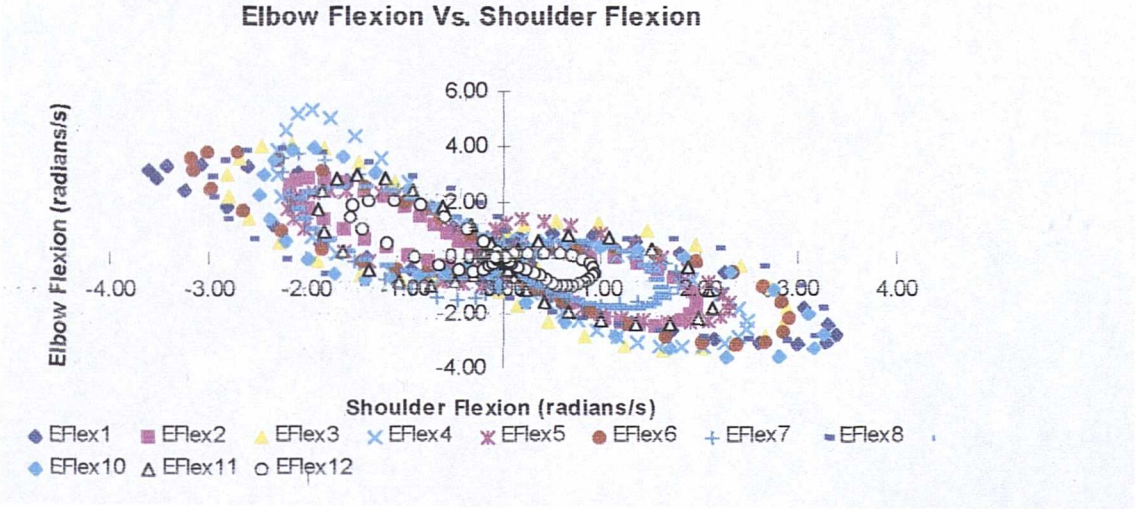

Fig.8.83 Elbow flexion Velocity Vs. Shoulder flexion Velocity during activity 9.

A clear pattern in the velocities from all subjects is visible, indicating similarity between the strategies adopted and again the reduction in the velocities for subject No.12 is obvious, particularly in the right hand loop for the raising of the block.

The acceleration plots in Fig.A.8.81 show the acceleration at all modelled joints for both subjects to have been less than the unimpaired mean. Subject No.11 had average maximum accelerations around 42% and 37% lower than the unimpaired mean at the shoulder and elbow respectively, with those for subject No.12 around 42% and 58% lower respectively.

Fig.8.84 shows the relationship between the shoulder flexion acceleration and angle for this activity with the upward and downward phases superimposed. The pattern indicates a high acceleration at low angles in the upward phase in order to move the block from its initial position, decreasing until around the mid-point in the raising of the block before deceleration occurred to bring the block to rest on the shelf. The similarity of the pattern for the lowering phase indicates a similar process in reverse. The marked reduction in angular range and in the flexion accelerations for subject No.12 is apparent.

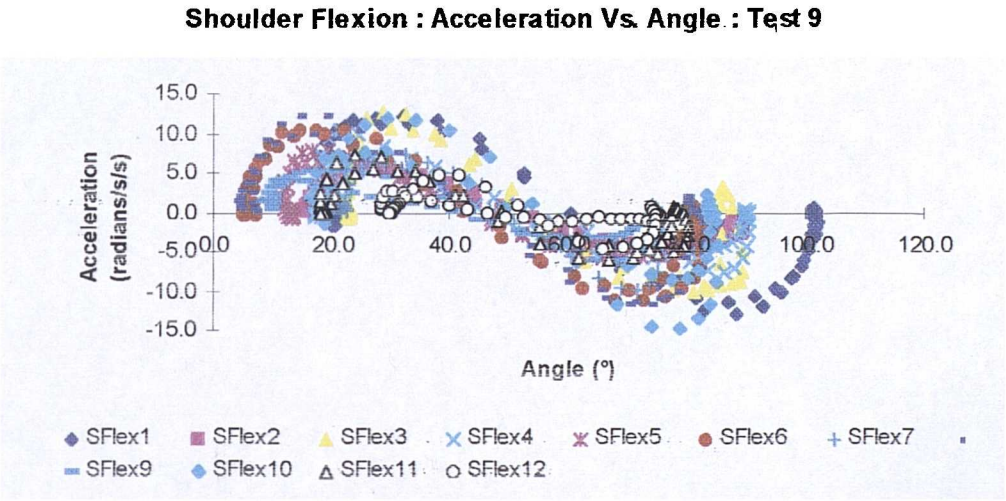

Fig.8.84 Shoulder flexion Acceleration Vs. Angle during block raise to shoulder height.

8.5.11 Activity 10 - Lift block to head height (repetition from Cheng (1996))

The trajectories of the elbow and wrist joint centres during this task are shown in Fig.A.8.85. The most consistent trajectory is that of the elbow in the coronal plane which shows the tendency for the elbow to move laterally as the shoulder abducts during raising of the block.

Figs.A.8.86 and A.8.87 show the angles, forces and moments at the shoulder and elbow with these data also summarised along with the joint angular velocities and accelerations in Tables 8.58 - 8.62. The mean flexion range at the shoulder was by some way the largest from the unimpaired subjects for any of the ten activities tested, having a lower minimum value and larger maximum value than for any other activity. The greatest abduction from

		Sh.Add.	Sh.Flex.	Sh.Int.Rot	Elb. Add.	Elb.Flex.	Elb.Pron.
Activity 10	Max.	-7.4	111.9	79.3	-16.6	102.6	44.3
	SD	7.6	7.4	12.0	7.8	12.1	14.9
	Min.	-39.7	14.7	18.7	-33.3	15.6	-18.5
	SD	6.9	7.6	7.8	9.5	6.6	13.9

Table 8.58 Mean maximum and minimum joint rotations (°).

		Sh.X	Sh.Y	Sh.Z	Elb.X	Elb.Y	Elb.Z	Wr.X	Wr.Y	Wr.Z
Activity 10	Max.	5.4	5.5	51.5	20.1	13.7	25.3	8.7	-1.7	-0.8
	SD	2.2	1.7	4.4	2.7	2.7	2.0	1.6	2.4	1.4
	Min.	-6.2	-7.5	32.5	5.9	2.1	-6.6	-1.6	-10.4	-8.0
	SD	3.1	3.7	5.6	3.9	1.8	2.3	3.2	1.5	1.1

Table 8.59 Mean maximum and minimum joint forces (N).

		Sh.Add.	Sh.Flex.	Sh.Int.Rot.	El.Flex.	Wr.U.Dev.	Wr.Flex.
Activity 10	Max.	4.2	13.5	-0.8	5.8	0.2	-0.2
	SD	1.8	1.1	0.4	0.5	0.3	0.2
	Min.	-3.7	6.5	-3.9	0.1	-0.6	-0.8
	SD	1.2	1.0	0.6	1.1	0.1	0.1

Table 8.60 Mean maximum and minimum joint moments (Nm).

		Sh.Flex.	Sh.Add.	Sh.Int.Rot.	Elb.Flex.	Elb.Pron.
Activity 10	Max.	3.4	1.4	2.4	4.1	2.9
	SD	0.8	0.2	0.6	1.1	1.3
	Min.	-3.5	-1.4	-2.5	-3.4	-2.5
	SD	0.5	0.4	0.6	0.9	0.8

Table 8.61 Mean maximum and minimum joint angular velocities ($rads^{-1}$).

		Sh.Flex.	Sh.Add.	Sh.Int.Rot.	Elb.Flex.	Elb.Pron.
Activity 10	Max.	11.9	9.2	13.3	17.1	15.3
	SD	3.9	2.5	3.8	7.2	7.0
	Min.	-12.6	-6.4	-10.4	-19.8	-16.5
	SD	3.7	2.4	3.4	6.5	8.1

Table 8.62 Mean maximum and minimum joint angular accelerations ($rads^{-2}$).

the unimpaired subjects for any of the ten activities tested was also achieved as well as the lowest minimum and greatest range of internal rotation. The Z axis force at the shoulder reached the greatest maximum from any of the ten activities early in the cycle, with the Y axis force reaching its greatest negative magnitude. The mean unimpaired flexion moment at the shoulder reached the second greatest maximum from any of the ten activities. The relationship between the shoulder flexion moment and angle is shown in Fig.8.88. The mean range of the shoulder adduction moment was the greatest from the unimpaired subjects for any of the ten activities tested, having the greatest magnitudes of moment in both positive and negative directions. The greatest mean unimpaired shoulder external rotation moment was also achieved, this activity involving the greatest range for this moment.

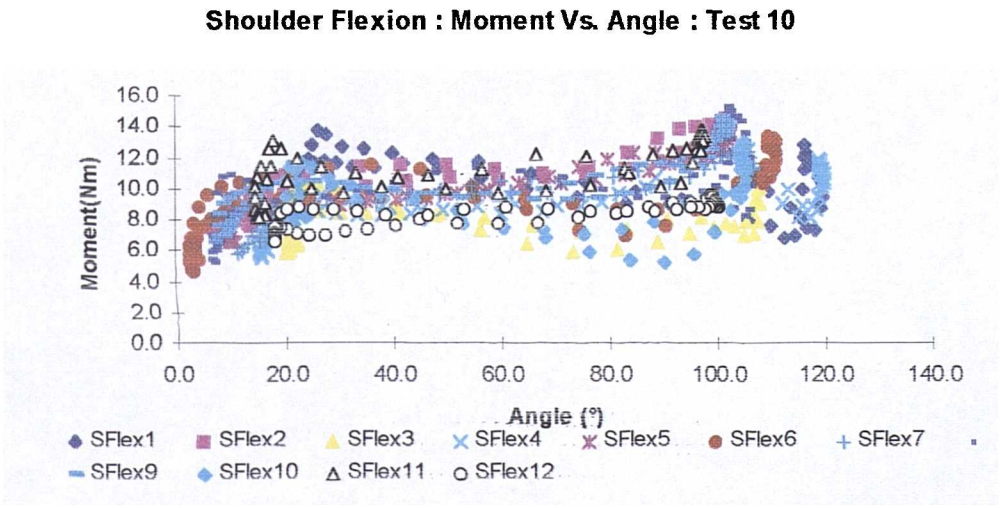

Fig.8.88 Shoulder flexion Moment Vs. Angle during raising of block to head height.

At the elbow the major component of rotation was flexion with the most extended position from any of the ten activities being reached around mid-cycle as the block was placed on the shelf. The major force components at the elbow were along the Z and X axes, with the magnitudes of the maxima and minima along both these axes being the greatest from any of the ten activities for the unimpaired mean. A negative force occurred along the Z axis due to flexion of the shoulder above 90°. The high X axis force was due to the mass of the block and the vertical orientation of the axis as the shoulder abducted. The

mean range of the elbow flexion moment included the highest value from the unimpaired subjects for any of the ten activities.

The angle against angle plots in Fig.8.89 exhibited interesting patterns for this activity, these including data from all unimpaired and impaired subjects. Repeated relationships are particularly clear for shoulder adduction and internal rotation angles and elbow flexion angles, all in relation to the shoulder flexion angles. Shoulder internal rotation and abduction increase as the shoulder flexes, while elbow flexion and pronation decrease.

This activity involved additional loading due to the mass of the wooden block and Fig.A.8.90 shows the maxima and minima of the contributions of this hand held load to the forces and moments at each of the modelled joints. The contribution of the mass of the block was around 20%-25% on average to the forces and moments at the shoulder, around 15%-20% on average to the forces and moments at the elbow and around 47%-49% to the forces and moments at the wrists.

The shoulder and elbow angle and moment data were compared with graphs presented by Cheng (1996), the values from which were corrected as discussed in the previous section. Data from the relevant portions of the cycle are shown in Tables 8.63 and 8.64 in relation to the axes defined for the current study. No standard deviation or uncertainty boundaries were given.

	Mean Range
Shoulder Flexion	2° → 98°
Shoulder Adduction	-13° → -111°
Shoulder Internal Rotation	5° → 65°

Table 8.63 Approximate mean shoulder angle ranges from Cheng (1996).

The mean angular ranges of flexion and internal rotation at the shoulder from Cheng (1996) are similar to the mean unimpaired values from the current study, though the extreme values are slightly offset. Both the flexion and internal rotation ranges of Cheng (1996) at the shoulder lie comfortably within the ±2SD boundaries from the current study. The shoulder adduction from

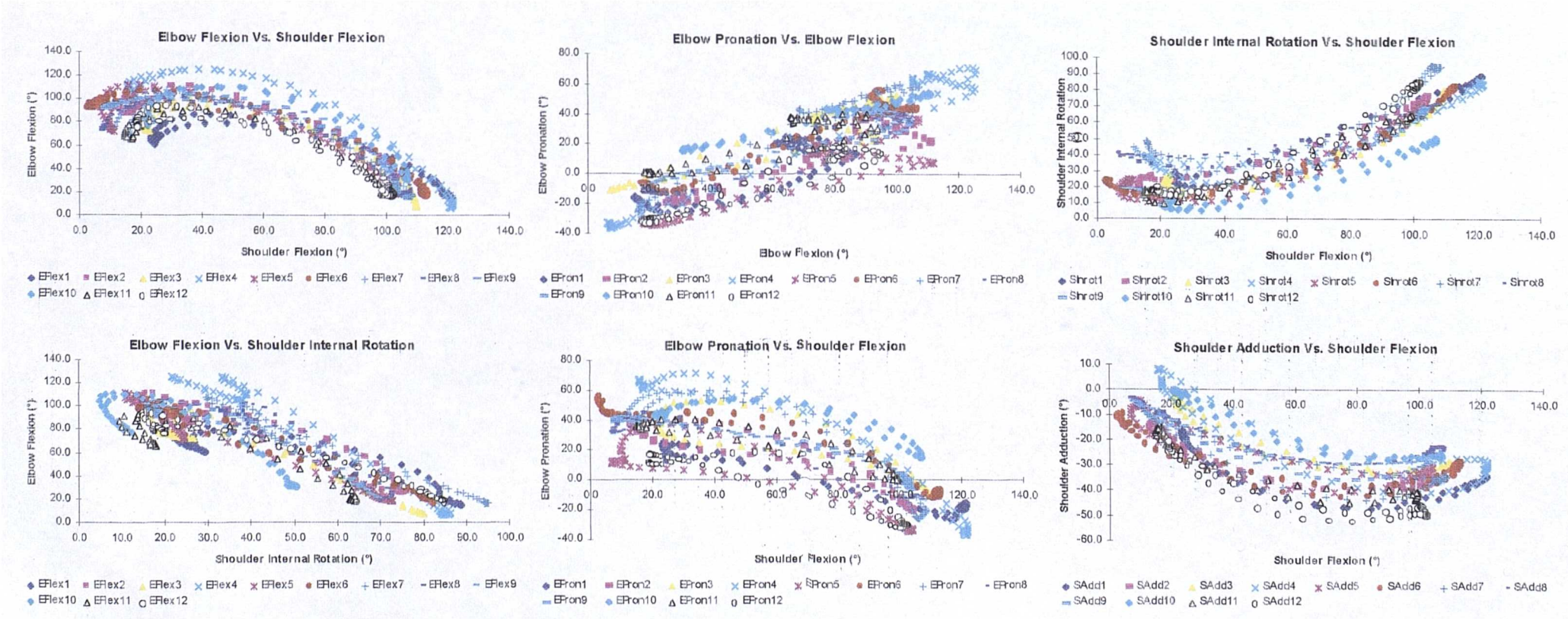

Fig.8.89 Angle Vs. Angle relationships during performance of Test 10. (Δ - Subject 11, o - Subject 12)

Cheng (1996) shows a very large range in comparison to the unimpaired mean from the current study. The initial adduction angles are similar but the mean of Cheng (1996) becomes around 70° more abducted in mid-cycle than the unimpaired mean and some two and a half times greater than that obtained by the same author for the raising of the block to shoulder height.

	Mean Range
Shoulder Flexion	3Nm → 13Nm
Shoulder Adduction	-10Nm → -3Nm
Shoulder Internal Rotation	-3Nm → 1Nm

Table 8.64 Approximate mean shoulder moment ranges from Cheng (1996).

For the principal moments at the shoulder, flexion and internal rotation, the mean ranges from Cheng (1996) are similar to those from the current study. The flexion moment of Cheng (1996) had a lower minimum value due to the greater extension of the shoulder in the initial position and the maximum value from the current study was greater due to the greater shoulder flexion and elbow extension in mid-cycle. Values for the abduction moment from Cheng (1996) were outside the ±2SD boundaries from the current study, corresponding with the greater abduction angles from that study.

For elbow flexion Cheng (1996) obtained an approximate mean range between 96.7° and 41.6°. The maximum corresponds well with that obtained in the current study though the higher minimum of Cheng (1996) indicates a greater flexion in mid-cycle. Cheng (1996) obtained an approximate mean range for the elbow flexion moment starting at around 7Nm, dropping to around 1Nm before rising to around 4Nm in mid-cycle, slightly greater than the unimpaired mean from the current study, probably due to the greater hand held mass. Cheng (1996) did not present elbow adduction angles and forearm pronation was presented in terms of a rotation from an initial position and thus could not be compared.

Figs.A.8.91 and A.8.92 show the angles, forces and moments at the shoulder and elbow, obtained from the impaired subjects, with the unimpaired and impaired maxima and minima of these data shown in Fig.A.8.93.

Subject No.11 was less internally rotated at the shoulder initially and reached a considerably lower maximum value in mid-cycle than the unimpaired mean while also reaching a lower maximum of flexion. The shoulder of subject No.11 was more abducted than the unimpaired mean throughout the cycle and reached a greater maximum than the unimpaired mean from any activity. The elbow of subject No.11 was considerably less supinated in mid-cycle than the unimpaired mean and did not reach as extended an elbow position.

Subject No.12 had a lower initial shoulder internal rotation than the unimpaired mean with a greater maximum in mid-cycle where shoulder flexion reached a lower maximum. Subject No.12 was considerably more abducted throughout the cycle than the unimpaired mean, reaching a maximum greater than subject No.11 and greater than the unimpaired mean from any activity. The elbow was less pronated initially and more supinated in mid-cycle than the unimpaired mean, while flexion reached a similar minimum at that point.

The shoulder Z axis force for Subject No.11 varied in the upper level of the mean unimpaired force range with that for subject No.12 being below the mean unimpaired range and reaching a lower maximum than the unimpaired mean from any activity. The forces along each of the shoulder X and Y axes for both impaired subjects reached lower maxima than the unimpaired mean. At the elbow subject No.11 reached a greater maximum along the X and Z axes than the unimpaired mean from any activity, while subject No.12 had lower forces along all axes than the unimpaired mean. The shoulder flexion moment for subject No.11 was of similar magnitude to the unimpaired mean with that of subject No.12 being lower. Both impaired subjects had lower maximum and minimum adduction moments than the unimpaired mean with subject No.11 reaching a greater maximum abduction moment than the unimpaired mean from any activity. At the elbow the flexion moment of subject No.11 reached a greater maximum than the unimpaired mean from any activity while that of subject No.12 was considerably lower.

The absolute and mean unimpaired maxima and minima of the angular velocities and accelerations about each joint axis, along with the maxima and minima from the impaired subjects are given in Fig.A.8.94.

With the exception of the shoulder internal rotation angular velocity during lowering for subject No.11, the maximum angular velocity for all the modelled rotations from both impaired subjects was lower than the unimpaired mean. The average maximum shoulder angular velocities were around 16% and 22% less than the unimpaired mean for subjects No.11 and No.12 respectively. The phase plane relationship between shoulder flexion velocity and angle is shown in Fig.8.95, in which the area above the X axis represents increasing shoulder flexion as the wooden block was raised to the shelf and the area below represents shoulder extension as the block was returned to its initial position on the table. A symmetry across the X axis is visible for all subjects.

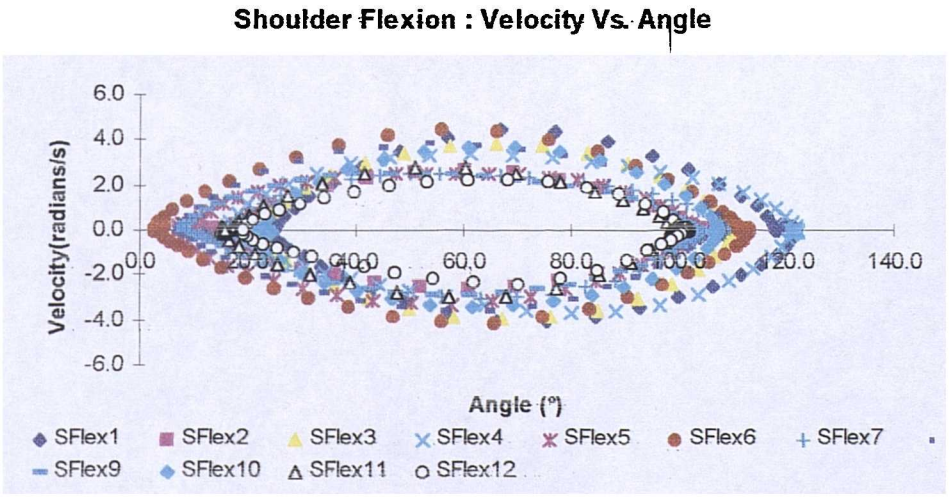

Fig.8.95 Shoulder flexion Velocity Vs. Angle during raising of block to head height.

The average maximum elbow angular velocities were around 30% and 34% less than the unimpaired mean for subjects No.11 and No.12 respectively. Fig.8.96 shows the elbow flexion velocity against shoulder flexion velocity, where the right hand loop represents the raising of the block to the shelf and the left hand loop represents the lowering of the block to its initial position. The

upper portion of each loop represents the acceleration phase in that direction, with the lower portion representing deceleration to rest.

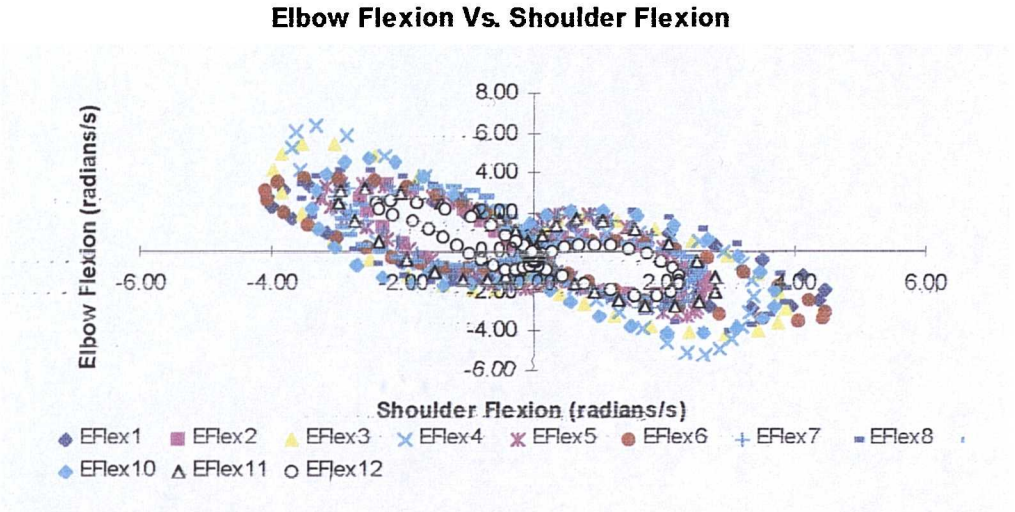

Fig.8.96 Elbow flexion Velocity Vs. Shoulder flexion Velocity during activity 10.

A clear pattern is visible in the velocities from all subjects, indicating similarity between the strategies adopted. The velocities for subject No.12 can be seen to be relatively low in comparison to the other subjects from the reduced size of the loops though the misshapen left hand loop for this subject indicates a more rapid reduction in elbow flexion velocity on lowering.

Fig.8.97 shows the shoulder adduction velocity against shoulder flexion velocity in which the right hand loop represents the raising of the block to the shelf and the left hand loop represents the lowering of the block to its initial position. The lower portion of each loop represents the acceleration phase in that direction, with the upper portion representing deceleration to rest. A clear pattern in the velocities from all subjects is visible, again indicating similarity between the strategies adopted. The size of the loops are relatively small for subject No.12, indicating the lower joint angular velocities for this subject.

With the exception of the shoulder internal rotation angular acceleration during lowering for subject No.11, Fig.A.8.94 shows the acceleration at all modelled joints for both subjects to have been less than the unimpaired mean. Subject No.11 had average maximum accelerations around 22% and 27%

lower than the unimpaired mean at the shoulder and elbow respectively, with those of subject No.12 around 45% lower at both the shoulder and elbow.

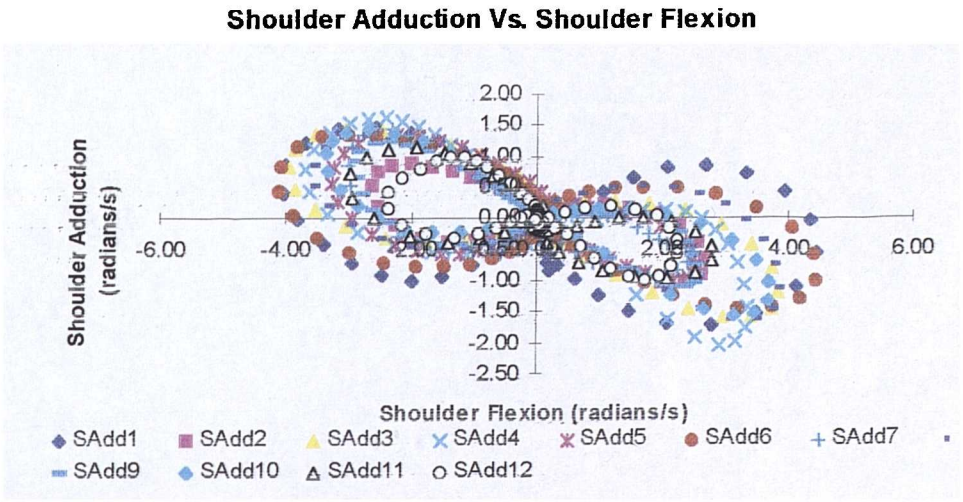

Fig.8.97 Shoulder adduction Velocity Vs. Shoulder flexion Velocity during activity 10.

Fig.8.98 shows the relationship between the shoulder flexion acceleration and angle for this activity with the upward and downward phases superimposed. The pattern indicates a high acceleration at low angles in the upward phase in order to move the block from its initial position, decreasing until around the mid-point in the raising of the block before deceleration occurred to bring the block to rest on the shelf, with a similar process occurring in reverse for the lowering phase. Reduced ranges of flexion and lower maximum acceleration values can be seen for the impaired subjects.

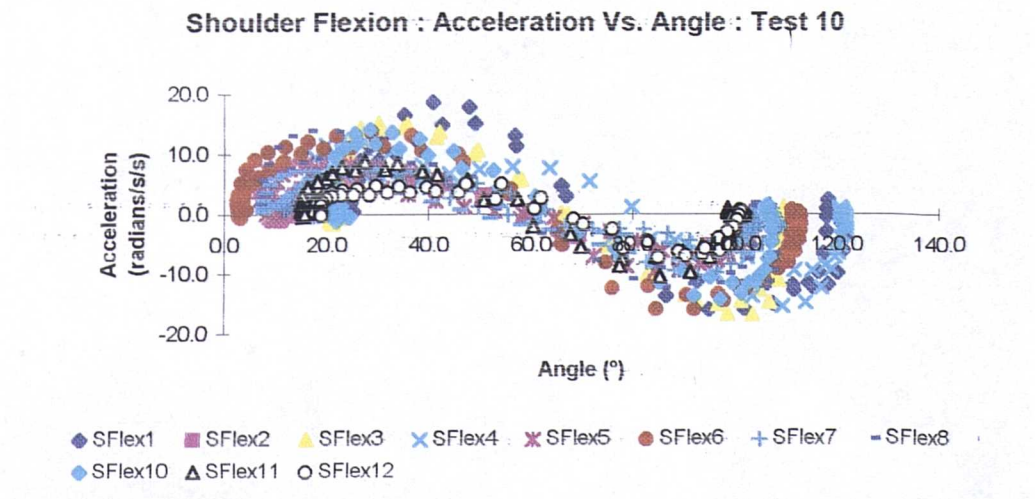

Fig.8.98 Shoulder flexion acceleration Vs. Angle during activity 10.

8.6 Discussion of results obtained for ten selected everyday activities

8.6.1 Introduction

The following section contains a discussion of the key aspects and general patterns of the results presented in Section 8.5.

Initially the preliminary assessment of twenty three activities based on marker visibility and joint ranges of motion allowed the selection of ten that would be suitable for testing. Those selected were involved in feeding, personal hygiene and the use of simple everyday objects and were performed by twelve subjects, two of whom had shoulder impairment. Body segment parameters, cadences, elbow and wrist trajectories, joint angles, joint angular velocities and joint angular accelerations were calculated. In addition the external forces and moments at and around the joints were calculated as well as the contributions to these forces and moments of any hand held load.

8.6.2 Cadences

The cadence results showed that for five of the ten activities, both impaired subjects performed the activities slower than the slowest of the unimpaired subjects. For four of the remaining five activities the unimpaired subjects performed slower than the mean of the unimpaired subjects. This indicated a reduction in speed of performance by the subjects with shoulder impairment, either through a conscious decision or a reduced functional capacity.

8.6.3 Elbow and wrist trajectories

The trajectory of the wrist centres for the reach to opposite side of the neck and answer the telephone activities was relatively consistent in all three planes with the elbow centre trajectory being less consistent. These patterns indicated the ability of different subjects to achieve the same task using different combinations of the multiple degrees of freedom available to the upper limb.

The consistent pattern of the wrist sagittal plane trajectory, particularly for those activities such as the drink from a mug which involved primarily elbow

flexion, also indicated the adoption of a strategy whereby the precise location of the hand in the target position was the key objective.

More consistent trajectories occurred for both the elbow and wrist for those activities involving more complex motion and placing of the hand in a more extreme position in its workspace, such as the reach to the opposite side of the neck and the raising of the block to shoulder and head heights. These activities made greater demands on the degrees of freedom available to the upper extremity that were exhibited in the trajectories for other activities.

For the raising of the block to shoulder and head heights the elbow coronal plane trajectories showed a tendency to curve laterally. This was due to the abduction of the shoulder in order to avoid impingement at the shoulder.

8.6.4 Joint rotations

From most activities the angle data were reasonably smooth with narrow ±2SD boundaries. Table 8.65 contains a ranking of the maximum unimpaired mean rotations at each joint. The lower the score for an activity, the greater the rotation required about the axis to which it refers in comparison to the other activities. It can be seen for instance that the reach to the opposite axilla required the greatest shoulder internal rotation maximum from all activities but among the lowest maxima for shoulder and elbow flexion. Where both positive and negative rotations occurred about an axis, columns were included for each. Where no rotation occurred about an axis for one or more activity, they were each given an equal ranking one below the previous true ranking. The 'Total' and 'Posn.' columns in Table 8.65 give the sum of the ranking scores for each activity and the resultant overall ranking of their relative complexity.

The most demanding activities in terms of rotation at the shoulder were the raising of the block to head height, reach to head side and back and reach to opposite side of the neck activities, the least demanding being the eat with hand to mouth and eat with spoon activities.

	Sh.Add.	Sh.Abd.	Sh.Flex.	Sh.Int.Rot	Elb.Flex.	Elb.Pron.	Elb.Sup.	Total	Posn.
Opposite Axilla	2	6	8	1	8	4	2	31	4
Opposite side of Neck	1	7	5	2	6	3	1	25	2
Head Side and Back	4=	2	2	5	1	1	9=	24	1
Eat Hand to Mouth	4=	10	9	7	5	5	5	45	10
Eat with Spoon	4=	3	10	10	3	10	3	43	8
Drink from Mug	4=	4	7	9	4	8	8	44	9
Answer Telephone	4=	8	6	8	2	2	9=	39	5
Brush Left of Head	3	9	4	4	7	9	4	40	6
Block to Shld. Height	4=	5	3	6	10	7	7	42	7
Block to Head Height	4=	1	1	3	9	6	6	30	3

Table 8.65 Ranking of maximum unimpaired mean joint rotations for each activity.

No activity involved extension or external rotation of the shoulder, with shoulder flexion reaching a maximum level for the raise of the block to head height and the reach to head side and back activities. The maximum internal rotation occurred for the reach to opposite axilla and opposite side of the neck activities. The minimum internal rotation occurred for the eat with spoon and drink from mug activities due to the targeting of an extended hand held object to the mouth as opposed to the hand itself. The reach to the opposite side of the neck activity involved a more considerable adduction of the shoulder than any other activity, the shoulder being in abduction throughout seven of the ten activities. The greatest abduction occurred for the raising of the block to head height, leading to the laterally curved trajectory of the elbow in the coronal plane. The least amount of abduction occurred for the eat with hand to mouth activity.

The most demanding activities in terms of rotation at the elbow were the reach to opposite side of the neck, reach to head side and back and answer the telephone activities, the least demanding being the raising of the block and drink from a mug activities.

For all except the last activity, elbow flexion was the major rotation component. The greatest angles occurred during the reach to head side and back and the answer the telephone activities, with the most extended positions being reached for the raise of the block to shoulder and head heights due to

the positioning of the shelf at arms length. Maximum pronation at the elbow occurred during the reach to the head side and back activity and the answer a telephone activity, with maximum supination occurring for the reach to opposite axilla and reach to the opposite side of the neck activities.

The reach to head side and back activity involved the greatest elbow flexion and pronation as well as relatively high shoulder abduction and flexion and consequently can be seen to have been ranked as the most complex task overall. The next most complex were the block raise to head height with high relative maxima for shoulder abduction, flexion and internal rotation and the reach to the opposite side of the neck with high relative maxima for shoulder adduction and internal rotation and forearm pronation and supination. The activities ranked as the least demanding overall were the drink from mug, eat with spoon and eat with hand to mouth activities, being primarily dependent on elbow motion with relatively little shoulder involvement.

Among the results of interest was the low maximum shoulder adduction for the brush of the left side of the head in comparison to the reach to opposite side of neck activity when these activities would appear to be similar. The difference was due to a tendency for the subjects to turn their head slightly to meet the brush as well as the extension to the hand afforded by the brush. In contrast the hand required to be placed fully on the opposite side of the neck around the mid-cycle of the reach to the opposite side of the neck. High levels of shoulder abduction were noticeable for the eat with a spoon and drink from a mug activities due to the extension of the hand by these objects, requiring the final position of the hand to be slightly lateral to the mouth.

8.6.5 External joint forces

The joint force data, as well as the joint moment data discussed in the next section were less smooth than the joint angle data, having been based on velocities and accelerations obtained by differentiating the angle data, a process which magnified its random noise components. When considering the external forces it was expected that the primary force component would act in the direction of the gravitational acceleration. This was indeed the case, the maximum force for all activities occurring along the vertical shoulder Z axis,

maintaining a similar level at around 5% of the mean unimpaired subject body weight which corresponds with the data of de Leva (1996a) from which the mass of the arm and hand was 4.94% of the body mass.

	Sh.X+	Sh.X-	Sh.Y+	Sh.Y-	Sh.Z+	El..X+	El..Y+	El..Y-	El..Z+	El..Z-	Total	Posn.
Opposite Axilla	2	3	6=	8	8=	7=	10	2	7	4=	57	6
Opposite side of Neck	1	1	4	1	6	3	9	1	4	3	33	3
Head Side and Back	4	5=	3	5	3	7=	1	3=	3	2	36	4
Eat Hand to Mouth	8=	8	6=	7	8=	10	7	3=	9	4=	70	9
Eat with Spoon	10	9	8	9	10	9	6	3=	10	4=	78	10
Drink from Mug	8=	10	9	6	4	5	5	3=	5	4=	59	7
Answer Telephone	7	7	1	4	7	6	4	3=	8	4=	51	5
Brush Left of Head	5	5=	10	10	5	4	8	3=	6	4=	60	8
Block to Shd. Height	6	4	2	3	2	2	2=	3=	2	4=	30	2
Block to Head Height	3	2	5	2	1	1	2=	3=	1	1	21	1

Table 8.66 Ranking of maximum unimpaired mean joint forces for each activity.

Similar to the summary table for the angles, Table 8.66 ranks the joint force data. Where both positive and negative forces occurred along an axis, columns were included for each. Where more than one value were equal they were given the same ranking and the next lower ranking value was missed out. Where no force occurred along an axis in a particular direction it was regarded as zero and all such values were given a ranking one below the previous true ranking.

At the shoulder the maximum Z axis force occurred for the raising of the block to shoulder and head heights, these involving the greatest hand-held load. The maximum positive and negative X axis forces and the maximum negative Y axis force occurred for the reach to the opposite side of the neck activity where the shoulder was flexed, adducted and internally rotated. The maximum positive Y axis force occurred for the answer the telephone activity.

At the elbow the maximum positive and negative forces again occurred along the Z axis direction for the raising of the block to head height. The only considerable forces in the negative Z axis direction were for the reach to head

side and back and raise block to head height activities, both involving flexion of the shoulder greater than 90°. The X and Y axis forces at the elbow reach greater maximum values than those at the shoulder due to these axes becoming vertically oriented during motion. The maximum force in the X axis direction occurred for the raising of the block to head height due to the flexion and internal rotation of the shoulder. No activity involved a negative force along the X axis as no shoulder external rotation occurred. The maximum positive force along the Y axis occurred for the reach to head side and back activity due to the high flexion at the shoulder and elbow. The maximum negative force along this axis occurred for the reach to opposite side of the neck activity as the hand reached the neck and moved away from it.

8.6.6 External joint moments

When considering the joint moments, the maximum values were expected to occur for horizontal axes about which the rotations were most affected by gravity. This would tend to be the axes perpendicular to the longitudinal axes of the upper limb segments and displaced from the segment mass centres, but would also apply to the humeral longitudinal axis when horizontal with the elbow flexed. The application of a moment would be required in such a position to counteract the action of gravity on the mass of the forearm.

The shoulder flexion moment was the greatest for all activities, being responsible for the motion of the combined masses of the upper limb segments through relatively large rotations. The elbow flexion moment was the next greatest for all tests, with the shoulder adduction moment generally lower due to the small range of motion about this axis. The internal rotation moments at the shoulder were small and all negative as the upper limb segment positions in all activities led to a gravitational internal rotation moment that required to be opposed.

Table 8.67 shows a ranking of the maximum unimpaired mean shoulder and elbow moment data. Forearm pronation moments were not included as the forearm centre of mass was defined to lie on its longitudinal axis leading to

negligible elbow pronation moments. Where moments were applied in both directions about an axis, two columns were included.

	Sh.Add.	Sh.Abd.	Sh.Flex.	Sh.Ext.Rot	Elb.Flex.	Elb.Ext.	Total	Posn.
Opposite Axilla	3	5	10	5=	8	8=	39	8
Opposite side of Neck	2	4	6=	7	6=	7	32	6
Head Side and Back	6	3	8	9=	3	1	30	3=
Eat Hand to Mouth	7	10	6=	9=	9	6	47	10
Eat with Spoon	9=	6	9	8	10	4=	46	9
Drink from Mug	9=	7	4	3	4	3	30	3=
Answer Telephone	8	8	3	4	5	2	30	3=
Brush Left of Head	4	9	5	5=	6=	4=	33	7
Block to Shd. Height	5	2	1	2	2	8=	20	2
Block to Head Height	1	1	2	1	1	8=	14	1

Table 8.67 Ranking of maximum unimpaired mean joint moments for each activity.

As might be expected the raising of the block to shoulder and head heights were ranked as requiring the greatest moments, these involving the greatest hand held mass, the greatest elbow extension and among the greatest levels of flexion at the shoulder. The raise to head height can be seen to involve the greatest unimpaired mean shoulder adduction, abduction and external rotation moments from any activity as well as the greatest elbow flexion moment, the latter being applied in mid-cycle to control extension of the elbow under the influence of gravity as the block was lowered onto the shelf. Although the shoulder was abducted in mid-cycle, the block was held in such a position that an adduction moment was required in order to oppose an abduction moment due to gravity.

The drink from mug activity was also ranked as requiring relatively large moments, along with the answer the telephone activity which involved an extension of the elbow and flexion of the shoulder in the initial position. The moments for these were similar due to the comparable hand loads involved. The eat with hand to mouth and with spoon activities were ranked as requiring the lowest moments, a result of the limited ranges of motion during these activities and the lack of any major additional hand load. These activities also

involved flexion of the elbow, bringing the forearm centre of mass closer to the shoulder flexion axis, resulting in a lower moment about this axis.

Elbow extension moments were required to maintain the forearm position in mid-cycle for all but the reach to opposite axilla and raising of the block to shoulder and head height activities. These were required where the forearm reached a position in which the action of gravity tended to cause elbow flexion. The largest occurred for the reach to head side and back and answer telephone activities due to flexion at the shoulder and elbow.

8.6.7 Joint angular velocities and accelerations

Angular velocities and accelerations about each of the modelled upper limb axes were calculated in order to try and establish variations in performance between subjects which may have been masked during calculation of the forces and moments due to differences in their masses. The maximum unimpaired mean values are ranked in Tables 8.68 and 8.69.

	S.F.	S.E.	S.Ad.	S.Ab.	S.I.R.	S.E.R.	E.F.	E.E.	E.P.	E.S.	Total	Posn.
Opposite Axilla	6	6	3	3	2=	5	10	10	2	2	49	5
Opposite side of Neck	3	5	1	1	2=	2	7=	7=	1	1	30	2
Head Side and Back	5	2	5=	7=	5=	3	2=	1	5	5	40	3
Eat Hand to Mouth	7=	10	9=	9=	8	8	5	3=	3	3	65	7
Eat with Spoon	7=	9	7	7=	9	9=	9	5	8	8	78	9
Drink from Mug	7=	8	8	6	10	9=	7=	6	9	9	79	10
Answer Telephone	7=	7	9=	9=	7	7	4	3=	10	10	73	8
Brush Left of Head	4	4	5=	4=	5=	4	6	9	7	6	54	6
Block to Shd. Height	2	3	4	4=	4	6	2=	7=	6	7	45	4
Block to Head Height	1	1	2	2	1	1	1	2	4	4	19	1

Table 8.68 Ranking of maximum unimpaired mean joint angular velocities for each activity.

The magnitudes of the angular velocities and accelerations were generally found to be greater for axes about which there were large ranges of motion. The greatest maximum unimpaired mean velocity from any activity occurred about the pronation axis for the reach to opposite side of neck activity, this rotation having the second greatest mean angular range from any activity.

The lowest maximum angular velocities occurred about the shoulder adduction axis for the eat with hand to mouth and answer the telephone activities, these having the narrowest mean ranges from any of the activities. This pattern suggested that in order to complete large joint rotations while maintaining the joint co-ordination pattern, the rate of rotation was increased.

	S.F.	S.E.	S.Ad.	S.Ab.	S.I.R.	S.E.R.	E.F.	E.E.	E.P.	E.S.	Total	Posn.
Opposite Axilla	7	6	3=	3	4	5	10	8	2	2	50	5
Opposite side of Neck	4	4	2	1	2	1	7	4	1	1	27	2
Head Side and Back	2	2	6	6	3	3	1=	3	4	4	34	3
Eat Hand to Mouth	8	9	8	9=	8	8	4	5	3	3	65	7
Eat with Spoon	9	8	7	9=	9	9	9	9	9	7	85	9
Drink from Mug	10	10	9=	7	10	10	8	10	10	10	94	10
Answer Telephone	6	7	9=	8	7	7	5	6	8	9	72	8
Brush Left of Head	5	5	5	5	5	4	6	7	6	6	54	6
Block to Shd. Height	3	3	3=	4	6	6	3	2	7	8	45	4
Block to Head Height	1	1	1	2	1	2	1=	1	5	5	20	1

Table 8.69 Ranking of maximum unimpaired mean joint angular accelerations for each activity.

The angular accelerations were found to follow a similar pattern, the greatest maximum occurring for the same rotation as the maximum velocity, with the lowest maximum occurring about the shoulder adduction axis for the drink from a mug activity which had a small angular range.

The raising of the block to head height was ranked as requiring the greatest angular velocities and accelerations, this activity involving the largest ranges of shoulder flexion and internal rotation from any activity as well as relatively large ranges about the other axes of rotation.

8.6.8 Ranking of activities for analysis or modelling purposes

In order to assess which of the activities analysed in the current study would be of most use in future studies of impaired upper limb motion, the ranking positions from the final columns in each of Tables 8.65 - 8.69 for each of the activities were totalled. The lowest possible overall total would be five if

an activity was ranked highest in all five tables, the highest possible total being fifty. The results are given in Table 8.70.

Overall Ranking	Activity	Overall Total
1	Block to Head Height	7
2	Head Side and Back	14
3	Opposite side of Neck	15
4	Block to Shd. Height	19
5	Opposite Axilla	28
6	Answer Telephone	29
7	Brush Left of Head	33
8	Drink from Mug	39
9	Eat Hand to Mouth	43
10	Eat with Spoon	45

Table 8.70 Overall ranking of activities.

It can be seen that the raising of the block to head height has the lowest total by some way, indicating that it involved the greatest combination of angles, forces, moments, velocities and accelerations from all the activities. This activity would therefore be proposed as the most suitable of the activities tested for assessment of impaired function in future studies.

8.6.9 Impaired subject data

From inspection of the angle patterns it can be seen that in general the impaired subjects managed to achieve ranges of motion that lay within the ± 2SD boundaries of the unimpaired subjects. The joint force and moment data also lay within these boundaries though there was a tendency for the moments of subject No.11 to be slightly greater than the unimpaired mean while those of subject No.12 were slightly lower.

When comparing patterns of force and moment between subjects, a contribution to any variations will be made by differences in their segment masses. It is therefore important when looking at data from impaired subjects in particular, that variations must not be automatically attributed to impairment. Subject No.11 had a body mass around 3.5 Kg greater than the unimpaired

mean with that for subject No.12 some 12.45Kg below this mean. Such widely differing body masses would easily account for variation in data such as that seen for the block raise to shoulder height activity, during which subject No.11 generated a greater maximum shoulder flexion moment than the unimpaired mean from any activity, with the maximum of subject No.12 lower by a considerable margin.

Looking at the patterns of shoulder motion for the impaired subjects from all the activities tested, subject No.11 reached a considerably lower maximum shoulder adduction and slightly lower internal rotation than the unimpaired mean, while subject No.12 reached a considerably lower maximum shoulder flexion and adduction than the unimpaired mean. For the raising of the block to head height both impaired subjects reached greater shoulder abduction than the unimpaired mean perhaps indicating a requirement for greater protective measures in order to avoid discomfort due to impingement. Both impaired subjects were seen to employ a lowering of the head to allow the completion of the reach to head side and back and brush the left side of head activities. A further compensatory mechanism was a greater elbow flexion than the unimpaired mean, employed in six of the ten activities by subject No.11 and in two by subject No.12.

Subject No.11 adopted a grip of the mug handle between thumb and extended fingers, as opposed to encircling the handle with the fingers as was performed by all other subjects, resulting in an increased abduction due to the greater length afforded to the hand and mug. Both subjects clearly employed a greater forearm pronation in order to tilt the mug however, rather than internally rotating and flexing the shoulder as was the tendency with the unimpaired subjects.

For the activities which were dependent on elbow motion and required minimal involvement of the shoulder, the eat with hand to mouth, eat with a spoon and drink from a mug activities in particular, there was no appreciable variation between the shoulder rotations from the unimpaired and impaired subjects.

In general, greater differences between the unimpaired and impaired groups were noticeable for the velocity and acceleration data, there being a

tendency for the impaired subjects to show lower maxima, particularly for the accelerations. This indicated an inability to generate muscular forces comparable to those of the unimpaired subjects, due possibly to a deterioration in muscle capability through lack of use. Alternatively it may indicate a conscious reduction in muscular force as a protective measure, reducing the load on the tissues around the affected joint and therefore reducing the possibility of experiencing discomfort.

Clear reductions in the velocities and accelerations for subject No.12 in comparison to subject No.11 were shown in the plots of shoulder flexion angular velocity and acceleration against flexion angle and elbow flexion angular velocity against shoulder flexion angular velocity for the raising of the block to shoulder and head heights and in the shoulder adduction angular velocity against shoulder flexion angular velocity plot for the raise to head height. These results indicate that for these activities at least, greater protective measures were employed or a greater functional deficit was experienced, by subject No.12 than subject No.11.

8.6.10 Contribution of additional hand load

As expected, the contribution of the hand-held loads to the external joint forces and moments increased with their increasing mass. The greatest effect occurred at the wrist due to the comparable masses of the hand and the objects involved. The percentage contributions of the hand-held masses to the external forces and moments at the shoulder and elbow were of similar magnitude and some way below those at the wrist.

8.6.11 Comparison with Cheng (1996) and Williams (1996)

On repetition of the eat with hand to mouth activity of Williams (1996) and the raising of the block to shoulder and head height activities of Cheng (1996) the angular ranges and moment values at the shoulder and elbow were found to compare well with those from the current study, particularly those for the primary components of the motion involved. The good correspondence with the results from these previous studies emphasised the validity of the experimental methods and analysis techniques used.

8.6.12 Graphical data output formats

In discussing upper limb motion control strategies, Barker (1996) highlighted the difficulty in defining 'normal' and 'abnormal' upper limb motion and indeed suggested that such clear definitions may actually be unobtainable due to the mechanical degrees of freedom available. As discussed in the introduction to Section 8.4, various permutations of data output were made in an attempt to investigate their suitability in trying to shed some light on the identification of normal and abnormal patterns of motion. The plots of joint moment against joint moment and angular acceleration against angular acceleration were found to contribute no useful information during the analysis of any activity.

Where they were incorporated, the phase plane plots of the relationship between joint angular velocity and angle were of particular interest, showing patterns similar to two out-of-phase sinusoids. Relatively consistent patterns between subjects indicated the importance of the rotation involved and the similarity of the strategies adopted.

During the drinking from a mug, eating with hand to mouth, eating with a spoon and answering a telephone activities, patterns were obtained for elbow flexion angular velocity which were symmetrical across the X-axis, showing the similarity in the flexion and extension velocities for raising and lowering phases. Similar patterns were obtained for the shoulder flexion angular velocity during the raise of the block to shoulder and head height activities. For all these plots the maximum velocities during flexion or extension were seen to occur around the mid-point of the motion. For the raising of the block to shoulder height activity the plot of shoulder flexion angular velocity against angle shows a clear reduction in the velocities and accelerations for subject No.12 in comparison to subject No.11.

For the raising of the block to shoulder and head height activities, involving similar movement strategies and targeted reaching of the hand, the plots of angle against angle were found to be useful. Repeated relationships were visible for the elbow flexion angles, the shoulder internal rotation angles and the elbow pronation angles, all in relation to shoulder flexion.

These patterns indicated that the subjects adapted similar strategies in order to complete these activities. Also notable from these was the tendency for shoulder internal rotation to increase as the shoulder was flexed during both activities and the associated compensatory supination of the forearm in order to maintain the wooden block in an upright position.

For the same activities, the plots of angular velocity against angular velocity showed similar 'figure of eight' patterns. These patterns indicate that different velocities occurred about each of the axes plotted, had they been the same the expected pattern would have been closer to a straight line.

A reduction in the right hand, raising phase loop for subject No.12 was evident for the raising of the block to shoulder height. This may be due to the action of the muscles in this direction being opposed by gravity, whereas it assists the muscles during lowering of the block. Atkeson & Hollerbach (1985) previously suggested such an explanation for differences in joint displacement patterns between upward and downward cycles and it seems that it may be as valid for the angular velocities of these cycles.

The plots of moment against angle and angular acceleration against angle also contributed to the discussion of some activities. The patterns obtained for the plots of velocity, acceleration and moment against angle and velocity against velocity indicated that these may be useful tools in the identification of repeated patterns of motion and deviations from these patterns, particularly for activities involving targeted reaching of the hand in the anterior workspace.

8.6.13 Experimental arrangement

The initial positioning of the objects and the arrangement of the experimental environment would have an effect on the results obtained. This was perhaps best illustrated by the occurrence of the lowest minimum shoulder flexion angles from any activity for the raising of the block to shoulder and head heights. These low values were due to an initial position of the hand slightly posterior to that from the other activities in order to allow gripping of the block. Such small differences could explain the variations between the studies of Williams (1996) and Cheng (1996) and the current study. As discussed in

Section 8.5.10, if the shelf of Cheng (1996) was set at a lesser horizontal distance from the subjects than in the current study during performance of the block raise to shoulder and head heights, a greater shoulder abduction and lesser elbow extension would be necessary in order to move the elbow laterally and raise the block to the shelf. This would become more exaggerated as the horizontal distance between subject and shelf was reduced and would also explain the wide variation in the maximum shoulder abduction between the two block raising activities of Cheng (1996).

8.6.14 General observations

During analysis of the reach to head side and back activity, the most complex tested in terms of upper limb joint motion, it was necessary to discard three data sets due to poor results from interpolation across missing marker paths. This highlighted the difficulty in using four cameras to film motions where both anterior and posterior views were required.

When raising the wooden block anteriorly to shelves at shoulder and head heights, the results indicate abduction and internal rotation at the shoulder and a simultaneous associated supination of the forearm for all subjects. The shoulder motion is necessary to avoid impingement, with that of the forearm acting as a compensatory mechanism to maintain the hand-held block in an upright position.

The differences in body mass between subjects were seen to cause variation in the results obtained. This was particularly obvious in the results from the two impaired subjects where the maximum force and moment values obtained for subject No.11 tended to be some way above those of the much lighter subject No.12.

The tendency for the angle, force and moment data to show insignificant differences between unimpaired and impaired subjects is consistent with results obtained in previous studies. Williams (1996) found that looking at angles alone allowed poor discrimination between unimpaired elbow function and that from patients with arthritic conditions. Fazel-Rezai et al (1998) found that no kinematic parameter showed a clear difference between unimpaired subjects and those with rheumatoid arthritis of the shoulder during performance

of five lifting and reaching tasks similar to those from the current study. Schmidt et al (1999b) tested patients with different shoulder disorders for maximal ranges of motion at the shoulder and during four reaching tasks. Young (16-25 y) patients with unstable shoulder conditions were found to differ little from an unimpaired control group, while older subjects (45-70y) with degenerative shoulder conditions were found to show obvious differences in joint angles, trajectories and velocities.

8.7 Activities performed by subject No.1 only

As earlier discussed and shown in Table 8.2, Subject No.1 performed six activities in addition to those discussed in Sections 8.5. Three of these were the brushing of the right side, back and top of the head, the others being a reach to the throat, reach to the top of the head and the placing of the hand over the mouth.

In the same manner as for the first ten activities, two repetitions of each of the three brushing activities performed by Subject No.1 were analysed. Similarly three repetitions of each of the other additional activities were analysed. The angles, forces and moments at the shoulder, elbow and wrist during performance of these activities are given in Appendix IV. As only a small number of repetitions of each were performed and by a single subject, these results cannot be held to be representative of the 'normal' patterns of motion for these activities.

As can be seen in Appendix IV, the brushing activities and the reach to the top of the head had similar patterns of motion and associated forces and moments as those from the brushing of the left side of the head and reach to side and back of head activities performed by all subjects. The placing of the hand over the mouth and the reach to the neck activities had very similar patterns of motion and associated forces and moments to those from the eating with hand to mouth activity. These additional activities were not performed by all subjects as the motions involved were considered to be similar to those of other activities. The results obtained, though from one subject only, would seem to support their exclusion on these grounds.

CHAPTER 9 : FURTHER INDICATED EXPERIMENTAL WORK

9.1 The influence of the non-rigid-body behaviour of the forearm

9.1.0 Introduction

During analysis of some of the activities discussed in Sections 8.4 and 8.5, the measured abduction angles at the elbow had greater ranges and variability than might have been expected. The maximum abduction values for some of the activities reached some way beyond the average adult carrying angle found by Beals (1976) to be around 17.8°, or the figure of 15.4° from Deland (1987).

Pronation and supination of the forearm does not occur at the elbow joint but along the length of the forearm between elbow and wrist. It would therefore be possible for relative rotation between the markers attached on the proximal and distal forearm to occur during pronation and supination.

As discussed in Section 6.3.11, anatomical calibration of the epicondyles was carried out with the forearm in a 'neutral' position, pronated 90° from its fully supinated 'anatomical' position.

From such a position it is clear that if the forearm is rotated again into full supination, the marker on the proximal ulna (marker 3 in Fig.6.5) will remain largely in the same position while those on the ulnar and radial styloids (markers 1 and 2 in Fig.6.5) will be rotated in the negative direction about the forearm longitudinal axis.

The rotation between proximal and distal forearm will lead to a deformation of the affixed marker pattern, the proximal ulna marker being posteriorly and laterally displaced relative to the styloid markers after supination from the neutral position.

Subsequent least squares fitting of the original marker configuration to this deformed marker pattern as described in Section 5.3, would cause the orientation of the technical embedded frame to be determined in greater adduction and flexion than it had actually reached. This would in turn cause the anatomical embedded frame to be defined in a similarly adducted and

flexed position, influencing the accuracy of the angular values obtained for the rotations at the elbow.

A similar effect would be introduced if no least squares fitting were used, the embedded technical frame being defined from the raw marker co-ordinates. In this instance if the proximal ulna and ulnar styloid markers were used to define the primary axis of the forearm technical frame in the initial position, on supination of the forearm this frame would again be identified both flexed and adducted from its true position as shown in Fig.9.1.

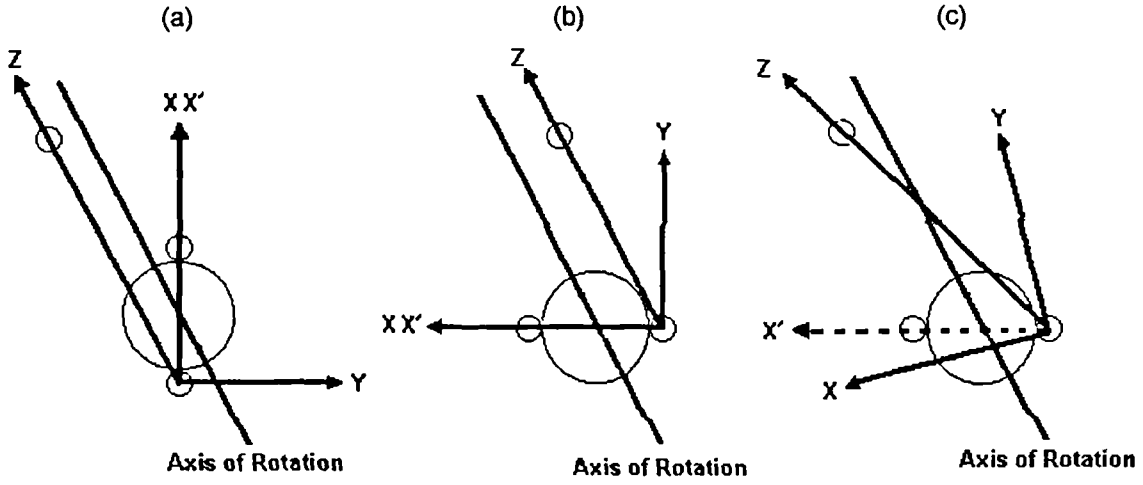

Fig.9.1 Flexion and adduction of embedded frame due to relative motion between proximal and distal forearm markers. (a) Frame defined in neutral position, (b) Frame defined in supinated position if proximal forearm marker also rotates, (c) Frame defined in supinated position if proximal forearm marker remains stationary.

Fig.9.1. is simplified so that the axis of rotation passes midway between the radial and ulnar styloid markers and is offset equally from the proximal ulna marker and each of the styloid markers. In reality this rotation axis would pass through the centre of the radial and ulnar heads (Nakamura et al (1999)).

Alternatively if no least squares fitting were used and the radial and ulnar styloid markers were used to define the primary axis of the forearm technical frame in the initial position, the offset from its true position on supination of the forearm would involve flexion only. In this case the adduction component would be removed in the process of finding the cross-products to define the axes.

This last solution might seem to be the best but relies on the initial forearm technical axis defined between the radial and ulnar styloid markers. The short distance between these markers would increase the influence of any marker digitising errors when defining the axes, an effect reduced by the selection of wider spaced markers when defining the primary technical axis. Also, although the error introduced to the measured elbow adduction angle would be removed using this last method, any correction of the error introduced to the flexion angle would be difficult.

Least squares fitting of the original marker configuration was used in the current study. The anatomical calibration of the epicondyles with the forearm in 90° of pronation from its fully supinated 'anatomical' position was adopted. Forearm pronation was found to vary fairly evenly about this point, the maximum unimpaired mean values from all tests being 65.3° of pronation and 53.7° of supination.

In order to investigate what contribution the forearm frame deformation might make to errors in the measured properties during analysis of upper limb activities, some additional tests were incorporated during filming of subject No.10, the final unimpaired subject.

9.1.1 Epicondyle anatomical calibration for varying forearm pronation

The first additional test was to carry out anatomical calibration of the lateral and medial epicondyles with the elbow in three positions of pronation, these being full supination, full pronation and a position midway between, defined as 'neutral' and adopted during subject testing.

The aim in performing this test was to assess the effect on the resulting angles, forces and moments when the initial relationship between the forearm embedded technical and anatomical frames was defined in the varying positions of forearm rotation. The relationship between these frames would be different for each position of forearm pronation.

The assessment was carried out using the data from the right hand reach to the left side of the neck activity for subject No.10, this activity being analysed using the three sets of epicondyle anatomical calibration data in

turn. The reach to the left side of the neck activity was selected as it exhibited the largest unimpaired mean range of forearm pronation from any of the activities tested, between -53.7° and 52.0°. The results obtained for the shoulder, elbow and wrist are given in Figs.9.2, 9.3 and 9.4 respectively.

At the shoulder there is little apparent variation in the angles or the major force and moment values on performing the analysis for each of the three positions of forearm anatomical calibration. Some of the lesser force and moment values are more affected though the magnitudes are small.

At the elbow a far greater variation in the angles than that shown for the shoulder is apparent. In particular the elbow adduction angle and elbow flexion angle can be seen to be affected as suggested in Section 9.1.0.

The results obtained for the extremes of pronation and supination are more exaggerated than any data obtained during subject testing as such extreme positions were never reached in practice. The results in Fig.9.3 do indicate however, that slight variations in the position of the forearm during anatomical calibration for the subjects and therefore differences in the relationship established between the embedded technical and anatomical frames, are almost certainly a contributory factor to the variations seen in the elbow adduction values during testing.

The forces and moments at the elbow and wrist can be seen in Fig.9.3 and Fig.9.4 to be less severely affected than the angles at the elbow, this due to the fact that the measured adduction angles were not included in the dynamic model, as discussed in Section 9.1.4.

9.1.2 C7 anatomical calibration for varying forearm pronation

The second additional test was to carry out anatomical calibration of the seventh cervical vertebra (C7) with the forearm again in positions of full supination, full pronation and a neutral position midway between.

For this test calibration of the epicondyles and therefore initial definition of the relationship between the embedded technical and anatomical frames was carried out with the forearm in the neutral position as was adopted during subject testing.

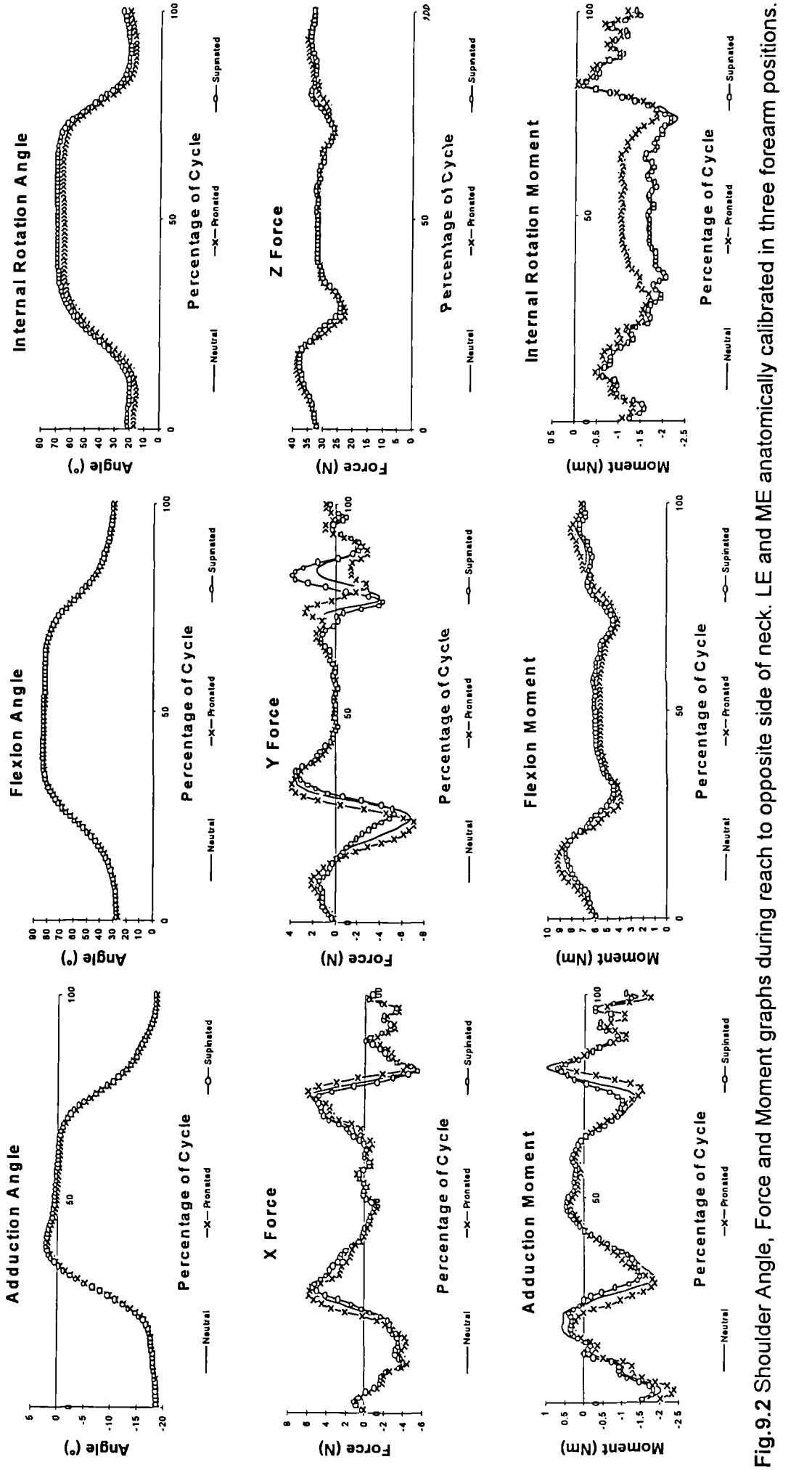

Fig.9.2 Shoulder Angle, Force and Moment graphs during reach to opposite side of neck. LE and ME anatomically calibrated in three forearm positions.

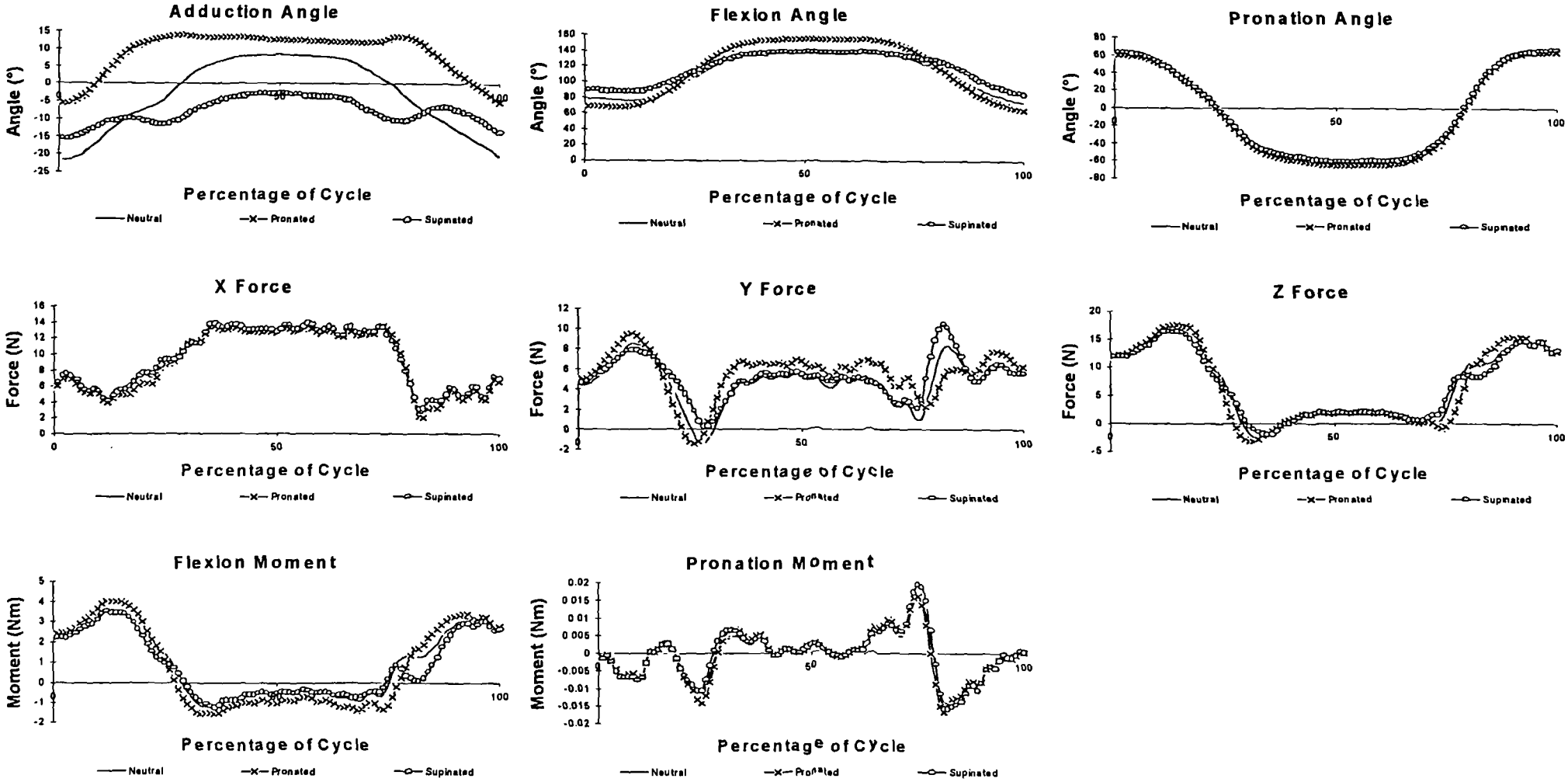

Fig.9.3 Elbow Angle, Force and Moment graphs during reach to opposite side of neck. LE and ME anatomically calibrated in three forearm positions.

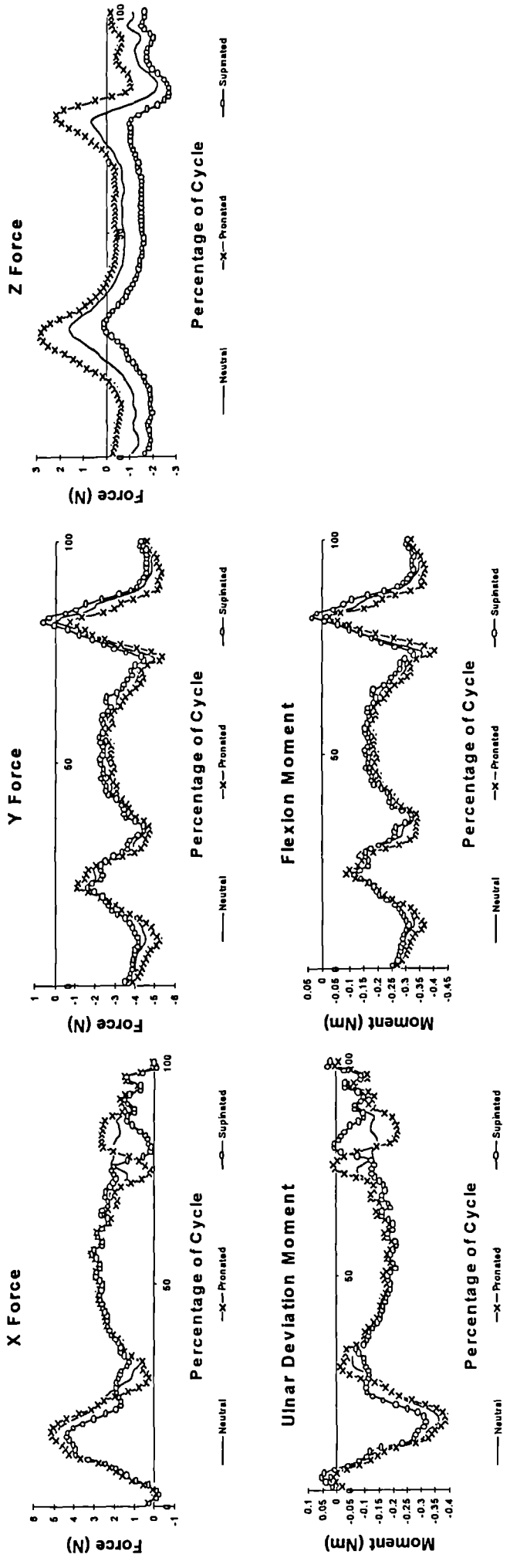

Fig.9.4 Wrist Force and Moment graphs during reach to opposite side of neck. LE and ME anatomically calibrated in three forearm positions.

As discussed in Section 6.5.5 the initial configuration of the markers used as the reference for the SVD least squares fitting in subsequent frames was defined from the position of the upper limb during anatomical calibration of the C7 landmark. The aim was to assess the effect on the resulting angles, forces and moments when the reference marker configuration for the SVD process was defined in varying positions of forearm rotation.

Again this assessment was made for the data from the right hand reach to the left side of the neck activity, incorporating the greatest range of forearm pronation measured for any of the activities. The results obtained for the shoulder, elbow and wrist are given in Figs.9.5, 9.6 and 9.7 respectively.

These show no significant differences in the results obtained at any of the three joints and are identical to the results obtained for the neutral forearm anatomical calibration in the previous section and shown in Figs.9.2, 9.3 and 9.4.

This indicates that the initial marker configuration for the SVD fitting is not the source of the poor results at the elbow but that these are due to variations in the initially defined relationship between technical and anatomical embedded frames or changes in this relationship during motion.

The similarity between the results of this test and those for the neutral forearm position from the previous test indicates that having established the relationship between the embedded technical and anatomical frames the errors introduced by subsequent deformation of the frame are 'locked in' irrespective of the position taken to define the initial configuration of the markers for the SVD fitting process.

The selection of the initial position has no effect on the initially defined relationship between the embedded technical and anatomical frames and each forearm position during the cycle would introduce the same distortion to the marker pattern irrespective of which position is used to define the initial configuration.

It was therefore established that the variation in the elbow adduction values was not due to any variation in the position of the forearm in which the initial marker configuration for the SVD fitting was defined.

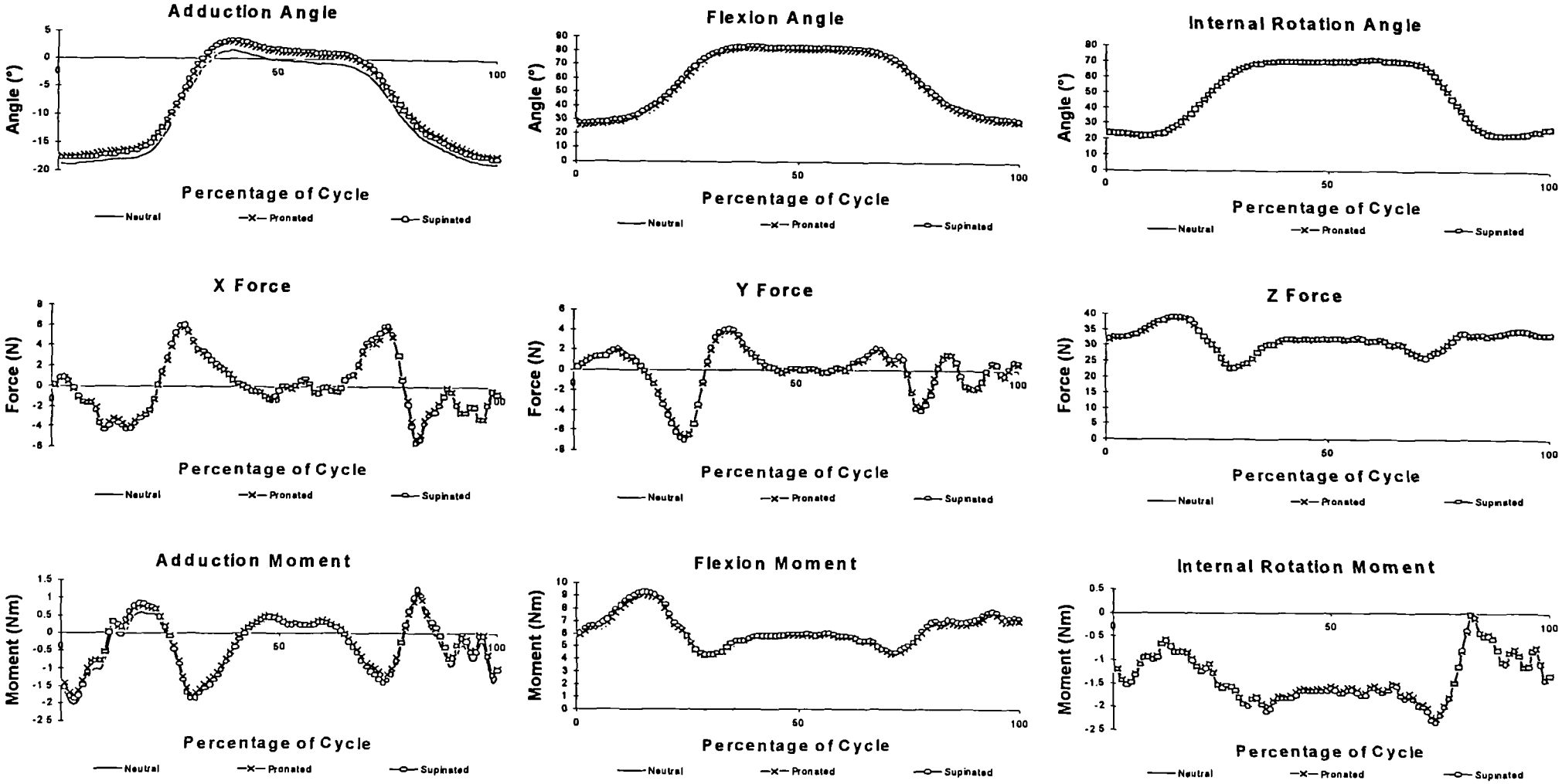

Fig.9.5 Shoulder Angle, Force and Moment graphs during reach to opposite side of neck. C7 anatomically calibrated with forearm in three positions.

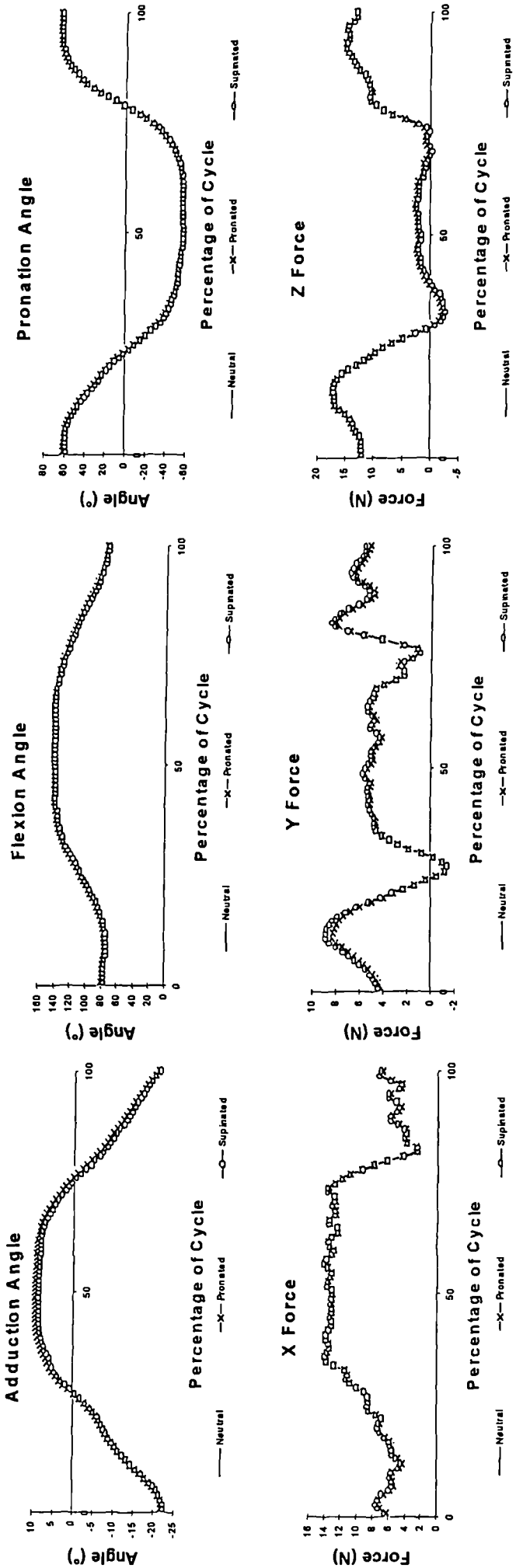

Fig.9.6 Elbow Angle, Force and Moment graphs during reach to opposite side of neck. C7 anatomically calibrated with forearm in three positions.

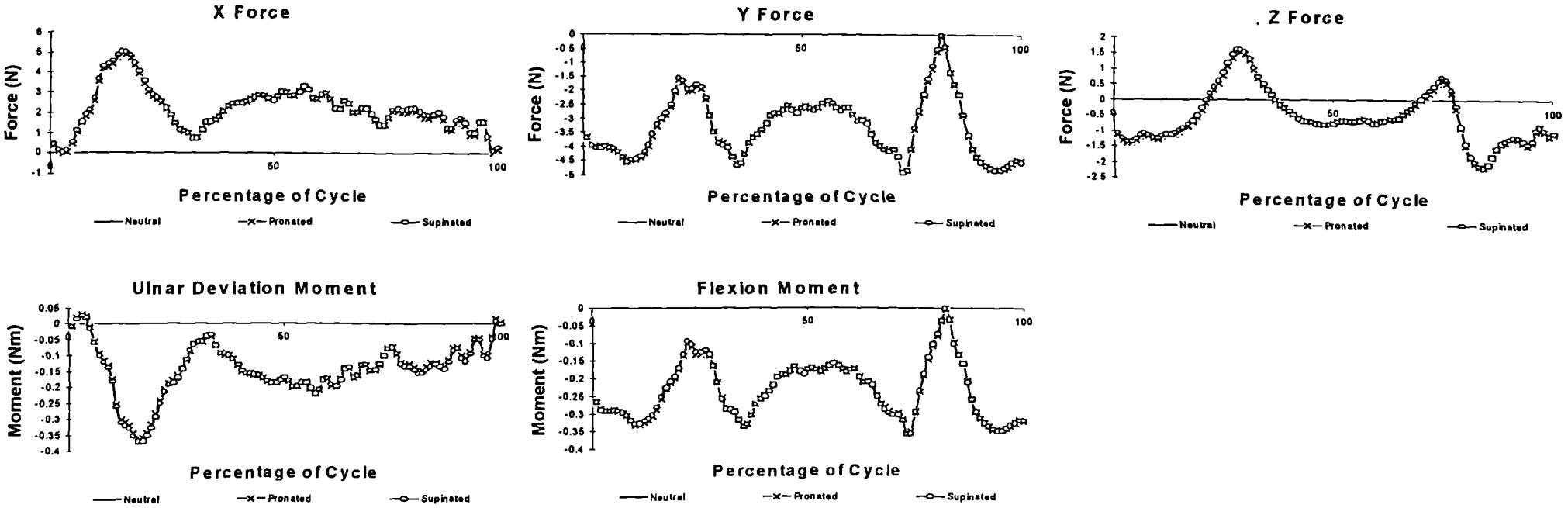

Fig.9.7 Wrist Force and Moment graphs during reach to opposite side of neck. C7 anatomically calibrated with forearm in three positions.

9.1.3 Effect of frame deformation during pure forearm pronation

The third additional test was for the subject to perform elbow pronation and supination across their maximal range while the upper arm was maintained in a constant position.

The aim in performing this test was to assess the level of elbow adduction/ abduction that was measured during pure forearm pronation and supination due to deformation of the surface marker pattern from the initial pattern used to define the embedded axes.

As for the first test discussed in Section 8.6.1, anatomical calibration of the lateral and medial epicondyles was carried out with the elbow in full supination, full pronation and in the neutral position midway between. The results obtained are given in Fig.9.8 and show the results from the forearm pronation activity for each of three anatomical calibration positions.

Fig.9.8 shows similar results to those in Fig.9.3, a difference between the results for the three data sets being shown. This supports the earlier finding, that changing the initial relationship between embedded technical and anatomical frames leads to changes in the results obtained.

On considering the traces for the three anatomical calibration positions independently, it is clear that an adduction was measured during forearm pronation and supination, though such an adduction motion was not performed by the subject.

The results form this test support the earlier result that the definition of the initial relationship between the embedded technical and anatomical frames has an effect on the results obtained. They also show that once the relationship between the embedded technical and anatomical frames has been defined, subsequent deformation in the marker pattern due to forearm pronation leads to a similar change in this relationship, resulting in the measurement of an adduction angle that did not occur.

Again as in Section 9.1.1 an effect is also apparent for the flexion results indicating cross-talk due to misalignment between the embedded axes and the underlying true anatomical rotation axes. As discussed in Chapter 7

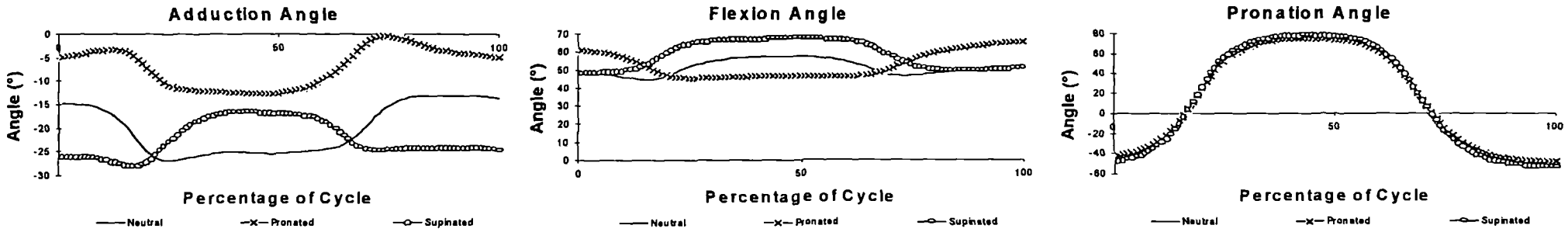

Fig.9.8 Elbow Angle graphs during pure forearm rotation. LE and ME anatomically calibrated in three forearm positions.

such cross-talk is unavoidable when defining orthogonal embedded frames for a system of rotations that do not necessarily occur about orthogonal axes.

9.1.4 Influence of elbow adduction/ abduction on dynamic results

The final additional test involved the insertion of predefined elbow abduction or 'carrying' angles into the linkage model used for calculation of the limb dynamics.

Four values considered representative of the true anatomical values were tested, these being 0°, 10°, 20° and the average adult carrying angle of 17.8° from Beals (1976). All other angles at the shoulder and elbow were kept constant in the dynamic model throughout, the only change being in the defined value of the elbow carrying angle.

The aim of this test was to assess how the amount of carrying angle defined in the dynamic model affected the final force and moment results. This would indicate the relevance of the problem with the elbow adduction angles for a dynamic study. As before, the data from the right hand reach to the left side of the neck activity was used. As well as a large range of forearm pronation this activity involved a large range of elbow flexion thus maximising the effect of any carrying angle included in the dynamic model. The results obtained for the shoulder, elbow and wrist are given in Figs.9.9, 9.10 and 9.11 respectively.

These results show that defining a carrying angle in the dynamic model has little effect on the major forces and moments at each of the joints in comparison to those obtained with no defined carrying angle. This suggests that the problem with the forearm marker pattern deformation and adduction angles at the elbow is of greatest importance to those studies where accurate measurement of this adduction is a key aim.

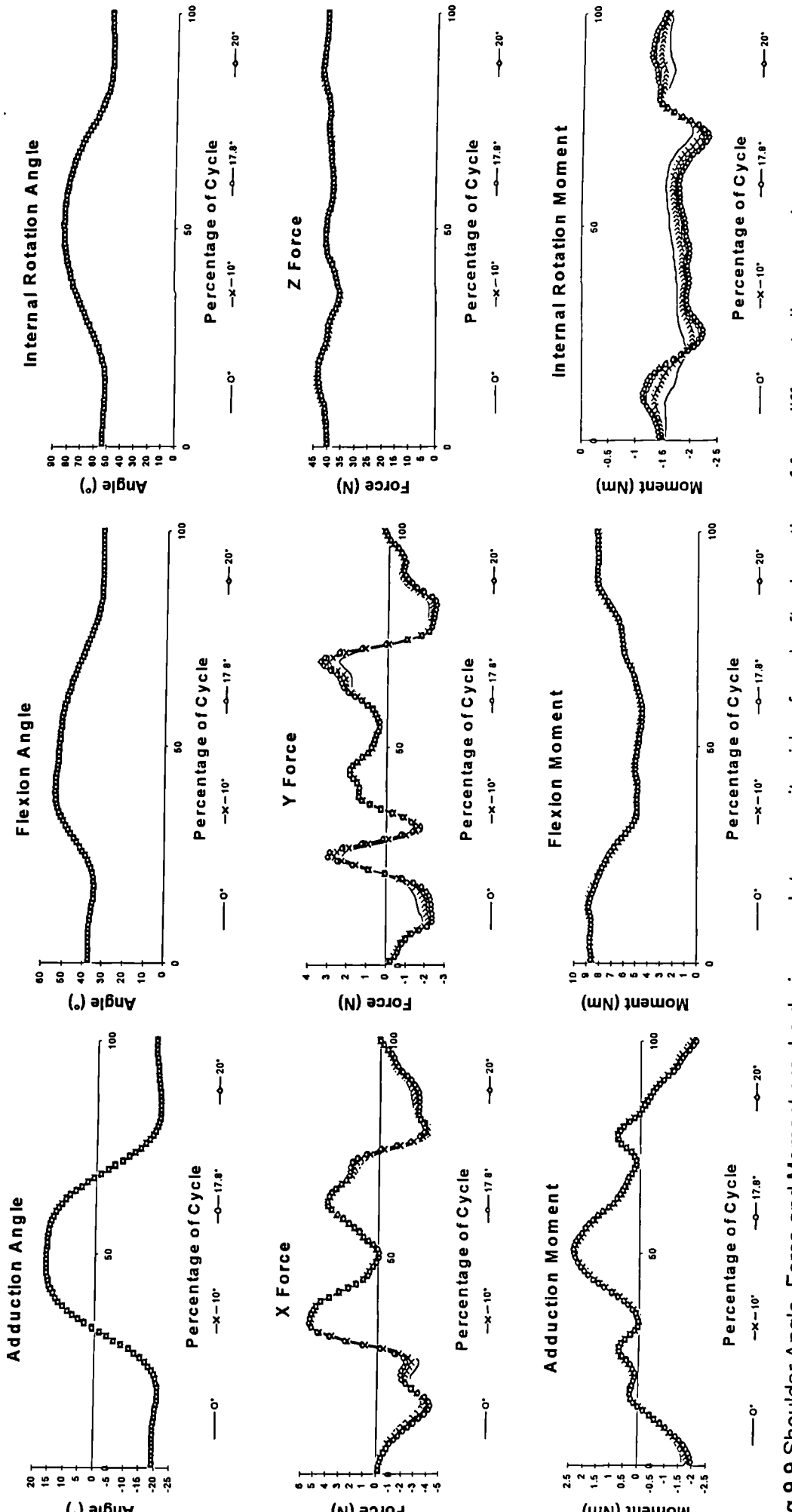

Fig.9.9 Shoulder Angle, Force and Moment graphs during reach to opposite side of neck after insertion of four different elbow carrying angle values.

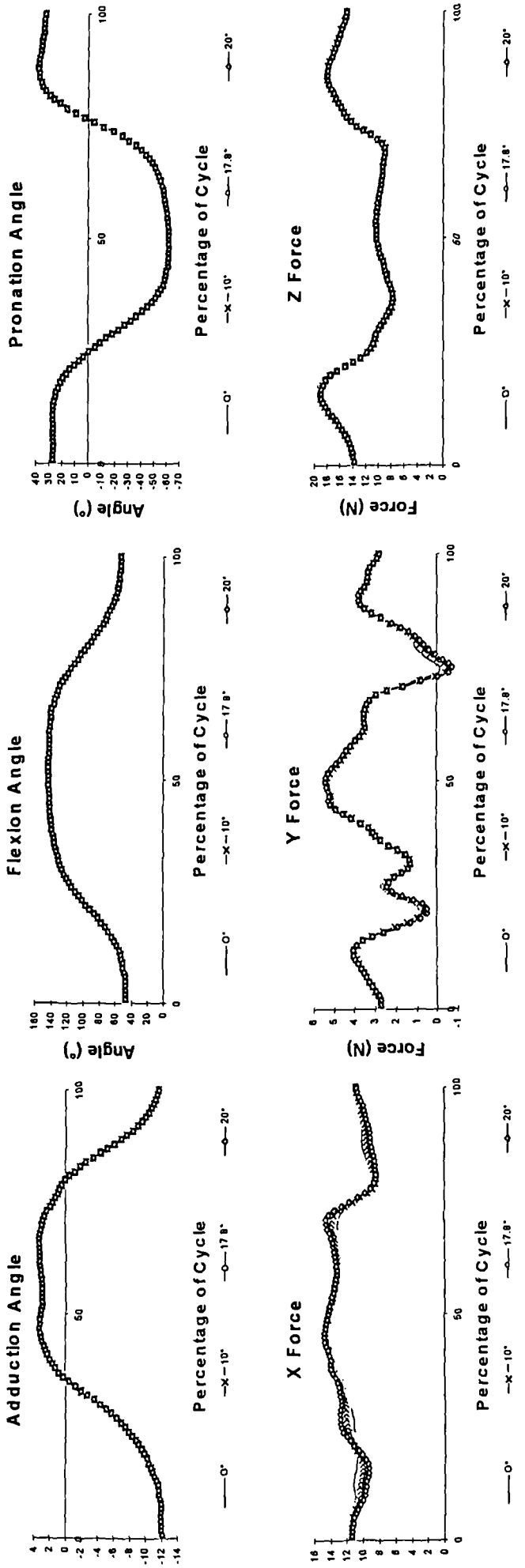

Fig.9.10 Elbow Angle, Force and Moment graphs during reach to opposite side of neck after insertion of four different elbow carrying angle values.

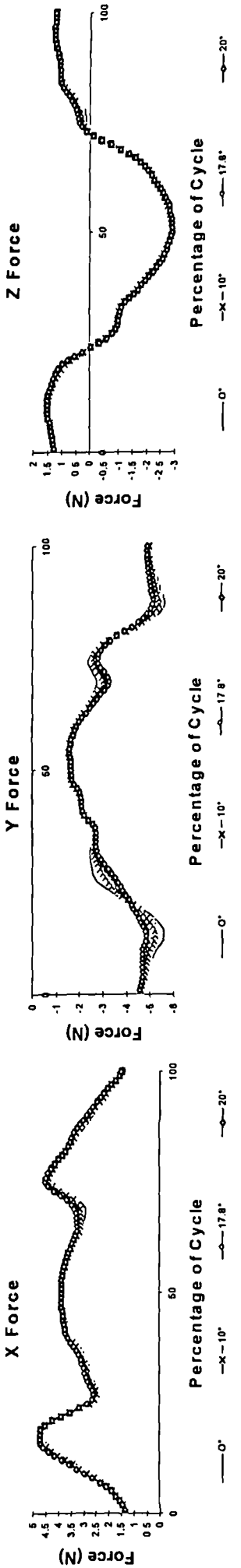

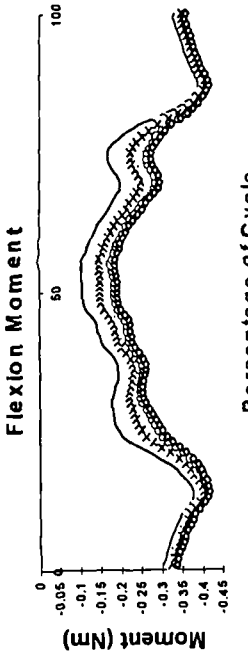

Fig.9.11 Wrist Force and Moment graphs during reach to opposite side of neck after insertion of four different elbow carrying angle values.

9.1.5 Summary of testing of non-rigid-body behaviour of the forearm

The tests discussed in Sections 9.1.1-9.1.4 allowed an insight into the problems introduced during upper limb testing due to the deviation of the forearm from the rigid body assumption.

The first three tests were performed by a single subject only and for the performance of a single activity and thus their significance must not be overstated. The reach to the opposite side of the neck activity had the greatest range of forearm pronation/ supination from all those tested however and thus allowed an idea of 'worst case scenario' to be obtained.

The first and third tests indicate that different initial definitions of the relationship between the embedded technical and anatomical frames, lead to differences in the results obtained, in particular for adduction and flexion at the elbow.

From these same tests it is also clear that variability in the values of adduction and flexion at the elbow are caused by the fitting of the initial marker configuration to a marker pattern subsequently deformed during forearm pronation and supination. This is due to the deformation of the marker pattern from that used to define the relationship between the embedded frames.

It can be seen that the variation in elbow adduction angles apparent during subject testing could easily have been caused by slight differences in the initial forearm pronation between subjects and subsequent differences in the deformation of the marker pattern during performance of the upper limb activities.

The results of the third test indicate that the variation in elbow adduction angles during testing was not due to variation in the position of the forearm selected for the definition of the initial marker configuration for SVD fitting.

The final test indicates that the input of carrying angles with magnitudes similar to those accepted as being true anatomical values has little effect on the principal force and moments measured at the joints of the upper limb during performance of a standard daily task.

It is clear that further work is required on this aspect of upper limb studies, particularly for those that wish to focus on the motion of the elbow and forearm. The inherent problems of trying to model the forearm as a single rigid body when it actually consists of two and trying to track its motion using skin fixed markers make a complete solution to this problem very difficult.

Greater consideration of the locations and patterns of the markers fixed to the forearm and the definitions of embedded frames from these markers is required.

These additional tests have shown that for the current study the adoption of the neutral forearm position for anatomical calibration was the most suitable in terms of minimising the deformation problems, Figs.9.3, 9.4 and 9.8 showing the results for the neutral forearm position to lie somewhere in between those for the extremes of pronation.

CHAPTER 10 : CONCLUSIONS AND FURTHER WORK

10.1 Conclusions

10.1.1 Development and validation of the measurement technique

This thesis has presented the development, validation and application of a technique for the measurement of upper limb kinematics and dynamics during the performance of everyday tasks.

A set of analysis routines were written to enable the calculation of joint angles, angular velocities, angular accelerations, cadences and external forces and moments during the performance of ten activities by twelve subjects.

It has been shown that the attachment of deformable skin fixed marker arrays on the segments of the trunk and upper limb may be used in conjunction with a pointer based anatomical calibration procedure and optimised fitting of the marker configurations in order to obtain upper limb kinematic information during everyday activities.

A novel configuration of markers for the trunk was established, the trunk vertical axis being defined directly through the vertical alignment of markers over the manubrium and xiphoid with the trunk in an upright position.

A novel method for the location of the rotation centre of the glenohumeral joint was established, a normalised vector between the most superior point on the acromioclavicular joint and the glenohumeral rotation centre being defined, based on the cadaver studies of Veeger et al (1997) and Pronk (1991).

10.1.2 Results

The techniques developed for the measurement of upper limb motion and the dynamic modelling of this motion have been shown to be valid, based on the results of rigorous validation studies and favourable comparisons with the results of previous studies. Through testing of both unimpaired and impaired subjects it has been shown that the techniques developed were

sensitive enough to identify deficits in upper limb motion for the impaired subjects.

It can be concluded that the experimental methods and analysis techniques developed and applied are suitable for the investigation of upper limb kinematics and dynamics, for establishing standard patterns of motion and any deviations from these.

From the assessment of the six available JCS sequences in relation to the upper limb, it can be concluded that the selection of the Flexion-Adduction-Rotation JCS axis sequence is the most suitable for the description of shoulder and elbow motion.

Considering the kinematics and dynamics of the upper limb during everyday tasks, the following conclusions may be drawn:

1. Elbow flexion was the major component for successful completion of the selected everyday tasks, with flexion of the shoulder the next most important.
2. During anterior targeted lifting the shoulder abducts and internal rotation occurs to maintain the hand on the targeted path. Supination of the forearm is then required to preserve the upright position of the hand-held object.
3. Subjects with shoulder impairment generally exhibit lower joint angular velocities and accelerations than unimpaired subjects.
4. The degrees of freedom available to the upper limb allow the adoption of varied motion strategies for everyday activities.

10.1.3 General issues

Four cameras were found to be suitable for studies of complex upper limb motion occurring primarily in the anterior workspace, though difficulties occurred where both anterior and posterior views of the subject were required.

Changes in the configuration of the markers attached to the forearm during pronation and supination introduced errors in the results obtained for the angular values at the elbow.

It was also found that the major forces and moments measured at the joints of the upper limb during performance of standard daily tasks were unaffected by the inclusion of anatomically representative carrying angles in the dynamic modelling process.

The phase plane plots of joint angular velocity against joint angle and the plots of angular velocity against angular velocity were found to be useful in determining standard motion patterns for targeted reaching tasks in the anterior workspace and any deviations from these patterns.

10.2 Recommendations for further work

10.2.1 Overcoming marker deformation during forearm rotation

Further work is required into the problem of defining a reliable embedded frame from markers attached on the forearm. It may be that for accurate measurement of forearm motion, a rigid marker array attached to the distal forearm might be more suitable than deformable skin-fixed arrays or that more than one forearm frame should be defined.

Alternatively if these problems cannot be overcome then their characteristics should be found. Schmidt (1998), (1999a) looked at wrist and elbow motion with markers attached to a foam rubber cuff on the forearm. Problems were found at the wrist due to the attached markers not following the pronation/ supination movement. Suggested were the inclusion of 'pure' rotations to correct the rotation axes, remove crosstalk and explicitly establish the skin movement.

Such a procedure could be adopted in order to characterise the deformation of the configuration of markers attached on the proximal and distal forearm. Pure forearm pronation/ supination with a flexed elbow and straight wrist could be measured using a potentiometer or goniometer while simultaneously filming attached markers. The relationship between the

deformed marker pattern and the true rotation angles could then be established and corrections applied.

10.2.2 Further upper limb testing during everyday tasks

A replication of the activity analysis incorporating multiple repetitions from each subject would allow further validation of the results presented here and would further establish the characteristic kinematic and dynamic patterns from both unimpaired and impaired subjects.

Such studies should incorporate additional activities in order to allow the development of a comprehensive database of upper limb kinematic and dynamic information. This may then be used to aid in the differentiation of pathological effects on upper limb kinematics and dynamics from the typical variations which occur within a group of unimpaired subjects.

Testing of both left and right sides of the subjects should be carried out in order to assess the difference between impaired and unimpaired limbs, while also allowing comparison of the movement patterns for the dominant and non-dominant sides. Activities involving the simultaneous use of both upper limbs could be included.

Pre-operative and post-operative studies of impaired upper limb kinematics have previously been performed and similar studies incorporating the dynamics of the upper limb are required. The inclusion of both elderly and younger subjects would allow any differences between these groups to be determined.

10.2.3 Upper limb motion during targeted anterior reaching

Further investigation into the relationship between abduction and internal rotation at the shoulder and the associated supination of the forearm during targeted anterior lifting is necessary. The effect of lifting to varying heights could be investigated as could the lifting of different masses and objects with varying offset positions of centre of mass. The difference in patterns between impaired and unimpaired subjects for such activities also requires further investigation.

10.2.4 Further assessment of data presentation methods

Further investigation of the various permutations for data output is required. Characteristic patterns in the plots of joint angular velocity against joint angular velocity and against joint angle, as obtained for the block raising tasks, may occur for a variety of similar activities. The identification of such characteristic patterns could then be used in the identification of motion strategies and their variations and deviations from these patterns for impaired subjects.

The presentation of dimensionless measurements, commonly utilised during gait studies should be investigated for suitability in upper limb studies. As discussed by Sutherland (1996), Zijlstra et al (1996) and Hof (1996) these dimensionless quantities may be obtained by taking the physical quantity and dividing it by a constant quantity which is a relevant measure of the size of the subject, i.e. body mass or height. The most suitable dimensions for scaling data from upper limb studies should be found as these may differ from those for gait studies.

10.2.5 Utilising the advance in technology

Rhoad et al (1998) describe the use of magnetic resonance imaging in a study of the glenohumeral translations during shoulder internal and external rotation as a series of five static positions. Similarly Nakamura et al (1999) describe the use of magnetic resonance imaging in a study of forearm pronation and supination again as a series of five static positions.

The most accurate solution for the process of anatomically calibrating the relationship between surface fixed markers and underlying anatomical features prior to filming motion studies would seem to involve this technology. Relationships between centres of rotation and surface markers could be accurately specified as could the effects of skin movement and deformation of marker clusters.

The possible incorporation of such technology in the process of upper limb analysis requires to be investigated, particularly if the advancement of

such technology leads to MRI systems with greater internal volume allowing studies of more extensive motion of the upper limb than simply internal and external rotation.

10.3 Concluding Statement

In order to enable the measurement and modelling of upper limb kinematics and dynamics during performance of everyday tasks, a set of experimental methods and analysis techniques were developed. These have allowed patterns of upper limb motion to be determined and variations between unimpaired and impaired subjects to be established.

The data obtained during this study are now being used in the development of a detailed musculoskeletal model which will include both passive and active soft tissues and which will subsequently be used for the prediction of internal joint forces in both static and dynamic activities, further aiding the understanding of upper limb function.

APPENDIX I

References

Abdel-Aziz, Y.I., & Karara, H.M. (1971). Direct Linear Transformation from Comparator Coordinates into Object Space Coordinates. *Proc ASP/UI Symp on Close-range Photogrammetry (Urbana, Ill/USA 1975)*, 1-18.

Alaways, L.W., Hubbard, M., Conlan, T.M., & Miles, J.A. (1996). Static and Dynamic Accuracy Determination of a Three-Dimensional Motion Analysis System. *The Engineering of Sport, Haake(ed.)*, 289-296.

Allum, J.H.J., & Young, L.R. (1976). The Relaxed Oscillation Technique for the Determination of the Moment of Inertia of the Limb Segments. *Journal of Biomechanics, 9,* 21-26.

An, K.N., Browne, A.O., Korinek, S., Tanaka, S., & Morrey, B., F. (1991). Three Dimensional Kinematics of Glenohumeral Elevation. *Journal of Orthopaedic Research*, 9(1), 143-149.

Angeles, J. (1996). On Robustness and Invariance in Motion-Estimation Algorithms. *Proc Fourth International Symposium on 3-D Analysis of Human Movement, June 30th - July 3rd, Grenoble, France.*

Anglin, C., Wyss, U.P., & Pichora, D.R. (1996). Glenohumeral contact forces during five activities of daily living. *The First Conference of the International Shoulder Group, 26 and 27 August 1996, Delft University of Technology, Delft, The Netherlands.*

Arun, K.S., Huang, T.S., & Blostein, S.D. (1987). Least-Squares Fitting of Two 3-D Point Sets. *IEEE Trans Pattern Anal Machine Intell, 9,* 698-700.

Atkeson, C.G., & Hollerbach, J.M. (1985). Kinematic Features of Unrestrained Vertical Arm Movements. *The Journal of Neuroscience, 5,* 2318-2330.

Backhouse, K.M., & Hutchings, R.T. (1998). *Clinical Surface Anatomy.* Mosby-Wolfe.

Bao, H., & Willems, P.Y. (1999). On the Kinematic Modelling and Parameter Estimation of the Human Shoulder. *Journal of Biomechanics, 32,* 943-950.

Barker, T., Burkett, B., Kirtley, C., & Ratanapinunchai, J. (1996). Calculation of Multi-Segment Rigid Body Human Joint Dynamics Using MATLAB™. *Proceedings of the First Australasian Biomechanics Conference, Sydney*, 32-33.

Barker, T.M., Kirtley, C., & Ratanapinunchai, J. (1997). Calculation of Multi-Segment Rigid Body Joint Dynamics Using MATLAB. *Proc Instn Mec Engrs, 211,* 483-487.

Barker, T.M., Nicol, A.C., Kelly, I.G., & Paul, J.P. (1996). Three-dimensional joint co-ordination strategies of the upper limb during functional activities. *Journal of Engineering in Medicine, 210,* 17-26.

Barnett, N.D. (1996) Measurement and Modelling of Three Dimensional Scapulohumeral Kinematics. PhD Thesis, University of Newcastle upon Tyne.

Barnett, N.D., Duncan, R.D.D., & Johnson, G.R. (1999). The Measurement of Three Dimensional Scapulohumeral Kinematics -A Study of Reliability. *Clinical Biomechanics, 14,* 287-290.

Barter, J.T. (1957). Estimation of the Mass of Body Segments. *WADC Technical Report (TR-57-260),* Wright-Patterson Air Force Base, Ohio.

Barth, W., Reinschmidt, C., & Stussi, E. (1998). Comparison of Different Techniques to Determine Orientation, Angular Velocity and Acceleration of a Rigid Body, With Special Consideration of End Point Errors. *Proceedings of the Fourth International Symposium on the 3-D Analysis of Human Movement, July 2nd-5th, Chatanooga, Tennessee, USA*, 58-61.

Beals, R.K. (1976). The Normal Carrying Angle of the Elbow A Radiographic Study of 422 Patients. *Clinical Orthopaedics and Related Research, 119,* 194-196.

Benati, M., Gaglio, S., Morasso, P., Tagliasco, V., & Zaccaria, R. (1980). Anthropomorphic Robots. 1.Representing Mechanical Complexity. *Biological Cybernetics, 38,* 125-140.

Bernstein, N.A. (1947). On The Construction of Movements. *Moscow, Medgiz (In Russian),*

Biryukova, E.V., Frolov, A.A., Mokhtari, M., & Roby-Brami, A. (1996). Reconstruction of Joint Centres and Axes of Rotations from Spatial Tracking System Recordings. *Proceedings of the Fourth international Symposium on 3D Analysis of Human Movement, June 30th-July3rd, Grenoble, France.*

Biryukova, E.V., Frolov, A.A., Mokhtari, M., & Roby-Brami, A. (1998). 3D Reaching Movement Analysis: Kinematics Reconstruction by Using the Spatial Tracking System. *Proceedings of the Fifth international Symposium on 3D Analysis of Human Movement, July 2nd-July5th, Chatanooga, Tennessee, USA,* 26-29.

Bisshopp, K.E. (1969). Rodrigues' Formula and the Screw Matrix. *Journal of Engineering for Industry Transactions of the ASME,* February 1969, 179-185.

Bouisett, S., & Pertuzon, E. (1967). Experimental Determination of the Moment of Inertia of Limb Segments. *Biomechanics I Kargel, Basel,* 106-109.

Braune, W., & Fischer, O. (1889). The Centre of Gravity of the Human Body as Related to the Equipment of the German Infantryman. *Treat of the Math -Phys Class fo the Royal Acad Of Sci of Saxony (In German), 26,* 561-672.

Buckley, M.A., Yardley, A., Johnson, G.R., & Carus, D.A. (1996). Dynamics of the Upper Limb During Performance of the Tasks of Everyday Living - A Review of the Current Knowledge Base. *Proc Instn Mech Engrs, 210,* 241-247.

Busby, H.R., & Trujillo, D.M. (1985). Numerical Experiments With a New Differentiation Filter. *Journal of Biomechanical Engineering, 107,* 293-299.

Cappozzo, A. (1984). Gait Analysis Methodology. *Human Movement Science, 3,* 27-50.

Cappozzo, A. (1991). Three-dimensional Analysis of Human Walking: Experimental Methods and Associated Artifacts. *Human Movement Science, 10,* 589-602.

Cappozzo, A., Cappello, A., Della Croce, U., & Pensalfini, F. (1997). Surface-Marker Cluster Design Criteria for 3-D Bone Movement Reconstruction. *IEEE Transactions on Biomedical Engineering, 44,* 1165-1174.

Cappozzo, A., Catani, F., Della Croce, U., & Leardini, A. (1995). Position and Orientation in Space of Bones During Movement : Anatomical Frame Definition and Determination. *Clinical Biomechanics, 10,* 171-178.

Cappozzo, A., Catani, F., & Leardini, A. (1993). Skin Movement Artefacts in Human Movement Photogrammetry. *Int Soc Biomechanics 14th Congress, Paris 4th-8th July 1993,* 238-239.

Cerveri, P., Borghese, N.A., & Pedotti, A. (1998). Complete Calibration of Stereo Photogrammetric System Through Control Points of Unknown Co-ordinates. *Journal of Biomechanics, 31,* 935-940.

Challis, J.H. (1995b). A Multiphase Calibration Procedure for the Direct Linear Transform. *Journal of Applied Biomechanics, 11,* 351-358.

Challis, J.H., & Kerwin, D.G. (1992). Accuracy Assessment and Control Point Configuration When Using the DLT for Photogrammetry. *Journal of Biomechanics, 25,* 1053-1058.

Chandler, R.F., Clauser, C.E., McConville, J.T., Reynolds, H.M., & Young, J.W. (1975). Investigation of the Inertial Properties of the Human Body. (DOT HS-801-430), Wright-Patterson Air Force Base, Ohio.

Charlton,I.W. (1999). Biomechanical Model of the Elbow. Internal Report (1st Year PhD), Department of Mechanical, Materials and Manufacturing Engineering, University of Newcastle upon Tyne, September 1999.

Chen, L., Armstrong, C.W., & Raftopoulos, D.D. (1994). An Investigation on the Accuracy of Three-dimensional Space Reconstruction Using the Direct Linear Transformation Technique. *J Biomechanics, 27,* 493-500.

Cheng, P.L. (1996) Biomechanical Study of Upper Limb Activities of Daily Living. PhD Thesis, University of Strathclyde, Glasgow, Scotland.

Cheng, P.L., & Pearcy, M. (1999). A Three-dimensional Definition for the Flexion/ Extension and Abduction/ Adduction Angles. *Medical & Biological Engineering & Computing, 37,* 440-444.

Chèze, L., Fregly, B.J., & Dimnet, J. (1995). A Solidification Procedure to Facilitate Kinematic Analyses Based on Video System Data. *J Biomechanics, 28,* 879-884.

Chèze, L., Fregly, B.J., & Dimnet, J. (1998). Determination of Joint Functional Axes from Noisy Marker Data Using the Finite Helical Axis. *Human Movement Science, 17,* 1-15.

Chèze, L., Gutierrez, C., San Marcelino, R., & Dimnet, J. (1996). Biomechanics of the Upper Limb Using Robotic Techniques. *Human Movement Science, 15,* 477-496.

Clarys, J.P., & Marfell-Jones, M.J. (1986a). Anthropometric Prediction of Component Tissue Masses in the Minor Limb Segments of the Human Body. *Human Biology, 58,* 761-769.

Clarys, J.P., & Marfell-Jones, M.J. (1986b). Anatomical Segmentation in Humans and the Prediction of Segmental Masses from Intra-segmental Anthropometry. *Human Biology, 58,* 771-782.

Clauser, C.E., McConville, J.T., & Young, J.W. (1969). Weight, Volume and Centre of Mass of Segments of the Human Body. AMRL Technical Report (TR-69-70), Wright-Patterson Air Force Base, Ohio.

Codman, E.A. (1934). *The Shoulder. Rupture of the Supraspinatus Tendon and other Lesions in or about the Subacromial Bursa.* Boston: Thomas Todd Company.

Cole, G.K., Nigg, B.M., Ronsky, J.L., & Yeadon, M.R. (1993). Application of the Joint Coordinate System to Three-Dimensional Joint Attitude and Movement Representation: A Standardization Proposal. *Journal of Biomechanical Engineering, 115,* 344-349.

Contini, R. (1970). Body Segment Parameters (Pathological). *Tech Rept 1584 03, New York Univ School of Engineering and Science,*

Contini, R. (1972). Body Segment Parameters, Part II. *Artificial Limbs, 16,* 1-19.

Cooper, J.E., Shweddyk, E., Quanbury, A.O., Miller, J., & Hildebrand, D. (1993). Elbow Joint Restriction: Effect on Functional Upper Limb Motion During Performance of Three Feeding Activities. *Arch Phys Med Rehabil, 74,* 805-809.

Corke, P.I. (1995). A Computer Tool for Simulation and Analysis: The Robotics Toolbox for MATLAB. *Proceedings of the 1995 Conference of the Australian Robot Association, Melbourne, Australia, July,* 319-330.

Corke, P.I. (1996). A Robotics Toolbox for MATLAB. *IEEE Robotics & Automation Magazine, 3 (March),* 24-32.

Corradini, M.L., Fioretti, S., & Leo, T. (1993). Numerical Differentiation in Movement Analysis: How to Standardise the Evaluation of Techniques. *Medical & Biological Engineering & Computing, 31,* 187-197.

Craig, J.J. (1989). *Introduction to Robotics, Mechanics and Control.* Addison-Wesley.

Craven, P., & Wahba, G. (1979). Smoothing Noisy Data with Spline Functions, Estimating the Correct Degree of Smoothing by the Method of Generalized Cross-Validation. *Numerical Mathematics, 31,* 377-403.

Crawford, N.R., Yamaguchi, G.T., & Dickman, C.A. (1999). A New Technique for Determining 3-D Joint Angles: The Tilt/Twist Method. *Clinical Biomechanics, 14,* 153-165.

Culham, E., & Peat, M. (1993). Functional Anatomy of the Shoulder Complex. *Journal of Orthop & Sports Physical Therapy, 18,* 342-350.

Dapena, J. (1985). Correction for 'Three-Dimensional Cinematography with Control Object of Unknown Shape'. *Journal of Biomechanics, 18,* 163.

Dapena, J., Harman, E.A., & Miller, J.A. (1982). Three-Dimensional Cinematography with Control Object of unknown Shape. *Journal of Biomechanics, 15,* 11-19.

Davis, J.L., Growney, E.S., Johnson, M.E., Iuliano, B.A., & An, K. (1998). Three-dimensional Kinematics of the Shoulder Complex During Wheelchair Propulsion: A Technical Report. *Journal of Rehabilitation Research and Development, 35,* 61-72.

de Leva, P. (1993). Validity and Accuracy of four Methods for Locating the Center of Mass of Young Male and Female Athletes. *International Society of Biomechanics XIVth Congress, Paris 4-8 July, Abstracts,* 318-319.

de Leva, P. (1996a). Adjustments to Zatsiorsky-Seluyanov Segment Inertia Parameters. *Journal of Biomechanics, 29,* 1223-1230.

de Leva, P. (1996b). Joint Center Longitudinal Positions Computed from a Selected Subset of Chandler's Data. *Journal of Biomechanics, 29,* 1231-1233.

Deland, J.T., Garg, A., & Walker, P.S. (1987). Biomechanical Basis for Elbow Hinge-Distractor Design. *Clinical Orthopaedics and Related Research, 215,* 303-312.

Deluzio, K.J., Wyss, U.P., Zee, B., Costigan, P.A., & Sorbie, C. (1997). Principal Component Models of Knee Kinematics and Kinetics: Normal Vs. Pathological Gait patterns. *Human Movement Science, 16,* 201-217.

Dempster, W.T. (1955). Space Requirements of the Seated Operator. *WADC Technical Report (TR-55-159)* Wright-Patterson Air Force Base, Ohio.

Denavit, J., & Hartenberg, R.S. (1955). A Kinematic Notation for Lower-Pair Mechanisms Based on Matrices. *Journal of Applied Mechanics, 77,* 215-221.

Djupsjobacka, M., Lonn, J., & Olsson, A. (1999). A Method for Calibration of Upper-Limb Kinematic Data from an Electromagnetic Tracker System, and Estimation of Reciever Movement Error. *Proceedings of the International Society of Biomechanics XVIIth Congress, Calgary, Canada, August 8 - 13th,* 218.

Dohrmann, C.R., Busby, H.R., & Trujillo, D.M. (1988). Smoothing Noisy Data Using Dynamic Programming and Generalized Cross-Validation. *ASME Journal of Biomechanical Engineering, 110,* 37-41.

Dol'nikov, Y.I. (1965). Experimental Research on the Movements in the Large Joints of the Arm. *NASA Report N72-33108, Russian Central Scientific Research Institute of Prosthetics and Orthopaedic Appliances.*

Drillis, R., & Contini, R. (1966). Body Segment Mass Properties. *Technical Report No 1166 03 New York University.*

Drillis, R., Contini, R., & Bluestein, M. (1964). Body Segment Parameters: A Survey of Measurement Techniques. *Artificial Limbs, 8:* (1). 44-66.

Elliott, B.C., & Grove, J.R. (1985). A Three-dimensional Cinematographic Analysis of Baseball Pitching Technique. *The Australian Journal of Science and Medicine in Sport*, 8-13.

Engin, A.E., & Chen, S.M. (1986). Statistical Data Base for the Biomechanical Properties of the Human Shoulder Complex. 1.Kinematics of the Shoulder Complex. *J Biomech Engr, 108,* 215-221.

Engin, A.E., Peindl, R.D., Berme, N., & Kaleps, I. (1984). Kinematic and Force Data Collection in Biomechanics by Means of Sonic Emitters - 1:Kinematic Data Collection Methodology. *Journal of Biomechanical Engineering, 106,* 204-211.

Fazel-Rezai, R., Shwedyk, E., Cooper, J.E., Ripat, J., & Onyshko, S. (1998). Changes in Upper Limb Dynamics in Patients with Rheumatoid Arthritis. *11th Conference of the ESB, July 8-11, Toulouse, France*, 15.

Fenn, W.O. (1938). The Mechanics of Muscular Contraction in Man. *J Appl Physics, 9,* 65-177.

Fischer, O. (1906). *Theoretical Fundamentals of the Mechanics of Living Bodies (In German).* Berlin: Teubner.

Forwood, M.R., Neal, R.J., & Wilson, B.D. (1985). Scaling Segmental Moments of Inertia for Individual Subjects. *Journal of Biomechanics, 18,* 755-761.

Gagnon, D., & Gagnon, M. (1992). The Influence of Dynamic Factors on Triaxial Net Muscular Moments at the L5/S1 Joint During Asymmetrical Lifting and Lowering. *Journal of Biomechanics, 25,* 891-901.

Gazzani, F. (1992). Performance of a 7-Parameter DLT Method for the Calibration of Stereophotogrammetric Systems Using 1-D Transducers. *J Biomed Eng, 14,* 476-482.

Gazzani, F. (1993). Comparative Assessment of Two Algorithms for Calibrating Stereophotogrammetric Systems. *J Biomechanics, 26,* 1449-1454.

Gerald, C.F., & Wheatley, P. (1989). *Applied Numerical Analysis.* Reading, Mass. : Addison-Wesley Pub. Co.

Ghosh, S.J. (1979). *Analytical Photogrammetry.* New York: Pergamon Press.

Giakas, G., & Baltzopoulos, V. (1997). A Comparison of Automatic Filtering Techniques Applied to Biomechanical Walking Data. *Journal of Biomechanics, 30,* 847-850.

Golub, G.H., & Van Loan, C.F. (1989). *Matrix Computations.* Baltimore: John Hopkins University Press.

Grood, E.S., & Suntay, W.J. (1983). A Joint Coordinate System for the Clinical Description of Three-Dimensional Motions: Application to the Knee. *Journal of Biomechanical Engineering, 105,* 136-144.

Hanson, R.J., & Norris, M.J. (1981). Analysis of Measurements Based on the Singular Value Decomposition. *SIAM J Sci Stat Comput, 2,* 363-373.

Harless, E. (1860). The Static Moments of Human Limbs. *Treatises of the Math -Phys Class of the Royal Acad Of Sc Of Bavaria, 8,* 257-294.

Hatze, H. (1980). A Mathematical Model for the Computational Determination of Parameter Values of Anthropometric Segments. *Journal of Biomechanics, 13,* 833-843.

Hatze, H. (1988). High Precision Three-dimensional Photogrammetric Calibration and Object Space Reconstruction Using a Modified DLT-Approach. *Journal of Biomechanics, 21,* 533-538.

Hildebrand, F.B. (1974). *Introduction to Numerical Analysis.* New York : McGraw-Hill.

Hinrichs, R.N. (1985). Regression Equations to Predict Segmental Moments of Inertia from Anthropometric Measurements: An Extension of the Data of Chandler et al. (1975). *Journal of Biomechanics, 18,* 621-624.

Hinrichs, R.N. (1990). Adjustments to the Segment Center of Mass Proportions of Clauser et al. (1969). *Journal of Biomechanics, 23,* 949-951.

Hinrichs, R.N., & McLean, S.P. (1995). NLT and Extrapolated DLT : 3-D Cinematography Alternatives for Enlarging the Volume of Calibration. *J Biomechanics, 28,* 1219-1223.

HMSO. (1986). *SI The International System of Units Le système International dunités.* National Physical Laboratory: HMSO.

Hodgson, A.J. (1994). Considerations in Applying Dynamic Programming Filters to the Smoothing of Noisy Data. *ASME Journal of Biomechanical Engineering, 116,* 528-531.

Hof, A.L. (1996). Letter to the Editor : Scaling Gait Data to Body Size. *Gait and Posture, 4,* 222-223.

Hollerbach, J.M. (1980). A Recursive Lagrangian Formulation of Manipulator Dynamics and a Comparative Study of Dynamics Formulation Complexity. *IEEE Trans Syst Man Cybern, SMC-10,* 730-736.

Hollerbach, K., & Hollister, A.M. (1995). Mathematical Analysis of Errors Inherent in the Use of Euler Angles in Measuring Joint Motion. *ISB Congress 1995, Book of Abstracts,* 396-397.

Hollinshead, W.H. (1991). *Functional Anatomy of the Limbs and Back.* Philadelphia: W.B.Saunders Company.

Iannotti, J.P., Gabriel, J.P., Schneck, S.L., Evans, B.G., & Misra, S. (1992). The Normal Glenohumeral Relationships. *The Journal of Bone and Joint Surgery, 74-A,* 491-500.

Inman, V.T., Ralston, H.J., & Todd, F. (1981). *Human Walking.* Baltimore: Williams & Wilkins.

Inman, V.T., Saunders, J.B.d.M., & Abbott, L.C. (1944). Observations on the Function of the Shoulder Joint. *The Journal of Bone and Joint Surgery, 26,* 1-30.

Jackson, J.E. (1991). *A User's Guide to Principal Components.* New York: John Wiley & Sons.

Johnson, G.R. (1990). A Study of the Muscles of the Shoulder Complex with Particular Emphasis on the Mechanism of the Shoulder Girdle. Internal report, Department of Mechanical, Materials and Manufacturing Engineering, University of Newcastle upon Tyne.

Jones, D.W. (1970). The Role of Shoulder Muscles in the Control of Humeral Position (an electromyographic study). Master's Thesis. Case Western Reserve University.

Kadaba, M.P., Ramakrishnan, H.K., Wootten, M.E., Gorton, G., & Cochran, G.V.B. (1989). Repeatability of Kinematic, Kinetic and Electromyographic Data in Normal Adult Gait. *Journal of Orthopaedic Research, 7,* 849-860.

Kanatani-Fujimoto, K., Lazareva, B.V., & Zatsiorsky, V.M. (1997). Local Proportional Scaling of Time-Series Data : Method and Applications. *Motor Control, 1,* 20-43.

Kane, T.R., & Levinson, D.A. (1983). The Use of Kane's Dynamical Equations in Robotics. *International Journal of Robotics Research, 2,* 3-21.

Kane, T.R., Likins, P.W., & Levinson, D.A. (1983). *Spacecraft Dynamics.* New York: McGraw-Hill.

Kapandji, I.A. (1999). *The Shoulder.* W.B.Saunders Company Limited.

Karlsson, D., & Peterson, B. (1992). Towards a Model for Force Predictions in the Human Shoulder. *Journal of Biomechanics, 25,* 189-199.

Keogh, B., & Ebbs, S. (1984). *Normal Surface Anatomy.* London: William Heinemann Medical Books.

Khoo, B.C.C., Goh, J.C.H., & Bose, K. (1995). A Biomechanical Model to Determine Lumbosacral Loads During Single Stance Phase in Normal Gait. *Med Eng Phys, 17,* 27-35.

Kreysig, E. (1983). *Advanced Engineering Mathematics.* New York : John Wiley & Sons.

Kromodihardjo, S., & Mital, A. (1987). Biomechanical Analysis of Manual Lifting Tasks. *Journal of Biomechanical Engineering, 109,* 132-138.

Lanczos, V. (1967). *Applied Analysis.* London: Pitman.

Langrana, N.A. (1981). Spatial Kinematic Analysis of the Upper Extremity Using a Biplanar Videotaping Method. *Journal of Biomechanical Engineering, 103,* 11-17.

Larivière, C., & Gagnon, D. (1999). The Influence of Trunk Modelling in 3D Biomechanical Analysis of Simple and Complex Lifting Tasks. *Clinical Biomechanics, 14,* 449-461.

Laursen, B., Jensen, B.R., Nemeth, G., & Sjogaard, G. (1998). A Model Predicting Individual Shoulder Muscle Forces Based on Relationships Between Electromyographic and 3D External Forces in Static Position. *Journal of Biomechanics, 31,* 731-739.

Lawson, C.L., & Hanson, R.J. (1974). *Solving Least Squares Problems.* Englewood Cliffs, N.J. Prentice-Hall.

Lenhoff, M.W., Santner, T.J., Otis, J.C., Peterson, M.G.E., Williams, B.J., & Backus, S.I. (1999). Bootstrap Prediction and Confidence Bands: A Superior Statistical Method for Analysis of Gait Data. *Gait and Posture, 9,* 10-17.

Likins, P.W. (1973). *Elements of Engineering Mechanics.* New York: McGraw-Hill.

Luh, J.Y.S., Walker, M.W., & Paul, R.C.P. (1980). On-Line Computational Scheme for Mechanical Manipulators. *Journal of Dynamic Systems, Measurement, and Control, 102,* 69-76.

Mann, R.W., & Antonsson, E.K. (1983). Gait Analysis - Precise, Rapid, Automatic, 3-D Position and Orientation Kinematics and Dynamics. *Bulletin of the Hospital for Joint Diseases Orthopaedic Institute, 43,* 137-146.

Marion, J.B. (1979). *General Physica With Bioscience Essays.* New York: John Wiley & Sons.

Martini, F.H. (1995). *Fundamentals of Anatomy and Physiology.* New Jersey: Prentice Hall.

McConville, J.T., Clauser, C.E., Churchill, T.D., Cuzzi, J., & Kaleps, I. (1980). Anthropometric Relationships of Body and Body Segment Moments of Inertia. AMRL TR-80-119, Wright-Patterson Air Force Base, Ohio.

McCullagh, P.J.J. (1995). Biomechanics and Design of Shoulder Arthroplasty. *Journal of Engineering in Medicine, 209,* 207-213.

McWilliam, R.P.J.G. (1970). A List of Everyday Tasks for Use in Prosthesis Design and Development. *Bulletin of Prosthetic Research, 10,* 135-164.

Meskers, C.G.M., Van Der Helm, F.C.T., Rozendaal, L.A., & Rozing, P.M. (1998). In Vivo Estimation of the Glenohumeral Joint Rotation Center from Scapular Bony Landmarks by Linear Regression. *Journal of Biomechanics, 31,* 93-96.

Meskers, C.G.M., Vermeulen, H.M., de Groot, J.H., van Der Helm, F.C.T., & Rozing, P.M. (1998). 3D Shoulder Position Measurements Using a Six-degree-of-freedom Electromagnetic Tracking Device. *Clinical Biomechanics, 13,* 280-292.

Meskers, C.G.M., Fraterman, H., Van Der Helm, F.C.T., Vermeulen, H.M., & Rozing, P.M. (1999). Calibration of the "Flock of Birds" Electromagnetic Tracking Device and its Application in Shoulder Motion Studies. *Journal of Biomechanics, 32,* 629-633.

Moore, K.L., & Agur, A.M.R. (1996). *Essential Clinical Anatomy.* Baltimore: William & Wilkins.

Morrey, B.F., Askew, L.J., An, K.N., & Chao, E.Y. (1981). A Biomechanical Study of Normal Functional Elbow Motion. *The Journal of Bone and Joint Surgery, 63-A,* 872-877.

Morrey, B.F., & Chao, E.Y.S. (1976). Passive Motion of the Elbow Joint A Biomechanical Analysis. *The Journal of Bone and Joint Surgery, 58-A,* 501-508.

Nakamura, T., Yabe, Y., Horiuchi, Y., & Yamazaki, N. (1999). In Vivo Motion Analysis of forearm Rotation Utilizing Magnetic Resonance Imaging. *Clinical Biomechanics, 14,* 315-320.

Nicol, A.C. (1977) Elbow Joint Prosthesis Design: Biomechanical Aspects. PhD Thesis, Strathclyde University, Glasgow, Scotland.

Nigg, B.M. (1995). Inertial Properties of the Human or Animal Body. In B.M. Nigg & W. Herzog (Eds.), *Biomechanics of the Musculo-Skeletal System.* (pp. 337-364). Chichester, England: John Wiley & Sons Ltd.

Nigg, B.M., & Herzog, W. (1995). *Biomechanics of the Musculo-Skeletal System.* Chichester, England: John Wiley & Sons Ltd.

Olshen, R.A., Biden, E.N., Wyatt, M.P., & Sutherland, D.H. (1989). Gait Analysis and the Bootstrap. *The Annals of Statistics, 17,* 1419-1440.

Packer, T.L., Peat, M., Wyss, U., & Sorbie, C. (1990). Examining the Elbow During Functional Activities. *The Occupational Therapy Journal of Research, 10,* 323-333.

Palastanga, N., Field, D., & Soames, R. (1994). *Anatomy and Human Movement. Structure and Function.* Oxford: Butterworth Heinemann.

Pandyan, A.D., Price, C.I.M., Barnes, M.I.P. & Johnson, G.R. (1999). Assessing resistance to passive movement: Are repeated measures necessary? *European Journal of Neurology, 6,* 66.

Payton, C.J., & Bartlett, R.M. (1995). Estimating Propulsive Forces in Swimming from Three-dimensional Kinematic Data. *Journal of Sports Sciences, 13,* 447-454.

Pearl, M.L., Harris, S.L., Lippitt, S.B., Sidles, J.A., Harryman, D.T., & Matsen, F.A. (1992). A System for Describing Positions of the Humerus Relative to the Thorax and its use in the Presentation of Several Functionally Important Arm Positions. *J Shoulder Elbow Surg, 1,* 113-118.

Pearsall, D.J., & Reid, J.G. (1994). The Study of Human Body Segment Parameters in Biomechanics An Historical Review and Current Status Report. *Sports Medicine, 18,* 126-140.

Peterson, B., & Palmerud, G. (1996). Measurement of Upper Extremity Orientation by Video Stereometry System. *Medical & Biological Engineering & Computing,* 34(2), 149-154.

Peyton, A.J. (1986). Determination of the Moment of inertia of Limb Segments by a Simple Method. *Journal of Biomechanics, 19,* 405-410.

Pheasant, S.T. (1986). *Bodyspace : Anthropometry, Ergonomics and Design.* London and Philadelphia: Taylor & Francis.

Politti, J.C., Goroso, G., Valentinuzzi, M.E., & Bravo, O. (1998). Codman's Paradox of the Arm Rotations is Not a Paradox: Mathematical Validation. *Medical Engineering & Physics, 20,* 257-260.

Poppen, N.K., & Walker, P.S. (1976). Normal and Abnormal Motion of the Shoulder. *Journal of Bone and Joint Surgery, 58-A,* 195-201.

Poppen, N.K., & Walker, P.S. (1978). Forces at the Glenohumeral Joint in Abduction. *Clinical Orthopaedics and Related Research, 135,* 165-170.

Pronk, G.M. (1991) The Shoulder Girdle. PhD Thesis, Faculty of Mechanical Engineering and Marine Technology, Delft University of Technology, Delft.

Pronk, G.M., & Van Der Helm, F.C.T. (1991). The Palpator: an Instrument for Measuring the Position of Bones in Three Dimensions. *Journal of Medical Engineering & Technology, 15,* 15-20.

Ramakrishnan, H.K., & Kadaba, M.P. (1991). On the Estimation of Joint Kinematics During Gait. *Journal of Biomechanics, 24,* 969-977.

Ramey, M.R., & Yang, A.T. (1981). A Simulation Procedure for Human Motion Studies. *Journal of Biomechanics, 14,* 203-213.

Rao, S.S., Bontrager, E.L., Gronley, J.K., Newsam, C.J., & Perry, J. (1996). Three-Dimensional Kinematics of Wheelchair Propulsion. *IEEE Transactions on Rehabilitation Engineering, 4,* 152-160.

Reinschmidt, C., & Van den Bogert, T. (1997). KineMat: A MATLAB Toolbox for Three-Dimensional Kinematic Analyses, Human Performance Laboratory, The University of Calgary. *http://isb ri ccf org/software/kinemat/*

Reynolds, H.M. (1978). The Inertial Properties of the Body and its Segments. *In NASA (1978), op cit , Vol I, Chapter IV.*

Reynolds, H.M., Clauser, C.E., McConville, J.T., Chandler, R.F., & Young, J.W. (1975). Mass Distribution Properties of the Male Cadaver. Automotive Engineering Congress and Exposition, Detroit, Michigan, February 24-28. SAE 750424.

Rhoad, R.C., Klimkiewicz, J.J., Williams, G.R., Kesmodel, S.B., Udupa, J.K., Kneeland, J.B., & Iannotti, J.P. (1998). A New In Vivo Technique for Three-dimensional Shoulder Kinematics Analysis. *Skeletal Radiology, 27,* 92-97.

Richards, J.G. (1998). The Measurement of Human Motion: A Comparison of Commercially Available Systems. *Proceedings of the Fifth International Symposium on the 3D Analysis of Human Movement, Chattanooga, Tennessee, July, 2nd - 5th,* 1-9.

Roberson, R.E., & Schwertassek, R. (1988). *Dynamics of Multibody Systems.* Berlin: Springer-Verlag.

Romilly, D.P., Anglin, C., Gosine, R.G., Hershler, C., & Raschke, S.U. (1994). A Functional Task Analysis and Simulation for the Development of a Powered Upper Limb-limb Orthosis. *IEEE Transactions on Rehabilitation Engineering, 2,* 119-128.

Runciman, R.J. (1993) Biomechanical model of the shoulder joint. PhD Thesis, University of Strathclyde, Glasgow, Scotland.

Runciman, R.J., & Nicol, A.C. (1994). Modelling Muscle and Joint forces at the Glenohumeral Joint: Overview of a Current Study. *Journal of Engineering in Medicine, 208,* 97-102.

Sadeghi, H., Allard, P., Shafie, K., & Duhaime, M. (1998). Muscle Power Curve Registration in Able-Bodied Gait Pattern. *Proc Fifth International Symposium on the 3-D Analysis of Human Movement, July 2nd - 5th, Chattanooga, USA,* 81-84.

Safaee-Rad, R., Shedyk, E., & Quanbury, A.O. (1990). Three-Dimensional Measurement System for Functional Arm Motion Studies. *Med & Biol Eng & Comput, 28,* 569-573.

Safaee-Rad, R., Shedyk, E., Quanbury, A.O., & Cooper, J.E. (1990). Normal Functional Range of Motion of Upper Limb Joints During Performance of Three Feeding Activities. *Arch Phys Med Rehabil, 71,* 505-509.

Samuelson, B., Wangenheim, M., & Wos, H. (1987). A Device for Three-Dimensional Registration of Human Movement. *Ergonomics, 30,* 1655-1670.

Schmid, O.A., & Beb, R. (1998). Preliminary Results Using a New Calibration Method for Biomechanical Studies. *Proc Fourth International Symposium on the 3-D Analysis of Human Movement, July 2nd - 5th, Chattanooga, USA*, 14-17.

Schmidt, R., Disselhorst-Klug, C., Silny, J., & Rau, G. (1998). A measurement Procedure for the Quantitative Analysis of Free Upper-Extremity Movements. *Proc Fifth International Symposium on the 3-D Analysis of Human Movement, July 2nd - 5th, Chattanooga, USA*, 47-50.

Schmidt, R., Disselhorst-Klug, C., Silny, J., & Rau, G. (1999). A Marker-Based Measurement Procedure for Unconstrained Wrist and Elbow Motions. *Journal of Biomechanics, 32,* 615-621.

Schmidt, R., Miltner, O., Disselhorst-Klug, C., Rau, G., & Niethard, F.U. (1999). Monitoring of Shoulder Rehabilitation by 3-D Motion Analysis. *Proceedings of the International Society of Biomechanics XVIIth Congress, Calgary, Canada, August 8 - 13th*, 849.

Scholz, J.P. (1989). Reliability and Validity of the WATSMART^{TM} Three-Dimensional Optoelectronic Motion Analysis System. *Physical Therapy, 69,* 679-689.

Scholz, J.P., & Millford, J.P. (1993). Accuracy and Precision of the PEAK Performance Technologies Motion Measurement System. *Journal of Motor Behaviour, 25,* 2-7.

Sears, F.W., Zemansky, M.W., & Young, H.D. (1987). *University Physics.* USA: Addison-Wesley.

Söderkvist, I., & Wedin, P. (1993). Determining the Movements of the Skeleton Using Well-configured Markers. *J Biomechanics, 26,* 1473-1477.

Spoor, C.W., & Veldpaus, F.E. (1980). Rigid Body Motion Calculated from Spatial Co-ordinates of Markers. *Journal of Biomechanics, 13,* 391-393.

Sprigings, E., Marshall, R., Elliott, B., & Jennings, L. (1994). A Three-dimensional Kinematic Method for Determining the Effectiveness of Arm Segment Rotations in Producing Racquet-head Speed. *J Biomechanics, 27,* 245-254.

Suntay, W.J., Grood, E.S., Noyes, F.R., & Butler, D.L. (1978). A Coordinate System for Describing Joint Position. *Advances in Bioengineering*, 59-62.

Sutherland, D.H. (1996). Editorial: Dimensionless Gait Measurements and Gait Maturity. *Gait and Posture, 4,* 209-211.

Thornton, M.J., Morrissey, M.C., & Coutts, F.J. (1998). Some Effects of Camera Placement on the Accuracy of the Kinemetrix Three-Dimensional Motion Analysis System. *Clinical Biomechanics, 13,* 452-454.

Tsai, R.Y. (1986). An Efficient and Accurate Camera Calibration Technique for 3D Machine Vision. *Proceedings Computer Vision and Pattern Recognition, IEEE, Miami Beach*, 364-374.

Turner-Stokes, L., & Reid, K. (1999). Three-Dimensional Motion Analysis of Upper Limb Movement in the Bowing Arm of String-Playing Musicians. *Clinical Biomechanics, 14,* 426-433.

Van Der Helm, F.C.T. (1994). Analysis of the Kinematic and Dynamic Behaviour of the Shoulder Mechanism. *J Biomechanics, 27,* 527-550.

Van Der Helm, F.C.T. (1997a). A standardized protocol for motion recordings of the shoulder. In H.E.J. Veeger, F.C.T. Van der Helm, & P.M. Rozing (Eds.), *Proc. 1st Conf. Int. Shoulder Group.* (pp. 7-12). Maastricht: Shaker Publishers.

Van Der Helm, F.C.T. (1997b). A standardized protocol for motion recordings of the shoulder: Standardization of Joint Rotations, New Recommendations.
http://www.fbw.vu.nl/research/Lijn_A4/shoulder/isg/proposal/protocol.html

Van Der Helm, F.C.T., & Dapena, J. (1993). Standardisation of Joint Rotations, Proposal to ISB.
http://www-mr wbmt tudelft nl/schouder/dsg/standardization.html

Van Der Helm, F.C.T., & Pronk, G.M. (1995). Three-Dimensional recording and Description of Motions of the Shoulder Mechanism. *Journal of Biomechanical Engineering, 117,* 27-40.

Van Der Helm, F.C.T., Pronk, G.M., Veeger, H.E.J., & van der Woude, L.H.V. (1989). The Rotation Centre of the Glenohumeral Joint. *XII International Congress of Biomechanics*, Los Angeles, USA, 676-677.

Van Der Helm, F.C.T., Veeger, H.E.J., Pronk, G.M., van der Woude, L.V.H., & Rozendal, R.H. (1992). Geometry Parameters for Musculoskeletal Modelling of the Shoulder System. *J Biomechanics, 25,* 129-144.

Van Der Helm, F.C.T., & Veenbaas, R. (1991). Modelling the Mechanical Effect of Muscles With Large Attachment Sites : Application to the Shoulder Mechanism. *J Biomechanics, 24,* 1151-1163.

Veeger, H.E.G., Yu, B., An, K., & Rozendal, R.H. (1997). Parameters for Modeling the Upper Extremity. *Journal of Biomechanics, 30,* 647-652.

Veeger, H.E.J., Van Der Helm, F.C.T., van der Woude, L.H.V., Pronk, G.M., & Rozendal, R.H. (1991). Inertia and Muscle Contraction Parameters for Musculoskeletal Modelling of the Shoulder Mechanism. *Journal of Biomechanics, 24,* 615-629.

Veldpaus, F.E., Woltring, H.J., & Dortmans, L.J.M.G. (1988). A Least-squares Algorithm for the Equiform Transformation from Spatial Marker Co-ordinates. *Journal of Biomechanics, 21,* 45-54.

Walker, M.W., & Orin, D.E. (1982). Efficient Dynamic Computer Simulation of Robotic Mechanisms. *Journal of Dynamic Systems, Measurement, and Control, 104,* 205-211.

Wang, K., & Gasser, T. (1997). Alignment of Curves by Dynamic Time Warping. *The Annals of Statistics, 25,* 1251-1276.

Wang, L., Wu, H., Chang, Y., & Su, F. (1996). Three-Dimensional Kinematic Analysis of Upper Extremity in the Soft-tennis Forehand Drive. *The Engineering of Sport, Haake(ed.),* Rotterdam: Balkema 141-146.

Wang, X.G. (1996). Construction of Arm Kinematic Linkage from External Surface Markers. *Proceedings of the Fourth international Symposium on 3D Analysis of Human Movement, June 30th-July3rd, Grenoble, France.*

Wang, X.G., Maurin, M., Mazet, F., Maia, N.D.C., Voinot, K., Verriest, J.P., & Fayet, M. (1998). Three-dimensional Modelling of the Motion Range of Axial Rotation of the Upper Arm. *Journal of Biomechanics, 31,* 899-908.

Whiting, W.C., Gregor, R.J., & Finerman, G.A. (1988). Kinematic Analysis of Human Upper Extremity Movements in Boxing. *The American Journal of Sports Medicine, 16,* 130-136.

Williams, J.R. (1996) Some Aspects of the Biomechanics of the Elbow Joint: Related to prosthetic Design. D.M. Thesis, University of Oxford.

Williams, J.R., Leardini, A., & Catani, F. (1996). The Study of Upper Limb Kinematics Using a "Technical Array" Marker Set, "Anatomical Calibration" and "Technical and Anatomical Axes". *Proc: Spring Meeting of the British Orthopaedic Research Society, Oswestry, March.*

Williams, R.J., & Seireg, A. (1979). Interactive Modeling and Analysis of Open or Closed Loop Dynamic Systems with Redundant Actuators. *ASME Journal of Mechanical Design, 101,* 407-416.

Winter, D.A. (1990). *Biomechanics and Motor Control of Human Movement.* New York: John Wiley & Sons.

Woltring, H.J. (1986). A Fortran Package for Generalized, Cross-validatory Spline Smoothing and Differentiation. *Advances in Engineering Software, 8,* 104-113.

Woltring, H.J. (1991). Representation and Calculation of 3-D Joint Movement. *Human Movement Science, 10,* 603-616.

Woltring, H.J. (1994). 3-D Attitude Representation of Human Joints : A Standardisation Procedure. *Journal of Biomechanics, 27,* 1399-1414.

Woltring, H.J., Huiskes, R., de Lange, A., & Veldpaus, F.E. (1985). Finite Centroid and Helical Axis Estimation from Noisy Landmark Measurements in the Study of Human Joint Kinematics. *Journal of Biomechanics, 18,* 379-389.

Wood, G.A., & Marshall, R.N. (1986). The Accuracy of the DLT Extrapolation in Three-dimensional Film Analysis. *Journal of Biomechanics, 19,* 781-785.

Worden, K. (1990). Data Processing and Experiment Design for the Restoring Force Surface Method, Part I: Integration and Differentiation of Measured Time Data. *Mechanical Systems and Signal Processing, 4,* 295-319.

Yakowitz, S., & Szidarovsky, F. (1989). *An Introduction to Numerical Computations.* New York : Macmillan.

Yeadon, M.R., & Morlock, M. (1989). The Appropriate Use of Regression Equations for the Estimation of Segmental Inertia Parameters. *Journal of Biomechanics, 22,* 683-689.

Yu, B., Koh, T.J., & Hay, J.G. (1993). A Panning DLT Procedure for Three-dimensional Videography. *Journal of Biomechanics, 26,* 741-751.

Zatsiorsky, V., & Seluyanov, V. (1983). The Mass and Inertia Characteristics of the Main Segments of the Human Body. *Biomechanics VIII-B 8th Intl Congress, VIII,* 1152-1159.

Zatsiorsky, V., & Seluyanov, V. (1985). Estimation of the Mass and Inertia Characteristics of the Human Body by Means of the Best Predictive Regression Equations. *Biomechanics IX-B 9th Intl Congress, IX,* 233-239.

Zatsiorsky, V.M., Seluyanov, V.N., & Chugunova, L.G. (1990). Methods of Determining Mass-Inertial Characteristics of Human Body Segments. In G.G. Chernyi & S.A. Regirer (Eds.), *Contemporary Problems of Biomechanics.* (pp. 272-291). Massachusetts: CRC Press.

Zijlstra, W., Prokop, T., & Berger, W. (1996). Adaptability of Leg Movements During Normal Treadmill Walking and Split-belt Walking in Children. *Gait and Posture, 4,* 212-221.

APPENDIX II

Results for Activities 2 - 10

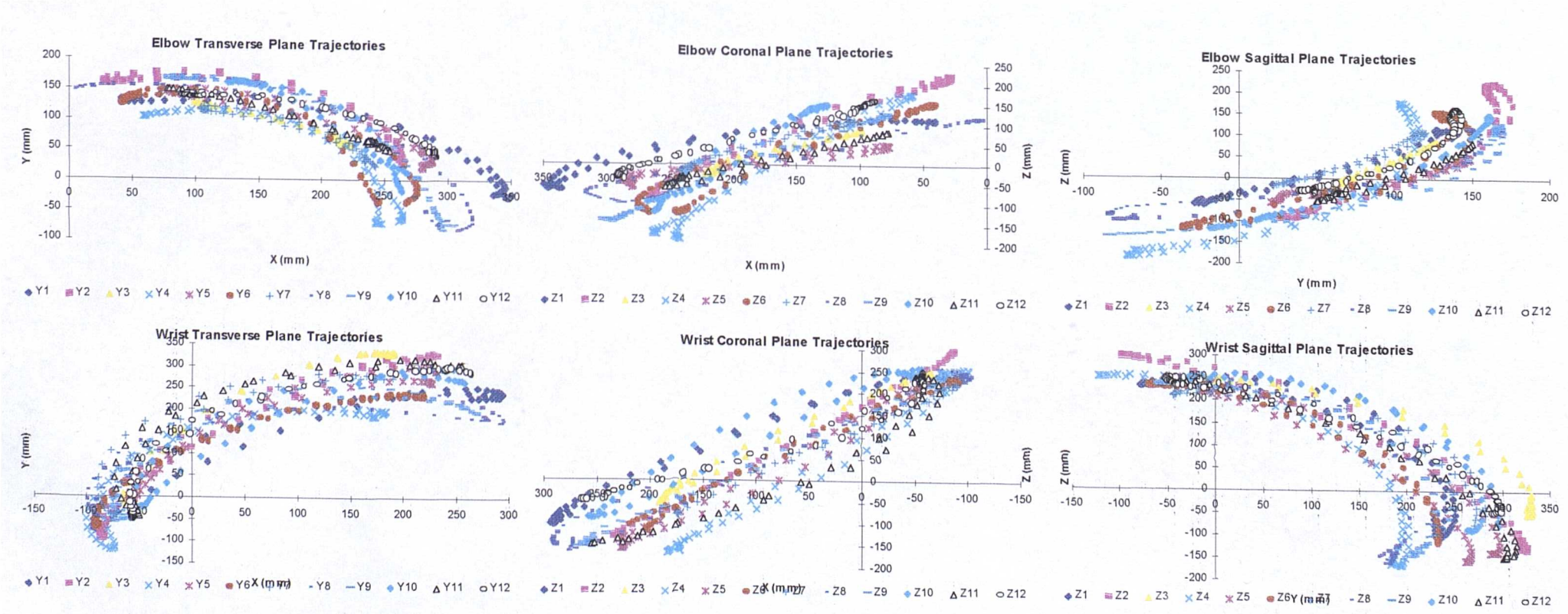

Fig.A.8.10 Trajectories of Elbow and Wrist in the Trunk Frame during performance of Activity 2.

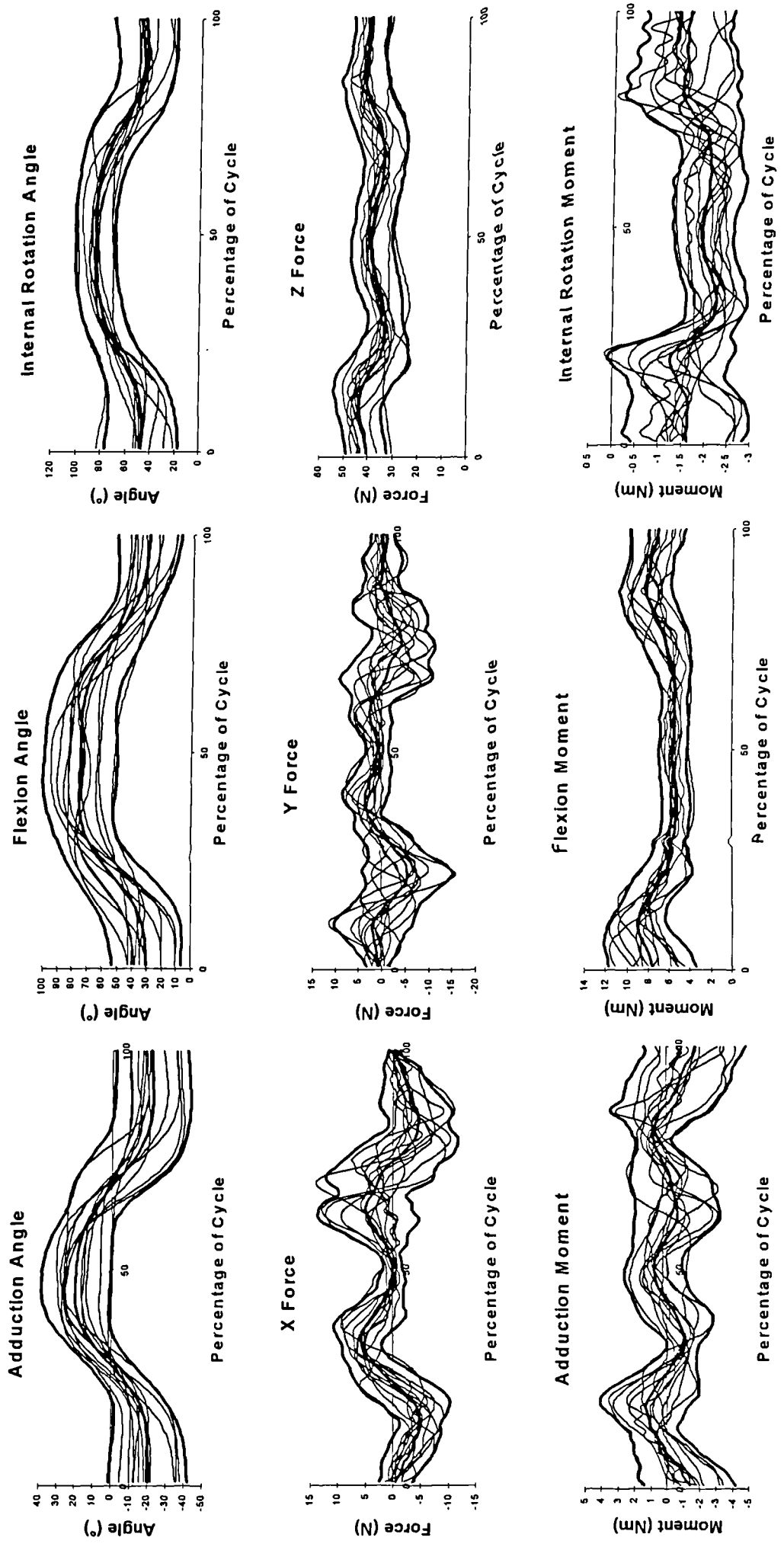

Fig.A.8.11 Angle, Force and Moment graphs for the Shoulder during Performance of Activity 2, showing mean +/- 2SD in bold.

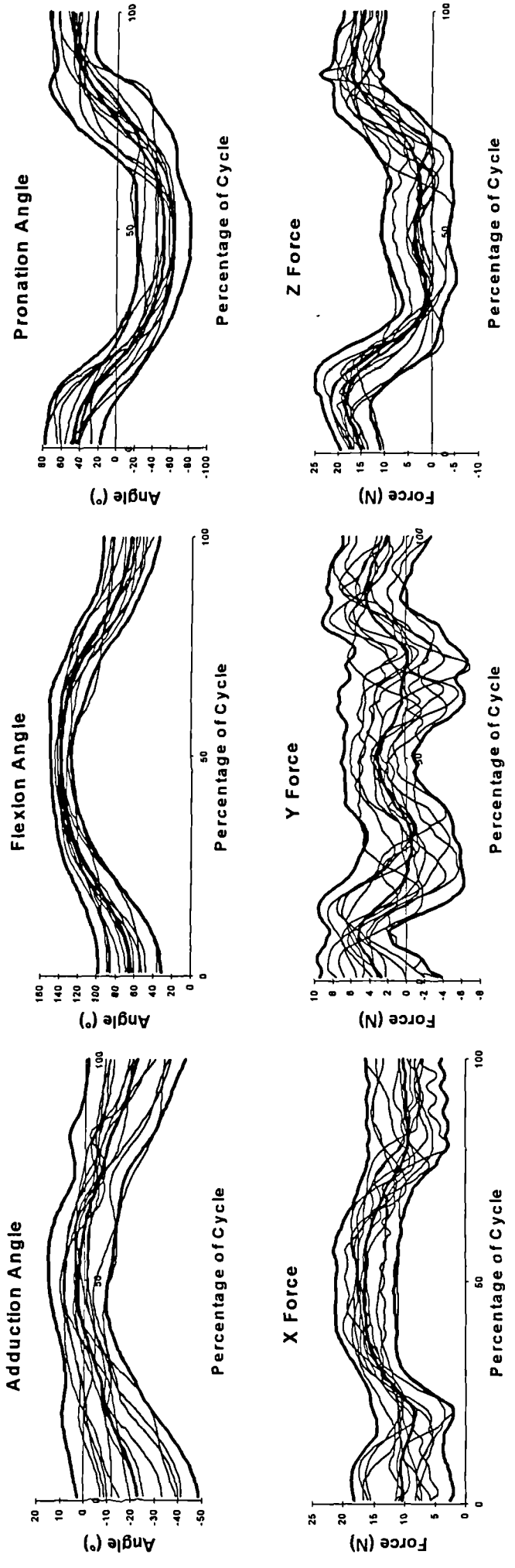

Fig.A.8.12 Angle, Force and Moment graphs for the Elbow during performance of Activity 2, showing mean +/- 2SD in bold.

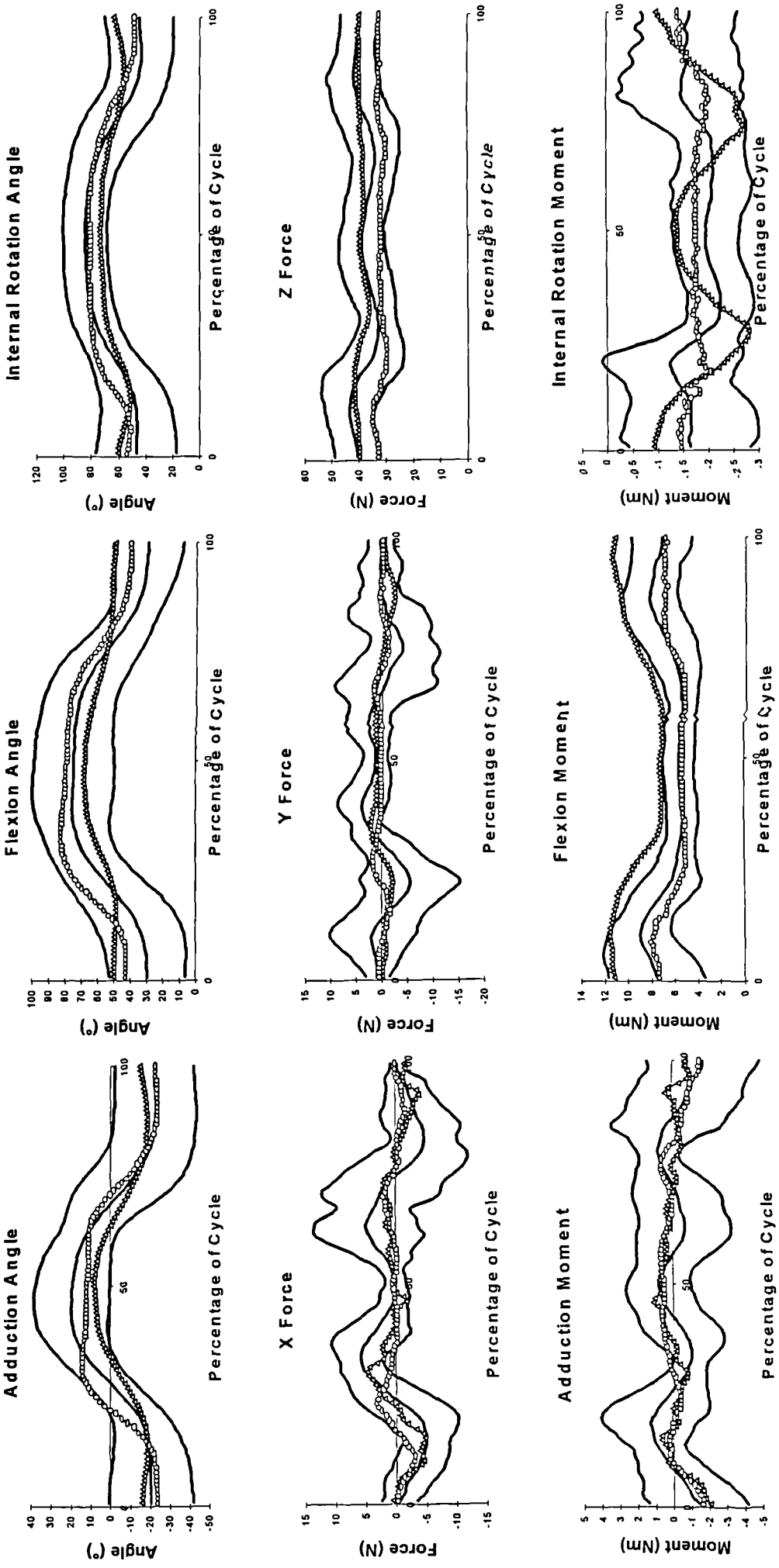

Fig.A.8.13 Comparison of impaired with unimpaired graphs for the Shoulder during performance of Activity 2. (Δ - Subject 11, o - Subject 12)

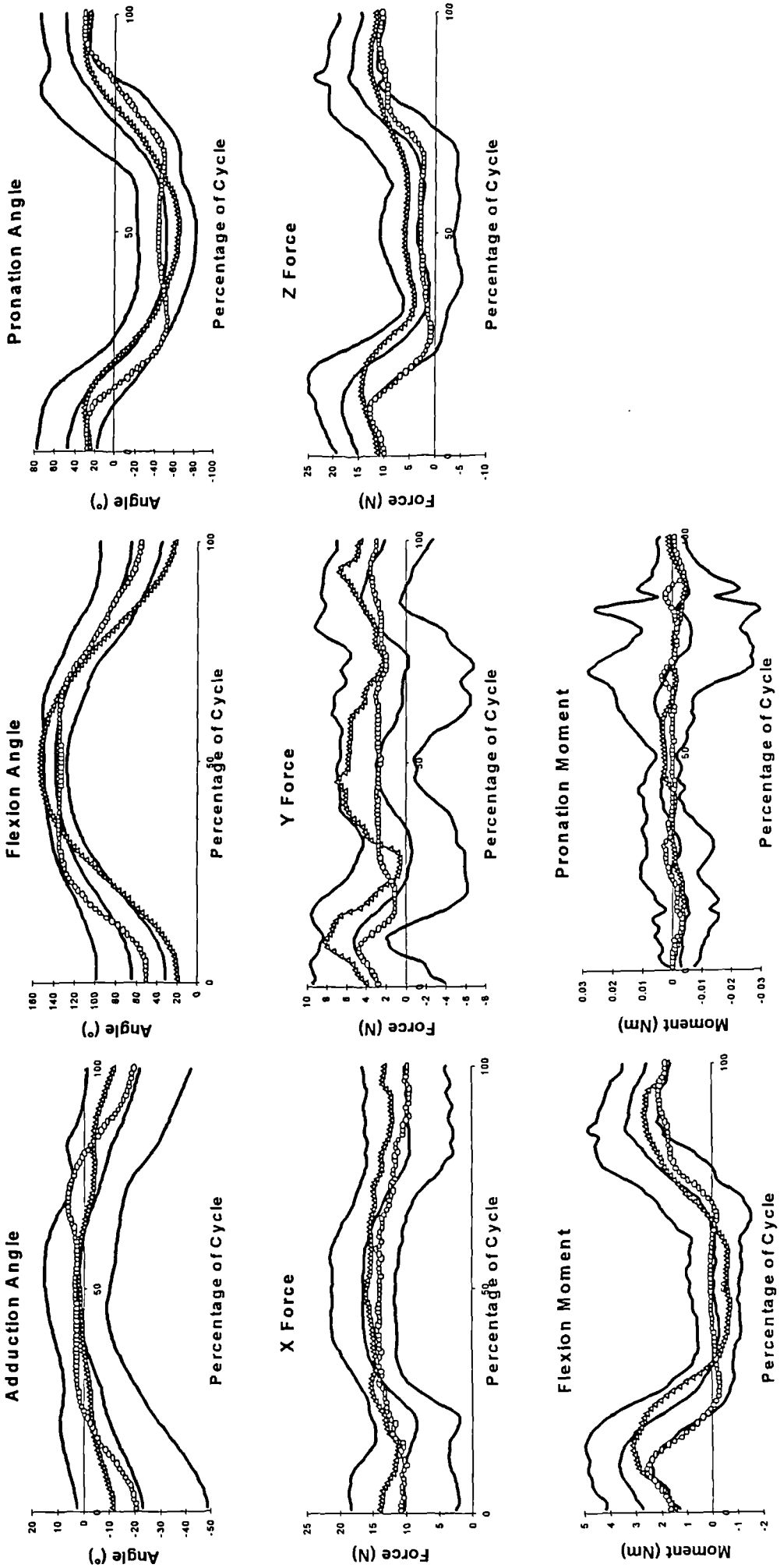

Fig.A.8.14 Comparison of impaired with unimpaired graphs for the Elbow during performance of Activity 2. (Δ - Subject 11, o - Subject 12)

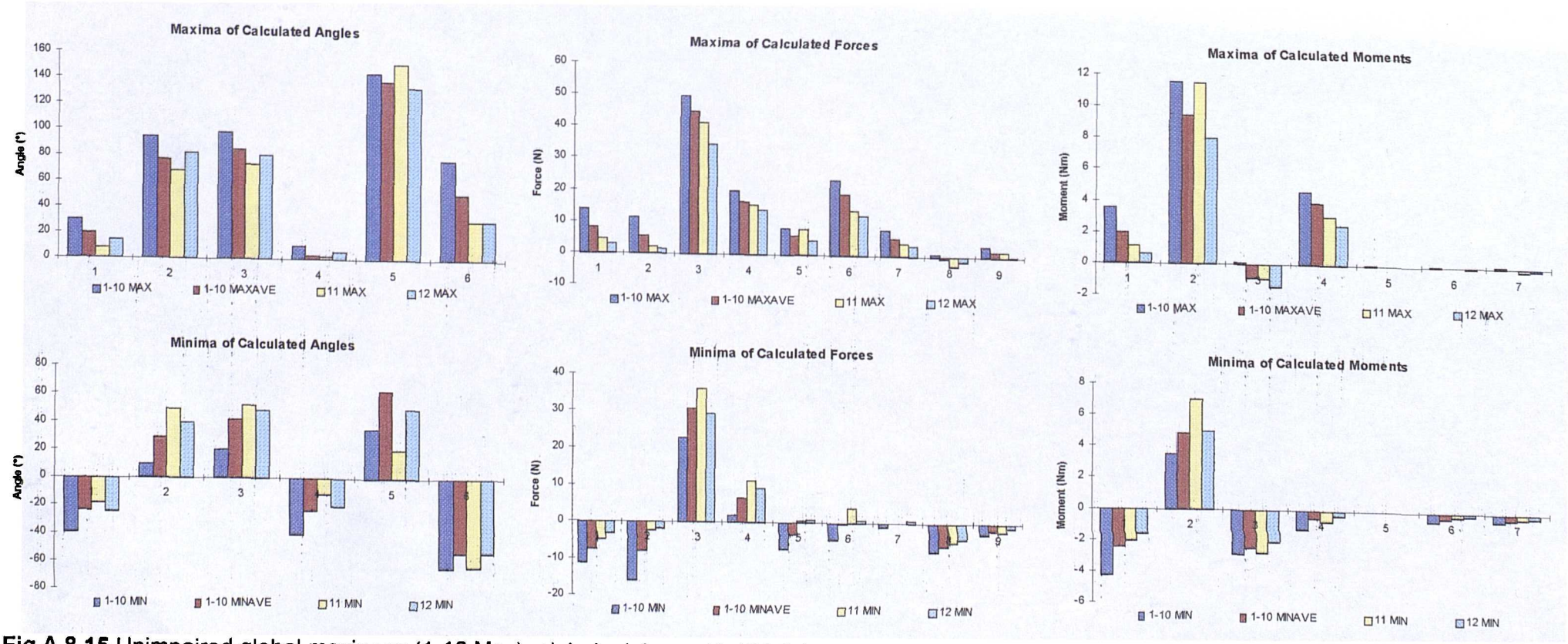

Fig.A.8.15 Unimpaired global maximum (1-10 Max), global minimum (1-10 Min), mean maximum (1-10 Maxave) and mean minimum (1-10 Minave) Angle, Force and Moment values, along with impaired maximum (11 Max, 12 Max) and minimum (11 Min, 12 Min) during performance of Activity 2. Key as in Table 8.12.

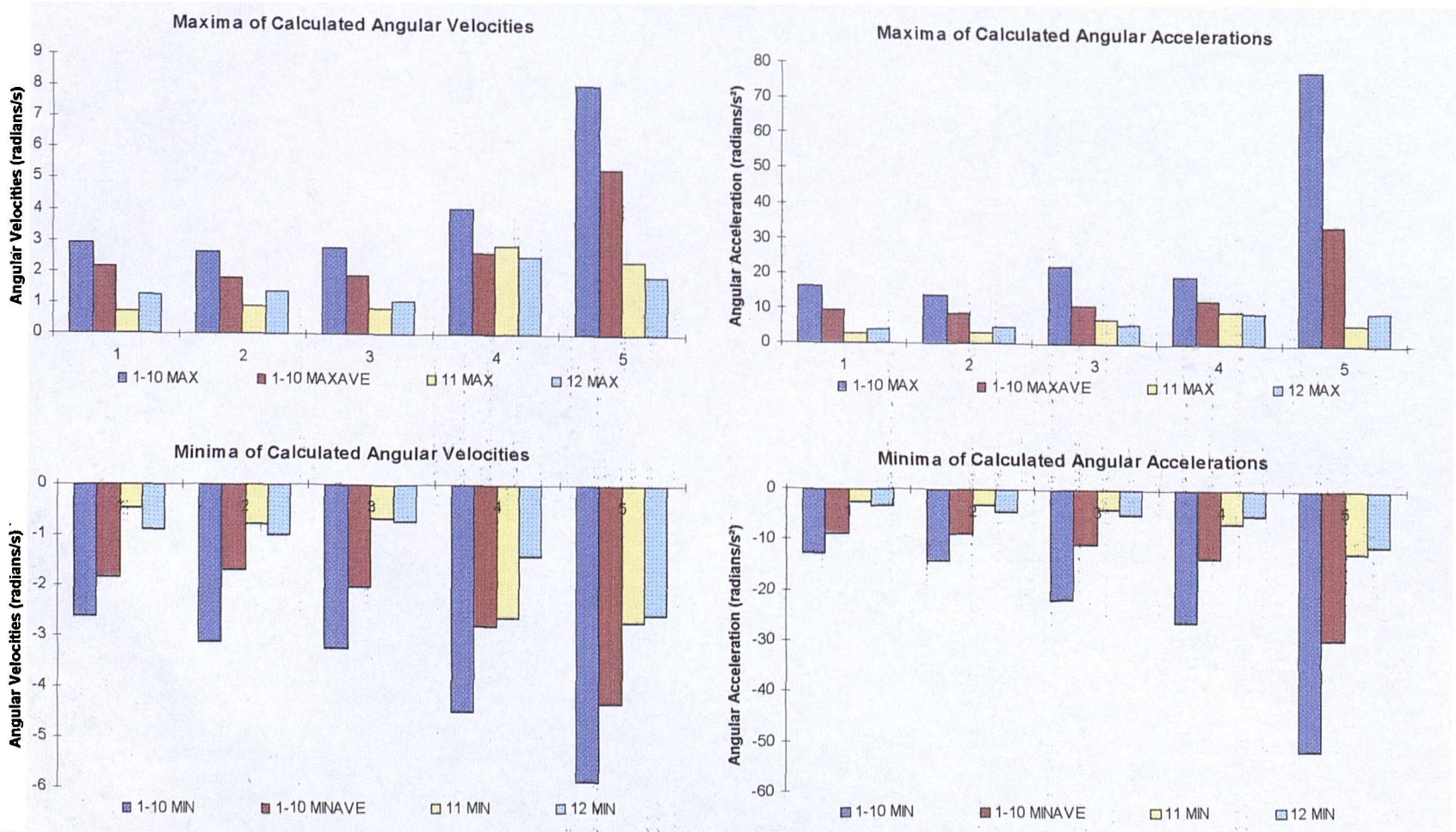

Fig.A.8.16 Unimpaired global maximum (1-10 Max), global minimum (1-10 Min), mean maximum (1-10 Maxave) and mean minimum (1-10 Minave) Angular Velocity and Acceleration, along with impaired maximum (11 Max, 12 Max) and minimum (11 Min, 12 Min) during performance of Activity 2. Key as in Table 8.13.

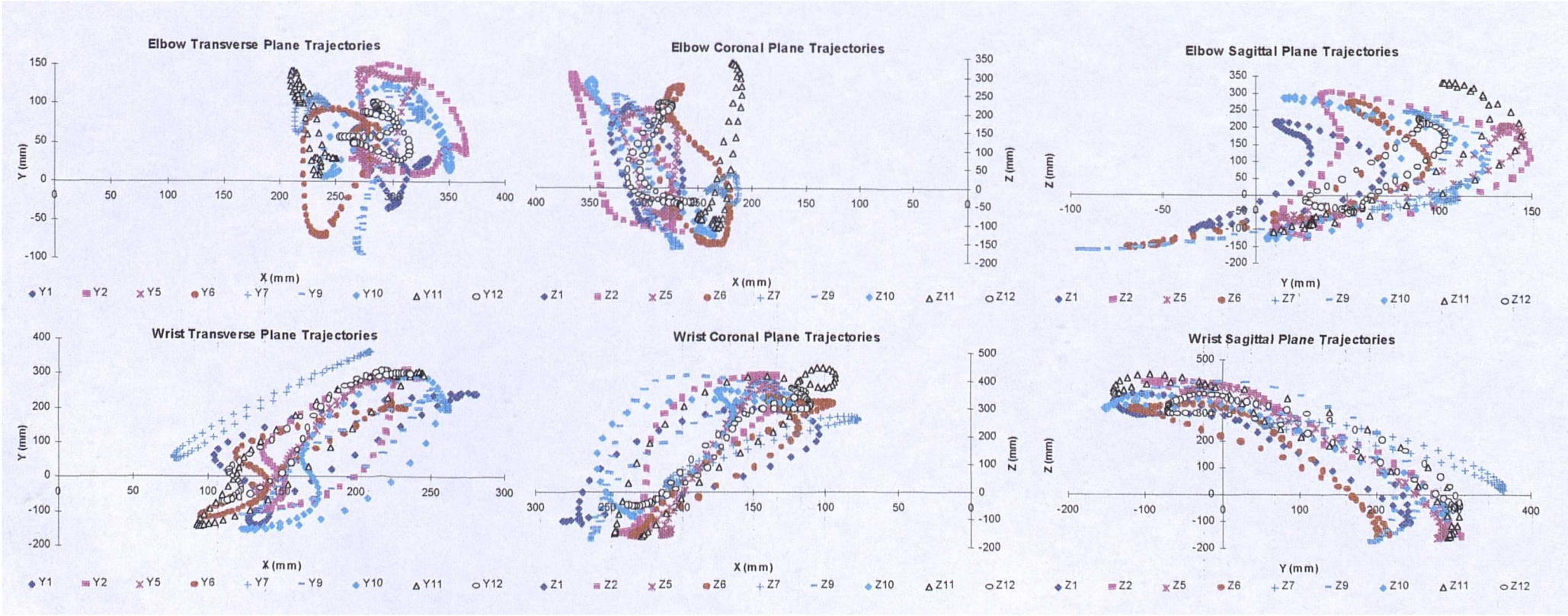

Fig.A.8.17 Trajectories of Elbow and Wrist in the Trunk Frame during performance of Activity 3.

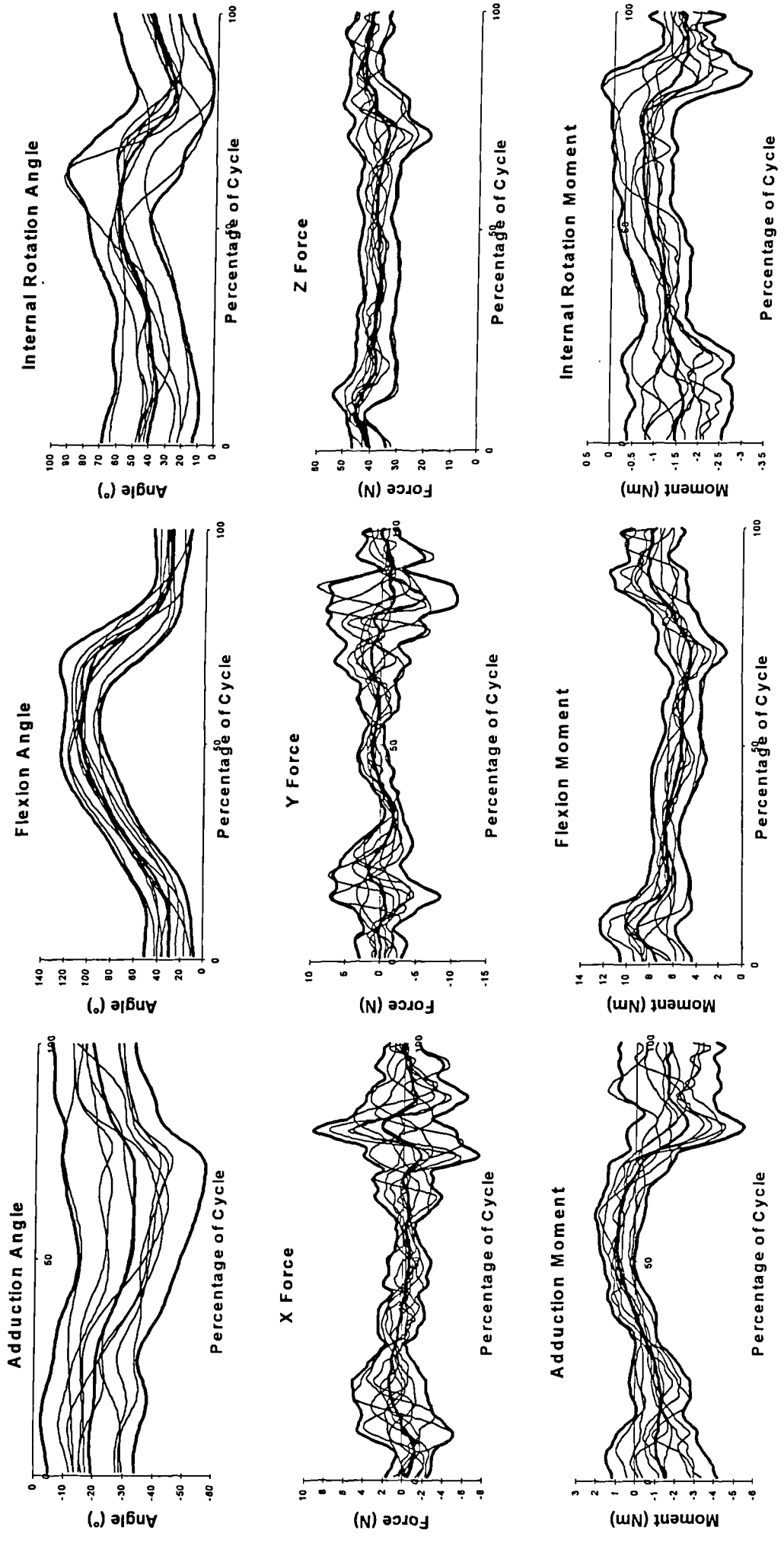

Fig.A.8.18 Angle, Force and Moment graphs for the Shoulder during performance of Activity 3, showing mean +/- 2SD in bold.

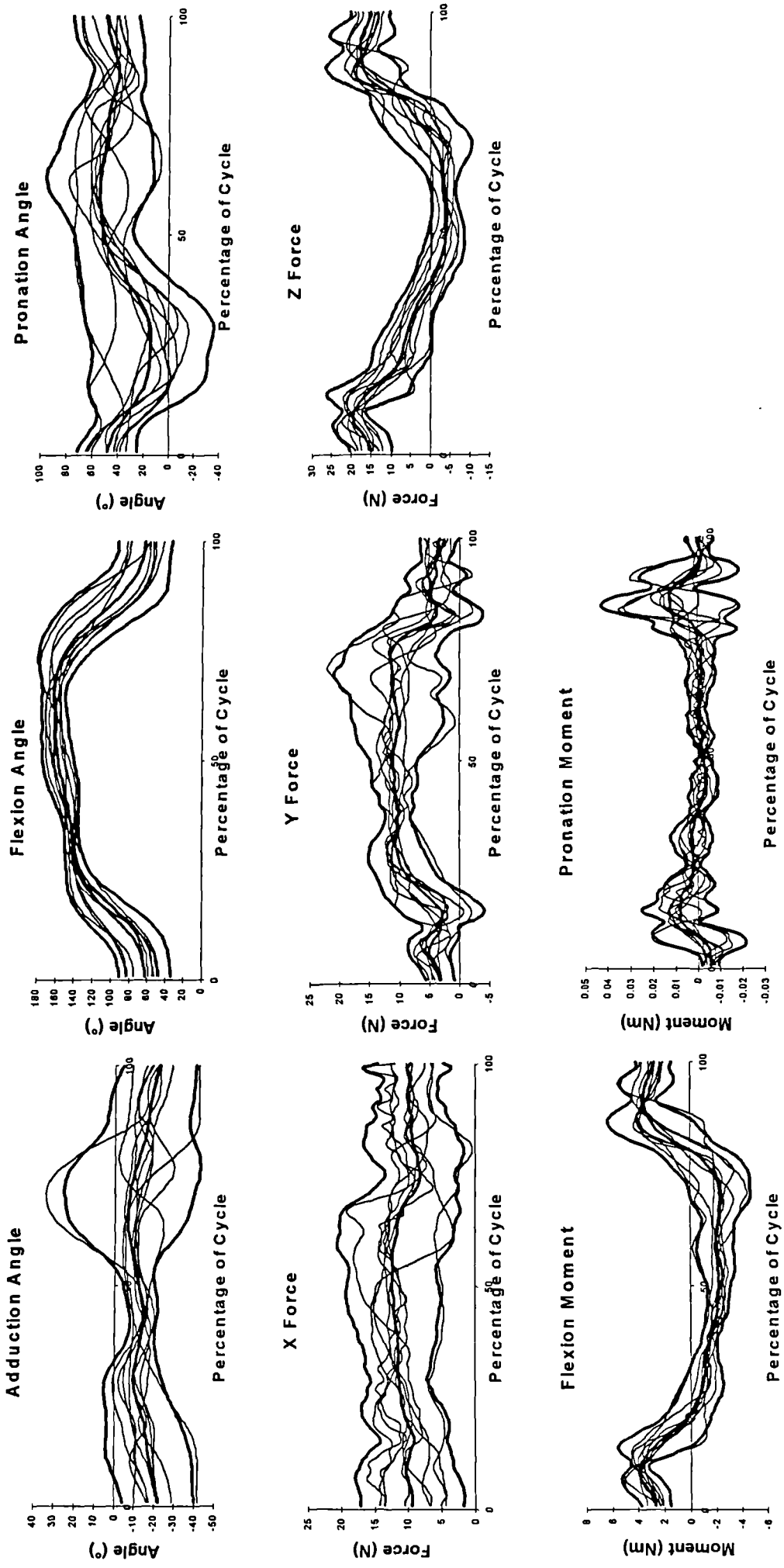

Fig.A.8.19 Angle, Force and Moment graphs for the Elbow during performance of Activity 3, showing mean +/- 2SD in bold.

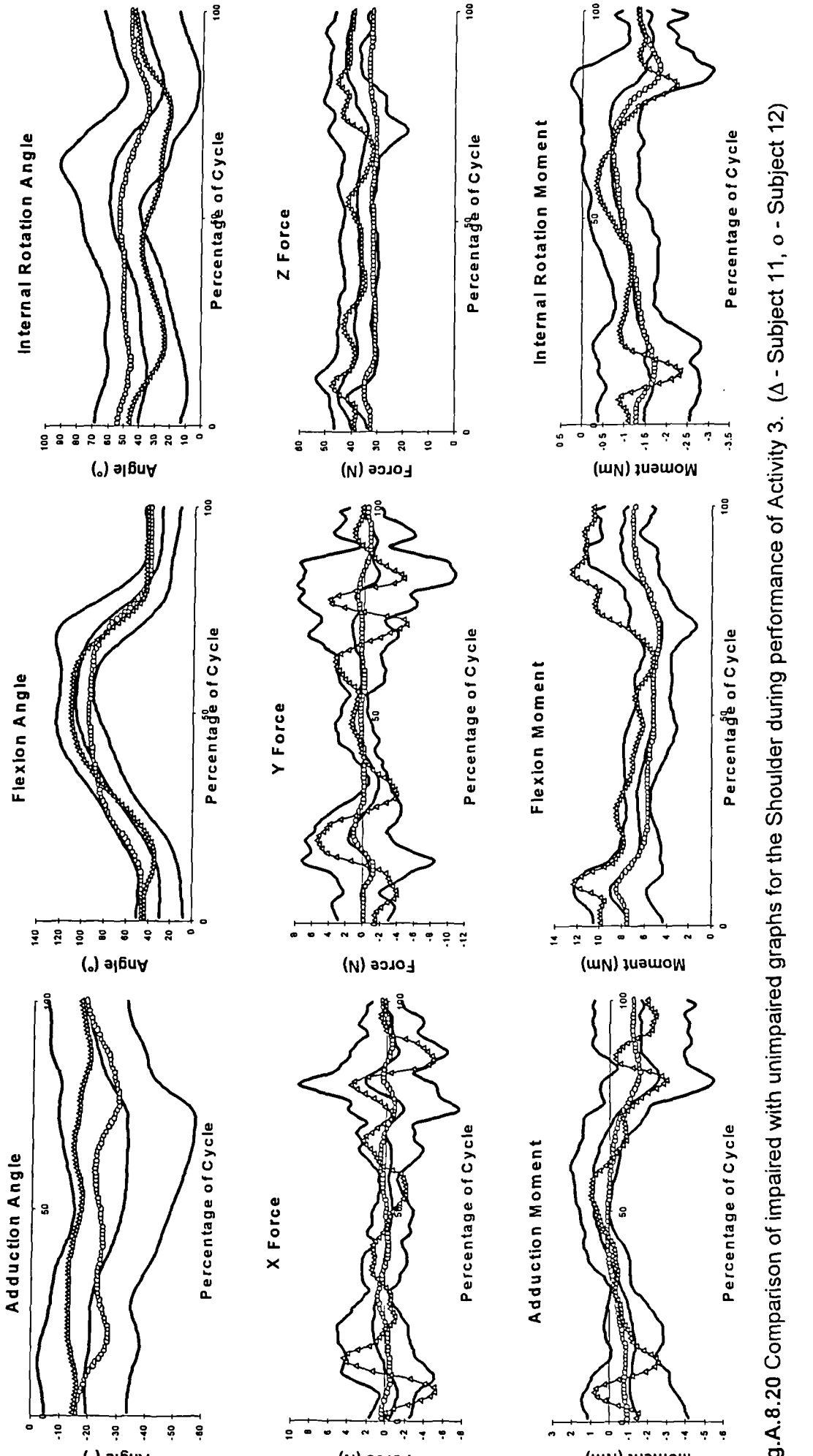

Fig.A.8.20 Comparison of impaired with unimpaired graphs for the Shoulder during performance of Activity 3. (Δ - Subject 11, o - Subject 12)

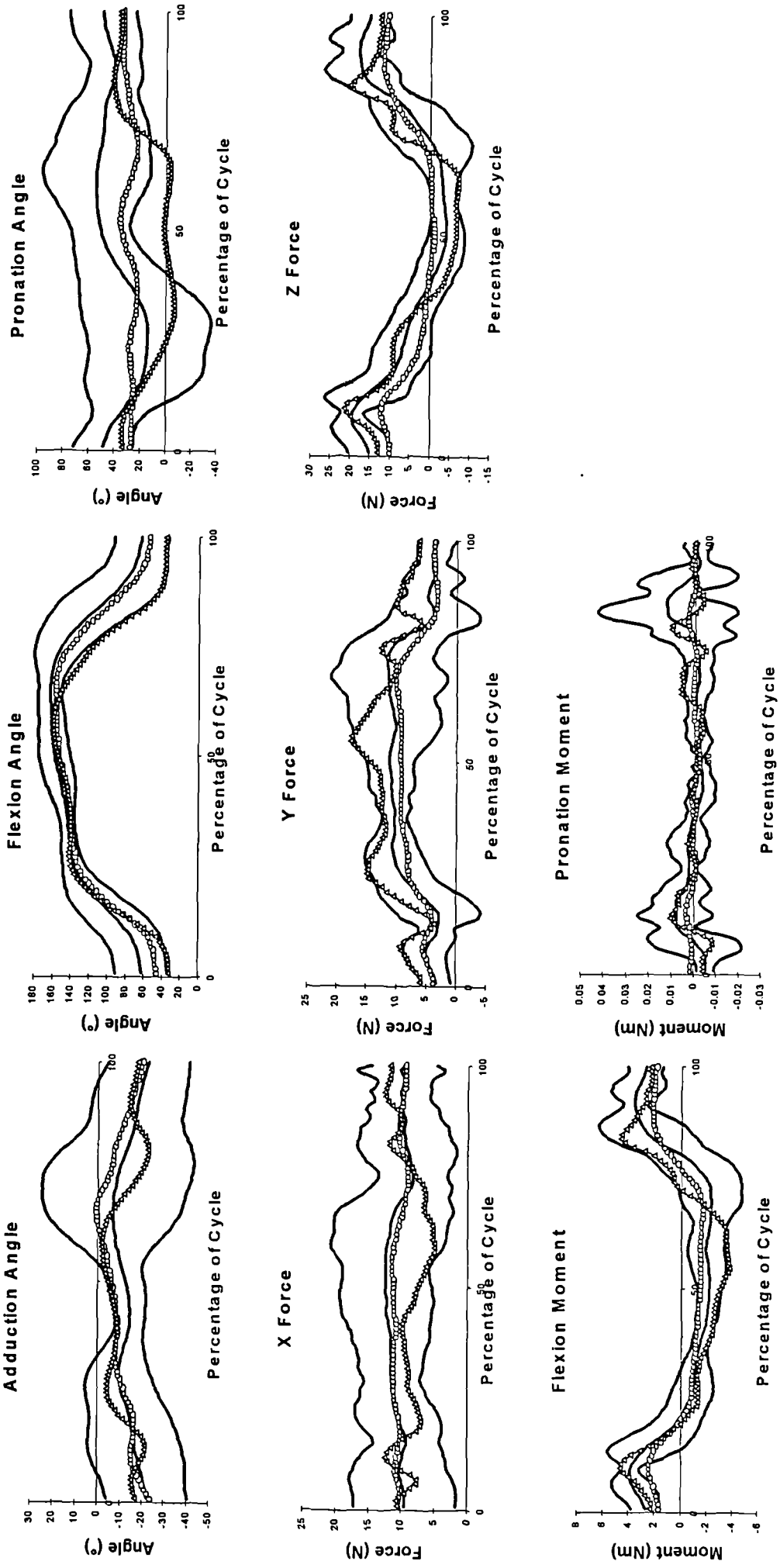

Fig.A.8.21 Comparison of impaired with unimpaired graphs for the Elbow during performance of Activity 3. (Δ - Subject 11, o - Subject 12)

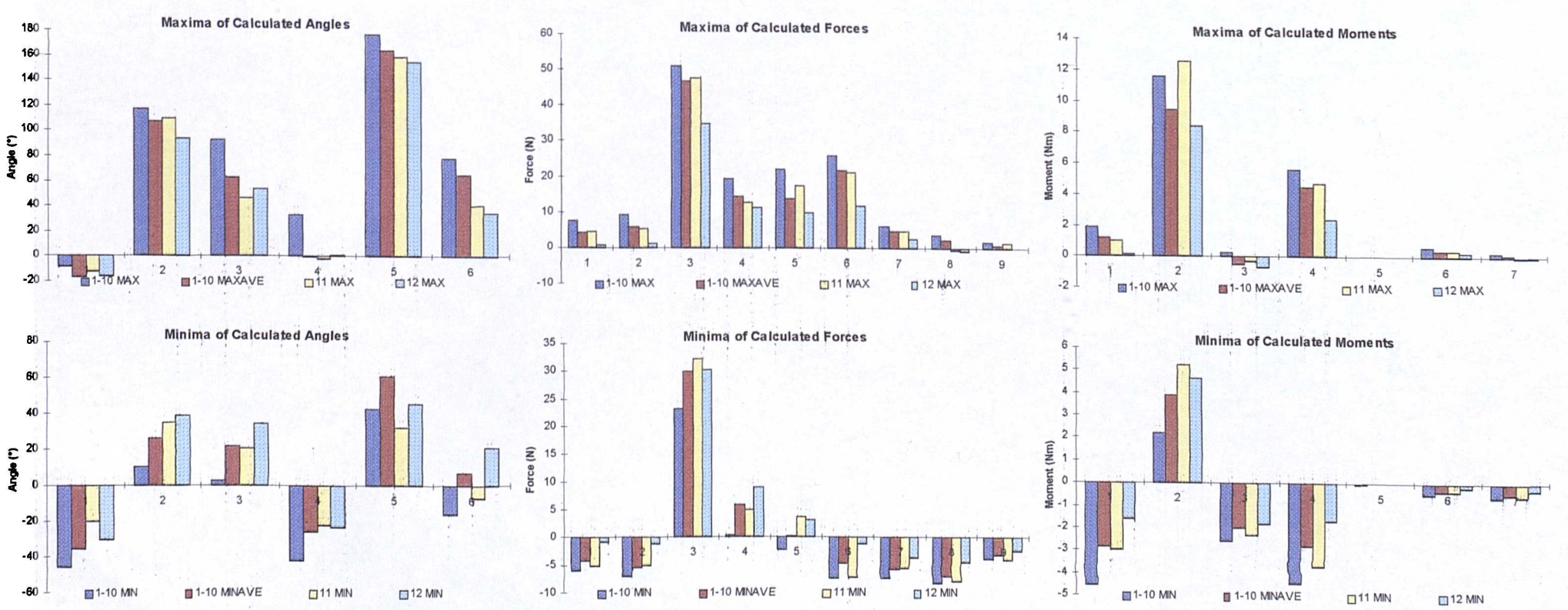

Fig.A.8.22 Unimpaired global maximum (1-10 Max), global minimum (1-10 Min), mean maximum (1-10 Maxave) and mean minimum (1-10 Minave) Angle, Force and Moment values, along with impaired maximum (11 Max, 12 Max) and minimum (11 Min, 12 Min) during performance of Activity 3. Key as in Table 8.12.

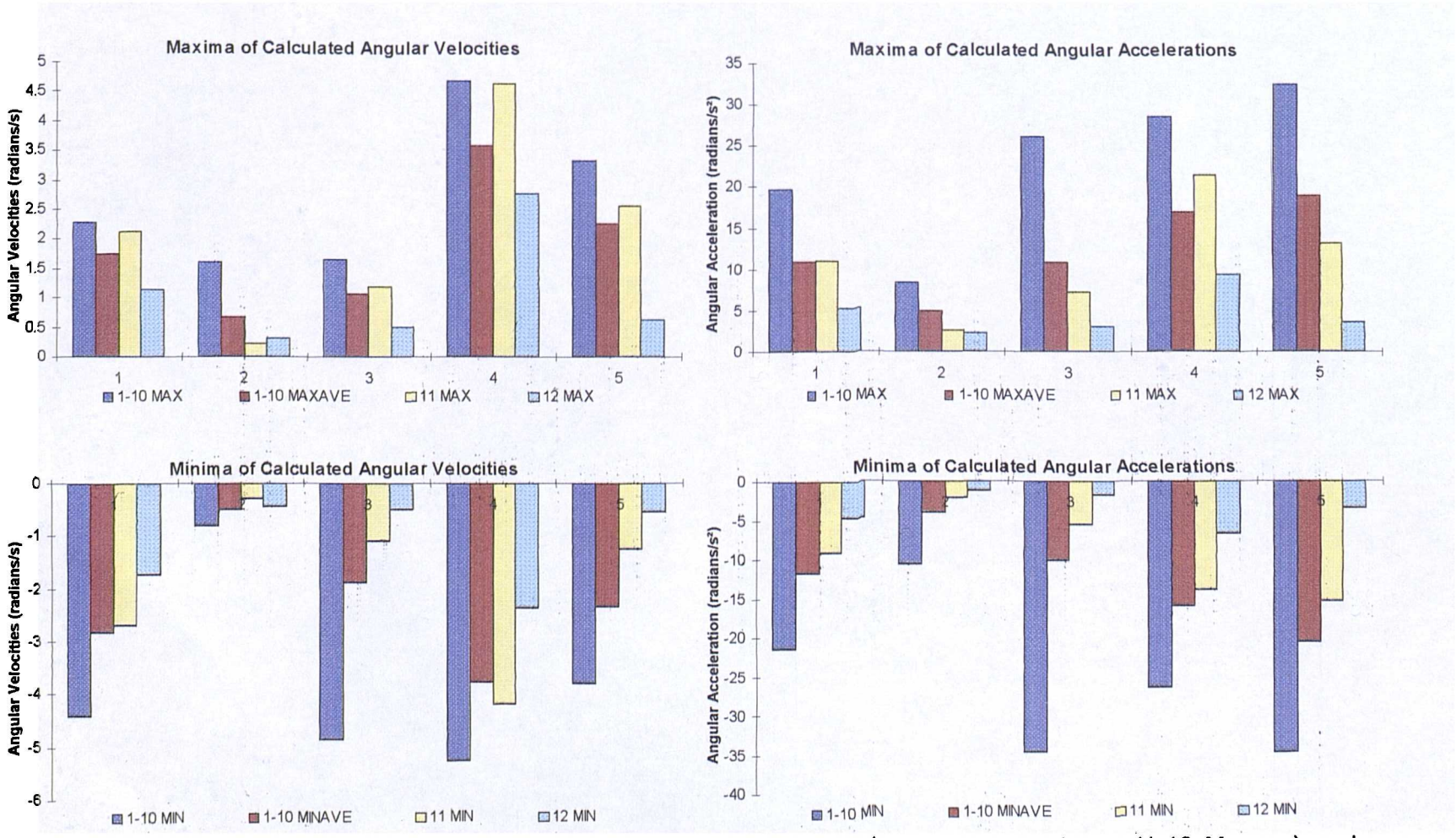

Fig.A.8.23 Unimpaired global maximum (1-10 Max), global minimum (1-10 Min), mean maximum (1-10 Maxave) and mean minimum (1-10 Minave) Angular Velocity and Acceleration, along with impaired maximum (11 Max, 12 Max) and minimum (11 Min, 12 Min) during performance of Activity 3. Key as in Table 8.13.

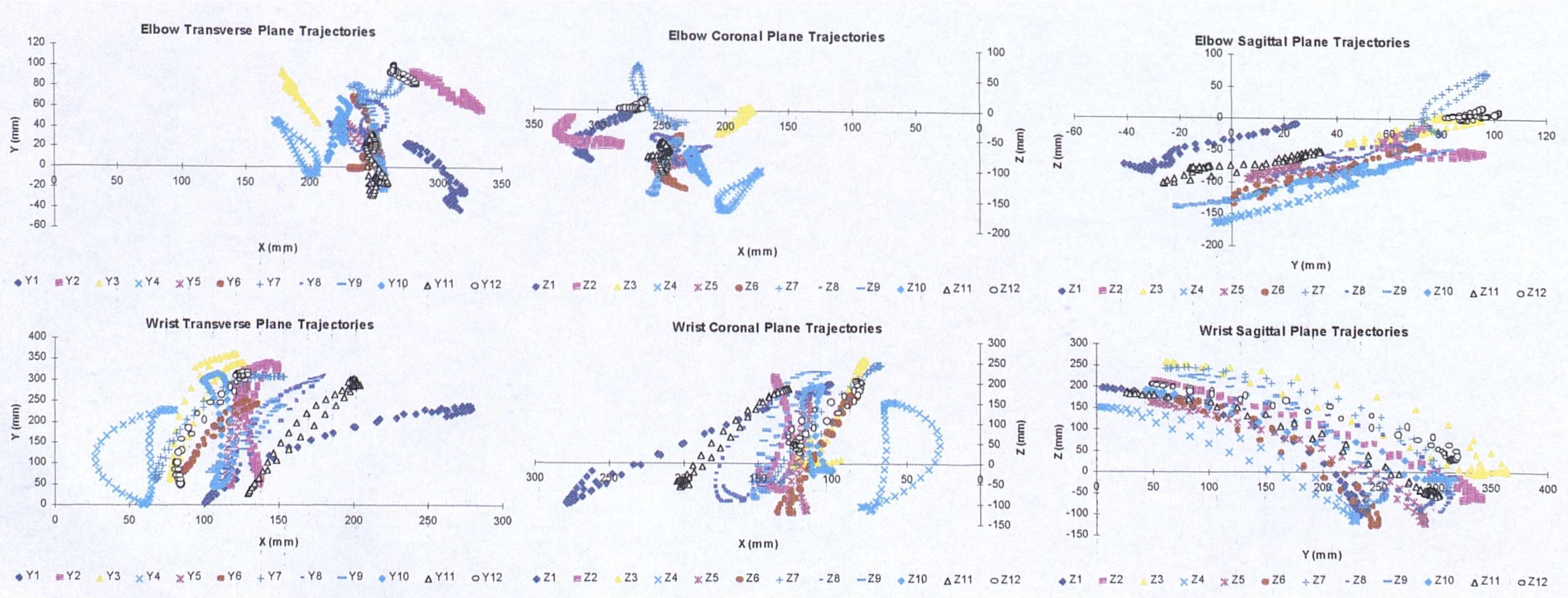

Fig.A.8.24 Trajectories of Elbow and Wrist in the Trunk Frame during performance of Activity 4.

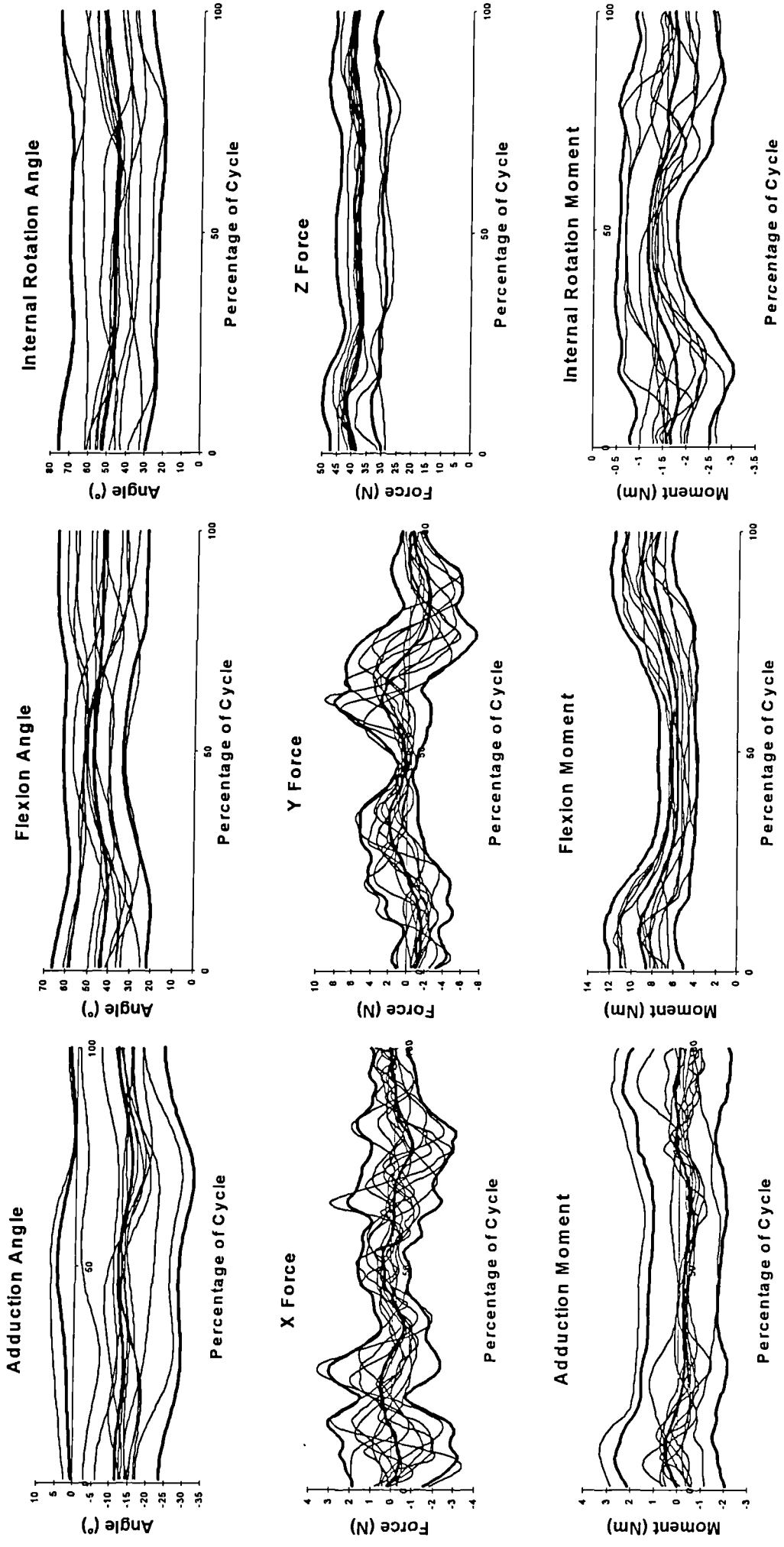

Fig.A.8.25 Angle, Force and Moment graphs for the Shoulder during performance of Activity 4, showing mean +/- 2SD in bold.

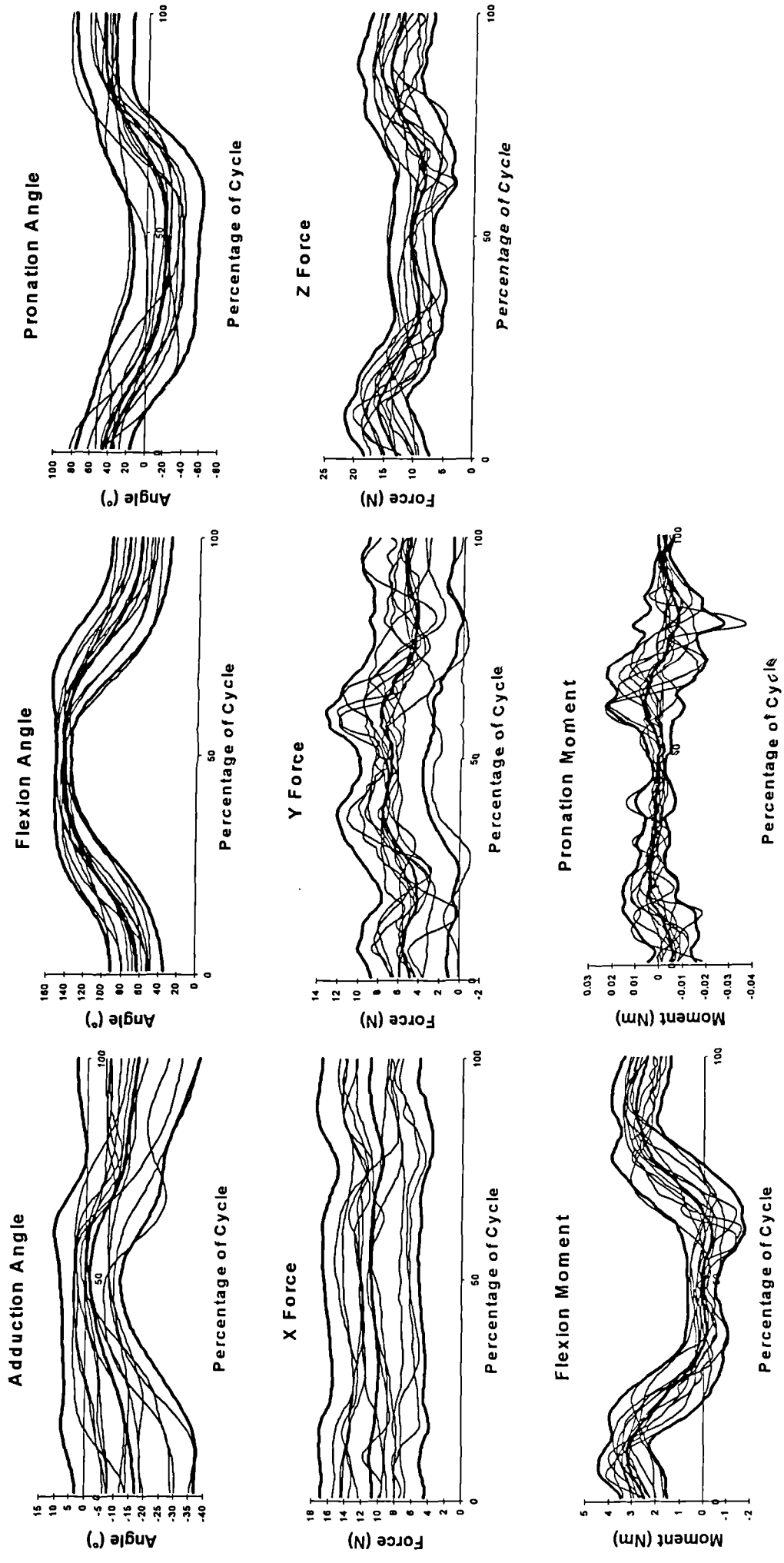

Fig.A.8.26 Angle, Force and Moment graphs for the Elbow during performance of Activity 4, showing mean +/- 2SD in bold.

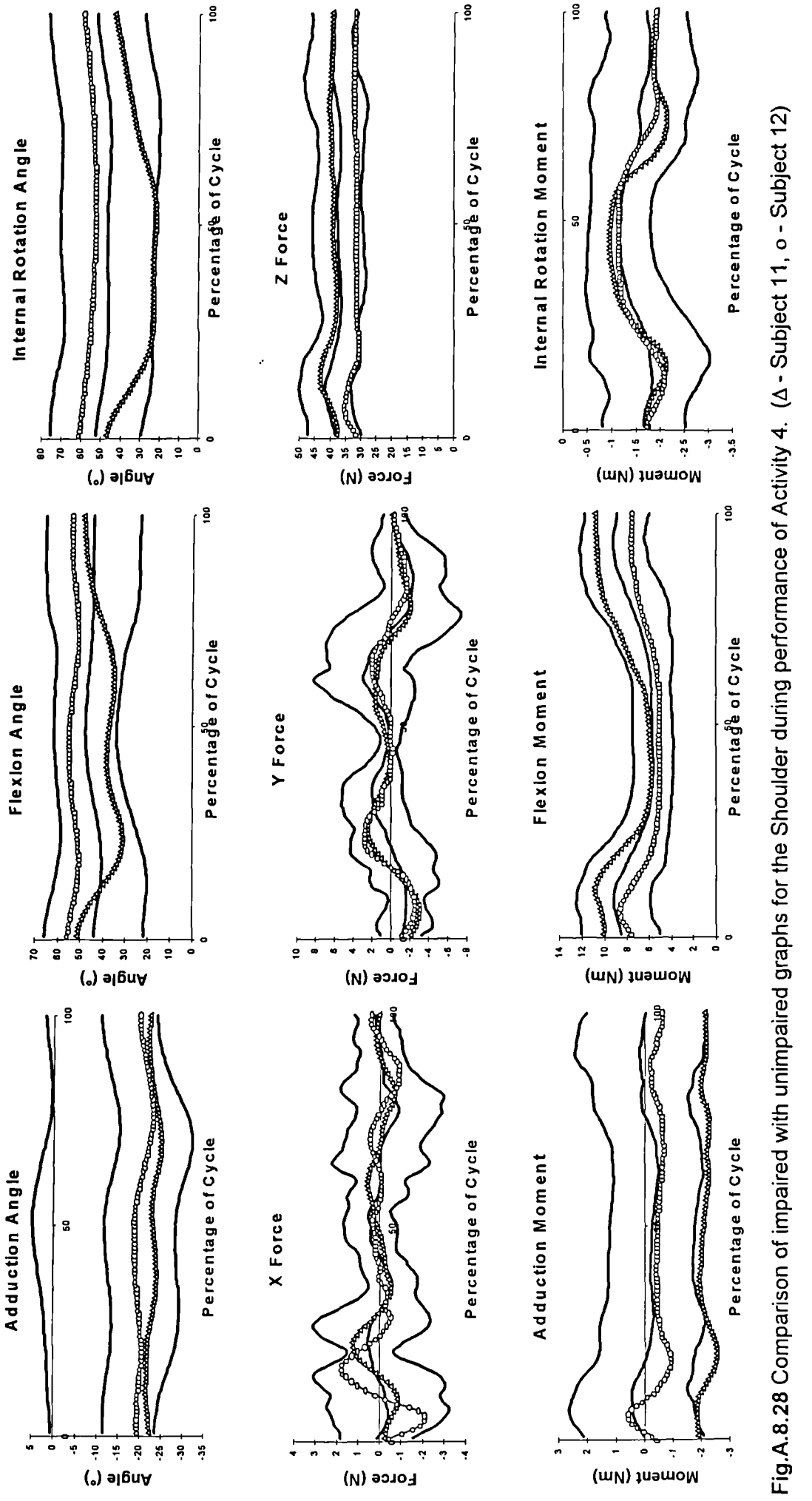

Fig.A.8.28 Comparison of impaired with unimpaired graphs for the Shoulder during performance of Activity 4. (Δ - Subject 11, o - Subject 12)

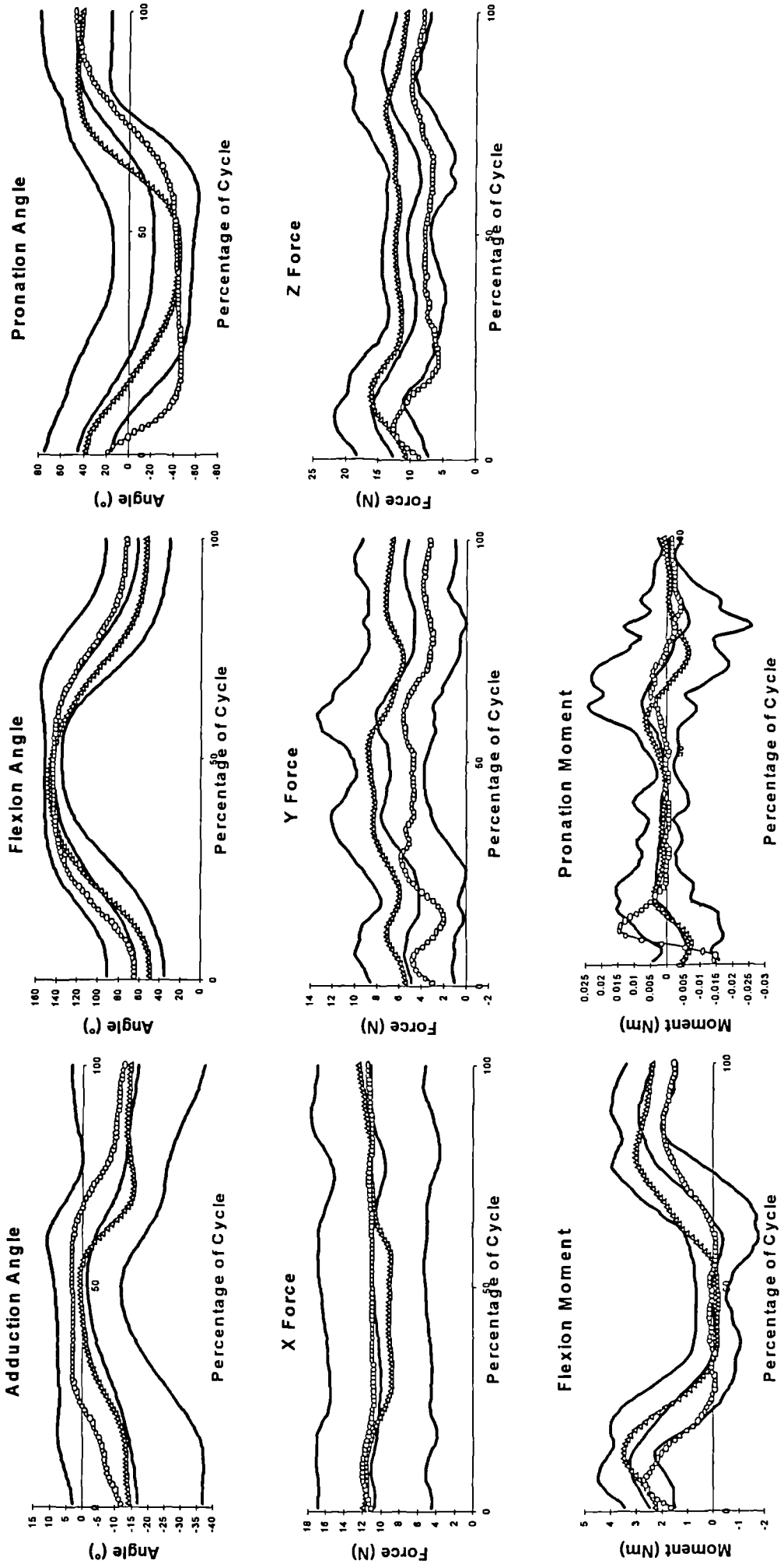

Fig.A.8.29 Comparison of impaired with unimpaired graphs for the Elbow during performance of Activity 4. (Δ - Subject 11, o - Subject 12)

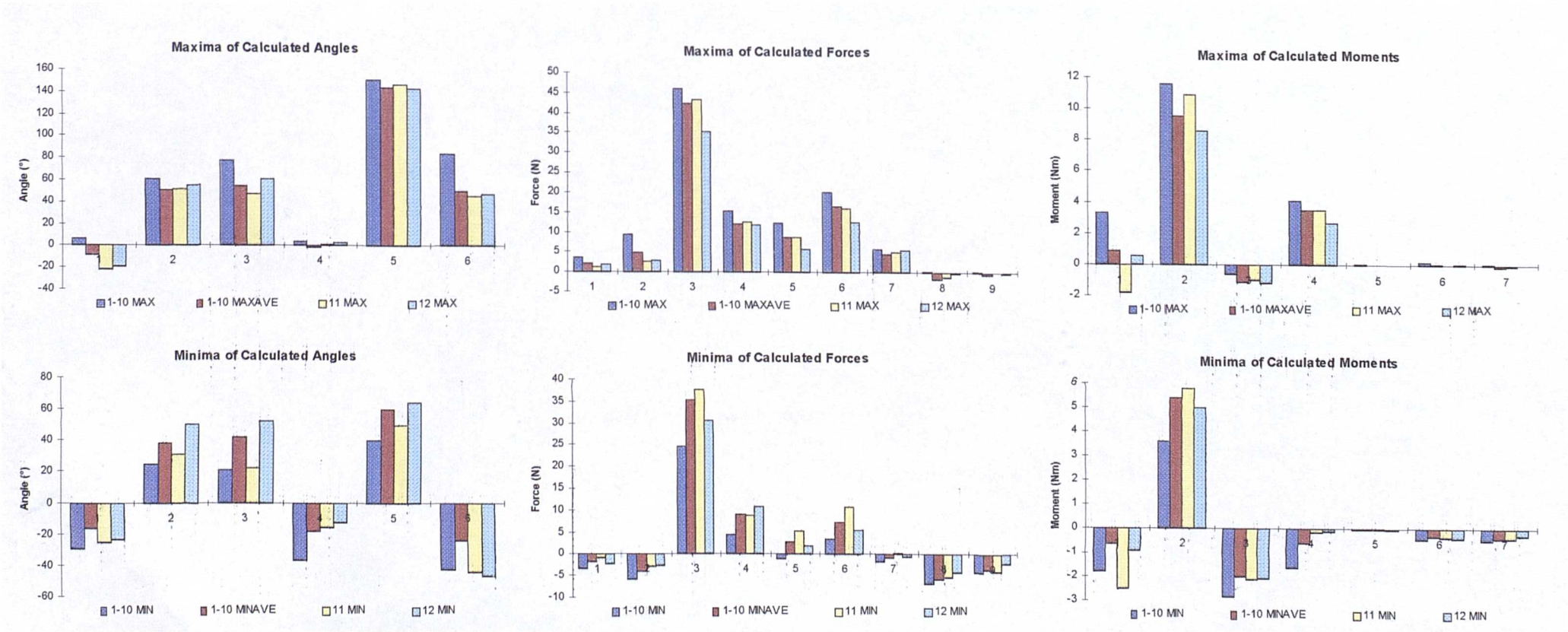

Fig.A.8.30 Unimpaired global maximum (1-10 Max), global minimum (1-10 Min), mean maximum (1-10 Maxave) and mean minimum (1-10 Minave) Angle, Force and Moment values, along with impaired maximum (11 Max, 12 Max) and minimum (11 Min, 12 Min) during performance of Activity 4. Key as in Table 8.12.

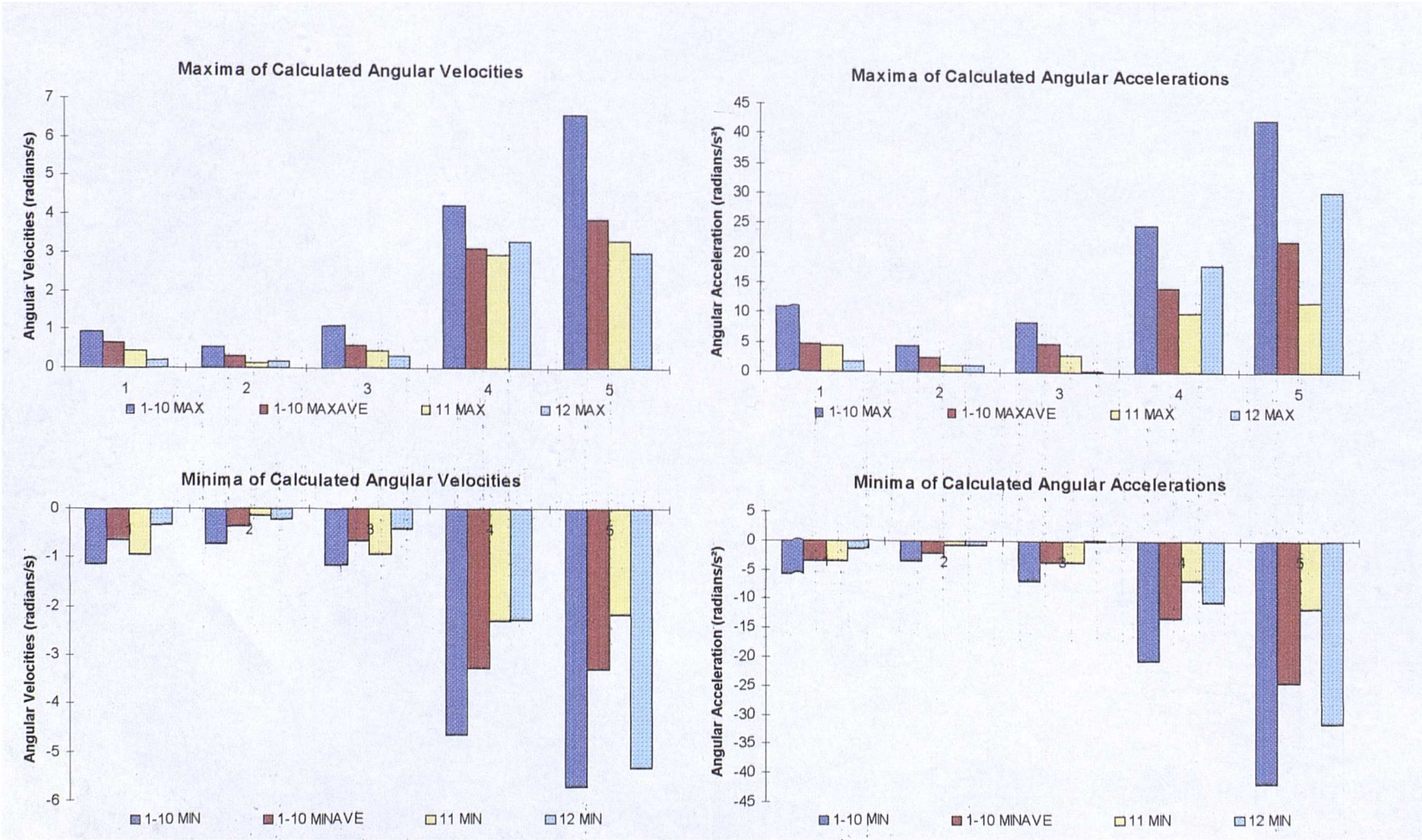

Fig.A.8.31 Unimpaired global maximum (1-10 Max), global minimum (1-10 Min), mean maximum (1-10 Maxave) and mean minimum (1-10 Minave) Angular Velocity and Acceleration, along with impaired maximum (11 Max, 12 Max) and minimum (11 Min, 12 Min) during performance of Activity 4. Key as in Table 8.13.

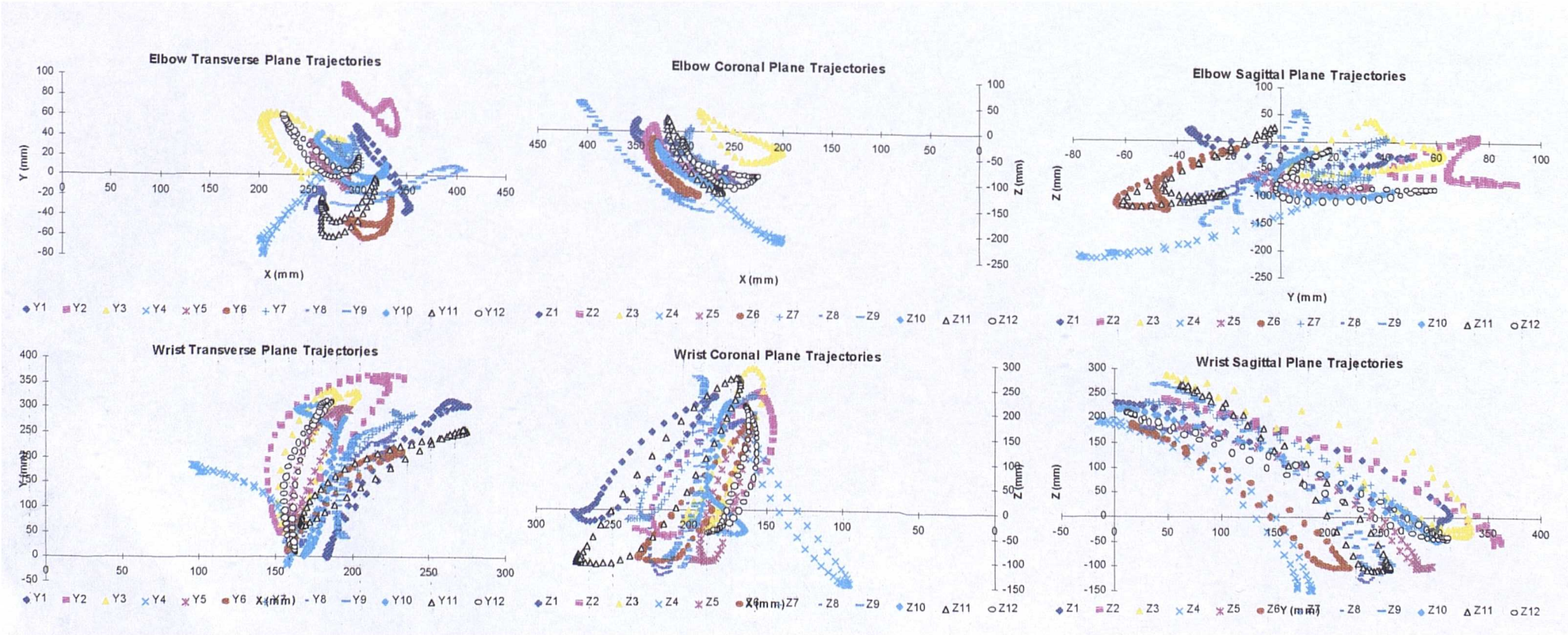

Fig.A.8.33 Trajectories of Elbow and Wrist in the Trunk Frame during performance of Activity 5.

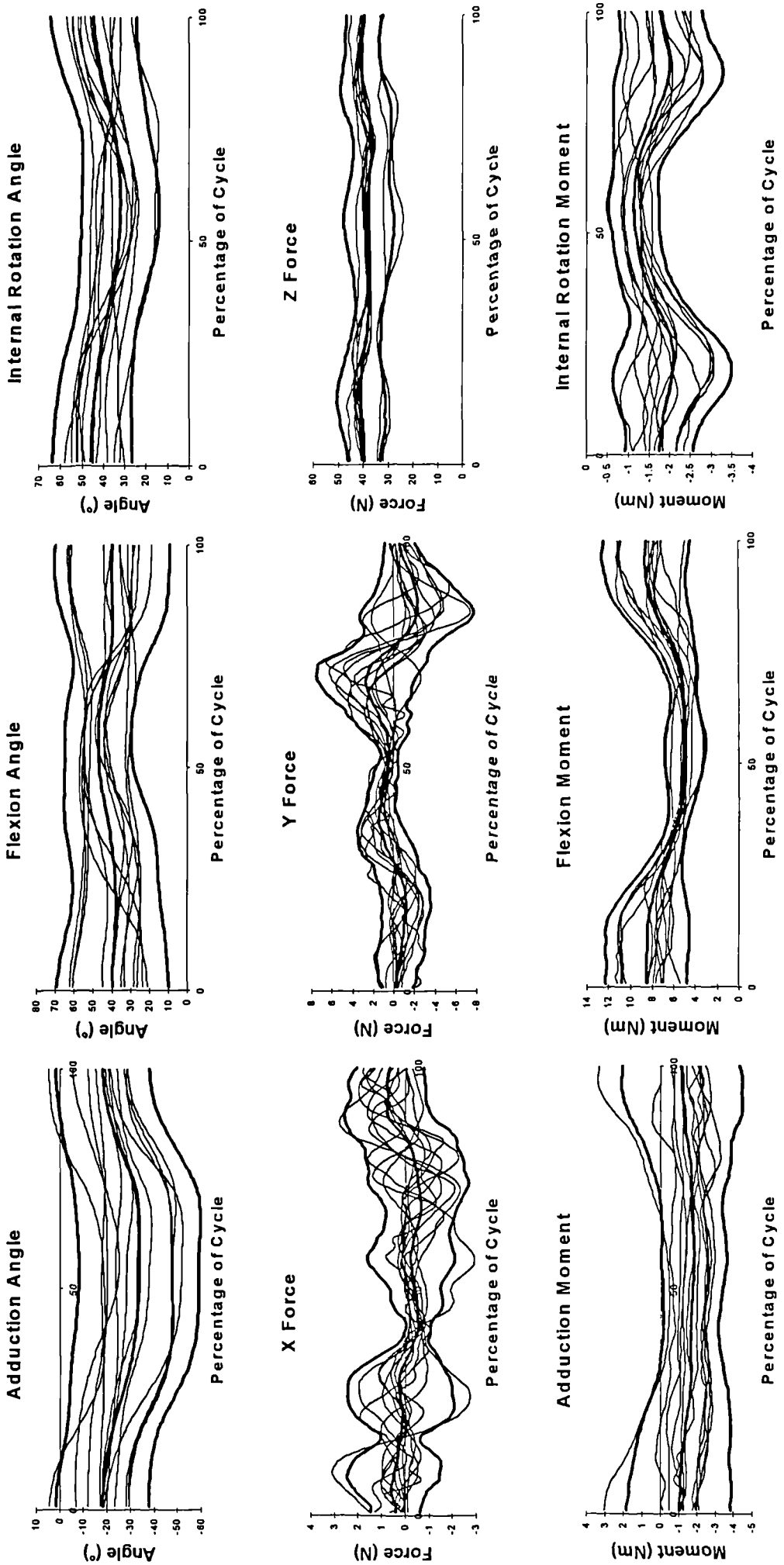

Fig.A.8.34 Angle, Force and Moment graphs for the Shoulder during performance of Activity 5, showing mean +/- 2SD in bold.

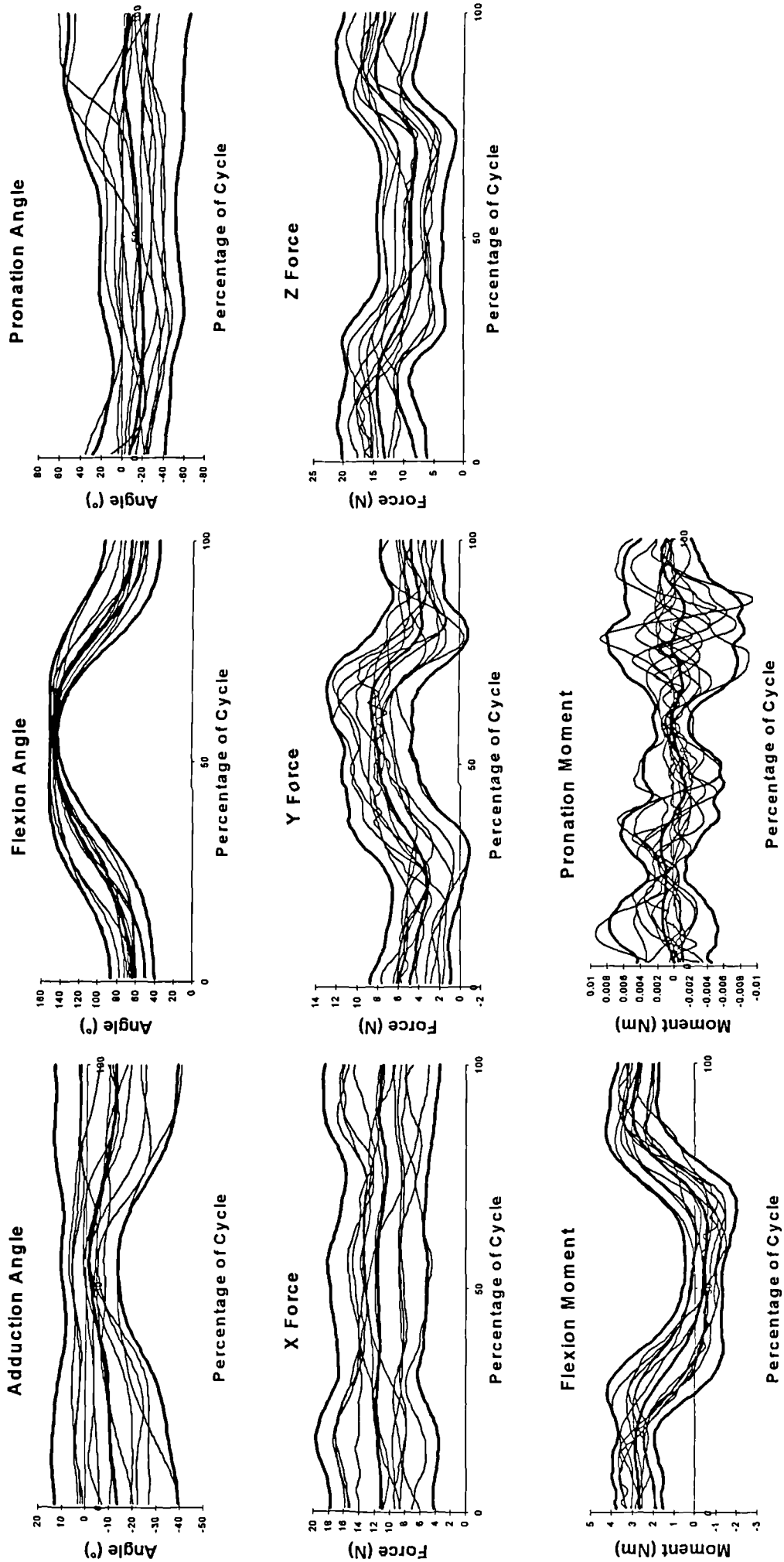

Fig.A.8.35 Angle, Force and Moment graphs for the Elbow during performance of Activity 5, showing mean +/- 2SD in bold.

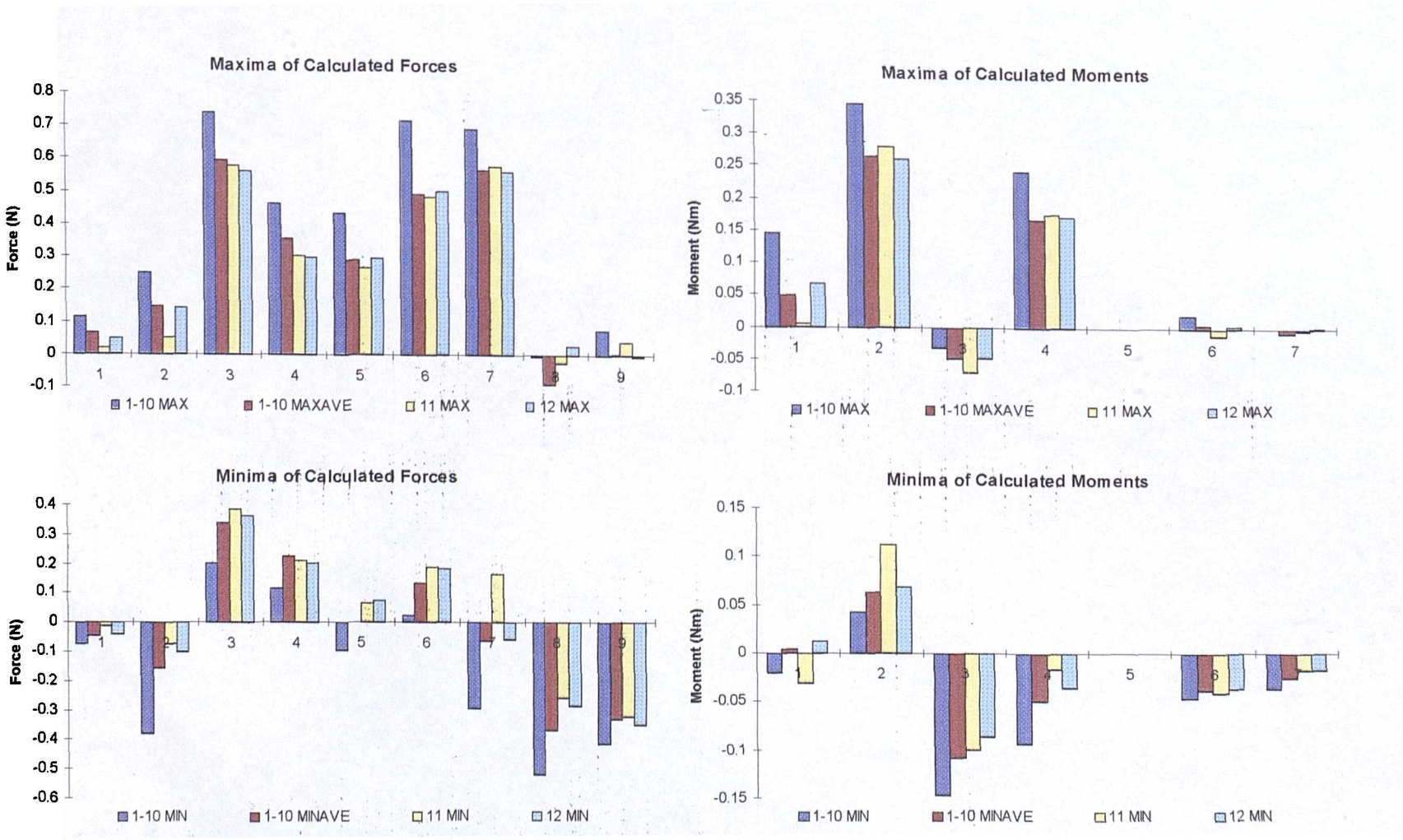

Fig.A.8.37 Unimpaired global maximum (1-10 Max), global minimum (1-10 Min), mean maximum (1-10 Maxave) and mean minimum (1-10 Minave) Force and Moment values due to hand load, along with impaired maximum (11 Max, 12 Max) and minimum (11 Min, 12 Min), during performance of Activity 5. *Key as in Table 8.12.*

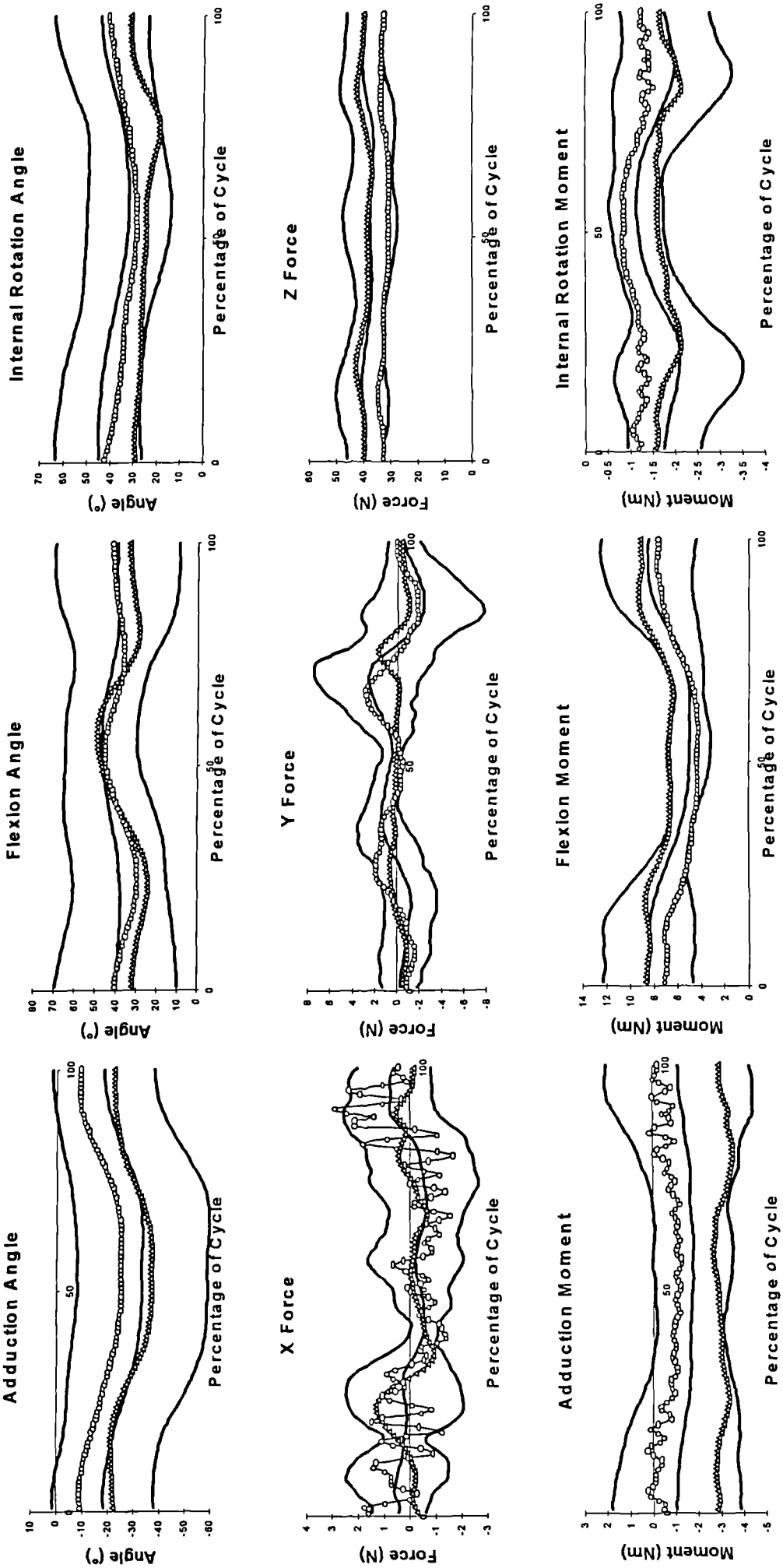

Fig.A.8.38 Comparison of impaired with unimpaired graphs for the Shoulder during performance of Activity 5. (Δ - Subject 11, o - Subject 12)

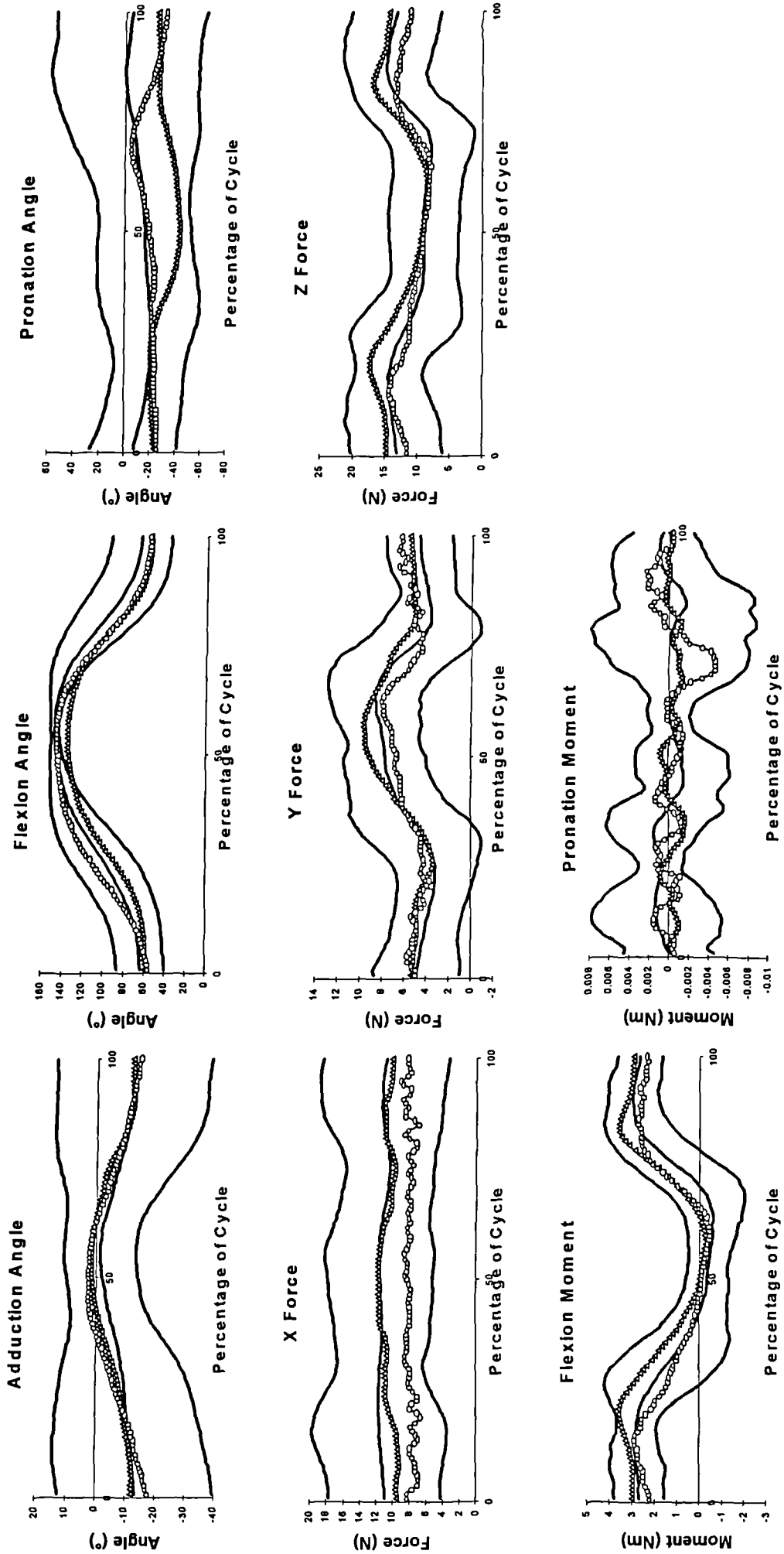

Fig.A.8.39 Comparison of impaired with unimpaired graphs for the Elbow during performance of Activity 5. (Δ - Subject 11, o - Subject 12)

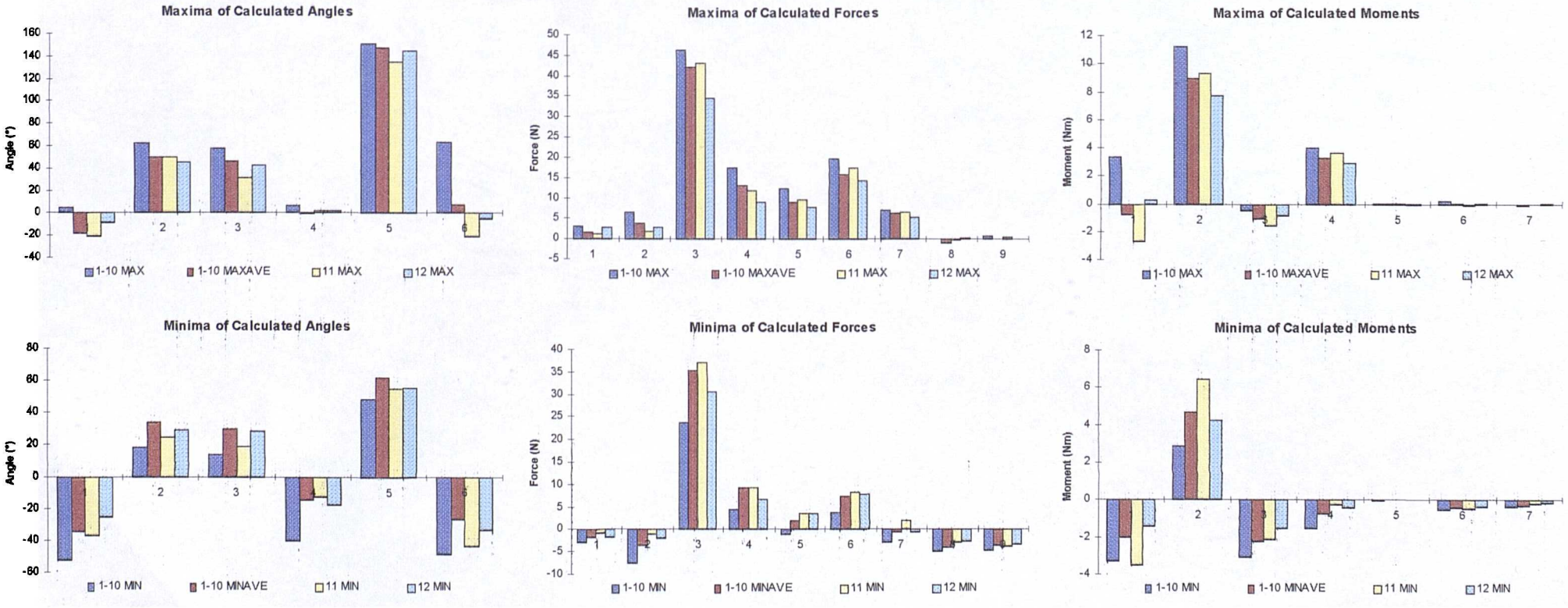

Fig.A.8.40 Unimpaired global maximum (1-10 Max), global minimum (1-10 Min), mean maximum (1-10 Maxave) and mean minimum (1-10 Minave) Angle, Force and Moment values, along with impaired maximum (11 Max, 12 Max) and minimum (11 Min, 12 Min) during performance of Activity 5. Key as in Table 8.12.

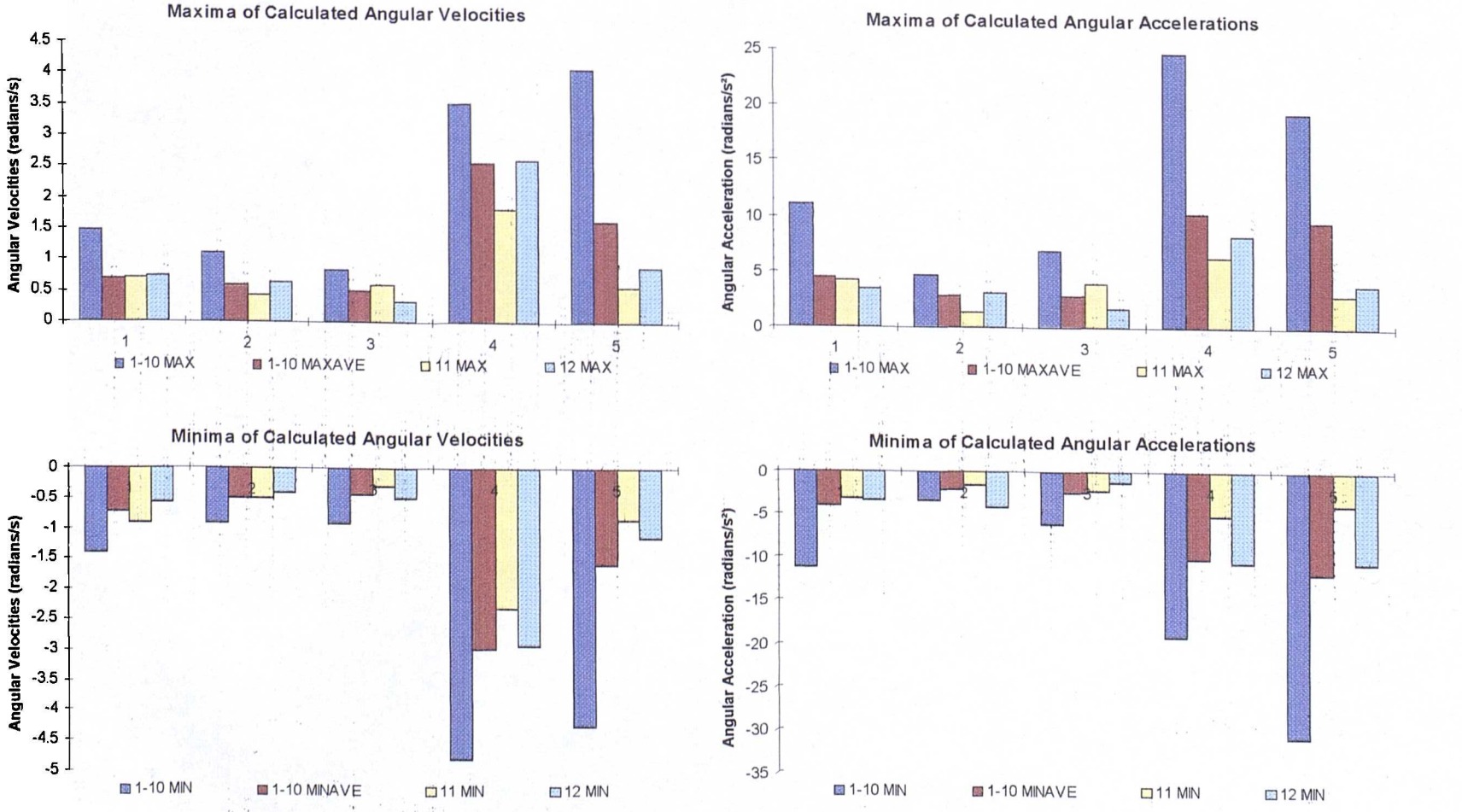

Fig.A.8.41 Unimpaired global maximum (1-10 Max), global minimum (1-10 Min), mean maximum (1-10 Maxave) and mean minimum (1-10 Minave) Angular Velocity and Acceleration, along with impaired maximum (11 Max, 12 Max) and minimum (11 Min, 12 Min) during performance of Activity 5. Key as in Table 8.13.

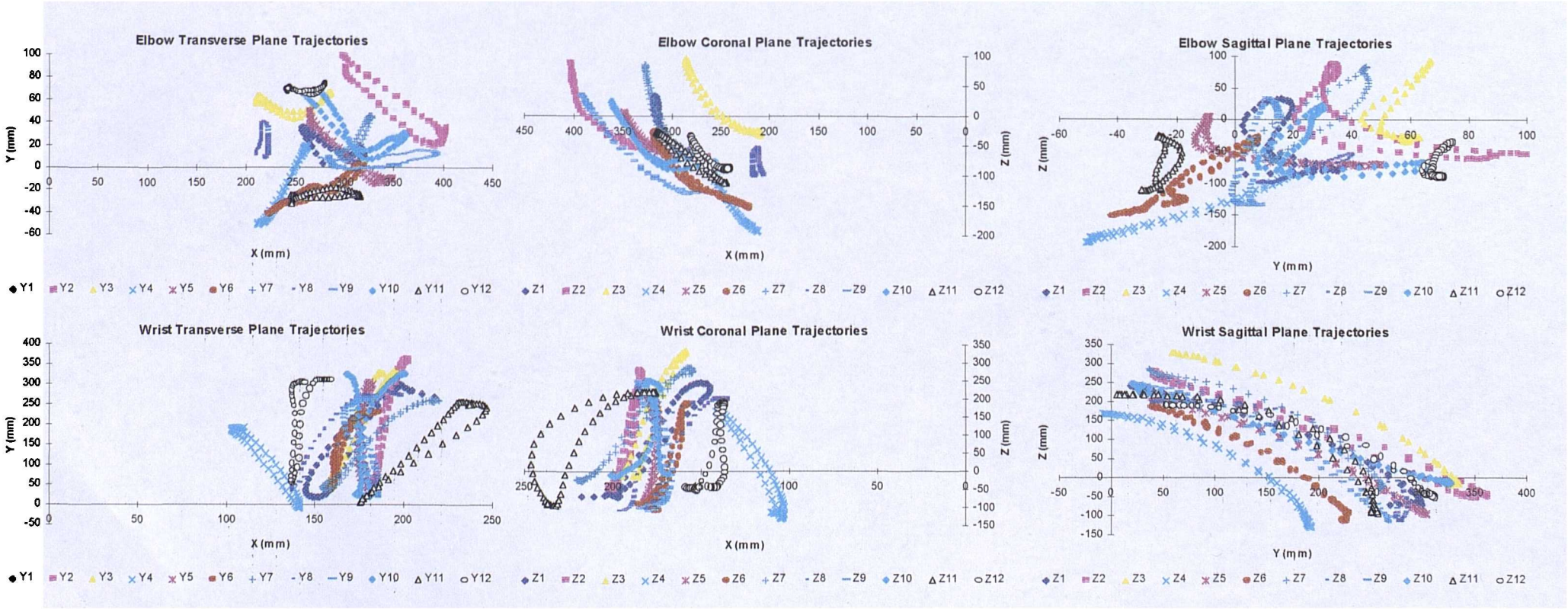

Fig.A.8.43 Trajectories of Elbow and Wrist in the Trunk Frame during performance of Activity 6.

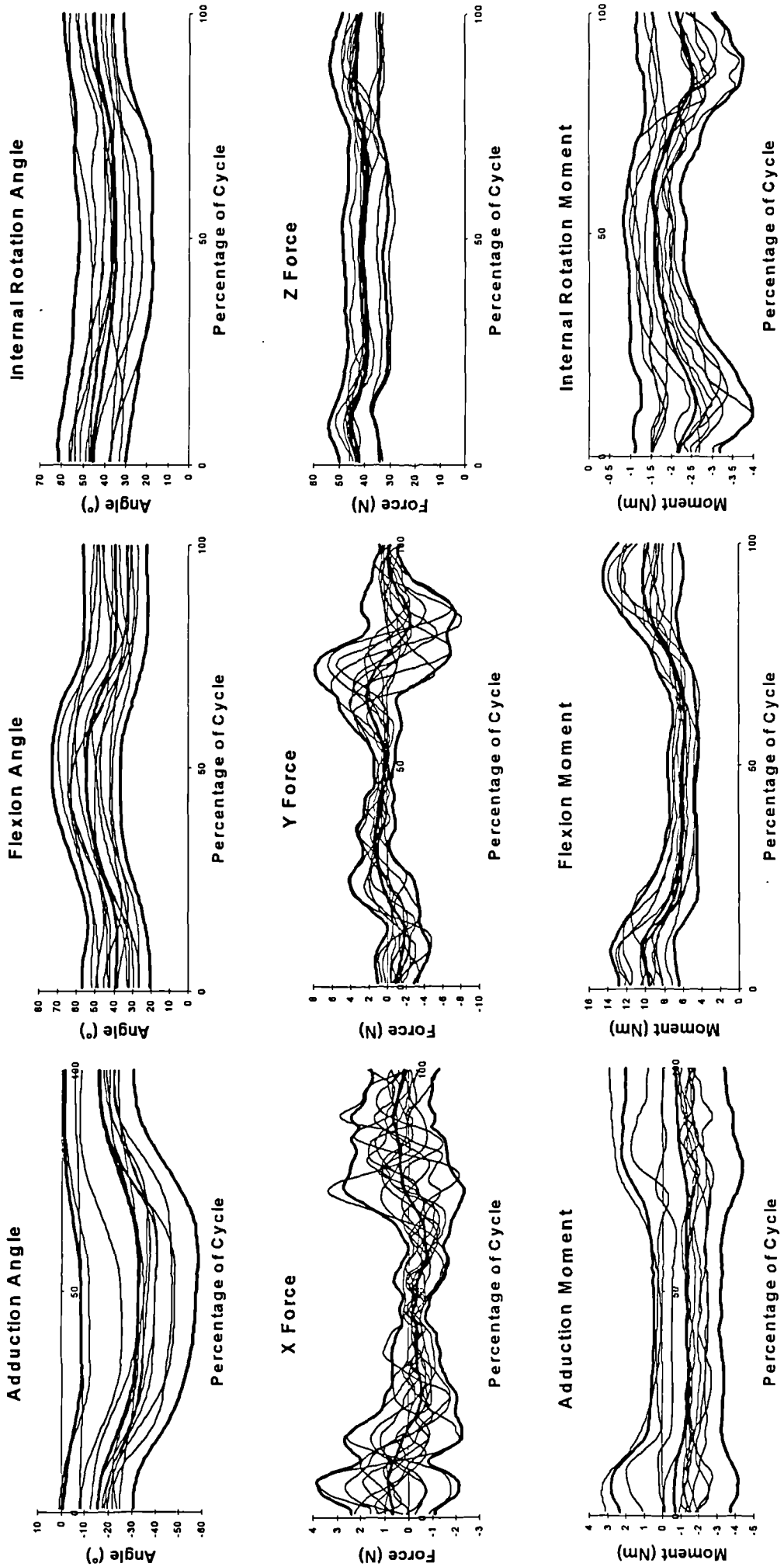

Fig.A.8.44 Angle, Force and Moment graphs for the Shoulder during performance of Activity 6, showing mean +/- 2SD in bold.

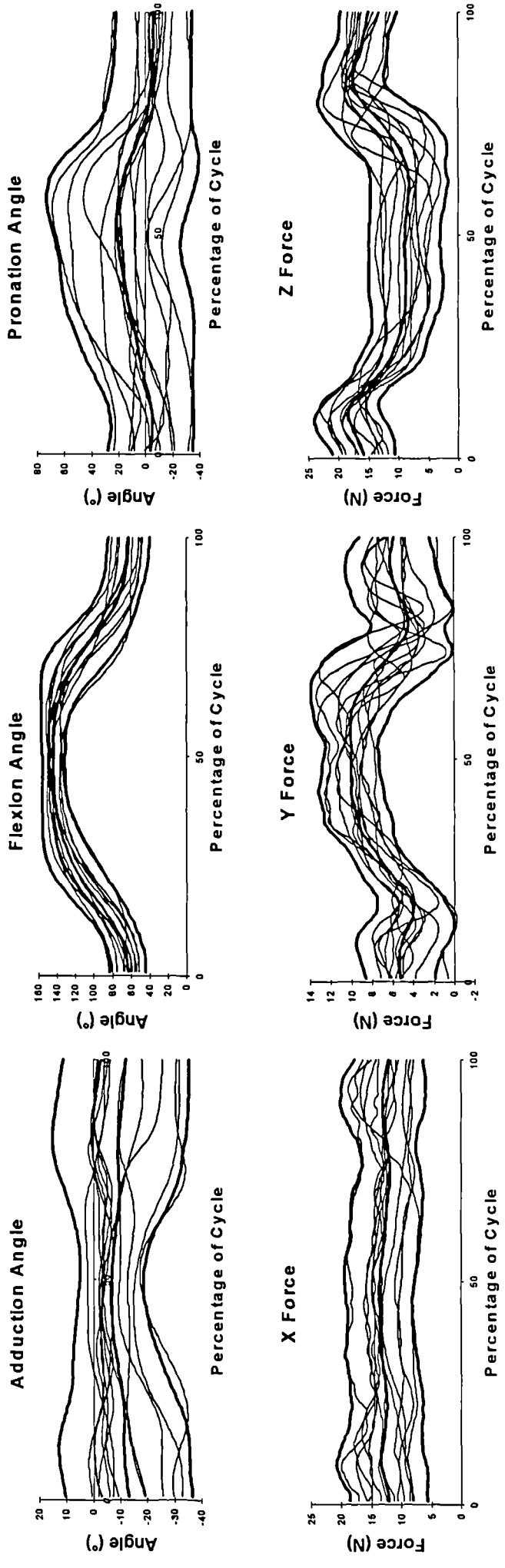

Fig.A.8.45 Angle, Force and Moment graphs for the Elbow during performance of Activity 6, showing mean +/- 2SD in bold.

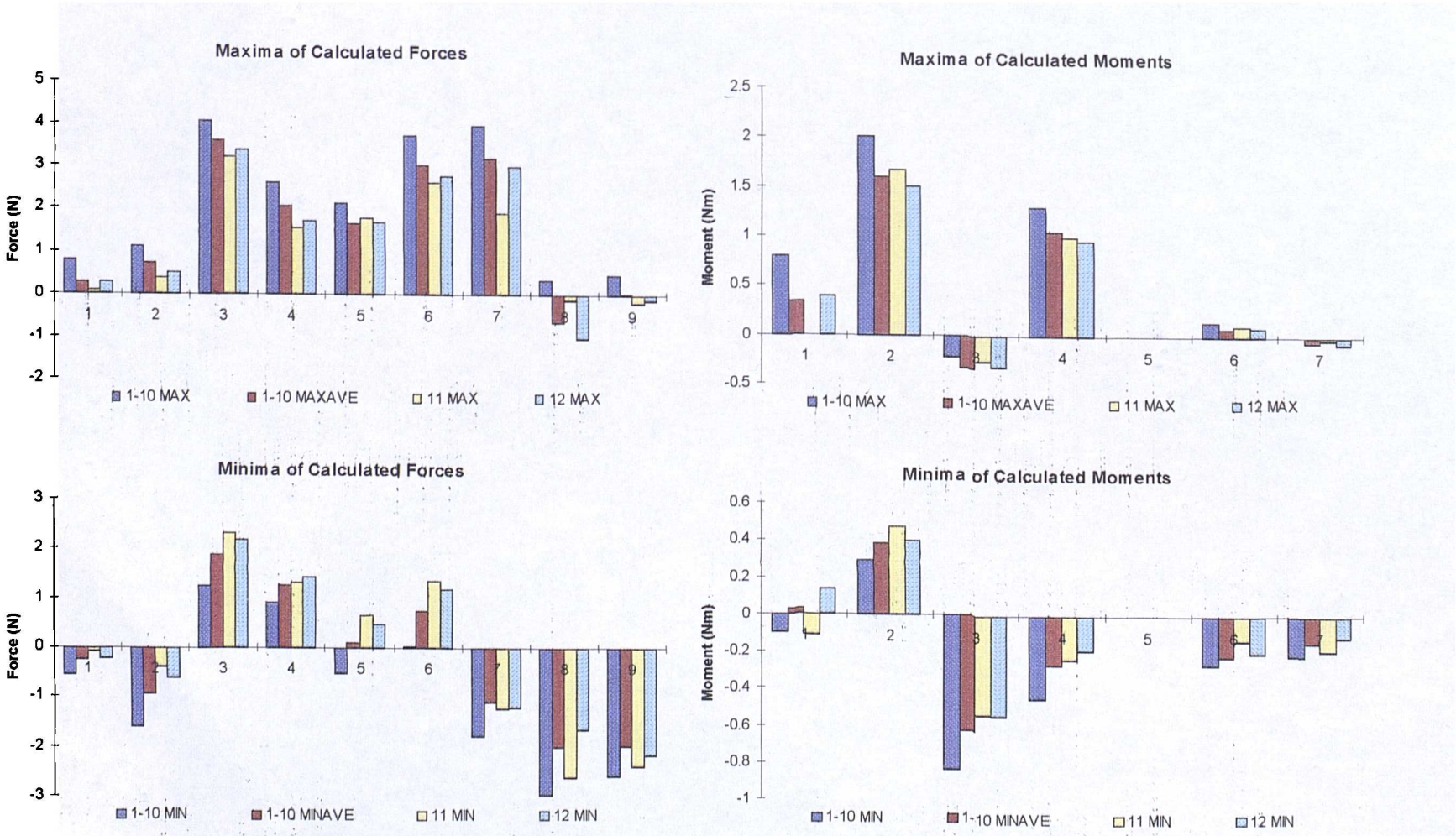

Fig.A.8.47 Unimpaired global maximum (1-10 Max), global minimum (1-10 Min), mean maximum (1-10 Maxave) and mean minimum (1-10 Minave) Force and Moment values due to hand load, along with impaired maximum (11 Max, 12 Max) and minimum (11 Min, 12 Min), during performance of Activity 6. Key as in Table 8.12.

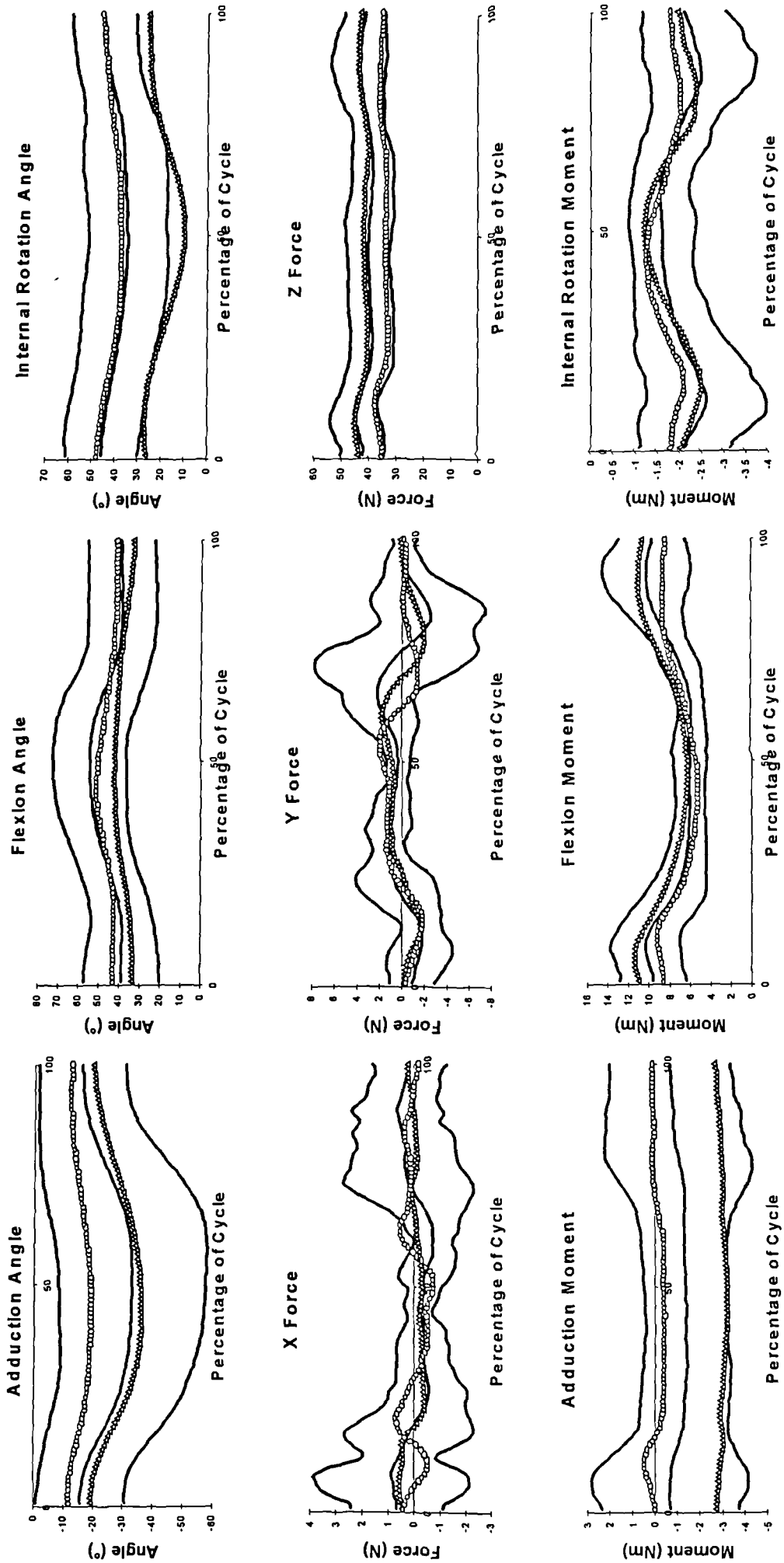

Fig.A.8.48 Comparison of impaired with unimpaired graphs for the Shoulder during performance of Activity 6. (Δ - Subject 11, o - Subject 12)

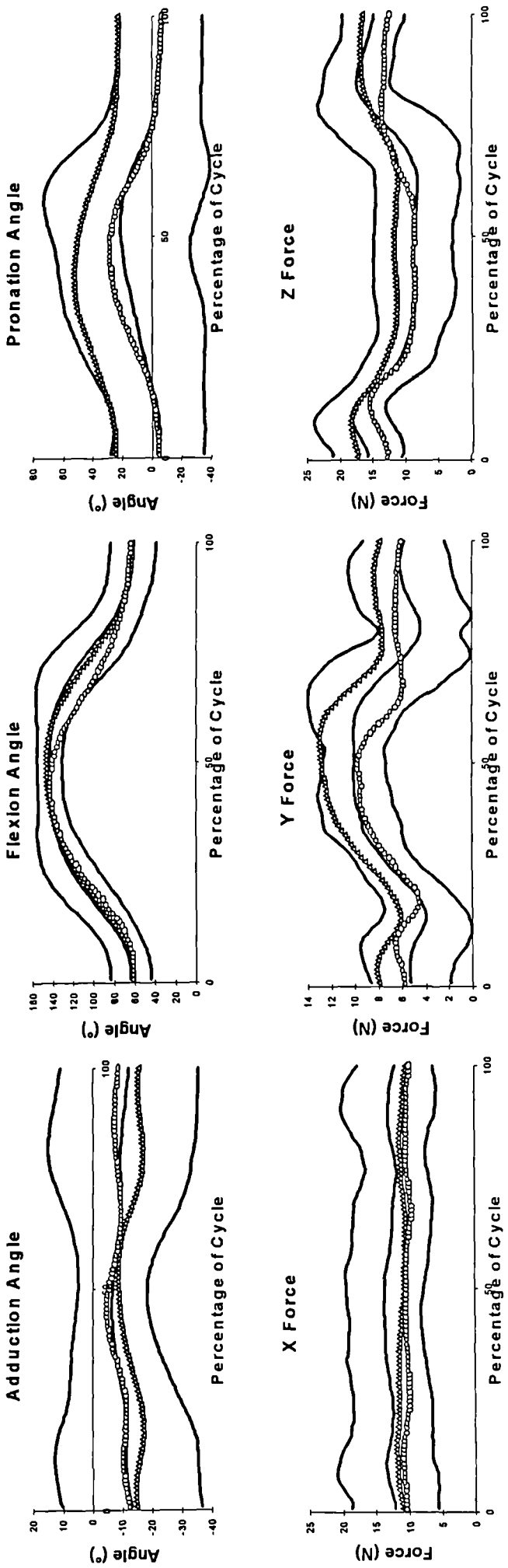

Fig.A.8.49 Comparison of impaired with unimpaired graphs for the Elbow during performance of Activity 6. (Δ - Subject 11, o - Subject 12)

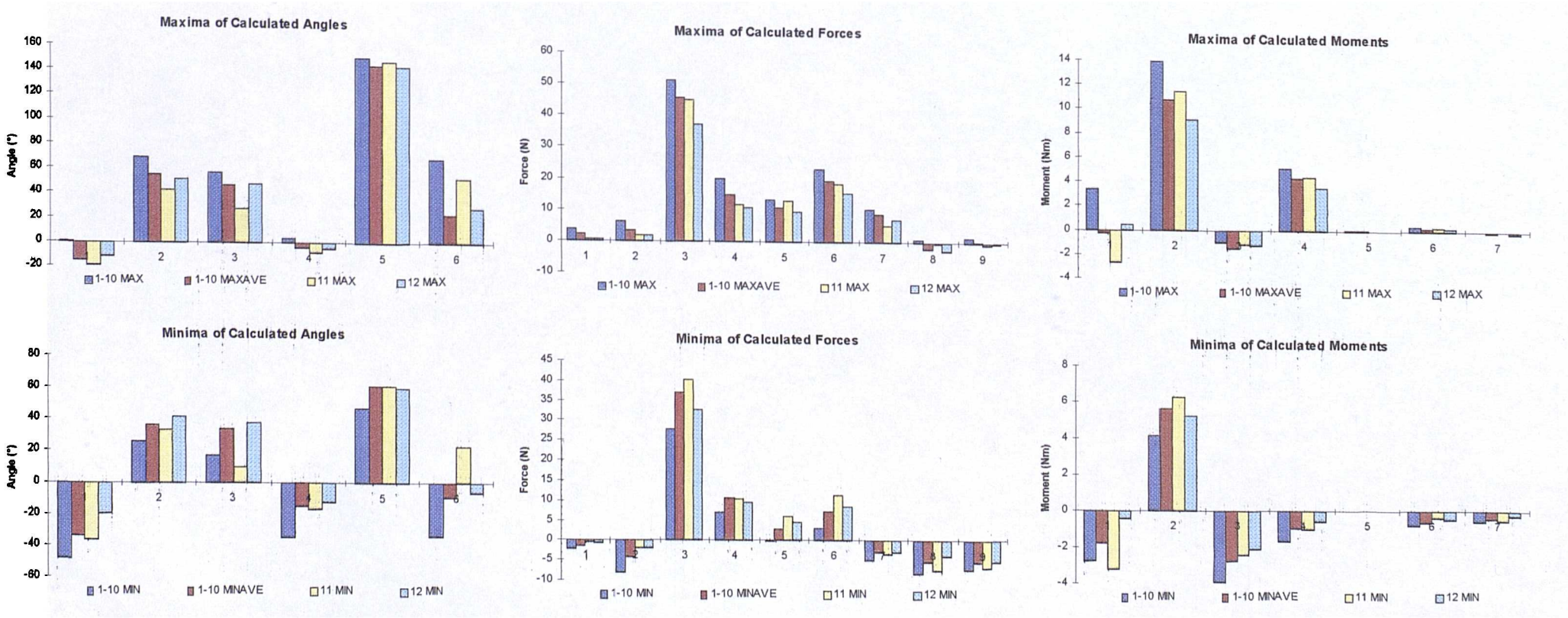

Fig.A.8.50 Unimpaired global maximum (1-10 Max), global minimum (1-10 Min), mean maximum (1-10 Maxave) and mean minimum (1-10 Minave) Angle, Force and Moment values, along with impaired maximum (11 Max, 12 Max) and minimum (11 Min, 12 Min) during performance of Activity 6. Key as in Table 8.12.

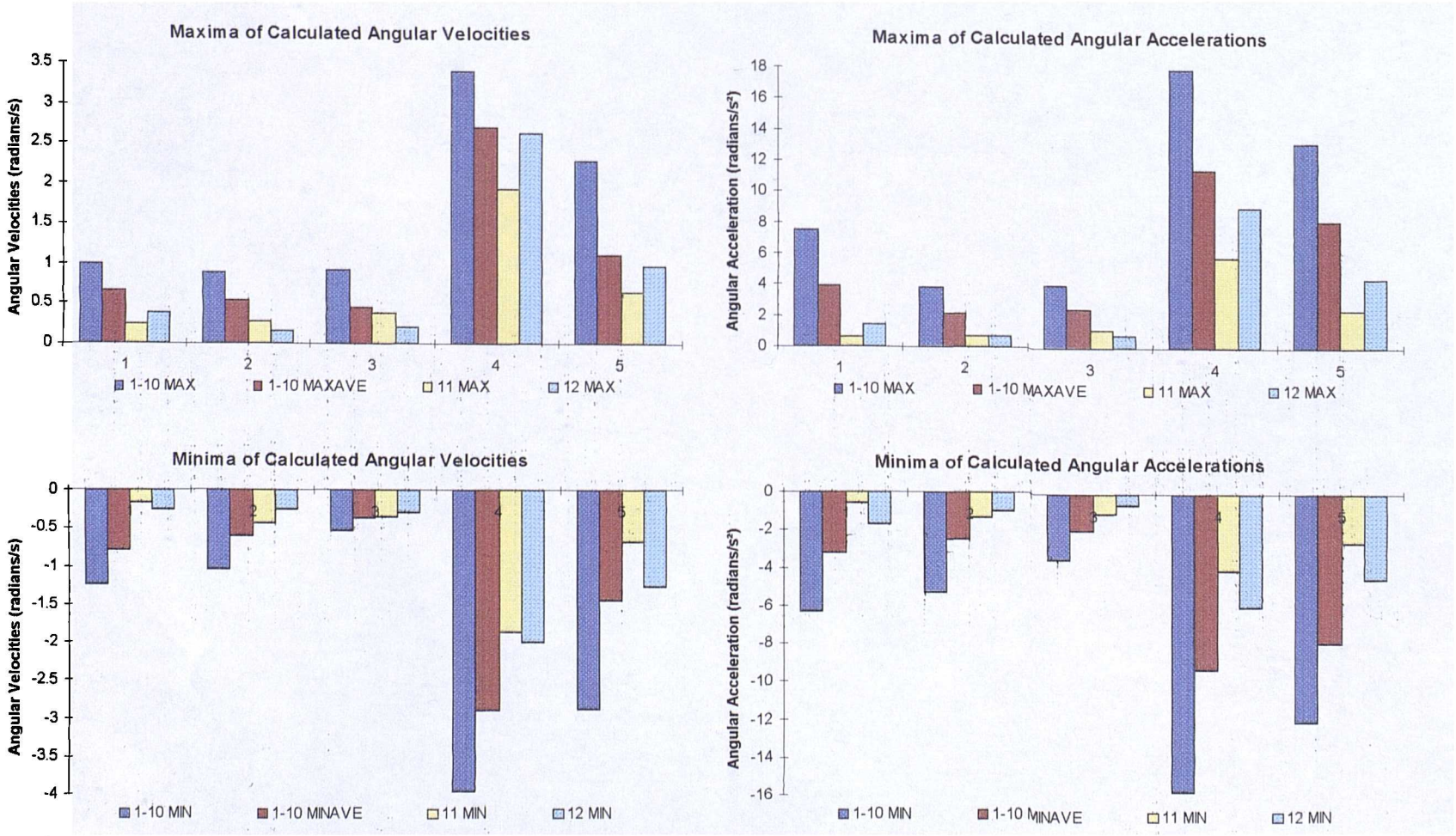

Fig.A.8.51 Unimpaired global maximum (1-10 Max), global minimum (1-10 Min), mean maximum (1-10 Maxave) and mean minimum (1-10 Minave) Angular Velocity and Acceleration, along with impaired maximum (11 Max, 12 Max) and minimum (11 Min, 12 Min) during performance of Activity 6. Key as in Table 8.13.

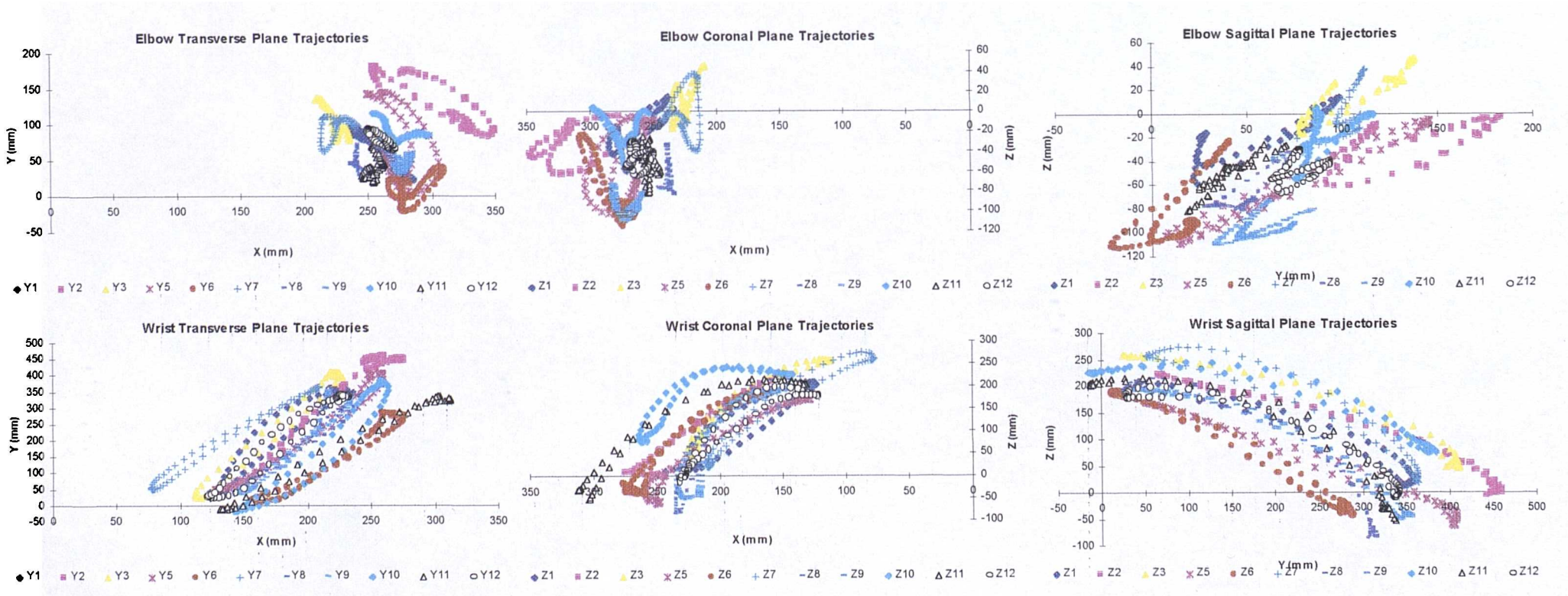

Fig.A.8.53 Trajectories of Elbow and Wrist in the Trunk Frame during performance of Activity 7.

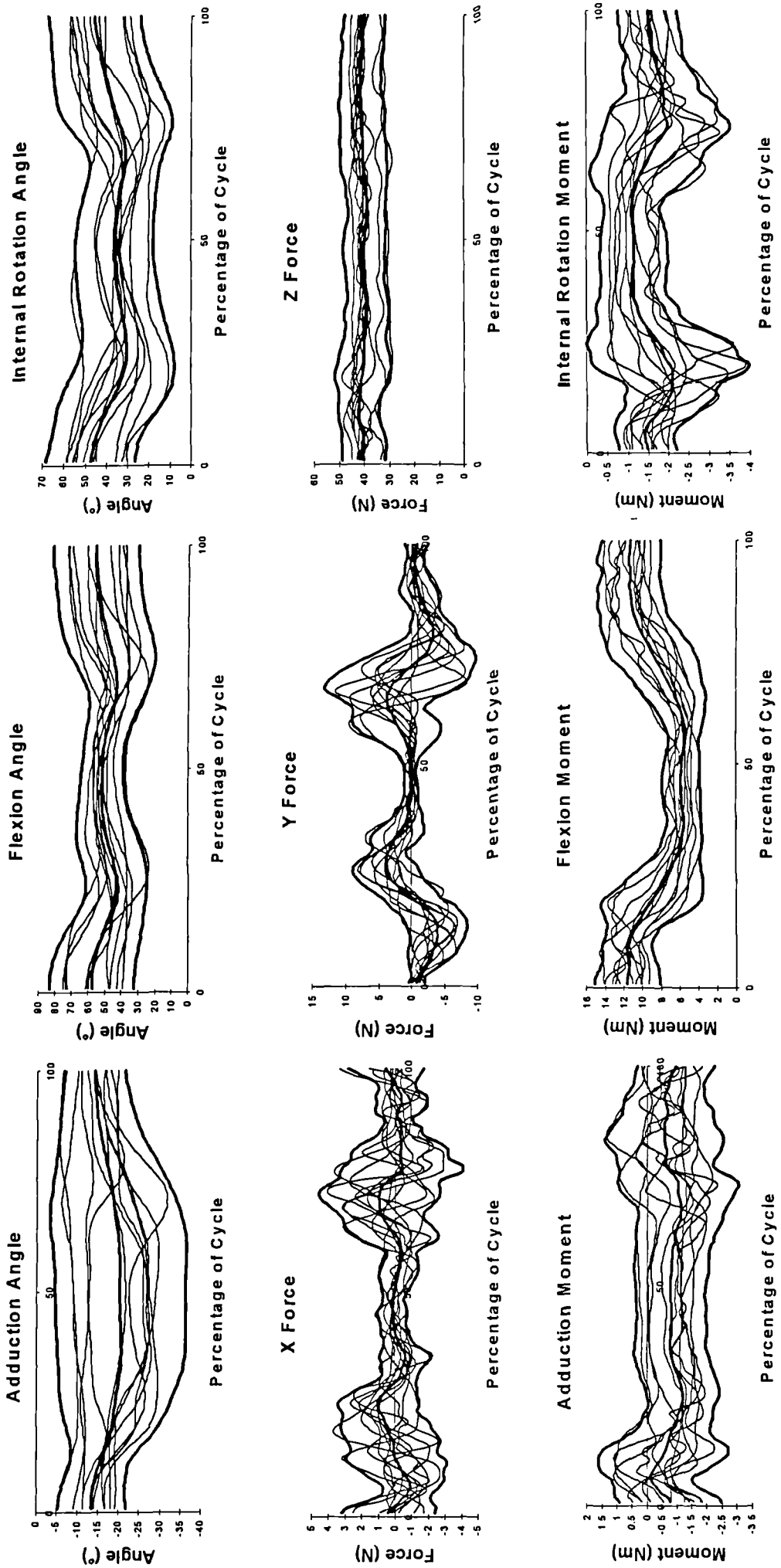

Fig.A.8.54 Angle, Force and Moment graphs for the Shoulder during performance of Activity 7, showing mean +/- 2SD in bold.

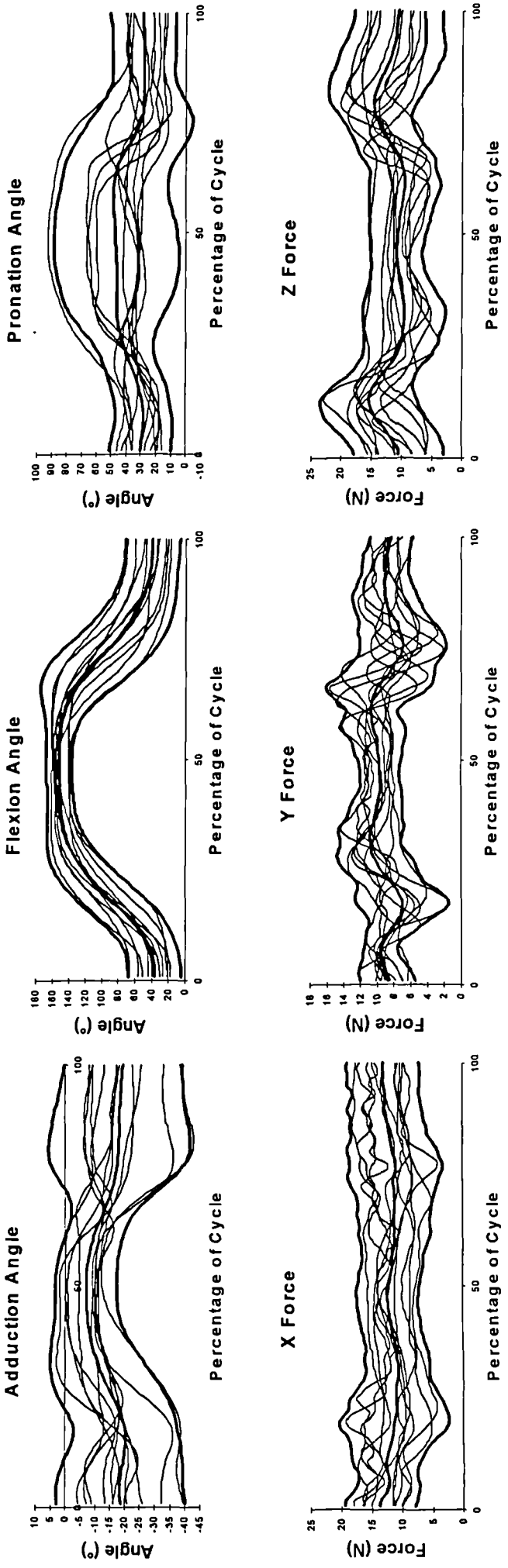

Fig.A.8.55 Angle, Force and Moment graphs for the Elbow during performance of Activity 7, showing mean +/- 2SD in bold.

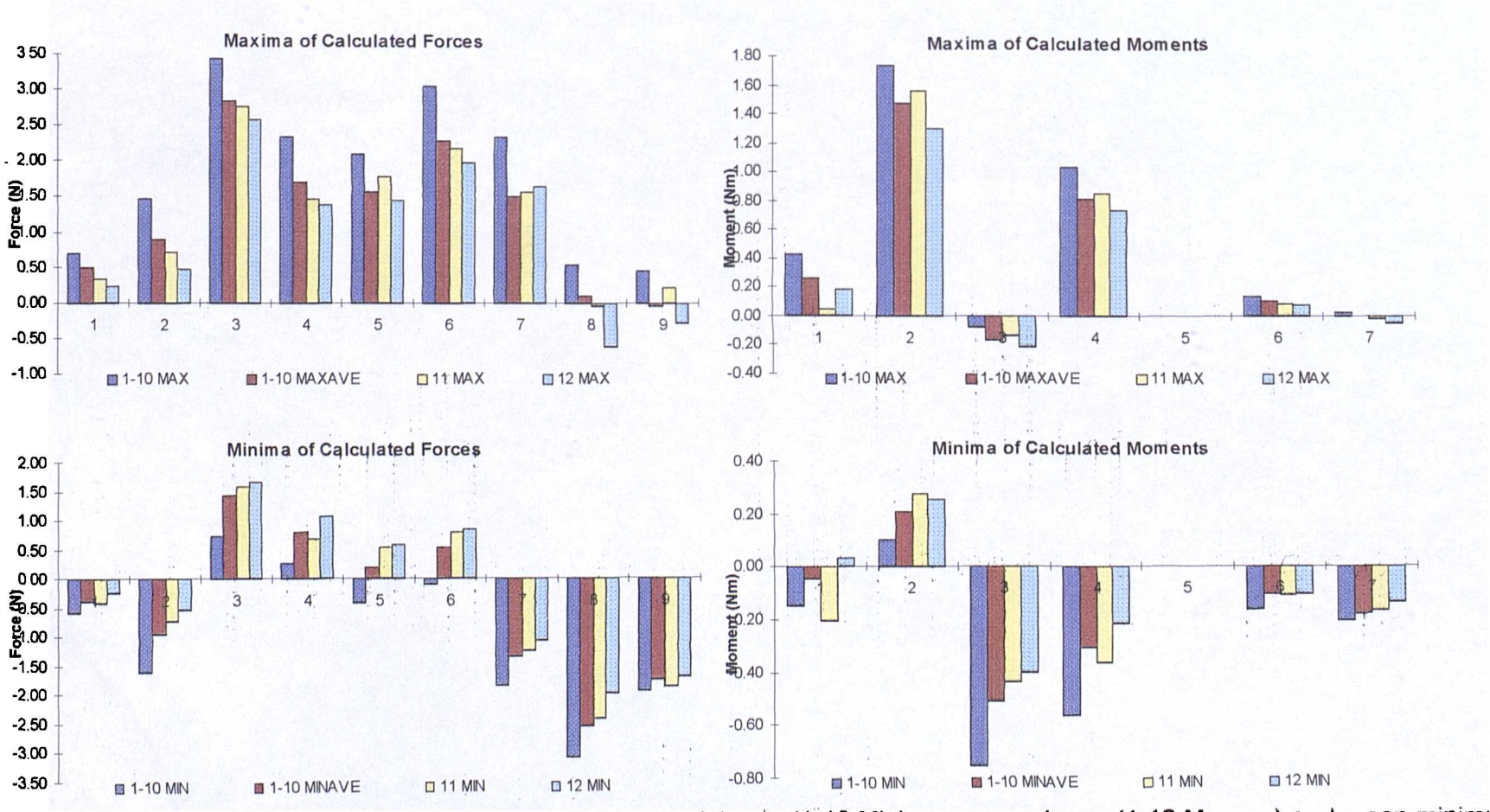

Fig.A.8.57 Unimpaired global maximum (1-10 Max), global minimum (1-10 Min), mean maximum (1-10 Maxave) and mean minimum (1-10 Minave) Force and Moment values due to hand load, along with impaired maximum (11 Max, 12 Max) and minimum (11 Min, 12 Min), during performance of Activity 7. Key as in Table 8.12.

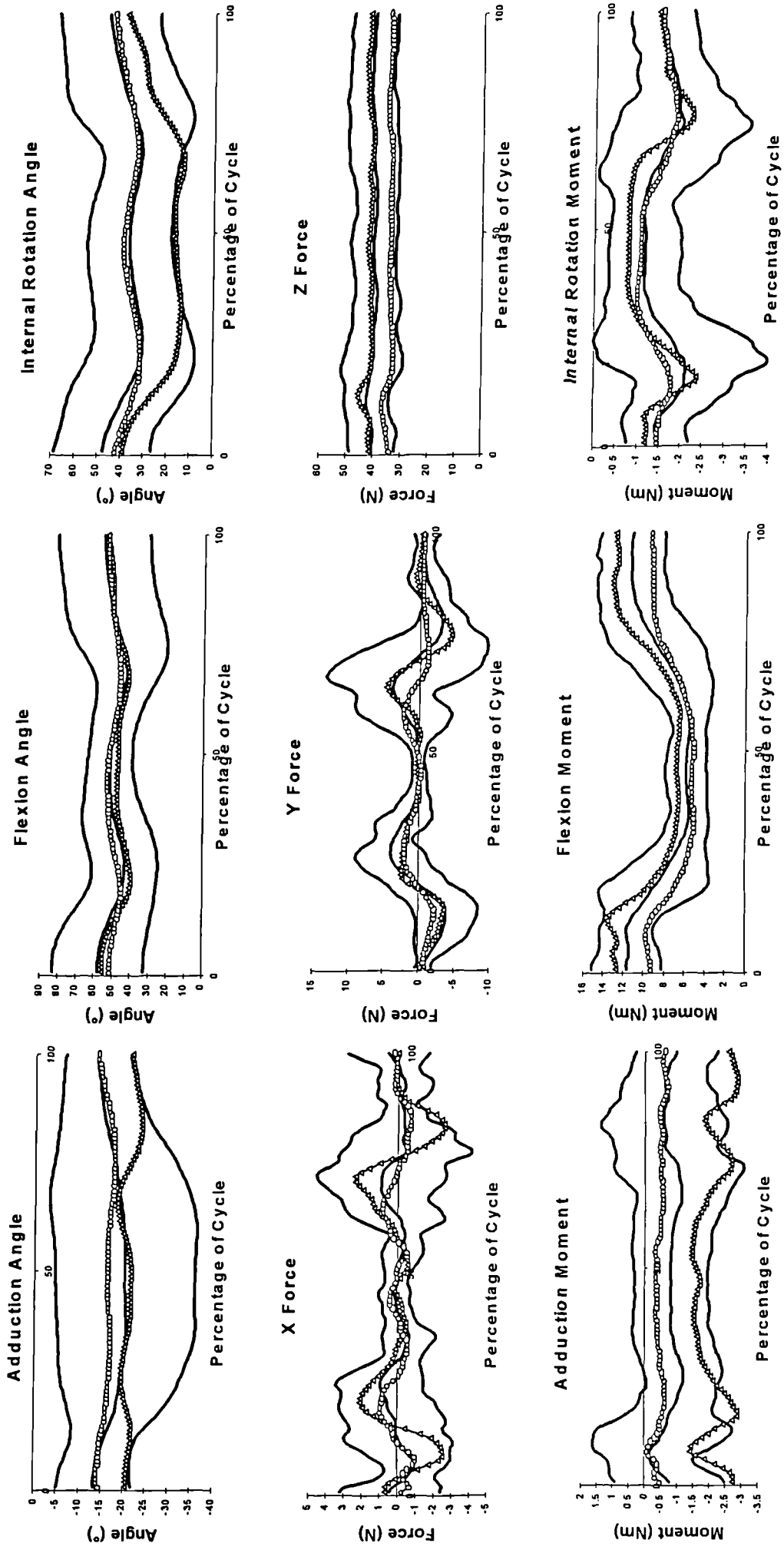

Fig.A.8.58 Comparison of impaired with unimpaired graphs for the Shoulder during performance of Activity 7. (Δ - Subject 11, o - Subject 12)

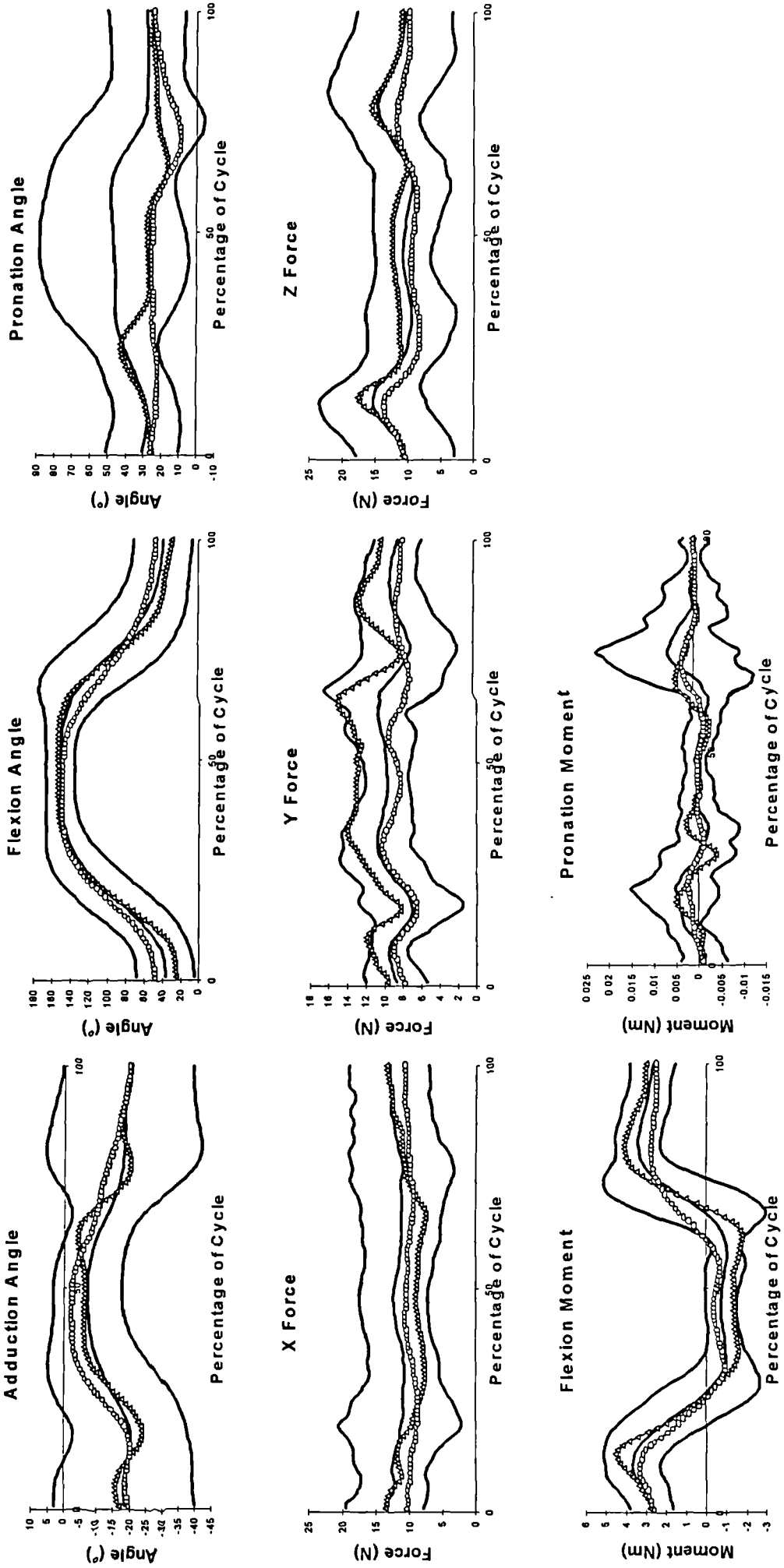

Fig.A.8.59 Comparison of impaired with unimpaired graphs for the Elbow during performance of Activity 7. (Δ - Subject 11, o - Subject 12)

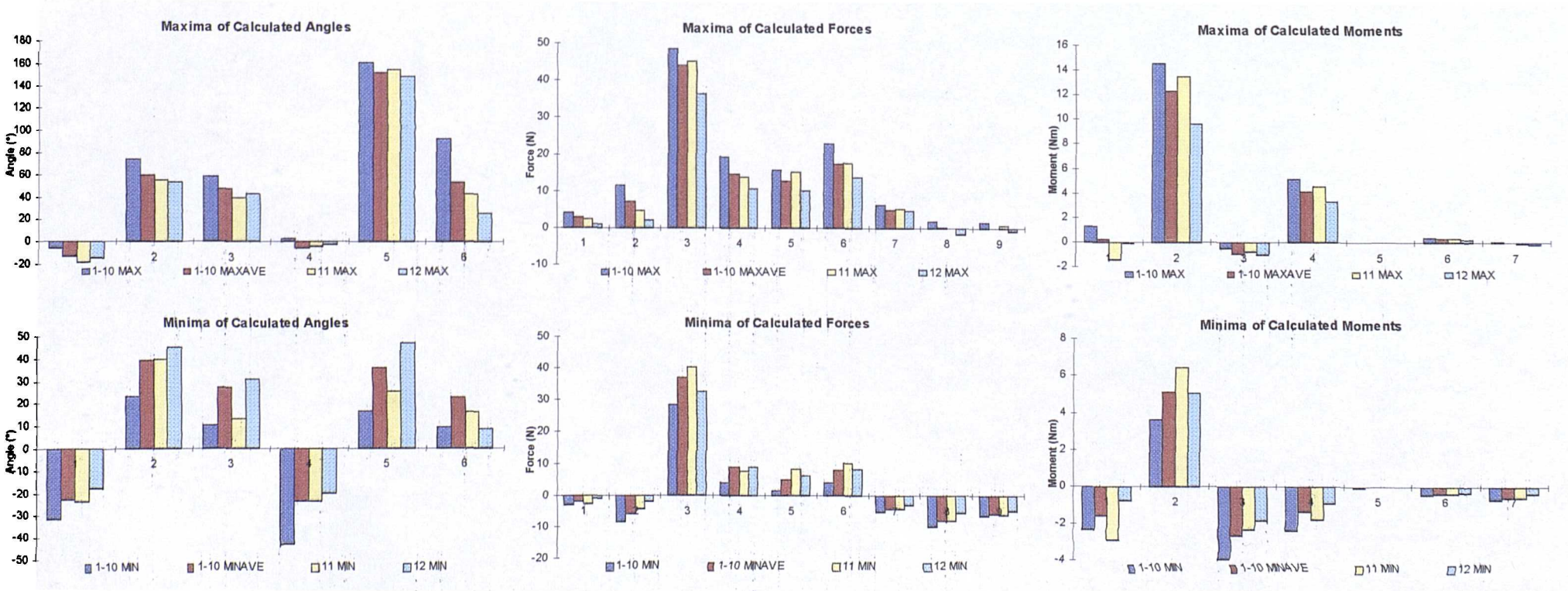

Fig.A.8.60 Unimpaired global maximum (1-10 Max), global minimum (1-10 Min), mean maximum (1-10 Maxave) and mean minimum (1-10 Minave) Angle, Force and Moment values, along with impaired maximum (11 Max, 12 Max) and minimum (11 Min, 12 Min) during performance of Activity 7. Key as in Table 8.12.

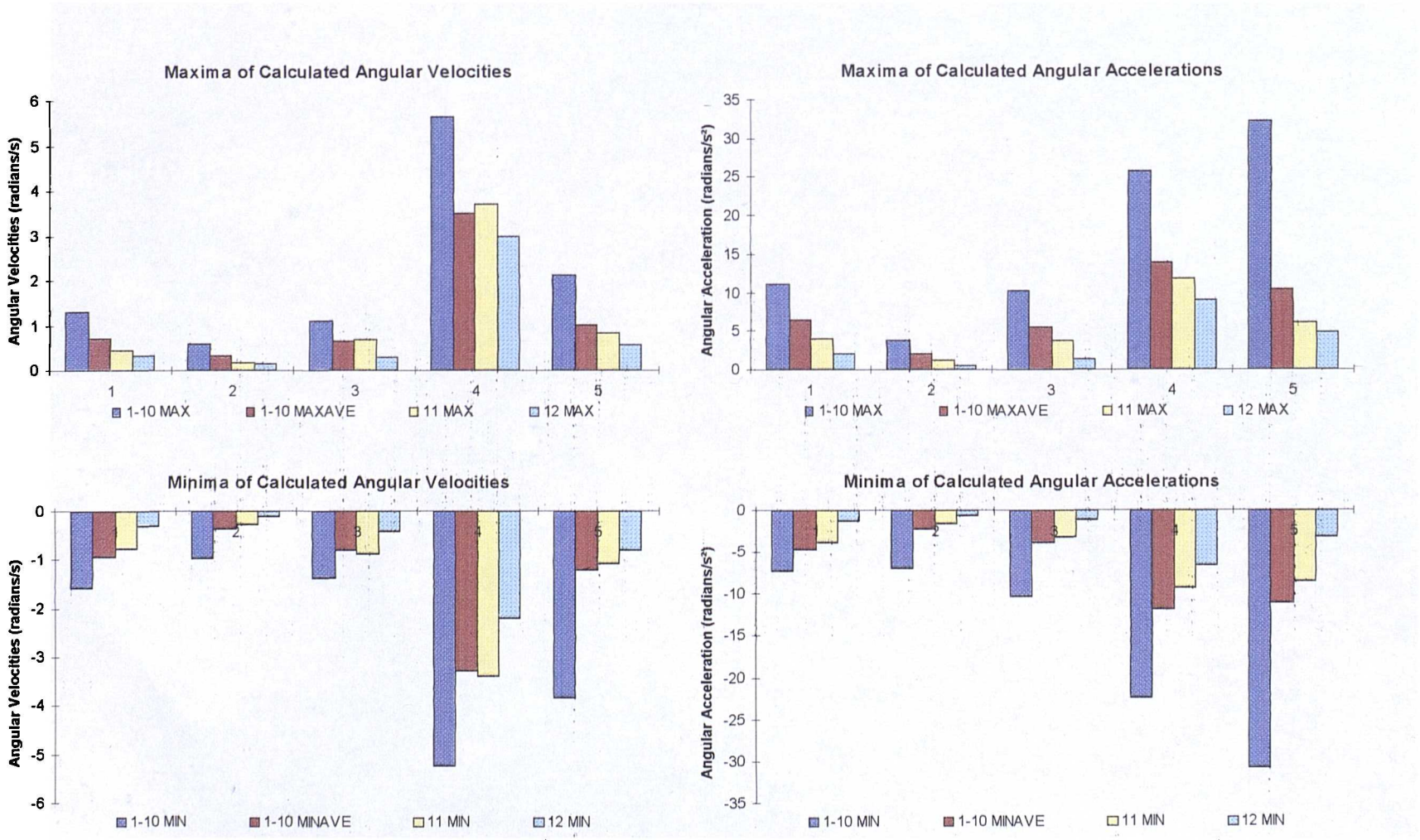

Fig.A.8.61 Unimpaired global maximum (1-10 Max), global minimum (1-10 Min), mean maximum (1-10 Maxave) and mean minimum (1-10 Minave) Angular Velocity and Acceleration, along with impaired maximum (11 Max, 12 Max) and minimum (11 Min, 12 Min) during performance of Activity 7. Key as in Table 8.13.

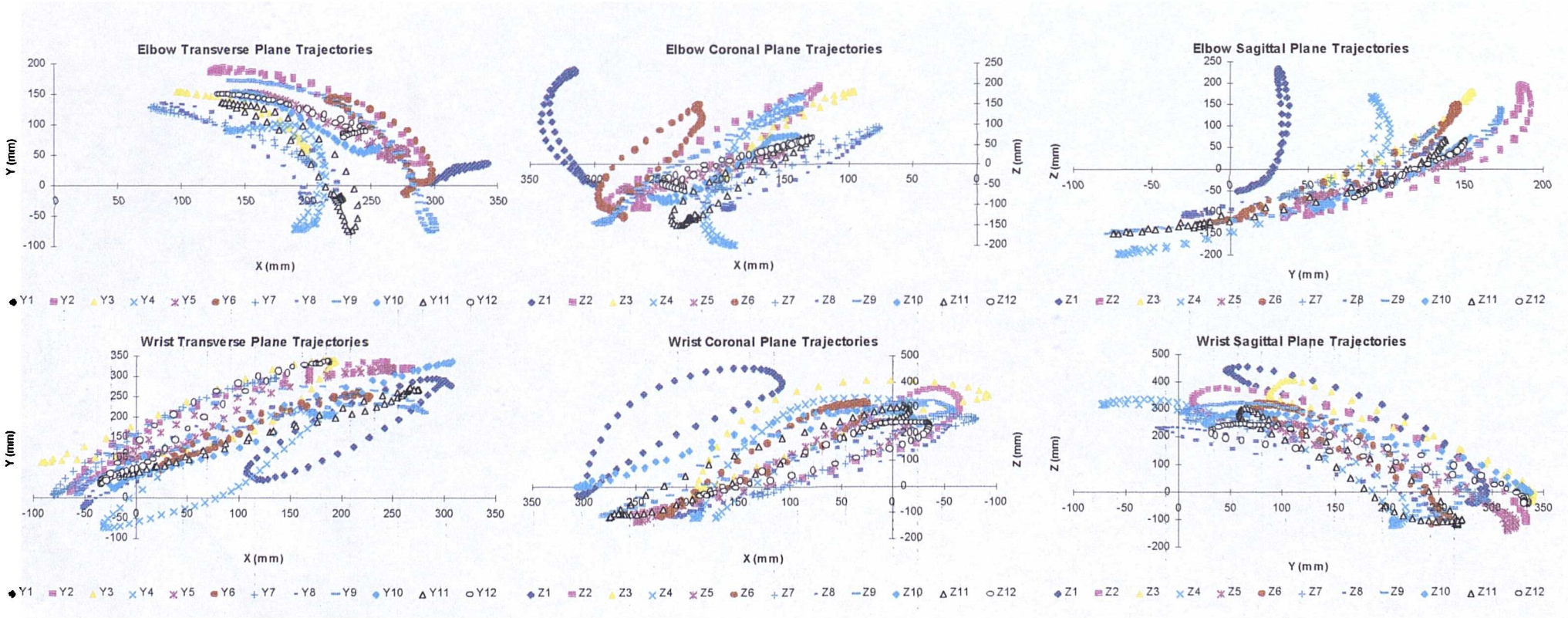

Fig.A.8.63 Trajectories of Elbow and Wrist in the Trunk Frame during performance of Activity 8.

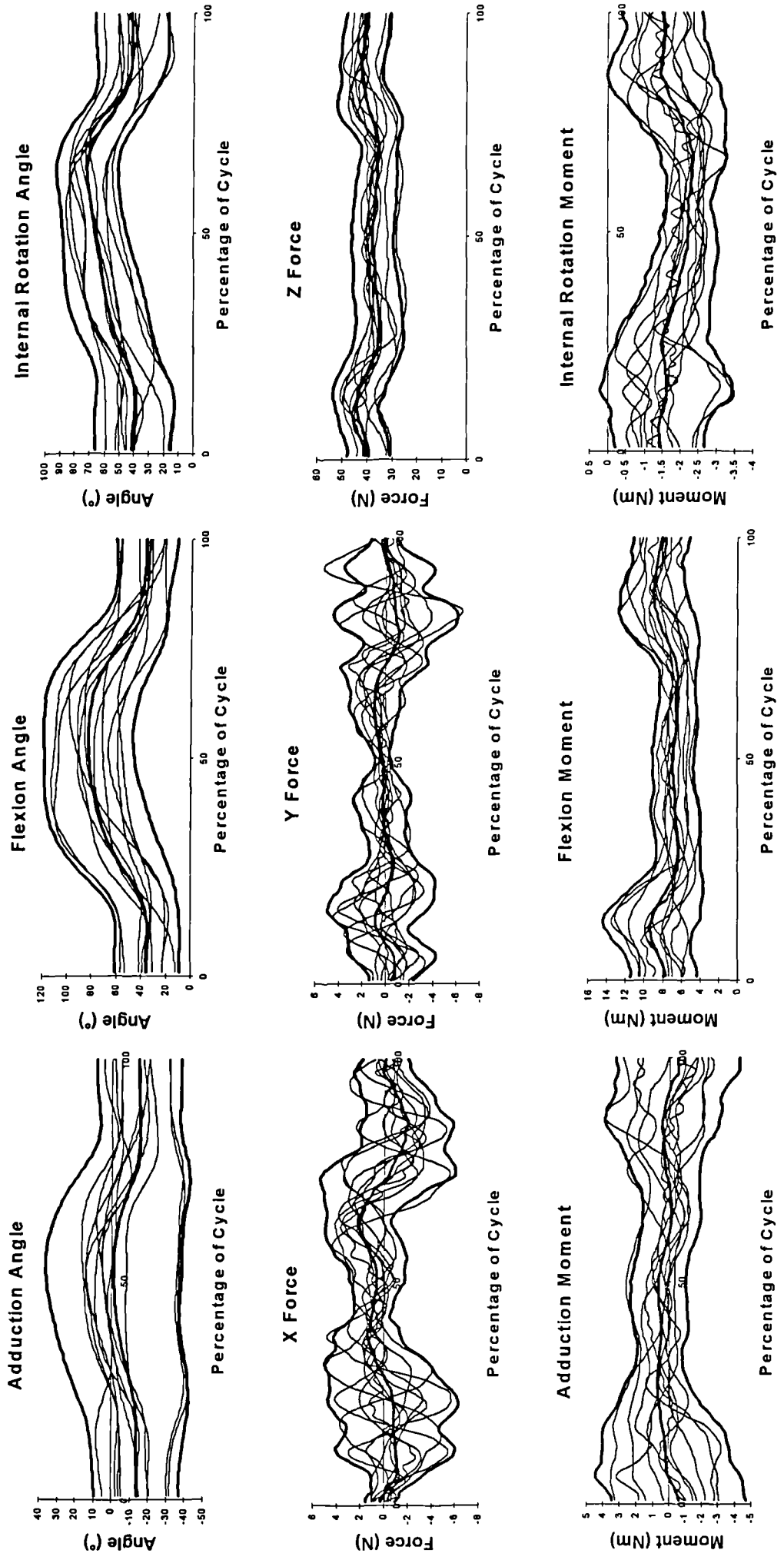

Fig.A.8.64 Angle, Force and Moment graphs for the Shoulder during performance of Activity 8, showing mean +/- 2SD in bold.

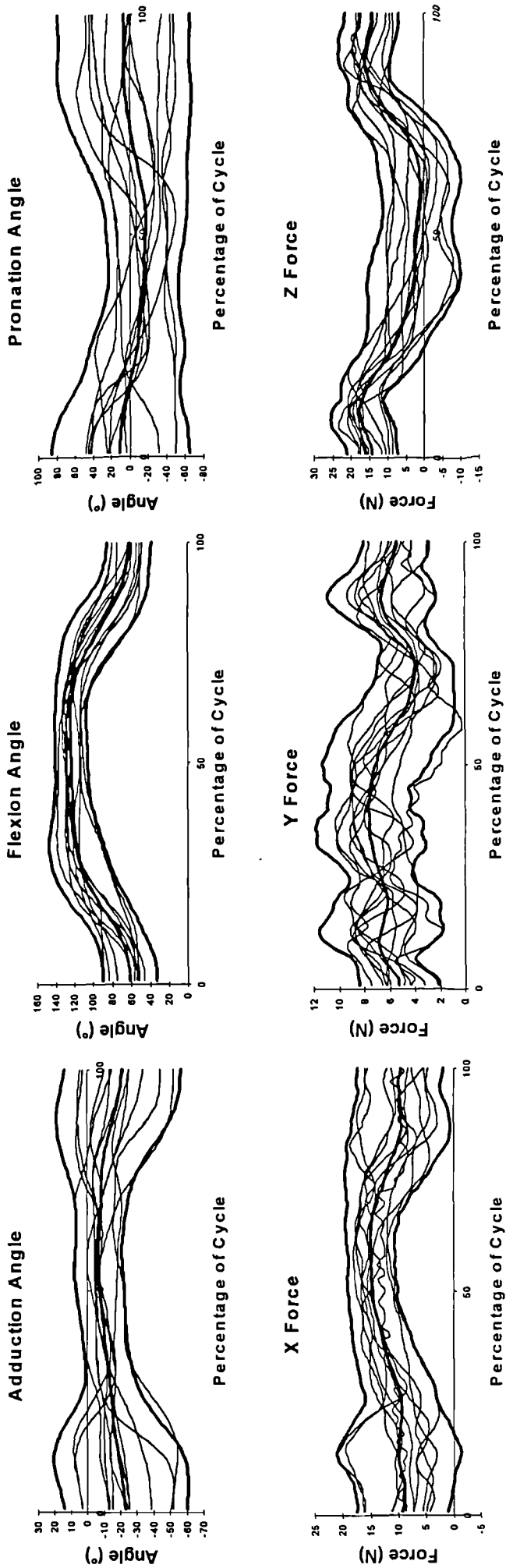

Fig.A.8.65 Angle, Force and Moment graphs for the Elbow during performance of Activity 8, showing mean +/- 2SD in bold.

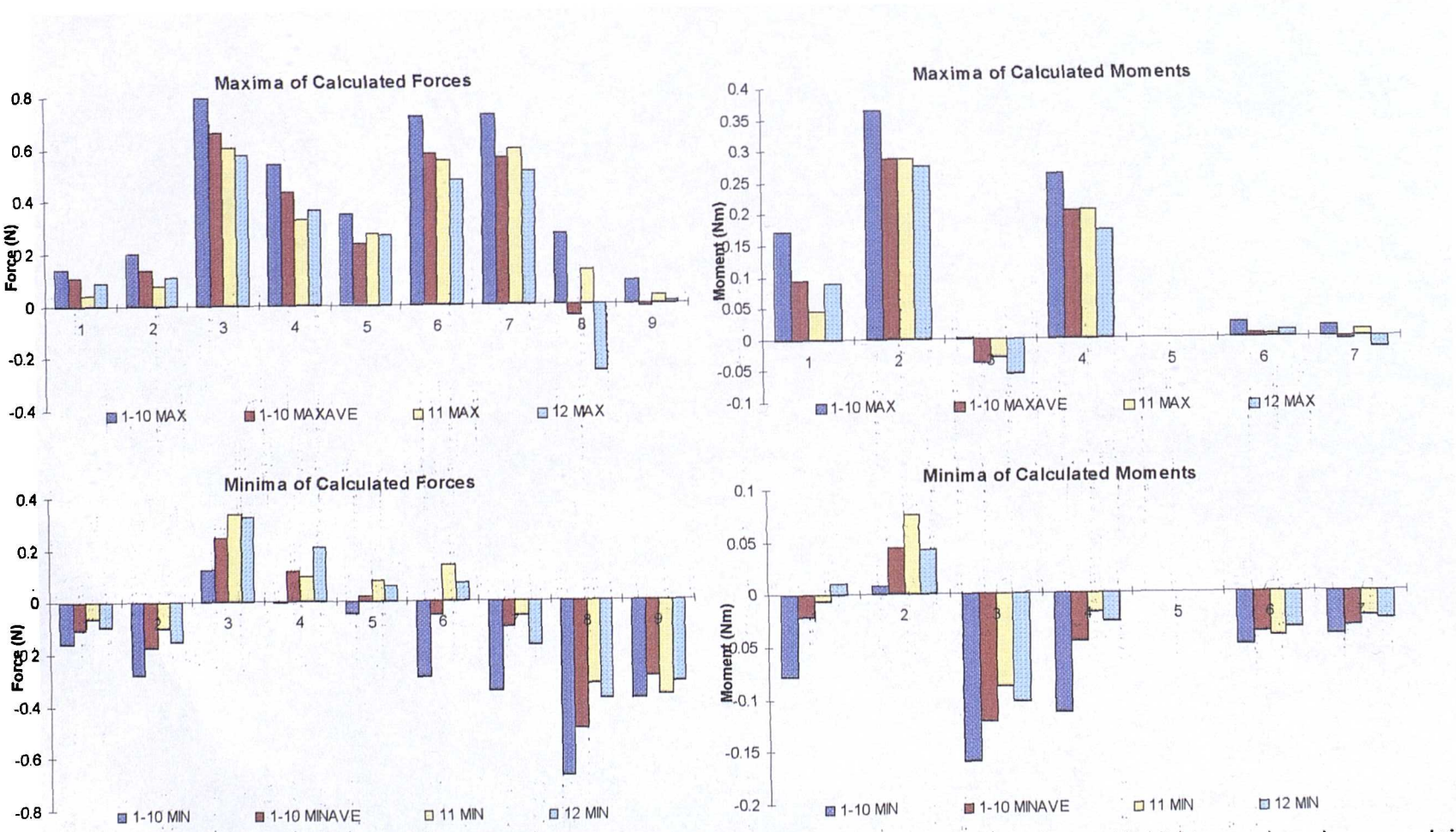

Fig.A.8.67 Unimpaired global maximum (1-10 Max), global minimum (1-10 Min), mean maximum (1-10 Maxave) and mean minimum (1-10 Minave) Force and Moment values due to hand load, along with impaired maximum (11 Max, 12 Max) and minimum (11 Min, 12 Min), during performance of Activity 8. Key as in Table 8.12.

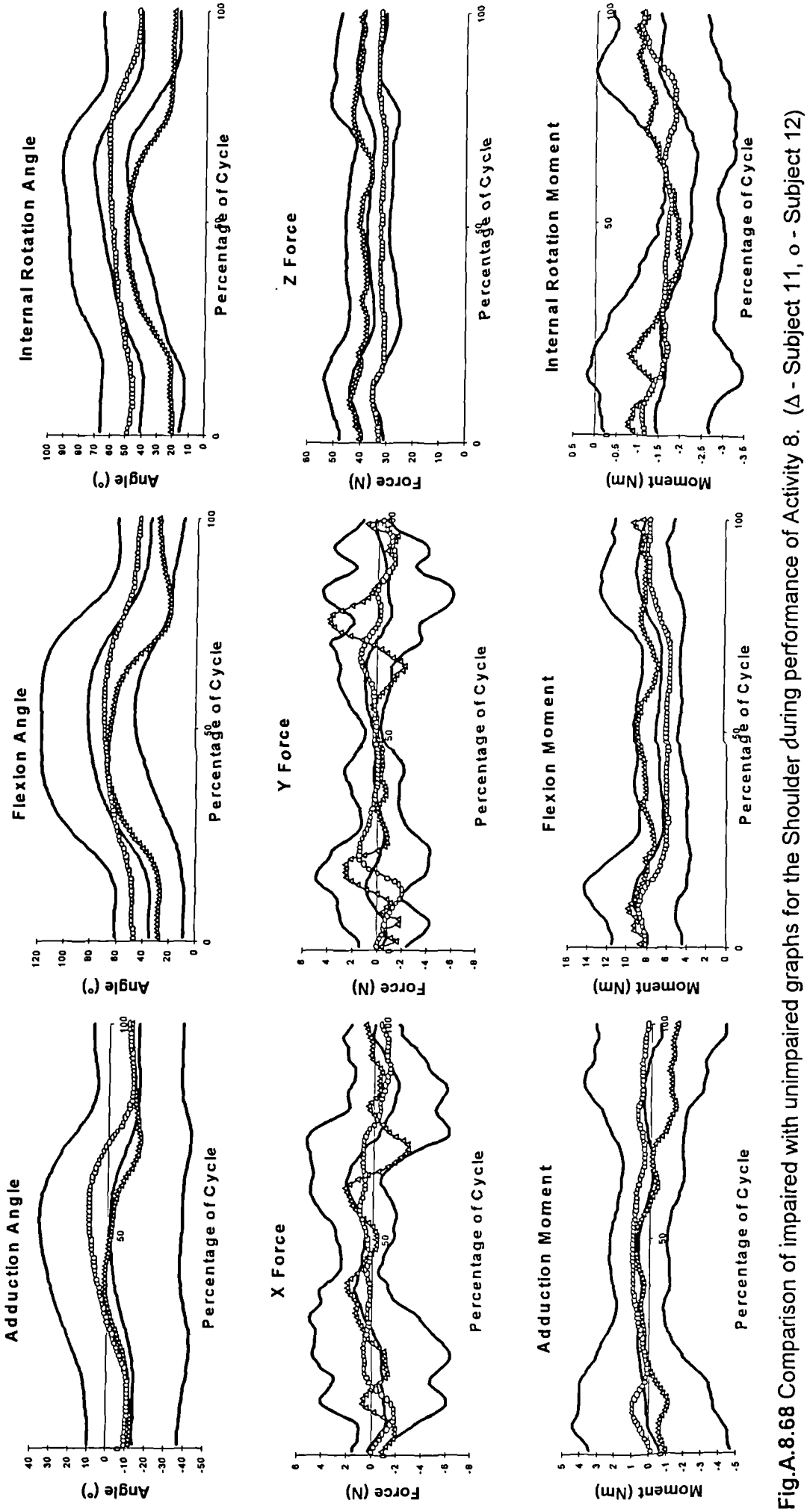

Fig.A.8.68 Comparison of impaired with unimpaired graphs for the Shoulder during performance of Activity 8. (Δ - Subject 11, o - Subject 12)

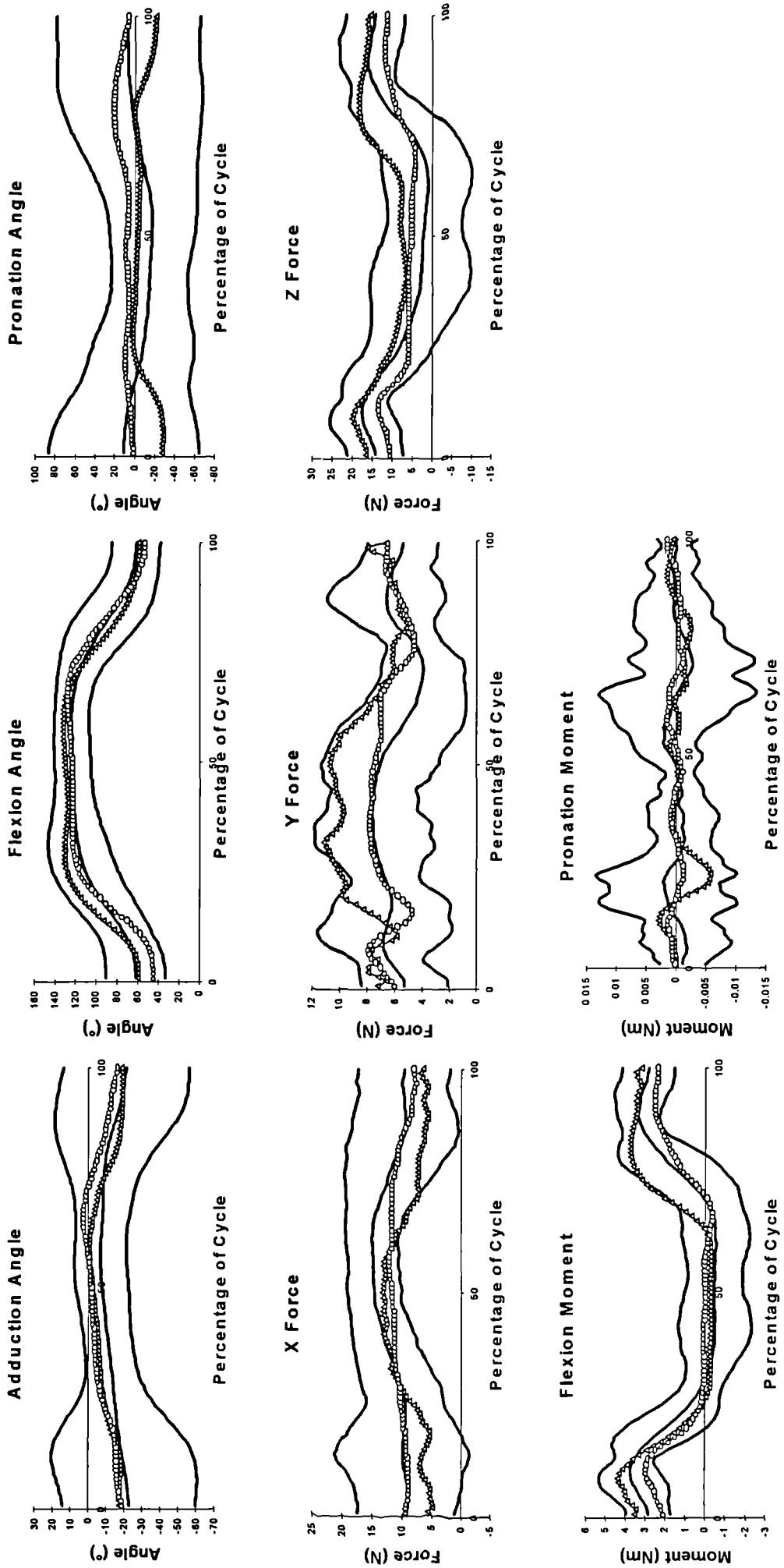

Fig.A.8.69 Comparison of impaired with unimpaired graphs for the Elbow during performance of Activity 8. (Δ - Subject 11, o - Subject 12)

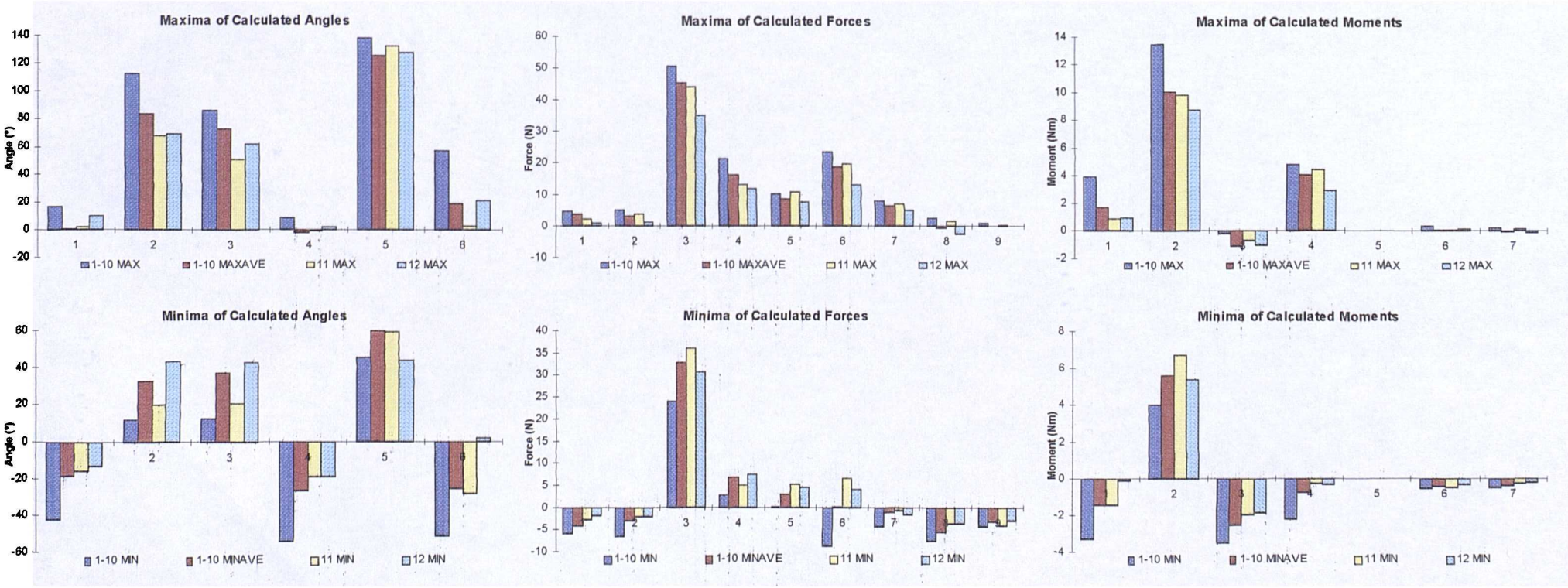

Fig.A.8.70 Unimpaired global maximum (1-10 Max), global minimum (1-10 Min), mean maximum (1-10 Maxave) and mean minimum (1-10 Minave) Angle, Force and Moment values, along with impaired maximum (11 Max, 12 Max) and minimum (11 Min, 12 Min) during performance of Activity 8. Key as in Table 8.12.

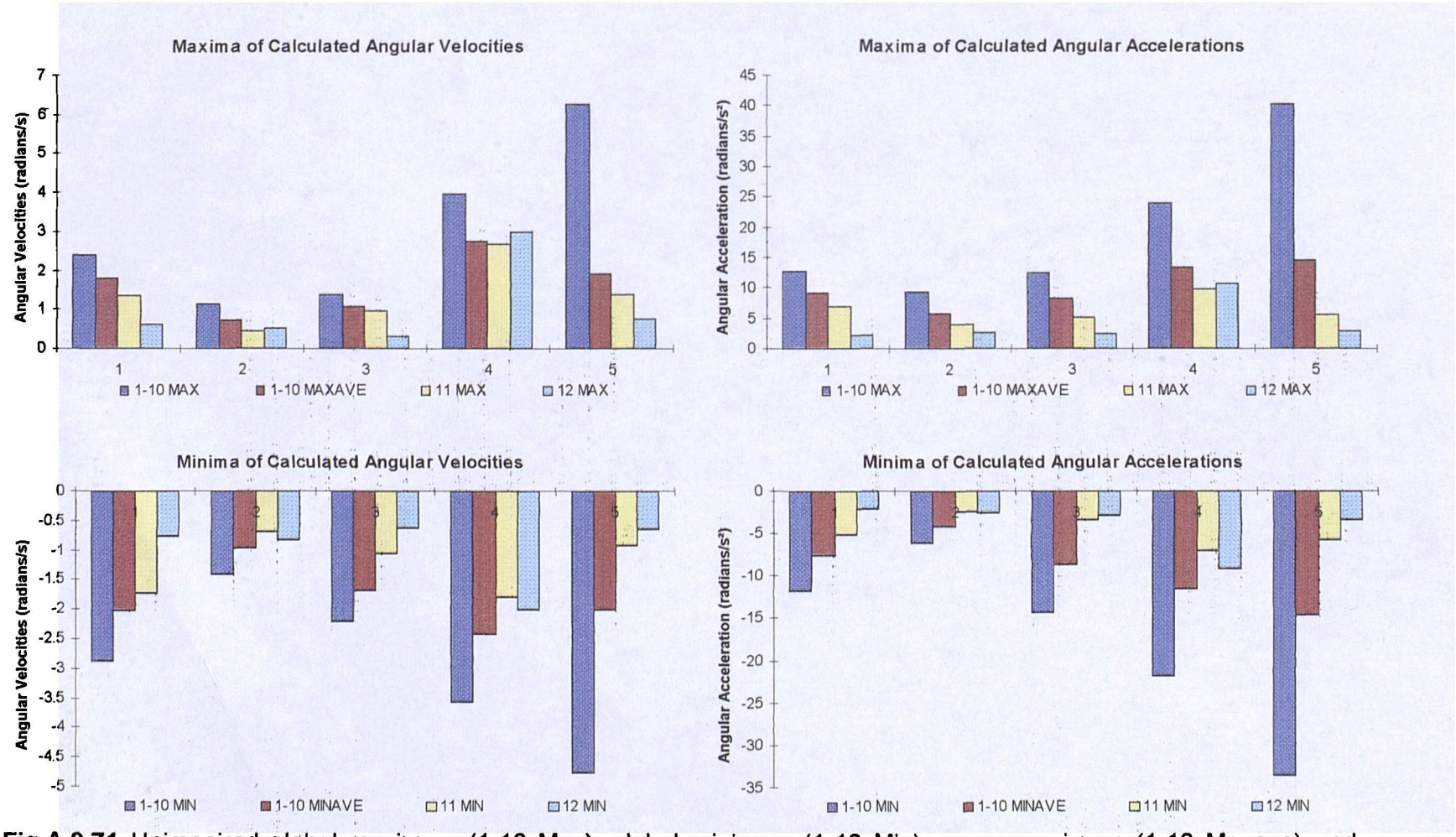

Fig.A.8.71 Unimpaired global maximum (1-10 Max), global minimum (1-10 Min), mean maximum (1-10 Maxave) and mean minimum (1-10 Minave) Angular Velocity and Acceleration, along with impaired maximum (11 Max, 12 Max) and minimum (11 Min, 12 Min) during performance of Activity 8. Key as in Table 8.13.

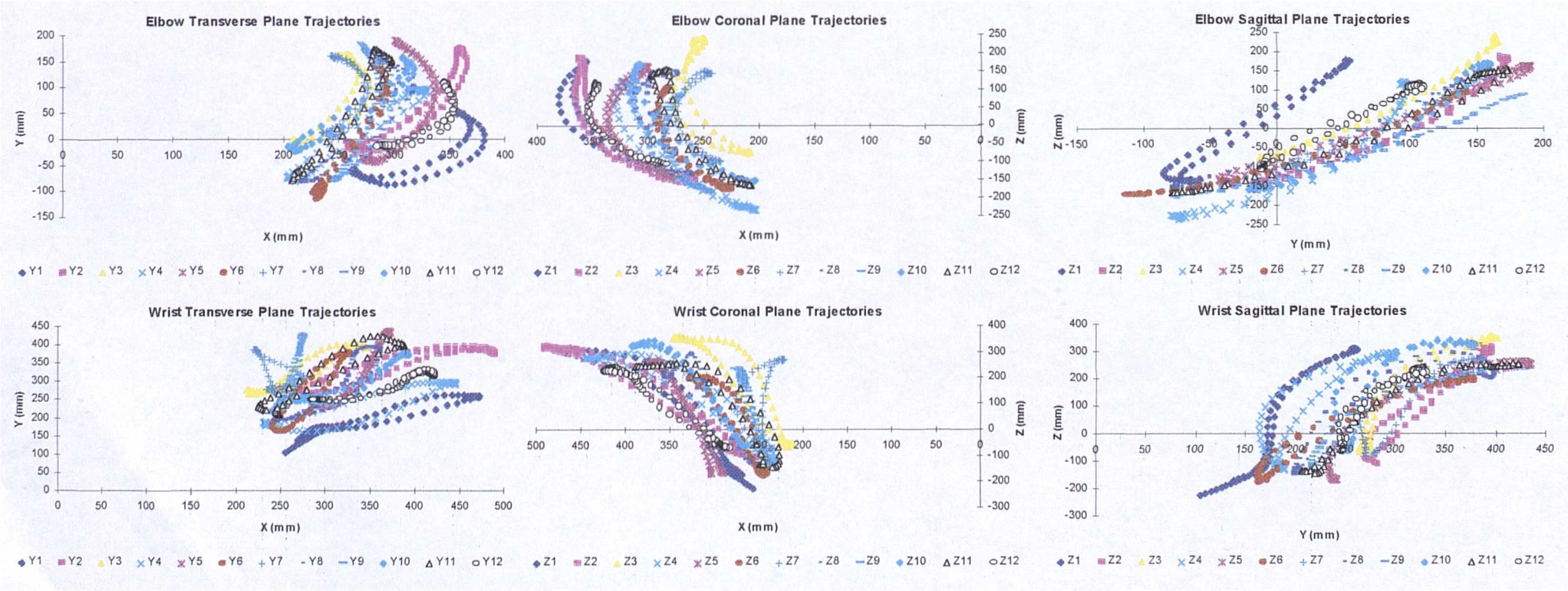

Fig.A.8.72 Trajectories of Elbow and Wrist in the Trunk Frame during performance of Activity 9.

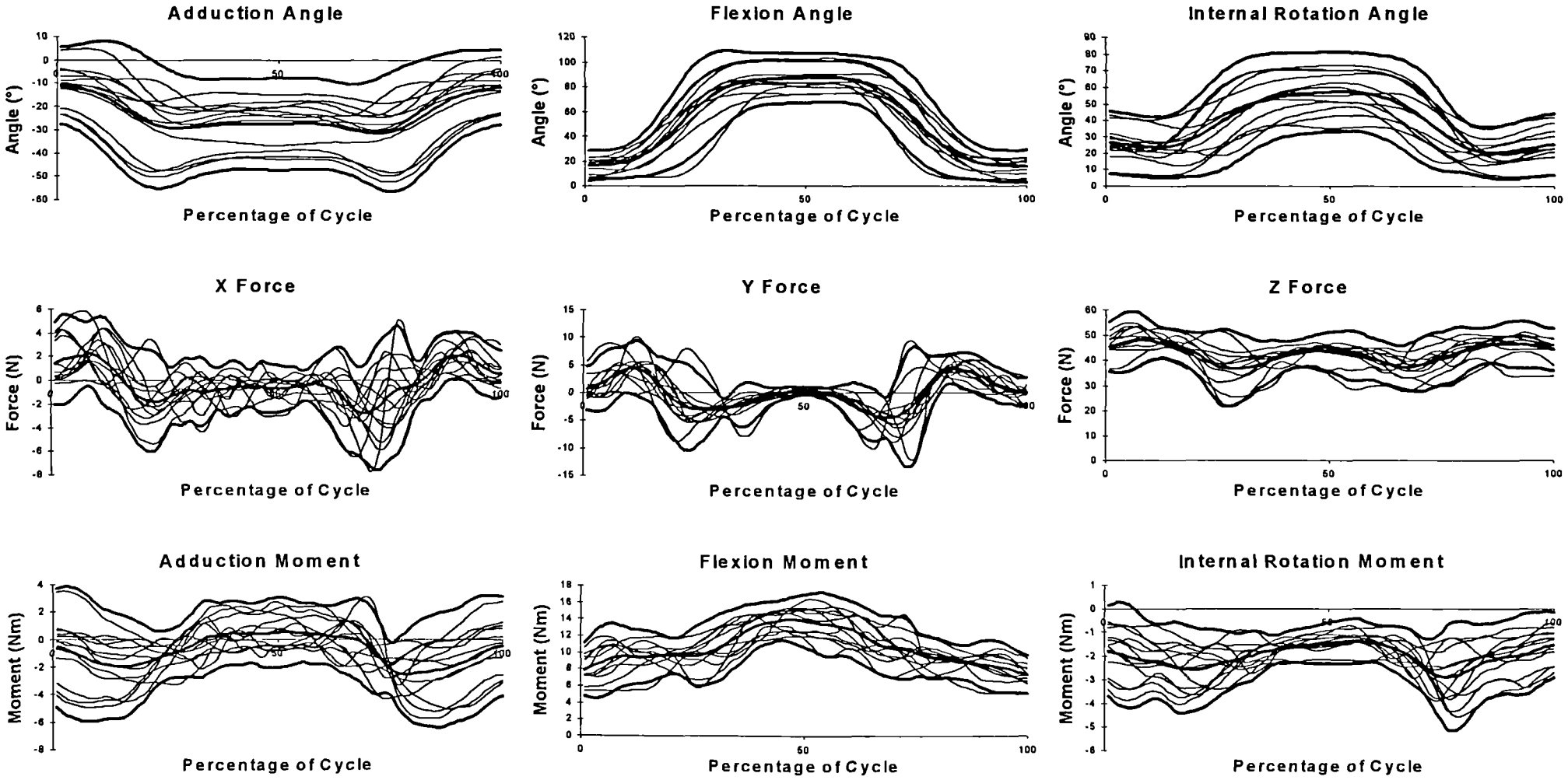

Fig.A.8.73 Angle, Force and Moment graphs for the Shoulder during performance of Activity 9, showing mean +/- 2SD in bold.

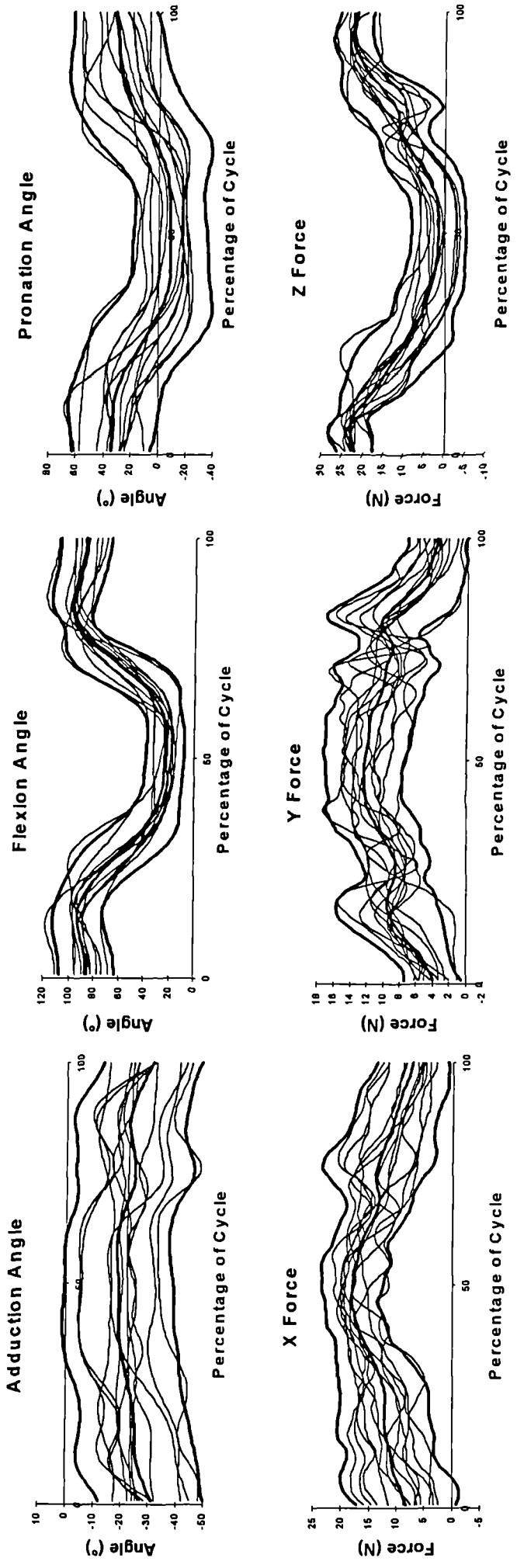

Fig.A.8.74 Angle, Force and Moment graphs for the Elbow during performance of Activity 9, showing mean +/- 2SD in bold.

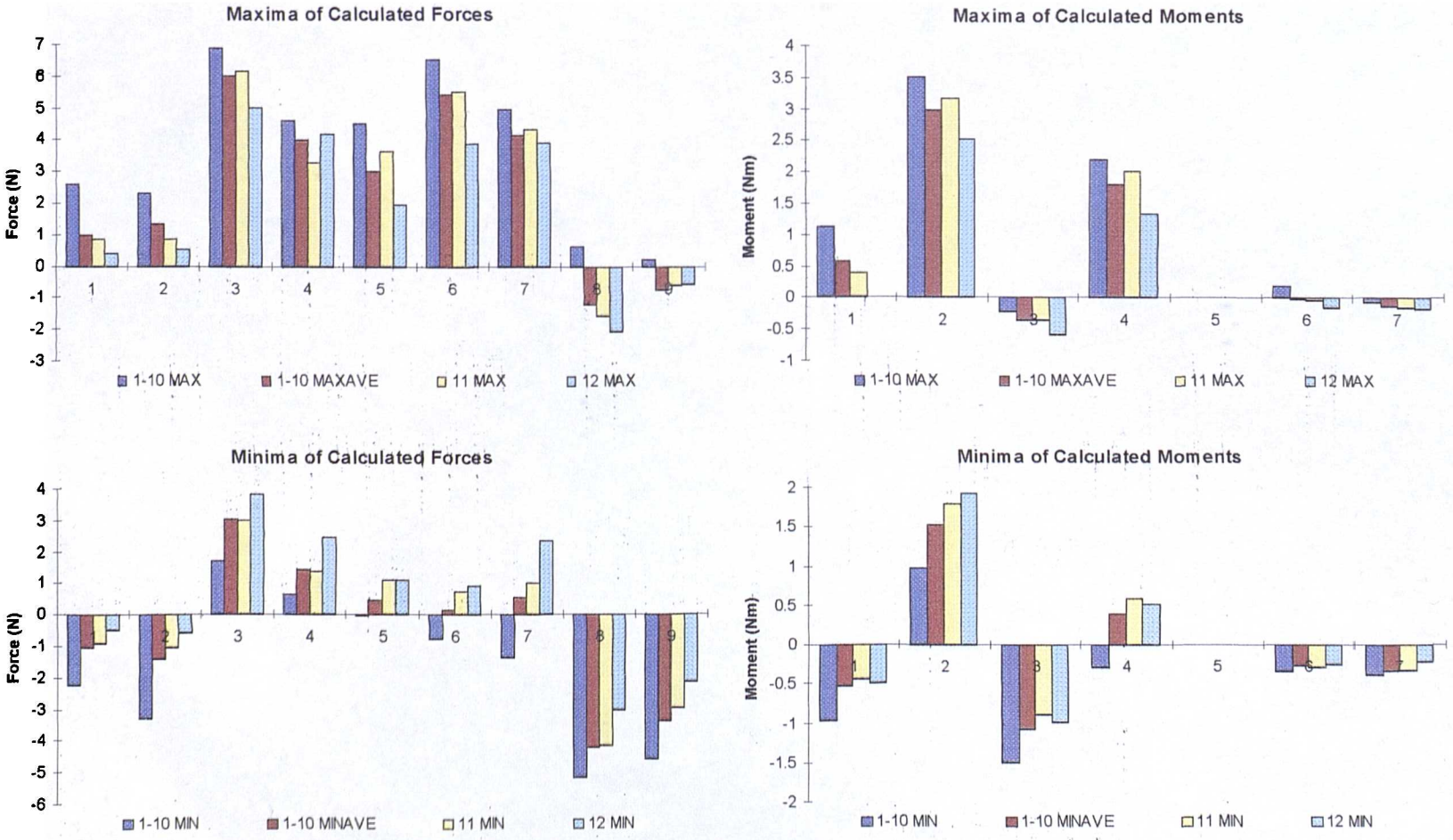

Fig.A.8.77 Unimpaired global maximum (1-10 Max), global minimum (1-10 Min), mean maximum (1-10 Maxave) and mean minimum (1-10 Minave) Force and Moment values due to hand load, along with impaired maximum (11 Max, 12 Max) and minimum (11 Min, 12 Min), during performance of Activity 9. Key as in Table 8.12.

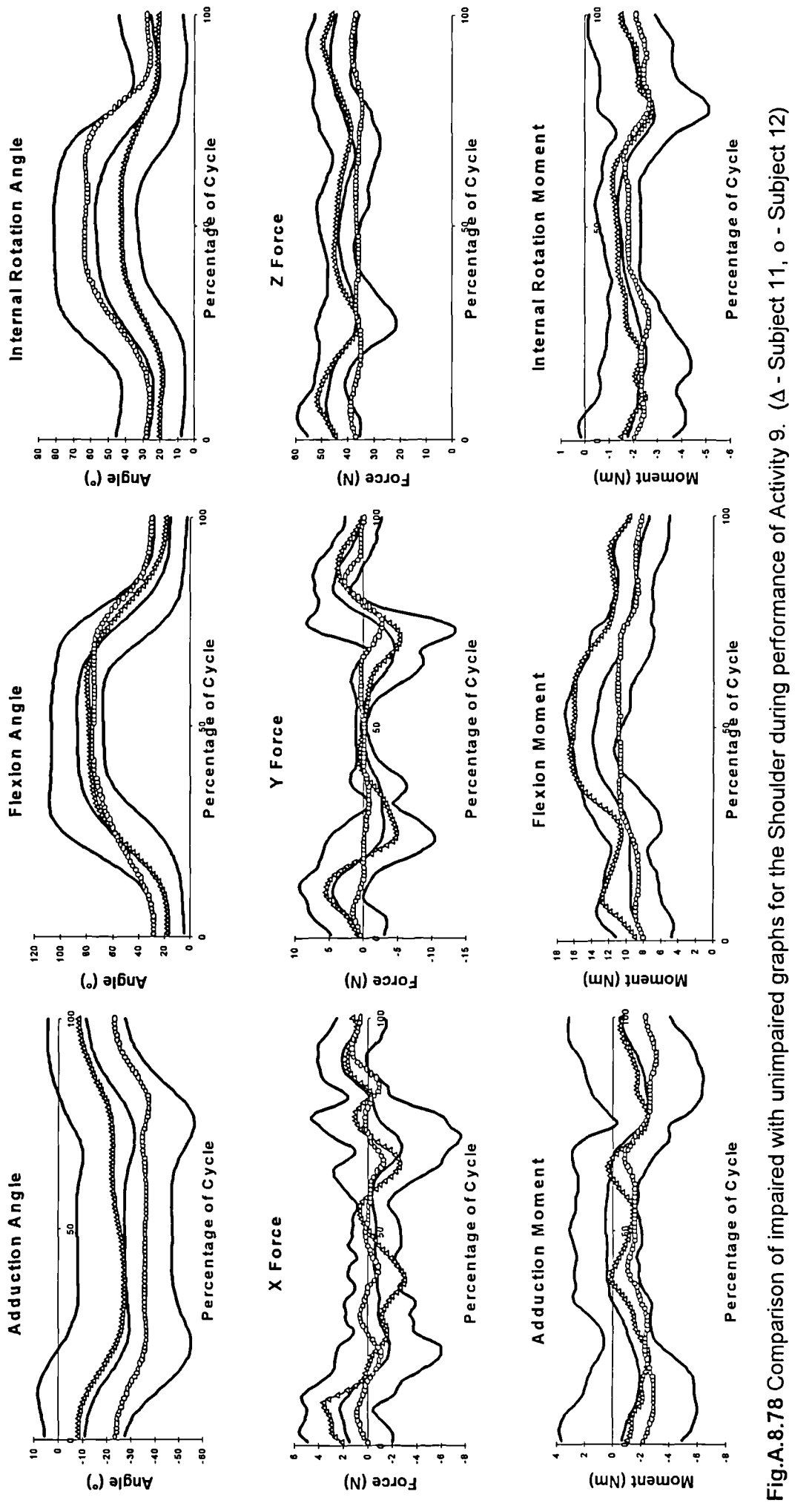

Fig.A.8.78 Comparison of impaired with unimpaired graphs for the Shoulder during performance of Activity 9. (Δ - Subject 11, o - Subject 12)

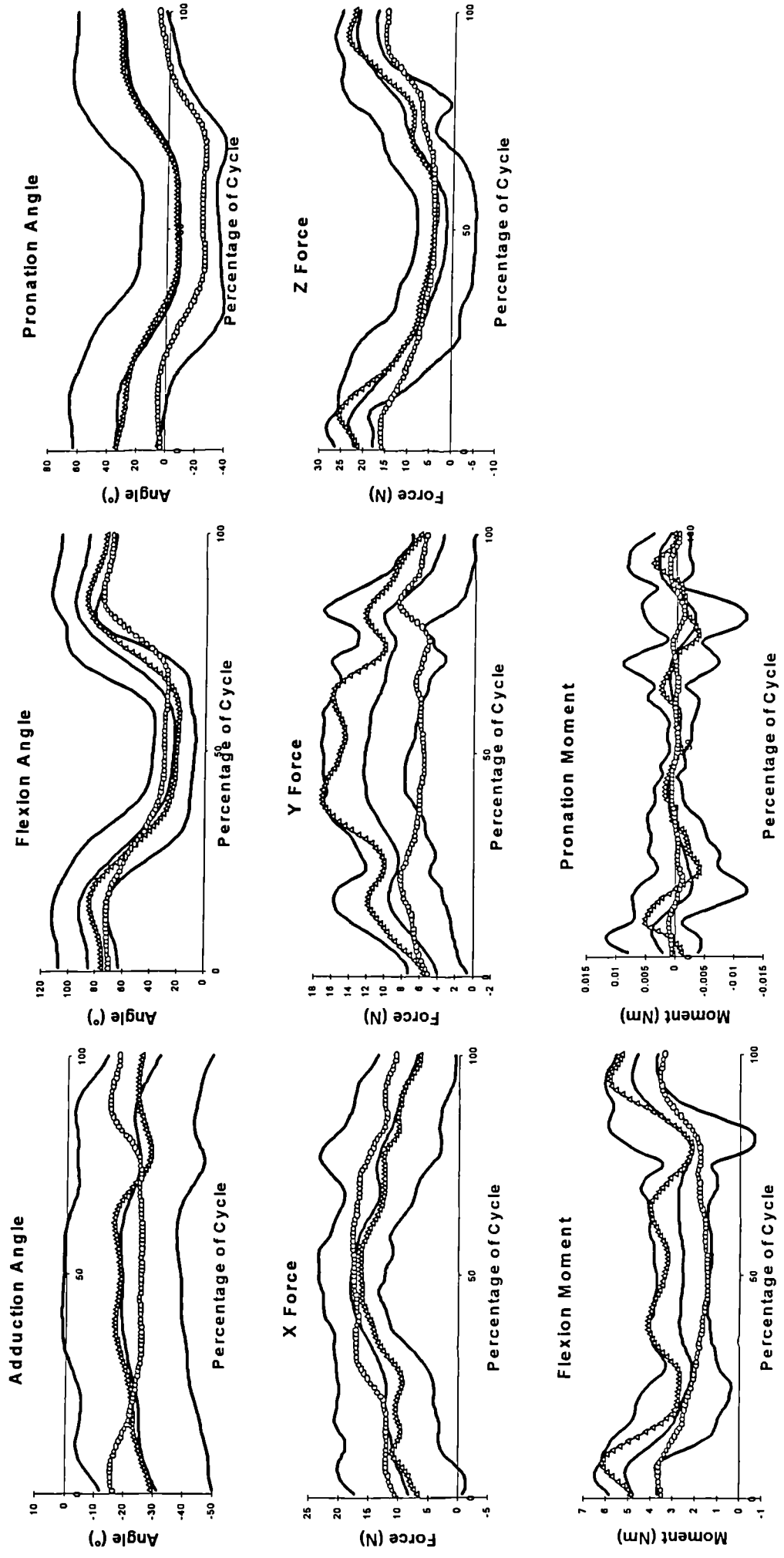

Fig.A.8.79 Comparison of impaired with unimpaired graphs for the Elbow during performance of Activity 9. (Δ - Subject 11, o - Subject 12)

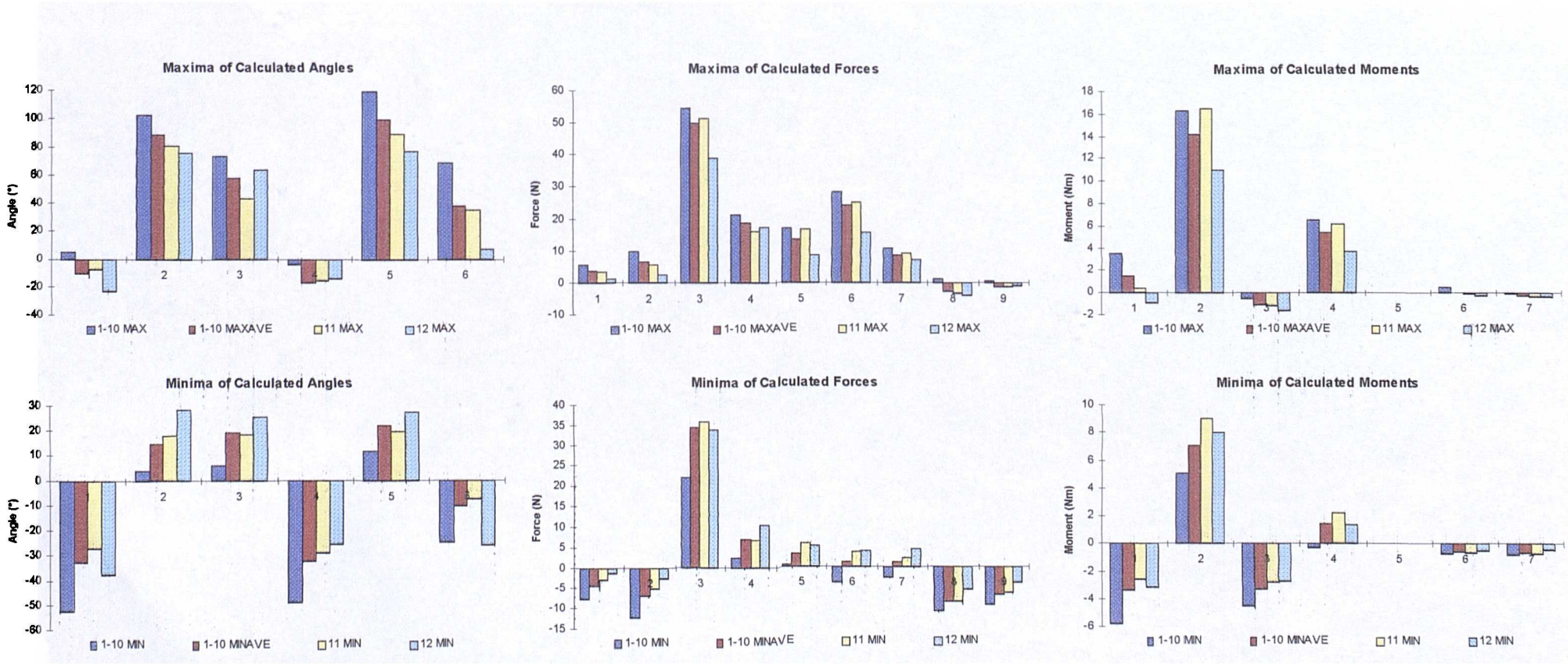

Fig.A.8.80 Unimpaired global maximum (1-10 Max), global minimum (1-10 Min), mean maximum (1-10 Maxave) and mean minimum (1-10 Minave) Angle, Force and Moment values, along with impaired maximum (11 Max, 12 Max) and minimum (11 Min, 12 Min) during performance of Activity 9. Key as in Table 8.12.

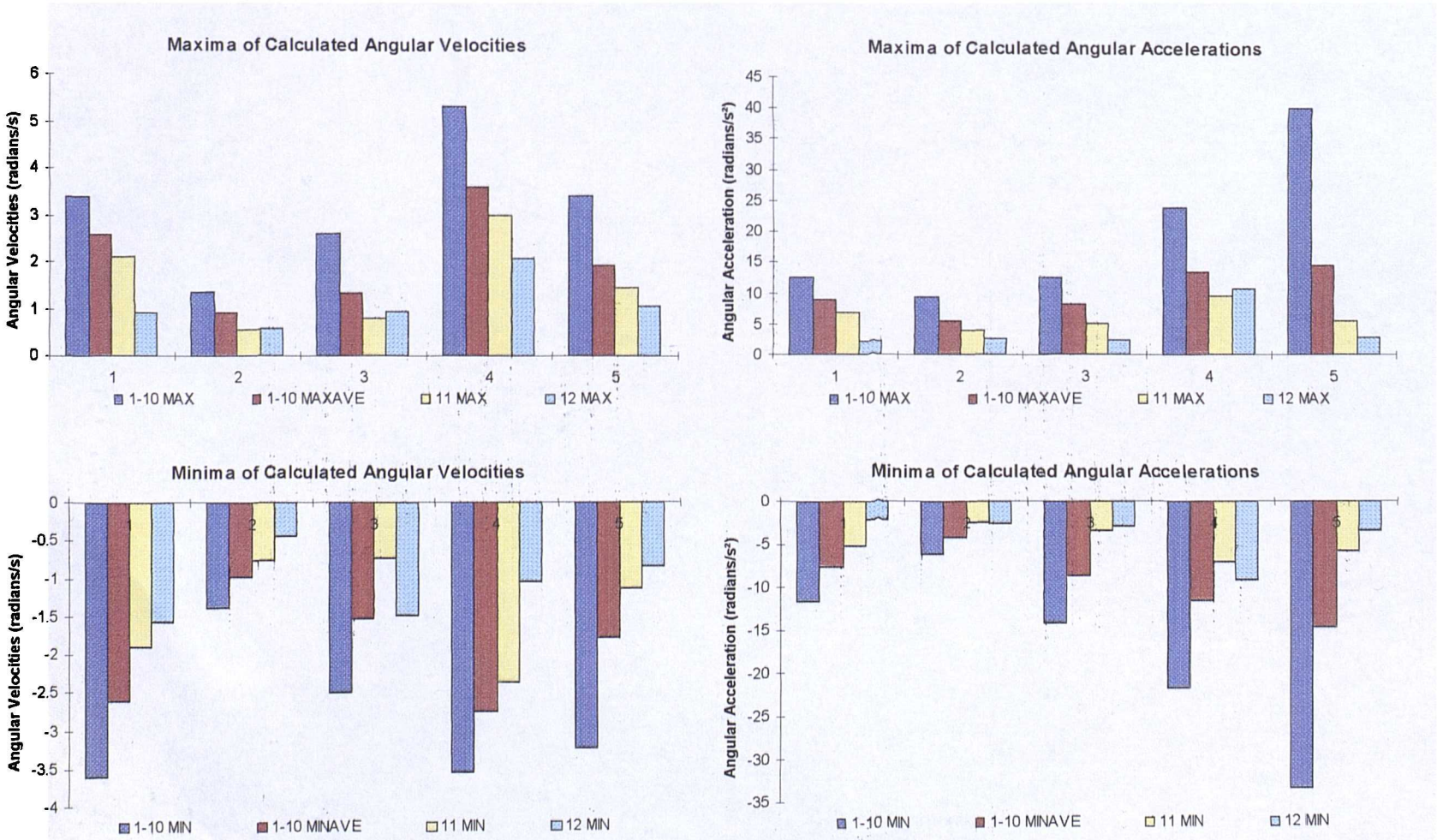

Fig.A.8.81 Unimpaired global maximum (1-10 Max), global minimum (1-10 Min), mean maximum (1-10 Maxave) and mean minimum (1-10 Minave) Angular Velocity and Acceleration, along with impaired maximum (11 Max, 12 Max) and minimum (11 Min, 12 Min) during performance of Activity 9. Key as in Table 8.13.

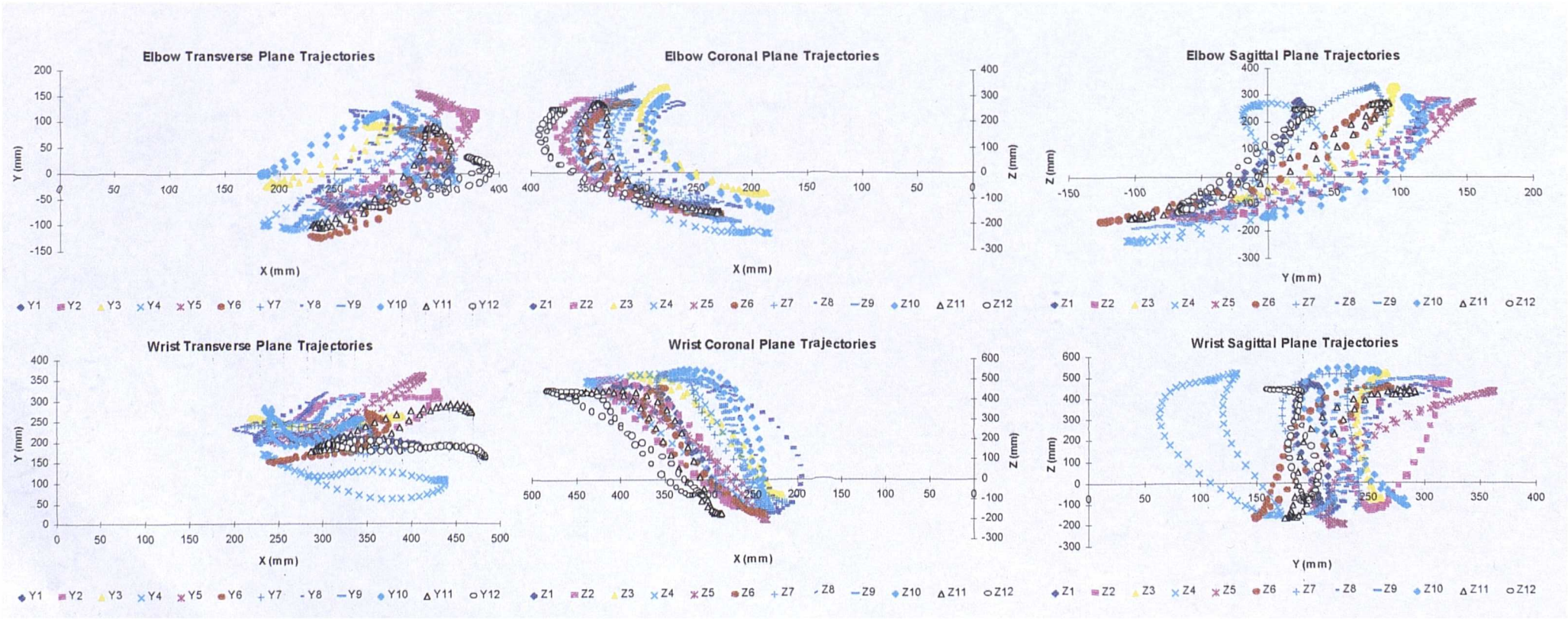

Fig.A.8.85 Trajectories of Elbow and Wrist in the Trunk Frame during performance of Activity 10.

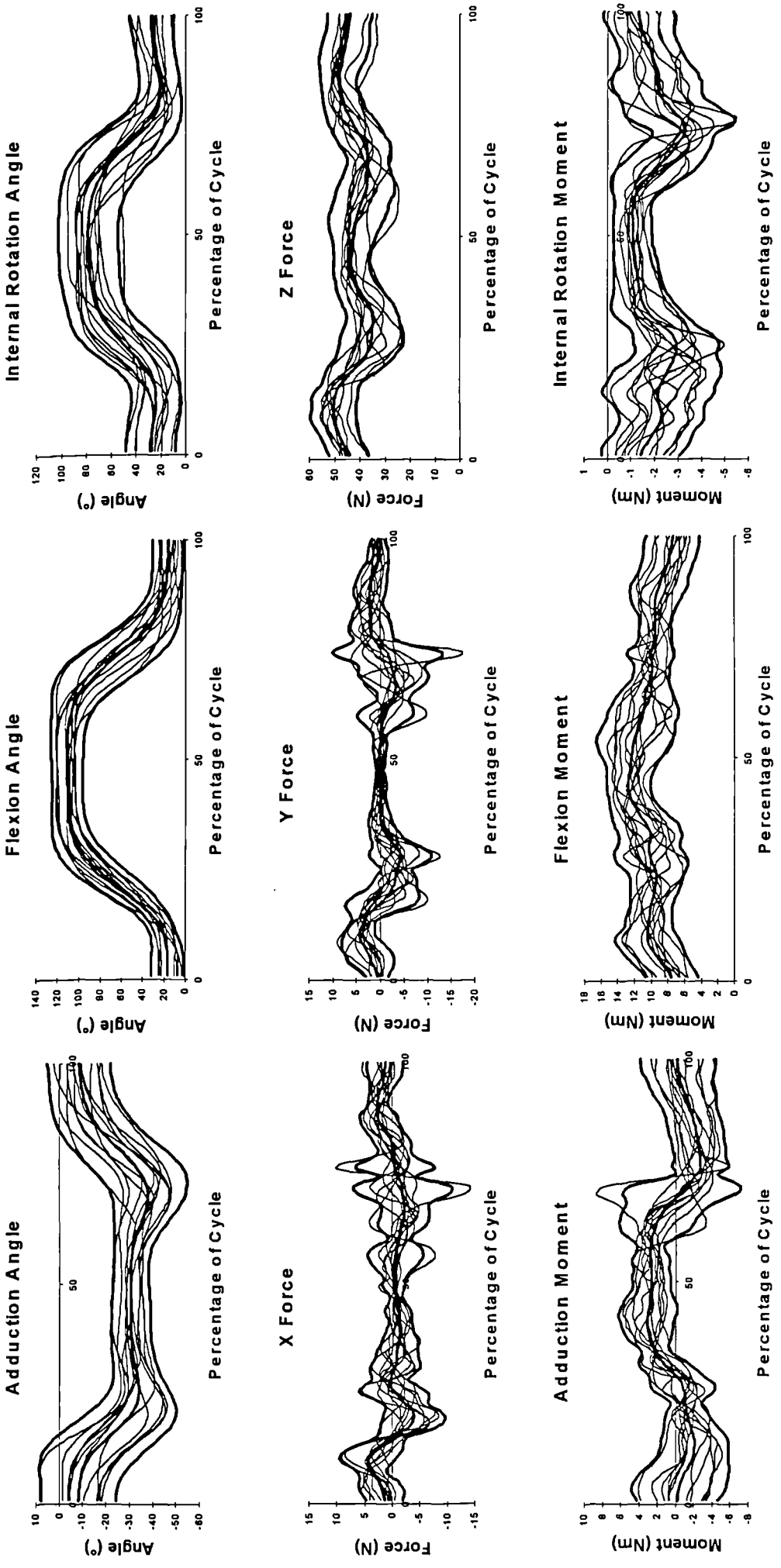

Fig.A.8.86 Angle, Force and Moment graphs for the Shoulder during performance of Activity 10, showing mean +/- 2SD in bold.

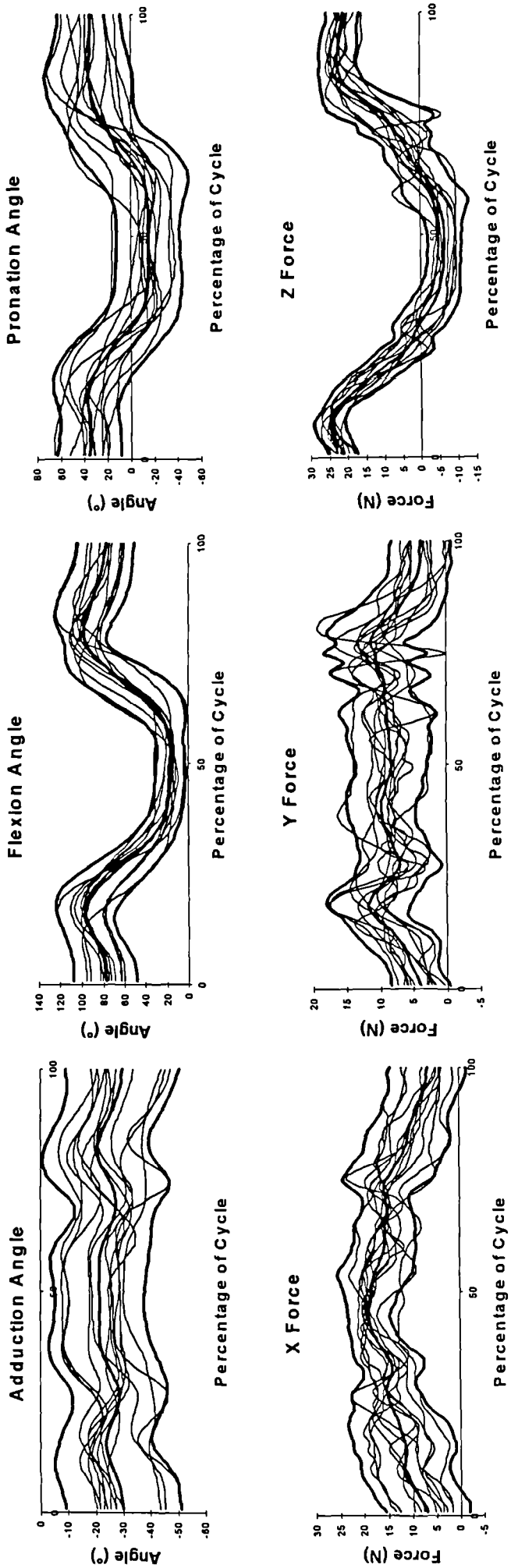

Fig.A.8.87 Angle, Force and Moment graphs for the Elbow during performance of Activity 10, showing mean +/- 2SD in bold.

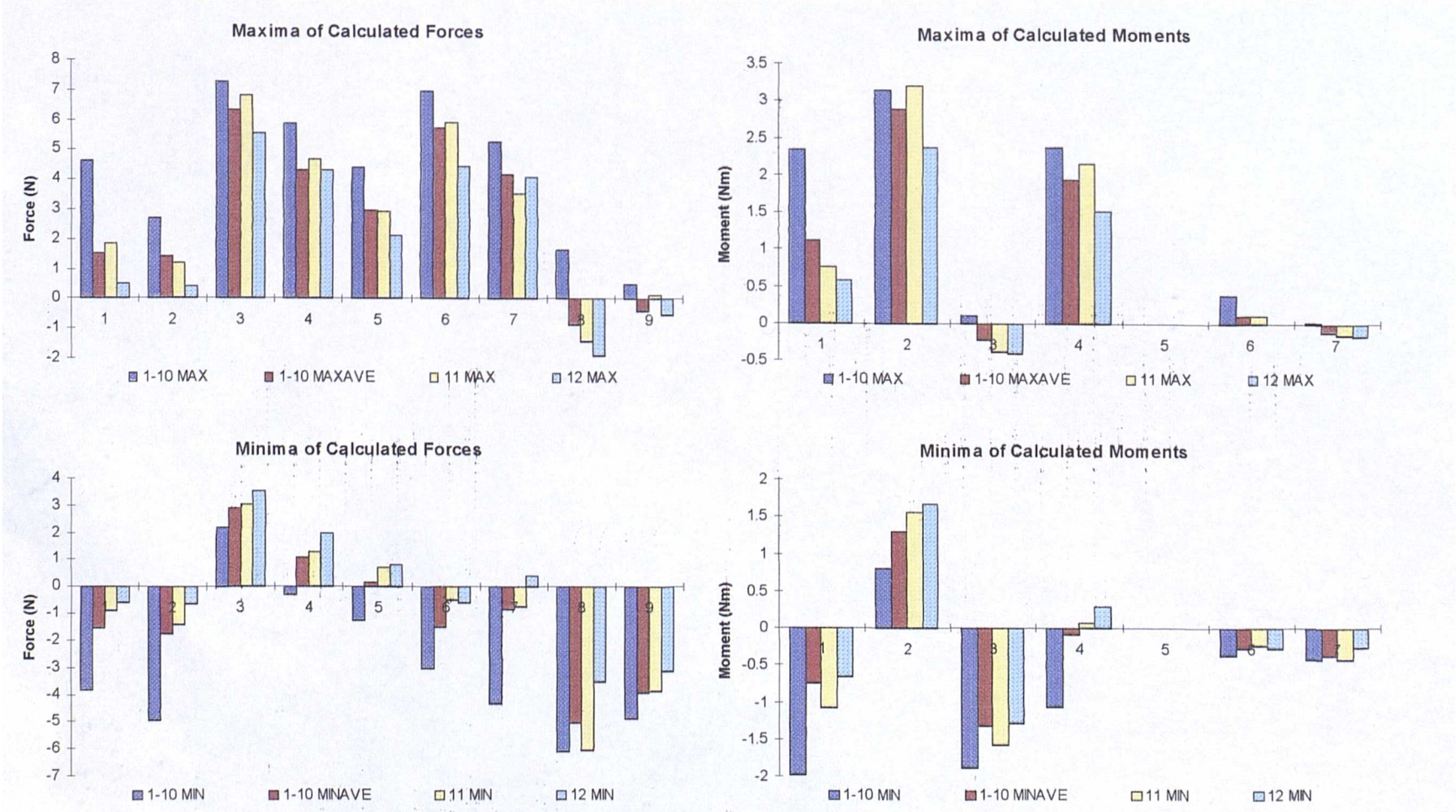

Fig.A.8.90 Unimpaired global maximum (1-10 Max), global minimum (1-10 Min), mean maximum (1-10 Maxave) and mean minimum (1-10 Minave) Force and Moment values due to hand load, along with impaired maximum (11 Max, 12 Max) and minimum (11 Min, 12 Min), during performance of Activity 10. Key as in Table 8.12.

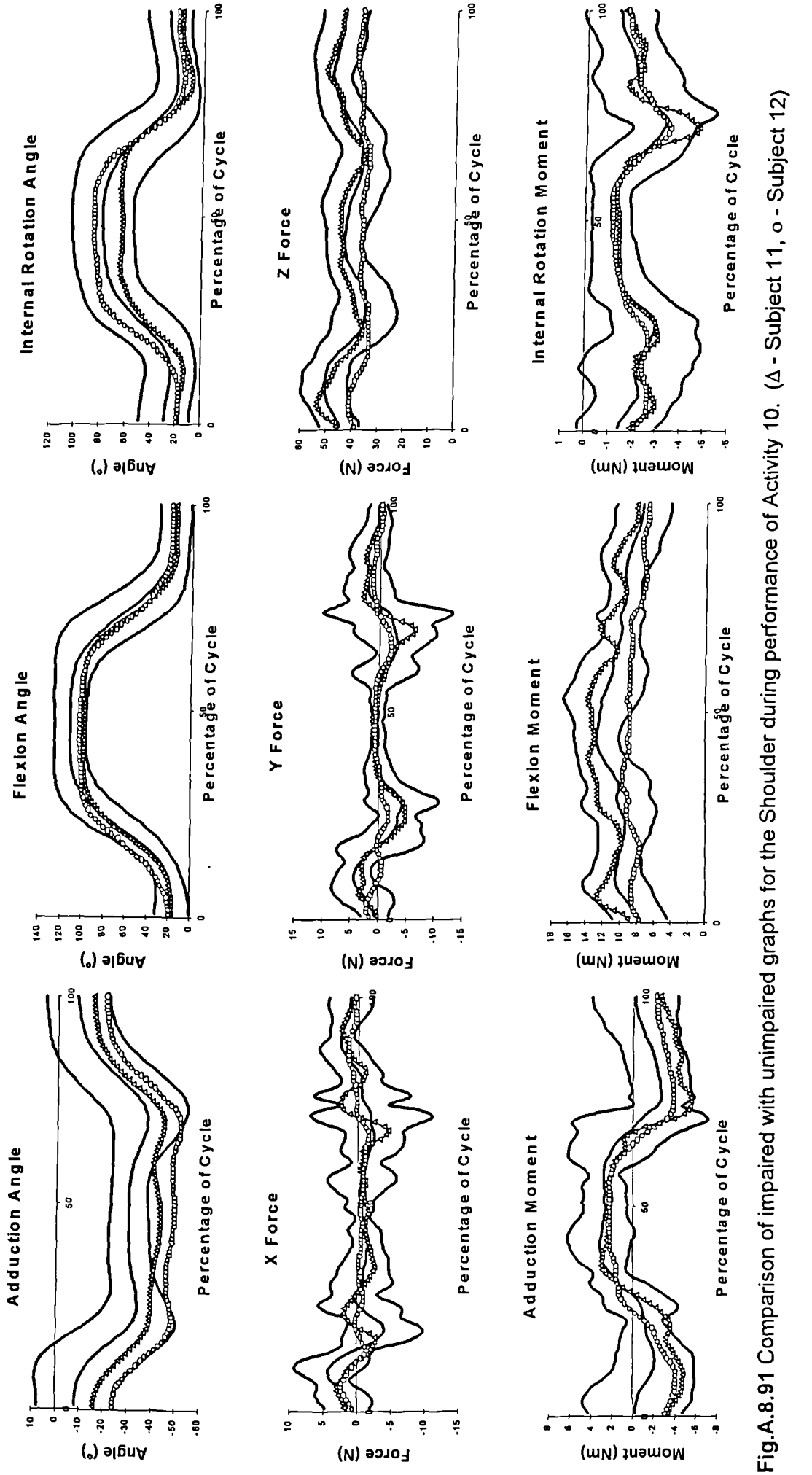

Fig.A.8.91 Comparison of impaired with unimpaired graphs for the Shoulder during performance of Activity 10. (Δ - Subject 11, o - Subject 12)

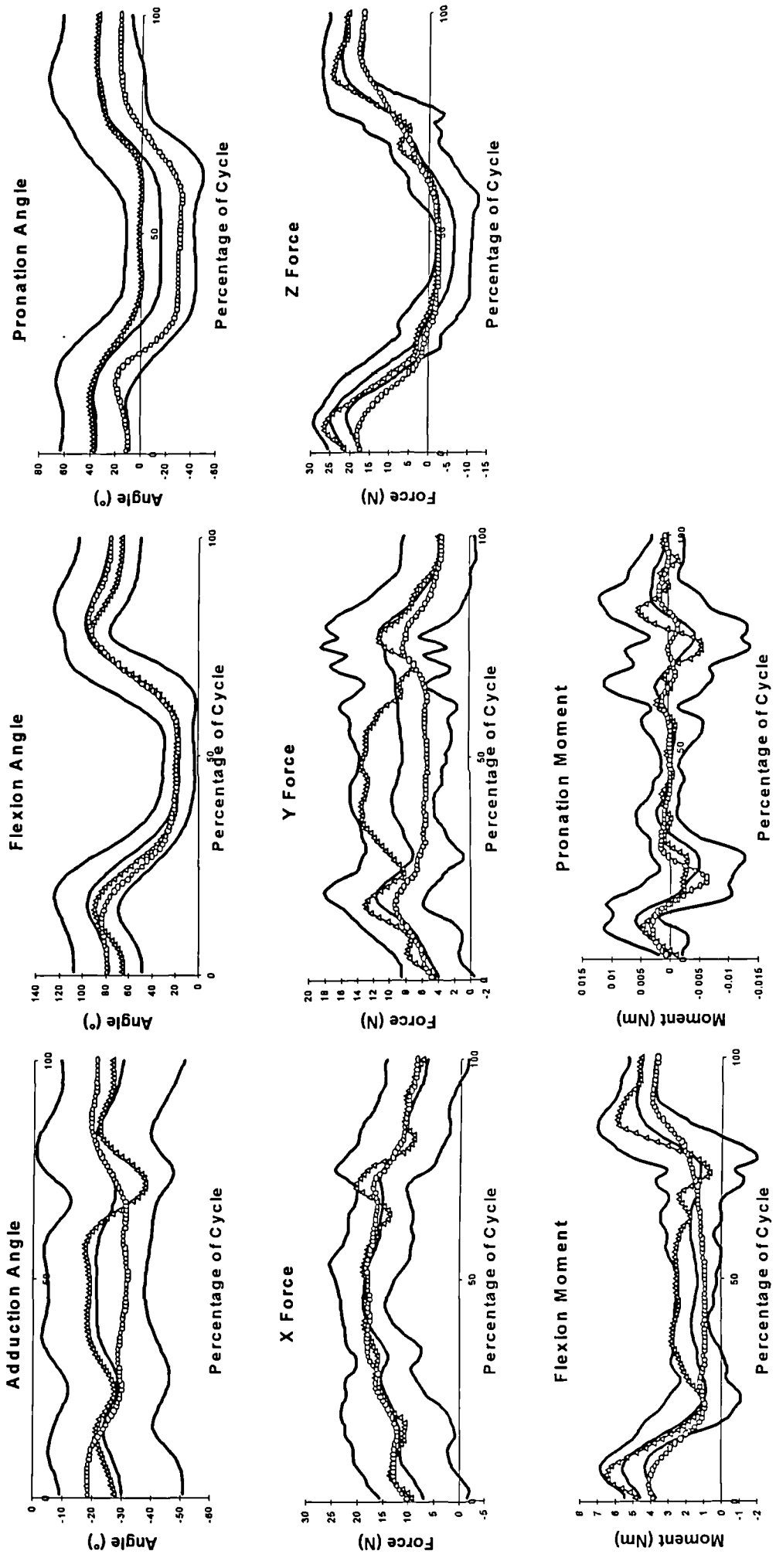

Fig.A.8.92 Comparison of impaired with unimpaired graphs for the Elbow during performance of Activity 10. (Δ - Subject 11, o - Subject 12)

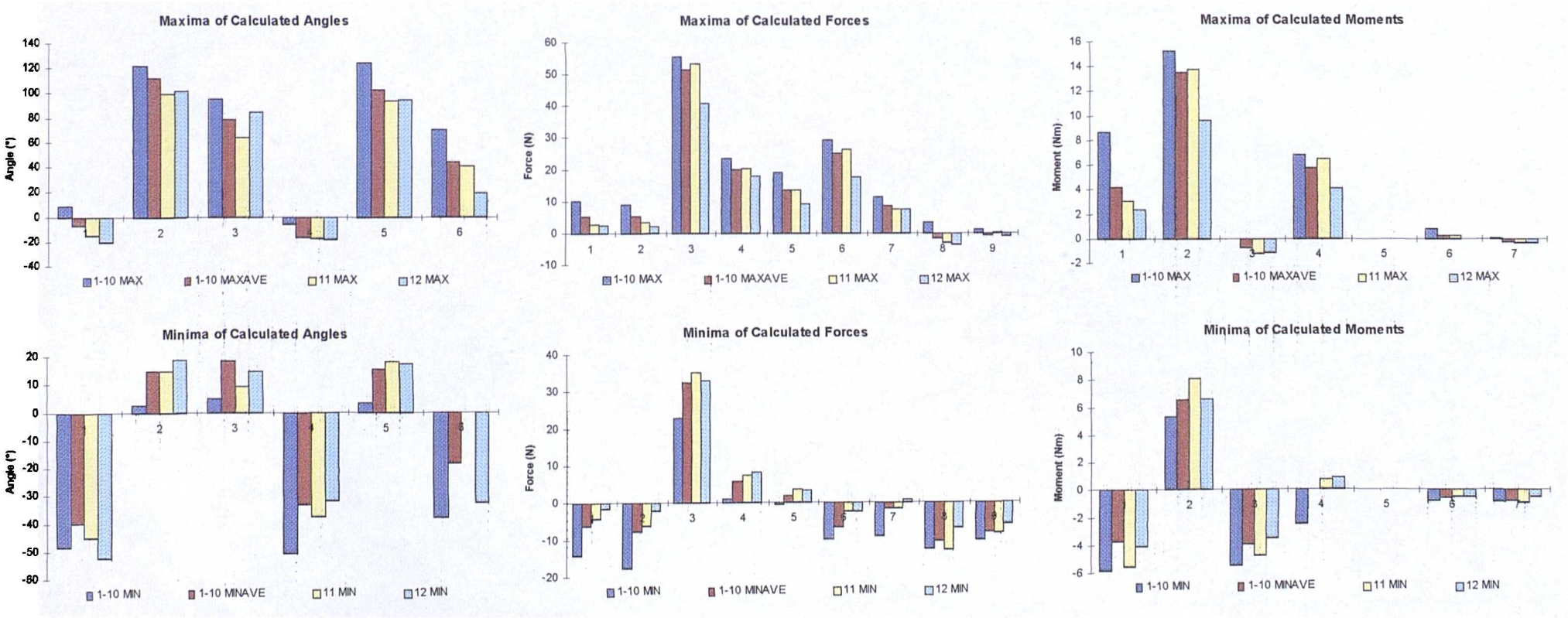

Fig.A.8.93 Unimpaired global maximum (1-10 Max), global minimum (1-10 Min), mean maximum (1-10 Maxave) and mean minimum (1-10 Minave) Angle, Force and Moment values, along with impaired maximum (11 Max, 12 Max) and minimum (11 Min, 12 Min) during performance of Activity 10. Key as in Table 8.12.

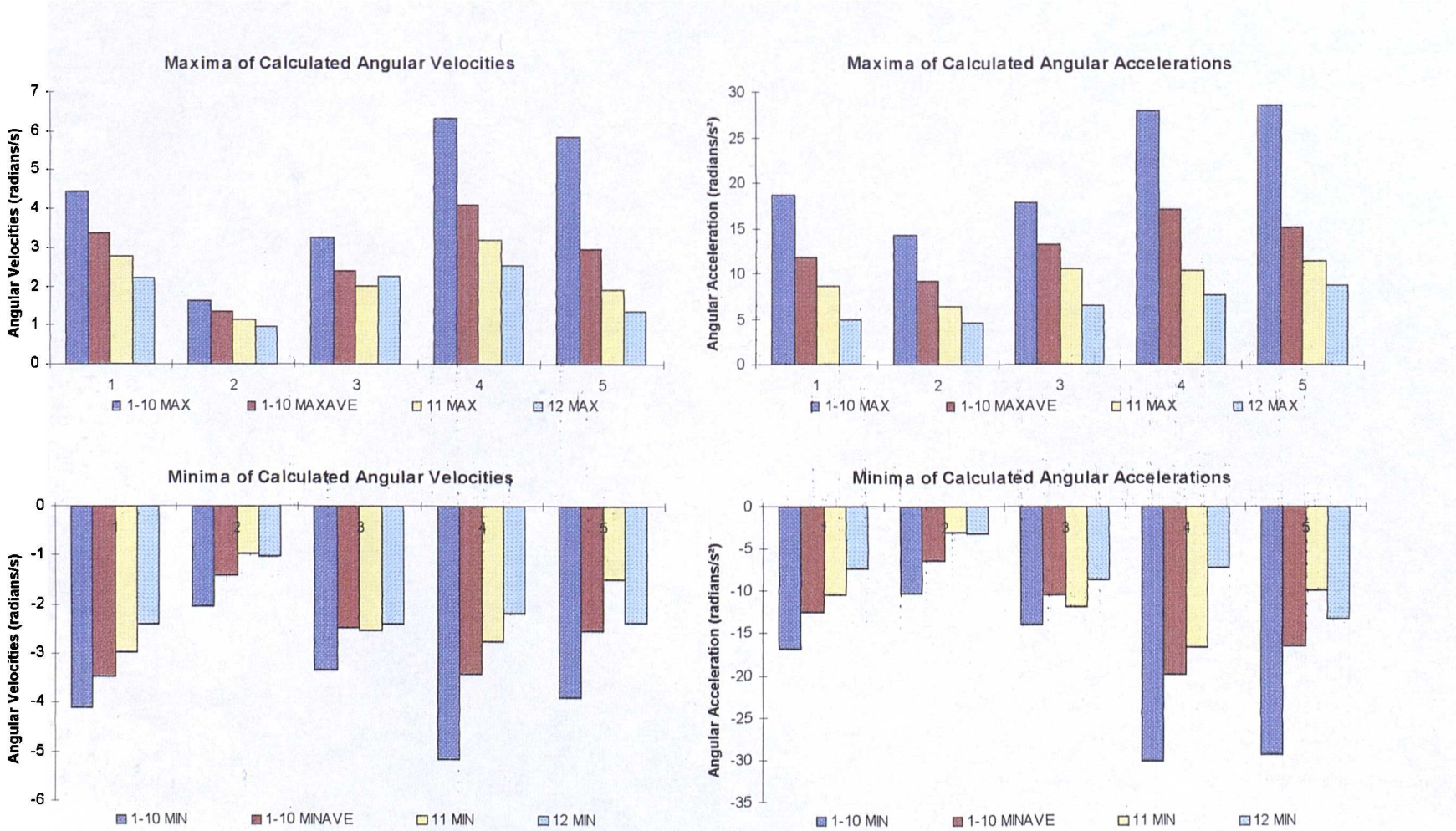

Fig.A.8.94 Unimpaired global maximum (1-10 Max), global minimum (1-10 Min), mean maximum (1-10 Maxave) and mean minimum (1-10 Minave) Angular Velocity and Acceleration, along with impaired maximum (11 Max, 12 Max) and minimum (11 Min, 12 Min) during performance of Activity 10. Key as in Table 8.13.

APPENDIX III

Results for wrist - All activities

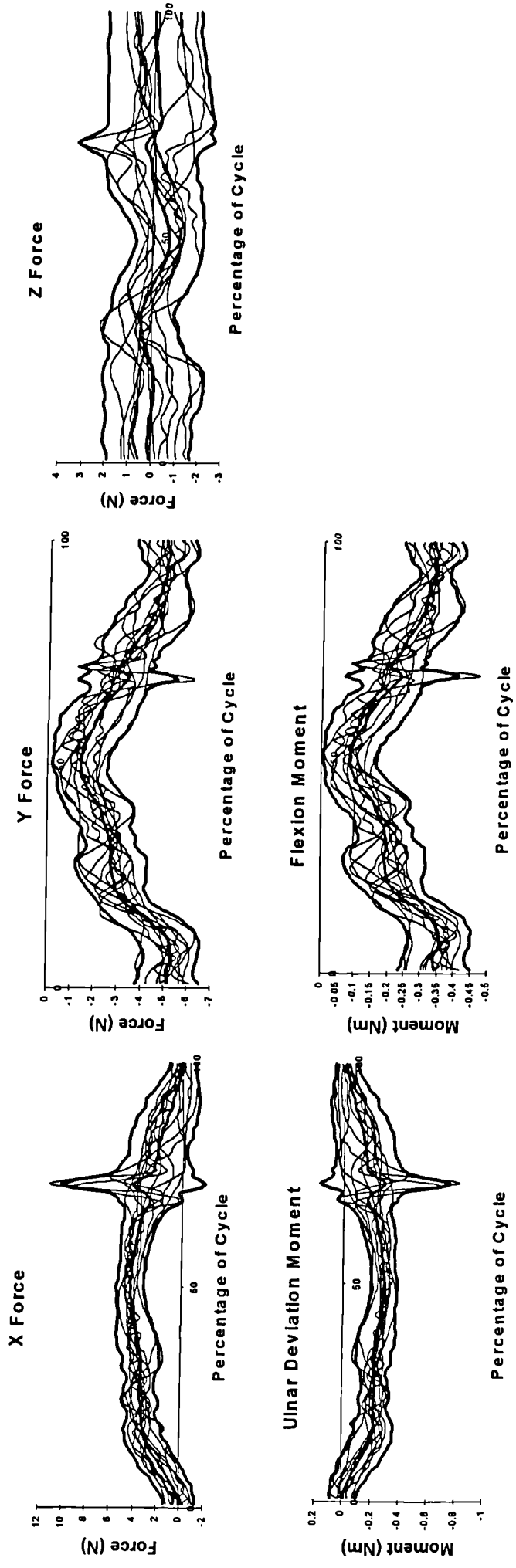

Fig.W.1 Force and Moment graphs for the Wrist during performance of Activity 1, showing mean +/- 2SD in bold.

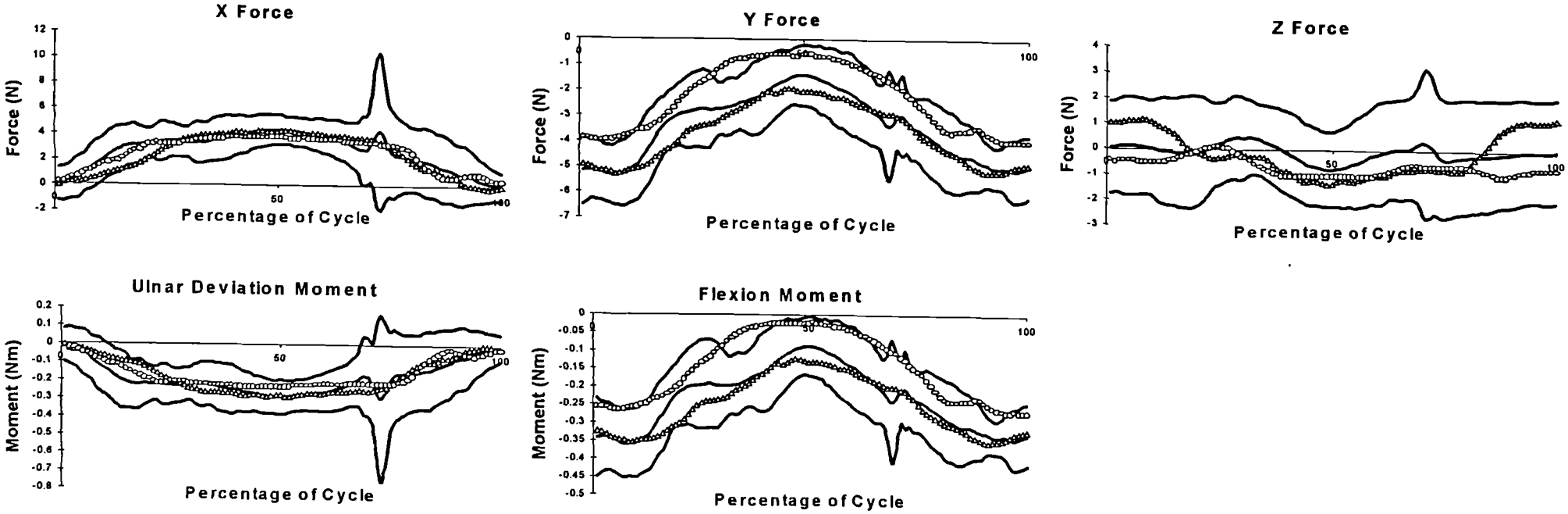

Fig.W.2 Comparison of impaired with unimpaired graphs for the Wrist during performance of Activity 1. (Δ - Subject 11, o - Subject 12)

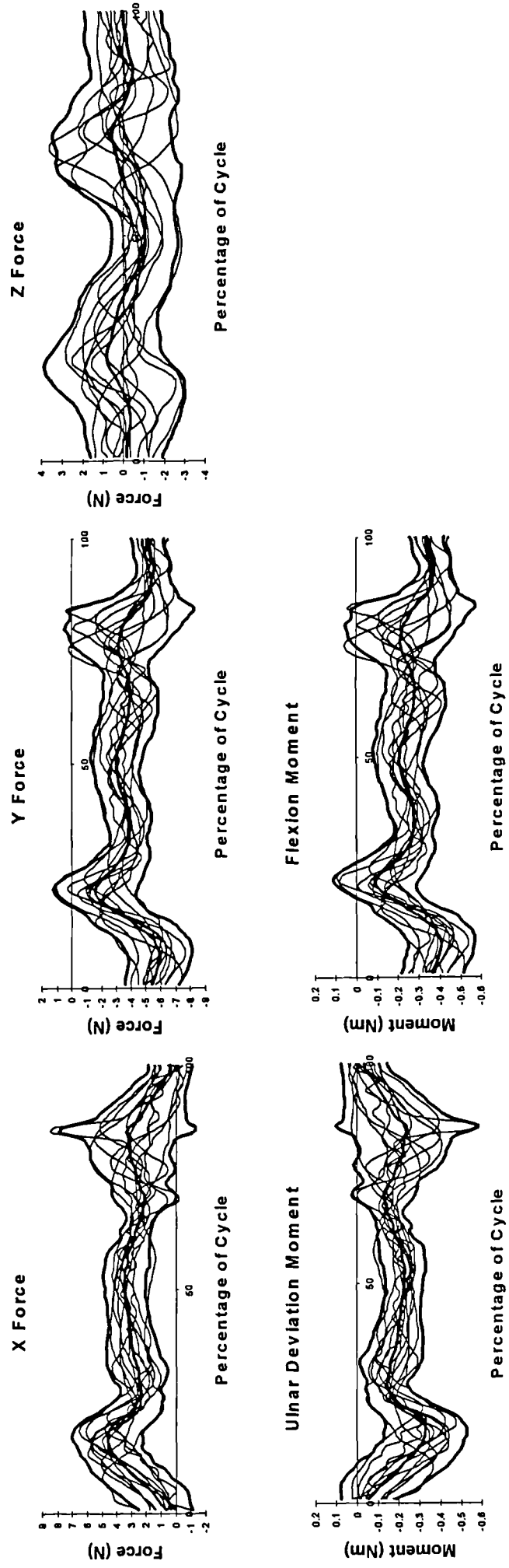

Fig.W.3 Force and Moment graphs for the Wrist during performance of Activity 2, showing mean +/- 2SD in bold.

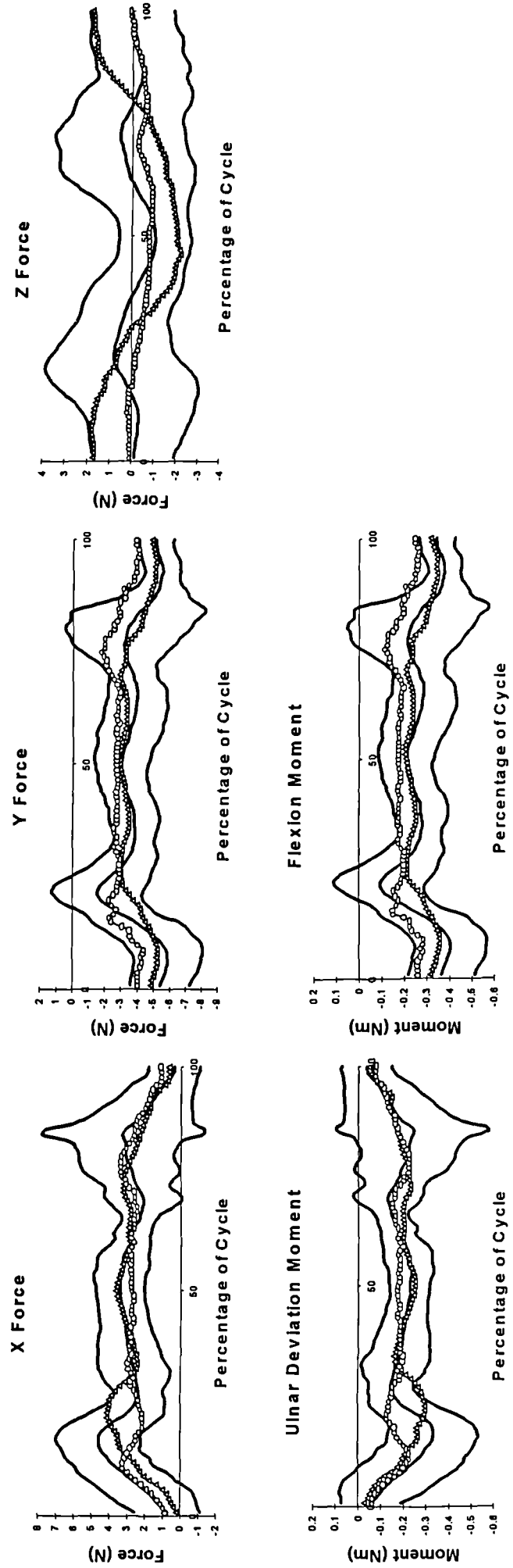

Fig.W.4 Comparison of impaired with unimpaired graphs for the Wrist during performance of Activity 2. (Δ - Subject 11, o - Subject 12)

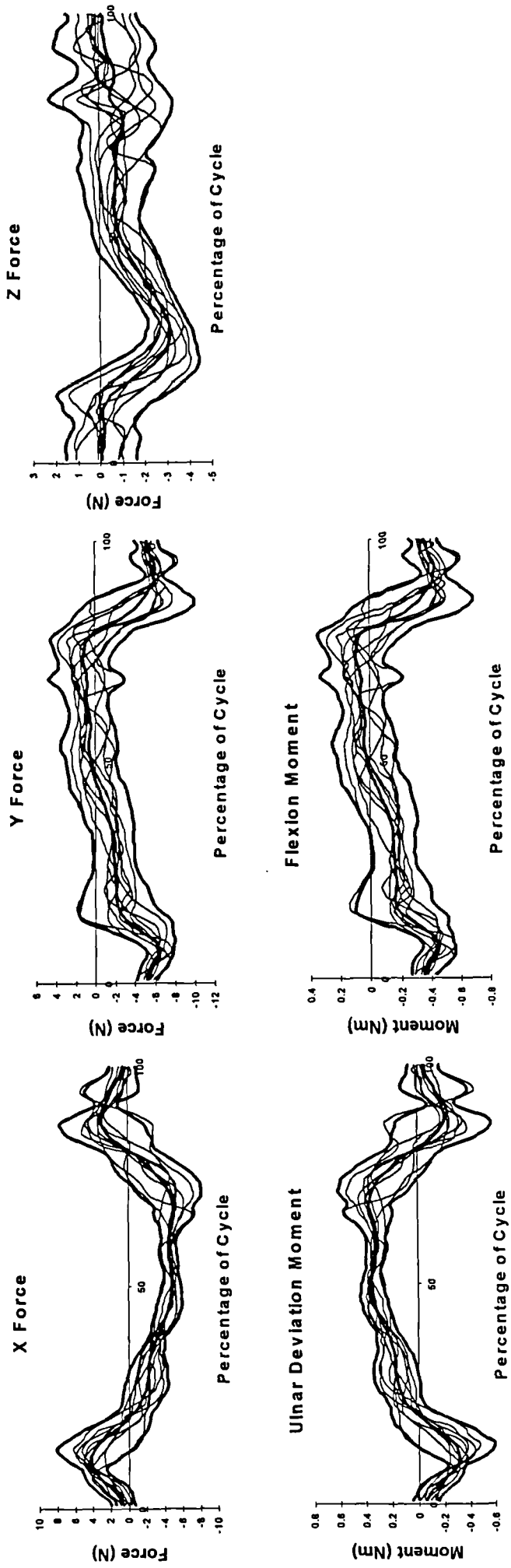

Fig.W.5 Force and Moment graphs for the Wrist during performance of Activity 3, showing mean +/- 2SD in bold.

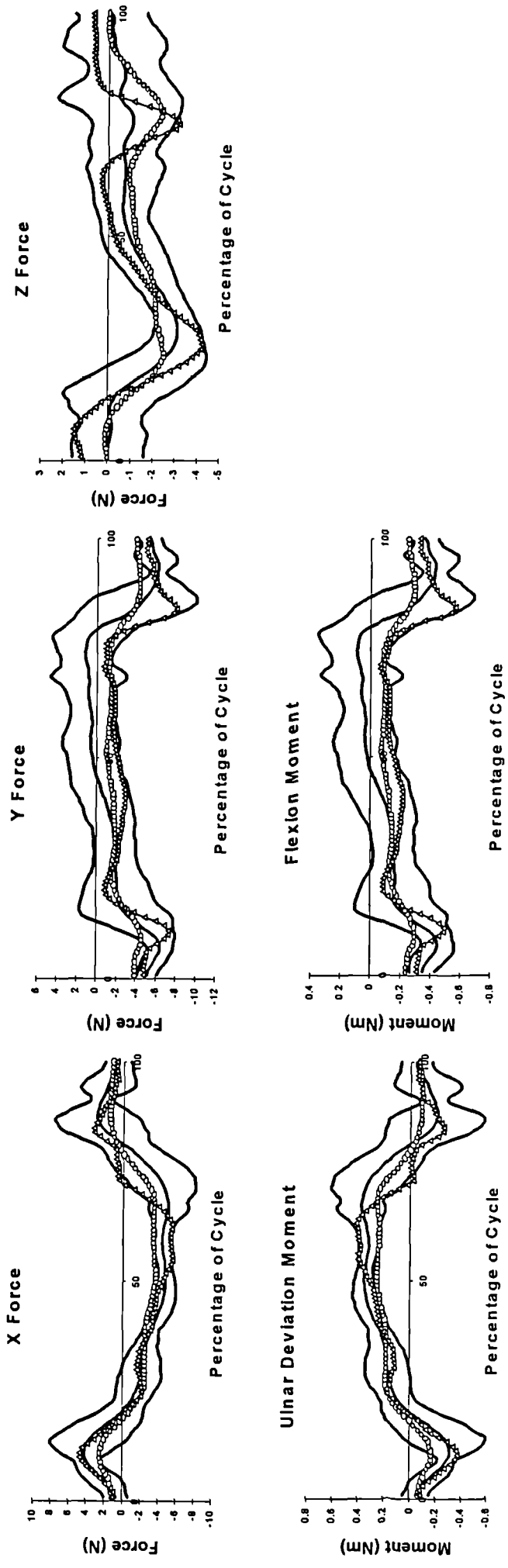

Fig.W.6 Comparison of impaired with unimpaired graphs for the Wrist during performance of Activity 3. (Δ - Subject 11, o - Subject 12)

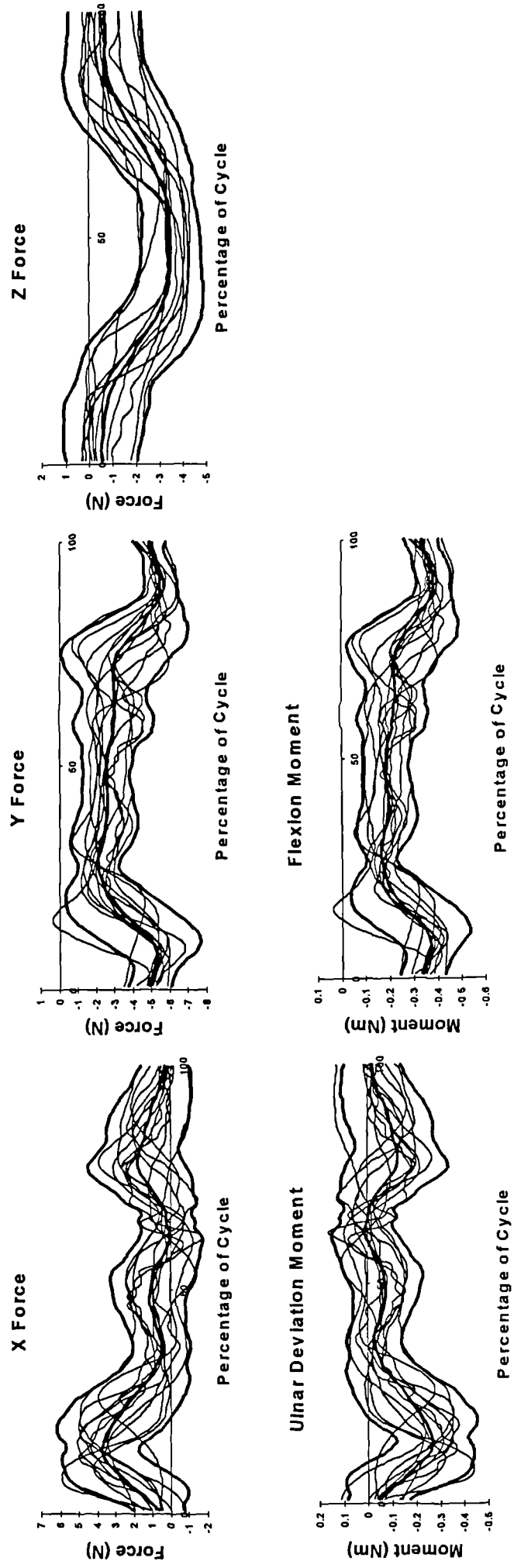

Fig.W.7Force and Moment graphs for the Wrist during performance of Activity 4, showing mean +/- 2SD in bold.

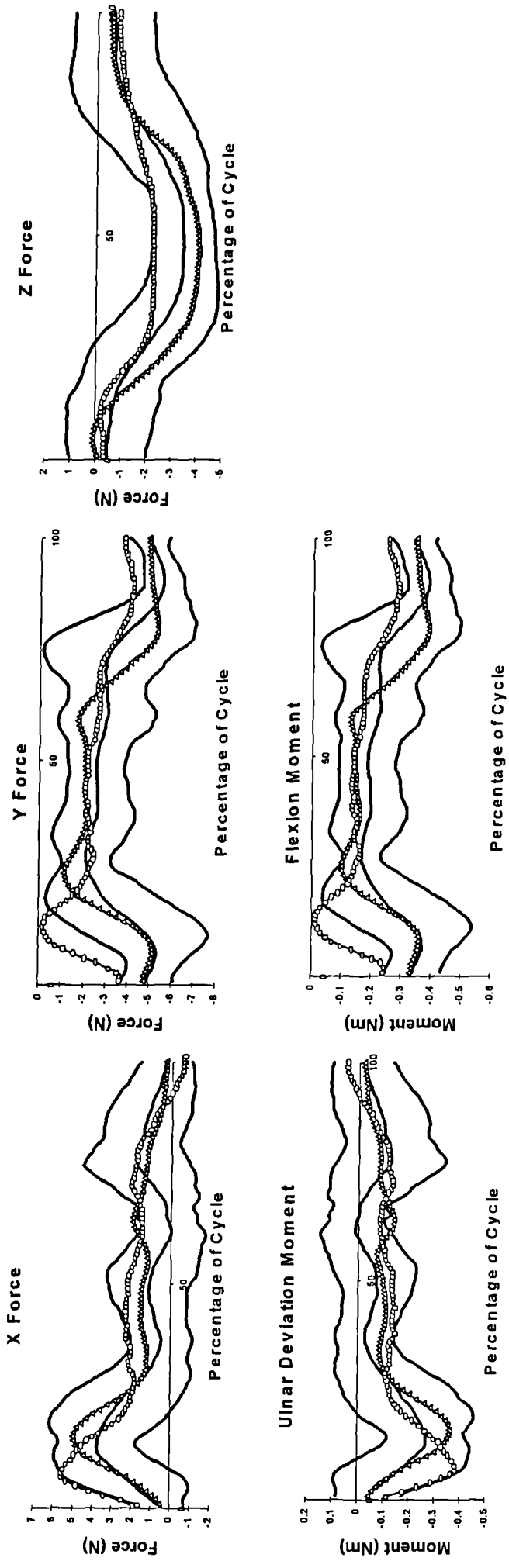

Fig.W.8 Comparison of impaired with unimpaired graphs for the Wrist during performance of Activity 4. (Δ - Subject 11, o - Subject 12)

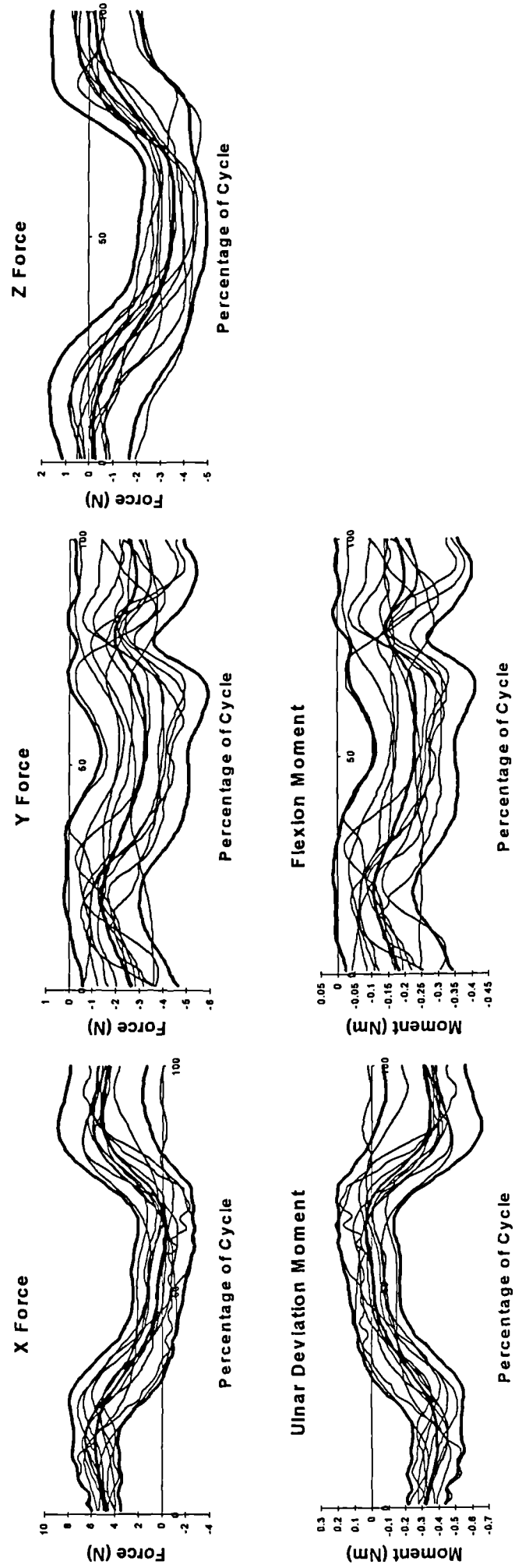

Fig.W.9Force and Moment graphs for the Wrist during performance of Activity 5, showing mean +/- 2SD in bold.

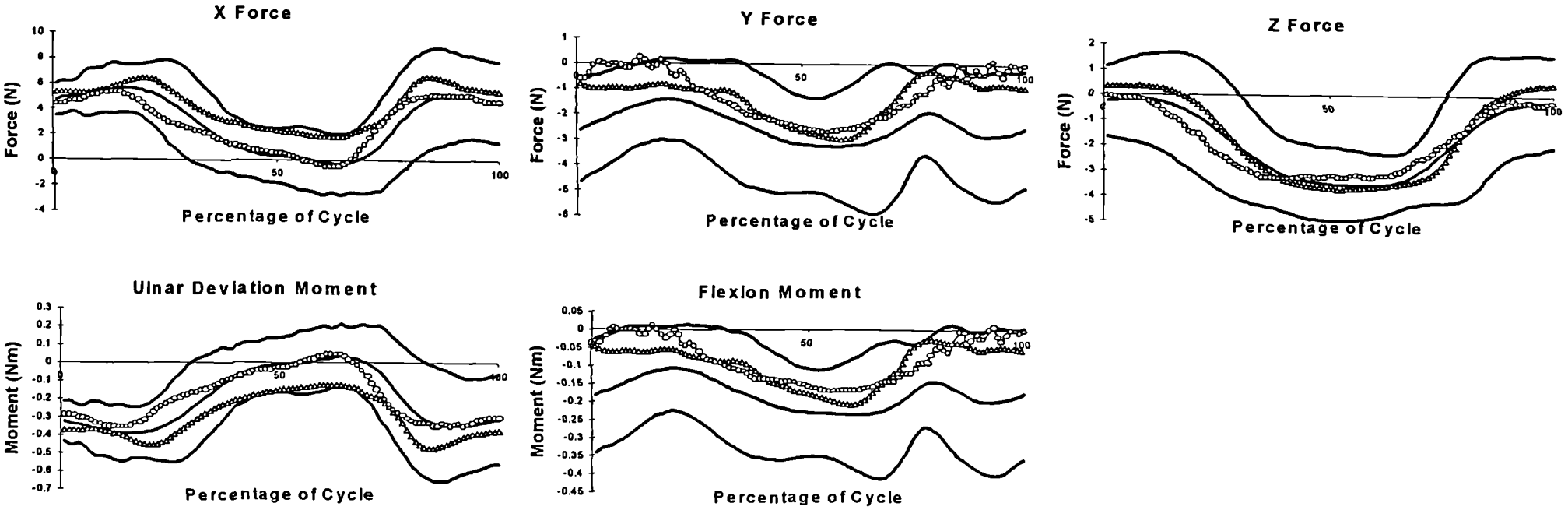

Fig.W.10 Comparison of impaired with unimpaired graphs for the Wrist during performance of Activity 5. (Δ - Subject 11, o - Subject 12)

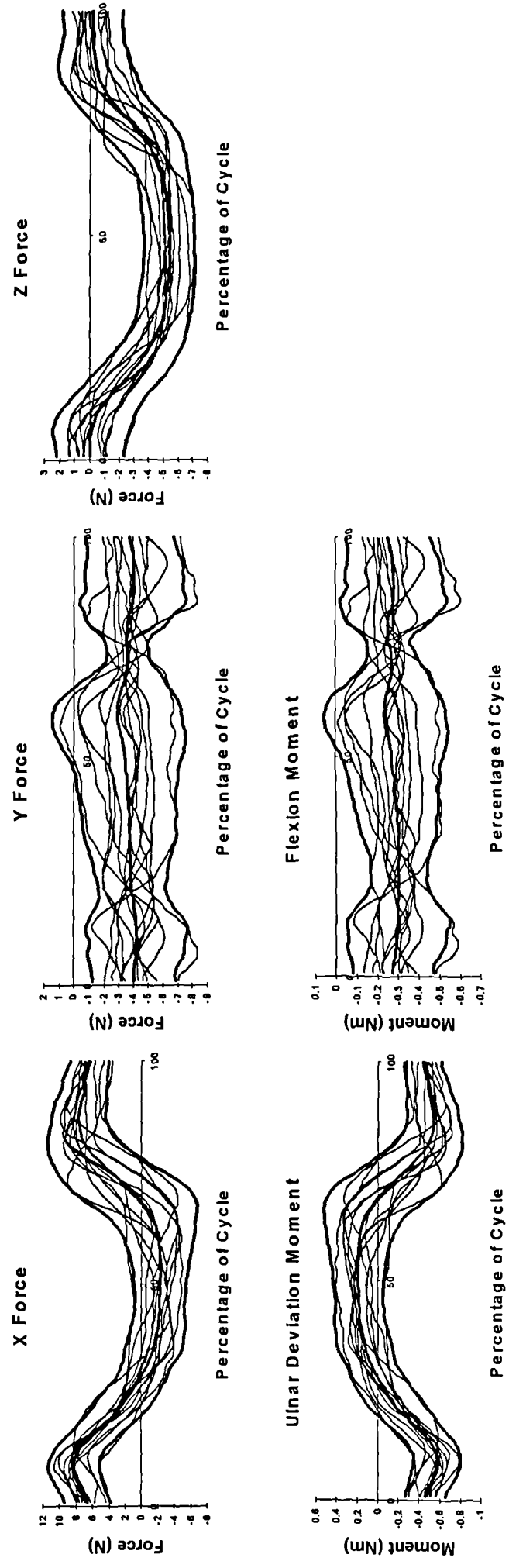

Fig.W.11 Force and Moment graphs for the Wrist during performance of Activity 6, showing mean +/- 2SD in bold.

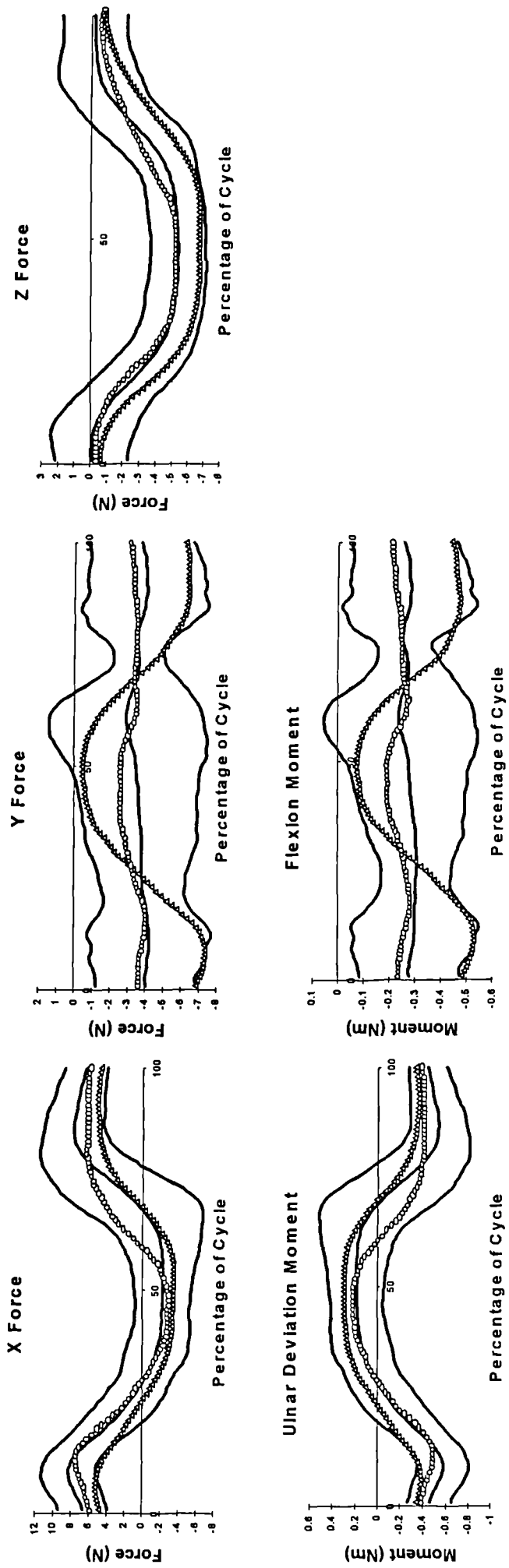

Fig.W.12 Comparison of impaired with unimpaired graphs for the Wrist during performance of Activity 6. (Δ - Subject 11, o - Subject 12)

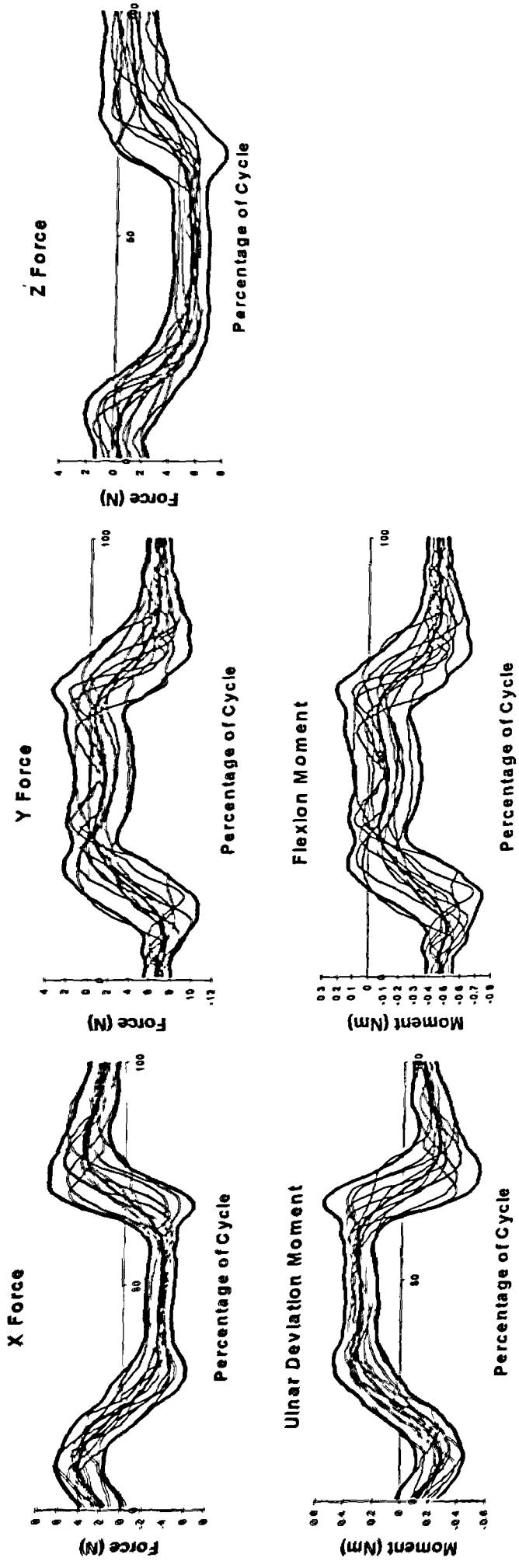

Fig.W.13 Force and Moment graphs for the Wrist during performance of Activity 7, showing *mean* +/- 2SD in *bold*.

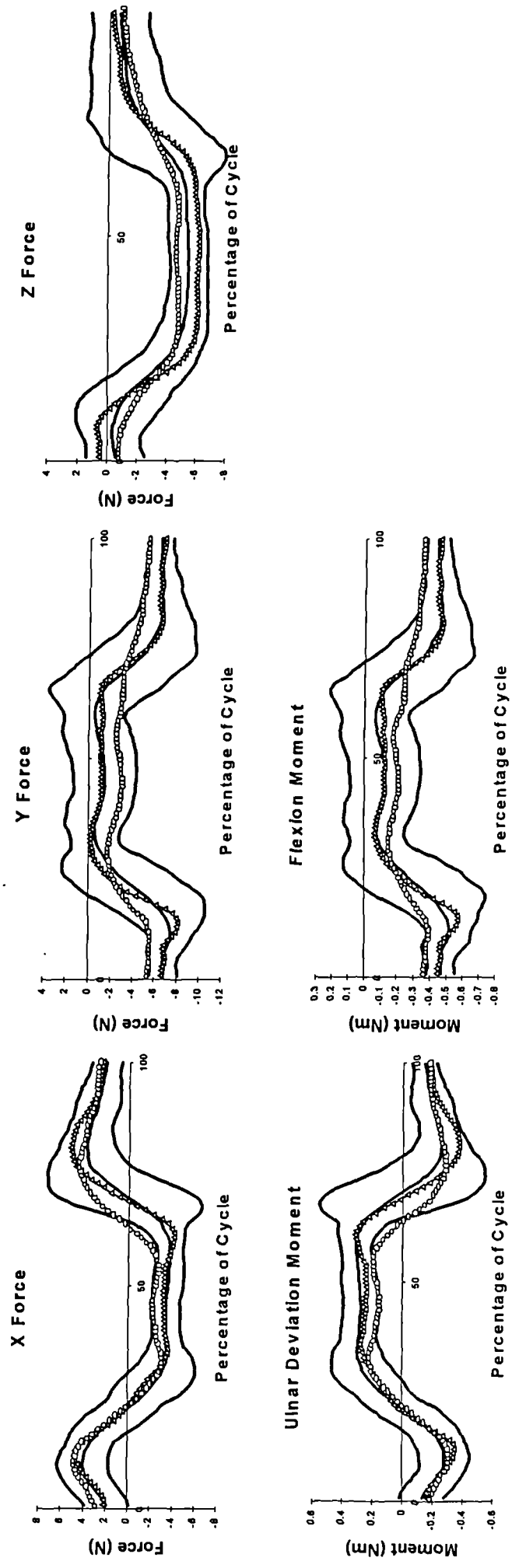

Fig.W.14 Comparison of impaired with unimpaired graphs for the Wrist during performance of Activity 7. (Δ - Subject 11, o - Subject 12)

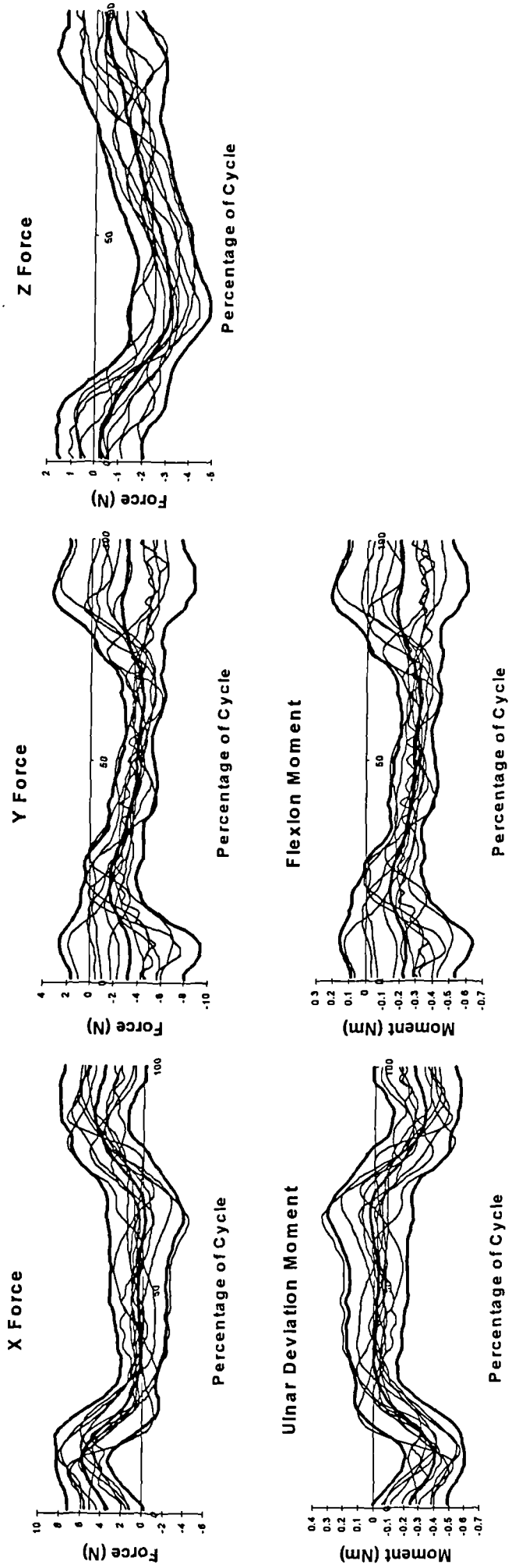

Fig.W.15 Force and Moment graphs for the Wrist during performance of Activity 8, showing mean +/- 2SD in bold.

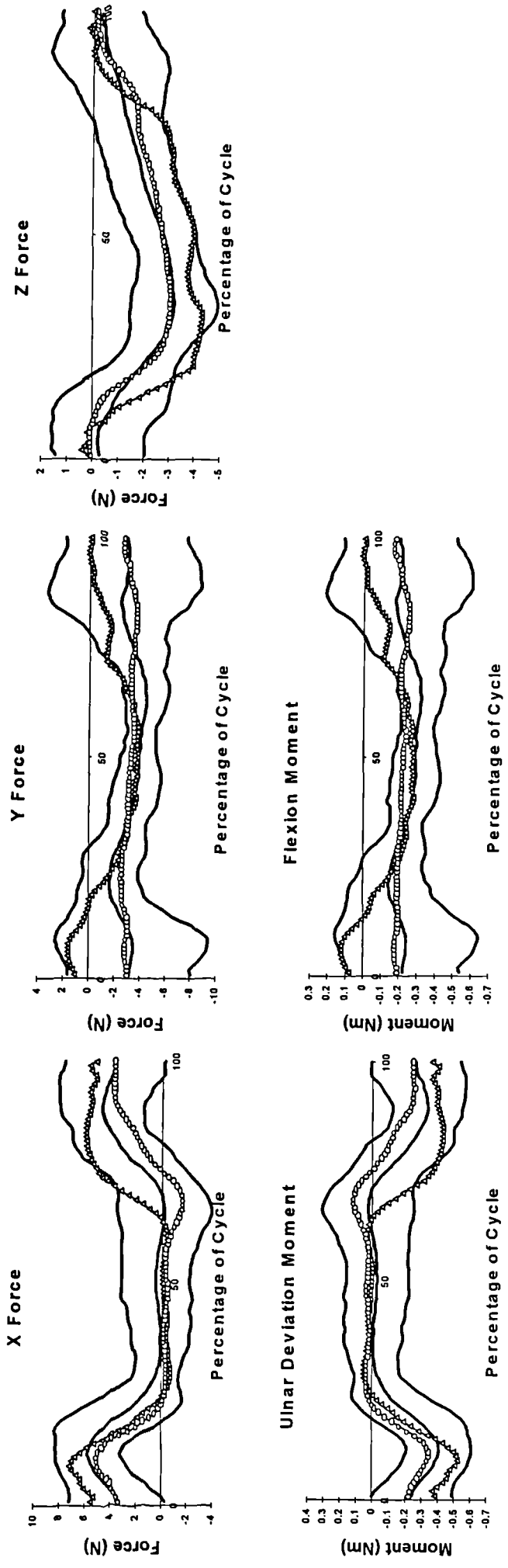

Fig.W.16 Comparison of impaired with unimpaired graphs for the Wrist during performance of Activity 8. (Δ - Subject 11, o - Subject 12)

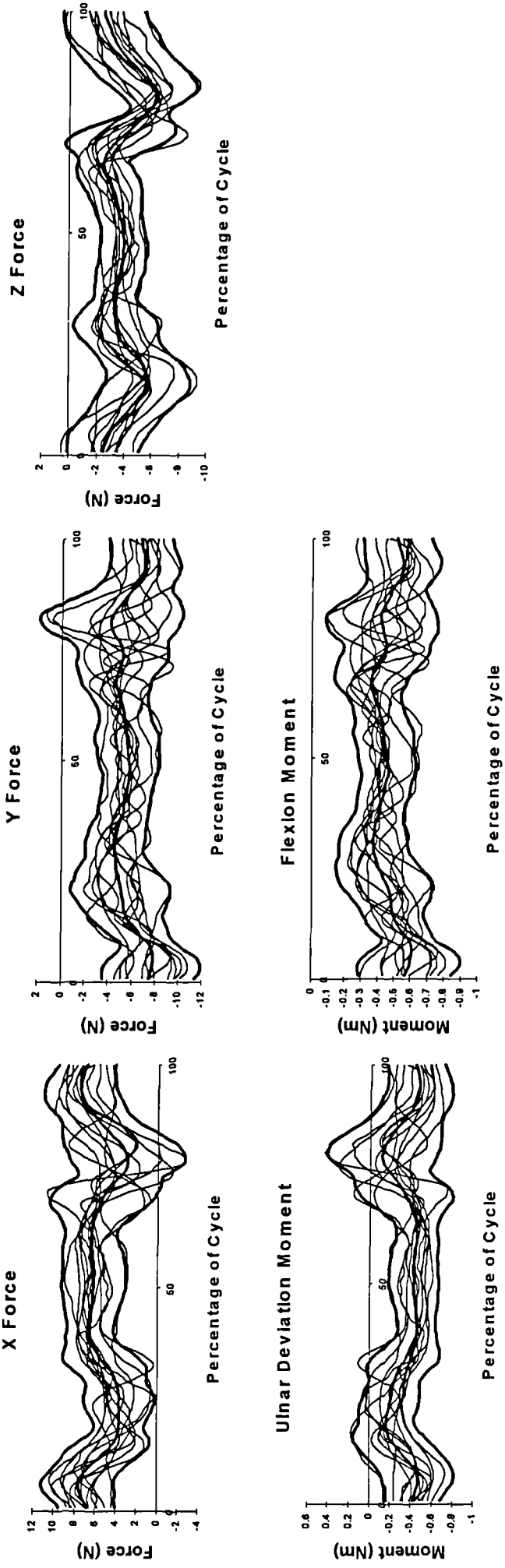

Fig.W.17 Force and Moment graphs for the Wrist during performance of Activity 9, showing mean +/- 2SD in bold.

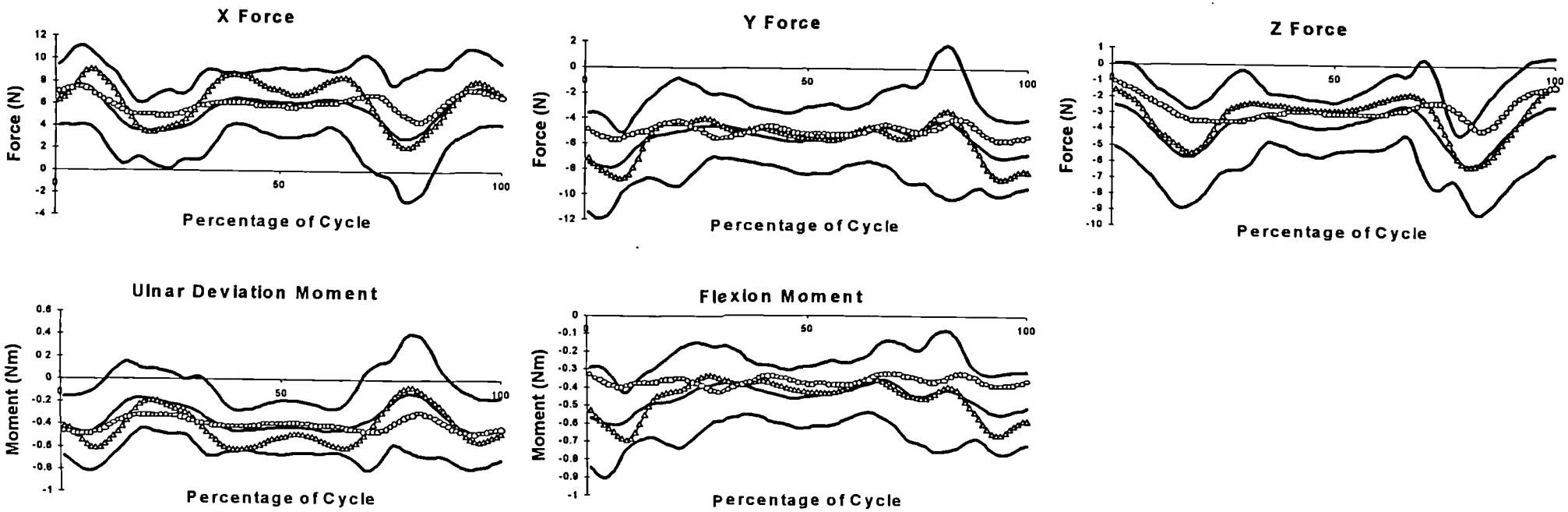

Fig.W.18 Comparison of impaired with unimpaired graphs for the Wrist during performance of Activity 9. (Δ - Subject 11, o - Subject 12)

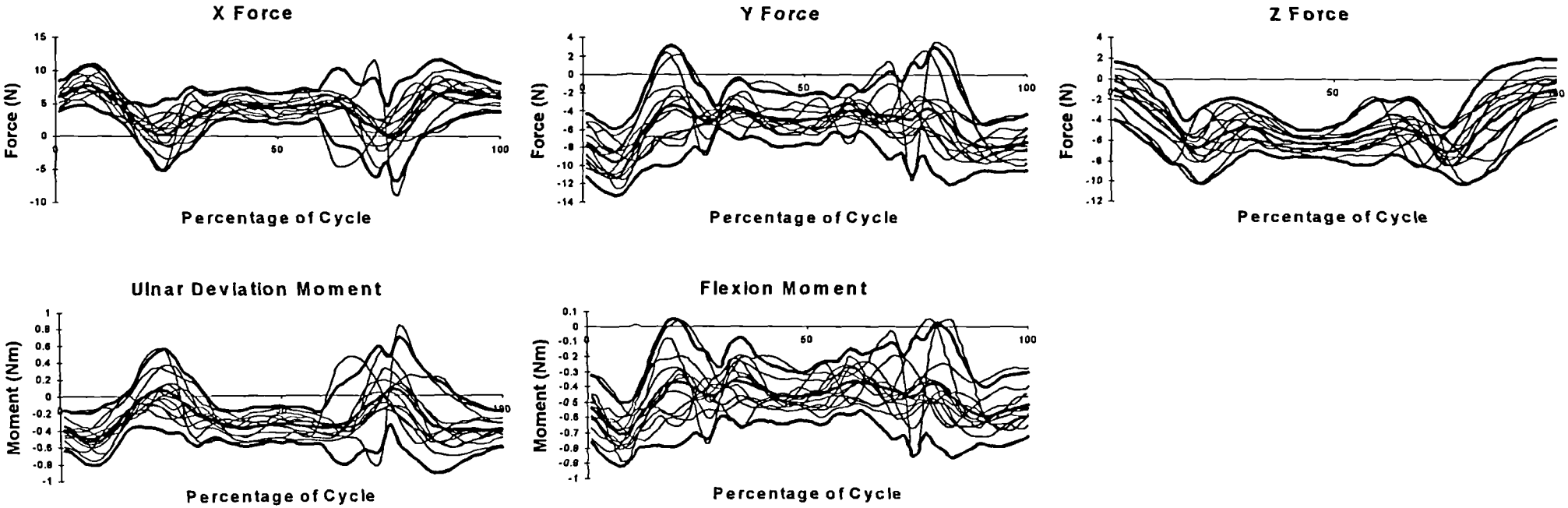

Fig.W.19 Force and Moment graphs for the Wrist during performance of Activity 10, showing mean +/- 2SD in bold.

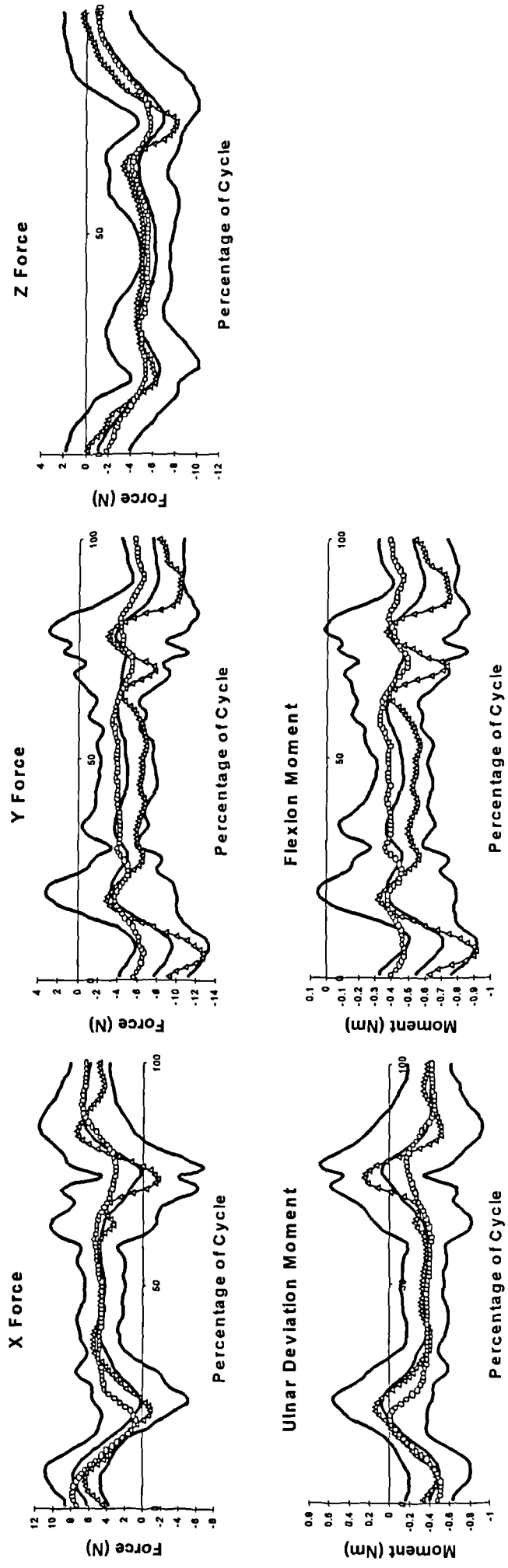

Fig.W.20 Comparison of impaired with unimpaired graphs for the Wrist during performance of Activity 10. (Δ - Subject 11, o - Subject 12)

APPENDIX IV

Results for tests performed by subject No.1 only

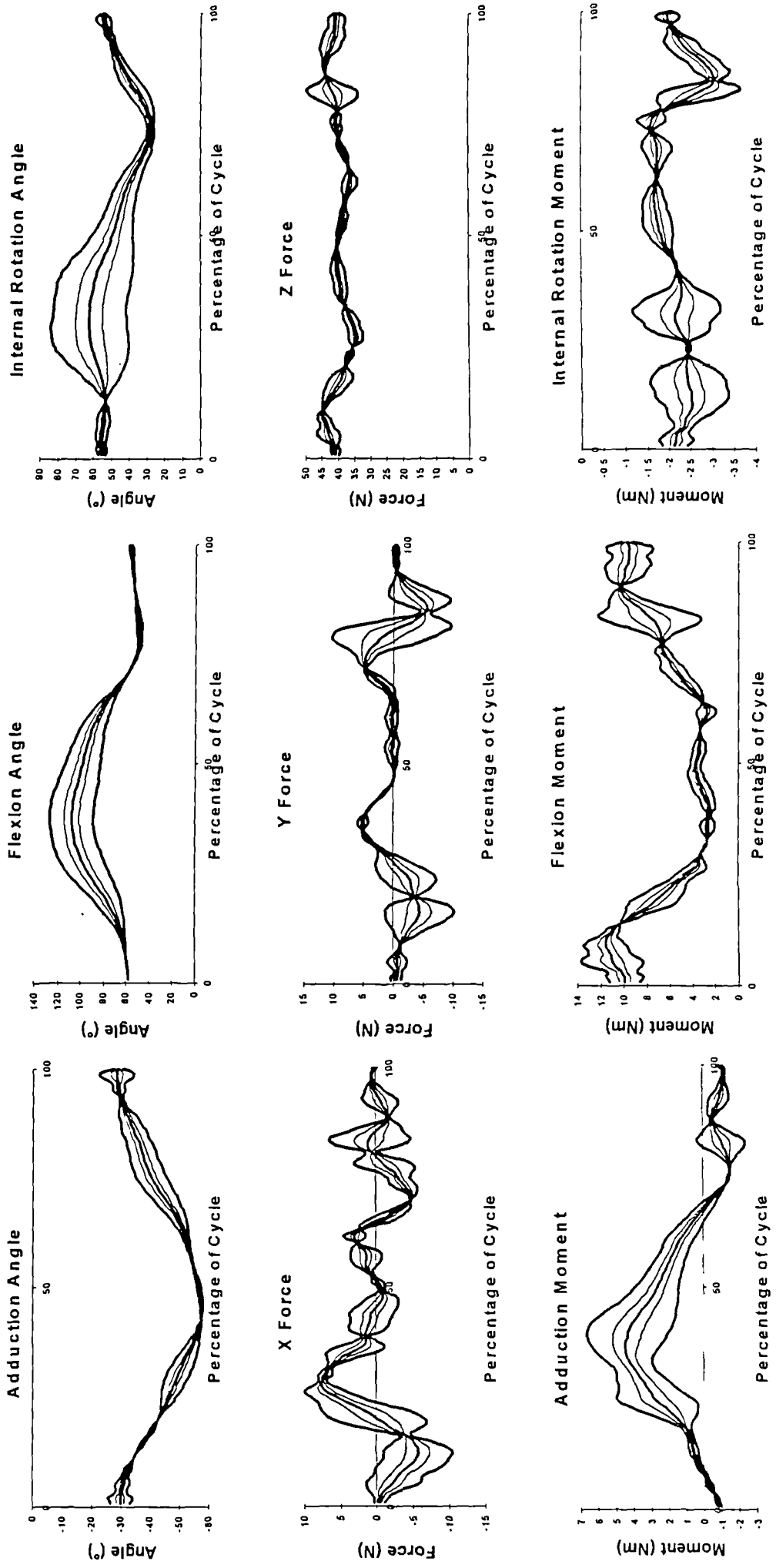

Fig.S1.1 Angle, Force and Moment graphs for the Shoulder during performance of brushing posterior of head, showing mean +/- 2SD in bold.

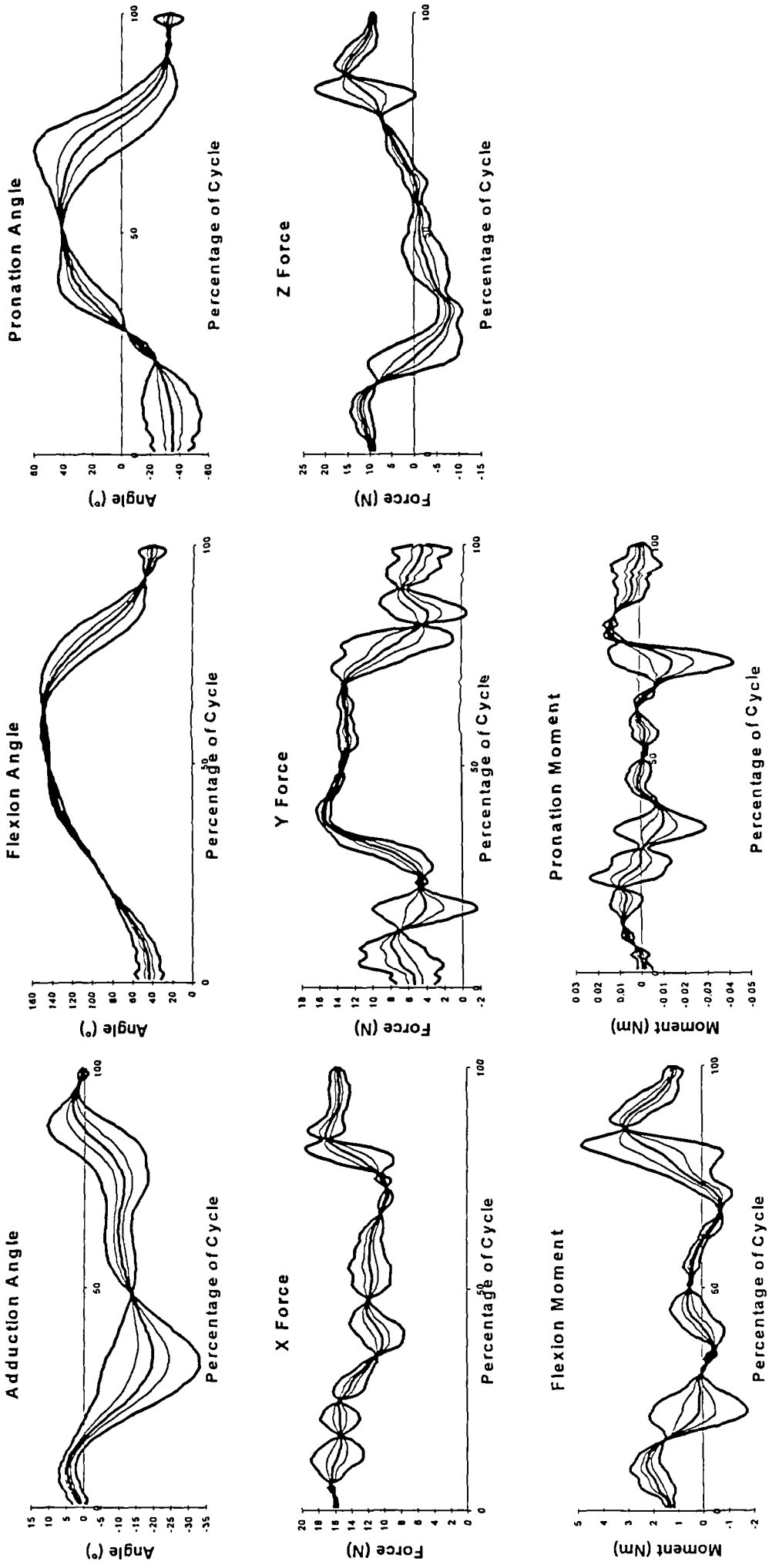

Fig.S1.2 Angle, Force and Moment graphs for the Elbow during performance of brushing posterior of head, showing mean +/- 2SD in bold.

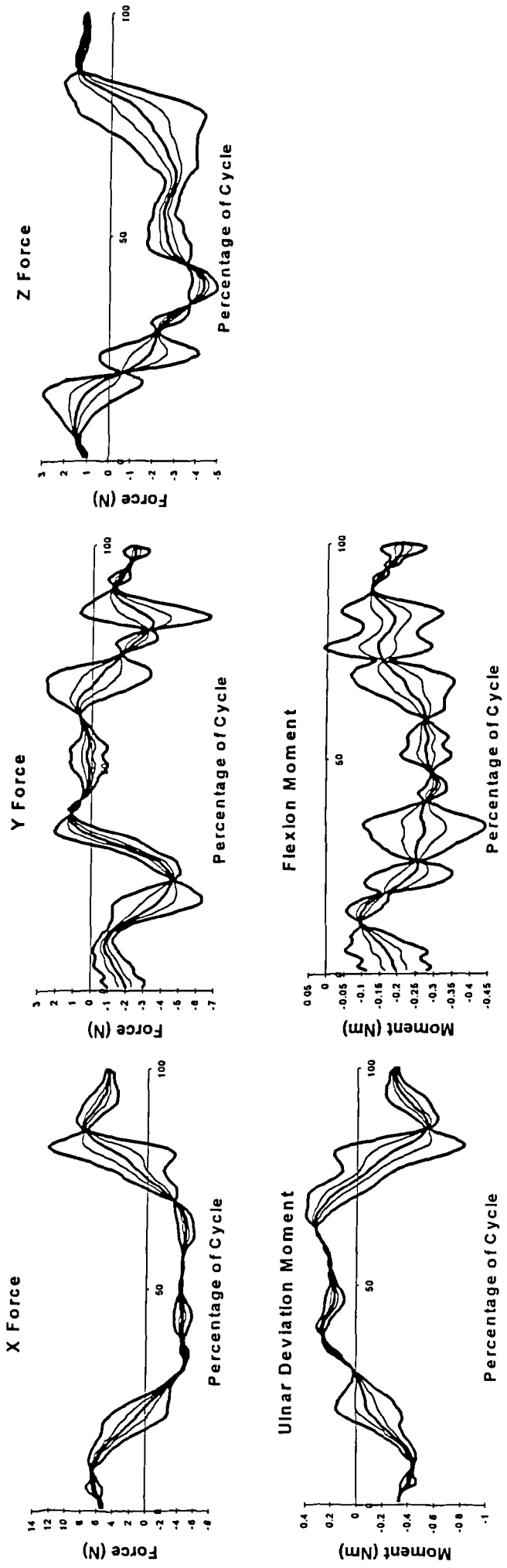

Fig.S1.3 Force and Moment graphs for the Wrist during performance of brushing posterior of head, showing mean +/- 2SD in bold.

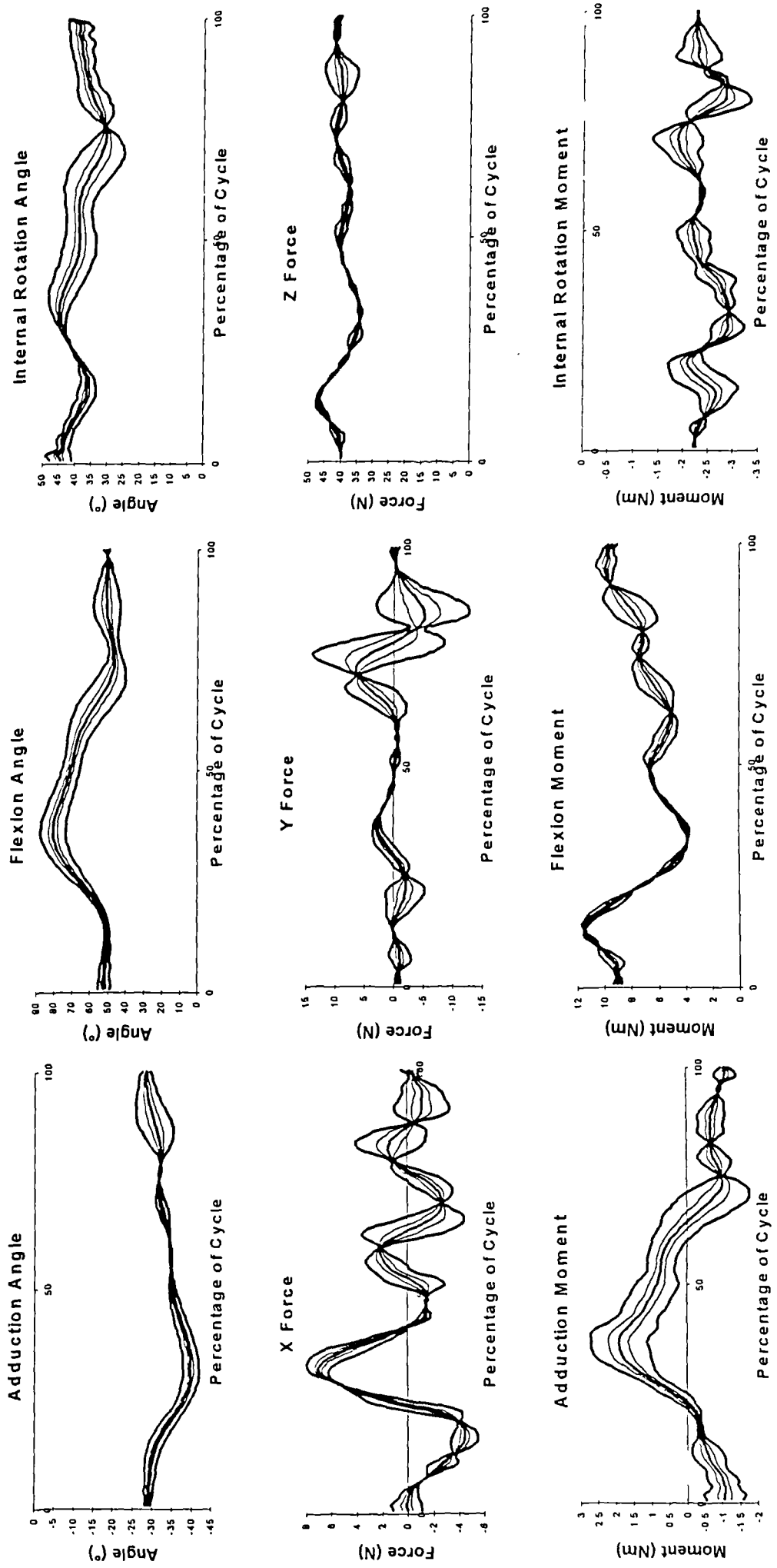

Fig.S1.4 Angle, Force and Moment graphs for the Shoulder during performance of brushing right side of head, showing mean +/- 2SD in bold.

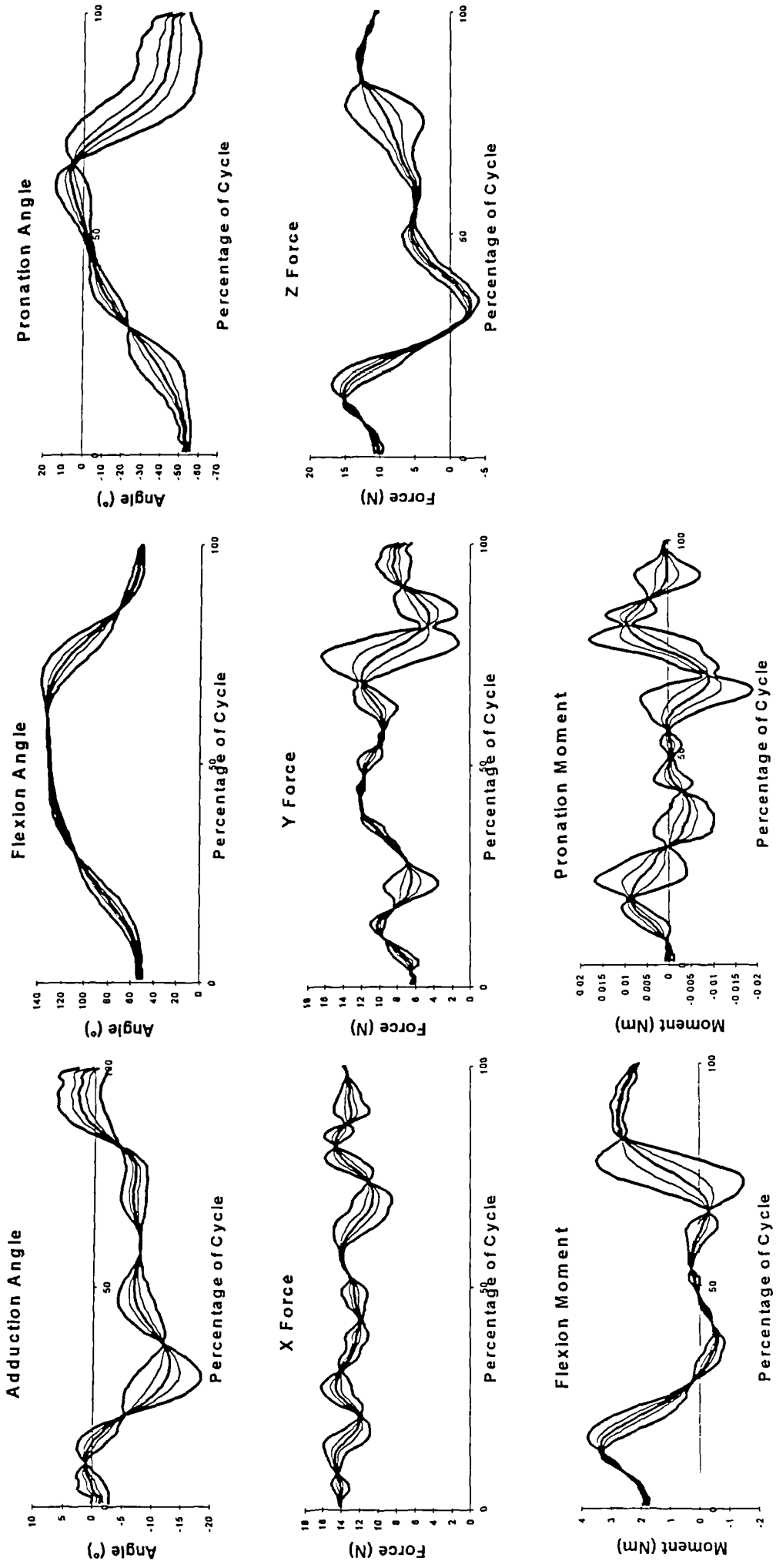

Fig.S1.5 Angle, Force and Moment graphs for the Elbow during performance of brushing right side of head, showing mean +/- 2SD in bold.

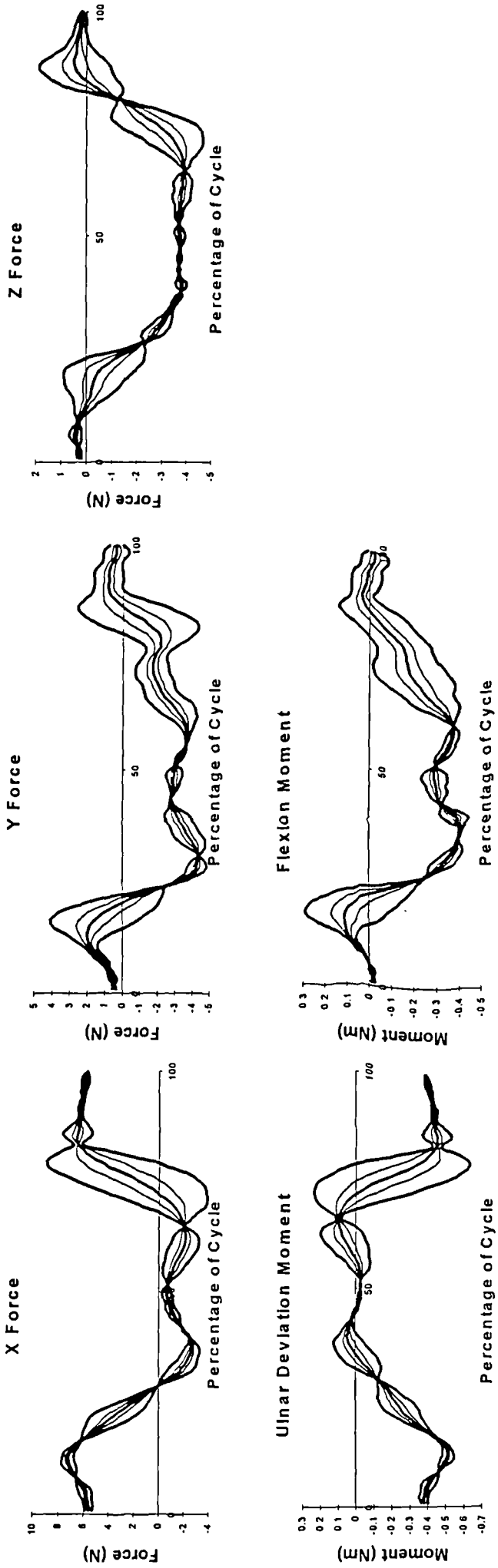

Fig.S1.6 Force and Moment graphs for the Wrist during performance of brushing right side of head, showing mean +/- 2SD in bold.

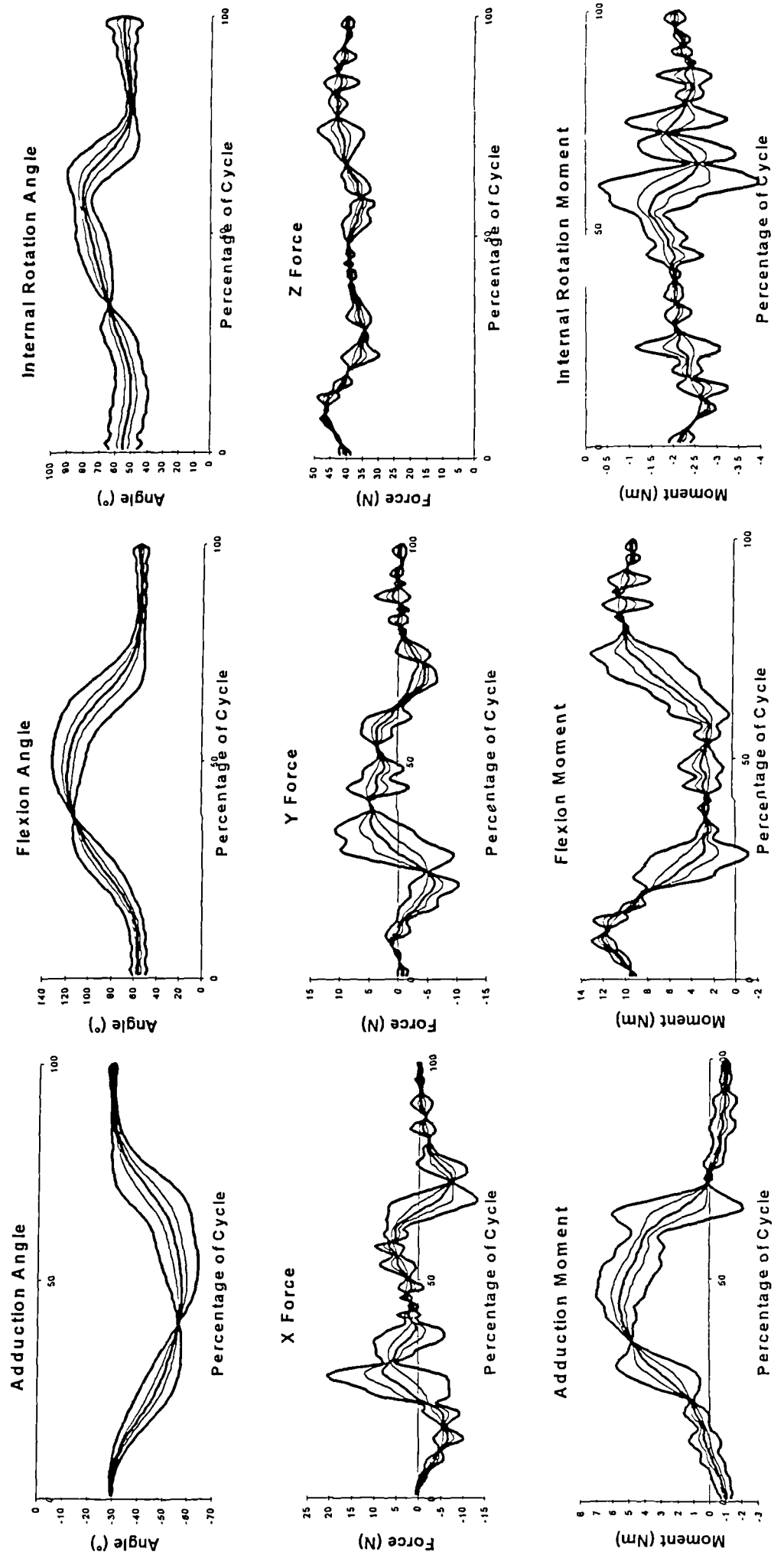

Fig.S1.7 Angle, Force and Moment graphs for the Shoulder during performance of brushing top of head, showing mean +/- 2SD in bold.

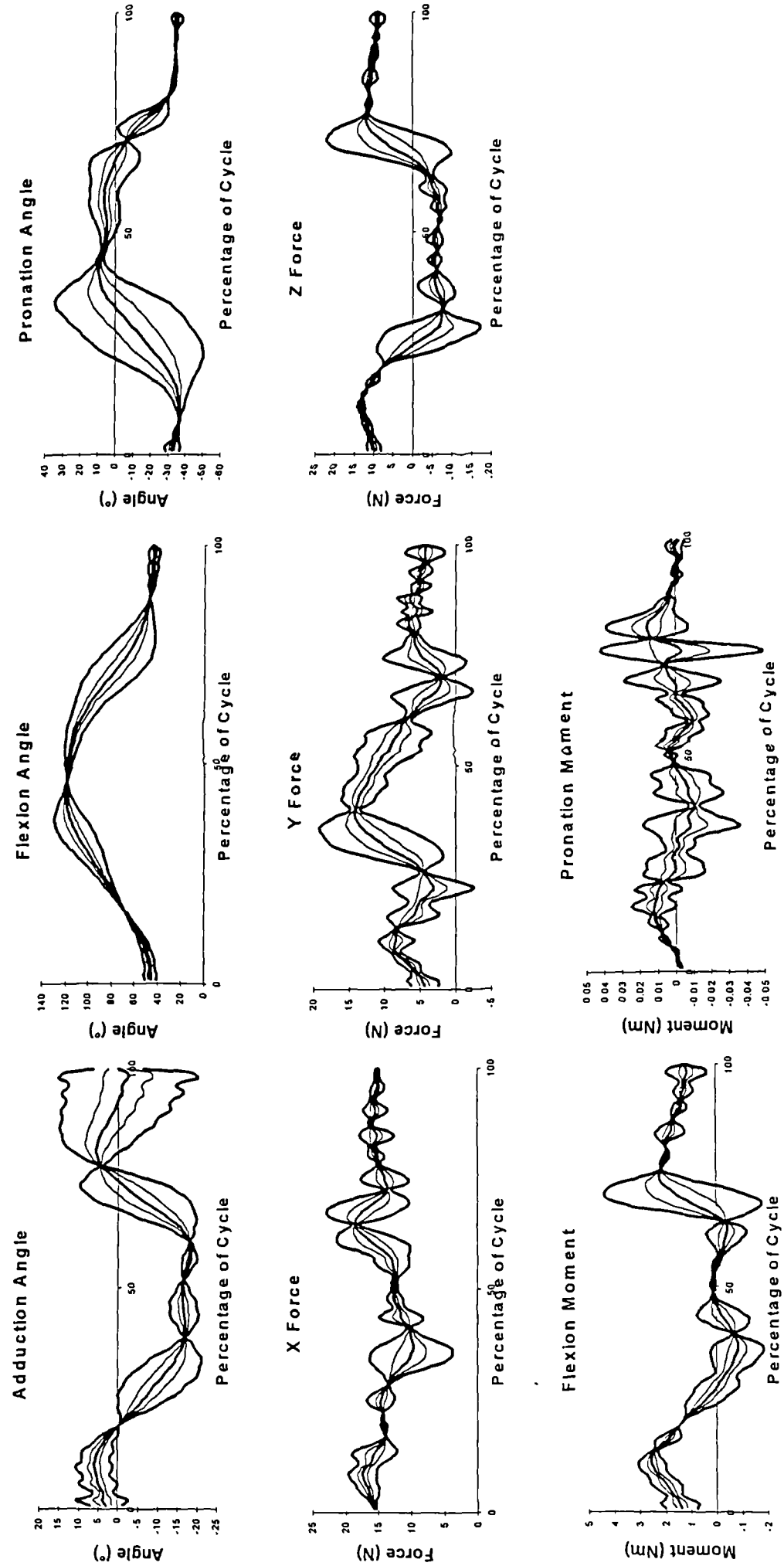

Fig.S1.8 Angle, Force and Moment graphs for the Elbow during performance of brushing top of head, showing mean +/- 2SD in bold.

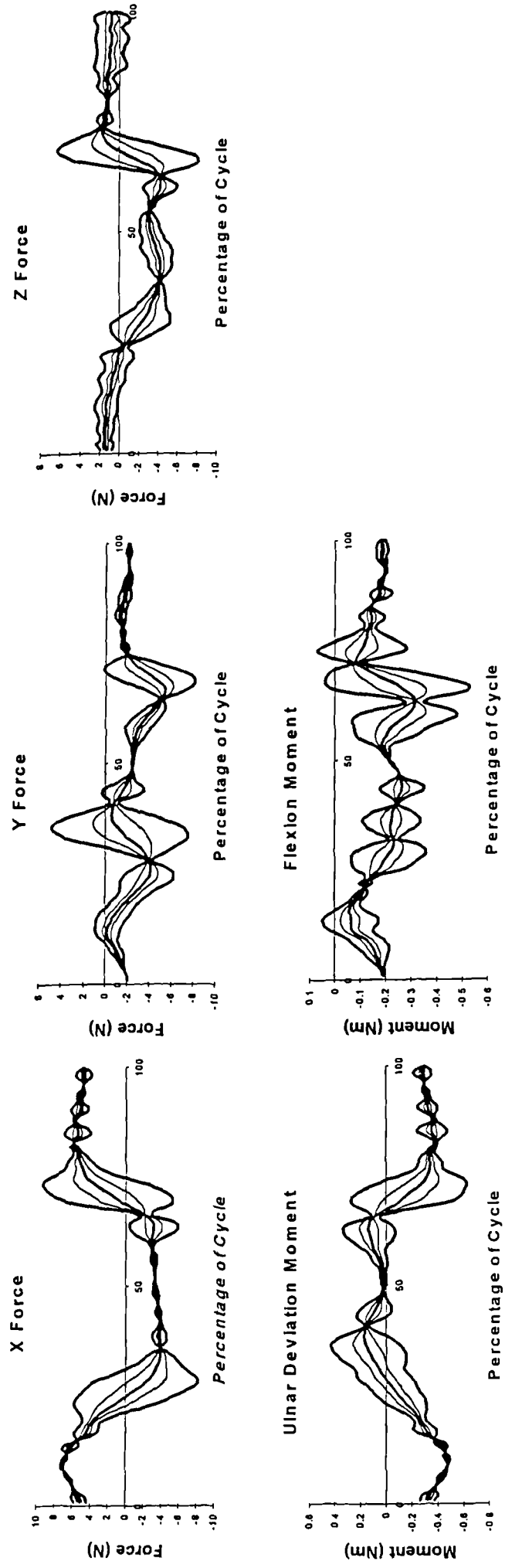

Fig.S1.9 Force and Moment graphs for the Wrist during performance of brushing top of head, showing mean +/- 2SD in bold.

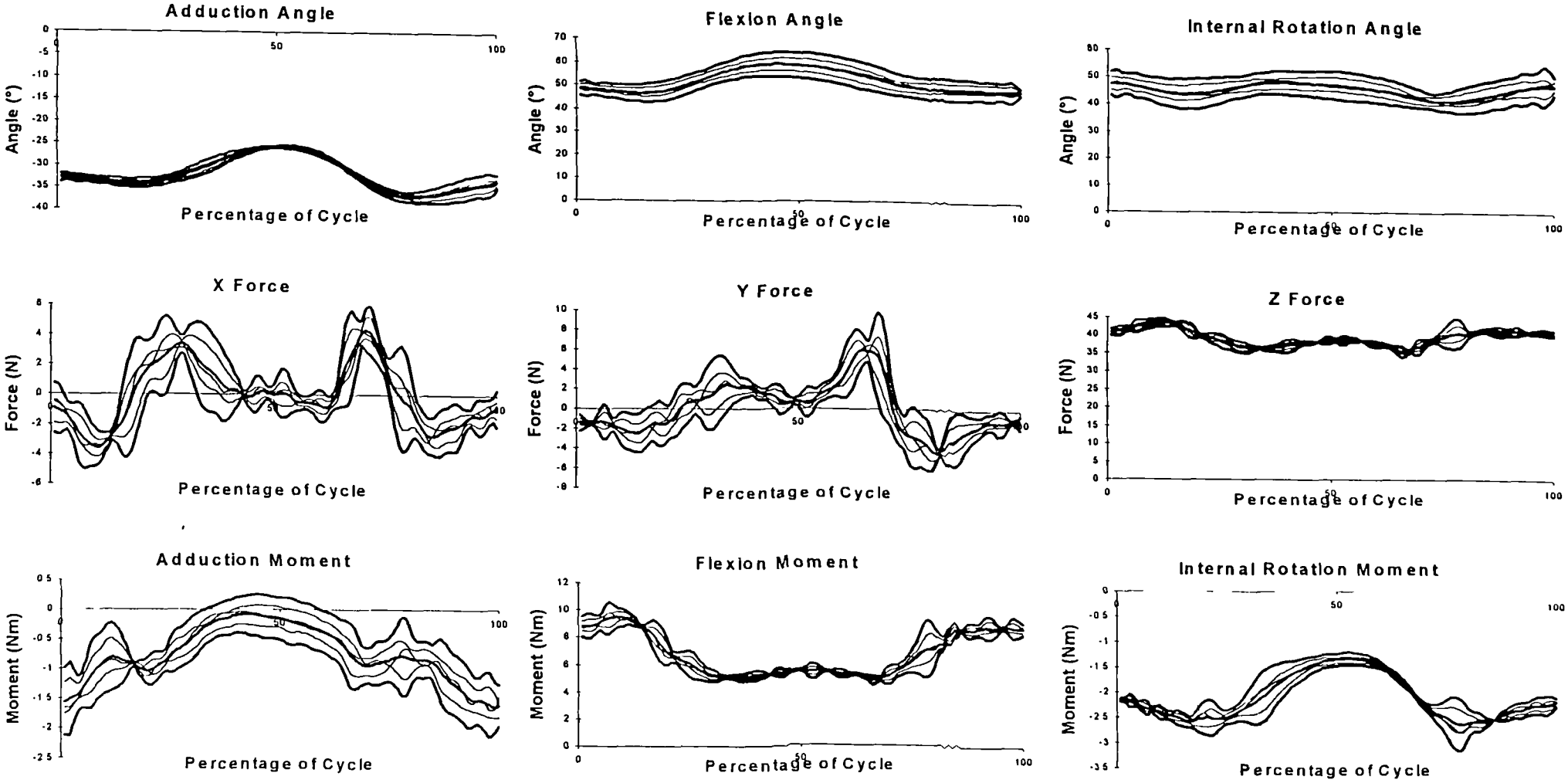

Fig.S1.10 Angle, Force and Moment graphs for the Shoulder during performance of placing hand over mouth, showing mean +/- 2SD in bold.

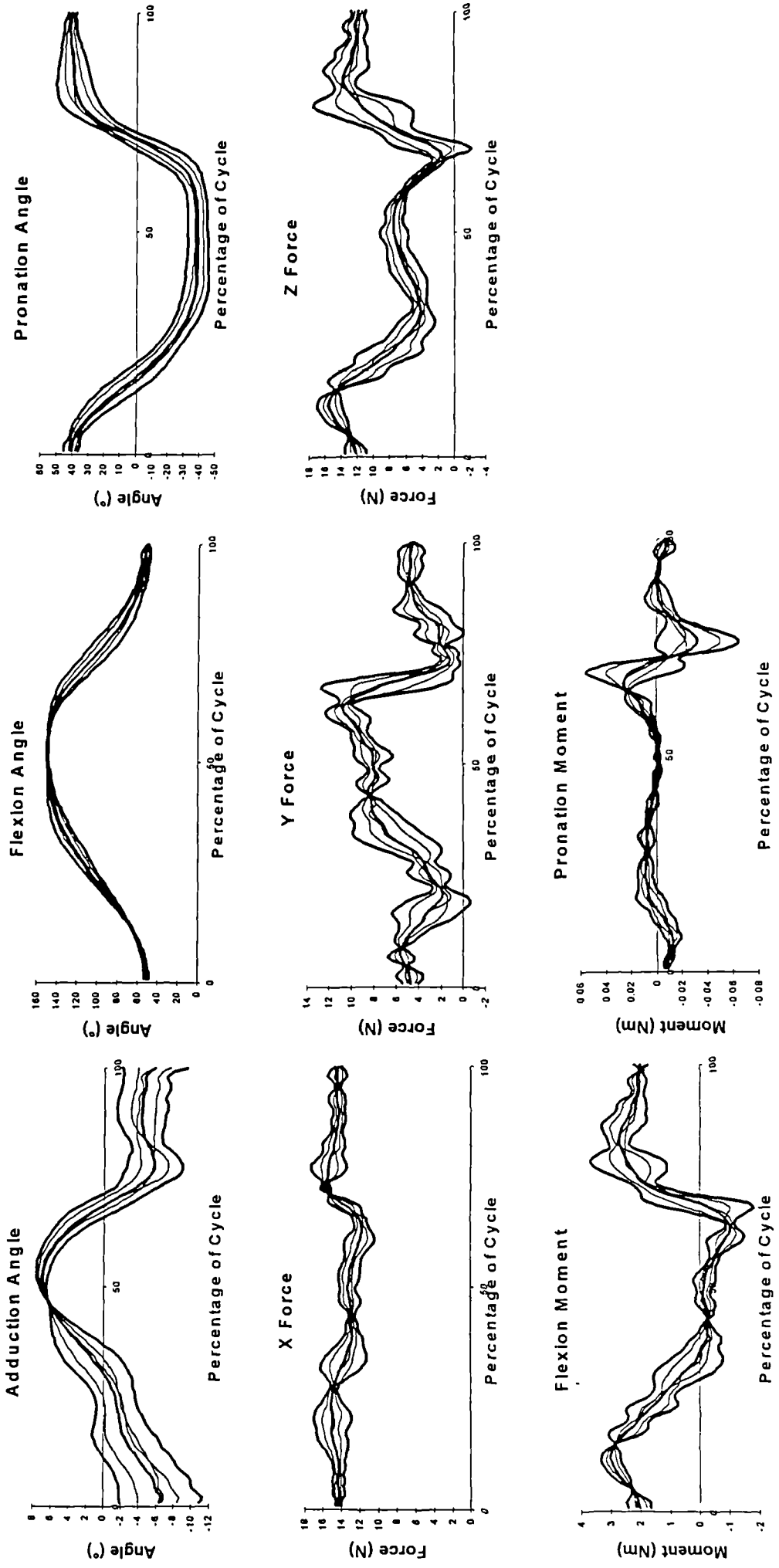

Fig.S1.11 Angle, Force and Moment graphs for the Elbow during performance of placing hand over mouth, showing mean +/- 2SD in bold.

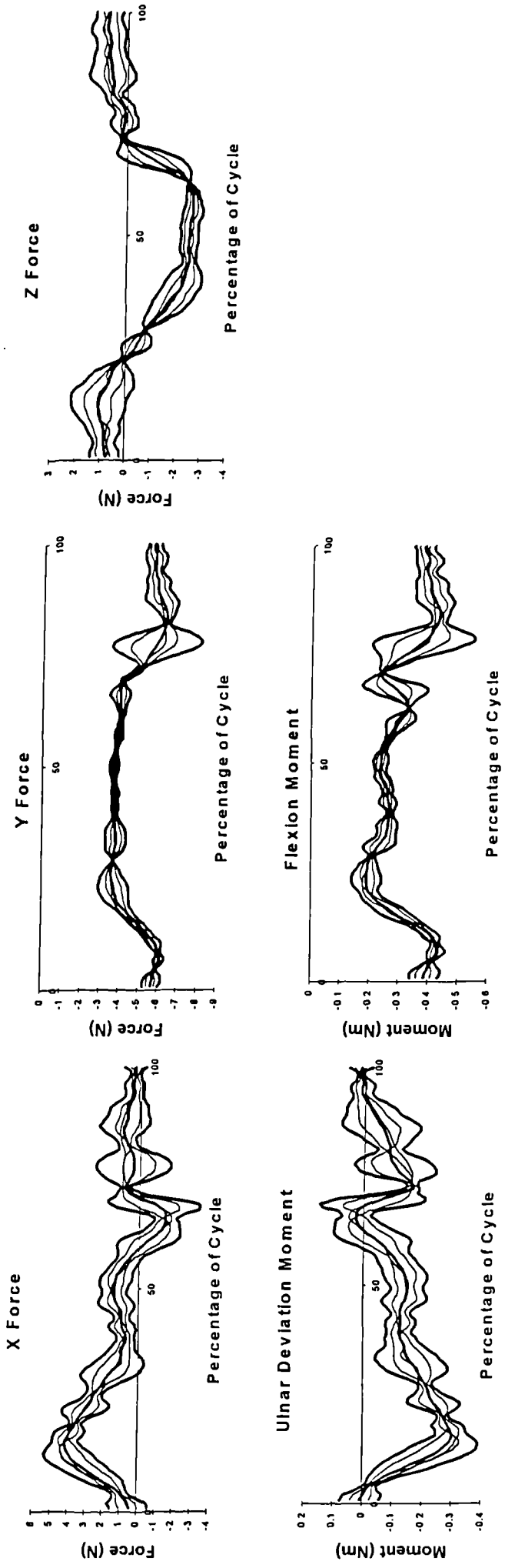

Fig.S1.12 Force and Moment graphs for the Wrist during performance of placing hand over mouth, showing mean +/- 2SD in bold.

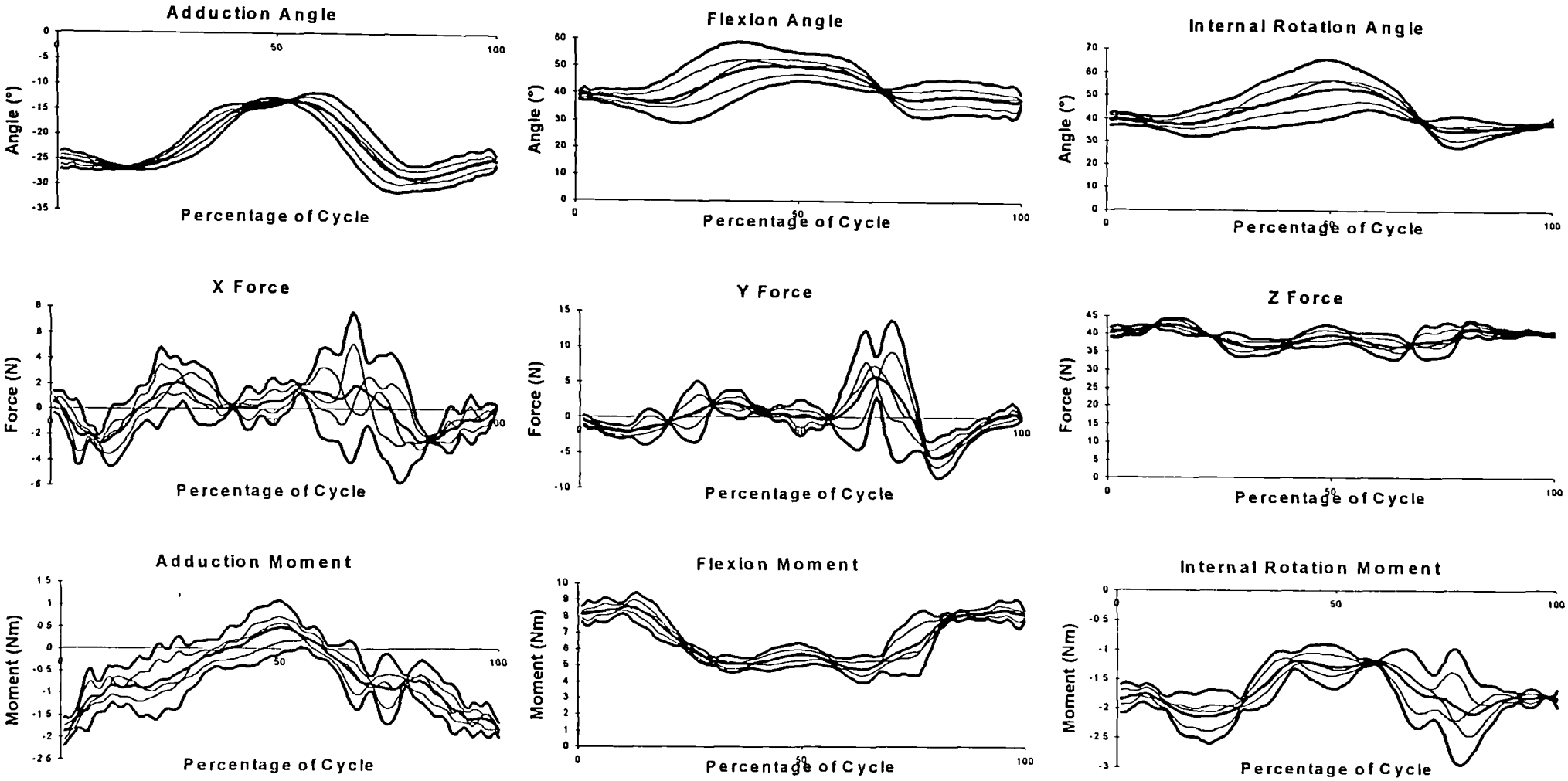

Fig.S1.13 Angle, Force and Moment graphs for the Shoulder during performance of reaching to neck, showing mean +/- 2SD in bold.

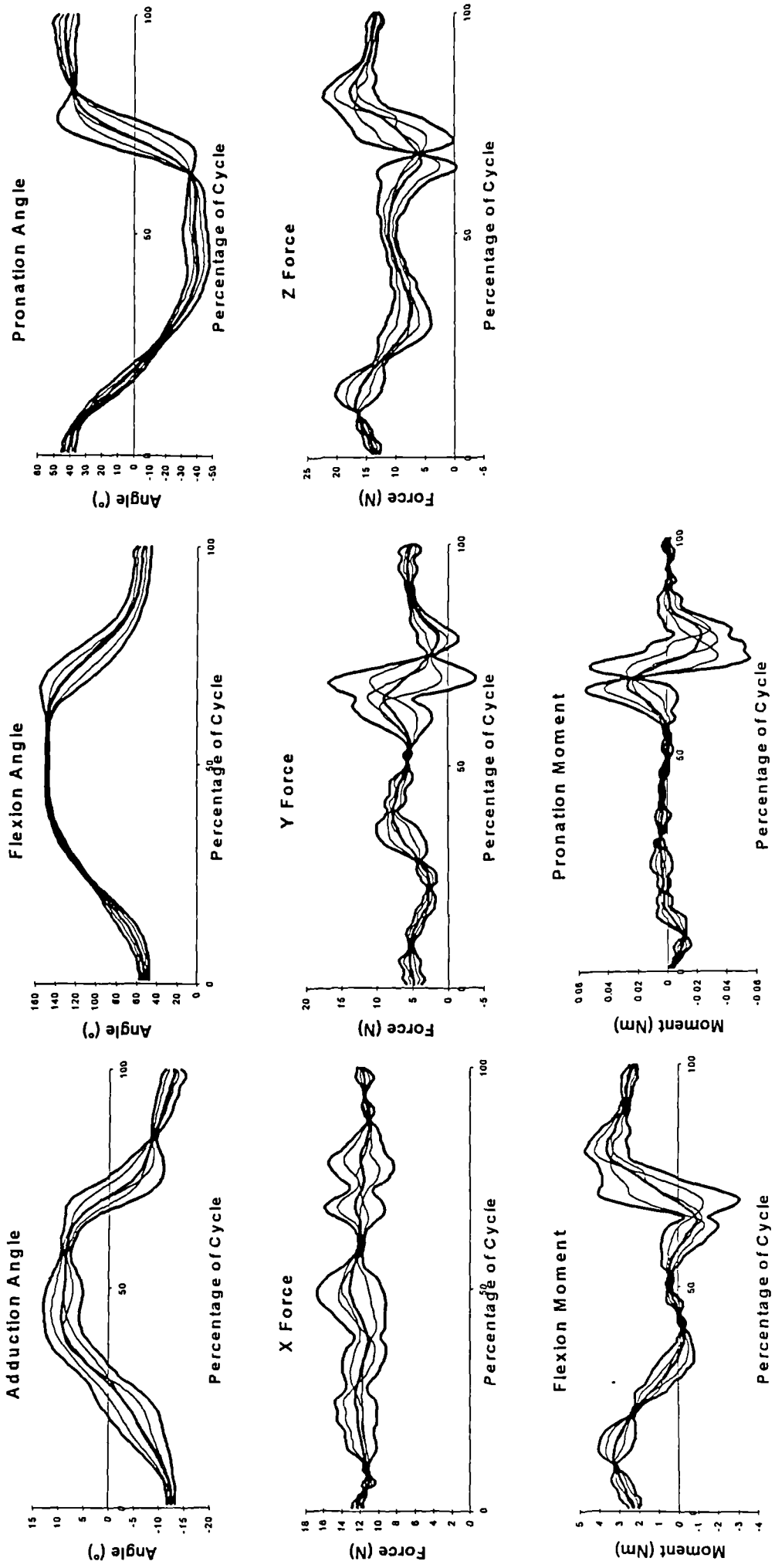

Fig.S1.14 Angle, Force and Moment graphs for the Elbow during performance of reaching to neck, showing mean +/- 2SD in bold.

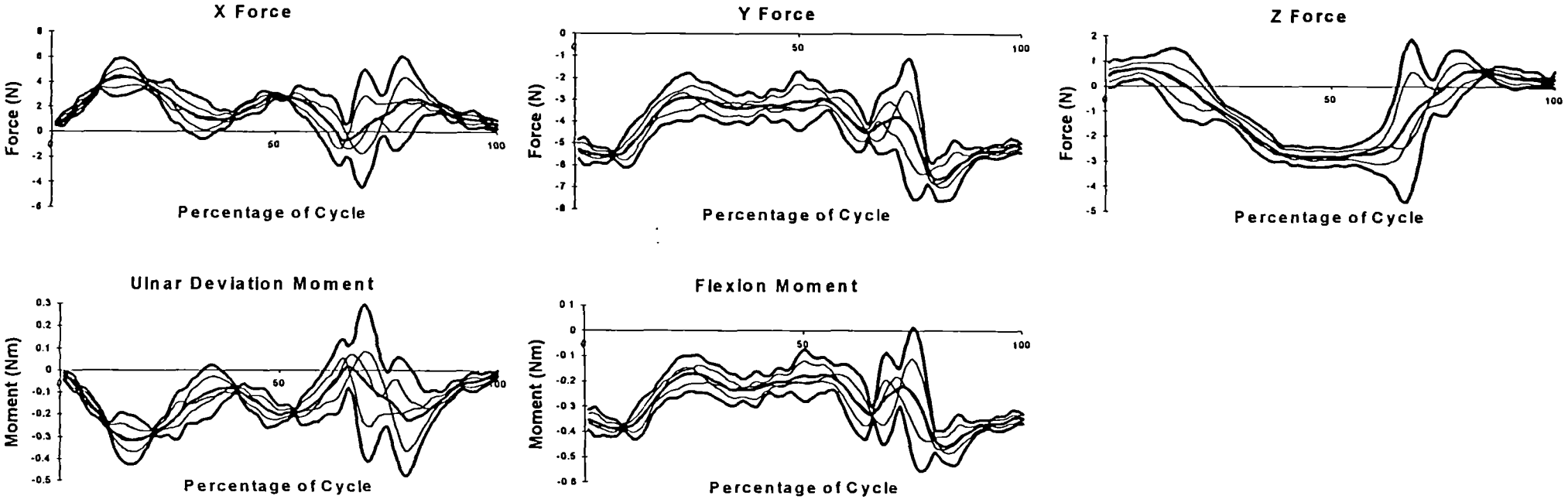

Fig.S1.15 Force and Moment graphs for the Wrist during performance of reaching to neck, showing mean +/- 2SD in bold.

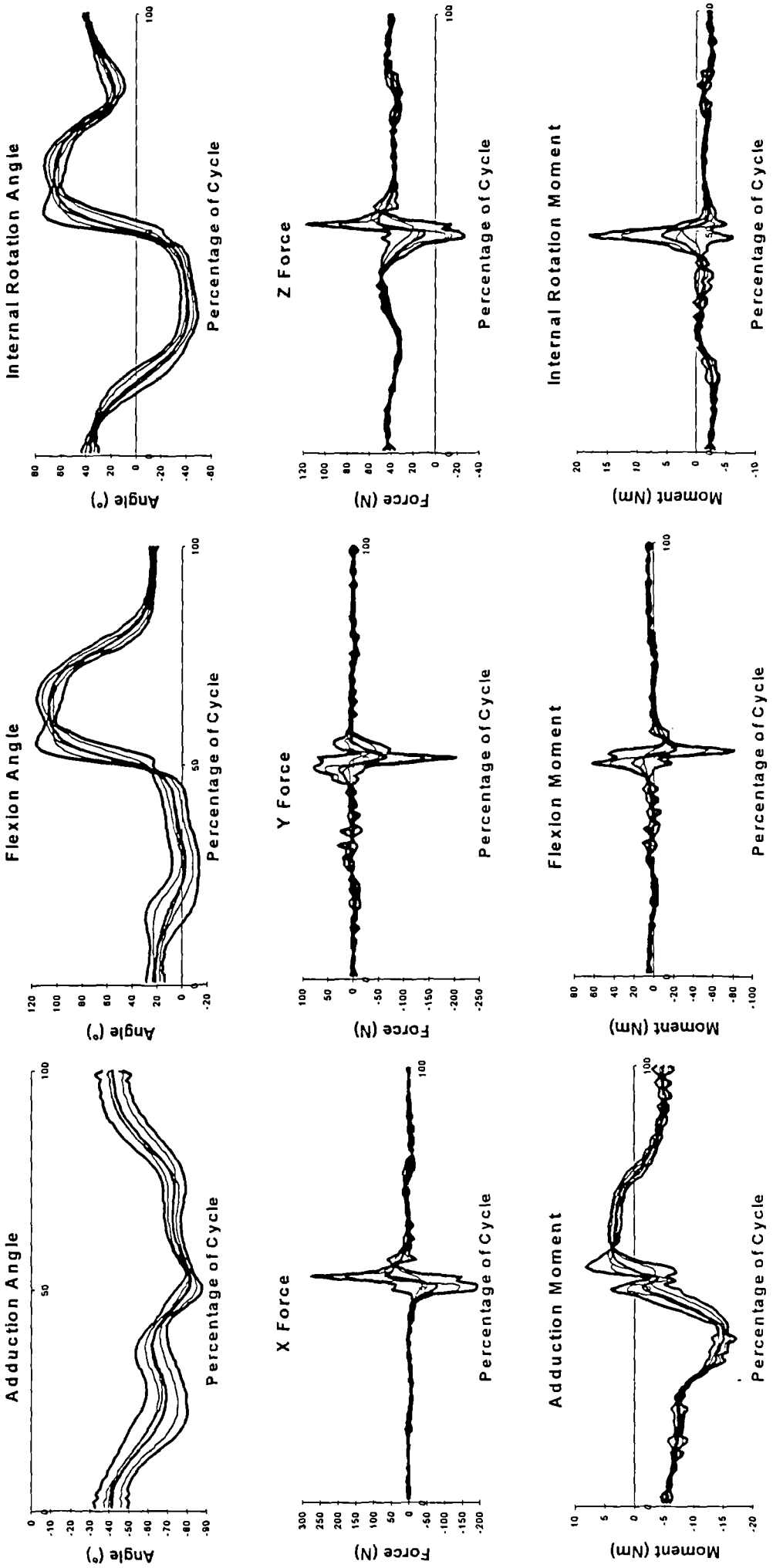

Fig.S1.16 Angle, Force and Moment graphs for the Shoulder during performance of reaching to top of head, showing mean +/- 2SD in bold.

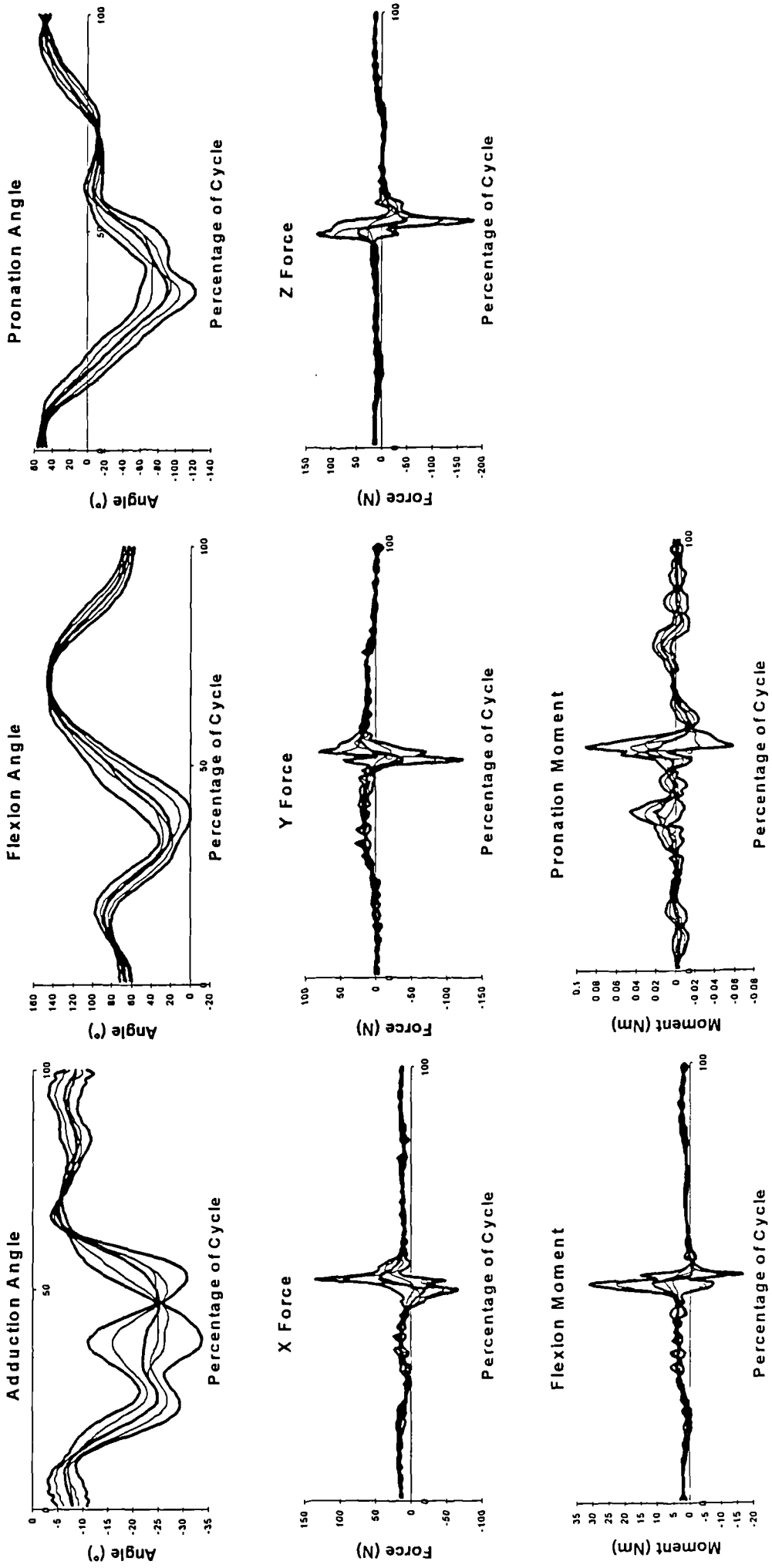

Fig.S1.17 Angle, Force and Moment graphs for the Elbow during performance of reaching to top of head, showing mean +/- 2SD in bold.

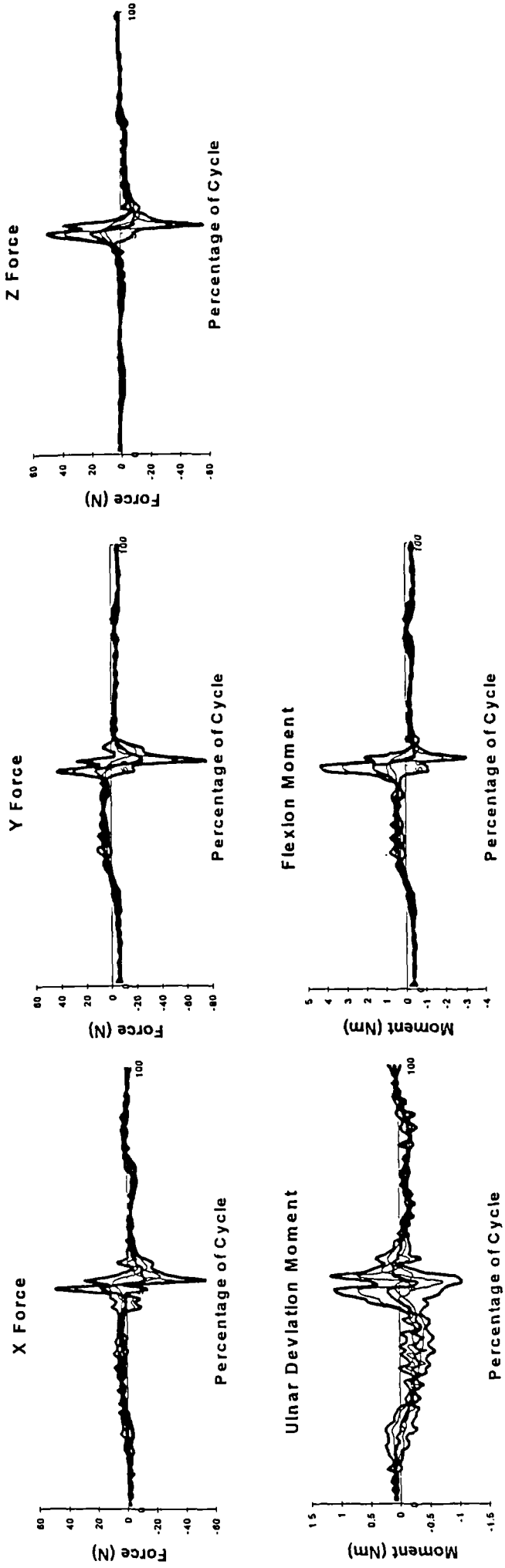

Fig.S1.18 Force and Moment graphs for the Wrist during performance of reaching to top of head, showing mean +/- 2SD in bold.

APPENDIX V

MATLAB™ analysis routines in alphabetical order:

```
%Procedure to allow the running of the APAS analysis functions on typing
%the instruction "APAS" at the >> prompt.  The analysis option should be run
which
%will produce and save files of data.
%Then the 'plots' or 'normalise' option can be run as many times as required.
%
%Written by Ingram Murray, CREST, University of Newcastle upon Tyne.
%
%Date: June 1998
%Modifications:     Largely re-written 02/12/98 to allow quicker data analysis
%            by running tech, tech2 and numdiff automatically.
%
%Input:      handvec - a row vector containing the values of hand load for each
test in order.
%      srvec  - a row vector containing the values of the time between samples
for each test.
%Output: Runs selected script m-file.
%
%load(input('Type the name of the subject file you wish to analyse: ','s'))
%
%
antsts=menu('Which option do you require ?','ANALYSE ALL ACTIVITIES','ANALYSE A
SPECIFIC ACTIVITY','PLOT RESULTS','NORMALISE RESULTS','CLOSE WINDOW');
%
if antsts==1
%
handvec=[0 0 0 0 0.048 0.2755 0.215 0.045 0.452 0.452]
srvec=[0.04 0.06 0.06 0.06 0.04 0.06 0.06 0.06 0.06 0.06]
%
%Ask for segement parameters.
M=input('What is the body mass of the subject in kilograms ? ');
H=input('What is the height of the subject in metres ? ');
%
LSQF=input('Do you wish to use the SVD least squares fitting of marker
positions? Y/N [Y]: ','s');
       if isempty(LSQF)
       LSQF='Y';
       end
%
       load le.txt
       load me.txt
       load tv.txt
%
rps=input('How many activities were tested ?: ');
for files=1:rps
       file = 'Test';
       load([file,num2str(files),'.txt']);
       should=eval(['Test' num2str(files)]);
       disp(['Test' num2str(files)]);
       Hload=handvec(files)
       h=srvec(files)
       tech
       tech2
       numdiff
       clear global
       hmnumdif
       clear global
%
       testres=[ALLANGLE ALLFORCE ALLMOMENTS];
       eval(['Tstres' num2str(files) '=testres']);
       File = 'Tstres';
       save([File,num2str(files)],[File,num2str(files)],'-ascii','-tabs')
%
       hlodres=[ALLHLFRCS ALLHLMOMS];
       eval(['Hldres' num2str(files) '=hlodres']);
       FilE = 'Hldres';
       save([FilE,num2str(files)],[FilE,num2str(files)],'-ascii','-tabs')
%
       inrtres=[INERTIAMOMS];
       eval(['Ineres' num2str(files) '=inrtres']);
       fiLe = 'Ineres';
       save([fiLe,num2str(files)],[fiLe,num2str(files)],'-ascii','-tabs')
%
       trajvel=[straj etraj wtraj q qd qdd];
       eval(['Trjvel' num2str(files) '=trajvel']);
       fIle = 'Trjvel';
```

```
       save([fIle,num2str(files)],[fIle,num2str(files)],'-ascii','-tabs')
%
       omomdot=[OMEGAS OMEGADOTS];
       eval(['Omegs' num2str(files) '=omomdot']);
       fILe = 'Omegs';
       save([fILe,num2str(files)],[fILe,num2str(files)],'-ascii','-tabs')
%
       if files==1
       bsps=[ual fal hl;uam fam hm;uac fac hc;uaIa uaIt uaIl;faIa faIt faIl;hIa
hIt hIl];
       eval(['BSPs' num2str(files) '=bsps']);
       filE = 'BSPs';
       save([filE,num2str(files)],[filE,num2str(files)],'-ascii','-tabs')
       end
end
apas
end
%
if antsts==2
%
%Ask for segement parameters.
M=input('What is the body mass of the subject in kilograms ? ');
H=input('What is the height of the subject in metres ? ');
%
LSQF=input('Do you wish to use the SVD least squares fitting of marker
positions? Y/N [Y]: ','s');
       if isempty(LSQF)
       LSQF='Y';
       end
%
       load le.txt
       load me.txt
       load tv.txt
%
       nxtest=input('Which activity do you wish to analyse?: ');
       file = 'Test';
       load([file,num2str(nxtest),'.txt']);
       should=eval(['Test' num2str(nxtest)]);
       disp(['Test' num2str(nxtest)]);
       Hload=handvec(nxtest);
       h=srvec(nxtest);
       tech
       tech2
       numdiff
       clear global
       testres=[ALLANGLE ALLFORCE ALLMOMENTS];
       eval(['Tstres' num2str(nxtest) '=testres'])
       file = 'Tstres';
       save([file,num2str(nxtest)],[file,num2str(nxtest)],'-ascii','-tabs')
       apas
end
if antsts==3
        plots
end
if antsts==4
       rpps=input('How many activities were tested ?: ');
       cadence=[];
       for ffiles=1:rpps
       disp(['Results' num2str(ffiles)])
              ffile = 'Tstres';
              load([ffile,num2str(ffiles)]);
              Whatest=eval(['Tstres' num2str(ffiles)]);
              fFiLe = 'Hldres';
              load([fFiLe,num2str(ffiles)]);
              Whahl=eval(['Hldres' num2str(ffiles)]);
              data_sdd
%
              eval(['Nrmres',num2str(ffiles),'=normres']);
              fiile = 'Nrmres';
              save([fiile,num2str(ffiles)],[fiile,num2str(ffiles)],'-ascii','-
tabs');
%
              eval(['Nrhlrs',num2str(ffiles),'=norhlrs']);
              fIiLe = 'Nrhlrs';
              save([fIiLe,num2str(ffiles)],[fIiLe,num2str(ffiles)],'-ascii','-
tabs');
       end
              Cadnce=cadence;
```

```
                save Cadnce Cadnce -ascii -tabs;
apas
end
if antsts==5
close
end
```

```
function [out] = cole(data)
%Procedure to calculate the rotations about defined embedded axes using
%the joint co-ordinate system.
%
%Written by Ingram Murray, CREST, University of Newcastle upon Tyne.
%
%Date: March 1998
%
%References: Cole,G.K. et al (1993).  Application of the Joint Co-
ordinate System
%             to Three-dimensional Joint Attitude and Movement
Representation : A
%             Standardization Proposal.  Journal of Biomechanical
Engineering.
%             November 1993 : Vol 115 : pp 344-349
%
%e(k)=unit vector describing the attitude of the kth axis of the joint
%     co-ordinate system between the reference segment (1) and the target
segment (2),
%     relative to an inertial reference system
%F, L, T = breakdown of the axes of a body segment co-ordinate system
into an
%          axis of flexion, a longitudinal axis and a third axis.
%fi, li, ti = unit vectors that describe the attitude of the F, L and T
axes
%              respectively, in an inertrial reference system
%
%Input: Matrix C= [f1 l1 t1;f2 l2 t2], containing the unit vectors
describing the
%       attitude of the axes of the co-ordinate systems embedded in each
segment.
%       Vector [f1 l1 t1] describes the flexion, longitudinal and third
co-ordinate
%       axes of the proximal segment.
%       Vector [f2 l2 t2] describes the flexion, longitudinal and third
co-ordinate
%       axes of the distal segment.
%
%Output: Angles of rotation about axes e1, e2, e3, flexion, abduction and
rotation
%        respectively.
%
f1=data(1,1:3);,l1=data(1,4:6);,t1=data(1,7:9);
f2=data(2,1:3);,l2=data(2,4:6);,t2=data(2,7:9);
e1=f1;
e3=l2;
a=cross(e3,e1);
b=vecsize(cross(e1,e3));
if (dot((cross(e3,e1)),t2)<0) & (dot((cross((cross(e3,e1)),e3)),f2)>0)
   A=-1;
else
   A=1;
end
e2=(a/b)*A;
r=(cross(f1,e2))/(vecsize(cross(f1,e2)));
theta1=(acos(dot(e2,t1)))*(signd(dot(e2,l1)));
theta2=(acos(dot(r,l2)))*(signd(dot(f1,l2)));
theta3=(acos(dot(e2,t2)))*(signd(dot(e2,f2)));
out=[rad2deg(theta1),rad2deg(theta2),rad2deg(theta3)];
```

```
%THIS MATLAB ROUTINE STANDARDISES THE DATA CYCLE LENGTHS TO 100 POINTS
%
%*********************************************************************
%Adapted from code first written 24/11/95 by John R. Williams and given
in;
%Williams,J.R. (1996)  Some Aspects of the Biomechanics of the Elbow
Joint:
%Related to Prosthetic design.
%
%Modified to include Force and Moment normalisation by I. Murray 21/7/98
%Modified to allow loading and saving of particular test by I. Murray
02/12/98
%Modified to normalise with interp1 instead of interpft by I. Murray
04/03/99
%*********************************************************************
%
%
cyclea=[];
cyclef=[];
cyclem=[];
cyclhl=[];
ANGLES_dg=Whatest(:,1:6);
FORCES_dg=Whatest(:,7:15);
MOMENTS_dg=Whatest(:,16:22);
HLFMOM_dg=Whahl(:,1:16);
%
%Plot Shoulder and Elbow Flexion curves.
%
%
figure(1)
clf reset
plot(ANGLES_dg(:,2))
hold
plot(ANGLES_dg(:,5),'r')
plot([0,(max(length(ANGLES_dg)))+10],[0,0],'m');
%
%Identify start and end points of cycle.
%
disp(['Test' num2str(ffiles)])
disp('   "Use cursor to click on start of each cycle, then press "return"
"')
l=ginput;   %reads point from cursor
l=l(:,1);   %discards y values
%
%Calculation of cadence in cycles per minute
cadence(ffiles,1)=(1/((l(2,1)-l(1,1))*srvec(1,ffiles)))*60;
%
%
%spread the field range up and down one frame.
%
l_up=ceil(l);            %rounds towards +infinity
l_down=floor(l);  %rounds towards -infinity
%
%
figure(2);     %prepare figure for data
clf reset;
hold;
%
angle_data=zeros(100,6);
%
%define the start and finish frames of each cycle
      start=l_down(1,1);
      finish=l_up(2,1);
%
%define cycle.
      cyclea=ANGLES_dg(start:finish,:);
%
%standardise data to 100 sample points per cycle
```

```
      sizcyca=size(cyclea,1);
      oldXa=(1:1:sizcyca);
      newXa=linspace(1,sizcyca,100);
      for cyang=1:6;
      oldYa=cyclea(:,cyang);
      newYa(:,cyang)= interp1 (oldXa, oldYa, newXa, 'spline');
      end;
      cy_data=newYa;
%
%alternatively use:
%cy_data=interpft(cyclea,100);
%
      plot(cy_data);
      grid
      angle_data=cy_data;
%
%
figure(3)
clf reset;
%
force_data=zeros(100,9);
%
%define the start and finish frames of each cycle
%
      start=l_down(1,1);
      finish=l_up(2,1);
%
%define cycle.
      cyclef=FORCES_dg(start:finish,:);
%
%standardise data to 100 sample points per cycle
      sizcycf=size(cyclef,1);
      oldXf=(1:1:sizcycf);
      newXf=linspace(1,sizcycf,100);
      for cyfor=1:9;
      oldYf=cyclef(:,cyfor);
      newYf(:,cyfor)= interp1 (oldXf, oldYf, newXf, 'spline');
      end;
      for_data=newYf;
%
%Alternatively use :
%for_data=interpft(cyclef,100);
%
      plot(for_data);
      grid
      force_data=for_data;
%
%
figure(4)
clf reset;
%
moment_data=zeros(100,7);
%
%define the start and finish frames of each cycle
%
      start=l_down(1,1);
      finish=l_up(2,1);
%
%define cycles.
      cyclem=MOMENTS_dg(start:finish,:);
%
%standardise data to 100 sample points per cycle
      sizcycm=size(cyclem,1);
      oldXm=(1:1:sizcycm);
      newXm=linspace(1,sizcycm,100);
      for cymom=1:7;
      oldYm=cyclem(:,cymom);
      newYm(:,cymom)= interp1 (oldXm, oldYm, newXm, 'spline');
      end;
      mom_data=newYm;
```

```
%
%Alternatively use :
%mom_data=interpft(cyclem,100);
%
      plot(mom_data);
      grid
      moment_data=mom_data;
%
%
figure(5)
clf reset;
%
hlfmom_data=zeros(100,16);
%
%define the start and finish frames of each cycle
%
      start=l_down(1,1);
      finish=l_up(2,1);
%
%define cycles.
      cyclhl=HLFMOM_dg(start:finish,:);
%
%standardise data to 100 sample points per cycle
      szcychl=size(cyclhl,1);
      olXhl=(1:1:szcychl);
      nwXhl=linspace(1,szcychl,100);
      for cyhl=1:16;
      olYhl=cyclhl(:,cyhl);
      nwYhl(:,cyhl)= interp1 (olXhl, olYhl, nwXhl, 'spline');
      end;
      hlfmom_data=nwYhl;
%
%Alternatively use :
%hlfmom_data=interpft(cyclhl,100);
%
      plot(hlfmom_data);
      grid
      hndlfmom_data=hlfmom_data;
%
normres=[angle_data  force_data  moment_data];
norhlrs=[hndlfmom_data];
```

```
function [out]=deg2rad(in)

% function [out]=deg2rad(in)

% Description:    Conversion of degrees to radians applied to the entire
matrix

% Input:    in (values in degrees)

% Output:   out (values in radians)

% Author:   Christoph Reinschmidt, HPL, The University of Calgary

% Date:           October, 1994

% Last Changes:   November 29, 1996

% Version:  1.0

out=in./(180/pi);
```

```
function [ds,Sopt,gcv] = dpf( data, delT, S, maxiter )

%  DPF:
%
%  A straightforward, but inefficient, implementation of the Dohrmann
%  dynamic programming filter using the built-in matrix programming
%  abilities of Matlab.  To improve speed, either recode the filter
%  using the optimized algorithms contained in the C version or compile
%  the C version as a DLL and call the DLL from Matlab.  Note that this
%  routine simply orchestrates the search for the optimal smoothing
%  parameter;  the real work is done by the routine DPFSWEEP.M.
%
%  Usage:   [ds,Sopt,gcv] = dpf( data, delT, S, maxiter )
%
%  Inputs:
%       data:   a vector of noisy data
%       delT:   sampling interval
%       S:      a smoothing parameter (0 if optimization is requested)
%       maxiter:the maximum number of iterations used to find the
optimum;
%               if maxiter = 0, then no optimization is performed and the
%               data is smoothed using the supplied value of S
%  Outputs:
%       ds:     smoothed position, velocity and acceleration vectors,
%               arranged by row
%       Sopt:   the optimal smoothing parameter
%       gcv:    the generalized cross-validation value
%
%   Copyright 1993  Antony Hodgson (ahodgson@hstbme.mit.edu)
%   All rights reserved


    disp('DPF notice:  This routine is quite slow.  Please be patient.');
    npts = length(data);

    epsiln = 1e-4;  % termination criterion on smoothing parameter range
    if (S <= 0), S = 1e5; end
    x1 = log10(S);
    dx = 1;

    if maxiter == 0
        [ds,gcvnew] = dpfsweep( data, S );

    else % find an optimum
        disp('DPF:  Smoothing using first guess at smoothing
parameter.');
        [ds,f1] = dpfsweep( data, S );  % ds = smoothed data;  f1 =
gcv(x1)
        x2 = x1 + dx;       S = 10^x2;
        disp('DPF:  Smoothing using second guess at smoothing
parameter.');
        [ds,f2] = dpfsweep( data, S );
        if (f2 > f1)    %  swap so that f1 > f2 is guaranteed
            dx = -dx;
            tmp = f1;  f1 = f2;  f2 = tmp;  %  swap(f1, f2);
            tmp = x1;  x1 = x2;  x2 = tmp;  %  swap(x1, x2);
        end
            % disp('DPF:  First points:');
            % [ x1 x2; f1 f2 ]
        %  the following will be executed at least once since f1 > f2
        %  as ensured by the above code
        while f1 > f2   %  go downhill until we bound the minimum
            x0 = x1;  x1 = x2;  f1 = f2;  x2 = x1 + dx;  S = 10^x2;
            disp('DPF:  Stepping downhill to try to bracket minimum.');
            [ds,f2] = dpfsweep( data, S );
        end
            % disp('DPF:  bounding points (note: f1 is repeated):' );
            % [ x0 x1 x2; f1 f1 f2 ]  % uncomment to display
```

```
        %  FOUND A BOUND AND STARTING POINTS
        aa = x0;    bb = x2;    GoldenRatio = (sqrt(5.) - 1) * 0.5;
        range = bb - aa;  x1 = bb - GoldenRatio * range;  S = 10^x1;
        disp('DPF:  Closing in.');
        [ds,f1] = dpfsweep( data, S );
        x2 = aa + GoldenRatio * range;  S = 10^x2;
        disp('DPF:  Closing in.');
        [ds,f2] = dpfsweep( data, S );
        gcvold = 0; gcvnew = f2;    if (f1 < f2) gcvnew = f1;  end

        %% CHECK CONVERGENCE OF GCV
        del = (gcvnew - gcvold) / gcvnew;
        TERMINATION_CRITERION = 1e-5;   %  criterion on generalized
                        %  cross-validation value

        while abs(del) > TERMINATION_CRITERION
            gcvold = gcvnew;
            if (f1 > f2)
                aa = x1;  x1 = x2;  f1 = f2;  range = bb - aa;
                x2 = aa + GoldenRatio * range;  oldS = S;  S = 10^x2;
                if abs( (S - oldS) / S ) > epsiln
                disp('DPF:  Closing in.');
                    [ds,f2] = dpfsweep( data, S );  gcvnew = f2;
                end
            else
                bb = x2;  x2 = x1;  f2 = f1;  range = bb - aa;
                x1 = bb - GoldenRatio * range;  oldS = S;  S = 10^x1;
                if abs( (S - oldS) / S ) > epsiln
                disp('DPF:  Closing in.');
                    [ds,f1] = dpfsweep( data, S );  gcvnew = f1;
                end
            end
            del = (gcvnew - gcvold) / gcvnew;
        end
    end  % optimization

    %  now that we've got the optimal S, return the GCV and convert the
    %  velocity and acceleration estimates to their correct time units.
    disp('DPF:  Done.');
    gcv = gcvnew; Sopt = S;
    ds(2,:) = ds(2,:) / delT;   ds(3,:) = ds(3,:) / delT^2;
%   end of dpf
```

```
function [ds,gcv] = dpfsweep( d, b )

%  DPFSWEEP:
%
%  Performs the forward and reverse sweeps of the Dohrmann algorithm
given
%  a smoothing parameter.  The data is assumed to be uniformily sampled
%  with a sampling interval of one time unit.  If the actual sampling
rate
%  was different from 1, divide the velocity by delT and the acceleration
%  by delT^2.  Normalizing in time makes it a little easier to
consistently
%  find the order of magnitude of the optimal smoothing parameter because
%  this parameter is a function of both the non-dimensional noise
amplitude
%  and the sampling interval.  If we set the sampling interval to 1, then
%  the optimal smoothing parameter is only a function of the non-
dimensional
%  noise amplitude and we can estimate this more easily.
%
%  Usage:   [ds,gcv] = dpfsweep( d, b )
%
%  Inputs:
%   d:  noisy data
%   b:  smoothing parameter
%
%  Outputs:
%   ds:     a matrix containing the smoothed data:  position, velocity
%           and acceleration histories organized by row
%   gcv:    the generalized cross-validation value (roughly equivalent
%           to the estimated mean squared error)
%
%   Note:   as implemented, this routine is fairly slow.  It does not
%           take advantage of the symmetry of various matrices involved
%           in the computations.
%
%   Copyright 1993  Antony Hodgson  (ahodgson@hstbme.mit.edu)
%   All rights reserved


N = length(d);  %  number of sample points
delT = 1;   %  set to 1 by default;  velocity and acceleration vectors
can
        %  be divided by delT and delT^2 respectively later
U = zeros(3,3);  U(1,1) = 1;

%  the update equation for the position estimate is X(k+1) = M*X(k) +
P*g(k)
M = [ 1 delT delT^2/2; 0 1 delT; 0 0 1 ];
P = [ delT^3/6; delT^2/2; delT ];
g = zeros(1,N-1);   %  history of third derivatives


%  ********** BACKWARD SWEEP **********

%  Notes:  (1)  the subscript 'all' in the following variables refers to
%  the fact that we are storing these values at all sampling intervals
%  because they are needed in the computations of the forward sweep.
%  (2)  the matrix R is always symmetric, so it really only needs 6
%  independent entries, rather than 9 as shown here.
Rall = zeros(9,N);  sall = zeros(3,N);  %  for the dynamic programming
filter
MThall = zeros(9,N);    Eall = zeros(9,N);  %  for computing the
generalized
                                            %  cross-validation

%  initialize the recursion variables
R = U;
```

```
e = [ d(N); 0; 0 ];
s = -2*U*e;
for j = 1:3, Rall(3*j-2:3*j,N) = R(1:3,j);  end
sall(:,N) = s;

for i = N-1:-1:1
    HT = 2*R*P;
    D = 1/(2*b+P'*HT);
    R = U + M'*(R-0.5*HT*D*HT')*M;
    e = [ d(i); 0; 0 ];
    %s = -2*U*e + M'*(eye(3)-HT*D*P')*s;  % since U = [ 1 0 0; 0 0 0; 0 0
0 ]
                          %  and e = [ e(1); 0; 0 ] we can simplify:
    s = -2*e + M'*(eye(3)-HT*D*P')*s;

    %  keep track of R and s
    for j = 1:3, Rall(3*j-2:3*j,i) = R(1:3,j);  end
    sall(:,i) = s;

    %  also, for the cross validation procedure, keep track of MTh and E
    MTh = M'*(eye(3)-HT*D*P');
    E = -P*D*P';
    for j = 1:3
        MThall(3*j-2:3*j,i+1) = MTh(1:3,j);
        Eall(3*j-2:3*j,i+1) = E(1:3,j);
    end
end

%  ********** FORWARD SWEEP **********

%  initialize the recursion variables
ds = zeros(3,N);
%  for maximum programming safety, we should regenerate R(1) and s(1)
from
%  the record of the backward sweep, but since we know that we haven't
%  changed them, we can just use them directly.
X = -0.5*inv(R)*s;  %  the position, velocity, acceleration vector
ds(:,1) = X;
Q = inv(R);      %  used to compute the trace of the influence matrix
traceA = Q(1,1);

for i = 1:N-1
    for j = 1:3, R(1:3,j) = Rall(3*j-2:3*j,i+1);  end    %  regenerate R
    s = sall(:,i+1);                                     %  regenerate s
    g(i) = -1/(2*(b+P'*R*P))*P'*(s+2*R*M*X);
    X = M*X + P*g(i);
    ds(:,i+1) = X;  %  gather up the position, velocity, and
            %  acceleration estimates

    %  update the Q matrix
    for j = 1:3 %  regenerate MTh and E
        MTh(1:3,j) = MThall(3*j-2:3*j,i+1);
        E(1:3,j) = Eall(3*j-2:3*j,i+1);
    end
    Q = MTh'*Q*MTh-2*E;
    traceA = traceA + Q(1,1);
end


%  ********** COMPUTE GENERALIZED CROSS-VALIDATION PARAMETER **********
%  Start by making sure that the data vector is a row vector
[rows,cols] = size(d);
if cols == 1, d = d';  end
delx = d - ds(1,:);
gcv = delx * delx' * N / ( N - traceA )^2;
```

```
%Procedure to find the normalised average vector from the most cranial
point on the
%acromioclavicular joint to the glenohumeral rotation centre, from the
data presented
%by Veeger et al (1997) after repositioning their scapulae in the resting
position
%defined by Pronk (1991).
%
%Written by Iain Charlton, Ingram Murray, CREST, University of Newcastle
upon Tyne.
%
%Date: February 1999
%
%References : Pronk,G.M. (1991).  The shoulder girdle: analyzed and
modelled kinematically.
%             Doctoral Thesis, Delft University Technology, The
Netherlands.
%             Veeger,H.E.G., Yu,B., An,K., Rozendal,R.H. (1997).
Parameters for Modeling
%             the upper Extremity.  J. Biomech. Vol.30 pp.647-652
%
%Output: Matrix "AC_GHvec" containing vectors between acromion and
glenohumeral
%        rotation centre in global reference frame.
%        Matrix "ANGLES" containing the positions of the scapulae of
Veeger et al (1997)
%        in terms of rotations about the global axes from Pronk's resting
position
%        Matrix "NewAC" containing new Acromion positions after rotation
of scapulae
%        Vectors "szACGHg", "szACGHs", "szACGHgn" included as a check of
the consistency
%        of the magnitude of the vector between acromion and Ghc in
global, scapular and
%        finally new global frames.
%        Vector AVVEC, the average, normalised vector from acromion to
glenohumeral rotation
%        centre in the global frame.  Normalised to the distance between
acromion and elbow
%        centre in the resting position.
%
%
Xg=[1 0     0];
Yg=[0 1     0];
Zg=[0 0     1];

%From Pronk (1991) the rotation matrix describing the location of the
scapula with
%respect to his global frame (rotated +90 degrees about my X)

Sp=[-0.82 0.2632 0.5083 0;-0.1919 -0.963 0.1892 0;0.5393 0.0576 0.8401
0;0 0 0 1];

%correction to apply +90 degree rotation of my frame to that of Pronk.

Rpv=[1 0 0 0;0 0 -1 0;0 1 0 0;0 0 0 1];

%rotation matrix describing resting location of the scapula in MY global
frame.

RR=Rpv*Sp;

%Co-ordinates of necessary anatomical landmarks from Veeger in global
frame, after
%correcting third set of data (left arm specimen) for reversal of Y axis.

ACg =[      26.38 5.69  37.6
      24.11 5.57  41.26
```

```
      24.26 1.85  42.15
      23.5  5.03  40.74
      25.29 1.28  40.96];

AAg =[      27.55 4.39  36.5
      25.16 2.24  40.65
      24.73 -0.88 41.43
      24.4  2.35  41.52
      24.85 -1.93 39.22];

TSg =[      12.66 4.11  35.69
      12.31 2.07  35.8
      12.19 1.96  36.19
      12.56 2.96  36.04
      12.87 1.47  36.92];

AIg =[      11.28 1.78  23.2
      14.79 1.22  22.68
      15.25 1.62  22.79
      15.83 0.88  22.77
      13.86 3.09  22.91];

GHg =[      26.13 5.16  32.88
      25.5  4.51  38.15
      25.49 1.3   38.41
      24.69 4.04  37.9
      25.92 2.66  36.44];

LEg =[27.51    5.48    3.96
      28.51    1.45    5.56
      26.47    -0.55    6.46
      29.54    2.5    8.99
      30.75   -1.13    5.18];

MEg =[20.81    3.18    4.22
      22.23    4.43    5.02
      22.87    5.6    6.45
      22.69    0.31    8.99
      23.49   -0.9    5.31];

%Calcuate the co-ordinates of the mid-point of the lateral and medial
epicondyles from the
%data of Veeger et al (1997), after rotation of the humerus about the
glenohumeral centre
%so that the mid-point of the epicondyles lies below the glenohumeral
rotation centre.

for i=1:5;
MP(i,1:3)=(LEg(i,1:3)+MEg(i,1:3))/2;
mag(i,1)=vecsize(GHg(i,:)-MP(i,:));
MPP(i,1:3)=[GHg(i,1:2) (GHg(i,3)-mag(i,1))];
end;
MPg=MPP

for i=1:5;
ACng=[];
TSng=[];
AIng=[];
RG=[];

%Defining Pronk's embedded scapular plane from Veeger data.
Xs1 = unit(TSg(i,1:3)-AAg(i,1:3));
Zs1 = unit(cross(Xs1,(AIg(i,1:3)-AAg(i,1:3))));
Ys1 = unit(cross(Zs1,Xs1));

%calculate transformation from global to scapular frame
Rgs=soder([Xg Yg Zg;Xs1 Ys1 Zs1]);

%calculate transformation from scapular to global frame
Rsg=inv(Rgs);
```

```
%Calculate acromion and glenohumeral centre in scapular co-ordinates.
ACs=Rsg*[ACg(i,1:3) 1]';
GHs=Rsg*[GHg(i,1:3) 1]';
TSs=Rsg*[TSg(i,1:3) 1]';
AIs=Rsg*[AIg(i,1:3) 1]';

%Calculate vector from acromion to glenohumeral centre in Veeger scapular
frame.
AC_GHs(i,1:4)=(GHs-ACs)';

%Calculate vector from acromion to glenohumeral centre in global frame
using Pronk(Veeger)
%frame and Pronk's matrix.
AC_GHng(i,1:4)=(RR*AC_GHs(i,1:4)')';

%calculate landmark locations in my global frame
ACng=(RR*ACs)';
TSng=(RR*TSs)';
AIng=(RR*AIs)';

%calculate rotation between Pronk's resting and Veeger's positions for
each set of data
RG=soder([ACng(1,1:3) TSng(1,1:3) AIng(1,1:3);ACg(i,1:3) TSg(i,1:3)
AIg(i,1:3)]);

%calculate angles of rotation from resting position to Veeger's position
ANGS(i,1:9)=rzxysolv(RG);

%Calculate new positions of acromion after rotation about glenohumeral
centre
ACgh(i,1:3)=ACg(i,1:3)-GHg(i,1:3);
ACGh(i,1:4)=((inv(RG))*[ACgh(i,1:3) 1]')';
ACGH(i,1:3)=ACGh(i,1:3)+GHg(i,1:3);

%Alternative calculation of new acromion positions from reversal of
acromion to
%glenohumeral rotation centre vectors.
ACGH2(i,1:3)=(AC_GHng(i,1:3)*(-1))+GHg(i,1:3);

%calculate vectors and their magnitude from elbow mid-point to acromion
MPAC(i,1:3)=ACGH(i,1:3)-MPg(i,1:3);
EAC(i,1)=vecsize(MPAC(i,1:3));

%calculate normalised vector between acromion and glenohumeral centre
normvecs(i,1:3)=(AC_GHng(i,1:3))/EAC(i,1);

%calculate magnitudes of the ACGH vectors in global, scapular and
modified global as check
szACGHg(i,1)=vecsize(ACg(i,1:3)-GHg(i,1:3));
szACGHs(i,1)=vecsize(AC_GHng(i,1:3));
szACGHgn(i,1)=vecsize(ACGh(i,1:3));

end

AC_GHvec=AC_GHng(1:5,1:3)
ANGLES=ANGS(1:5,1:3);
NewAC=ACGH
NewAC2=ACGH2
szACGHg
szACGHs
szACGHgn

%average vector from acromion to glenohumerla rotation centre
AVVEC1=(sum(AC_GHvec))/5
STDEVEC=std(AC_GHvec)
%average normalised vector from acromion to glenohumerla rotation centre
AVVEC2=(sum(normvecs))/5
STDNORMVEC=std(normvecs)
```

```
%Procedure to calculate the moments due to hand-held mass only,about the
flexion,
%adduction and rotation axes of the shoulder and flexion and rotation
axes of the
%elbow, using the Robotics Toolbox of Corke (1996).  Using sequence
%Flexion/Adduction/Internal rotn.
%
%Written by Ingram Murray, CREST, University of Newcastle upon Tyne.
%
%Date: Sept 1999
%
%Input: Output from "tech2.m" and various user inputs.
%
%Output: Moments and Forces about each of the shoulder and elbow axes in
Nm through
%       time due to Hand-held mass.
%
%
%References: Corke P.I. (1996) A Robotics Toolbox for MATLAB.  IEEE
Robotics and
%Automation Magazine.  Vol 3 (March) No 1 pp 24-32
%
hlm=[];
HLFORCSHLDER=[];
HLFORCwrst=[];
HLFORClbo=[];
%Construct the "dyn" matrix for input to "rne.m".
%       alpha       A        theta     D     sigma  mass    rx      ry      rz
Ixx  Iyy  Izz    Ixy    Iyz    Ixz    Jm    G    B    Tc+    Tc-
dyn= [-pi/2        0         01       0       0      0       0      0       0
0    0    0      0      0      0      0    0    0     0      0  ;
         0          0       -pi/2      0       0      0       0      0       0
0    0    0      0      0      0      0    0    0     0      0  ;
       pi/2         0         03       0       0      0       0      0       0
0    0    0      0      0      0      0    0    0     0      0  ;
         0          0        pi/2      0       0      0       0      0      -uac
0    0    0      0      0      0      0    0    0     0      0  ;
       pi/2         0         05     -ual      0      0       0      0       0
0    0    0      0      0      0      0    0    0     0      0  ;
      -pi/2         0         06       0       0      0       0      0      -fac
0    0    0      0      0      0      0    0    0     0      0  ;
      -pi/2         0         07     -fal      0      0       0      0       0
0    0    0      0      0      0      0    0    0     0      0  ;
         0          0        pi/2      0       0      0       0      0       0
0    0    0      0      0      0      0    0    0     0      0  ;
       pi/2         0         09       0       0      0       0      0       0
0    0    0      0      0      0      0    0    0     0      0  ;
         0          hl       010       0       0    Hload    -hc     0       0
0    0    0      0      0      0      0    0    0     0      0  ];
%
%
%Carry out "rne.m" to calculate the moments.
tau=rne(dyn,q,qd,qdd,grav);
%
%
%Display the results in a reasonable format.
hlm(:,1)=tau(:,3);
hlm(:,2)=tau(:,1);
hlm(:,3)=tau(:,5);
hlm(:,4)=tau(:,6);
hlm(:,5)=tau(:,7);
hlm(:,6)=tau(:,9);
hlm(:,7)=tau(:,10);
%disp('                THE MOMENTS ABOUT THE RESPECTIVE AXES ARE')
%disp('  adduction  flexion   int_rotn elbw_flex pronation ulnar_dev
wrist_flex')
%disp(hlm)
%
```

```
%
global FTUFH
global FTFH
global FTH
FTUFH;
EFTAll=EFTall;
ETHAll=ETHall;
for ff=1:size(FTUFH,1)
%For calculation of force at elbow
ETHH=ETHAll(1:3,3*ff-2:3*ff);
HLFORClbo(ff,1:3)=(ETHH\(FTFH(ff,1:3)'))';
HLFORCLBO=HLFORClbo(:,1:3);
%For calculation of force at wrist
EFTT=EFTAll(1:3,3*ff-2:3*ff);
HLFORCwrst(ff,1:3)=(EFTT\(FTH(ff,1:3)'))';
HLFORCWRST=HLFORCwrst(:,1:3);
%Force at shoulder
HLFORCSHLDER=FTUFH;
end
%disp('THE FORCES ALONG THE RESPECTIVE AXES DUE TO HAND-HELD LOAD ARE')
%disp('  ShoulderX ShoulderY ShoulderZ')
%disp(HLFORCSHLDER)
%disp('   ElbowX    ElbowY    ElbowZ')
%disp(HLFORCLBO)
%disp('   WristX    WristY    WristZ')
%disp(HLFORCWRST)
ALLHLMOMS=hlm;
ALLHLFRCS=[HLFORCSHLDER HLFORCLBO HLFORCWRST];
```

```
%Procedure to calculate the moments about the flexion, adduction and
rotation
%axes of the shoulder and flexion and rotation axes of the elbow, using
the
%Robotics Toolbox of Corke (1996).  Using sequence
Flexion/Adduction/Internal rotn.
%
%Written by Ingram Murray, CREST, University of Newcastle upon Tyne.
%
%Date: April 1999
%
%MODIFICATIONS
%
%Input: Output from "tech2.m" and various user inputs.
%
%Output: Moments about each of the shoulder and elbow axes in Nm through
time.
%
%
%References: Corke P.I. (1996) A Robotics Toolbox for MATLAB.  IEEE
Robotics and
%Automation Magazine.  Vol 3 (March) No 1 pp 24-32
%
%
%Some algorithms for numerical differentiation.
%f'(xi)=-x(i-1)+x(i+1)/2h
%f'(xi)=x(i-2)-8x(i-1)+8x(i+1)-x(i+2)/12h - used
%f''(xi)=-x(i-2)+16x(i-1)-30(xi)+16x(i+1)-x(i+2)/12h^2 - used
%f''(xi)=2x(i-2)-x(i-1)-2(xi)-x(i+1)+2x(i+2)/7h^2
%f''(xi)=x(i+1)-2(xi)+x(i-1)/h^2
%f''(xi)=x(i+2)-2(xi)+x(i-2)/4h^2
%
%
%Take inputs and calculate first and second numerical derivatives of the
angle data.
uat=[];
q=[];
qd=[];
qdd=[];
FORCESHOULDER=[];
FORCEwrist=[];
FORCelbow=[];
ALLANGLE=[];
INERTIAMOMS=[];
OMEGAS=[];
OMEGADOTS=[];
inau=[];
%ELB(:,3)=ing;
ELbw=ELB;
ELbw(:,3)=ELB(:,3)-90;
SHdr=SHD;
ELBw=deg2rad(ELbw);
SHDr=deg2rad(SHdr);
g=size(SHDr,1);
gg=size(ELBw,1);
qds1=(dpf( SHDr(:,1)',h,0,1))';
qds2=(dpf( SHDr(:,2)',h,0,1))';
qds3=(dpf( SHDr(:,3)',h,0,1))';
qde1=(dpf( ELBw(:,1)',h,0,1))';
qde2=(dpf( ELBw(:,2)',h,0,1))';
qde3=(dpf( ELBw(:,3)',h,0,1))';
%Construct q,qd,qdd matrices for "rne.m" input.
q=zeros(g,10);
q(:,1)=qds1(:,1);
q(:,2)=-pi/2*ones(g,1);
q(:,3)=qds2(:,1);
q(:,4)=pi/2*ones(g,1);
q(:,5)=qds3(:,1);
```

```
q(:,6)=qde1(:,1);
q(:,7)=qde3(:,1);
q(:,8)=pi/2*ones(g,1);
q(:,9)=zeros(g,1);
q(:,10)=zeros(g,1);
%
qd=zeros(g,10);
qd(:,1)=qds1(:,2);
qd(:,2)=zeros(g,1);
qd(:,3)=qds2(:,2);
qd(:,4)=zeros(g,1);
qd(:,5)=qds3(:,2);
qd(:,6)=qde1(:,2);
qd(:,7)=qde3(:,2);
qd(:,8)=zeros(g,1);
qd(:,9)=zeros(g,1);
qd(:,10)=zeros(g,1);
%
%
qdd=zeros(g,10);
qdd(:,1)=qds1(:,3);
qdd(:,2)=zeros(g,1);
qdd(:,3)=qds2(:,3);
qdd(:,4)=zeros(g,1);
qdd(:,5)=qds3(:,3);
qdd(:,6)=qde1(:,3);
qdd(:,7)=qde3(:,3);
qdd(:,8)=zeros(g,1);
qdd(:,9)=zeros(g,1);
qdd(:,10)=zeros(g,1);
%
%
%Define gravity vector for input to "rne.m".
%grav=[-9.80665;0;0];
grav=[0;0;0];
%
%This is equivalent to saying that the base of the linkage is
%accelerating upwards at 1g.  This ficticious upward acceleration
%causes exactly the same effect on the links as gravity would.
%(Craig (1989)).
%
%
%
q;
qd;
qdd;
%
%
%input fractions of body mass and calculate segment masses.
mu=0.0271;
mf=0.0162;
mh=0.0061;
uam=M*mu;
fam=M*mf;
hm=M*mh;
%Calculate segment lengths.
ual=vecsize(hanz)/1000;
fal=vecsize1(fanz)/1000;
hl=H*(0.1879/1.741);
%Calculate CoM positions
uac=(0.5772)*ual;
fac=(0.4574)*fal;
hc=(1-0.3624)*hl;
%Calculate Moments of inertia
uaIa=(uam)*(ual*0.285)^2;
uaIt=(uam)*(ual*0.269)^2;
uaIl=(uam)*(ual*0.158)^2;
faIa=(fam)*(fal*0.276)^2;
faIt=(fam)*(fal*0.265)^2;
faIl=(fam)*(fal*0.121)^2;
```

```
hIa=(hm)*(hl*0.288)^2;
hIt=(hm)*(hl*0.235)^2;
hIl=(hm)*(hl*0.184)^2;
disp('LENGTHS')
disp('  Upper arm  Forearm     Hand')
disp([   ual    fal    hl    ])
disp('MASSES')
disp('  Upper arm  Forearm     Hand')
disp([   uam    fam    hm    ])
disp('CoM LOCATIONS')
disp('  Upper arm  Forearm     Hand')
disp([   uac    fac    hc    ])
disp('MOMENTS OF INERTIA')
disp('      UAIap      UAIt       UAIl')
disp([   uaIa  uaIt  uaIl    ])
disp('      FAIap      FAIt       FAIl')
disp([   faIa  faIt  faIl    ])
disp('      HIap       HIt         HIl')
disp([    hIa   hIt   hIl    ])
%
%
%Construct the "dyn" matrix for input to "rne.m".
%       alpha       A        theta     D     sigma  mass    rx      ry      rz
Ixx   Iyy   Izz    Ixy    Iyz    Ixz    Jm    G    B    Tc+    Tc-
dyn= [-pi/2        0         01       0       0     0      0       0       0
0     0     0      0      0      0      0     0    0     0      0  ;
         0         0       -pi/2      0       0     0      0       0       0
0     0     0      0      0      0      0     0    0     0      0  ;
        pi/2       0         03       0       0     0      0       0       0
0     0     0      0      0      0      0     0    0     0      0  ;
         0         0        pi/2      0       0     0     uam      0       0      -uac
uaIa uaIt uaIl    0      0      0      0     0    0     0      0  ;
        pi/2       0         05     -ual      0     0      0       0       0
0     0     0      0      0      0      0     0    0     0      0  ;
       -pi/2       0         06       0       0     0     fam      0       0      -fac
faIa faIt faIl    0      0      0      0     0    0     0      0  ;
       -pi/2       0         07     -fal      0     0      0       0       0
0     0     0      0      0      0      0     0    0     0      0  ;
         0         0        pi/2      0       0     0      0       0       0
0     0     0      0      0      0      0     0    0     0      0  ;
        pi/2       0         09       0       0     0      0       0       0
0     0     0      0      0      0      0     0    0     0      0  ;
         0        hl        010       0       0   hm+Hload -hc     0       0
hIl   hIa   hIt    0      0      0      0     0    0     0      0  ];
%
%
%Carry out "rne.m" to calculate the moments.
tau=rne(dyn,q,qd,qdd,grav);
%
%
%Display the results in a reasonable format.
uat(:,1)=tau(:,3);
uat(:,2)=tau(:,1);
uat(:,3)=tau(:,5);
uat(:,4)=tau(:,6);
uat(:,5)=tau(:,7);
uat(:,6)=tau(:,9);
uat(:,7)=tau(:,10);
%disp('                THE MOMENTS ABOUT THE RESPECTIVE AXES ARE')
%disp('  adduction  flexion   int_rotn elbw_flex pronation ulnar_dev
wrist_flex')
%disp(uat)
%
%
global FTUFH
global FTFH
global FTH
global INMOM
global omega
global omegadot
```

```
FTUFH;
EFTAll=EFTall;
ETHAll=ETHall;
for ff=1:size(FTUFH,1)
%For calculation of force at elbow
ETHH=ETHAll(1:3,3*ff-2:3*ff);
FORCelbow(ff,1:3)=(ETHH\(FTFH(ff,1:3)'))';
FORCELBOW=FORCelbow(:,1:3);
%For calculation of force at wrist
EFTT=EFTAll(1:3,3*ff-2:3*ff);
FORCEwrist(ff,1:3)=(EFTT\(FTH(ff,1:3)'))';
FORCEWRIST=FORCEwrist(:,1:3);
%Force at shoulder
FORCESHOULDER=FTUFH;
end
%disp('THE FORCES ALONG THE RESPECTIVE AXES ARE')
%disp('  ShoulderX ShoulderY ShoulderZ')
%disp(FORCESHOULDER)
%disp('   ElbowX    ElbowY    ElbowZ')
%disp(FORCELBOW)
%disp('   WristX    WristY    WristZ')
%disp(FORCEWRIST)
ALLANGLE(:,1)=rad2deg(q(:,3));
ALLANGLE(:,2)=rad2deg(q(:,1));
ALLANGLE(:,3)=rad2deg(q(:,5));
ALLANGLE(:,4)=rad2deg(qde2(:,1));
ALLANGLE(:,5)=rad2deg(q(:,6));
ALLANGLE(:,6)=rad2deg(q(:,7));
ALLANGLE;
ALLMOMENTS=uat;
ALLFORCE=[FORCESHOULDER FORCELBOW FORCEWRIST];

%Rearranging matrix of inertial moments for all joints and all samples to
%give matrix whose first three columns are xyz moments for link 1, next
three
%columns are xyz moments for link 2 etc, rows are data points.
for lnks=1:10
INERTIAMOMS(:,3*lnks-
2:3*lnks)=(reshape(INMOM(:,lnks)',3,size(INMOM,1)/3))';
OMEGAS(:,3*lnks-2:3*lnks)=(reshape(omega(:,lnks)',3,size(omega,1)/3))';
OMEGADOTS(:,3*lnks-
2:3*lnks)=(reshape(omegadot(:,lnks)',3,size(omegadot,1)/3))';

%The following lines were added by I.Murray 10/11/99
%Display the results in a reasonable format.
global inau
INM(:,1)=inau(:,3);
INM(:,2)=inau(:,1);
INM(:,3)=inau(:,5);
INM(:,4)=inau(:,6);
INM(:,5)=inau(:,7);
INM(:,6)=inau(:,9);
INM(:,7)=inau(:,10);
end
```

```
%Procedure to calculate acceleration due to gravity from APAS co-ordinate
%data from pendulum tests.  NB For a swinging pendulum the horizontal co-
%ordinates will have one maximum per cycle, the vertical component will
%have two maxima per cycle.
%
%Written by Ingram Murray, CREST, University of Newcastle upon Tyne.
%
%Date: June 1998
%
%Input:     data - a column matrix of displacement data from the pendulum
tests.
%
%Output: Acceleration due to gravity.
%
SMOTH=input('Do you wish to smooth the data prior to calculating g? Y/N
[Y]: ','s');
      if isempty(SMOTH)
      SMOTH='Y';
      end
h=input('What is the sampling interval of the data ? ');
pl=input('What is the length of the pendulum ? ');
%
%Construct vector of time intervals.
x=(h:h:(size(data,1)*h))';
%
OUT=[]
for nn=1:3
t=[];
g=[];
%
DATA=data(:,nn);
%
if SMOTH=='Y'
%Smooth data.
smothd=(dpf(DATA,h,0,1))';
end
%
%Include loop to allow recalculation if unsatisfactory.
LOOP='Y';
while LOOP=='Y'
%
if SMOTH=='Y'
%Plot smoothed displacement against time vector.
figure(1);
clf reset;
plot(x,smothd(:,1));
hold;
%Identify maxima of each cycle.
disp('   "Use cursor to click on the maxima of each cycle, then press
"return"   "')
max=ginput;     %reads point from cursor
max=max(:,1);   %discards y values
else
plot(x,DATA);
hold;
%Identify maxima of each cycle.
disp('   "Use cursor to click on the maxima of each cycle, then press
"return"   "')
max=ginput;     %reads point from cursor
max=max(:,1);   %discards y values
end
%
%Calculate periods throughout trial.
n=size(max,1);
      for i=1:n-1;
      t(i,1)=max(i+1,:)-max(i,:);
      %Apply gravity calculation.
      g(i,1)=(4*(pl))*((pi/t(i,1))^2)
```

```
      end;
%

%
%Recalculate by starting loop again or exit routine.
LOOP=input('Do you wish to recalculate g ? Y/N [Y]: ','s');
      if isempty(LOOP)
      LOOP='Y';
      end
end
OUT(:,nn)=g;
end
OUT
mean(OUT)
std(OUT)
```

```
%Procedure to produce graphs of the data obtained from the APAS system.
%
%Written by Ingram Murray, CREST, University of Newcastle upon Tyne.
%
%Date: May 1998
%
%MODIFICATIONS
%18/8/98 Altered to output smoothed angular values rather than
unsmoothed.
%
%Input: User selection from menu of options.
%
%Output: Produces a graph of the selected variables.
%
%Define time vector for use in plotting graphs.
timesec=0;
timesec1=0;
for tt=1:g;
      time1(tt,1)=timesec;
      timesec=timesec+h;
end;
time1;
gs=menu('Which graphs do you wish to plot ?','ANGLE GRAPHS','MOMENT
GRAPHS','TRAJECTORY GRAPHS','FORCE GRAPHS','RESULTANT FORCES','CLOSE
WINDOW');
if gs==1
kak=menu('Which angle graph do you wish to plot ?','Shoulder Adduction
Angle Vs. Time','Shoulder Flexion Angle Vs. Time','Shoulder Int.Rotn.
Angle Vs. Time','Elbow Flexion Angle Vs. Time','Elbow Adduction Angle Vs.
Time','Forearm Pronation Angle Vs. Time','Ulnar Deviation Angle Vs.
Time','Wrist Flexion Angle Vs. Time','CLOSE WINDOW');
      if kak==1
        plot(time1,rad2deg(q(:,1)))
      title('Shoulder Adduction Angle Vs. Time'),xlabel('Time
(s)'),ylabel('Angle (degrees)')
      plots
      end
      if kak==2
        plot(time1,rad2deg(q(:,3)))
      title('Shoulder Flexion Angle Vs. Time'),xlabel('Time
(s)'),ylabel('Angle (degrees)')
      plots
      end
      if kak==3
        plot(time1,rad2deg(q(:,4)))
      title('Shoulder Int.Rotn. Angle Vs. Time'),xlabel('Time
(s)'),ylabel('Angle (degrees)')
      plots
      end
      if kak==4
        plot(time1,rad2deg(q(:,5)))
      title('Elbow Flexion Angle Vs. Time'),xlabel('Time
(s)'),ylabel('Angle (degrees)')
      plots
      end
      if kak==5
        plot(time1,rad2deg(qde2(:,1)))
      title('Elbow Adduction Angle Vs. Time'),xlabel('Time
(s)'),ylabel('Angle (degrees)')
      plots
      end
      if kak==6
        plot(time1,rad2deg(q(:,6)))
      title('Forearm Pronation Angle Vs. Time'),xlabel('Time
(s)'),ylabel('Angle (degrees)')
      plots
      end
      if kak==7
```

```
        plot(time1,rad2deg(q(:,8)))
      title('Ulnar Deviation Angle Vs. Time'),xlabel('Time
(s)'),ylabel('Angle (degrees)')
      plots
      end
      if kak==8
        plot(time1,rad2deg(q(:,9)))
      title('Wrist Flexion Angle Vs. Time'),xlabel('Time
(s)'),ylabel('Angle (degrees)')
      plots
      end
      if kak==9
        close
      end
end
if gs==2
kk=menu('Which moment graph do you wish to plot ?','Shoulder Adduction
Moment Vs. Time','Shoulder Flexion Moment Vs. Time','Shoulder Int.Rotn.
Moment Vs. Time','Elbow Flexion Moment Vs. Time','Elbow Adduction Moment
Vs. Time','Forearm Pronation Moment Vs. Time','Ulnar Deviation Moment Vs.
Time','Wrist Flexion Moment Vs. Time','CLOSE WINDOW');
      if kk==1
        plot(time1,uat(:,1))
%     curvefit(time2,uat(:,1),15)
      title('Shoulder Adduction Moment Vs. Time'),xlabel('Time
(s)'),ylabel('Moment (Nm)')
      plots
      end
      if kk==2
        plot(time1,uat(:,2))
      title('Shoulder Flexion Moment Vs. Time'),xlabel('Time
(s)'),ylabel('Moment (Nm)')
      plots
      end
      if kk==3
        plot(time1,uat(:,3))
      title('Shoulder Int.Rotn. Moment Vs. Time'),xlabel('Time
(s)'),ylabel('Moment (Nm)')
      plots
      end
      if kk==4
        plot(time1,uat(:,4))
      title('Elbow Flexion Moment Vs. Time'),xlabel('Time
(s)'),ylabel('Moment (Nm)')
      plots
      end
      if kk==5
        plot(time1,zeros(g,1))
      title('Elbow Adduction Moment Vs. Time'),xlabel('Time
(s)'),ylabel('Moment (Nm)')
      plots
      end
      if kk==6
        plot(time1,uat(:,5))
      title('Forearm Pronation Moment Vs. Time'),xlabel('Time
(s)'),ylabel('Moment (Nm)')
      plots
      end
      if kk==7
        plot(time1,uat(:,6))
      title('Ulnar Deviation Moment Vs. Time'),xlabel('Time
(s)'),ylabel('Moment (Nm)')
      plots
      end
      if kk==8
        plot(time1,uat(:,7))
      title('Wrist Flexion Moment Vs. Time'),xlabel('Time
(s)'),ylabel('Moment (Nm)')
      plots
      end
```

```
      if kk==9
        close
      end
end
if gs==3
      kkk=menu('How do you wish to plot the shoulder, elbow and wrist
trajectories ?','3-Dimensional','Sagittal plane','Frontal
plane','Transverse plane','CLOSE WINDOW');
%'flip' x and y axes as these axes in Matlab by default are the reverse
of mine.
      if kkk==1
      plot3(Straj(:,1),Straj(:,2),Straj(:,3),'ow',Etraj(:,1),Etraj(:,2),E
traj(:,3),'oy',Wtraj(:,1),Wtraj(:,2),Wtraj(:,3),'or')
      title('3D Shoulder, Elbow and Wrist
Trajectories'),xlabel('X'),ylabel('Y'),zlabel('Z')
      flipaxis('X');
      flipaxis('Y');
      plots
      end
      if kkk==2
      plot(Straj(:,2),Straj(:,3),'ow',Etraj(:,2),Etraj(:,3),'oy',Wtraj(:,
2),Wtraj(:,3),'or')
      title('Sagittal Plane Shoulder, Elbow and Wrist
Trajectories'),xlabel('Y'),ylabel('Z')
      plots
      end
      if kkk==3
      plot(Straj(:,1),Straj(:,3),'ow',Etraj(:,1),Etraj(:,3),'oy',Wtraj(:,
1),Wtraj(:,3),'or')
      title('Frontal Plane Shoulder, Elbow and Wrist
Trajectories'),xlabel('X'),ylabel('Z')
      flipaxis('X');
      plots
      end
      if kkk==4
      plot(Straj(:,1),Straj(:,2),'ow',Etraj(:,1),Etraj(:,2),'oy',Wtraj(:,
1),Wtraj(:,2),'or')
      title('Transverse Plane Shoulder, Elbow and Wrist
Trajectories'),xlabel('X'),ylabel('Y')
      flipaxis('X');
      flipaxis('Y');
      plots
      end
      if kkk==5
      close
      end
end
if gs==4
kkkk=menu('Which force graph do you wish to plot ?','Shoulder X-axis
Force Vs. Time','Shoulder Y-axis Force Vs. Time','Shoulder Z-axis Force
Vs. Time','Elbow X-axis Force Vs. Time','Elbow Y-axis Force Vs.
Time','Elbow Z-axis Force Vs. Time','Wrist X-axis Force Vs. Time','Wrist
Y-axis Force Vs. Time','Wrist Z-axis Force Vs. Time','CLOSE WINDOW');
      if kkkk==1
        plot(time1,FORCESHOULDER(:,1))
      title('Shoulder X-axis Force Vs. Time'),xlabel('Time
(s)'),ylabel('Force (N)')
      plots
      end
      if kkkk==2
        plot(time1,FORCESHOULDER(:,2))
      title('Shoulder Y-axis Force Vs. Time'),xlabel('Time
(s)'),ylabel('Force (N)')
      plots
      end
      if kkkk==3
        plot(time1,FORCESHOULDER(:,3))
      title('Shoulder Z-axis Force Vs. Time'),xlabel('Time
(s)'),ylabel('Force (N)')
      plots
```

```
      end
      if kkkk==4
        plot(time1,FORCELBOW(:,1))
      title('Elbow X-axis Force Vs. Time'),xlabel('Time
(s)'),ylabel('Force (N)')
      plots
      end
      if kkkk==5
        plot(time1,FORCELBOW(:,2))
      title('Elbow Y-axis Force Vs. Time'),xlabel('Time
(s)'),ylabel('Force (N)')
      plots
      end
      if kkkk==6
        plot(time1,FORCELBOW(:,3))
      title('Elbow Z-axis Force Vs. Time'),xlabel('Time
(s)'),ylabel('Force (N)')
      plots
      end
      if kkkk==7
        plot(time1,FORCEWRIST(:,1))
      title('Wrist X-axis Force Vs. Time'),xlabel('Time
(s)'),ylabel('Force (N)')
      plots
      end
      if kkkk==8
        plot(time1,FORCEWRIST(:,2))
      title('Wrist Y-axis Force Vs. Time'),xlabel('Time
(s)'),ylabel('Force (N)')
      plots
      end
      if kkkk==9
        plot(time1,FORCEWRIST(:,3))
      title('Wrist Z-axis Force Vs. Time'),xlabel('Time
(s)'),ylabel('Force (N)')
      plots
      end
      if kkkk==10
        close
      end
end
if gs==5
kkkkk=menu('Which resultant force do you wish to plot ?','Resultant
Shoulder Force in 3-D','Resultant Shoulder Force in Sagittal
plane','Resultant Shoulder Force in Frontal plane','Resultant Shoulder
Force in Transverse plane','Resultant Elbow Force in 3-D','Resultant
Elbow Force in Y-Z plane','Resultant Elbow Force in X-Z plane','Resultant
Elbow Force in X-Y plane','Resultant Wrist Force in 3-D','Resultant Wrist
Force in Y-Z plane','Resultant Wrist Force in X-Z plane','Resultant Wrist
Force in X-Y plane','CLOSE WINDOW');
      if kkkkk==1
        plot3(FORCESHOULDER(:,1),FORCESHOULDER(:,2),FORCESHOULDER(:,3),':
')
      title('Resultant Shoulder Force in 3D'),xlabel('XForce
(N)'),ylabel('YForce (N)'),zlabel('ZForce (N)')
      flipaxis('X');
      flipaxis('Y');
            for ddd=1:size(FORCESHOULDER,1)
            ARROW([0 0
0],[FORCESHOULDER(ddd,1),FORCESHOULDER(ddd,2),FORCESHOULDER(ddd,3)])
            end
      plots
      end
      if kkkkk==2
        plot(FORCESHOULDER(:,2),FORCESHOULDER(:,3),'k')
      title('Resultant Shoulder Force in Sagittal Plane'),xlabel('YForce
(N)'),ylabel('ZForce (N)')
            for ar=1:size(FORCESHOULDER,1)
            a=FORCESHOULDER(ar,2);b=FORCESHOULDER(ar,3);
            ARROW([0 0 ],[a,b])
```

```
            end
       plots
       end
       if kkkkk==3
       plot(FORCESHOULDER(:,1),FORCESHOULDER(:,3),'k')
       title('Resultant Shoulder Force in Frontal Plane'),xlabel('XForce
(N)'),ylabel('ZForce (N)')
       flipaxis('x')
             for arr=1:size(FORCESHOULDER,1)
             aa=FORCESHOULDER(arr,1);bb=FORCESHOULDER(arr,3);
             ARROW([0 0],[aa,bb])
             end
       plots
       end
       if kkkkk==4
         plot(FORCESHOULDER(:,1),FORCESHOULDER(:,2),'k')
       title('Resultant Shoulder Force in Transverse
Plane'),xlabel('XForce (N)'),ylabel('YForce (N)')
       flipaxis('x')
       flipaxis('y')
             for arrr=1:size(FORCESHOULDER,1)
             aaa=FORCESHOULDER(arrr,1);bbb=FORCESHOULDER(arrr,2);
             ARROW([0 0],[aaa,bbb])
             end
       plots
       end
       if kkkkk==5
         plot3(FORCELBOW(:,1),FORCELBOW(:,2),FORCELBOW(:,3),':')
       title('Resultant Elbow Force in 3D'),xlabel('YForce
(N)'),ylabel('YForce (N)'),zlabel('ZForce (N)')
       flipaxis('X');
       flipaxis('Y');
             for ddd=1:size(FORCELBOW,1)
             ARROW([0 0
0],[FORCELBOW(ddd,1),FORCELBOW(ddd,2),FORCELBOW(ddd,3)])
             end
       plots
       end
       if kkkkk==6
         plot(FORCELBOW(:,2),FORCELBOW(:,3),'k')
       title('Resultant Elbow Force in Y-Z Plane'),xlabel('YForce
(N)'),ylabel('ZForce (N)')
             for ar=1:size(FORCELBOW,1)
             a=FORCELBOW(ar,2);b=FORCELBOW(ar,3);
             ARROW([0 0 ],[a,b])
             end
       plots
       end
       if kkkkk==7
       plot(FORCELBOW(:,1),FORCELBOW(:,3),'k')
       title('Resultant Elbow Force in X-Z Plane'),xlabel('XForce
(N)'),ylabel('ZForce (N)')
       flipaxis('x')
             for arr=1:size(FORCELBOW,1)
             aa=FORCELBOW(arr,1);bb=FORCELBOW(arr,3);
             ARROW([0 0],[aa,bb])
             end
       plots
       end
       if kkkkk==8
         plot(FORCELBOW(:,1),FORCELBOW(:,2),'k')
       title('Resultant Elbow Force in X-Y Plane'),xlabel('XForce
(N)'),ylabel('YForce (N)')
       flipaxis('x')
       flipaxis('y')
             for arrr=1:size(FORCELBOW,1)
             aaa=FORCELBOW(arrr,1);bbb=FORCELBOW(arrr,2);
             ARROW([0 0],[aaa,bbb])
             end
      plots
```

```
      end
      if kkkkk==9
        plot3(FORCEWRIST(:,1),FORCEWRIST(:,2),FORCEWRIST(:,3),':')
      title('Resultant Wrist Force in 3D'),xlabel('YForce
(N)'),ylabel('YForce (N)'),zlabel('ZForce (N)')
      flipaxis('X');
      flipaxis('Y');
            for ddd=1:size(FORCEWRIST,1)
            ARROW([0 0
0],[FORCEWRIST(ddd,1),FORCEWRIST(ddd,2),FORCEWRIST(ddd,3)])
            end
      plots
      end
      if kkkkk==10
        plot(FORCEWRIST(:,2),FORCEWRIST(:,3),'k')
      title('Resultant Wrist Force in Y-Z Plane'),xlabel('YForce
(N)'),ylabel('ZForce (N)')
            for ar=1:size(FORCELBOW,1)
            a=FORCEWRIST(ar,2);b=FORCEWRIST(ar,3);
            ARROW([0 0 ],[a,b])
            end
      plots
      end
      if kkkkk==11
      plot(FORCEWRIST(:,1),FORCEWRIST(:,3),'k')
      title('Resultant Wrist Force in X-Z Plane'),xlabel('XForce
(N)'),ylabel('ZForce (N)')
      flipaxis('x')
            for arr=1:size(FORCEWRIST,1)
            aa=FORCEWRIST(arr,1);bb=FORCEWRIST(arr,3);
            ARROW([0 0],[aa,bb])
            end
      plots
      end
      if kkkkk==12
        plot(FORCEWRIST(:,1),FORCEWRIST(:,2),'k')
      title('Resultant Wrist Force in X-Y Plane'),xlabel('XForce
(N)'),ylabel('YForce (N)')
      flipaxis('x')
      flipaxis('y')
            for arrr=1:size(FORCEWRIST,1)
            aaa=FORCEWRIST(arrr,1);bbb=FORCEWRIST(arrr,2);
            ARROW([0 0],[aaa,bbb])
            end
      plots
      end
      if kkkkk==13
        close
      end
end
if gs==6
      close
end
```

```
function [out]=rad2deg(in)

% function [out]=rad2deg(in)

% Description:    Conversion of radians to degrees applied to the entire
matrix

% Input:    in (values in radians)

% Output:   out (values in degrees)

% Author:   Christoph Reinschmidt, HPL, The University of Calgary

% Date:           October, 1994

% Last Changes:   November 29, 1996

% Version:  1.0


out=in.*(180/pi);
```

```
%RNE    Compute inverse dynamics via recursive Newton-Euler formulation
%
%       TAU = RNE(DYN, Q, QD, QDD)
%       TAU = RNE(DYN, [Q QD QDD])
%
%       Returns the joint torque required to achieve the specified joint
position,
%       velocity and acceleration state.
%
%       Gravity is assumed to be acting in the -Z direction with
acceleration of
%       9.81m/s/s, but this may be overriden by providing a gravity
acceleration
%       vector [gx gy gz].
%
%       TAU = RNE(DYN, Q, QD, QDD, GRAV)
%       TAU = RNE(DYN, [Q QD QDD], GRAV)
%
%       An external force/moment acting on the end of the manipulator may
also be
%       specified by a 6-element vector [Fx Fy Fz Mx My Mz].
%
%       TAU = RNE(DYN, Q, QD, QDD, GRAV, FEXT)
%       TAU = RNE(DYN, [Q QD QDD], GRAV, FEXT)
%
%       where   Q, QD and QDD are row vectors of the manipulator state;
pos, vel, and accel.
%
%       The torque computed also contains a contribution due to armature
%       inertia.
%
%       See also DYN, FDYN, ACCEL, GRAVLOAD, INERTIA.
%
%       Should be a MEX file.
%
% verified against MAPLE code, which is verified by examples
%

%       Copyright (C) 1992 Peter Corke

% MOD.HISTORY
%       6/95    make use of passed in FEXT
%       4/95    fix bug in use of passed FEXT
%       11/96   bug for prismatic case
function [tau] = rne(dyn, a1, a2, a3, a4, a5)
        z0 = [0;0;1];
        grav = 9.81*z0;
        fext = zeros(6, 1);

        n = numrows(dyn);
        if numcols(a1) == 3*n,
                Q = a1(:,1:n);
                Qd = a1(:,n+1:2*n);
                Qdd = a1(:,2*n+1:3*n);
                np = numrows(Q);
                if nargin >= 3,
                        grav = a2;
                end
                if nargin == 4,
                        fext = a3;
                end
        else
                np = numrows(a1);
                Q = a1;
                Qd = a2;
                Qdd = a3;
                if numcols(a1) ~= n | numcols(Qd) ~= n | numcols(Qdd) ~=
n | ...
```

```
                numrows(Qd) ~= np | numrows(Qdd) ~= np,
                error('bad data');
        end
        if nargin >= 5,
                grav = a4;
        end
        if nargin == 6,
                fext = a5;
        end
end

%
% create local vars for mass, COG and inertia matrices
%
m = dyn(:,6);           % column vector of link mass
r = dyn(:,7:9);         % matrix of COM data; row per link
Jm = [];
for j=1:n,
        J = [   dyn(j,10) dyn(j,13) dyn(j,15); ...
                dyn(j,13) dyn(j,11) dyn(j,14); ...
                dyn(j,15) dyn(j,14) dyn(j,12)  ];
        Jm = [Jm J];
end

tau = zeros(np,n);

for p=1:np,
        q = Q(p,:)';
        qd = Qd(p,:)';
        qdd = Qdd(p,:)';

        Fm = [];
        Nm = [];
        pstarm = [];
        Rm = [];
        w = zeros(3,1);
        wd = zeros(3,1);
        v = zeros(3,1);
        vd = grav;

%
% init some variables, compute the link rotation matrices
%
        for j=1:n,
                alpha = dyn(j,1);
                A = dyn(j,2);
                if dyn(j,5) == 0,
                        theta = q(j);
                        D = dyn(j,4);
                else
                        theta = dyn(j,3);
                        D = q(j);
                end
                sa = sin(alpha); ca = cos(alpha);
                st = sin(theta); ct = cos(theta);

                R = [   ct      -st*ca  st*sa
                        st      ct*ca   -ct*sa
                        0       sa      ca];
                Rm = [Rm R];
                pstar = [A; D*sa; D*ca];
                pstarm = [pstarm pstar];
        end
%The following lines were added by I.Murray 2/4/99
                TZo=[0 0 1;0 1 0;-1 0 0];
                TZ9=TZo*Rm(:,1:3)*Rm(:,4:6)*Rm(:,7:9)*Rm(:,10:12)
*Rm(:,13:15)*Rm(:,16:18)*Rm(:,19:21)*Rm(:,22:24)*Rm(:,25:27)*Rm(:,28:30);
                TZ5=TZo*Rm(:,1:3)*Rm(:,4:6)*Rm(:,7:9)*Rm(:,10:12)
*Rm(:,13:15)*Rm(:,16:18);
                TZ3=TZo*Rm(:,1:3)*Rm(:,4:6)*Rm(:,7:9)*Rm(:,10:12)
```

```
;
        %
        %  the forward recursion
        %
                for j=1:n,
                        R = Rm(:,3*j-2:3*j)';
                        pstar = pstarm(:,j);

                        %
                        % statement order is important here
                        %
                        if dyn(j,5) == 0,
                                % revolute axis
                                wd = R*(wd + z0*qdd(j) + ...
                                        cross(w,z0*qd(j)));
                                w = R*(w + z0*qd(j));
                                %v = cross(w,pstar) + R*v;
                                vd = cross(wd,pstar) + ...
                                        cross(w, cross(w,pstar)) +R*vd;

                        else
                                % prismatic axis
                                w = R*w;
                                wd = R*wd;
                                %v = R*(z0*qd(j) + v) + cross(w,pstar);
                                vd = R*(z0*qdd(j)+vd) + ...
                                        cross(wd,pstar) + ...
                                        2*cross(w,R*z0*qd(j)) +...
                                        cross(w, cross(w,pstar));
                        end

                        J = Jm(:,3*j-2:3*j);
                        vhat = cross(wd,r(j,:)') + ...
                                cross(w,cross(w,r(j,:)')) + vd;
                        F = m(j)*vhat;
                        N = J*wd + cross(w,J*w);
                        Fm = [Fm F];
                        Nm = [Nm N];
%
%Angular velocities and accelerations
omega(3*p-2:3*p,j)=w;
omegadot(3*p-2:3*p,j)=wd;
%
                end
%
%The following lines were added by I.Murray 2/4/99
%Applying inertial moment to all angular rotations.
Nm(:,1)=Rm(:,4:6)*Rm(:,7:9)*Rm(:,10:12)*Nm(:,4);      %INSF
Nm(:,3)=Rm(:,10:12)*Nm(:,4);                          %INSA
Nm(:,5)=Rm(:,13:15)\Nm(:,4);                          %INSR
Nm(:,7)=Rm(:,19:21)\Nm(:,6);                          %INFP
Nm(:,9)=Rm(:,28:30)*Nm(:,10);                         %INUD
%
%Inertial moments
INMOM(3*p-2:3*p,:)=Nm;
%
%Forces
                        FZ9=TZ9*Fm(:,10);
                        FZ5=TZ5*Fm(:,6);
                        FZ3=TZ3*Fm(:,4);
                        FTUFH(p,1:3)=FZ9'+FZ5'+FZ3';
                        FTFH(p,1:3)=FZ9'+FZ5';
                        FTH(p,1:3)=FZ9';
        %
        %  the backward recursion
        %

                f = fext(1:3);          % force/moments on end of arm
                nn = fext(4:6);
```

```
                for j=n:-1:1,
                        pstar = pstarm(:,j);

                        %
                        % order of these statements is important, since
both
                        % nn and f are functions of previous f.
                        %
                        if j == n,
                                R = eye(3,3);
                        else
                                R = Rm(:,3*j+1:3*j+3);
                        end
                        nn = R*(nn + cross(R'*pstar,f)) + ...
                                cross(pstar+r(j,:)',Fm(:,j)) + ...
                                Nm(:,j);
                        f = R*f + Fm(:,j);
                        R = Rm(:,3*j-2:3*j);
                        if dyn(j,5) == 0,
                                % revolute
                                tau(p,j) = nn'*(R'*z0) +
dyn(j,16)*qdd(j)*dyn(j,17)^2;
%The following line was added by I.Murray 10/11/99
inau(p,j) = (cross(pstar+r(j,:)',Fm(:,j)))'*(R'*z0);
                        else
                                % prismatic
                                tau(p,j) = f'*(R'*z0) +
dyn(j,16)*qdd(j)*dyn(j,17)^2;
                        end
                end
        end
%Following lines added by I Murray 2/6/98
global FTUFH;
global FTFH;
global FTH;
%
%The following lines were added by I.Murray 21/9/99
global INMOM;
global omega;
global omegadot;
%The following line was added by I.Murray 10/11/99
global inau
```

```
function [out] = rzyxsolv(T)

% Description:    Solves for alpha,beta,gama,Hx,Hy,Hz of the
transformation

%               matrix with the order Rzyx (Rzyx = [rx] [ry] [rz])

%

% Input:    - T      Transformation matrix

% Output:   - out    [alpha,beta,gama,Hx,Hy,Hz]

%                       Note that the angles are given in the range

%                       from -180 to +180 deg.

%                       gama is not a typo: gamma could not be used
because

%                       it is an existing matlab function

% Author:   Christoph Reinschmidt, HPL, The University of Calgary

% Date:           October, 1994

% Last changes: February 13, 1995

% Version:  1.0

if size(T)~=[4,4];

   disp('Error: transformation matrix has to be a 4x4 matrix')

   break;

end;

if sum(isnan(T(:)))~=0, out=[NaN,NaN,NaN,NaN,NaN,NaN]; return; end

beta  = asin(T(1,3));  %'assumption' that cos(beta)>0

alphasin = asin(-T(2,3)/cos(beta));

alphacos = acos(T(3,3)/cos(beta));

if (alphacos>pi/2 & alphasin>0); alpha=pi-alphasin; end;

if (alphacos>pi/2 & alphasin<0); alpha=-pi-alphasin; end;

if (alphacos<=pi/2); alpha=alphasin; end;

gamasin = asin(-T(1,2)/cos(beta));

gamacos = acos(T(1,1)/cos(beta));

if (gamacos>pi/2 & gamasin>0); gama=pi-gamasin;  end;

if (gamacos>pi/2 & gamasin<0); gama=-pi-gamasin; end;

if (gamacos<=pi/2);            gama=gamasin;     end;
```

```
% Calculation of Hx,Hy,Hz

A=[1, 0, sin(beta);...
   0, cos(alpha), -sin(alpha)*cos(beta);...
   0, sin(alpha), cos(alpha)*cos(beta)];
H=A\T(1:3,4); H=H';

out=[rad2deg(alpha),rad2deg(beta),rad2deg(gama),H];
```

```
function[sid]=signd(value)
%
%Procedure to return a positive or negative unit value depending on
%sign of input.
%
%Written by Ingram Murray, CREST, University of Newcastle upon Tyne.
%
%Date: March 1998
%
%Input: value
%
%Output: +1 if 'value' >= 0, -1 if 'value' < 0
%
if value >=0
   sid=1;
end
if value<0
   sid=-1;
end
```

```
function [T,res]=soder(data)
% function [T,res]=soder(data)
%
% Description:    Program calculates the transformation matrix T
containing
%           the rotation matrix (3x3) and the translation translation
%           vector d (3x1) for a rigid body segment using a singular
%           value decomposition method (Soederkvist & Wedin 1993).
%
% Input:    data:   columns represent the XYZ positions and the rows
%                   represent time.
% Output:   T:      4x4 Matrix containing the rotation matrix R and the
%                   translation d: T = [R,d; 0 0 0 1]
%           res:    norm of residuals (measure of fit; "rigidity" of body
%
% References:     Soderkvist I. and Wedin P. -A., (1993). Determining the
%                 movements of the skeleton using well-configured
markers.
%                 Journal of Biomechanics, 26:1473-1477
%
% Author:   Christoph Reinschmidt, HPL, The University of Calgary
%               (Matlab code adapted from Ron Jacobs, 1993)
% Date:           February, 1995
% Last Changes: December 09, 1996
% Version:      3.1

if (size(data,2)/3)~=fix(size(data,2)/3),
   disp('ERROR: input has to be multiple of 3 (XYZ coordinates)'); return
end


A=[reshape(data(1,:)',3,size(data,2)/3)]';
B=[reshape(data(2,:)',3,size(data,2)/3)]';

% Checking for NaNs and also checking if still 3 pts left and if not
% T=[NaN...];
```

```
cut=[0];

qA=isnan(A); qB=isnan(B); qAB=[qA,qB];

qsum=sum(qAB'); cut=find(qsum~=0);

A([cut],:)=[]; B([cut],:)=[];

if size(A,1)<3,

 T=[NaN,NaN,NaN,NaN;NaN,NaN,NaN,NaN;NaN,NaN,NaN,NaN;NaN,NaN,NaN,NaN;];
return;

end


Amean=mean(A)'; Bmean=mean(B)';


for i=1:size(A,1)-size(cut,2),

        Ai(:,i)=[A(i,:)-Amean']';

        Bi(:,i)=[B(i,:)-Bmean']';

end


C=Bi*Ai';

[P,T,Q]=svd(C);

R=P*diag([1 1 det(P*Q')])*Q';

d=Bmean-R*(Amean);


T=[R,d;0 0 0 1];


% Calculating the norm of residuals

A=A'; A(4,:)=ones(1,size(A,2));

B=B';

Bcalc=T*A; Bcalc(4,:)=[]; Diff=B-Bcalc; Diffsquare=Diff.^2;

%DOF=3*(number of points)-6 unknowns (Hx,Hy,Hz,alpha,beta,gamma):

DOF=size(B,1)*size(B,2)-6;

res=[sum(Diffsquare(:))/DOF].^0.5;
```

```
%Procedure to find the rotation between the technical and anatomical
%frames in each segment.
%
%Written by Ingram Murray, CREST, University of Newcastle upon Tyne.
%
%Date: May 1998
%
%Modifications : 11/98 to include scaled vector from Veeger et al (1996)
%                       for location of Gh centre.
%            November 1998- to allow SVD optimisation of marker positions
%                       Soderkvist & Wedin (1993).
%
%            13/05/99-  forearm technical frame altered to make z-axis
%                       between proximal ulnar marker and wrist centre.
%
%Input: Matrices: le, me, tv, these being the matrices containing
%the co-ordinate data from the pointer calibration video sample (lateral
epicondyle,
%medial epicondyle and thoracic vertebra respectively.
%
%Output: Transformation matrix between the technical and anatomical
frames
%on the forearm, upper arm and trunk (Tfta, Thta and Ttta respectively).
%
%
%Average out the landmark data
L1=le;, L2=me;, L3=tv;
for i=1:3
x=eval(['L' int2str(i)]);
%X=x
X=mean(x);
%
%
%select position vectors for pointer markers
p11=X(:,31:33);
p12=X(:,34:36);
%calculate vector from p12 to p11 which corresponds to the vector
%between p11 and the tip of the pointer
pvec=p11-p12;
%calculate location of pointer tip
ptp=(p11+pvec)';
ptip=[ptp;1];
%
%
%LE : Select procedure for upper arm markers
if i==1
      %select position vectors for humeral (upper arm) markers
      h4=X(:,10:12);
      h5=X(:,13:15);
      h6=X(:,16:18);
      %define vectors h4h6 and h4h5, the former of which is taken as the
      %technical humeral z axis
      hz=h6-h4;
      h4h5=h5-h4;
      %define cross product of these to give humeral x axis and then
cross
      %z and x axes to give y-axis.
      hx=cross(h4h5,hz);
      hy=cross(hz,hx);
      %unitise the vectors representing the humeral technical axes
      Hx=unit(hx);
      Hy=unit(hy);
      Hz=unit(hz);
      %add these to the original co-ordinates for the origin, marker h4
to
      %give the technical axis unit vectors in terms of the global frame.
      HX=h4+Hx;
      HY=h4+Hy;
```

```
      HZ=h4+Hz;
      %Calculate transformation between global and technical frame.
      HUtl3=soder([1 0 0 0 1 0 0 0 1;HX HY HZ]);
      Le=HUtl3\ptip;
      LE=Le(1:3,:);
      ach=X(:,28:30)';
      Ach=HUtl3\[ach;1];
      ACh=Ach(1:3,:);
%
%select position vectors for forearm markers
      f1=X(:,1:3);
      f2=X(:,4:6);
      f3=X(:,7:9);
%define wrist mid-point for origin of forearm technical frame.
      f1a=(f1+f2)/2;
      %define vectors f1af3 and f1f2, the former of which is taken as the
      %forearm z axis
      fz=f3-f1a;
      f1f2=f2-f1;
      %define cross product of these to give forearm y axis and then
cross
      %y and z axes to give x-axis.
      fy=cross(fz,f1f2);
      fx=cross(fy,fz);
      %unitise the vectors representing the forearm technical axes
      Fx=unit(fx);
      Fy=unit(fy);
      Fz=unit(fz);
      %add these to the original co-ordinates for the origin, marker f1a
to
      %give the technical axis unit vectors in terms of the global frame.
      FX=f1a+Fx;
      FY=f1a+Fy;
      FZ=f1a+Fz;
      %Calculate transformation between global and technical frame.
      FAtl3=soder([1 0 0 0 1 0 0 0 1;FX FY FZ]);
      Lef=FAtl3\ptip;
      LEF=Lef(1:3,:);
      us=X(:,1:3)';
      rs=X(:,4:6)';
      Us=FAtl3\[us;1];
      Rs=FAtl3\[rs;1];
      RS=Rs(1:3,:);
      US=Us(1:3,:);
%
%
%ME: Select procedure for upper arm markers
elseif i==2
      %select position vectors for humeral (upper arm) markers
      h4=X(:,10:12);
      h5=X(:,13:15);
      h6=X(:,16:18);
      %define vectors h4h6 and h4h5, the former of which is taken as the
      %technical humeral z axis
      hz=h6-h4;
      h4h5=h5-h4;
      %define cross product of these to give humeral x axis and then
cross
      %z and x axes to give y-axis.
      hx=cross(h4h5,hz);
      hy=cross(hz,hx);
      %unitise the vectors representing the humeral technical axes
      Hx=unit(hx);
      Hy=unit(hy);
      Hz=unit(hz);
      %add these to the original co-ordinates for the origin, marker h4
to
      %give the technical axis unit vectors in terms of the global frame.
      HX=h4+Hx;
      HY=h4+Hy;
```

```
      HZ=h4+Hz;
      %Calculate transformation between global and technical frame.
      HUtl4=soder([1 0 0 0 1 0 0 0 1;HX HY HZ]);
      Me=HUtl4\ptip;
      ME=Me(1:3,:);
      ecenh=(LE+ME)/2;
      scaler=(vecsize(ACh-ecenh))-13.5;
%
%select position vectors for forearm markers
      f1=X(:,1:3);
      f2=X(:,4:6);
      f3=X(:,7:9);
%define wrist mid-point for origin of forearm technical frame.
      f1a=(f1+f2)/2;
      %define vectors f1af3 and f1f2, the former of which is taken as the
      %forearm z axis
      fz=f3-f1a;
      f1f2=f2-f1;
      %define cross product of these to give forearm y axis and then
cross
      %y and z axes to give x-axis.
      fy=cross(fz,f1f2);
      fx=cross(fy,fz);
      %unitise the vectors representing the forearm technical axes
      Fx=unit(fx);
      Fy=unit(fy);
      Fz=unit(fz);
      %add these to the original co-ordinates for the origin, marker f1a
to
      %give the technical axis unit vectors in terms of the global frame.
      FX=f1a+Fx;
      FY=f1a+Fy;
      FZ=f1a+Fz;
      %Calculate transformation between global and technical frame.
      FAtl4=soder([1 0 0 0 1 0 0 0 1;FX FY FZ]);
      Mef=FAtl4\ptip;
      MEF=Mef(1:3,:);
%
%
%TV : Select procedure for trunk markers
elseif i==3
      %select position vectors for trunk markers
      ac7=X(:,19:21);
      t8=X(:,22:24);
      t9=X(:,25:27);
      %define vectors t9t8 and t9ac7, the former of which is taken as the
      %trunk z axis
      tz=t8-t9;
      t9ac7=ac7-t9;
      %define cross product of these to give trunk y axis and then cross
      %z and y axes to give x-axis.
      ty=cross(t9ac7,tz);
      tx=cross(ty,tz);
      %unitise the vectors representing the trunk technical axes
      Tx=unit(tx);
      Ty=unit(ty);
      Tz=unit(tz);
      %add these to the original co-ordinates for the origin, marker t9
to
      %give the technical axis unit vectors in terms of the global frame.
      TX=t9+Tx;
      TY=t9+Ty;
      TZ=t9+Tz;
      %Calculate transformation between global and technical frame.
      TRtl5=soder([1 0 0 0 1 0 0 0 1;TX TY TZ]);
      Tv=TRtl5\ptip;
      TV=Tv(1:3,:);
      man=X(:,22:24)';
      xif=X(:,25:27)';
      Man=TRtl5\[man;1];
```

```
      MAN=Man(1:3,:);
      Xif=TRtl5\[xif;1];
      XIF=Xif(1:3,:);
%Define Trunk anatomical frame.
      tanz=MAN-XIF;
      tany1=TV-XIF;
      tanx=cross(tanz,tany1);
      tany=cross(tanz,tanx);
%unitise the vectors representing the trunk anatomical axes
      Tanz=unit(tanz);
      Tany=unit(tany);
      Tanx=unit(tanx);
%add these to the original co-ordinates for the origin, XIF to
%give the anatomical axis unit vectors in terms of the technical frame.
      TanX=XIF+Tanx;
      TanY=XIF+Tany;
      TanZ=XIF+Tanz;
%Calculate transformation between trunk technical and anatomical frame.
      Ttta=soder([1 0 0 0 1 0 0 0 1;TanX' TanY' TanZ']);
%Calculate transformation between global frame and trunk anatomical
frame.
      Tgta=TRtl5*Ttta;
%Calculate AC with respect to trunk anatomical frame
      act=X(:,28:30)';
      Act=Tgta\[act;1];
      ACt=[Act(1,1) Act(2,1) Act(3,1)-13.5];
%Calculate GH rotation centre with respect to trunk anatomical frame
      GHrt=ACt+(scaler*[0.020495 -0.02463 -0.10802]);
%
%select position vectors for humeral (upper arm) markers
      h4=X(:,10:12);
      h5=X(:,13:15);
      h6=X(:,16:18);
      %define vectors h4h6 and h4h5, the former of which is taken as the
      %technical humeral z axis
      hz=h6-h4;
      h4h5=h5-h4;
      %define cross product of these to give humeral x axis and then
cross
      %z and x axes to give y-axis.
      hx=cross(h4h5,hz);
      hy=cross(hz,hx);
      %unitise the vectors representing the humeral technical axes
      Hx=unit(hx);
      Hy=unit(hy);
      Hz=unit(hz);
      %add these to the original co-ordinates for the origin, marker h4
to
      %give the technical axis unit vectors in terms of the global frame.
      HX=h4+Hx;
      HY=h4+Hy;
      HZ=h4+Hz;
%Calculate transformation between global and technical frame.
      HUtl5=soder([1 0 0 0 1 0 0 0 1;HX HY HZ]);
%Calculate transformation between humerus technical frame and trunk
%anatomical frame.
      HTTG=HUtl5\Tgta;
%calculate location of glenohumeral rotation centre with respect to
%humeral technical axis.
      GHRC=HTTG*[GHrt';1];
%select position vectors for forearm markers
      f1=X(:,1:3);
      f2=X(:,4:6);
      f3=X(:,7:9);
%define wrist mid-point for origin of forearm technical frame.
      f1a=(f1+f2)/2;
      %define vectors f1af3 and f1f2, the former of which is taken as the
      %forearm z axis
      fz=f3-f1a;
      f1f2=f2-f1;
```

```
      %define cross product of these to give forearm y axis and then
cross
      %y and z axes to give x-axis.
      fy=cross(fz,f1f2);
      fx=cross(fy,fz);
      %unitise the vectors representing the forearm technical axes
      Fx=unit(fx);
      Fy=unit(fy);
      Fz=unit(fz);
      %add these to the original co-ordinates for the origin, marker f1a
to
      %give the technical axis unit vectors in terms of the global frame.
      FX=f1a+Fx;
      FY=f1a+Fy;
      FZ=f1a+Fz;
      %Calculate transformation between global and technical frame.
      FAt15=soder([1 0 0 0 1 0 0 0 1;FX FY FZ]);
end
end
%
%
%Humerus
ecenh=(LE+ME)/2;
hanz=GHRC(1:3,1)-ecenh;
hanx1=LE-ME;
hany=cross(hanz,hanx1);
hanx=cross(hany,hanz);
%unitise the vectors representing the forearm anatomical axes
Hanz=unit(hanz);
Hany=unit(hany);
Hanx=unit(hanx);
%add these to the original co-ordinates for the origin, ecenh to
%give the anatomical axis unit vectors in terms of the technical frame.
HanX=ecenh+Hanx;
HanY=ecenh+Hany;
HanZ=ecenh+Hanz;
%Calculate transformation between humerus technical and anatomical frame.
Thta=soder([1 0 0 0 1 0 0 0 1;HanX' HanY' HanZ']);
%
%Forearm
wcenf=(US+RS)/2;
ecenf=(LEF+MEF)/2;
fanz=ecenf-wcenf;
fanx1=RS-US;
fany=cross(fanz,fanx1);
fanx=cross(fany,fanz);
%unitise the vectors representing the forearm anatomical axes
Fanz=unit(fanz);
Fany=unit(fany);
Fanx=unit(fanx);
%add these to the original co-ordinates for the origin, wcenf to
%give the anatomical axis unit vectors in terms of the technical frame.
FanX=wcenf+Fanx;
FanY=wcenf+Fany;
FanZ=wcenf+Fanz;
%Calculate transformation between forearm technical and anatomical frame.
Tfta=soder([1 0 0 0 1 0 0 0 1;FanX' FanY' FanZ']);
Ttta;
```

```
%Procedure to find the flexion, adduction and internal rotation at the
elbow
%and shoulder
%
%Written by Ingram Murray, CREST, University of Newcastle upon Tyne.
%
%Date: May 1998
%
%Modifications : November 1998-     To cater for new method of GH centre
location.
%
%            24/11/98-  to allow SVD optimisation of marker positions
%                       Soderkvist & Wedin (1993).
%
%            13/05/99-  forearm technical frame altered to make z-axis
%                       between proximal ulnar marker and wrist centre.
%
%Input: Output from "tech.m" plus the matrix 'should' containing the co-
ordinate
%data for the nine body-fixed markers through time.
%
%Output: The angles of flexion, adduction and int.rotation at the
shoulder and
%elbow through time, using two methods.(1)  The step-by-step method of
%transformation matrix multiplication.(2) The algorithm of Cole et al
(1993).
%
%References: Cole,G.K. et al (1993).  Application of the Joint Co-
ordinate System
%            to Three-dimensional Joint Attitude and Movement
Representation : A
%            Standardization Proposal.  Journal of Biomechanical
Engineering.
%            November 1993 : Vol 115 : pp 344-349
%
%
%
%
wtraj=[];
etraj=[];
straj=[];
ELBOW=[];
SHOULDER=[];
SHD=[];
ELB=[];
EFTall=[];
ETHall=[];
t=size(should,1);
for k=1:t
%select position vectors for forearm markers
      f1=should(k,1:3);
      f2=should(k,4:6);
      f3=should(k,7:9);
%define wrist mid-point for origin of forearm technical frame.
      f1a=(f1+f2)/2;
%define vectors f1af3 and f1f2, the former of which is taken as the
      %forearm z axis
      fz=f3-f1a;
      f1f2=f2-f1;
      %define cross product of these to give forearm y axis and then
cross
      %y and z axes to give x-axis.
      fy=cross(fz,f1f2);
      fx=cross(fy,fz);
      %unitise the vectors representing the forearm technical axes
      Fx=unit(fx);
      Fy=unit(fy);
      Fz=unit(fz);
```

```
      %add these to the original co-ordinates for the origin, marker f1a
to
      %give the technical axis unit vectors in terms of the global frame.
      FX=f1a+Fx;
      FY=f1a+Fy;
      FZ=f1a+Fz;
      %Calculate transformation between global and technical frame.
      FGT=soder([1 0 0 0 1 0 0 0 1;FX FY FZ]);
      %Calculate transformation between global and anatomical frame.
      FGA=FGT*Tfta;
%
%
%select position vectors for humeral (upper arm) markers
      h4=should(k,10:12);
      h5=should(k,13:15);
      h6=should(k,16:18);
      %define vectors h4h6 and h4h5, the former of which is taken as the
      %technical humeral z axis
      hz=h6-h4;
      h4h5=h5-h4;
      %define cross product of these to give humeral x axis and then
cross
      %z and x axes to give y-axis.
      hx=cross(h4h5,hz);
      hy=cross(hz,hx);
      %unitise the vectors representing the humeral technical axes
      Hx=unit(hx);
      Hy=unit(hy);
      Hz=unit(hz);
      %add these to the original co-ordinates for the origin, marker h4
to
      %give the technical axis unit vectors in terms of the global frame.
      HX=h4+Hx;
      HY=h4+Hy;
      HZ=h4+Hz;
      %Calculate transformation between global and technical frame.
      HGT=soder([1 0 0 0 1 0 0 0 1;HX HY HZ]);
      %Calculate transformation between global and anatomical frame.
      HGA=HGT*Thta;
%
%
%select position vectors for trunk markers
      ac7=should(k,19:21);
      t8=should(k,22:24);
      t9=should(k,25:27);
      %define vectors t9t8 and t9ac7, the former of which is taken as the
      %trunk z axis
      tz=t8-t9;
      t9ac7=ac7-t9;
      %define cross product of these to give trunk y axis and then cross
      %z and y axes to give x-axis.
      ty=cross(t9ac7,tz);
      tx=cross(ty,tz);
      %unitise the vectors representing the trunk technical axes
      Tx=unit(tx);
      Ty=unit(ty);
      Tz=unit(tz);
      %add these to the original co-ordinates for the origin, marker t9
to
      %give the technical axis unit vectors in terms of the global frame.
      TX=t9+Tx;
      TY=t9+Ty;
      TZ=t9+Tz;
      %Calculate transformation between global and technical frame.
      TGT=soder([1 0 0 0 1 0 0 0 1;TX TY TZ]);
      %Calculate transformation between global and anatomical frame.
      TGA=TGT*Ttta;
%
%
if LSQF=='Y'
```

```
Ttcmov=soder([X(:,19:21) X(:,22:24) X(:,25:27);ac7 t8 t9]);
Thcmov=soder([X(:,10:12) X(:,13:15) X(:,16:18);h4 h5 h6]);
Tfcmov=soder([X(:,1:3) X(:,4:6) X(:,7:9);f1 f2 f3]);
TGA=Ttcmov*TRtl5*Ttta;
HGA=Thcmov*HUtl5*Thta;
FGA=Tfcmov*FAtl5*Tfta;
end
%
%
%Calculate relative motion using algorithm of Cole et al (1993).
%Calculate wrist centre, elbow centre and xiphoid wrt global frame.
%Gwcen1=FGT*[wcenf;1];
Gwcen2=FGA(1:4,4);
%Gecen1=HGT*[ecenh;1];
Gecen2=HGA(1:4,4);
%Gxif1=TGT*[XIF;1];
Gxif2=TGA(1:4,4);
%Calculate vector of anatomical frames wrt global frame.
Gfx=FGA*[1;0;0;1];
Gfy=FGA*[0;1;0;1];
Gfz=FGA*[0;0;1;1];
Ghx=HGA*[1;0;0;1];
Ghy=HGA*[0;1;0;1];
Ghz=HGA*[0;0;1;1];
Gtx=TGA*[1;0;0;1];
Gty=TGA*[0;1;0;1];
Gtz=TGA*[0;0;1;1];
%Calculate vectors of each of the axes wrt to global frame.
GFx=Gfx-Gwcen2;
GFX=GFx(1:3,1);
GFy=Gfy-Gwcen2;
GFY=GFy(1:3,1);
GFz=Gfz-Gwcen2;
GFZ=GFz(1:3,1);
GHx=Ghx-Gecen2;
GHX=GHx(1:3,1);
GHy=Ghy-Gecen2;
GHY=GHy(1:3,1);
GHz=Ghz-Gecen2;
GHZ=GHz(1:3,1);
GTx=Gtx-Gxif2;
GTX=GTx(1:3,1);
GTy=Gty-Gxif2;
GTY=GTy(1:3,1);
GTz=Gtz-Gxif2;
GTZ=GTz(1:3,1);
%Calculate shoulder angle using "Cole.m".
C1=[GTX' GTZ' GTY';GHX' GHZ' GHY'];
SHOULDER(k,1:3)=cole(C1);
%Calculate elbow angle using "Cole.m".
C2=[GHX' GHZ' GHY';GFX' GFZ' GFY'];
ELBOW(k,1:3)=cole(C2);
%
%
%Calculate relative motion at elbow my way
EHF=HGA\FGA;
%Calculate relative motion at shoulder my way
ETh=HGA\TGA;
ETH=inv(ETh);
%
%
%For calculation of wrist trajectory, need forearm frame wrt trunk frame.
EFt=FGA\TGA;
EFT=inv(EFt);
%
%
%Construct big matrices containing all EFT and ETH matrices.
EFTall=[EFTall EFT(1:3,1:3)];
ETHall=[ETHall ETH(1:3,1:3)];
%
```

```
%Calculate AC with respect to trunk anatomical frame
      actt=should(k,28:30)';
      Actt=TGA\[actt;1];
      ACtt=[Actt(1,1) Actt(2,1) Actt(3,1)-13.5];
%Calculate GH rotation centre with respect to trunk anatomical frame
      GHrtt=ACtt+(scaler*[0.026092 -0.012583 -0.111488]);
%
%Compile wrist, elbow and humeral head centre trajectories wrt trunk
axes.
wtraj(k,:)=EFT(1:3,4)';
etraj(k,:)=ETH(1:3,4)';
straj(k,:)=GHrtt(1,1:3);
%
%
%Break transformation matrices into Euler angles.
Elb=rzyxsolv(EHF);
ELb=Elb(1,1:3);
ELB(k,1:3)=ELb;
Shd=rzyxsolv(ETH);
SHd=Shd(1,1:3);
SHD(k,1:3)=SHd;
end
%
%
%Results from my method
%disp('               ELBOW')
%disp('   Flexion  Adduction Int.Rotn.')
%disp(ELB)
%disp('              SHOULDER')
%disp('   Flexion  Adduction Int.Rotn.')
%disp(SHD)
%
%
%Results from the algorithm of Cole et al (1993)
%disp('      ELBOW-COLE ET AL (1993)')
%disp('   Flexion  Adduction Int.Rotn.')
%disp(ELBOW)
%disp('    SHOULDER-COLE ET AL (1993)')
%disp('   Flexion  Adduction Int.Rotn.')
%disp(SHOULDER)
%
%
Wtraj=wtraj/1000;
Etraj=etraj/1000;
Straj=straj/1000;
```

```
%UNIT Unitize a vector
%
%     UNIT(V) returns a unit vector aligned with V.

%     Copright (C) Peter Corke 1990
function u = unit(v)
      u = v / norm(v,'fro');
```

```
function [S]=vecsize(data)
%Procedure vecsize.m gives the magnitude of a 1*3 vector
%
%Written by Ingram Murray, CREST, University of Newcastle upon Tyne.
%
%Date: February 1998
%
%Input: Vector X
%
%Output: Magnitude of the vector X
%
if size(data,1)==1
a=data(1,1);
b=data(1,2);
c=data(1,3);
elseif size(data,1)==3
a=data(1,1);
b=data(2,1);
c=data(3,1);
end
A=a*a;
B=b*b;
C=c*c;
S=sqrt(A+B+C);
```